FAILURE OF STEEL GUSSET PLATES

by

Stephen Robinson BSc

A thesis submitted for the degree of

Doctor of Philosophy

Department of Civil Engineering and Construction

The University of Aston in Birmingham

December 1983

Department of Civil Engineering and Construction
The University of Aston in Birmingham

FAILURE OF STEEL GUSSET PLATES

by
Stephen Robinson BSc

A thesis submitted for the degree of
Doctor of Philosophy

December 1983

SYNOPSIS

This thesis examines the parameters associated with the failure of triangular steel gusset plates. Eighty two results are presented investigating the position of the applied load, the gusset plate height to length ratio, size, thickness, internal angle and the removal of the inside corner. The thickness of the loaded plate and its influence on the gusset plates failure is also investigated. Twenty two similar gusset plates were tested to investigate the welds connecting the gusset plate to the adjacent loaded and support edges.

The experimental results are compared with existing methods, none of which cover all the variables tested. Some methods do not consider buckling and most of those that do are inadequate. Most of the methods do not accurately take account of the load position. An alternative method based on experimental observations is presented for design purposes. The method covers any combination of the variables tested. To test assumptions made in the theoretical work forty seven strut tests took place to investigate buckling characteristics and fifteen special gusset plates were also tested.

The gusset plates were found to fail in an elastic-plastic buckling manner. A gusset plate has a specific moment of resistance capacity about its inside corner and the ultimate load that can be applied is dependent upon the position of the load relative to the supported edge. There is an optimum height to length ratio for strength and any increase in the internal angle from 90 degrees produces little change in moment capacity. The removal of small portions of the inside corner of a gusset plate has little effect upon its moment capacity. The loaded plate does not provide any significant moment of resistance to the applied load at failure. The main functions of the loaded and supported edge welds is to prevent the gusset plate from slipping from between the plates.

Gusset plate Buckling Steel Welded Bracket

ACKNOWLEDGEMETNS

The author would like to express his sincere gratitude to:

The late Professor M. Holmes, BSc, PhD, DSc, CEng. FICE, FIStructE, formerly Head of the Department of Civil Engineering at the University of Aston in Birmingham for allowing this research to be carried out in the laboratories.

L.H. Martin, BSc, PhD, MICE, CEng, for his encouraging and helpful supervision.

Mr W. Parsons, formerly Chief Technician in the Civil Engineering Department and the staff of the Structural Laboratories and workshops for the invaluable help they provided during the fabrication and testing of the specimens.

Miss G.R. Thomas and Mrs G. Jones for typing the thesis neatly and efficiently.

Miss L. Pottiti and Mrs J. Hall for their help in completing the typing.

I would like to take this opportunity of thanking my wife Mary for being so patient and helpful while I have been completing my thesis.

CONTENTS

TABLE OF CONTENTS

CHAPTER SEVEN THEORETICAL ANALYSIS OF THE WELDS

CHAPTER EIGHT DESIGN

CHAPTER NINE CONCLUSIONS AND RECOMMENDATIONS FOR FUTURE WORK

LIST OF FIGURES

LIST OF TABLES

CHAPTER ONE

INTRODUCTION

1.1 General introduction

The majority of steel buildings consist basically of a main structural framework of beams and columns connected together by joints. This framework forms a skeleton which supports the floors, roof, external and internal walls etc., together with the external and internal applied loads.

In previous decades it was usually the main structural framework that was designed to take all these dead and live loads, and not the infilling walls and floors etc. Architectural and engineering trends produced structures with many internal partitioning walls consisting of materials, such as brick and stone which possesed strength and mass. The external walls were also of similar materials. In many situations the strength of the walls was not taken into consideration in the design calculation, but because of their weight, the member sections of the framework were relatively large. The main structural framework was therefore designed to provide the structural rigidity, and the joints were designed accordingly. However, a considerable amount of extra bracing and rigidity was provided by the numerous strong partitions and external walls which made the joints partly redundant. The design of the joints was therefore not so critical because any inadequacies would have been supplemented by the stiffness provided by these strong partitions etc.

The continuing demand for more economical structures necessitates reducing the quantity of material used and only incorporating heavy structural materials where absolutely necessary. This has led to structures being designed on an "open plan" basis with fewer internal partitioning walls, which are made from far lighter and weaker

materials with virtually no structural strength or rigidity. Similarly, external walls and decoration are of very much lighter and weaker materials, with the external decoration being in the form of cladding panels, which are hung onto the structural framework. In office blocks, for example, extensive use of glass has prevented any form of cross bracing being used. As a result, in modern structures, there is very little extra bracing or rigidity provided by these lighter partitions and cladding, and in some cases, where they do have some strength, as with corrugated steel panels on factory buildings, it is used in the design calculation. This means that far more reliance is placed upon the joints to take the loads for which they were designed, as the present day partitions are not capable of providing the necessary support to supplement any inadequately designed joint. Therefore a particular joint design which was used in an old structure will not necessarily be adequate in a structure of today and has led to the need for the joints to be justified in terms of their self strength.

In previous decades the design of steel structures was based on simple conservative assumptions regarding the behaviour of the members and the joints. The allowable stress design approach was used based on elastic analysis where the conditions of buckling or the initiation of yielding were recommended as design criteria. Plastic methods of design were not generally used. The design stresses obtained by these methods were generally conservative producing structures with relatively large member sizes.

The ability to produce steels of a far more consistant yield strength has facilitated the accurate specification of yield strengths allowing more efficient use of the material with a resulting reduction in the member sizes and materials factor. The specified allowable stresses are also higher than before, resulting in a further reduction of the overall safety factor.

Following the need to use materials more efficiently, it has been necessary to design the structural framework more efficiently, utilising the strength provided by the structural materials. This has resulted in research into the behaviour and design of the main members, involving the development of more elaborate structural analysis techniques, which make use of the plastic strength and the stiffness of the joints. These methods are more accurate at modelling the stresses in the structure, resulting in less conservative design stresses which are much closer to the actual stresses. For these methods to be accurate, further knowledge of the structural behaviour of the joints is required. Although there has been a considerable amount of research into the main members of a structure, providing engineers with a better understanding of their behaviour, the behaviour and design of the joints connecting these members has been neglected and there is a scarcity of information on real behaviour.

The British steel code 449(1) and more recently the proposed British draft steel code (2) give very little information on joint design and therefore encourage designers to spend the minimum time and effort on such details. The detailing in many design offices is allocated to those with lower academic and professional qualifications and in some cases is even left to the tracer/draughtsmen. In some circumstances the contractor who is involved in the fabrication and erection of the structure, and not directly involved in the design of members themselves, is either left to design the connections or may alter the design to suit his needs. Because of this, the basic assumptions in joint design are often not correct and the distribution of forces within the joints are not understood. This has become very apparent with the proposed introduction of the British draft steel code (2), where for the first time calculations are required at the ultimate limit state.

Designers still have to rely on the "rule of thumb" methods as

used for the structures of the past. Design of this nature may be attributed to engineering judgement and common sense based on years of experience. However, this experience was based on structures which had relatively large member sections with relatively low stresses. The structures also had a considerable reserve of strength and any inaccuracies in the joints would have been absorbed. In many cases the design was what looked right. The result is a reduction in the size of these details with the member sizes and therefore a corresponding reduction in their strength.

As the reserve strength is gradually reduced in the design of the new structures, then the actual safety factors for the individual components and the structure as a whole are reduced. In the old structures the actual factors of safety for each component may not have been the same, nor would they have been reduced by the same amount. The reserve strength has and still is continually being eroded.

1.2 Economic factors

Economic factors are also important in relation to design. Professor Van Dowen in a paper to the 2nd International ECCS Symposium in 1978(3), calculated that in the developed world the cost ratio of a man-hour of labour to a kilogram of steel had risen from 5 in 1945 to no less than 40 in 1978, a trend which is still continuing. Even allowing for doubled productivity flowing from the introduction of sophisticated machine tools, a factor of at least four is apparent. Thus Van Dowen maintains that in a steel structure designed, fabricated, painted and erected, material cost will only range from some 20% to 40% of the final cost of the structure. Further that a design fully optimising labour and material costs, will no longer be the optimum two years later. It therefore follows that a design based on achieving a minimum total weight considers only the minor part of

the problem, and is likely to be counter-productive if any increase in labour content is involved.

Generally in connections with an advanced technology, labour costs are high and it is therefore more economical to use more material and less labour. Professor Van Dowen, in his paper, presented relative material and fabrication costs for alternative design examples of some typical connections. One of the examples presented was the column base plate connection. He points out that many columns are designed with relatively thin base plates with stiffeners, instead of using a thick base plate. Although the former detail would require less material in the base plate it would require the use of additional material for the stiffeners and more manhours to cut the stiffeners and for the additional welding. He also points out that due to the economic situation in 1946 the stiffened base plate was then the most economical design overall. However, as the economic circumstances have changed, where a thick base plate is a possible alternative to the stiffened base plate, then the thick base plate without stiffeners will generally be the most economical design solution today. However there will be situations where a thick base plate would be totally inadequate and impractical, with the stiffened base plate being the most practical solution. In some of the developing countries where the labour is relatively cheap in comparison with the cost of materials the stiffened base plate connection is still the most economical solution.

1.3 Triangular steel gusset plates

The subject of joints in structural steelwork is extensive and complicated, which is probably why investigation has been limited in the past. This research is an attempt to provide a design method for one small aspect of the subject, namely the triangular steel gusset plate.

Triangular steel gusset plates consist of a flat, roughly triangular shaped plate which is usually welded in place. They occur in structures as a form of stiffener, mainly in joint construction such as support brackets for beams and crane girders, and as stiffeners in heavy bolted and welded frame joints and column bases. In the majority of cases they are required to sustain in-plane compressive loads, although in some cases they are loaded in tension. However, the compressive load condition is the least understood and therefore the most difficult to design for.

This work is concerned with the type of steel gusset plates found in the situations as shown in Figure 1.1. The basic shape of the gusset plate is triangular with two built in edges, and free on the third side as shown in Figure 1.2(a). The load is applied as a form of distributed compressive load and failure occurs by buckling as shown in Figure 1.2(b).

The following chapter contains a review of the relevant research and existing methods related to the design of steel gusset plates. Very little experimental work was found and most of the methods have no experimental verification. Experimental results were therefore necessary to complement the existing work and to determine the validity of the existing methods. Chapter 3 contains the test programme, testing and specimen details. Chapter 4 contains the experimental results and in Chapter 5 they are compared with the existing methods. An alternative method suggested by the author is developed for the gusset plates in Chapter 6 and for the welds in Chapter 7. Chapter 8 presents the method in a form suitable for use in design practice. The author's conclusions and recommendations for future work are given in Chapter 9.

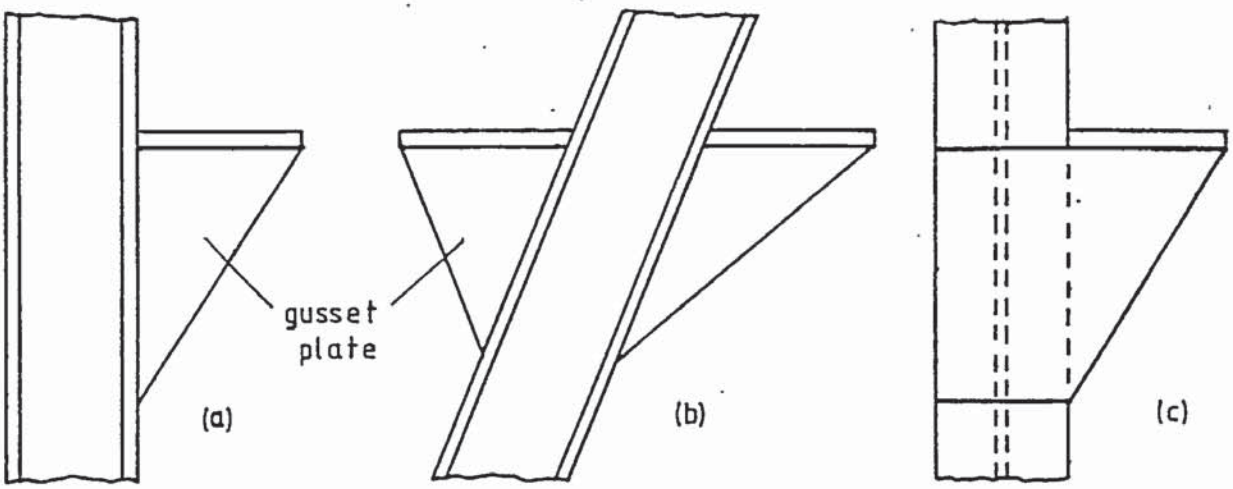

support brackets for beams and crane girders

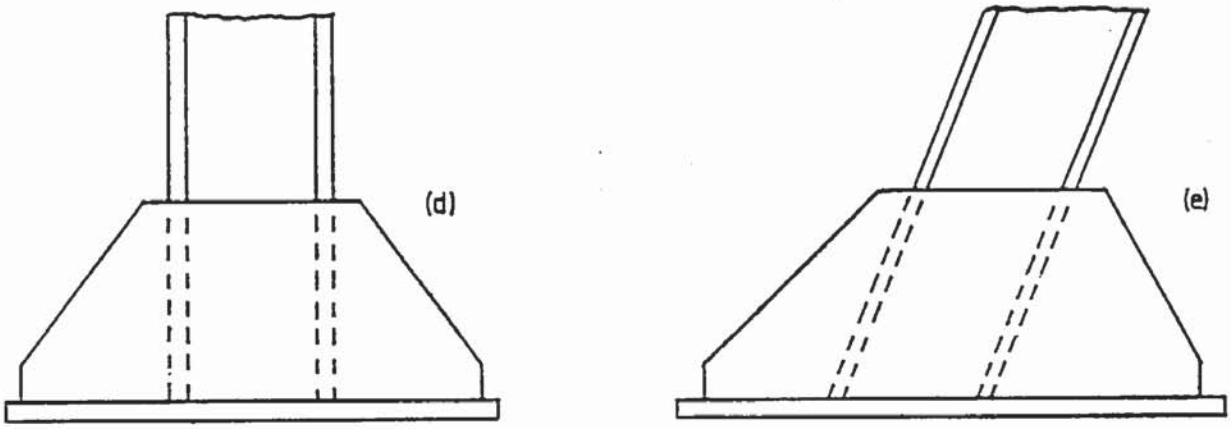

column bases

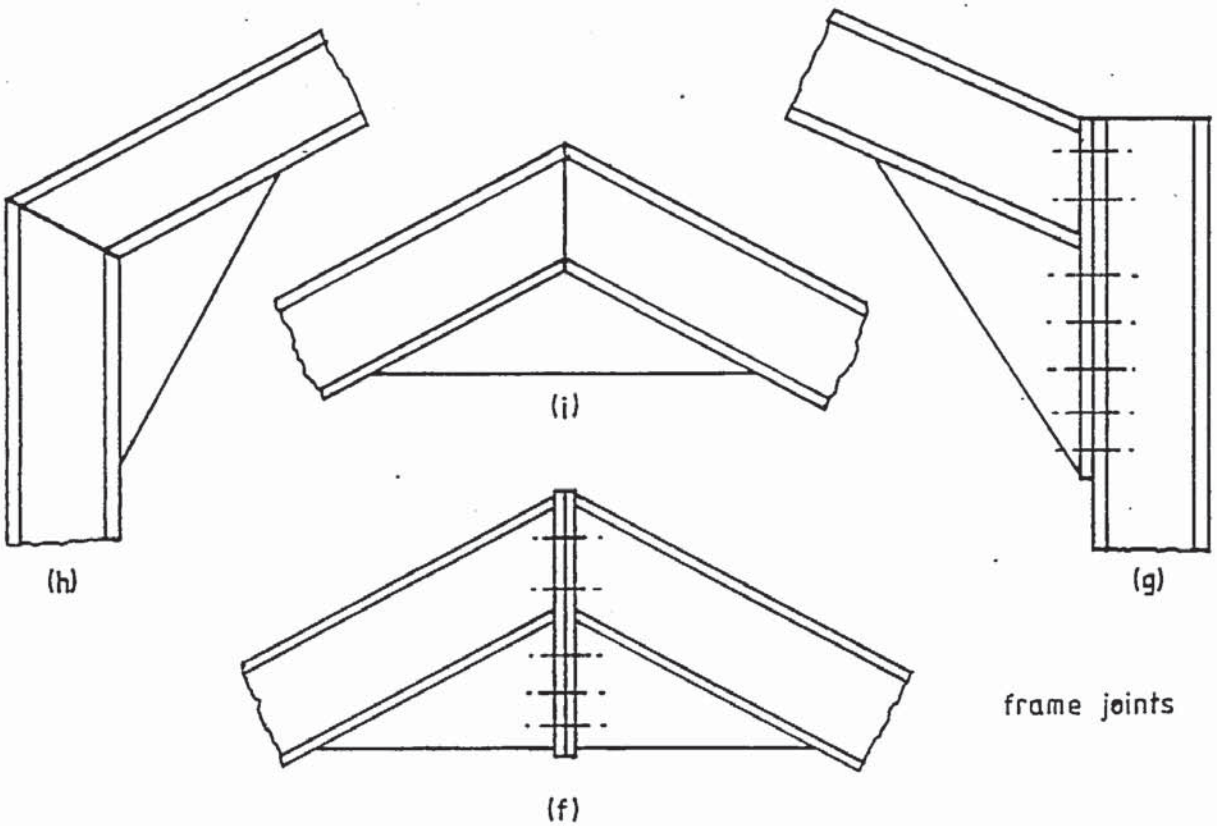

frame joints

Figure 1.1 Typical gusset plate applications.

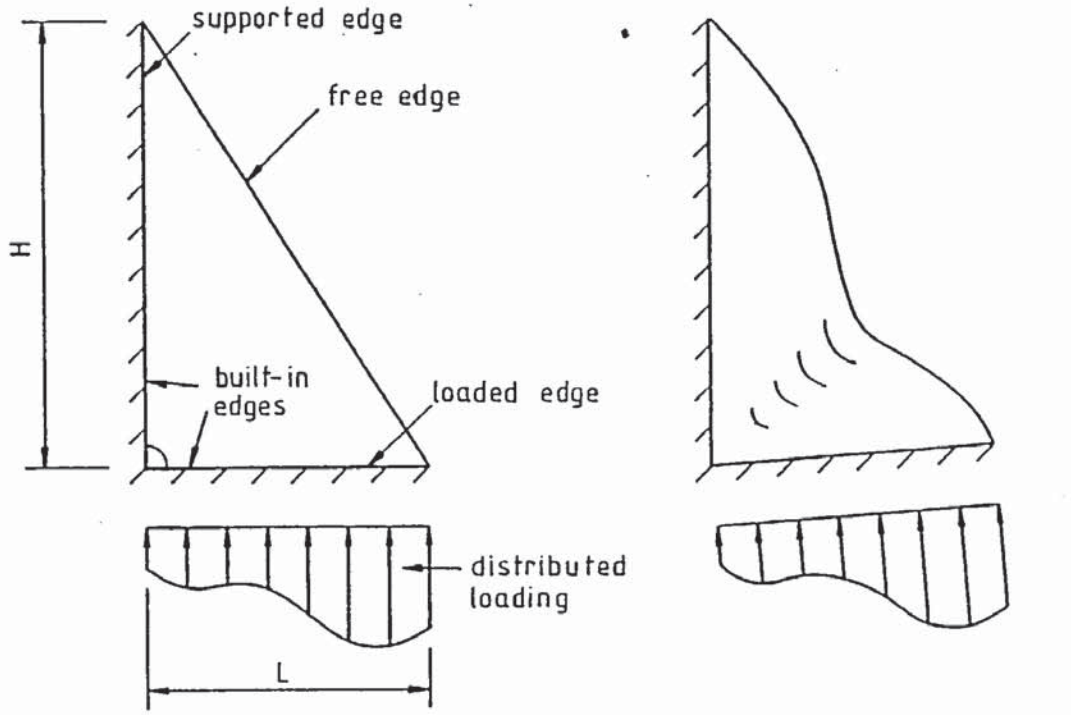

Figure 1.2 Typical gusset plate and failure mode.

CHAPTER TWO

LITERATURE REVIEW

2.1 Introduction

The behaviour of triangular gusset plates has received little attention and for many years the design of such plates was either based on experience without benefit of theory or tests. When in doubt, angle or plate stiffeners were used along the diagonal free edge of the plate rather than attempting to determine the thickness necessary to prevent buckling without diagonal edge stiffeners. As a consequence there is very little information on the design and behaviour of triangular gusset plates without edge stiffeners and the current British steel code B.S.449 (1) gives no advice on the design of such gusset plates. The following sections contain a review of the relevant research and existing methods.

2.2 Jensen's experimental & theoretical work

As far as can be determined the first work related to the design of triangular steel gusset plates was an experimental investigation by Jensen (4) in 1936, concerned with the design of the rigid type of welded steel brackets, of which there are many designs. The rigid type of bracket generally consists of two plates, a top loaded plate and a supporting gusset plate, or it may be a short section of an I or H section.

Jensen's (4) investigation was divided into three parts.

1. Eight celluloid models were tested by polarised light, to determine the lines of stress in the gusset plates.
2. Two brackets of steel were tested which were built to a linear scale of seven times the celluloid models, to measure more precisely the stresses in the gusset plates.
3. The testing of twenty-two small brackets, generally with 3/8 inch plates to determine the reserve strength of the bracket gusset plates,

the accuracy of a proposed method for designing the gusset plates and to check a method proposed by Priest (5) for designing the welds.

The Celluloid models of eight bracket shapes are shown in Figure 2.1, The loaded length, supported length, position of the applied load and its magnitude are assumed to be the same in each case. The results of these tests indicated very low stresses in the extra material added to the free edge of the basic triangular gusset plate shape and also on the inside corner of the gusset plate, indicating to Jensen (4) an excess of material. This suggests to the author that the removal of these portions would have little influence on the load carrying capacity of the brackets.

With the triangular shaped gusset plates, with and without the inside corner removed, specimens a and b in Figure 2.1, the line of action of the compressive stress in the gusset plate was roughly parallel to the diagonal free edge of the plate. The stress in the plates decreased from the outside edge inward along section BC and DE. This variation suggested to Jensen (4) the possibility of using the design formula for eccentric loads on prisms.

The plates with extra material added to the free edge, specimens c to e, in Figure 2.1, indicated that the section KL perpendicular to the applied load was the critical section and that specimens d, e and f would probably carry the same load as c.

Specimens g and h in Figure 2.1, represent brackets consisting of short sections of I-beam. Two methods of welding were used, (1) top and bottom welds as simulated by specimen g, and (2) top and bottom welds plus a web weld as simulated by specimen h. A better stress distribution was obtained for specimen h than for g. The section FG perpendicular to the applied load was taken as the critical section, the same as for specimens c, d, e and f.

The two steel prototype brackets, specimens a and b of Figure 2.1

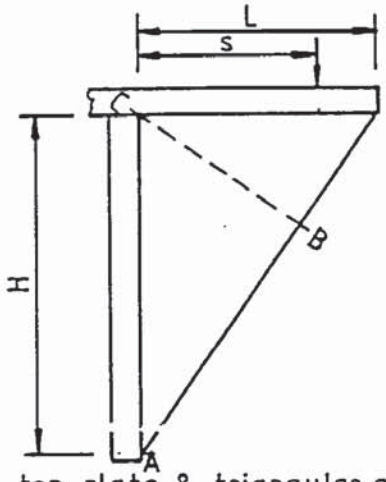

(a) top plate & triangular gusset plate.

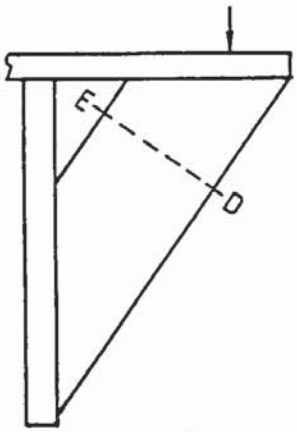

(b) top plate & partial gusset plate.

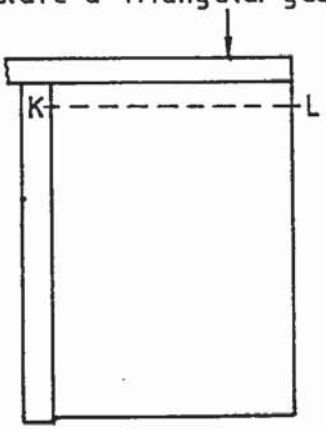

(c) top plate & rectangular gusset plate.

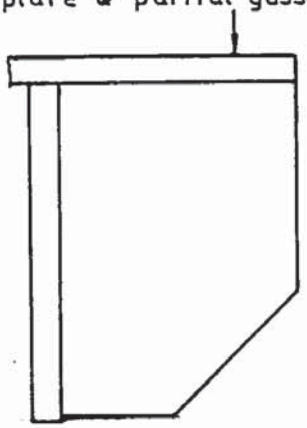

(d) same as "c" except corner cut off.

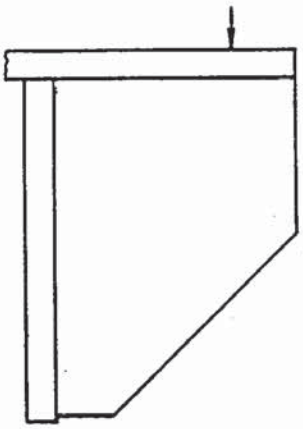

(e) same as "c" except corner cut off.

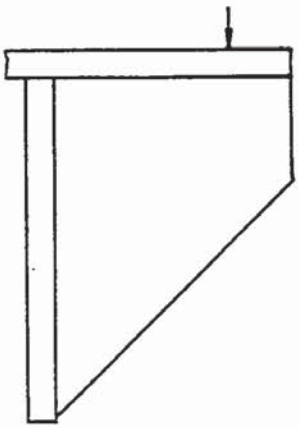

(f) same as "c" except corner cut off.

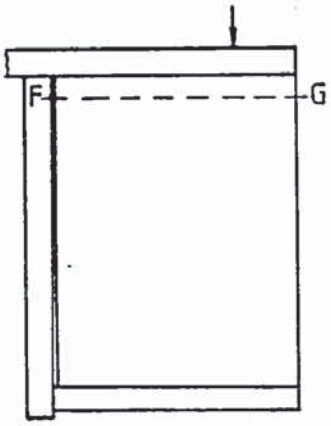

(g) short I-section.

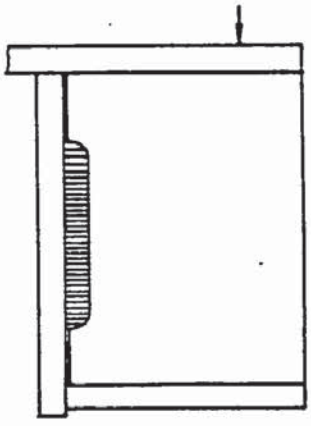

(h) same as "g" except center of web fixed.

Figure 2.1 Jensen's celluloid model bracket shapes.

were built to a linear scale of seven times the celluloid models. The loaded length, supported length and position of the applied load from the face of the column were 9, 12.74 and 6.55 inches respectively. The thickness of the plate was not given. The stress trajectories obtained from the celluloid models indicated that in the steel prototype the principal stresses in each gusset plate could be measured along the critical section. This was done by setting Huggenberger tensometers parallel to the free edge of the plates. The stresses perpendicular to the sections BC and DE were compared with those obtained from the model analysis and those computed by the eccentric loads on prism method suggested. The results are shown in Figure 2.2.

The steel prototypes were retested in an attempt to place the load so that a uniform stress distribution would be obtained in the gusset pates. However, this condition could not be obtained and was explained as ignorance as to where the applied load changed direction from the vertical to the direction parallel to the free edge of the gusset plate. The moment arms selected were based on the assumption that the load line extended vertically through the top plates and then suddenly change to a line parallel to the free edge as shown in Figure 2.2.

As a uniform stress distribution was not obtained, Jenson (4) concluded that the resultant force was not parallel to the free edge of the gusset plate but was inclined more steeply downward. This conclusion was confirmed by the abnormal strains in the region between G and the outer edge of the gusset plate from the tests, as shown in Figure 2.2. In addition the point of computed resultant compressive stress in the welds using the method suggested by Priest (5), is in the region of F and G, Figure 2.2.

Other conclusions made by Jenson (4) from these tests were that a large bending moment existed which subjected critical parts of the

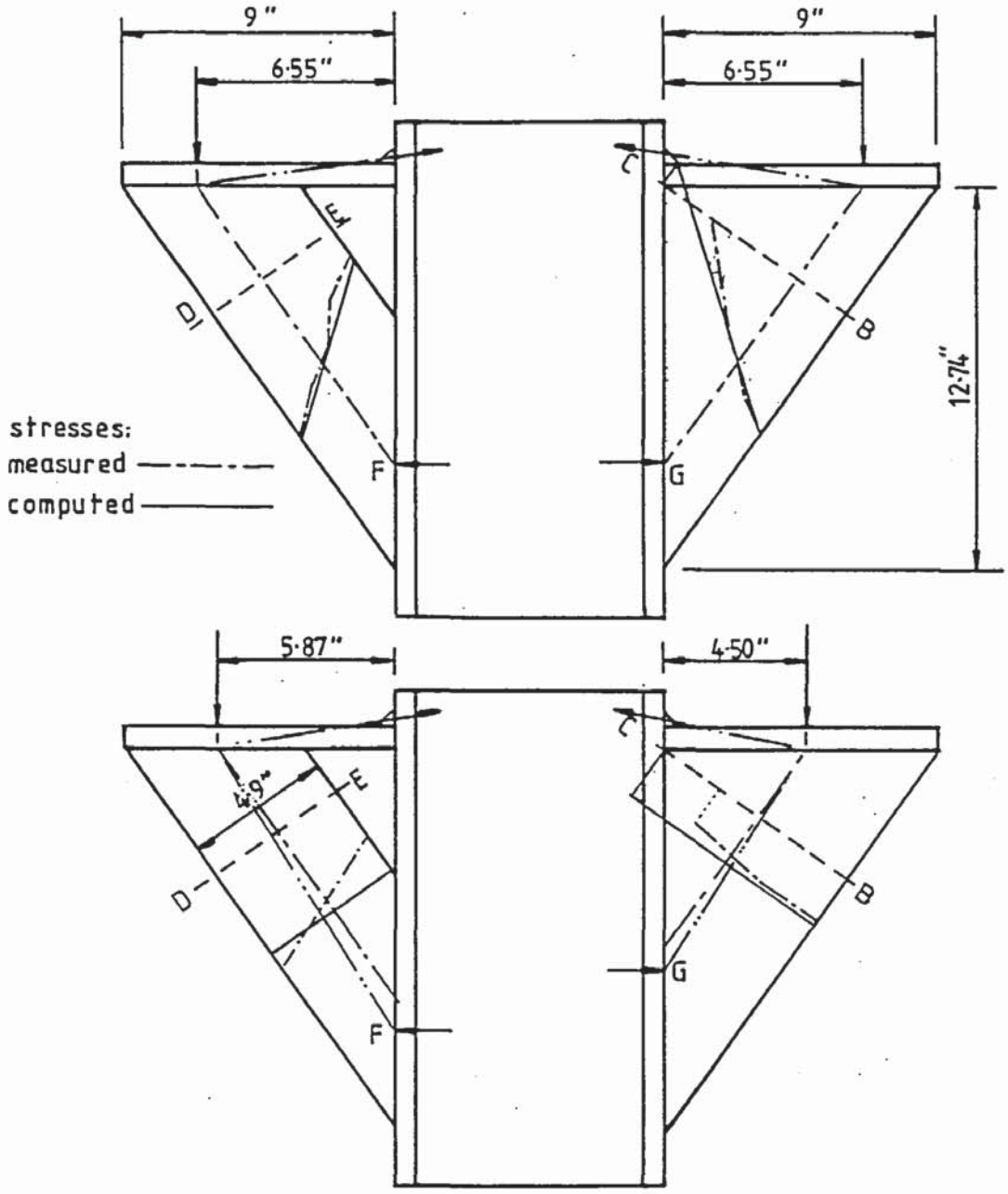

Figure 2.2 Comparison of stresses in Jensen's steel models.

gusset plate to compression, and the top plate to tension. The shearing load on the bracket was mainly carried by the gusset plate.

Jensen (4) went on to test to failure, sixteen small steel brackets constructed of 3/8 inch plates, two brackets with 1/8 inch gusset plates and four larger brackets. Two of these with 1.25 inch gusset plates and the other two of 8 inch I section.

In all of the small brackets the loaded edges were three inches long and the load was applied two inches from the face of the column.

The top plates were two inches wide with a 1/4 inch fillet weld across the top connecting it to the column. Other weld sizes were not specified and are therefore assumed to be the same. Two sets of the 3/8 inch thick specimens were made with different lengths of the weld connecting the top loaded plates to the column. One set had the weld all the way across the top loaded plate, the other only part the way across. The latter produced lower ultimate loads.

Another two sets of the 3/8 inch thick specimens were made up with the supported edge of the gusset plate not in contact with the column. It was thought that the plates in contact would be stronger, but this made very little difference to the ultimate loads. Each set of specimens consisted of three triangular gusset plate specimens with the supported edges of lengths 5.2, 4 and 3 inches respectively.

Another two 3/8 inch thick specimens were made up with rectangular profiles and with the lower corners cut off at 45°. The loaded lengths were the same as before, i.e. 3 inches, and the supported edges were 5.2 inches. The weld details for one of these specimens the same as the previous specimen, but the second specimen had a 3/8 inch fillet weld on the top loaded plate.

The two specimens made with 1/8 inch gusset plates were the only two specimens made to produce buckling of the gusset plate. The computed stresses on these plates at the buckling loads were slightly above the yield stress. These two gusset plates had loaded and supported edge lengths of 3 and 5.2 inches respectively. One specimen had a triangular gusset plate, the other had a rectangular gusset plate with the lower corner cut off at 45°.

Two specimens were made with the 3/8 inch gusset plates to investigate the effect of removing the inside corner and were compared with the two triangular gusset plate brackets with supported lengths of 5.2 and 4 inches respectively. The ultimate loads in both comparisons were approximately the same however, but the amount that

was removedwas not indicated.

The four larger size specimens were tested as a final check on the design formulas used in his paper. The two specimens with 1.25 inch thick gusset plates had loaded edge lengths of 4 inches and the load was applied at 3.2 inches from the face of the column. The top plates were 4 x 1.25 x 4.25 inches. The two specimens had rectangular gusset plates with the lower corners cut off at 45°. The supported edges were of lengths 8.6 and 10.0 inches respectively. The former had a 3/8 x 3.5 inch weld on top of the top plate and the latter had a 1/2 x 3 inch weld on the under side of the top plate. The fillet welds on the rest of the specimens were assumed to be of the same size.

The other two specimens were made from 8 inch I-sections with two different welding arrangements. The specimen with the extra weld along the web was stiffer, although the other specimen, in spite of the excessive deflection, carried 6.7 per cent more load.

The testing arrangement is not quite clear but, it is assumed that the column to which the brackets were welded was rigidly supported. The load was applied to the top plate as a point load in the form of a wedge and spanning it laterally. The loads at which the first appearance of strain lines on the whitewash coating and at which strain lines were generally distributed over the gusset plate were noted. With the exception of two plates which buckled, failure occurred in the top welds, with the gusset plates still carrying load, although in many cases there was excessive deformation.

The load at which the appearance of the first strain lines occurred was taken to be the load at which the yield at a point was first reached in the gusset plate. The load at which strain lines were generally distributed over the gusset plate was taken to be the plastic load of the gusset plate. This latter load condition was

compared with computed loads which assumed that the yield stress had been reached, presumably across the plate, and that a rectangular distribution of stress was obtained. The computed loads were slightly lower than the experimental values and was partly accounted for by the fact that the vertical load carried by the top welds was not considered.

It is understood from Jensen's (4) paper that after the plastic load of the gusset plate had been reached, the gusset plates deformed, whilst still taking load, until the top welds failed giving the ultimate load readings. The gusset plates at this point were still capable of sustaining a load. Therefore the predicted ultimate load based on weld strength should compare favourably with the actual ultimate load. Jensen (4) reasoned that the experimental values should be less than the theoretical values because the top welds were subjected to tearing stresses due to deformation of the gusset plate and the top plate. Jensen (4) concluded that these tearing stresses were not, however, so important as to cause actual failure before the predicted failure.

The method of designing the steel brackets proposed by Jensen (4) is as follows. A method suggested by Priest (5) was used to design the welds. The method treats the fillet welds as if they were single lines and the centroidal axis in the vertical plane is determined. The resultant stress in the top weld is then calculated, assuming that this is the most highly stressed weld, and combining the shearing and bending stresses at this point by vector addition.

Priest (5) placed his top weld on the under side of the top plate in order to avoid harmful contact between beam and weld. However, Jensen (4) in another paper, found that welds on the top of the plate are so much stronger than those at the bottom (tension instead of shear), that top welds should be used whenever possible.

For the design of gusset plates, Jensen (4) suggested the use of

the design formula for eccentric loads on prisms as follows. A section is chosen which is considered to be the most critical. For rectangular plates this section is taken to be the section perpendicular to the applied load, sections KL and FG in Figure 2.1 c and g. For triangular gusset plates it is usually the section taken across the plate from the inside corner and perpendicular to the free edge, sections CB and ED in Figure 2.1 a and b. It is also suggested that section CA in Figure 2.1 a, may be the critical section when the loaded length L is large in comparison with the supported edge H.

For the triangular gusset plates the general solution is as follows. The method assumes that the gusset plate acts as an eccentrically loaded prism and buckling does not occur as in Figure 2.3. The maximum stress in the plate is assumed to be along the free edge and the stress at the free edge on the critical section is computed from

$$f_{max} = P'/A + M'/z \qquad (2.1)$$

where f_{max} = compressive stress at B

P' = component of the applied load normal to section CB

A = area of section = $t(BC)$

M' = bending moment due to eccentricity of load = $P'e'$

z' = section modulus = $[t(BC)^2]/6$

It is not clear at which section Jensen (4) considered the change in direction of the applied vertical load, which affected the value of the eccentricity e' used. In one of Jensen's (4) diagrams the change in direction is shown to be at the centroid of the loaded plate. In the test it was assumed to be at the bottom of the loaded plate. The former assumption gives a smaller value for the eccentricity e' and a greater failure load for the same gusset plate the thicker the loaded plate. The theoretical values presented in Jensen's experimental work are not in agreement with either of these assumptions.

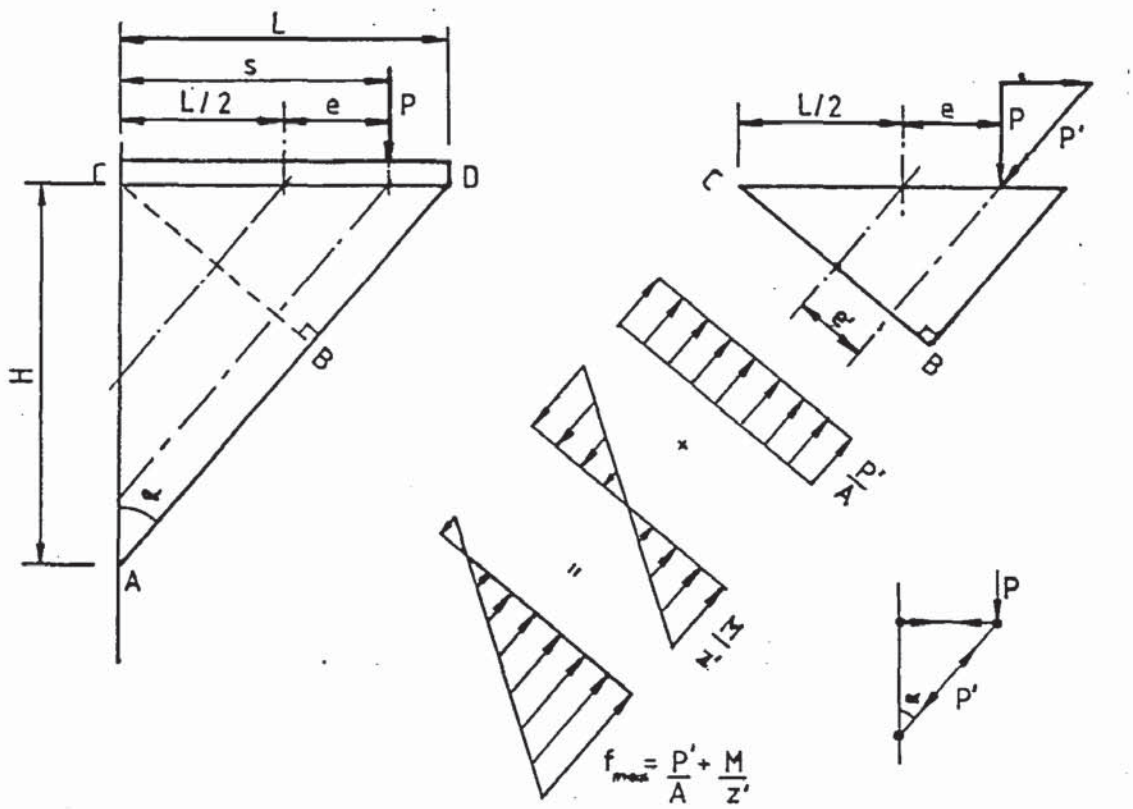

Figure 2.3 Stress distribution and geometry assumed by Jensen.

Jensen's (4) work was directed towards the testing and design of stiffened beam seat brackets. Although these brackets fall into the category of triangular gusset plates, they are so thick relative to the other dimensions that buckling is no problem. However, as these were the only tests available the method proposed by Jensen (4) for beam seats was adopted and extended for designing other gusset plates. Variations in this method have been developed to cope with the effects of buckling.

The method proposed by Jensen (4) is suggested for use by the A.W.S. Welding Handbook (6), Beedle et al (7) and Salmon et al (8). Each of these references takes the change in direction of the applied load as being at the bottom of the loaded plate, although the latter two references show the change in direction at the top of the loaded plate in their diagrams. Each of these references has expressed Jensen's (4) theory in a general equation form as follows.

Assuming that the change in direction is at the bottom of the

loaded plate, Equation 2.1 can be expressed in terms of the load eccentricity e as

$$f_{max} = \frac{P}{L.t.\cos^2\alpha}(1 + 6.e/L) \qquad (2.2)$$

or expressed in terms of the distance s, the position of the applied load along the loaded plate

$$f_{max} = \frac{P}{L.t.\cos^2\alpha}(6.s/L - 2) \qquad (2.3)$$

Equations 2.2 and 2.3 calculate the maximum stress along the free edge at the critical section. The problem is to determine this stress for design purposes. In an elastic allowable stress design this would be a factored elastic critical stress, which must be defined. If the plate fails by yielding then this stress would be the yield stress. If the plate fails by buckling then the stress should be an elastic critical buckling stress which is less than the yield stress. Jensen (4) takes the yield stress as the elastic critical stress which is factored to give an allowable stress for design purposes and ignores the effects of buckling.

The A.W.S. Welding Handbook (6) uses an allowable stress based on yielding and does not consider the possibility of buckling. Beedle et al (7) suggests that the possibility of buckling can be checked separately and conservatively. This is done by assuming that the component of the applied load P normal to the section CB being considered irrespective of its position along the loaded edge, acts concentrically on a strip of the gusset plate which is assumed to form a column of the length of the free edge AD ($=L/\sin\alpha$) and one quarter of the width of the critical section CB as shown in Figure 2.4.

The implications of this are not clear. Either the load that can be sustained by assuming this quarter width strip of plate is checked, assuming some slenderness ratio limitation and buckling equation or alternatively the buckling stress of this strip of plate is calculated

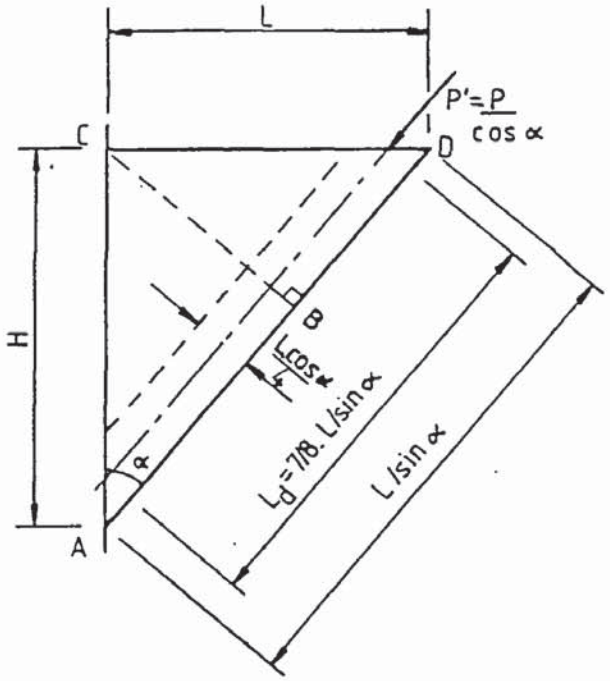

Figure 2.4 Beedle et al's stability check assumption.

and used as a limiting value for use in Jensen's equation.

The former method is in fact another method which, as shown later, is highly conservative. The latter method seems the most obvious, but requires the centre line length if considering a quarter width plate, otherwise a unit width is sufficient if considering the length of the free edge.

The problem is then to define the slenderness ratio limitation and buckling equation to be used to calculate the buckling stress. Beedle et al (7) gives no information but Salmon et al (8) suggests considering a similar strip of plate of the same width (L cos α /4) acting as a column and using the plate buckling equation

$$\frac{b}{t} \leqslant \sqrt{\frac{k\pi^2 E}{12(1-\nu^2)f_b}} \qquad (2.4)$$

with k = 1.0 for a pin-ended plate; letting b = Ld (=7/8 L/sin α), the centre line length of the strip of plate and putting the buckling stress f_b equal to the yield stress to give a limiting plate thickness to ensure yield occurs before buckling. However, assuming the load is

supported by a pin ended quarter width strip of plate appears to be a highly conservative way of ensuring that a plate thickness is not chosen that will buckle. This method will probably result in a very thick gusset plate.

Equations 2.2 and 2.3 express the maximum stress f_{max} at the outer free edge of the gusset plate, along the critical section with the load applied at an eccentricity e or a distance s along the loaded edge respectively. These equations imply that any value of s or e can be used with negative values of e for $s < L/2$, where the equation is expressed in terms of e. The theory, however, implies that at a value of $e = -L/6$ or $s = L/3$ there will be zero stress along the free edge and for values of $e < -L/6$ or $s < L/3$ there will be a tensile stress along the free edge.

The method assumes that the maximum load is governed by the stress along the free edge only. However, the theory implies that the stress at the inside corner could be critical if the load is applied at a distance of $s < L/2$ with plates that fail by yielding.

Equations 2.2 and 2.3 are usually re-arranged to give the plate thickness t, given the allowable stress p as follows

$$t > \frac{P}{L.p.\cos^2\alpha}(6.s/L - 2) \qquad (2.5)$$

This equation will give a rapidly decreasing plate thickness from $s = L/2$ to a value of zero at $s = L/3$. Negative plate thicknesses will be given for values of $s < L/3$. Even when the equation is given in the form of Equations 2.2 and 2.3, the same sort of pattern is given for the stress. Therefore Equations 2.2, 2.3 and 2.5, which are derived from Jensen's (4) theory, are limited to values of $s \geqslant L/2$. This limitation is not stipulated in the references.

2.3 Salmon's theoretical and experimental work

The buckling of non-symmetrical triangular plates with non-

symmetrical and non-uniform loading conditions was first analysed theoretically for stress distribution and elastic buckling properties by Salmon (9) in 1962. Salmon (9) chose to approach the problem using elastic plate buckling theories. Prior to Salmon (9) the buckling of triangular plates under various loadings and edge conditions had only been investigated analytically for special types of triangular plates, such as equilateral and isosceles, with regular or symmetrical edge loadings. The general results and conclusions being summarised by Bulson (10).

Salmon (9) pointed out that the problem differs from many buckling problems in that triangular plates have an unknown stress variation throughout the plate, thus making it difficult if not impossible to apply the well-known differential equation for the buckling of plates as given by Timoshenko (11). In addition, any expression used for the deflection perpendicular to the plate must satisfy the complete boundary conditions of the plate. Because of the diagonal free edge, Salmon (9) considered the determination of such an expression formidable if not impossible, although a finite difference approach using the differential equation might have conceivably led to a solution.

For solution, Salmon (9) chose to use the approximate Rayleigh-Ritz energy method, making use of the feature that the conditions of equilibrium need not be satisfied by the original displacement expression but, only the boundary geometry restrictions must initially be satisfied.

The theory assumed that the loaded and supported edges, $y = 0$ and $x = 0$ respectively, are acted on by unknown distributions of shear, normal forces and, in the case of fixed edge plates, moments. It was assumed that whatever the load distribution along the loaded edge of the plate, the edge remains a straight line during the elastic deformation, as well as during small buckling deflections. The

assumption was also made that no deformation occurs along the loaded or supported edges. These assumptions were selected in the belief that they approximated actual behaviour. The plate geometry as assumed by Salmon (9) is shown in Figure 2.5.

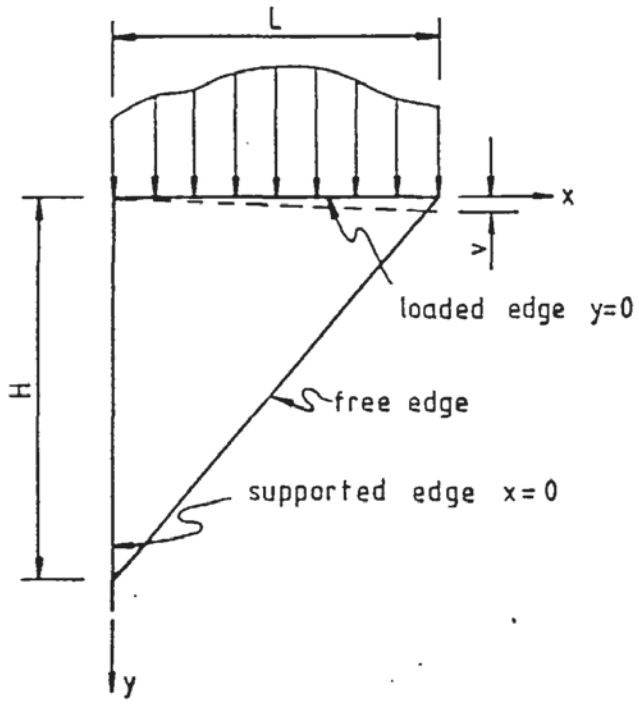

Figure 2.5 Triangular plate geometry assumed by Salmon.

The method of analysis was to assume double power series to approximate the displacements, u, v and w, in the direction of x, y and z respectively, of the plate that satisfied the following boundary conditions:

(i) at $x = 0$, $u = v = w = 0$,

(ii) at $y = 0$, $u = w = 0$, $v \propto x$ (2.6)

Expressions for the strain energy due to bending, and for the strain energy due to membrane stresses in the neutral plane of the plate could then be evaluated in terms of u, v and w. The total strain energy was then minimised by differentiating with respect to each of the arbitrary constants and setting the resulting expressions to zero. With many boundary conditions not inherently satisfied by

the displacement equations, a large number of terms of the power series had to be used to obtain sufficient accuracy. Utilisation of a very high-speed computer was therefore a necessity.

Large deflection theory using double power series expressions for displacements was used to determine the loaded edge deformation at which elastic buckling was imminent, so that the buckled deflection w could be determined. This was obtained by varying the loaded edge deformation until the buckled displacement just vanished. Once this had been obtained, general expressions for u, v and w were determined, and from these the distribution of supported load on edge x = 0 computed.

Two extremes for restraint of edge rotation along the loaded and supported edges, both simply supported and both fixed were investigated providing the maximum and minimum buckling strengths.

A large number of specific theoretical plates were investigated for stress distribution along each edge and the theoretical critical buckling stresses were compared to try and find some relationship between the various sizes. It was found, after trying various parameters, that the elastic critical buckling stress in the gusset plate for both the fixed edge and simply supported plates could be expressed by

$$f_{cr} = K.E/(L/t)^2 \qquad (2.7)$$

for any given L/H ratio. Where f_{cr} is the theoretical stress at which elastic buckling is imminent, and the constant K depends on the L/H ratio and Poisson's ratio. The constant K has a single value for all plates having the same L/H ratio and the same support condition.

The theoretical analysis also indicated that for a given L/H ratio:

1. the ratio of compressive stress along the diagonal to the stresses along the loaded and supported edges is a constant,
2. the maximum principal stress (compression) occurs along the

diagonal free edge, and

3. the critical stress occurs at the mid point of the diagonal for L/H equal to unity and at the edges of the diagonal for either a ratio of 0.5 and less, or a ratio of 2 and more.

Values of K were determined for ratios L/H from 0.25 to 4.0 for both simply supported and fixed edged plates. The accuracy of the approximate solution, which the energy method provides, was established by comparing the boundary stresses determined from the displacement equation with those necessary to satisfy equilibrium. The results were reasonably accurate for ratios of L/H from 0.5 to 2.0.

The results obtained were based on the assumption that the load was transmitted to the plate, such that the vertical deformation of the loaded edge would be linear, with no deformation in the direction of the axis of either the loaded or supported edges. The loading distribution required to produce such a deformation was found analytically to be essentially parabolic with its resultant approximately 0.6L from the supporting edge. This parabolic loading is of the type which in many practical engineering applications, is assumed to be uniform. Thus Salmon (9) considered the results to be useful for bracket plates, where the load is applied in a form of distributed load, with its resultant approximately in the middle and transmitted through a thick flange to the bracket.

Following Salmon's idealised theoretical study Salmon et al (12) tested eighteen triangular bracket plates and compared the results with Salmon's theory. The experimental aims were:

1. To determine the actual ultimate load that various size plates can sustain.

2. To determine whether yielding or buckling occurs first, and whether these are valid criteria for determining safe loads.

3. To locate the position of maximum stress along the free edge of the plate.

4. To establish the exact edge stress distribution to which the plates are subjected. (Effort was made in applying the load to achieve, along the top edge, the parabolic distribution derived from the theoretical study.)

5. To establish from the two preliminary tests whether or not the maximum stress occuring anywhere in the plate can be expected to occur along the free edge.

6. To determine the relationship between the maximum stress on the free edge and the applied load.

7. To adjust the design procedure suggested in the theoretical work to account for the expected deviations between assumed conditions and actual behaviour.

The test specimens were chosen with four L/H ratios ranging from 0.75 to 2.0. There were two plate sizes with the same L/H ratio and two plate thicknesses of 1/4 inches and 3/8 inches. The plate sizes and thicknesses were selected to include both plates which were expected to fail by yielding and by buckling. There was one duplication for the low range of L/H and one for the high range for preliminary testing.

The test specimens were designed to duplicate theoretical assumptions as nearly as possible. To prevent lateral movement of the bracket, a wide, thick, top plate was used, the dimensions of which were not given in the paper. To eliminate moment from being induced by the loading head and to confine the loads to the plane of the gusset plate, a bar was added to the top plate. It is understood that the load was applied at 0.6L from the supported edge to achieve, along the top edge, the parabolic distribution derived from the theoretical study. The predicted buckling or yielding loads were computed using curves derived from the theoretical study.

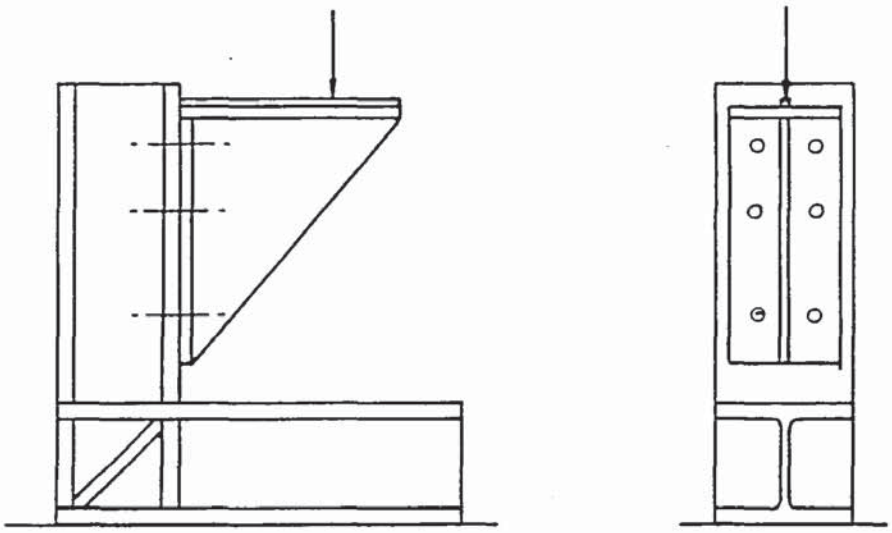

Figure 2.6 Testing frame and gusset plate bracket used by Salmon et al.

The gusset plates were made up in the form of brackets, the gusset plate being welded to a supporting plate and a loaded plate. The sizes of the welds were not given, and it is not clear whether the loaded plate was welded to the supporting plate. The brackets were supported in the testing machine by an L-shaped steel frame as shown in Figure 2.6. The brackets were attached to the frame with high tensile strength bolts passing through holes in the supporting plate of the bracket and in the flange of the vertical leg of the support frame.

As a large quantity of information was desired concerning the stress distribution throughout the plates, Salmon investigated the use of a brittle lacquer material that cracks under load at points of high stress, and a 3/4 inch wide photoelastic strip of material cemented along the free edge, to try to obtain a general stress distribution quickly and cheaply. However, neither of these methods was successful

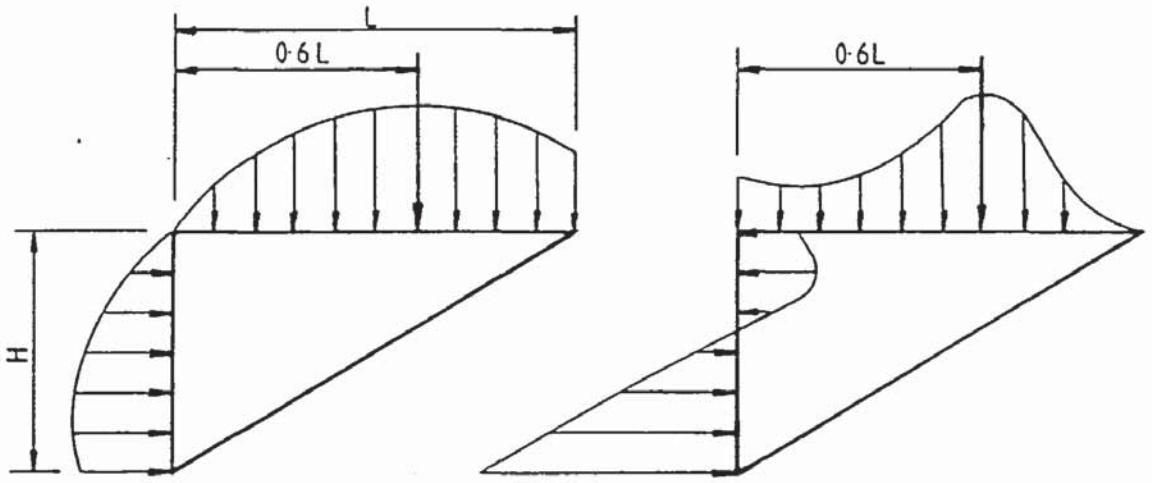

(a) typical theoretical normal stress distribution

(b) typical experimental normal stress distribution

Figure 2.7 Typical theoretical and experimental normal stress distributions presented by Salmon et al.

and he reverted to using strain gauges. The two preliminary specimens had strain gauge rosettes fixed on both sides of the plates along the loaded and supported edges. Strain gauges were also fixed on both sides of the plates along the free edge to measure the strains. Dial gauges were also used to measure the extension of the loaded plate, vertical deflection of the end of the loaded plate and the out-of-plane movement of the gusset plate.

The strain gauge results indicated that large shear stresses exist along the loaded edge, and tension stresses occur along the upper part of the supported edge. These stress distributions were not indicated by the theoretical study, however, Salmon et al (12) did not consider this deviation to be significant to invalidate the general theoretical findings and important relationships. Typical theoretical and experimental normal stress distributions are shown in Figure 2.7.

The theoretical work predicted the maximum stress in the plate to occur as compression along the free edge. The results of the strain gauge rosettes showed the lines of maximum compressive stress to be

essentially parallel to the free edge. From this Salmon et al (12) concluded that the maximum stress along the free edge was the maximum in the plate.

After the two preliminary tests to determine the general stress distribution a further sixteen were tested to determine the load-carrying capacity and type of failure i.e. yielding or buckling. As the maximum stress was believed to be on the free edge, only three or four strain gauges were used on each side of the plate along the free edge. Dial gauges were used only to determine out-of-plane movement.

The behaviour of the plates was variable, seemingly fitting into no predictable pattern. The test critical load was assumed to be at first yield for the yield type of failure, and for the buckled failure the buckling of the free edge as determined by the continuing out-of-plane movement of the gusset plate with no increase in load. The test critical load at which yielding along the free edge occurred and for cases in which elastic buckling occurred, did not agree with the predicted values. The experimental critical loads were closest to those predicted by the theory for L/H less than unity. As L/H increased, the test critical load was less than the theoretical values and became less accurate as L/H increased.

The experimental ultimate load, which Salmon et al (12) do not define, in all cases was higher than the test critical load, indicating that the critical load, especially yielding is not the proper criterion of strength. In cases in which elastic buckling occurred, the ultimate strength was approximately 10% higher, but where yielding of the free edge occurred, the ultimate strength was from 70% to 400% greater. Only one plate deviated from this, and it was considered that the yield load was essentially the buckling load as well, and that the plate should belong in the first category. The experimental ultimate loads in comparison to the theoretical critical loads were still lower for the plates with high values of L/H.

It is not clear what Salmon et al (12) adopted as the experimental ultimate load. Salmon et al (12) states that the attainment of the ultimate load, in most cases, occurred without large permanent, noticeable deformation and, upon reloading several times, approximately the same ultimate load was reached. As he adopted the load at which first yield or the elastic critical buckling load was reached as the critical load, then it is assumed that his ultimate load was possibly the plastic limit for plates failed by yielding. For plates which failed by buckling, the ultimate load is less clear.

No weld failures were detected, and the size and method of designing the welds is not stated.

In nearly all the tests, throughout the entire range of loading, the ratio of the compressive strains along the free edge from point to point continued to change during each succeeding increment of load. In other words, during the loading, the distribution of stresses throughout the plate was not constant. This effect was considered to be due to the loaded edge deforming downward and changing the direction of the machine load applied to the plate, rather than yielding occuring at a point other than along the free edge. The out-of-plane deformation, as well as compressive strain, caused the loaded edge downward deflection.

Many of the variations in results appeared to be directly related to the amount and type of out-of-plane deformation. Four plates buckled elastically and presented out-of-plane buckling deformation patterns. Two of the four plates buckled with two "loops", or typical higher mode shapes, but this was probably due to intitial imperfections.

The distribution of compressive stress along the free edge did not agree with the theoretical predictions and generally was in two categories. Either it was a maximum away from the support, as was

typical for the plates with L/H ratio 1.0 or less, or it reached a peak at the bottom of the plate, as was typical for the plates with L/H greater than 1.0.

Salmon's (9) idealised theoretical study showed that for any specific L/H ratio, there is a family of curves relating plate size to the elastic critical buckling stress in the diagonal free edge. Replacing K in Equation 2.7 by $k\pi^2/12(1-\nu^2)$ gives the expression

$$f_{cr} = k \frac{\pi^2 E}{12(1-\nu^2)(L/t)^2} \qquad (2.8)$$

where f_{cr} is the maximum stress along the free edge when elastic buckling is imminent, E is the modulus of elasticity, ν is Poisson's ratio and k represents the elastic buckling constant. From the theoretical study the curves for the two extremes of moment restraint at the loaded and supported edges were obtained, the upper bound with both edges fixed and the lower bound with both edges simply supported. Two other curves were presented in the experimental paper of Salmon et al (12), which were arbitrarily selected at a point equivalent to the plate being one-third fixed on both edges. It was one of these latter curves that was used to calculate the failure loads of the specimens.

In Salmon's theoretical paper he plotted the curves of the coefficient $K = k\pi^2/12(1-\nu^2)$ for values of the ratio L/H, where in the experimental paper the curves of the coefficient k for values of the ratio L/H have been plotted. It was also pointed out that the theoretical work was only considered reasonably accurate for the range of L/H = 0.5 to 2.0 and so only that range is included for the one third fixity curves.

In order to make the critical buckling stress a direct function of the total applied load, another curve was developed from his theoretical work giving the ratio (Z) between the average stress on the loaded edge and the maximum compressive stress on the free edge for values of the L/H ratio.

$$Z = \frac{\text{Average stress - loaded edge}}{\text{Max stress - free edge}} = \frac{f_{avg}}{f_{max}} = \frac{P/L.t}{f_{max}} \qquad (2.9)$$

The curve for Z based on the theoretical study however, gave somewhat higher values for Z than the experimental test results, i.e. the experimental stresses along the free edge were higher than theory predicted. This theoretical curve was therefore superseded by an experimental curve based on the test results. The following equation was given, which approximates to the experimental curve

$$Z = 1.39 - 2.20(L/H) + 1.27(L/H)^2 - 0.25(L/H)^3 \qquad (2.10)$$

for values of L/H from 0.75 to 2.0.

On the basis of this curve, the theoretical curves expressing the coefficient k for values of L/H, as used in determining the critical free edge buckling stress in Equation 2.8, were redrawn to give the coefficient k' for values of L/H, which would give the elastic buckling stress in terms of the average stress on the loaded edge.

The equation for the average stress on the loaded edge when buckling is imminent becomes

$$f_{avg} = \frac{P}{Lt} = \frac{k' \pi^2 E}{12(1 - \nu^2)(L/t)^2} \qquad (2.11)$$

From the experimental work a recommended k' curve was produced, the arbitrarily selected one-third fixety curve being abandoned. Unfortunately the plate sizes and thicknesses selected produced only four plates that failed by buckling and none of these failed with L/H ratios greater than 1.0. This latter part of the recommended k' curve was obtained by assuming the experimental yield loads in this region to be buckling loads. This gave a conservative curve for the region from L/H equal to 1.0 to L/H equal to 2.0, because the theoretical buckling stress is higher than the yield stress for those plates. This highlights an important point concerning Salmon's (9) theoretical work. The theoretical curves do not take into account yielding and

are based purely on the elastic buckling critical stress. The theory implies that plates with the same shape and size, but with different thicknesses, will all have the same k' value. However, as the plate thickness increases then the failure mode will transfer from buckling to yielding with the very thick plates and the k' value will only be the same for plates failing by buckling. The experimental value of k' for the yielded plates would then be less the thicker the plate.

The recommended k' curve is closely approximated by the following equation:

$$k' = 3.2 - 3.0(L/H) + 1.1(L/H)^2 \qquad (2.12)$$

for L/H from 0.75 to 2.0. This curve is applicable to the particular experimental results of Salmon et al (12). If for example, the plates were chosen of such a size and thickness that yielding occurred with plates having L/H ratios of less than one and buckling of plates with L/H ratios greater than one, then a recommended curve would have been produced with a lower value of k' for L/H ratios of less than one, and higher values of k' for L/H ratios greater than one, in comparison with the curve given.

To check for yielding the elastic critical buckling stress f_{cr} as calculated by Equation 2.8, is replaced by the yield stress f_y when used as f_{max} in Equation 2.9 to give

$$f_{avg} = \frac{P}{L.t} = Z.f_y \qquad (2.13)$$

To simplify design, the plate thickness is usually restricted to a thickness which should ensure that yielding is achieved without buckling, and therefore eliminating the use of Equation 2.11 for buckling design and using only Equation 2.13 for yield design. To do this the conditions of buckling and yielding, Equations 2.11 and 2.13, can be equated, and the following L/t requirement is derived.

$$Z.f_y \leqslant \frac{k'\pi^2 E}{12(1 - \nu^2)(L/t)^2} \qquad (2.14)$$

Therefore

$$\frac{L}{t} \leqslant \sqrt{\frac{k'\pi^2 E}{12(1-\nu^2)f_y.Z}} \qquad (2.15)$$

This equation together with Equations 2.10, 2.12 and 2.13 are recommended by Beedle et al (7) for the allowable stress design of plates to fail by yielding with the resultant load approximately in the middle of the loaded edge. Equation 2.11 is also given if plates are required to be designed for buckling failure. In the reference, the appropriate units are incorporated into Equations 2.11 and 2.15.

In the text book by Salmon et al (8) the recommended experimental curve or k' Equation 2.12 is no longer recommended, and neither is the use of Equation 2.11 for buckling design. The design method presented is to ensure that the plates do not fail by buckling and to design them for yielding. Equations 2.10 and 2.13 are still used but, Equation 2.15 has been re-arranged so that

$$\frac{L}{t} \leqslant \frac{Q}{\sqrt{f_y}} \qquad (2.16)$$

Separate linear values for $(L/t)\sqrt{f_y} = Q$ are then given for $0.5 < L/H < 1.0$ and $1.0 < L/H < 2.0$ in the appropriate units. The value of Q can be expressed as

$$Q = \sqrt{\frac{k\pi^2 E}{12(1-\nu^2)}} \qquad (2.17)$$

k is the same coefficient as in Equation 2.8 and replaces the value k'/Z in Equation 2.15. Effectively the new values of k recommended by Salmon et al (8) are

$0.5 < L/H < 1.0 \qquad k = 2.38$

$$\text{giving} \quad \frac{L}{t} \leqslant \frac{1}{\sqrt{f_y}}\sqrt{2.38\,\frac{\pi^2 E}{12(1-\nu^2)}}$$

$1.0 < L/H < 2.0 \qquad k = 2.38(L/H)^2$ (2.18)

$$\text{giving} \quad \frac{L}{t} \leqslant \frac{(L/H)}{\sqrt{f_y}}\sqrt{2.38\,\frac{\pi^2 E}{12(1-\nu^2)}}$$

which give a more conservative value for k than that given by the use of the experimental curve for k' Equation 2.12. That is, Equation 2.18 gives a greater limiting thickness than Equation 2.15.

To confuse the situation even more Salmon's old recommendations based on his original theoretical work (9) can still be found in old text books of Beedle et al (7) and is still used in Sweden. Salmon's (9) original theoretical equation for Z, which he found to be incorrect and ammended to Equation 2.10, is approximated by

$$Z = 0.6 - 0.21(L/H) \tag{2.19}$$

which when substituted in Equation 2.9 gives the Swedish equation

$$f_{max} = \frac{P}{L.t} \frac{1}{(0.6 - 0.21(L/H))} \tag{2.20}$$

By restricting the design to yielding then f_{max} would be f_y. (In allowable stress design this would be factored).

The design is restricted to yielding by limiting L/t ratios as in Salmon et al's text book (8). Expressing these limitations in terms of k to eliminate units, the original values of k are

$$0.5 \leqslant L/H \leqslant 1.0 \qquad k = 2.38$$

$$\text{giving} \quad \frac{L}{t} \leqslant \frac{1}{\sqrt{f_y}} \sqrt{2.38 \frac{\pi^2 E}{12(1 - \nu^2)}} \tag{2.21}$$

$$1.0 \leqslant L/H \leqslant 2.0 \qquad k = 2.38\left(\frac{1}{3} + \frac{2}{3}\frac{L}{H}\right)^2$$

$$\text{giving} \quad \frac{L}{t} \leqslant \frac{1}{\sqrt{f_y}}\left(\frac{1}{3} + \frac{2}{3}\frac{L}{H}\right) \sqrt{2.38 \frac{\pi^2 E}{12(1 - \nu^2)}}$$

which are similar, but slightly more conservative than Salmon's limitation. However, these limitations were reduced even further by dividing all of the curves for $(L/t)\sqrt{f_y} = Q$ with L/H by a factor of safety of 1.4.

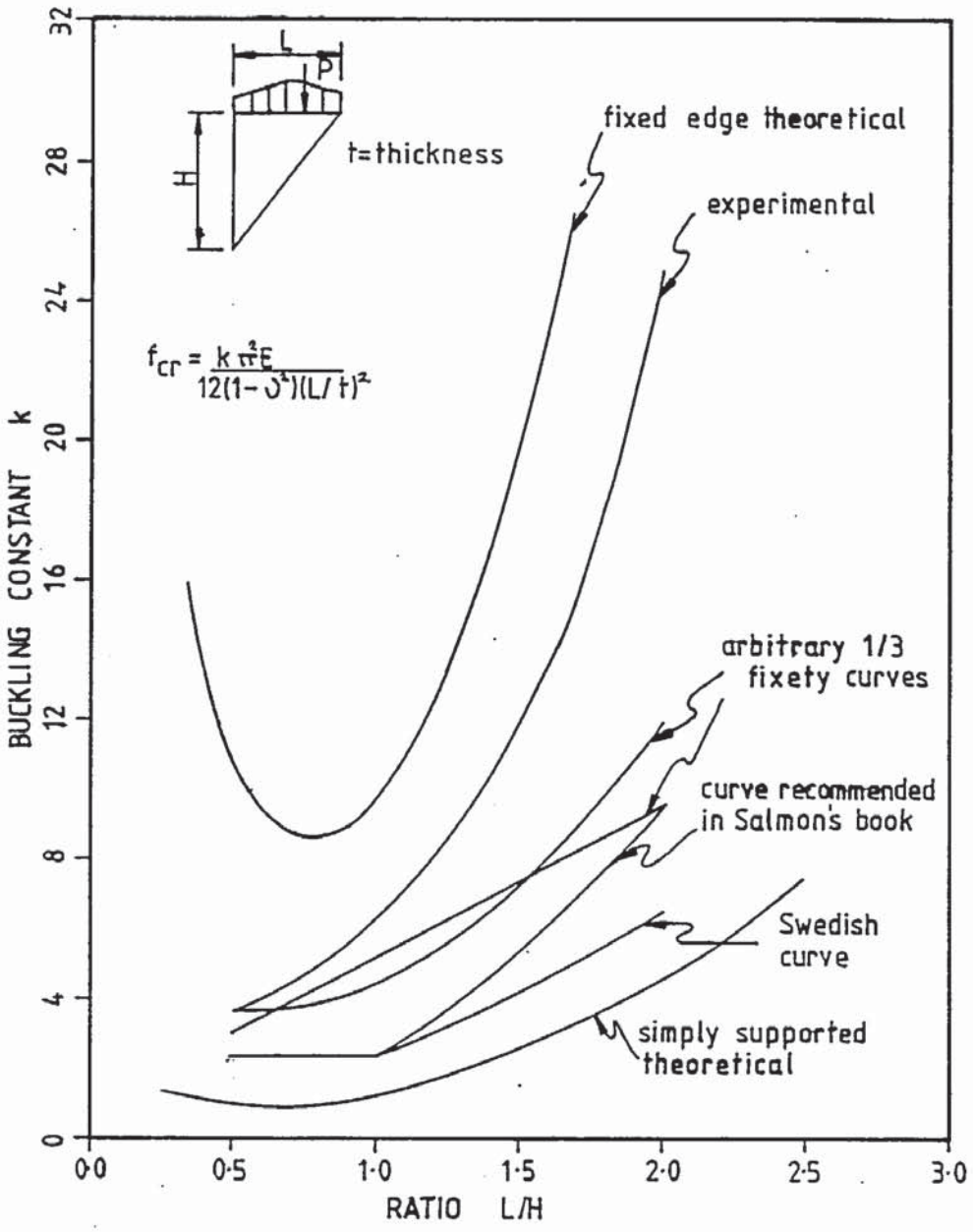

Figure 2.8 Comparison of k curves used by each variation of Salmon's method.

This effectively reduces the Equation 2.21 to

$$0.5 \leqslant L/H \leqslant 1.0 \qquad k = 1.21$$

$$\text{giving} \quad \frac{L}{t} \leqslant \frac{1}{\sqrt{f_y}} \sqrt{\frac{1.21\,\pi^2 E}{12(1-\nu^2)}}$$

$$1.0 \leqslant L/H \leqslant 2.0 \qquad k = 1.21\left(\frac{1}{3} + \frac{2}{3}\frac{L}{H}\right)^2 \qquad (2.22)$$

$$\text{giving} \quad \frac{L}{t} \leqslant \frac{1}{\sqrt{f_y}}\left(\frac{1}{3} + \frac{2}{3}\frac{L}{H}\right) \sqrt{\frac{1.21\,\pi^2 E}{12(1-\nu^2)}}$$

As a comparison the curves for k plotted against L/H for each variation of Salmon's method are given in Figure 2.8.

2.4 The beam method

One version of Salmon's method has been adopted for the allowable stress design of gusset plates where there is a form of distributed load on the loaded edge with its resultant acting approximately in the middle of that edge. When the resultant load is applied close to the free edge then either a version of Jensen's (4) method, as previously mentioned, is used or other methods are used as follows.

Other methods of designing gusset plates are used but they are not supported by experimental work. Some of these methods are given in books on structural steelwork and others are used in industry.

One method of designing gusset plates for stiffened column bases is based on a beam analysis. This method is given by the Steel Designers Manual 4th Edition, 1972 (13), MacGinley (14) and the British Draft Steel Code of Practice 1977 (2).

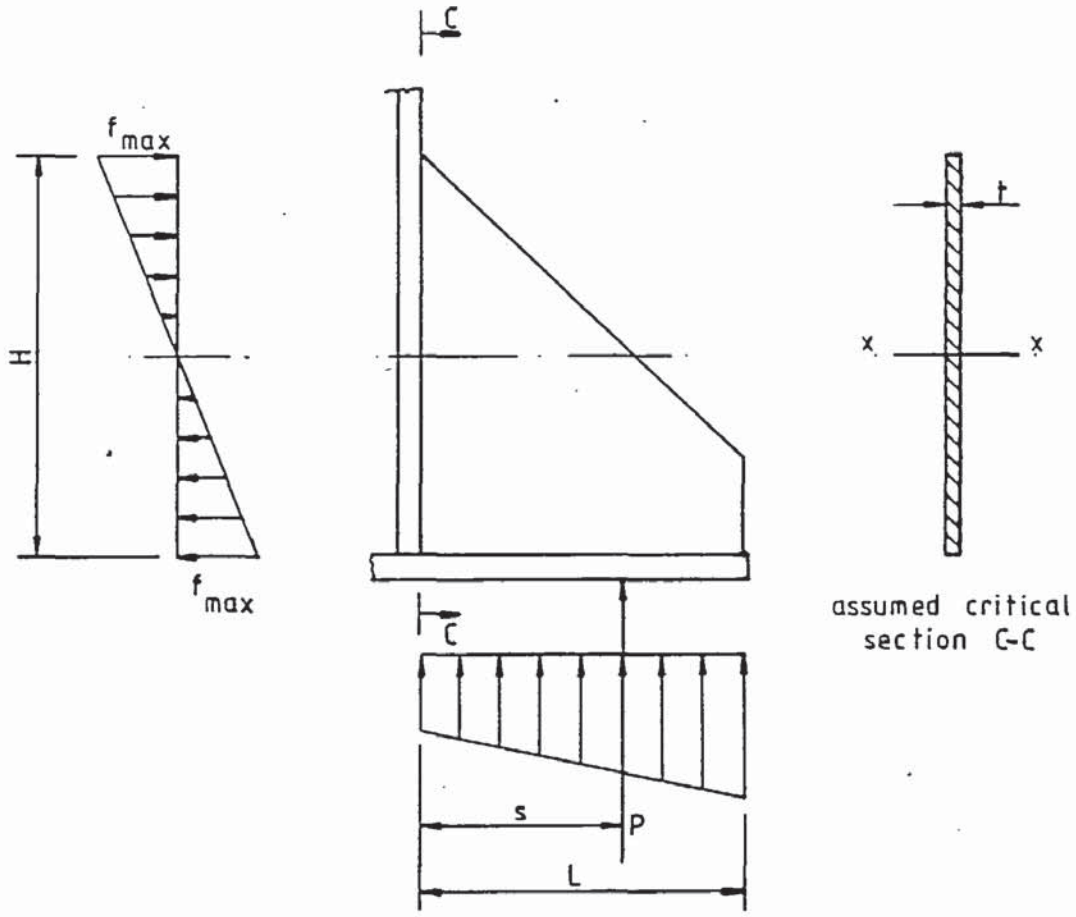

Figure 2.9 Stress distribution and geometry for the beam method of analysis

The main assumption is that the gusset plate acts as a beam with its critical section along the supported edge C-C as shown in Figure 2.9. The base plate is not considered to be part of the beam section and it is not assumed to take any horizontal loads or bending moments at the section concerned.

Moments are taken about section C-C for the gusset plate to give the maximum stress along this section.

$$f_{max} = \frac{M}{z'} \tag{2.23}$$

The bending moment M at section C-C for the gusset plate is

$$M = P.s$$

At section C-C of the gusset plate the section modulus is

$$z' = \frac{t.H^2}{6} \tag{2.24}$$

Therefore

$$f_{max} = \frac{6P.s}{t.H^2} \tag{2.25}$$

The British Draft Steel Code of Practice (1977) proposes only Equation 2.23 and presents it as the design formula

$$M < f_{max}.z' \tag{2.26}$$

The critical section is not defined and there is no guidance in the use of the equation.

The Steel Designer's Manual (13) uses Equation 2.25 to check the maximum stress f_{max} assuming values of t and H, L being governed by the size of the base plate required. The maximum value of f_{max} is not specified exactly but it is suggested that it should be less than the allowable bending stress f_{bc} as the gusset plate is unstiffened along the compression edge.

Therefore

$$\frac{6P.s}{t.H^2} < f_b \tag{2.27}$$

MacGinley (14) uses Equation 2.25 to calculate the depth of the plate H required assuming a value for t, and assuming f_{max} to be the allowable bending stress f_{bc}. No reduction is assumed for the compression edge i.e.

$$H = \sqrt{\frac{6P.s}{t.f_{bc}}} \qquad (2.28)$$

In each case the shear stresses along the section C-C in the gusset plate are checked and H adjusted accordingly, and not t. The shear stress f_q along section C-C in the gusset plate is checked as follows.

$$\frac{P}{H.t} < f_q \qquad (2.29)$$

The weld lengths and sizes are calculated and if necessary H is adjusted as required.

The design of the welds in the latter two references, is based on shear along the vertical edge and compression on the loaded edge L. In the Steel Designer's Manual (13) the derivation of the shear forces on the vertical edge is not based on Equation 2.29, as would be expected but, is based on the assumption that the column is supported by only the vertical welds connecting it to each of the gusset plates as shown in Figure 2.10. The combined shear force from both the vertical load and the bending moment is then calculated for each gusset plate vertical weld. The vertical load may be reduced to 60% for machined surfaces between the end of the column and the base plate. The vertical welds to the gusset plates are then designed to take the combined load in longitudinal shear.

It must be pointed out that the gusset plate along the same vertical edge adjacent to the vertical welds to the column, has only been designed to take the distributed load under the gusset plates and

$$P << [(V/2) + M/V]/2 \qquad (2.30)$$

A nominal sized fillet weld is then used for the other welds.

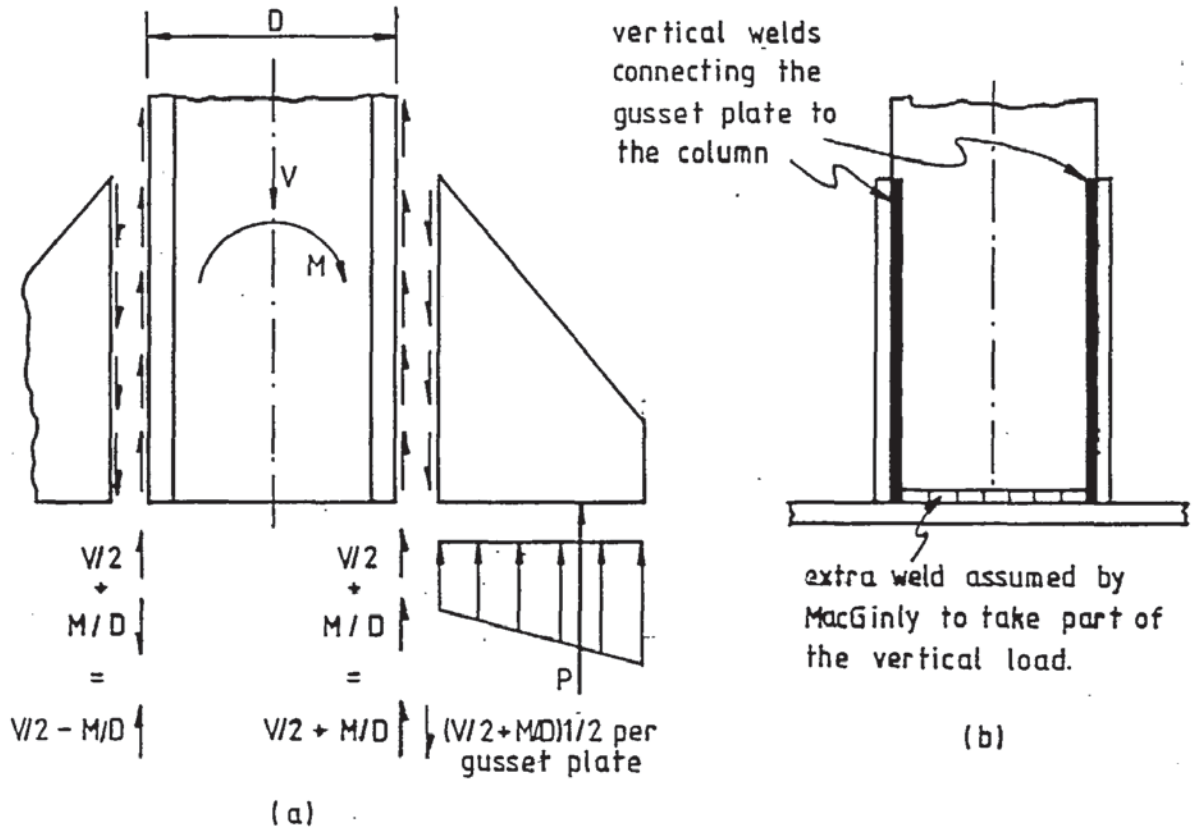

Figure 2.10 Shear forces on vertical weld as assumed by the steel designers manual.

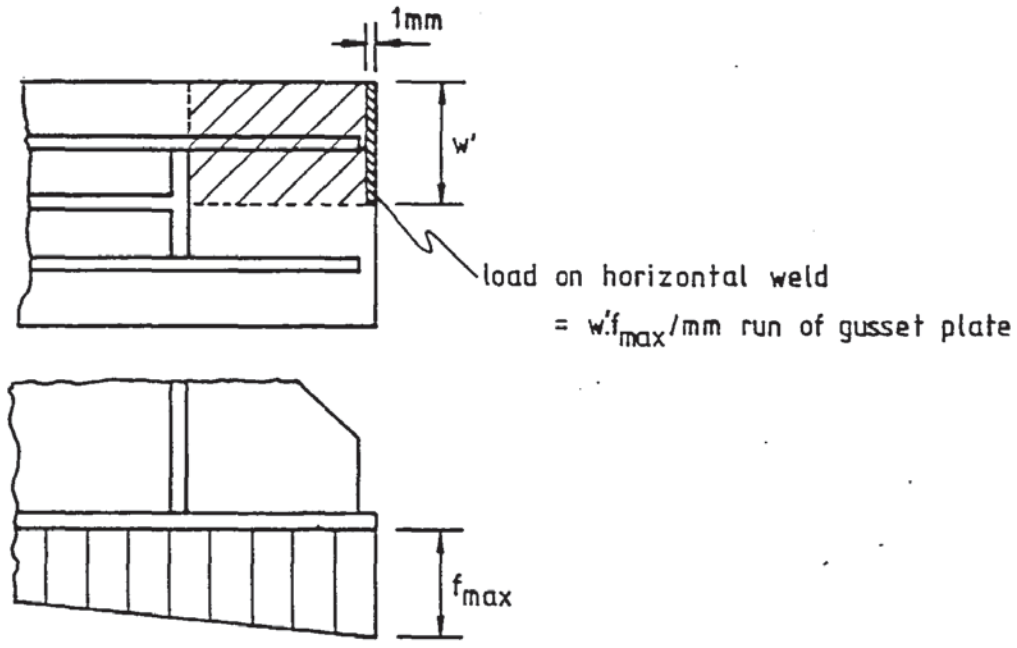

Figure 2.11 Max stress on horizontal weld of gusset plate as assumed by MacGinley.

MacGinley (14) assumes the same distribution of forces, but also assumes that the weld connecting the column to the base plate at the same section, see Figure 2.10(b) also resists part of the load as well as the gusset plate welds. The horizontal welds along the loaded edge of the gusset plates are then designed to resist the maximum pressure under the base. A strip 1mm wide at the edge of the base is considered as shown in Figure 2.11.

A modification of the beam method is to include the base plate in the assumed critical section C-C as shown in Figure 2.12. The section modulus z for section C-C including the base plate is obtained and substituted for Equation 2.24.

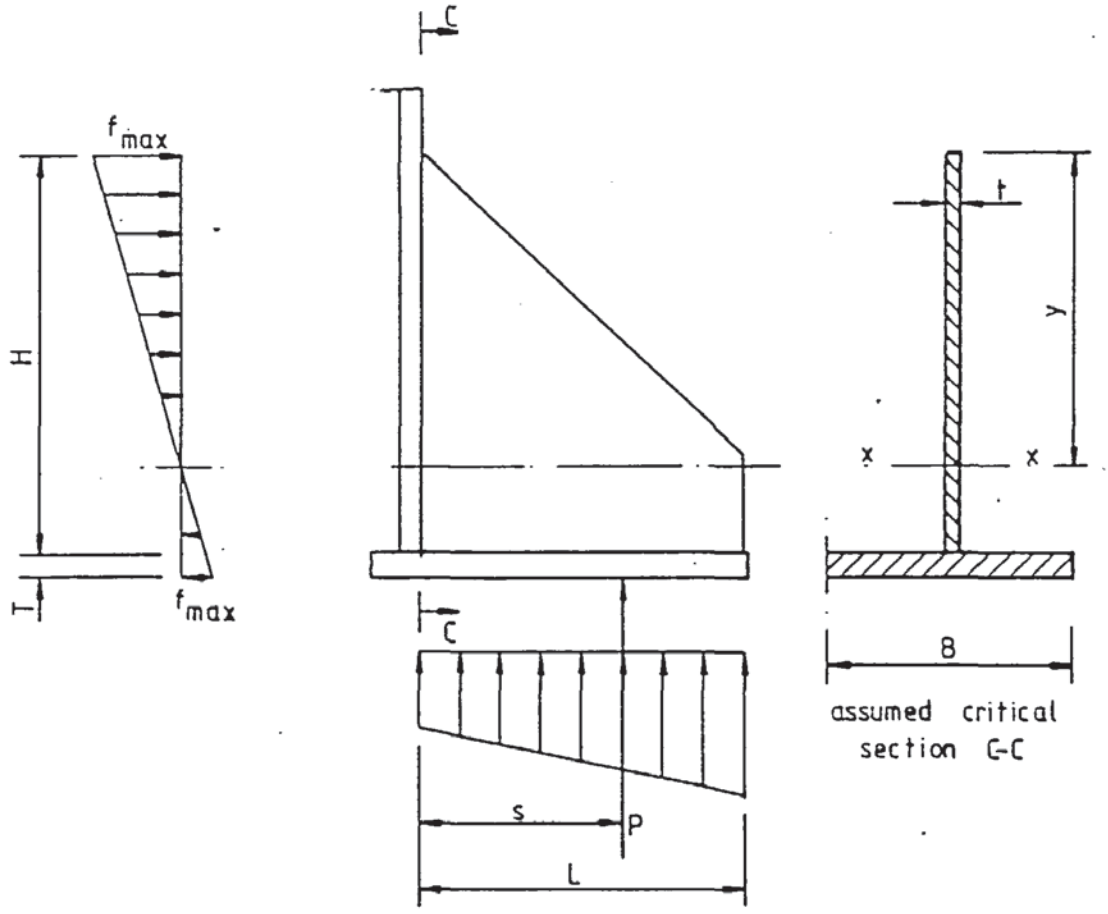

Figure 2.12 Stress distribution and geometry assumed for a beam method which includes the base plate.

2.5 The approximate strut methods

The approximate strut method has already been mentioned as a check for buckling with Jensen's (4) method. The method is also used separately and will be outlined again here for comparison with other methods. The stut method assumes that the component $P/\cos\alpha$ of the applied load P normal to the section AB, irrespective of its position along the loaded edge, acts concentrically on a strip of the gusset plate, which is assumed to form a column one quarter of the width of the section AB ($=L/4 \cos\alpha$) as shown in Figure 2.13.

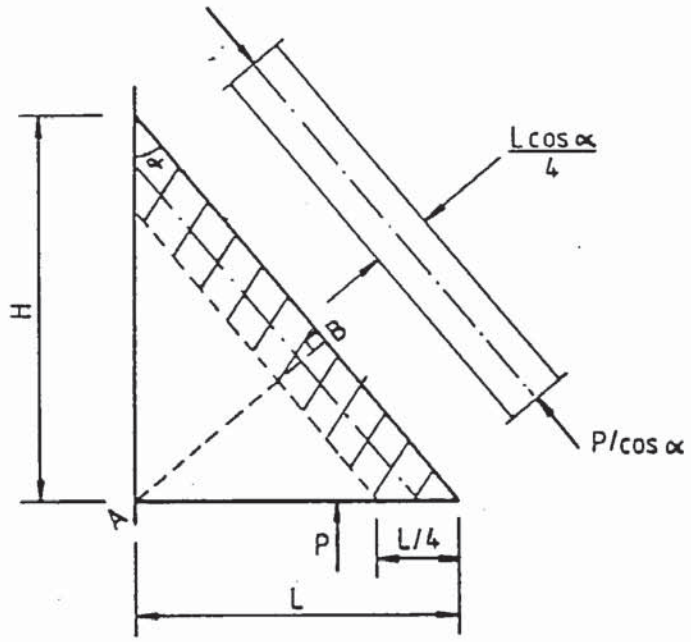

Figure 2.13 Approximate strut method assumption.

This then gives the design equation

$$\frac{4P}{L.t.\cos^2} \leq p_c \qquad (2.31)$$

The allowable stress p_c being the allowable buckling stress of the assumed strut.

A slenderness ratio limitation and buckling equation must be selected to calculate the allowable buckling stress. The effective lengths that are used vary from the length of the free edge to half of its length.

A modification to the strut method although less conservative is to assume that a unit strip along the free edge of the gusset plate acts as a strut. Calculate the maximum allowable buckling stress of this strip and assume that it applies to the full width of the section AB. Again, irrespective of the position of the applied load P, the component $P/\cos\alpha$ of the applied load is applied normal to the section AB. The design equation is

$$\frac{P}{L.t.\cos^2\alpha} \leqslant p_c \qquad (2.32)$$

Again the value of the allowable stress must be determined.

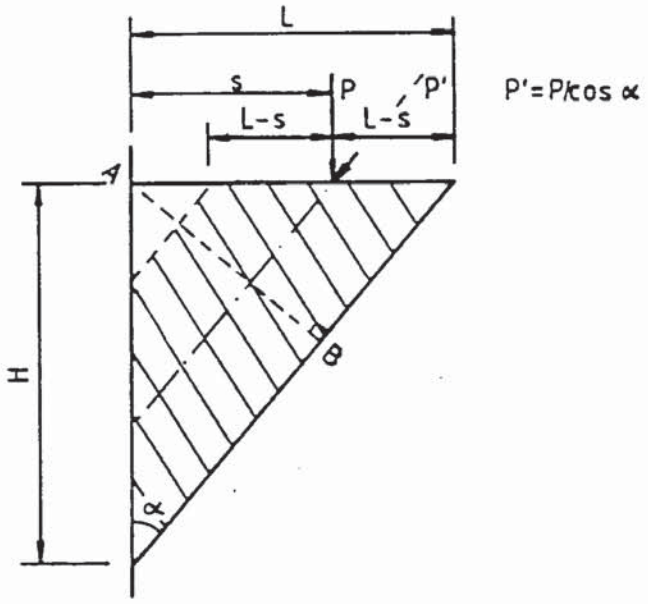

Figure 2.14 Approximate concentric strut assumption.

Another similar method is to assume a strip of the gusset plate of such a width that the load is applied concentrically as shown in Figure 2.14. The resulting design equation is

$$\frac{P}{2(L - s)t.\cos^2\alpha} \leqslant p_c \qquad (2.33)$$

Equation 2.33 is an attempt to take account of the effect of the position of the applied load P. The obvious limits are when s = L/2, the whole section AB is assumed to take the load, and when s = L, then

no part of the plate takes the load. If values of $s < L/2$ are taken then a section greater than AB is assumed to take the load, which is obviously not correct. One reference suggesting this method gives a limitation on the thickness of the plate used. First a thickness of t_1 is calculated by using Equation 2.33, assuming an allowable stress p_c based on the yield stress

$$t_1 = \frac{P}{2(L - s)p_c\cos^2\alpha} \tag{2.34}$$

If t_1 satisfies

$$\frac{t_1}{(L + H)/2} > 0.05 \tag{2.35}$$

which is effectively a limiting slenderness ratio based on the average lengths of the loaded and supported edges, then the plate is assumed to fail by yielding and Equation 2.34 is assumed to be correct, therefore

$$t \geqslant t_1 \tag{2.36}$$

If Equation 2.35 is not satisfied, then to prevent the risk of buckling, the plate thickness calculated by Equation 2.34 is increased by the following approximate equation

$$t \geqslant 0.65t_1 + 0.009(L + H) \tag{2.37}$$

The origins of Equations 2.35 and 2.37 are not known.

Another method is a combination of ideas. Salmon's (9) original Equation for Z, Equation 2.19, relating the average stress f_{avg} on the loaded edge to the maximum stress f_{max} along the free edge is used as a base to the equation giving

$$Z = \frac{f_{avg}}{f_{max}} = (0.6 - 0.21.L/H) \tag{2.38}$$

The load is applied concentrically to a width of strut to take account of the load position. The average stress f_{aveg} on the loaded edge is calculated on the assumption that the load only acts on this

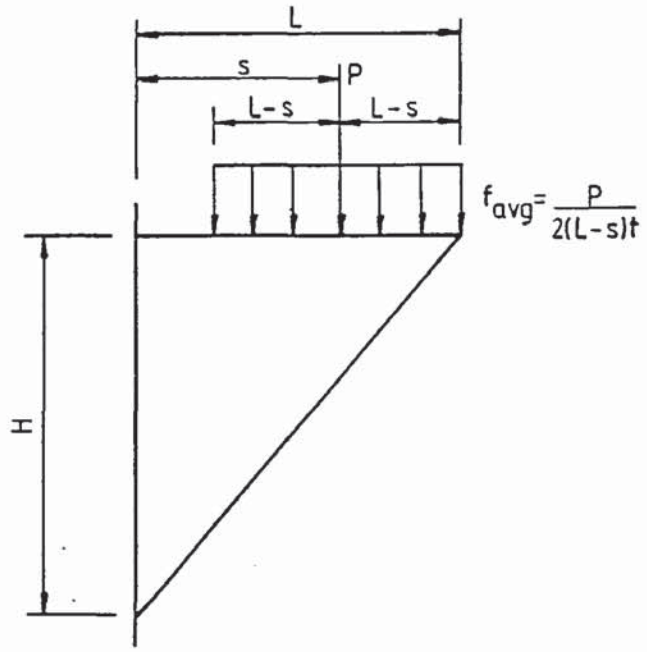

Figure 2.15 Adaption of Salmon's method to take account of load position.

area as shown in Figure 2.15. The resulting design equation is expressed in terms of the allowable stress along the free edge giving

$$\frac{P}{2(L - s)t(0.6 - 0.21.L/H)} \leqslant f_{all} \qquad (2.39)$$

The allowable stress is determined by considering a unit strip along the free edge which buckles as described in other methods.

2.6 Plastic design of triangular gusset plates

With the introduction of plastic design, a method was required of designing gusset plates at ultimate load. Jensen was concerned with allowable stress design at working load and although no equations or diagrams were given, it is understood that the ultimate loads calculated for gusset plates were based on an extension of his elastic design. At the ultimate load it is assumed that the full plastic strength in bending is developed on the critical section i.e. a rectangular stress distribution as shown in Figure 2.16. It appears that this assumption was also made by Beedle et al (7) and Salmon et

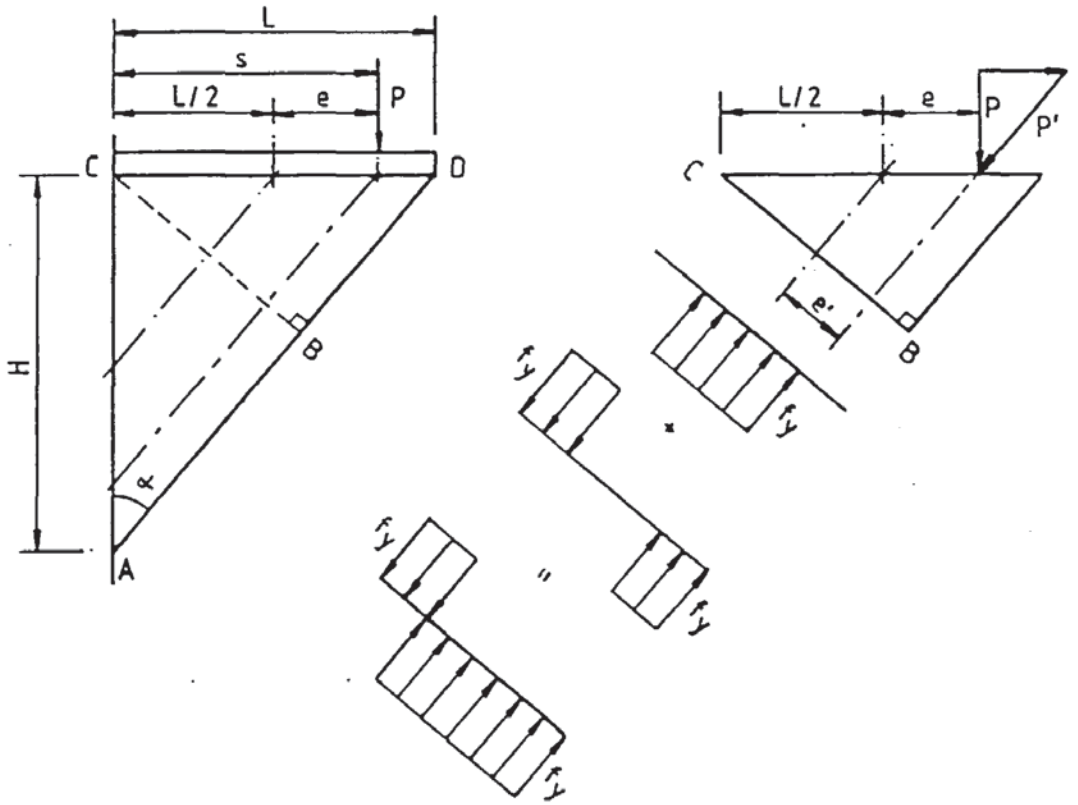

Figure 2.16 Plastic design assumption derived from Jensen's work.

al (8) in their plastic design methods.

The maximum value of P = P_{ult} consistent with this stress distribution, with the centroidal axis at the centre of the critical section, is computed by equating the resultant of the stresses on the critical section to the component P' which is parallel to the free edge and by taking the equilibrium of moments anywhere along the critical section produced by the stress and P'. The ultimate value of P is then given by

$$P = f_y.t.\cos^2\alpha \quad (-2e + \sqrt{4e^2 + L^2}) \qquad (2.40)$$

The top plate is assumed to carry the horizontal component ($P.\tan\alpha$) and thus its area is given by

$$A_{\text{top plate}} = \frac{P_{ult}\tan\alpha}{f_y} \qquad (2.41)$$

This method again is only applicable for values of $s \geqslant L/2$. According to the elastic theory and the plastic theory the maximum

load is obtained when the load is applied at the centre of the loaded edge. With Equation 2.40, if a negative value of e is put inserted for loads applied at s < L/2 then the load will increase. However, if positive values of e are inserted for s < L/2 then the equation gives the same load for the load applied at s = 0 as s = L. Similarly for positive e values in Equation 2.2 in the elastic design. If e in both methods is replaced by s then the equation breaks down for values of s < L/2.

Beedle et al (7) recommended that the plastic method only be used for triangular plates of sufficiently small L/t ratios where the full plastic strength can be developed without buckling. The limiting L/t ratio to be used varies with different references. Beedle et al (7) suggests that a conservative solution can be obtained by assuming that the material is isotropic and the modulus of elasticity in all directions is equal to the strain-hardening modulus. The limiting L/t ratios are then found by equating the buckling stress based on the strain-hardening modulus to the yield stress. Beedle et al (7) used Salmon's (9) equation for the average stress on the loaded edge, Equation 2.11, with the experimental Equation 2.12 for the value of k'. To ensure that yielding is achieved without buckling,

$$\frac{L}{t} \leqslant \sqrt{\frac{k'\pi^2 E}{12(1 - \nu^2) f_y}} \qquad (2.42)$$

This gives a thicker plate than for the elastic design based on the limiting thickness.

The text book of Salmon et al (12) suggests that to develop the plastic capacity of the bracket, it may be realistic to use half of the the value of L/t limitations as used in his elastic design method, that is reducing Equations 2.18 to

$$0.5 \leqslant L/H \leqslant 1.0 \qquad \frac{L}{t} \leqslant \frac{0.5}{\sqrt{f_y}}\sqrt{2.38\,\frac{\pi^2 E}{12(1-\nu^2)}}$$

$$1.0 \leqslant L/H \leqslant 2.0 \qquad \frac{L}{t} \leqslant 0.5\,\frac{(L/H)}{\sqrt{f_y}}\sqrt{2.38\,\frac{\pi^2 E}{12(1-\nu^2)}} \qquad (2.43)$$

2.7 Ultimate limit state design of triangular gusset plates

In 1979 Martin (15) investigated methods for the limit state design of triangular steel gusset plates. He reviewed the design methods of Salmon et al (12) and the Draft British Steel Code (2). These two methods were originally derived for the allowable stress design and the allowable stress was based on a failure load defined by either first yield or the elastic critical buckling load. The Draft British Steel Code (2) was based on first yield. For use in ultimate limit state design these failure loads were taken to be the ultimate loads. Salmon et al (12), however, concluded that this was not the proper criterion of strength as the actual ultimate load was much higher, especially with plates that failed by yielding. Martin (15) therefore presented an alternative theoretical approach for the ultimate limit state design based on experimental observation.

As there was little experimental work available for comparison, it was necessary initially for Martin (15) to provide further experimental evidence. Salmon et al (12) only presented 15 experimental results which were of the non-slender type of gusset, so Martin (15) concentrated on producing results for slender gusset plates. To produce gusset plates with high slenderness ratios, Martin (15) tested 43 slender non-welded model gusset plates made from mild steel sheet 0.263mm thick and yield strength of $350 N/mm^2$.

Each steel gusset plate was fastened along its supported and loaded edges to a timber frame using wood screws. A hinge was introduced in the frame at the junction of the loaded and supported edges to eliminate the resistance moment from the loaded plate that

occurs in many practical cases.

Three parameters were investigated. One series of experiments investigated the effect of varying the plate size by varying L(=H) from 25 to 125mm with s = L/2. To simulate specimens with and without the loaded plate, two types of specimens were used, one with the 90° corner removed to the level of the hinge to represent specimens without the loaded plate, and the other a complete triangle to represent specimens with the loaded plate.

The second series investigated the effect of varying the ratio H/L by varying H from 37.5 to 225mm with L fixed at 75mm and s = L/2. Again two types of specimens with and without the 90° corner were tested.

The third series investigated the effect of adding material parallel to the free edge with L = H = 75mm and s = L/2, for both specimens with and without the 90° corner.

Another 7 non-slender welded gusset plates of nominally 6mm thick plates, with different dimensions were tested to complement the experimental results by Salmon et al (12).

The gusset plates in the experiments appeared to buckle at failure, and after failure when the load was removed they did not regain their original shape, which indicated that part of the material of the gusset plate had yielded. From the behaviour of the specimens during the experiments Martin (15) developed the following theory.

Martin's (15) theoretical approach is based on assuming, for theoretical purposes, that the plate acts as a series of struts parallel to the free edge instead of assuming one strut as in other methods. However, with the loaded plate being fixed to the vertical support, the loaded plate was taken to rotate about this point, which was observed in the experiments and also assumed by Salmon et al (12). The theoretical point of rotation is referred to as the theoretical hinge in Martin's (15) work and is shown in Figure 2.17. By taking

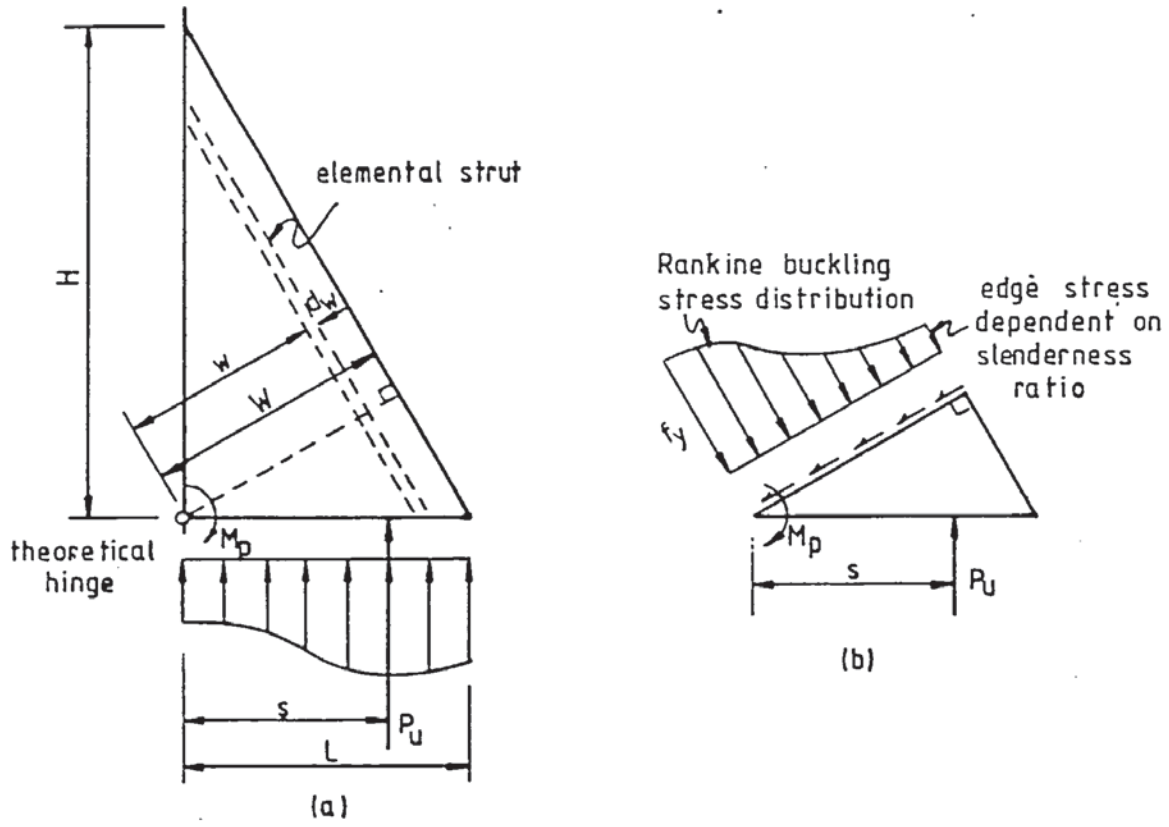

Figure 2.17 Geometry and stress distribution assumed by Martin.

moments about this theoretical hinge the forces passing through it are removed from the equilibrium equation. Therefore the moment P.s, about the theoretical hinge, produced by the applied load is resisted by the bending resistance of the loaded plate at the theoretical hinge and the summation of all the resistance moments produced by each of the assumed elemental struts about the theoretical hinge. It is then assumed that at the ultimate load the loaded plate reaches its plastic moment of resistance and all of the struts reach their ultimate load at the same time. If all of the struts fail by yielding then the stress distibution across the critical section can be plotted from the stress in each strut giving a rectangular stress distribution and the full plastic strength will have been reached. With the load applied at s = L/2 and neglecting the loaded plate, this would give the same result as the plastic design method derived from Jensen's (4) work. However for other values of s the two methods are different.

For the gusset plate that fails by buckling the maximum stress in each strut will be the buckling stress. The maximum stress in each strut is then dependent on its slenderness ratio and Martin (15) used the empirical Rankine (16) formula

$$f_{bw} = \frac{f_y}{1 + \frac{f_y}{E\pi^2}\left(\frac{l}{r}\right)^2} \tag{2.44}$$

to express the buckling stress. This formula was used because it is conservative and easily integrated. Therefore, the maximum axial stresses on the short struts close to the 90° corner will be at yield while at the free edge the stresses depend on the slenderness ratio. The stress distribution across the plate at the ultimate load will therefore be of the shape shown in Figure 2.17(b).

The main problem with any method for designing gusset plates assuming struts is to determine the effective lengths to be used for calculating the slenderness ratio. In other methods only the effective length of the free edge has been required. With Martin's (15) theory the effective lengths of all the assumed struts are required. Initially Martin (15) assumed all of the struts to be fixed ended struts. For the development of the theory the effective length l of each strut was expressed in terms of of the lever arm distance w from the theoretical hinge (see Figure 2.17). When $H/L \neq 1$, the actual length of each elemental strut is 2w, and the effective length l is half this value, i.e. of length w. When $H/L = 1$ the actual length of each elemental strut in terms of w is $w(L/H + H/L)$, but Martin (15) found from his experiments that the effective length was less than half this value, because the deflected shape had more than one "loop". The value adopted in his theoretical work was $l = w$. This would then give the slenderness ratio for the free edge of

$$\frac{l}{r} = \frac{2\sqrt{3}}{\sqrt{(L/H)^2 + 1}}\left(\frac{L}{t}\right) \tag{2.45}$$

Taking moments about the theoretical hinge and equating the applied moment produced by the load to the resistance moments assumed by the loaded plate and the gusset plate at the ultimate load P_u, an equation is formed relating P_u to the buckling stress f_{bw}

$$P_u s = \int_o^W f_{bw} t . w : dw + M_p \qquad (2.46)$$

M_p is the resistance moment at the hinge and varies depending on the experimental or practical conditions. Combining Equations 2.44 and 2.46 and solving gives

$$P_u = \frac{\pi^2 E\, t^3}{24 s} \ln\left[1 + \frac{12 f_y}{\pi^2 E} \frac{(L/t)^2}{[(L/H)^2 + 1]}\right] + \frac{M_p}{s} \qquad (2.47)$$

Martin's (15) experimental results showed a slight increase in strength was obtained by adding material to the free edge. He suggested that an approximate theoretical value of the increase in strength may be obtained by extending the previous stress distribution as shown in Figure 2.17. An arbitary parabolic stress distribution was assumed, extending the previous buckling stress at the original free edge to zero at the new free edge, as shown in Figure 2.18. The increase in buckling load P_u' is obtained by taking moments about the inside corner again, giving

$$P_u' = \frac{W' . t}{3s} \frac{f_y}{\left[1 + \frac{12 f_y}{E\pi^2}\left(\frac{W}{t}\right)^2\right]} \left(W + \frac{W'}{4}\right) \qquad (2.48)$$

where W is the original width of the critical section and W' is the extension produced by the added material. However, Martin (15) concluded that the relatively small increase resulting from this calculation is probably not worth considering practically.

The disadvantage of the previous theoretical approach is that Equation 2.47 is not easily arranged to obtain the value of t directly for design situations where the thickness t is the unknown. Martin

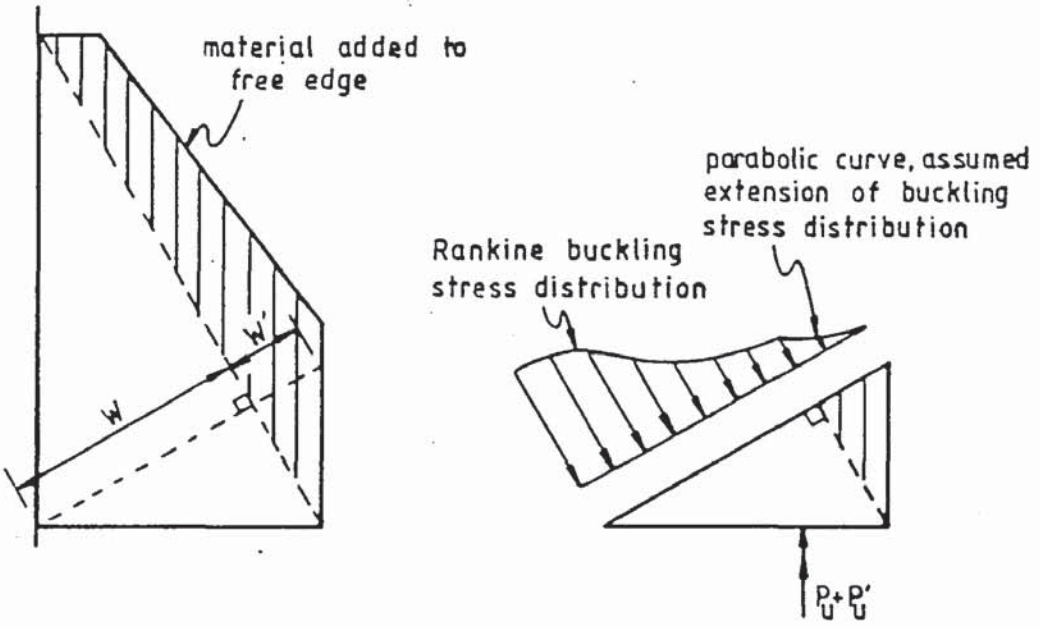

Figure 2.18 Extended stress distribution for material added to the free edge assumed by Martin.

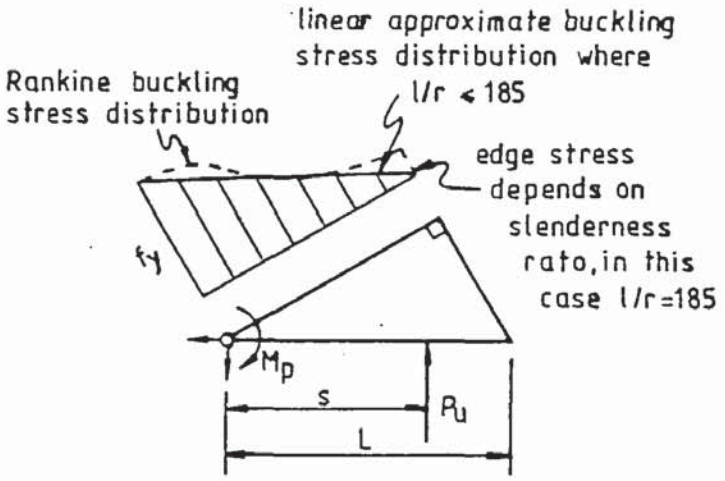

Figure 2.19 Martin's linear approximation to Rankine's buckling stress distribution

(15) therefore suggested an alternative approximate method for gusset plates of low slenderness ratio. The previous equilibrium Equation 2.46 remains the same but, the buckling stress distribution produced by using Rankine's (16) Equation 2.44 is approximated to a triangular distribution as shown in Figure 2.19. Provided the slenderness ratio of the free edge is less than 185, the buckling stress equation then becomes

$$f_{bw} = f_y\left[1 - \frac{(l/r)}{185}\right] = f_y\left[1 - \frac{(w/r)}{185}\right] \qquad (2.49)$$

Combining Equations 2.46 and 2.49 and integrating gives

$$P_u = \frac{f_y}{(s/L)} \frac{L.t}{[(L/H)^2 + 1]}\left[\frac{1}{2} - \frac{\sqrt{3}\,(L/t)}{277.5\sqrt{(L/H)^2 + 1}}\right] + \frac{M_p}{s} \qquad (2.50)$$

Rearranging to obtain t directly gives

$$t = \frac{2(P_u - M_p/s)(s/L)[(L/H)^2 + 1]}{f_y L} + \frac{3.L}{138.75\sqrt{(L/H)^2 + 1}} \qquad (2.51)$$

Alternatively the original design Equation 2.47 may be rearranged to a non-dimensional form for design purposes relating $(s/L)(Pu-M_p/s)/L^2E$ to H/L for values of t/L. This can then be plotted graphically or expressed in tabular form. A separate table or graph must be produced for each value of the design stress.

Martin (15) did an optimum weight analysis with his theoretical Equation 2.47 which produced an optimum value for $H/L \simeq 1$.

As for the value of M_p used in Martin's (15) equations, for his experimental work he used

$$M_p = B.T(T/2 + t_w)f_y \qquad (2.52)$$

based on experimental observations that the hinge appeared to form inside the welds. In practice he suggested that a conservative value of

$$M_p = B.T^2 f_y/4 \qquad (2.53)$$

may be more acceptable.

In comparing the design methods of Salmon et al (12), the Draft British Steel Code (2) and Martin (15), with the 15 experimental results by Salmon et al (15) and the 50 experimental results by Martin (15), the following conclusions were derived by Martin.

i) The Draft British Steel Code (2) method using the design equation

$$P_u s < p_y.z' \qquad (2.54)$$

was shown to be based on the wrong assumptions, i.e. bending, is

unsafe and inaccurate.

ii) The Salmon et a (12) method using the design equations

a) for stability, Equation 2.11, rearranged

$$P_u = \frac{k'\pi^2 E.t^2}{12(1 - \nu^2)L} \qquad (2.55)$$

where $k' = 3.2 - 3.0\ (L/H) + 1.1\ (L/H)^2$

b) for yielding, Equation 2.13, rearranged

$$P_u = Z.f_y L.t \qquad (2.56)$$

where $Z = 1.39 - 2.20\ (L/H) + 1.27\ (L/H)^2 - 0.25\ (L/H)^3$

is based on the correct mode of failure, i.e. buckling is considered, is conservative and not very accurate.

iii) The method developed by Martin (15), Equation 2.47, based on elastic-plastic buckling failure is less conservative and more accurate. The alternative approximate method, Equation 2.50, for gusset plates where the slenderness ratio of the free edge is less than 185 is also shown to be of comparable accuracy.

2.8 Conclusion of literature survey

From the literature survey of methods of designing triangular steel gusset plates the following conclusions were derived. Although triangular steel gusset plates have been used for many years and used in many different applications there are relatively few experimental results, and as a consequence little is known about their behaviour. This has led to many different design methods being suggested without any experimental evidence to support them.

Until 1962 the only experimental results that were related to triangular gusset plates were 22 experimental results on welded beam seat brackets presented in 1936 by Jensen (4). However, these brackets had gusset plates which were very small and thick, and had such a small slenderness ratio that buckling was no problem.

The design method suggested by Jensen (4) was specifically for

these small brackets and was intended for use in allowable stress design. However, as there were no other results available, the method was extended for the design of larger gusset plates. Some designers were aware of the possibility of buckling but, did not know how to deal with it, which is probably why there are so many empirical methods and variations.

The failure of gusset plates is essentially a plate buckling problem of a very complex nature. Although the classical plate buckling methods have been used to solve rectangular and circular plates with many loading and support conditions, there are not many solutions for triangular plates. The main reason is that the methods are very difficult to apply to triangular plates, especially non-symmetrical triangular plates with non-symmetrical and non-uniform loading conditions as found in triangular gusset plates. Salmon (9) took on the formidable task of using the most appropriate of these classical methods to produce a solution for such plates. However, after such an exercise he had to adjust his theoretical results to such an extent that he effectively produced an empirical equation from his 15 experimental results. It is important to note that Salmon et al (12) concluded from experimental work that the critical load, expecially yielding, is not the proper criterion of strength. The classical plate buckling theories produce solutions that are based on the elastic critical buckling load which do not take into account yielding or the post buckling strength.

The 15 experimental results presented by Salmon et al (12) were the first of practical sized welded gusset plates. However, they were of the non-slender type mainly failing by yielding and were of an exploratory nature. Salmon et al's (12) design recommendations have had several revisions, each revision is more conservative than the previous one and diverting further from the original theoretical work.

In 1979 Martin (15) presented 43 results for slender non-welded gusset plates and only 7 non-slender gusset plates together with an alternative theoretical approach for the ultimate limit state design. The slender gusset plates were of a model form and the non-slender gusset plates were of an exploratory nature. Where Salmon et al's (12) method was discontinuous from the buckling to the yield condition and was only based on the elastic critical loads, Martin's (15) method was continuous and was based on the ultimate failure load.

It is apparent that there is a scarcity of experimental results of practical sized welded gusset plates. There has not been any systematic experimental investigation of the various parameters on practical sized welded gusset plates. Martin (15) systematically investigated the effect of varying the size and the H/L ratio of his slender model tests but, these need to be repeated for practical sized welded gusset plates. The variation in the gusset plate thickness has not been investigated systematically. Salmon et al (12) only chose two values. The variation in the loaded plate thickness has not been investigated. Martin (15) is the only investigator to include a term for the loaded plate in his theoretical work. The effect of moving the position of the applied resultant load has not been investigated experimentally. Salmon's (9) theory does not allow for this as it assumes the loading to be of a certain type which would produce the required boundary conditions for its solution. Martin's (15) theory does cater for the resultant load position and so do some of the other theories to some degree, including Jensen's (4), however, they have not been checked experimentally. The effect of varying the internal angle between the two fixed edges has never been investigated. The effect of removing the inner corner of the gusset plate has only been investigated exploratory by Jensen (4) for one specimen and it therefore requires further investigation as it is sometimes necessary to remove this portion.

There is no adequate means of designing the welds in relation to the gusset plate. The method used by Jensen (4) which was proposed by Priest (5) is specifically for the small brackets with the load applied at approximately 0.8L along the loaded edge of the gusset plate. The design is also only for the combined weld attaching the gusset and loaded plate to the column. Any nominal weld size is suggested for the gusset plate to loaded plate weld. The design methods suggested by MacGinley (14) and the Steel Designers Manual (13) are not directly related to the gusset plate and there is an inconsistency in the design method adopted.

It is the aim of this research project to investigate systematically the parameters associated with practical welded triangular steel gusset plates and to recommend a design method that is simple enough to be used in design practice.

CHAPTER THREE

EXPERIMENTATION

3.1 Introduction

The main test program consisted of 82 triangular steel gusset plate tests which investigated parameters associated with the failure of triangular steel gusset plates. The parameters investigated were:-

a(i) gusset plate size L=H, s=L/2, H/L=1 (series 3)

a(ii) gusset plate ratio H/L, s=L/2 (series 4)

a(iii) variation of s, i.e. the point of application s of the resultant applied load P (series 5)

a(iv) continuation of the loaded plate (series 6)

a(v) loaded plate thickness T (series 7)

a(vi) gusset plate thickness t (series 12)

a(vii) removal of inside corner of gusset plate (series 8)

a(viii) variation of internal angle θ between loaded and supported edges (series 13).

To assist in the theoretical work various subsiduary tests were undertaken. A series of 47 strut tests investigated the buckling characteristics of the plate used in the gusset plates under various loading conditions. 15 special gusset plates were made to test assumptions used in the theoretical work. The subsiduary tests were as follows:-

b(i) pin ended directly loaded strut tests (series 1)

b(ii) fixed ended directly loaded strut tests (series 9)

b(iii) inclined indirectly loaded fixed ended strut tests (series 10)

b(iv) multiple strip plate test (series 11)

b(v) loaded plate bending resistance tests (series 2)

b(vi) rigid loaded plate strain gauge tests (series 5a).

Further series of tests were undertaken to investigate the

behaviour and influence of the welds connecting the gusset plate to its adjacent loaded and supported plates. A total of 22 similar gusset plates were tested with different weld sizes and arrangements as follows:-

c(i) the size of the loaded edge weld (series 14)

c(ii) the size of the supported edge weld (series 15)

c(iii) the size of both the loaded and supported edge welds simultaneously (series 16)

c(iv) the shear, normal and frictional forces on the welds (series 17).

Specimens, test rig and test procedure are described in this chapter and all relevant materials are referred to.

3.2 Main test program

3.2.1 Methods of testing

The main aim of the experimental work was to obtain the actual ultimate collapse load of welded gusset plates of a practical size used in industry. The gusset plates used in industry range from small thin gusset plates, as used in support brackets, to very large and thick gusset plates as used in large moment resisting column base plates. The limitations on the maximum thickness, size and shape of the gusset plates that could be tested were dependent on a combination of; the maximum load capacity of the testing machines and their availability; the maximum and minimum dimensions of the specimens that could be tested in each testing machine; the ease of manufacture, transporting, setting up and testing of the specimens and rig; and the relative costs of rigs and specimens. It was also considered that the worst case type of failure would be with the thinner gusset plates. The consideration of all these points led to the general use of 4mm steel plate.

In testing it was necessary (a) to produce simple consistant loading conditions which related to conditions and (b) to be able to isolate individual parameters without diverting too far from the practical situation.

Various testing arrangements were considered to simulate practical loading conditions. One method used by Salmon et al, was to construct a frame with a column supporting a single gusset plate in the form of a bracket, which was bolted to the column, as shown in Figure 3.1. For economic reasons it would have been desirable to construct one column for all tests. The column would therefore have to have been fairly large to withstand the testing of large plates and would have necessitated occupying one testing machine for the duration of the testing program. The size of the column would have also restricted testing to a rig with a capacity of just under 1000kN. It was also considered undesirable to bolt the gusset plates to the support as problems were foreseen in the testing of large plates. The possibility of bolt, flange or gusset support plate failure could not be ruled out. The size and shape of the gusset plates tested would be restricted by the position of the bolt holes in the column flange. With the repeated use of the same bolt holes in the column flange and the possible distortion of both the flange and the gusset support plate, problems in lining up bolt holes accurately were foreseen.

Another method considered was to bolt or weld a gusset plate in the form of a bracket to the end of an I beam, as shown in Figure 3.2. The same problems, concerning the bolting of the gusset plates to the end of the beam were expected. Alternatively the gusset plate could have been welded to the end of the beam and after testing, cut off and another gusset plate welded on. This method was, however, restricted to one machine with a capacity of just under 1000kN due to the size of the beam required.

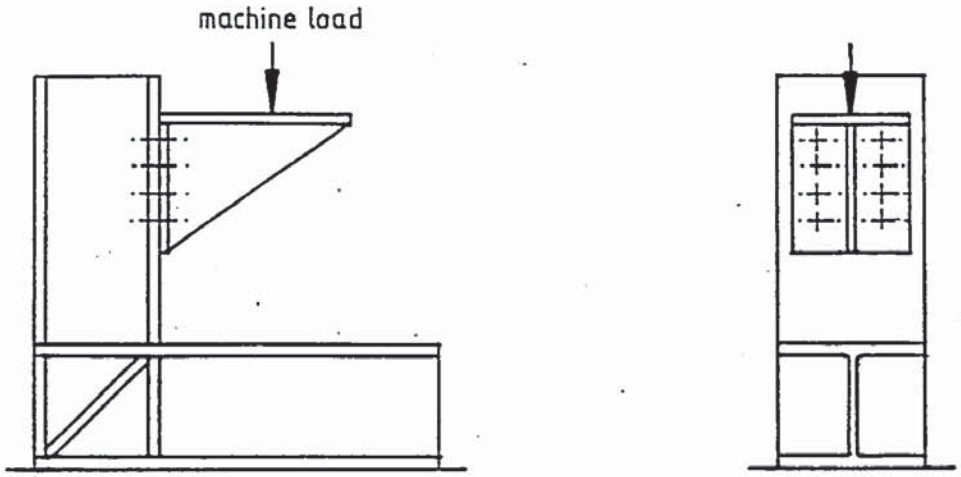

Figure 3.1 Column support testing arrangement as used by Salmon et al.

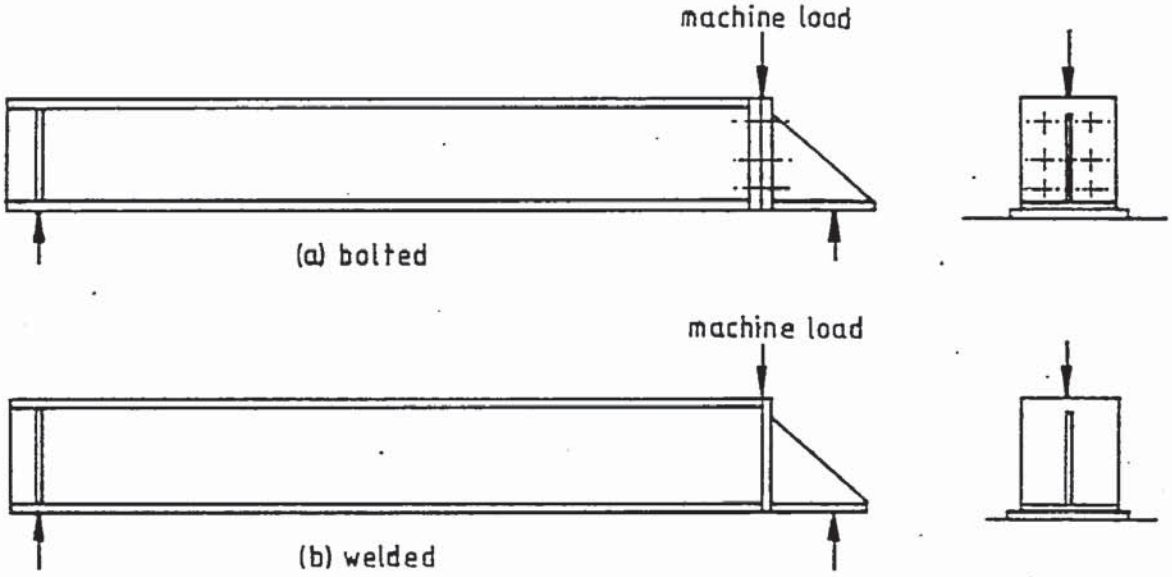

Figure 3.2 I-beam support testing arrangements.

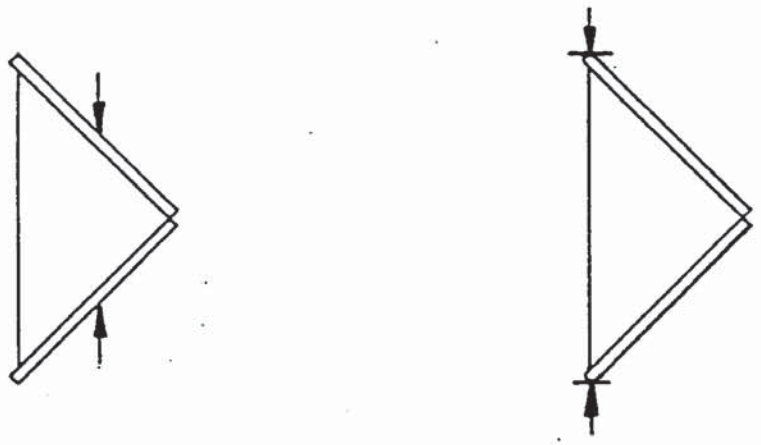

Figure 3.3 Other possible testing arrangements.

With both of the previous methods, difficulties were also expected with horizontal loads in the testing of gusset plates with varying internal angle between the loaded and supported edges.

Other methods considered were to test single gusset plate specimens as shown in Figure 3.3 but, these were not considered to be true representations of practical loading conditions as the loads were not applied perpendicular to the edges of the gusset plates.

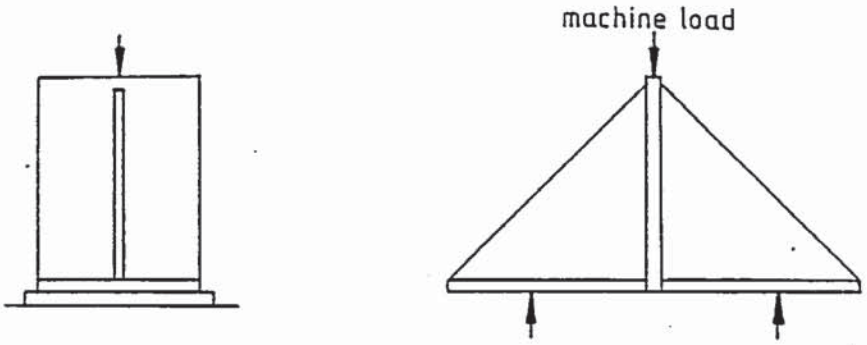

Figure 3.4 Back to back gusset plate testing arrangement adopted.

The method that was finally adopted was to weld two similar gusset plates back to back to the same vertical support, as shown in Figure 3.4. This had the advantage of producing a symmetrical specimen with very simple symmetrical loading requirements. By nature of its symmetry the vertical support was automatically as stiff as required with the forces on both sides of the vertical support being equal and opposite. This eliminated the need to design a vertical support that would have to withstand large bending moments or to be stiff enough to prevent distorting. As the specimens were self contained all connections were welded, eliminating the complications of using bolts. The support plate only had to be strong enough to prevent the top end, where the machine load was applied, from crushing. Any size or shape of gusset plate could be made and tested as the specimens were self contained. They were relatively easy to make, transport, set up and test due to their size and symmetry. Any

of the testing machines could be used as size and load required.

3.2.2 Testing arrangements

Three testing machines were utilized in the testing program. Most of the tests were performed on a Denison 500kN testing machine. Where the specimens were too tall to fit between the platens of this machine, a large portal frame testing rig with a Mitchell Hydraulics 1000kN hydraulic test ram was used. Where the capacity of these two machines was exceeded a Losenhausenwerk 5000kN hydraulic test ram and rig were used.

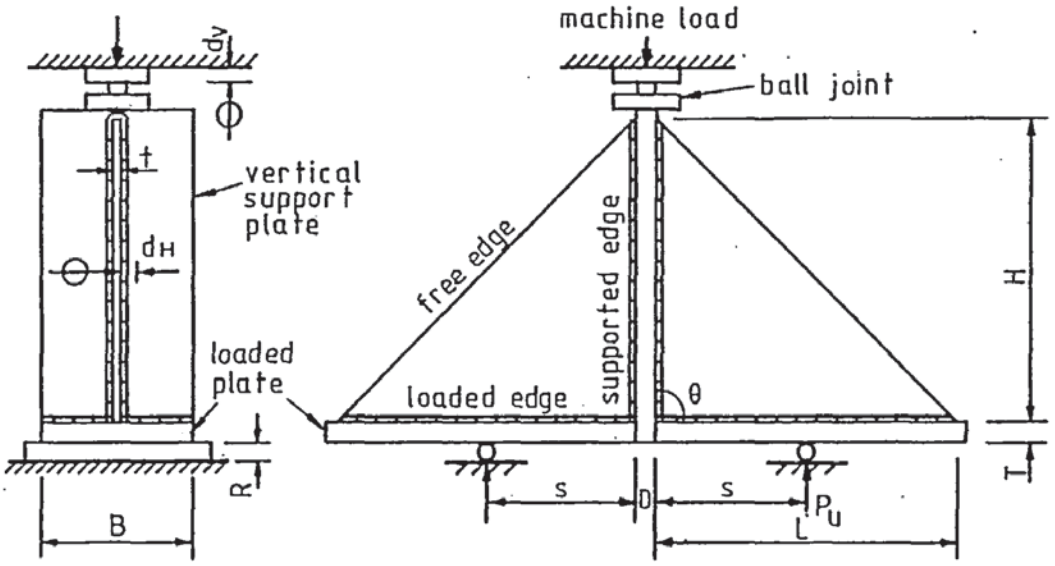

Generally

L = 300 mm	t = 4 mm	B = 150 mm
H = 300 mm	T = 20 mm	R = 20 mm
s = L/2	D = 20 mm	θ = 90°

Figure 3.5 General testing arrangement for main series.

The general testing arrangement is shown in Figure 3.5. The gusset plates were made from steel plate 4mm thick, except for the series investigating the variation in gusset plate thickness. Each steel gusset plate was fillet welded along the loaded and supported edges on both sides of the plate. Two similar gusset plates were welded back to back to the same vertical support. The loaded plates

and the vertical supports were made from mild steel section 20mm thick and 150mm wide. The exceptions to this were the series investigating the H/L ratio and the series investigating the loaded plate thickness. The loaded plates were terminated at the bottom of the vertical supports to eliminate the resistance moment of the loaded plate that occurs in many practical cases. The exceptions to this were the series investigating the effect of continuing the loaded plate through and the series investigating the thickness of the loaded plate. Each loaded plate was held in place laterally with a lateral fillet weld along its top edge to the vertical support. All fillet welds were 4mm except for the series investigating the gusset plate thickness.

The function of the loaded plate is to distribute the load to the loaded edge of the gusset plate. In practice the externally applied load is often in the form of a distributed load, but in the tests, to ensure accuracy in the positioning of the load, it was applied through a roller. This also ensured that it was only applied perpendicular to the loaded edge of the gusset plate. With all but the series investigating the position of the applied load, the rollers were placed at s=L/2. For the majority of tests, the internal angle θ between the loaded and supported edges was 90^{o}, and so the two rollers rested on the horizontal test bed of the testing machine.

In testing the variation of the internal angle θ between the loaded and supported edges, the loaded plates were not horizontal. Therefore a small rig was required to support the specimens on rollers in order to apply the load perpendicular to the loaded edge of the gusset plate. The rig was designed to support the specimens with the load applied at a distance s=L/2 for each angle tested. The rig details are shown in Figure 3.6 and two typical testing arrangements are shown in Figure 3.7.

For the majority of the tests the specimens were supported by two

20mm diameter steel rollers 150mm long, resting on the flat bed of the testing machine. The exceptions to this were the series investigating the thickness of the gusset plate and the variation of the internal angle between the loaded and supported edges. With the former, the loads were considerably high for the 9,11,13 and 15mm thick gusset plates and so 50mm diameter tool steel rollers 210 mm long, resting on the flat bed of the testing machine were used. Spreader plates 100 x 150 x 20mm thick were also used between the roller and the loaded plate for this series of gusset plate tests.

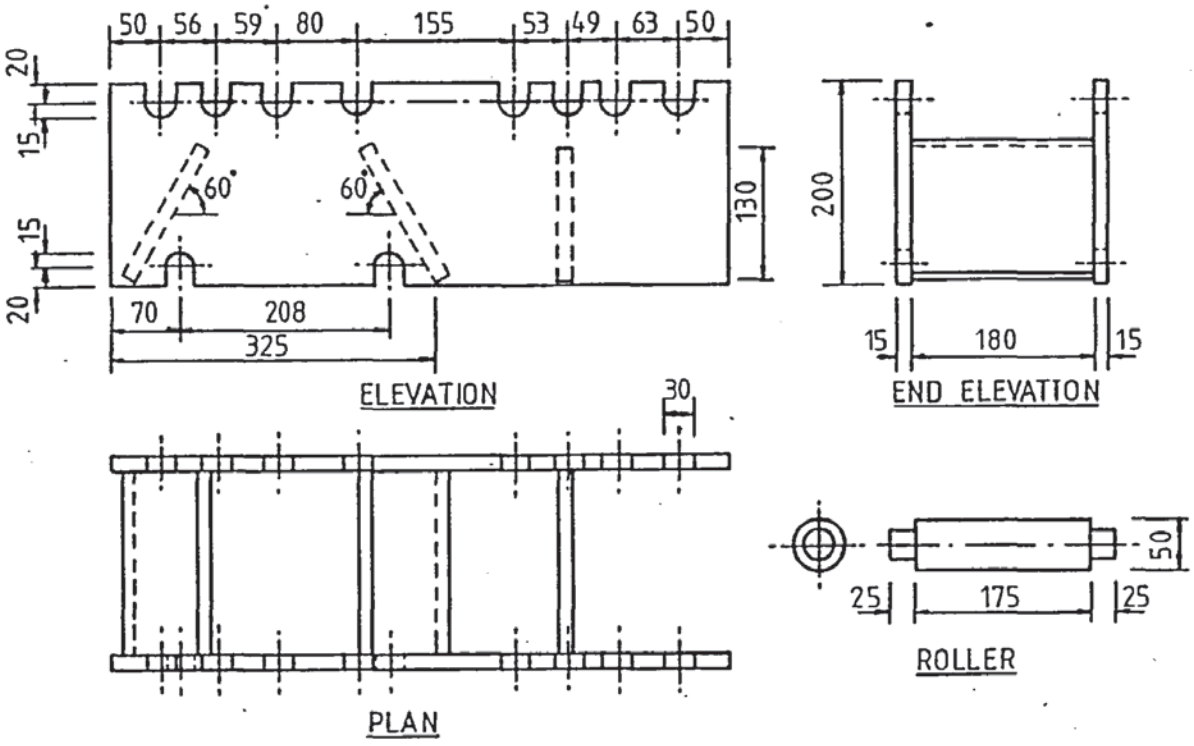

Figure 3.6 Details of roller support rig for series investigating the variation of the internal angle θ.

For the series investigating the variation of the internal angle, the rollers could only be supported by their ends. To prevent bending 50mm diameter tool steel rollers were used.

The machine load was applied through a ball joint to remove any eccentricity of loading caused by specimen inaccuracies and to allow accurate positioning of the machine load.

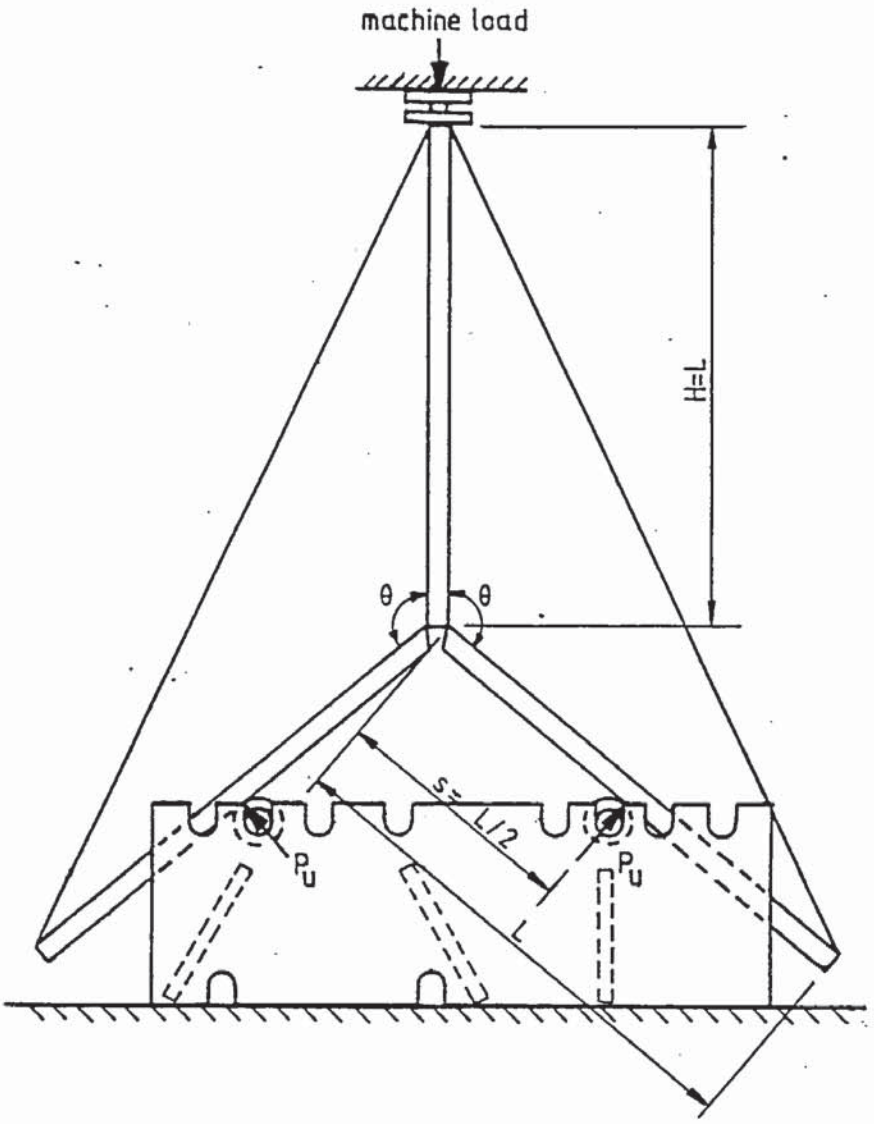

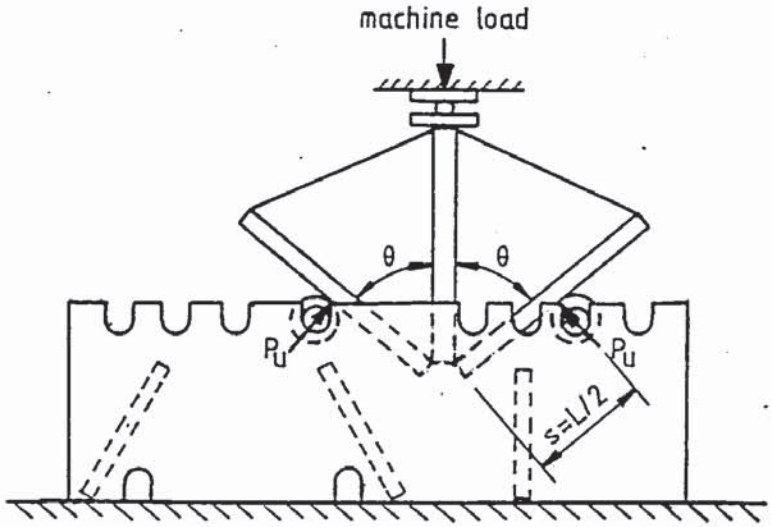

Figure 3.7 Typical testing arrangement for series investigating the variation of the internal angle θ.

3.2.3 Material and material tests

The material used for the test specimens was steel throughout. The gusset plates were generally made from rolled steel plate of 4mm nominal thickness. Only the series investigating the gusset plate thickness used gusset plates made from rolled mild steel section 15mm thick and 300 mm wide. The loaded plates and vertical support plates were generally made from mild steel section 20mm thick and 150mm wide, except when 150mm width was unavailable and was substituted with 100mm width. The series investigating the gusset plate thickness used blocks of mild steel 50mm thick for the vertical supports of the thicker plates and 25mm thick for the mid range plates to prevent them crushing.

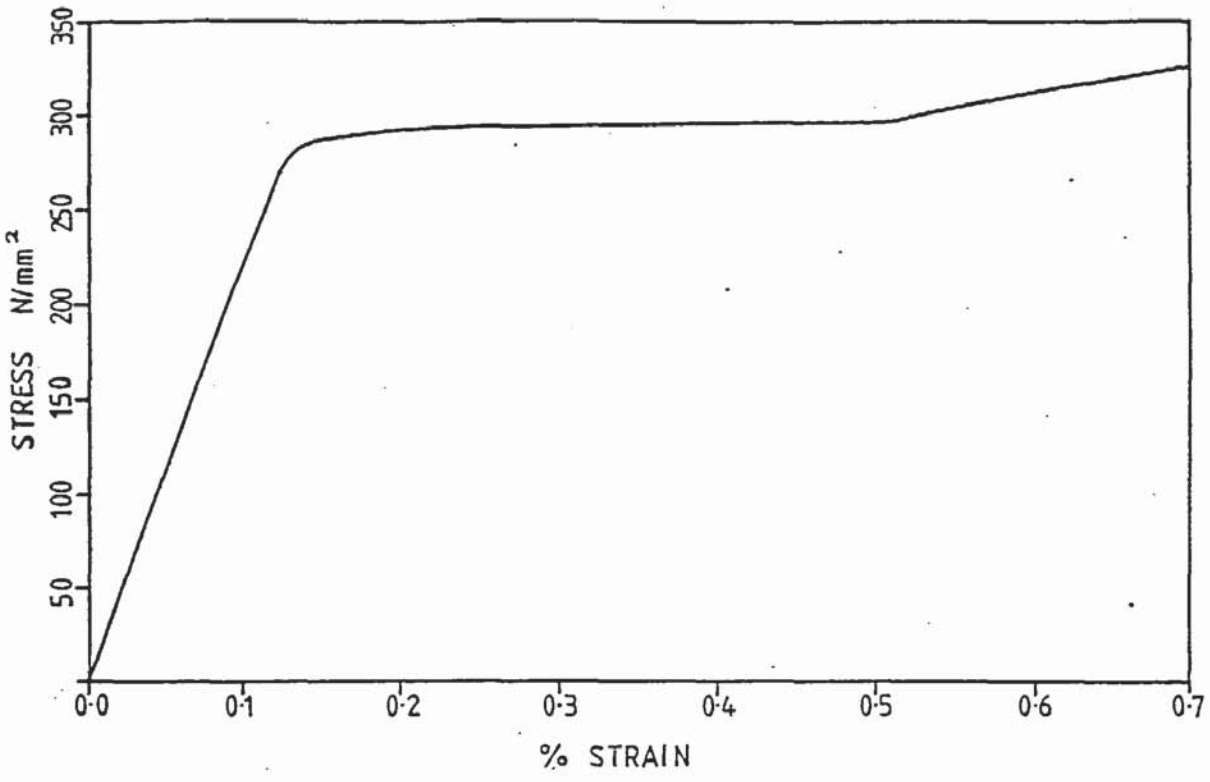

Figure 3.8 A typical stress-strain relationship for the steel used.

The thickness of each gusset plate was obtained by random sampling along the free edge of each specimen with a micrometer. The tensile yield strength of each batch of test specimens were determined by tensile tests on specimens 400mm long and 25mm wide using a Denison

500kN tensile testing machine. The tensile yield strengths of the loaded plates were also determined in a similar manner, where required.

The average value of Young's modulus of elasticity was found to be 206kN/mm^2. A typical stress-strain relationship for the gusset plate steel is shown in Figure 3.8.

3.2.4 Welding of the gusset plates

Each gusset plate was fillet welded on both sides of the plate along the loaded and supported edges. Two similar gusset plates were welded back to back to the same vertical support. To reduce the effects of distortions associated with welding the gusset plates were welded in the following manner.

For the specimens with the internal angle θ between the loaded and supporting edges equal to 90°, the loaded plates of the two gusset plates on one specimen were both clamped down to a horizontal, rigid, rotating work-bench. The vertical support plate was held vertically in place by clamping it to a steel block which was clamped to the loaded plate and work-bench as shown in Figure 3.9(a). Both gusset plates were tack welded into position. Each plate was then fillet welded into place using the step back technique in the order and direction shown in Figure 3.9(b). The loaded plate welds of both gusset plates were completed first followed by the vertical welds using the same technique. The lateral weld connecting the loaded plate to the vertical support was the last to be done. The only difference with the plates with an internal angle other than 90° was that they could not be clamped down to a work-bench.

All 4mm fillet welds were of single run, using 3.25mm Fastex electrodes made by B.O.C. The 6mm and 8mm welds used in the series investigating the gusset plate thickness were multi run welds using the same electrodes and technique. In the welding process the loaded

plates had a tendancy to lift and the welds pulled the gusset plate to the loaded plate and the support plates.

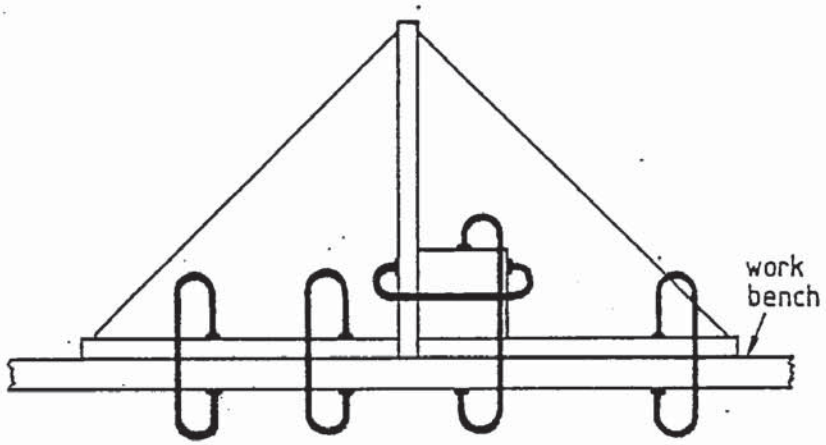

(a) method of clamping specimens for welding

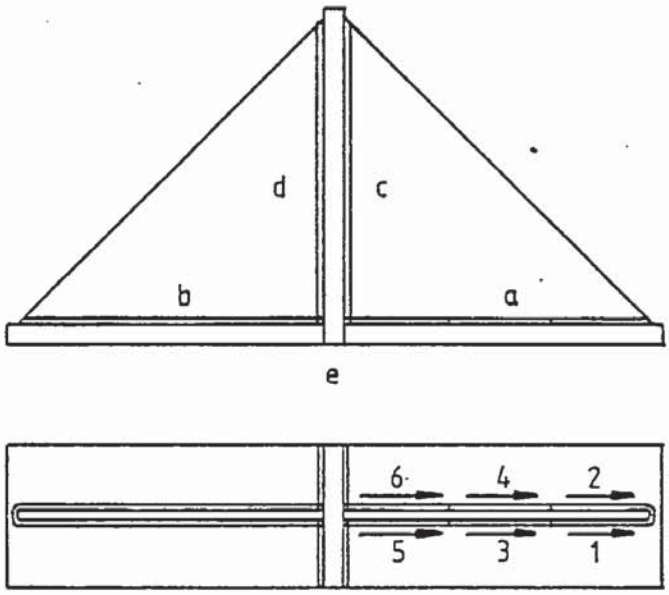

(b) order in which welds were done

Figure 3.9 Welding arrangement.

3.2.5 Instrumentation

Measurements of strain, deflection and rotation were possible with the use of electrical resistance strain gauges and mechanical

dial gauges. Types and method of fixing are described in this section.

3.2.5.1 Strain gauges

Three types of electrical resistance strain gauges were used in measuring strain on the steel; a one element strip strain gauge and two types of three element rosettes. All strain gauges were manufactured by Tokyo Sokki Kenkyujo Co., Ltd. The strain gauge details and the symbols used in the specimen descriptions are shown in Figure 3.10.

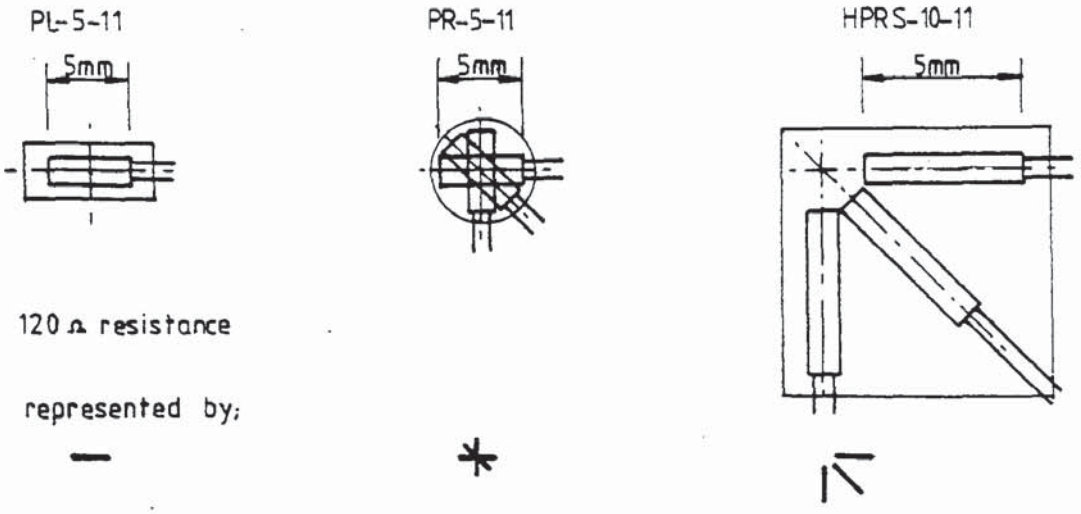

Figure 3.10 Details of the strain gauges used and their associated symbols.

The positions of the strain gauges were carefully prepared and the strain gauges were glued to the steel with M-Bond 200 adhesive, a Micro-Measurements product, and left to dry. The gauge wires were insulated from each other and the steel with adhesive tape. The exact positions and numbers of each gauge element on each specimen are given with the specimen details in Section 3.7.

3.2.5.2 Deflection measurement

Batty dial gauges of 0.01mm per division were used for the measurement of displacements of various points of the specimens. The exact positions and numbers of each dial gauge on each specimen is given with the details in Section 3.7. Generally the total vertical deflection of the specimen and the mid-lateral deflection of the gusset plate's free edge were measured.

3.2.6 Test procedure

One gusset plate was temporarily stiffened to produce failure of the other by clamping the gusset plate between two steel plates. With the testing of the second side of the 4mm gusset plates, the first side was flattened again when the steel stiffener plates were clamped in place. However, the thicker gusset plates of the series investigating the gusset plate thickness, could not be flattened and so stiffeners were welded in place on either side of the gusset plate that had previously been tested. The stiffeners also had to be welded in place with the very small angles of the series investigating the variation of the internal angle.

The specimens were set up in the testing machine with the vertical support plumbed and with the support rollers and ball joints in the correct positions. Shims were inserted between the rollers and loaded plate to remove any rocking or out of plumbness, ensuring the rolling action was not impaired.

Deflection gauges were positioned as required and the strain gauges connected to the junction box of the Compulog Alpha 16 Data Logger. This computer was utilized in reading and recording all strains during the test period. This computer was later replaced, during the testing program, by a new computer, Compulog System Four. The program from the Compulog Alpha 16 Data Logger had to be interpreted, updated and adapted for use on the Compulog System Four

computer, which used a different operating and data storage system. Installation and setting up problems were encountered with the new computer which took time to sort out. Details of the program and use of the new computer are given in Appendix 1.

The tests commenced by reading the initial dial and strain gauge readings. The load was applied in increments with dial and strain gauge readings taken at each increment, after allowing time for the gauges to settle. The magnitude of the increments was determined by the behaviour of the specimen. If the lateral or vertical deflections increased or took longer to settle, then the load increments were reduced. Deflection and strain gauge readings were taken as close to the actual failure as possible. The failure load was determined by the collapse of the specimen.

3.2.7 Specimen details

This section contains information on the parameters investigated, specimen dimensions, positions of strain gauges and deflection gauges for the main test series. A general account of the testing arrangements and specimen dimensions is set out in Section 3.2.2. Therefore only variations to this will be covered in detail.

The specimen numbers incorporate the series number, the value of the variable(s) being investigated and the sample number of that type of specimen. For example S5-300-2 is from series 5, which investigated the point of application s of the applied resultant load P. s is the variable being investigated and in this case is equal to 300mm. Three samples of this specimen were actually tested and the specimen referred to here is the second sample. Another example is S7-6-150-1 which is from series 7, which investigated the loaded plate thickness with the load applied at two different positions. In this case the loaded plate thickness is 6mm with the load at s=150mm and it is the first sample.

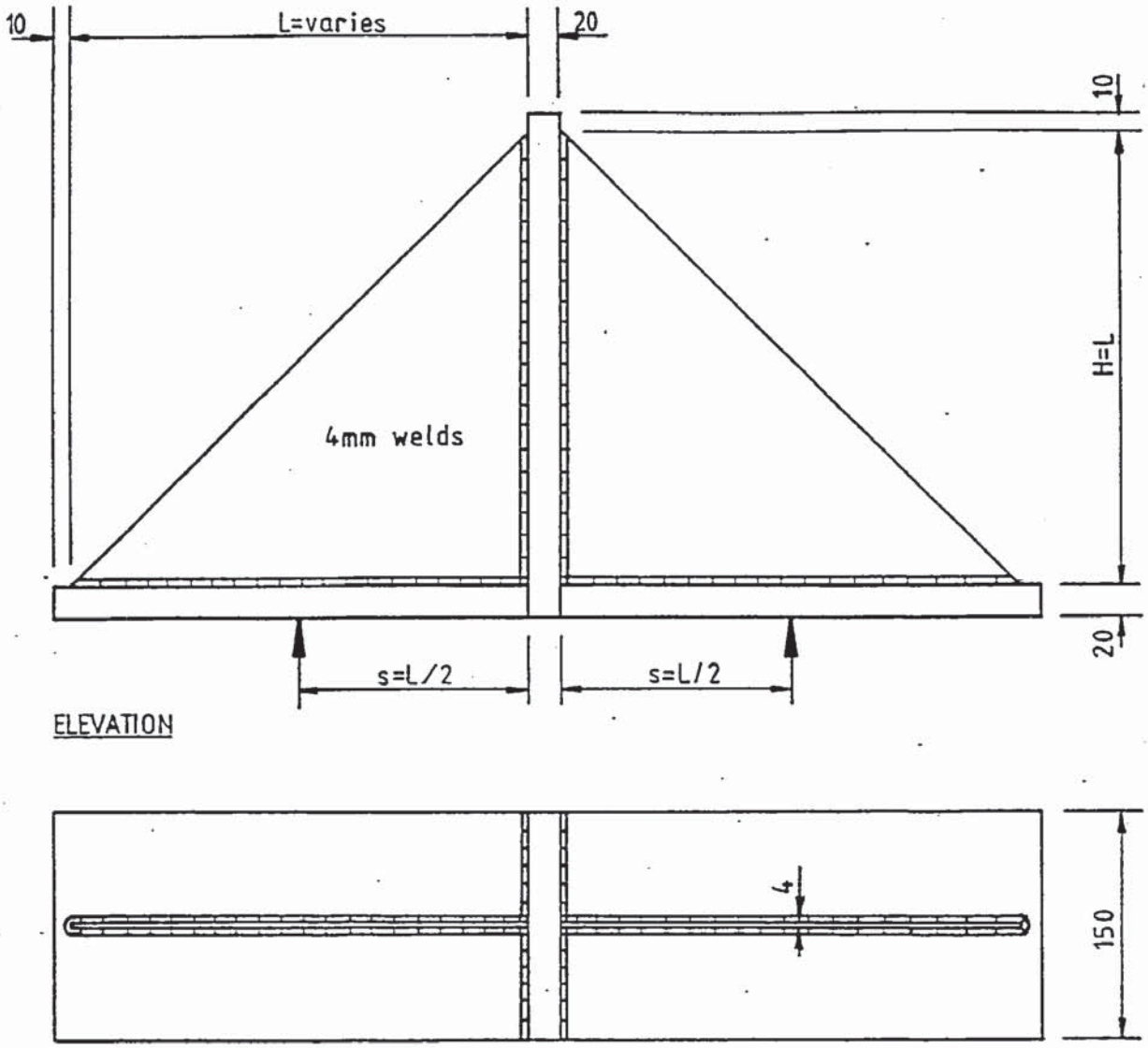

Figure 3.11 Specimen details for series investigating the gusset plate size L=H, s=L/2, (series 3).

3.2.7.1 Gusset plate size L=H,s=L/2, H/L=1 (series3)

This series of tests investigated the effect of varying the size of the gusset plate. This was achieved by varying the loaded edge L and the supported edge H with the ratio H/L=1. The plate thickness t remained constant and the load P was applied at a distance s=L/2. The values of L(=H) tested were 100, 200, 300, 400 and 500mm, with two plates of each size tested. Each specimen was made from the same batch of steel, with the gusset plates having a yield strength of 378 N/mm^2. The specimen details are shown in Figure 3.11.

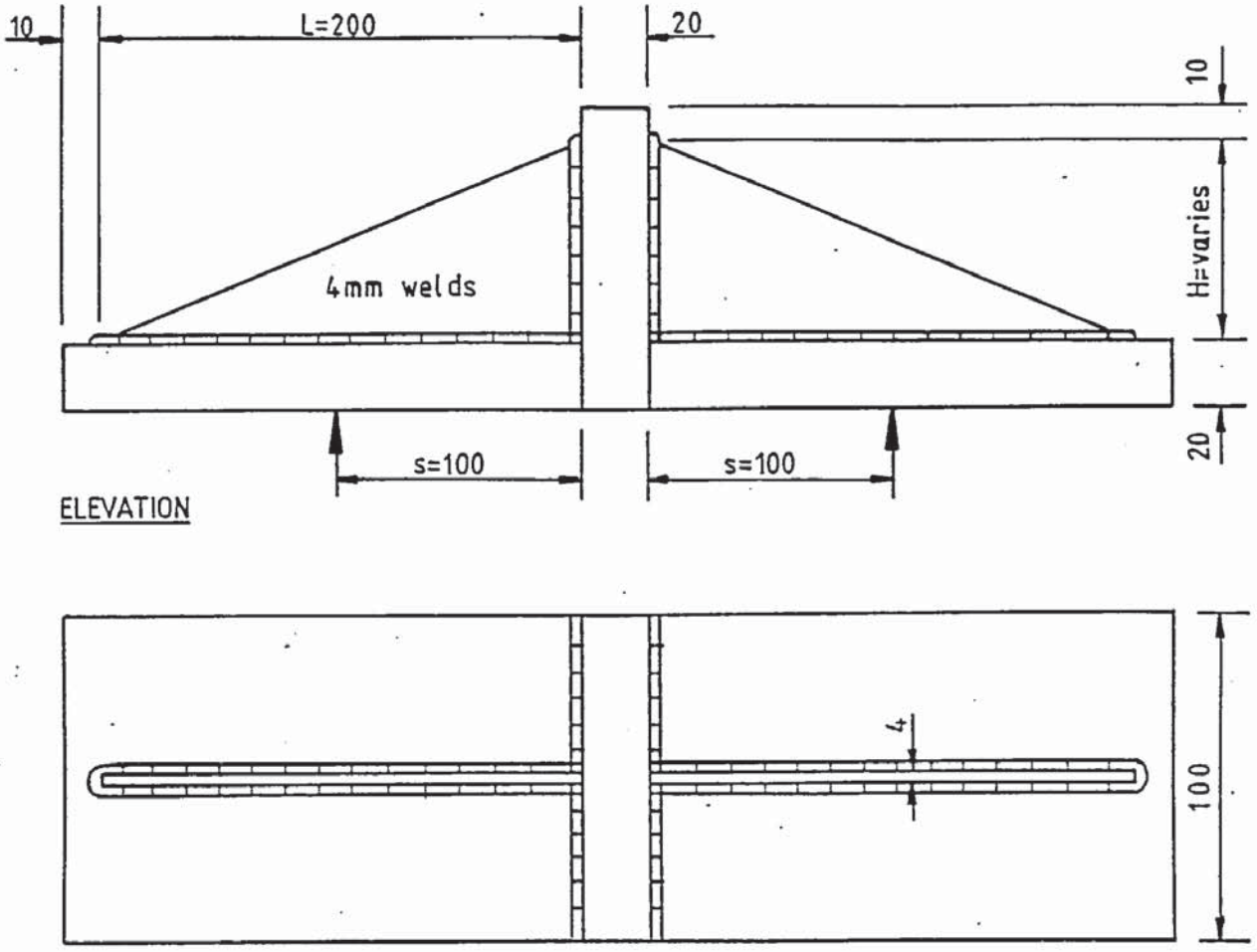

values of H=50, 100, 150, 200, 250, 300, 400, 500 & 600

Figure 3.12 Specimen details for series investigating the gusset plate ratio H/L, s=L/2 (series 4).

3.2.7.2 Gusset plate ratio H/L, s=L/2 (series 4)

This series of tests investigated the effect of varying the ratio H/L. The value of L was fixed at 200mm, with s=L/2 and the values of H tested were 50, 100, 150, 200, 250, 300, 400, 500 and 600mm, with two plates of each size tested. Each specimen was made from the same batch of steel as series 3 . The loaded plates, and the central vertical support were 100mm wide and not the general 150mm width. The specimen details are shown in Figure 3.12.

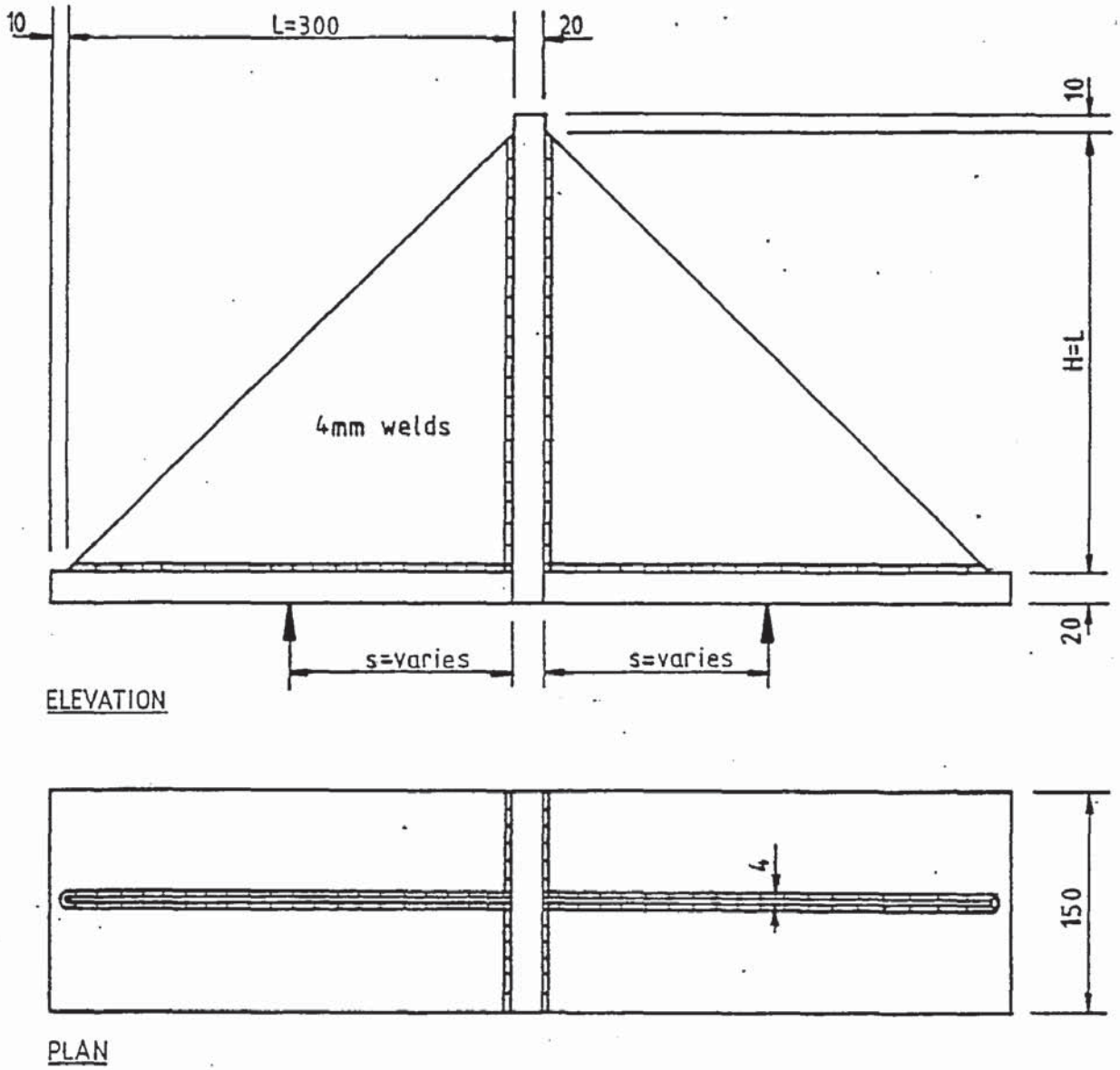

Figure 3.13 Specimen details for series investigating the point of application of the resultant applied load P i.e. varying s (series 5).

3.2.7.3 Point of application of the resultant applied load P (series 5)

This series of tests investigated the effect of varying the distance s which controlled the position of the resultant applied load P. All specimens tested were of the same general dimensions. The minimum practical value of s tested was 75mm because, as s decreases the load required to fail the specimen increases rapidly. The maximum

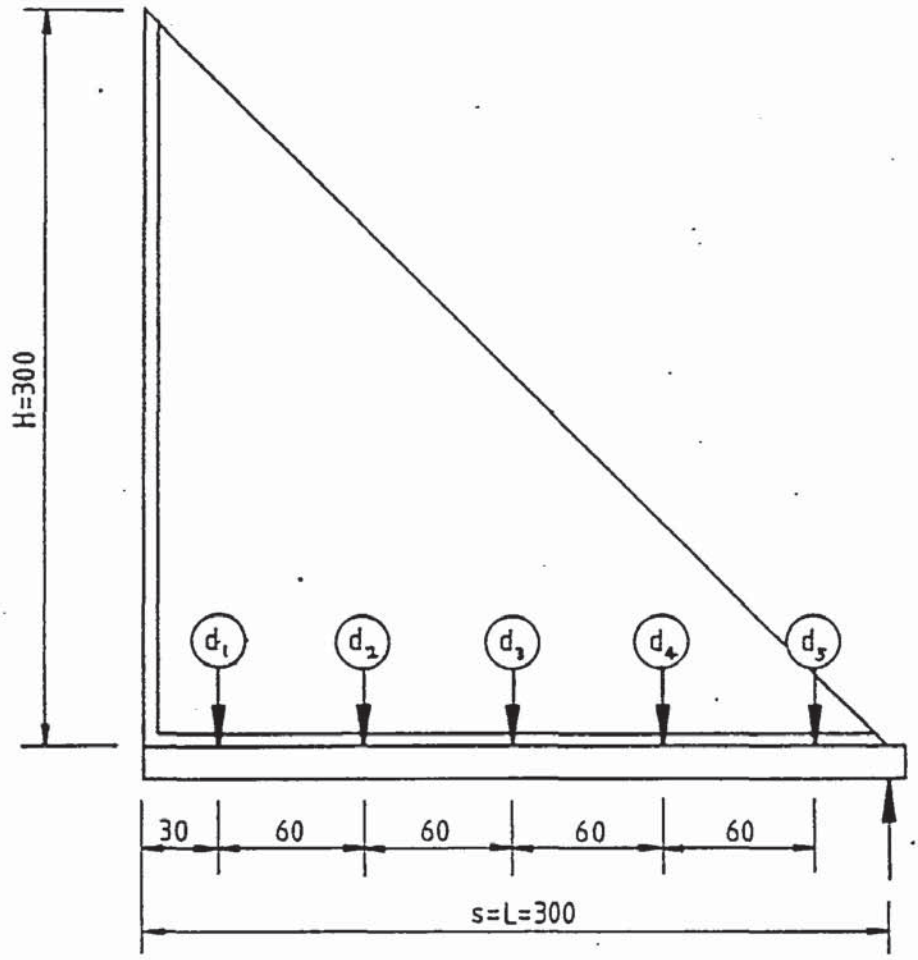

Figure 3.14 Extra dial gauge positions on the loaded plate of specimen S5-300-3.

value of s tested was 300 mm with the load applied at the end of the gusset plate. Other values of s tested were 100, 150, 200 and 250mm. Two more specimens were tested with s=150 and 300mm. Each specimen was made from the same batch of steel as series 3. The general specimen details are shown in Figure 3.13. Extra deflection gauges were put on specimen S5-300-3, as shown in Figure 3.14, to measure the loaded plate deflection profile.

Electrical resistance strain gauges were put on specimens S5-150-1, S5-150-2, S5-75-1, S5-300-1, S5-300-2 and S5-300-3 as shown in Figures 3.15, 3.16, 3.17, 3.18 and 3.19. Strain gauges were fixed along a line from the inside corner perpendicular to the free edge of the gusset plate on both faces of the plate for specimens S5-150-1,

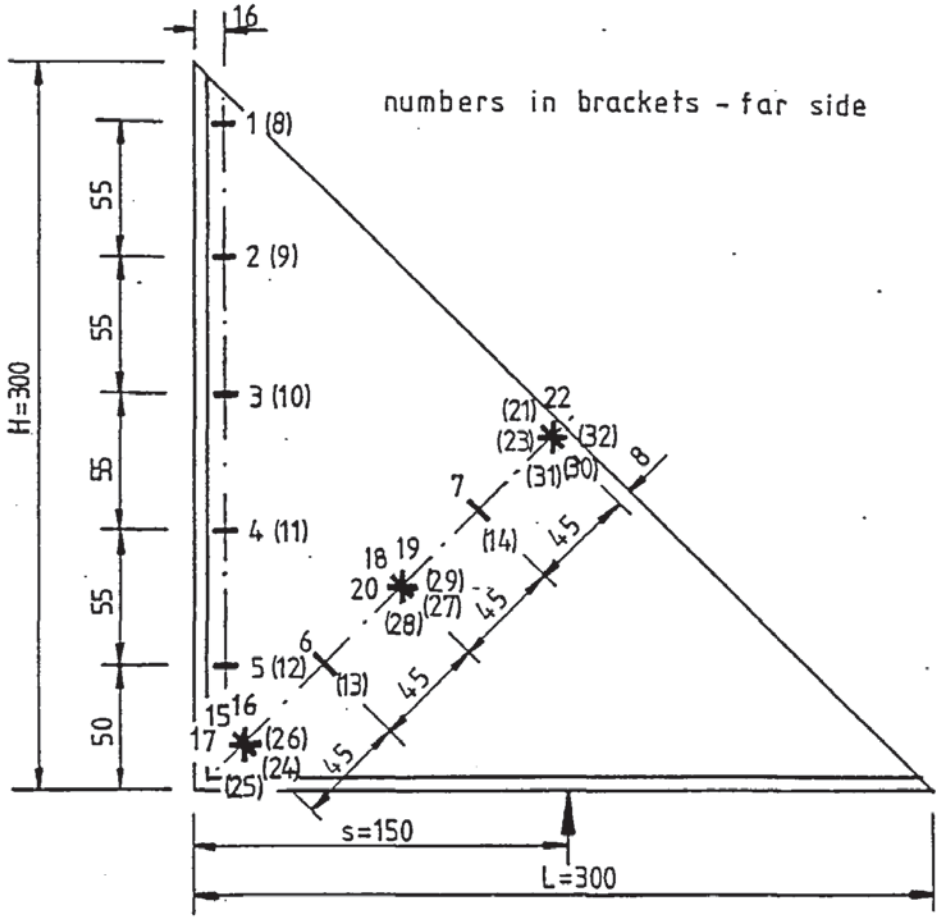

Figure 3.15 Strain gauge locations and numbers for specimen S5-150-1.

S5-150-2, S5-75-1, S5-300-1 and S5-300-2, to measure strains parallel to the free edge. Specimen S5-300-3 had a similar line of strain gauges to measure strains parallel to the free edge. These were offset from the perpendicular bisector, which was a fold line, in an attempt to obtain strain gauge readings as close to the failure load as possible without excessive bending strains. Specimen S5-150-2 had two other lines of gauges parallel to the perpendicular bisector for the same reasons, as shown in Figure 3.16.

Specimens S5-150-1 and S5-150-2 had strain gauges fixed along the supported edge of the gusset plate to measure strains perpendicular to the supported edge of the plate. Strain gauge rosettes were used to measure the magnitude and direction of the principle strains in the gusset plate, mainly along the perpendicular bisector but, also at

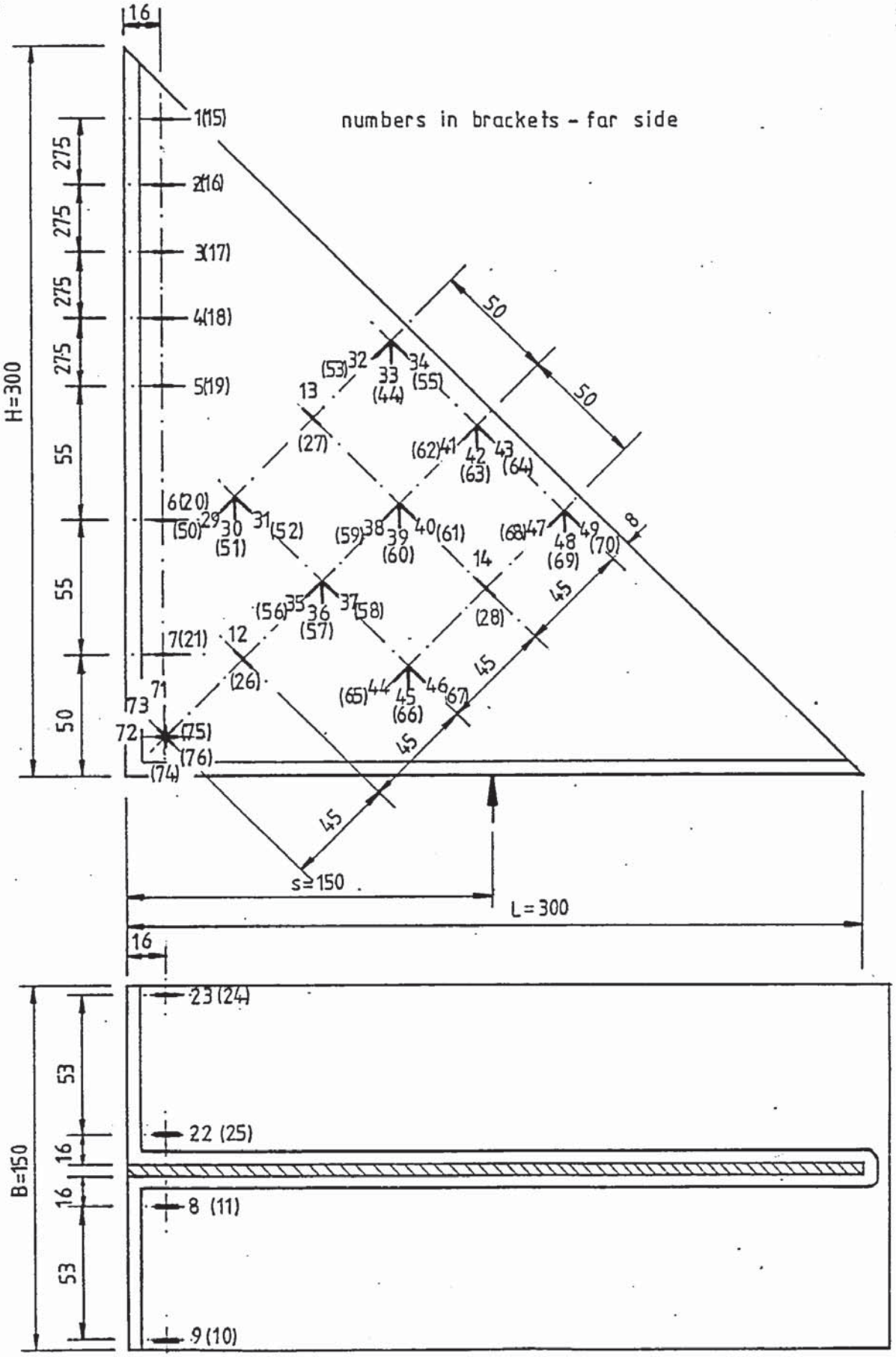

Figure 3.16 Strain gauge locations and numbers for specimen S5-150-2.

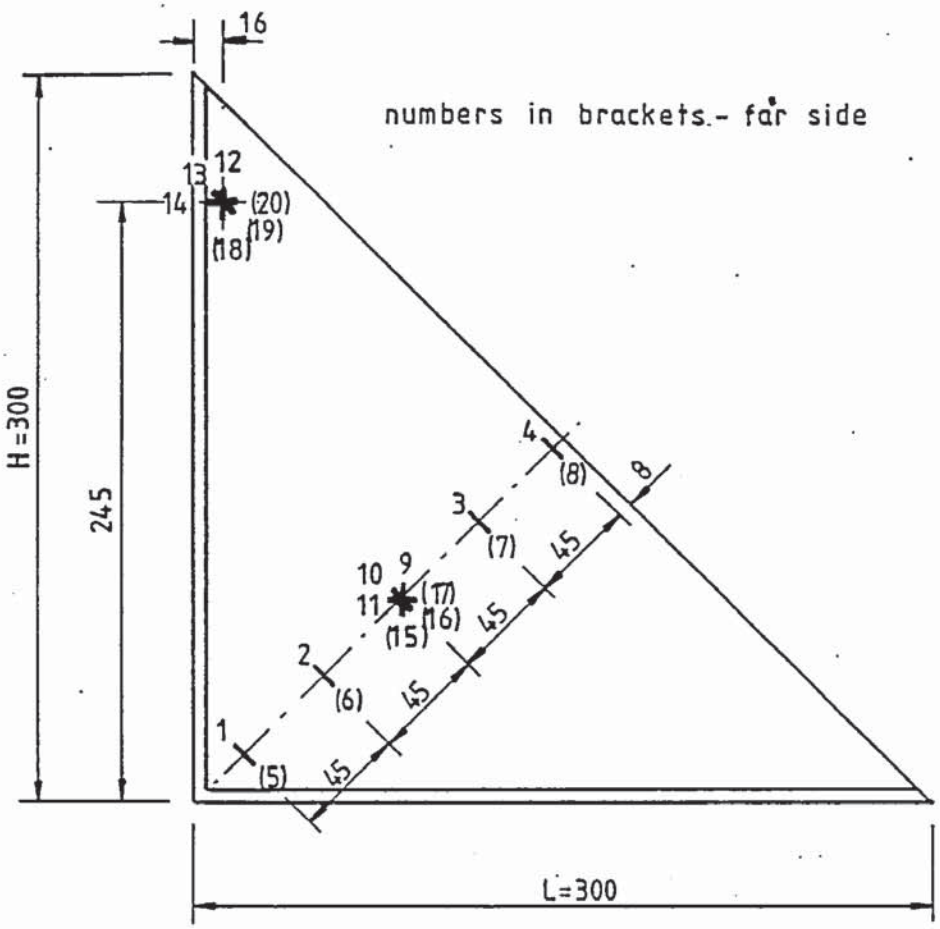

Figure 3.17 Strain gauge locations and numbers for specimens S5-75-1 and S5-300-1.

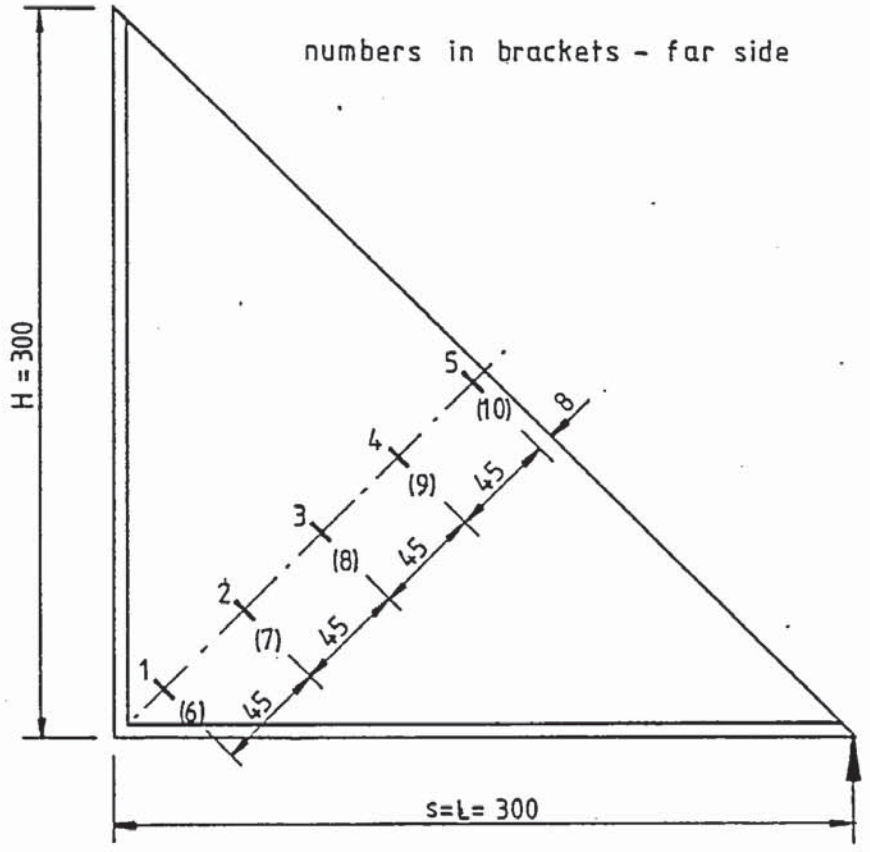

Figure 3.18 Strain gauge locations and numbers for specimen S5-300-2.

other points as indicated in Figures 3.15, 3.16 and 3.17.

Strain gauges were fixed to the loaded plate of specimen S5-150-2 across the inside corner adjacent to the vertical support, to measure the bending strains at this point. Strain gauges were also fixed to the loaded plate of specimen S5-300-3 in an attempt to measure the longitudinal strains in the loaded plate.

Strains were measured at each increment of load until failure of the gusset plate occurred and the readings were converted to average stress.

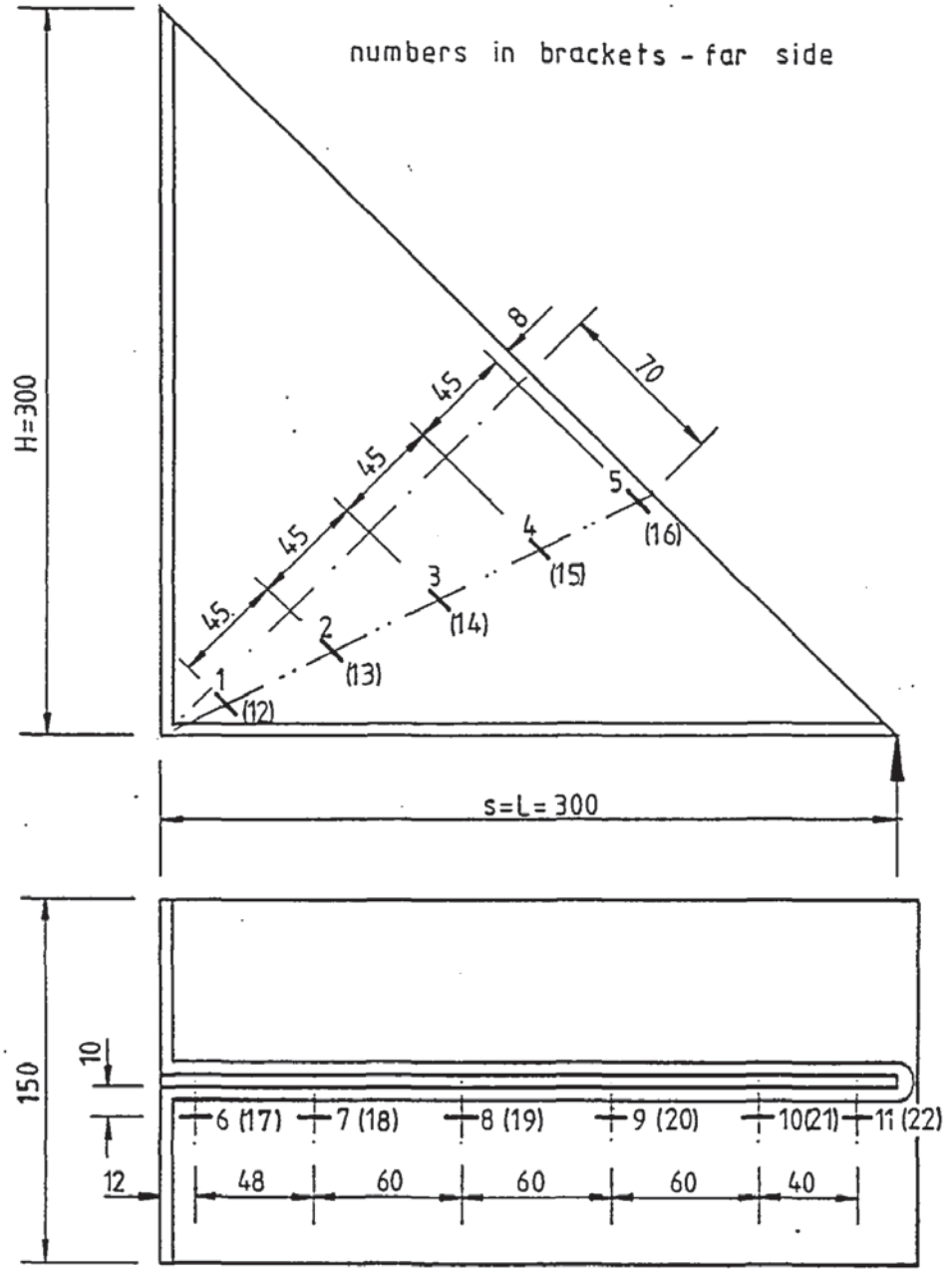

Figure 3.19 Strain gauge locations and numbers for specimen S5-300-3.

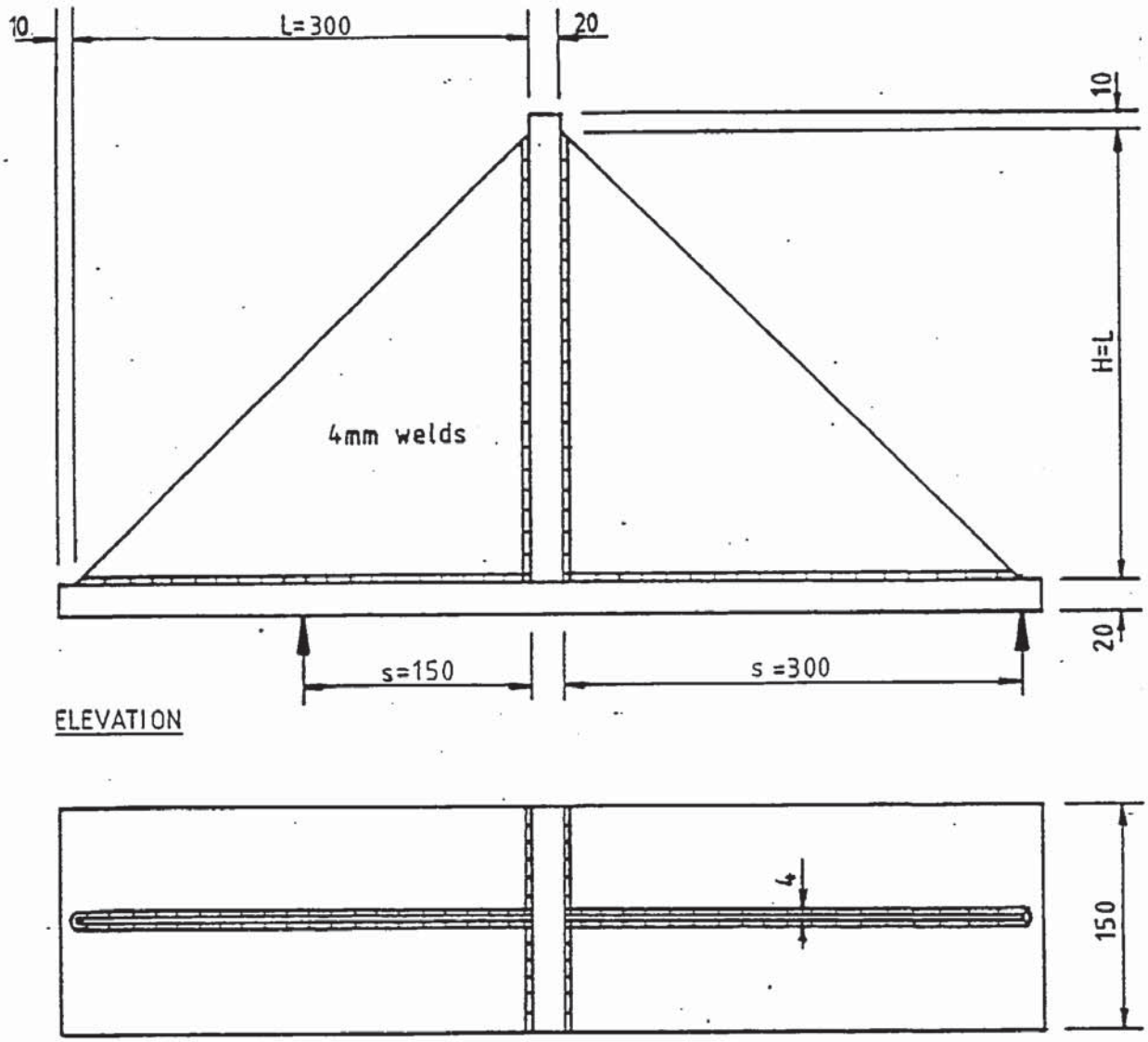

Figure 3.20 General specimen details for series investigating the effect of continuing the loaded plate (series 6).

3.2.7.4 Continuation of the loaded plate (series 6)

This series of tests investigated the effect of continuing the loaded plate through at the bottom of the vertical support. Only two gusset plates were tested for comparison with two tests from series 5, which were identical apart from the loaded plate being continued through at the bottom of the vertical support in this series. The dimensions of the gusset plates were the same as in series 5 with

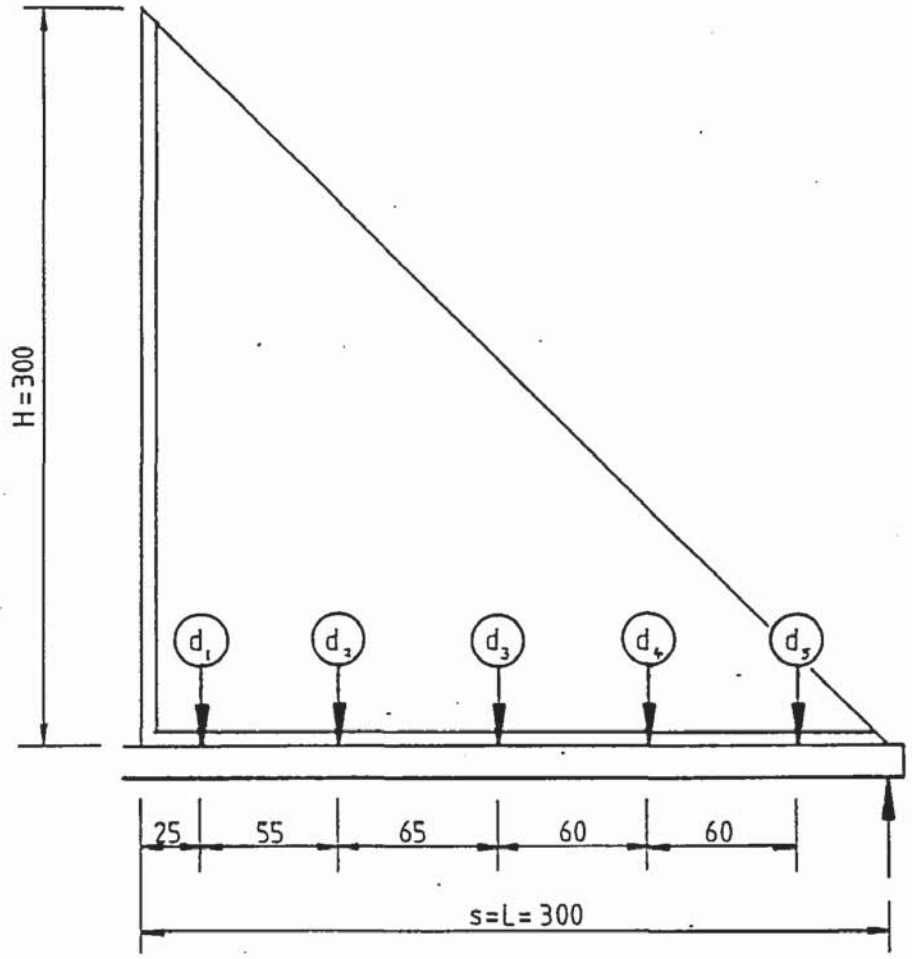

Figure 3.21 Extra dial gauge positions on loaded plate of specimen S6-300-1.

L=H=300mm and the values of s tested were 150 and 300mm. The test specimen was made from the same batch of steel as series 3. The general specimen details are shown in Figure 3.20. Extra deflection gauges were put on specimen S6-300-1 to measure the loaded plate deflection profile as shown in Figure 3.21.

Electrical resistance strain gauges were put on both specimens S6-150-1 and S6-300-1 as shown in Figure 3.22. Strain gauges were fixed along a line from the inside corner perpendicular to the free edge of the gusset plate on both faces of the plate to measure strains parallel to the free edge as in series 5. Strain gauges were fixed to the loaded plates to measure the longitudinal strain at various points along the loaded plate.

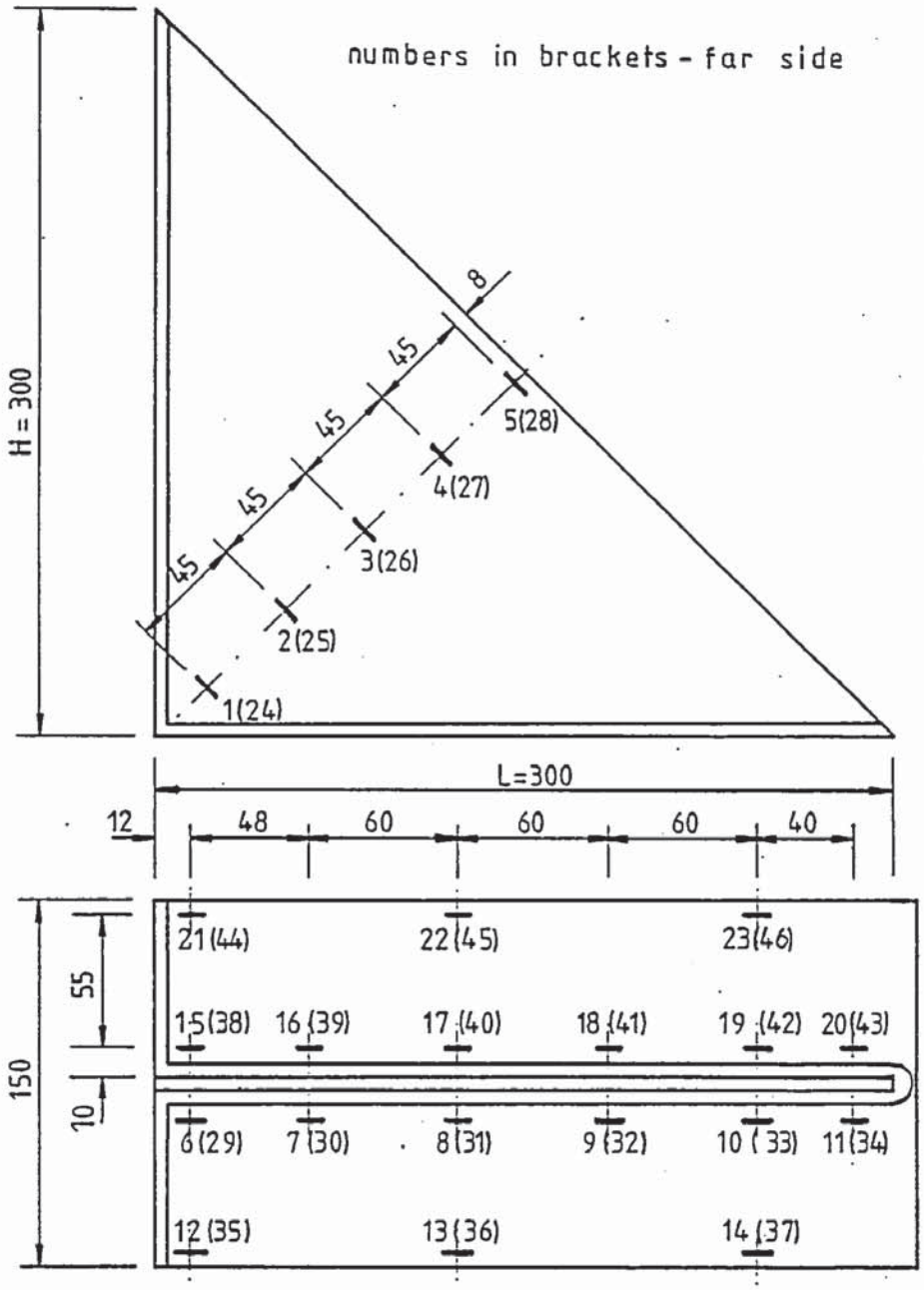

Figure 3.22 Strain gauge locations and numbers for specimen S6-150-1.

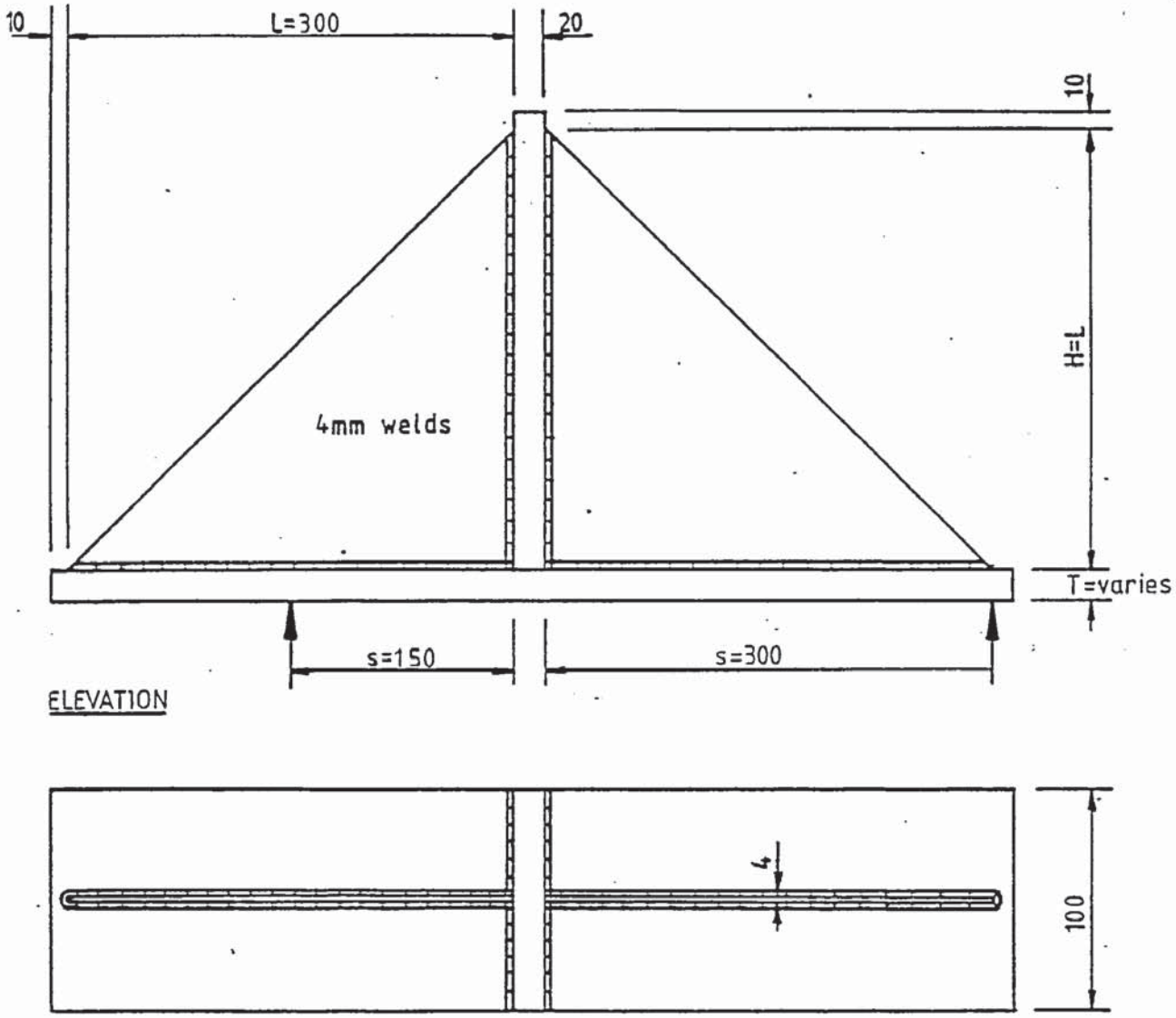

values of T = 6, 10, 13, 16 & 20

Figure 3.23 General specimen details for series investigating the loaded plate thickness T (series 7).

3.2.7.5 Loaded plate thickness T (series 7)

This series of tests investigated the effect of varying the thickness T of the loaded plate over its whole length, the loaded plate being continued through at the bottom of the vertical support. The dimensions of the gusset plates were the same as in series 6. The objective was to test as thin a loaded plate as practical to see if local buckling of the gusset plate would occur at the load point. The

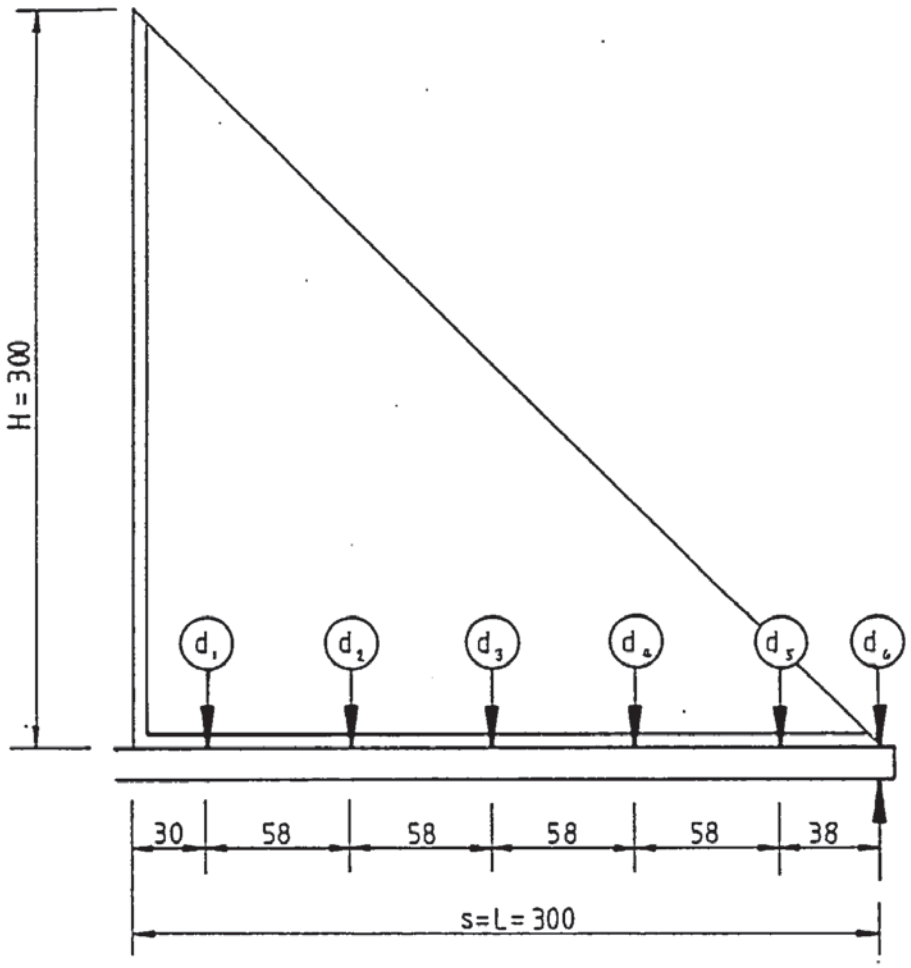

Figure 3.24 Extra dial gauge positions on loaded plate of specimen S7-6-300-1.

loaded plates were all made form the same 20mm x 100mm mild steel section and machined down to thicknesses of 16, 13, 10 and 6mm respectively, before being welded to the gusset plates. Practical limitations were found due to distortions associated with the welding. The distortions increased, the thinner the loaded plate and the larger the weld size. Using 4mm fillet welds the minimum thickness of loaded plate that could be used with an acceptable amount of distortion was 10mm. Using the smallest practical weld of 2mm it was possible to test a specimen with a loaded plate of 6mm thick. All the fillet welds for the 6mm thick loaded plate specimen were 2mm. One side of

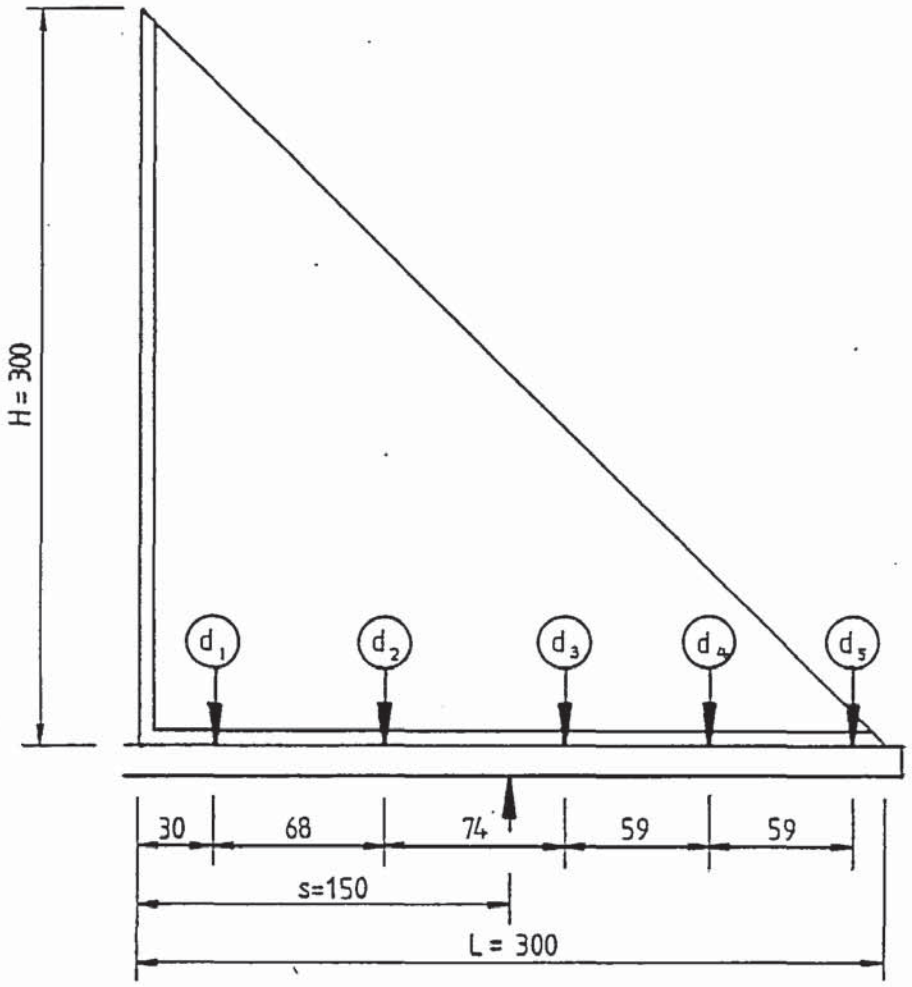

Figure 3.25 Extra dial gauge positions on loaded plate of specimen S7-10-150-1.

each specimen was tested with s=150mm(s=L/2) and the second side of each specimen was tested with s=300mm(s=L). The gusset plates were made from the same batch of steel as series 3. The central vertical support was made from the same 20x100mm mild steel section as the loaded plates.

The general specimen details are shown in Figure 3.23. Extra dial gauges were put on specimens S7-6-300-1, S7-10-150-1 and S7-13-300-1 to measure the loaded plate deflection profile as shown in Figures 3.24, 3.25 and 3.26.

Electrical resistance strain gauges were put on plates

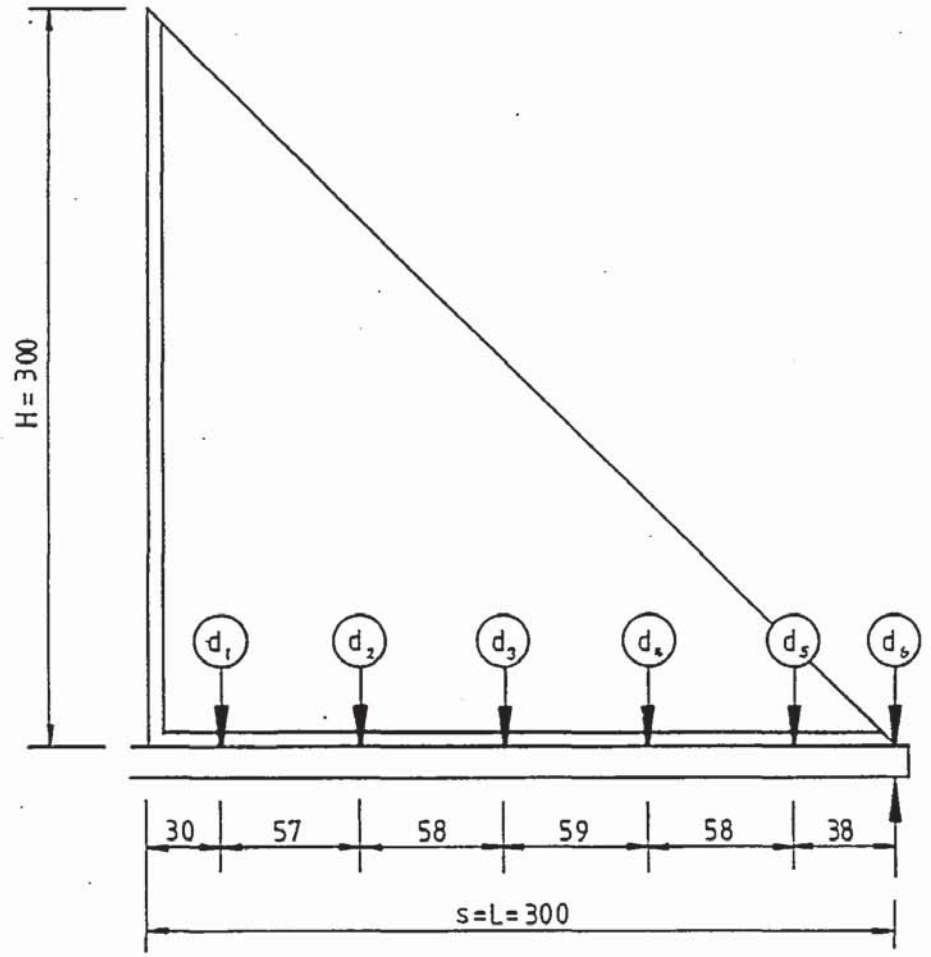

Figure 3.26 Extra dial gauge positions on loaded plate of specimen S7-13-300-1.

S7-10-150-1, S7-6-150-1, S7-13-150-1 and S7-16-150-1 as shown in Figures 3.27 and 3.28. Strain gauges were put on specimen S7-10-150-1 along the offset from the perpendicular bisector of the gusset plate to measure strains parallel to the free edge. Strain gauges were also put on the gusset plate of this specimen to measure the longitudinal strains in the loaded plate at the inside corner of the loaded plate adjacent to the vertical support and along the length of the loaded plate. With the other specimens, strain gauges were only put on the loaded plate adjacent to the vertical support, to measure the bending strains at this point.

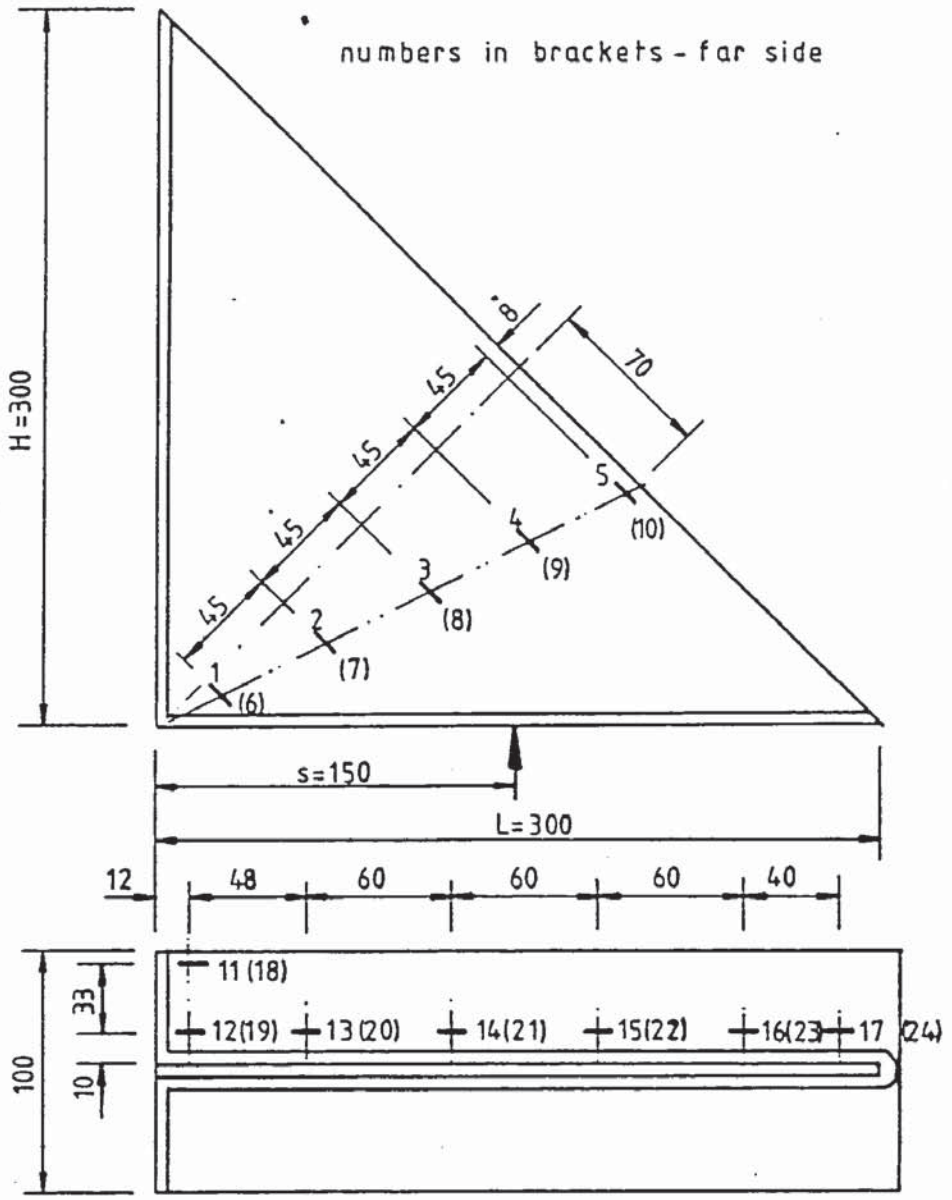

Figure 3.27 Strain gauge locations and numbers for specimen S7-10-150-1.

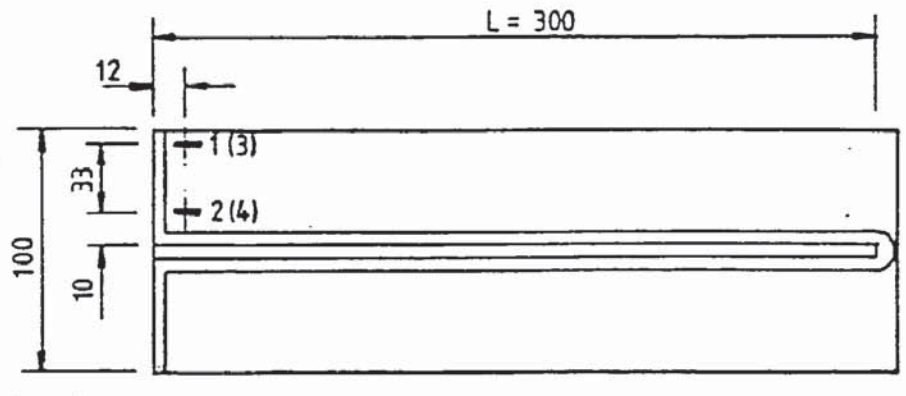

Figure 3.28 Strain gauge locations and numbers for specimens S7-6-150-1, S7-13-150-1 and S7-16-150-1.

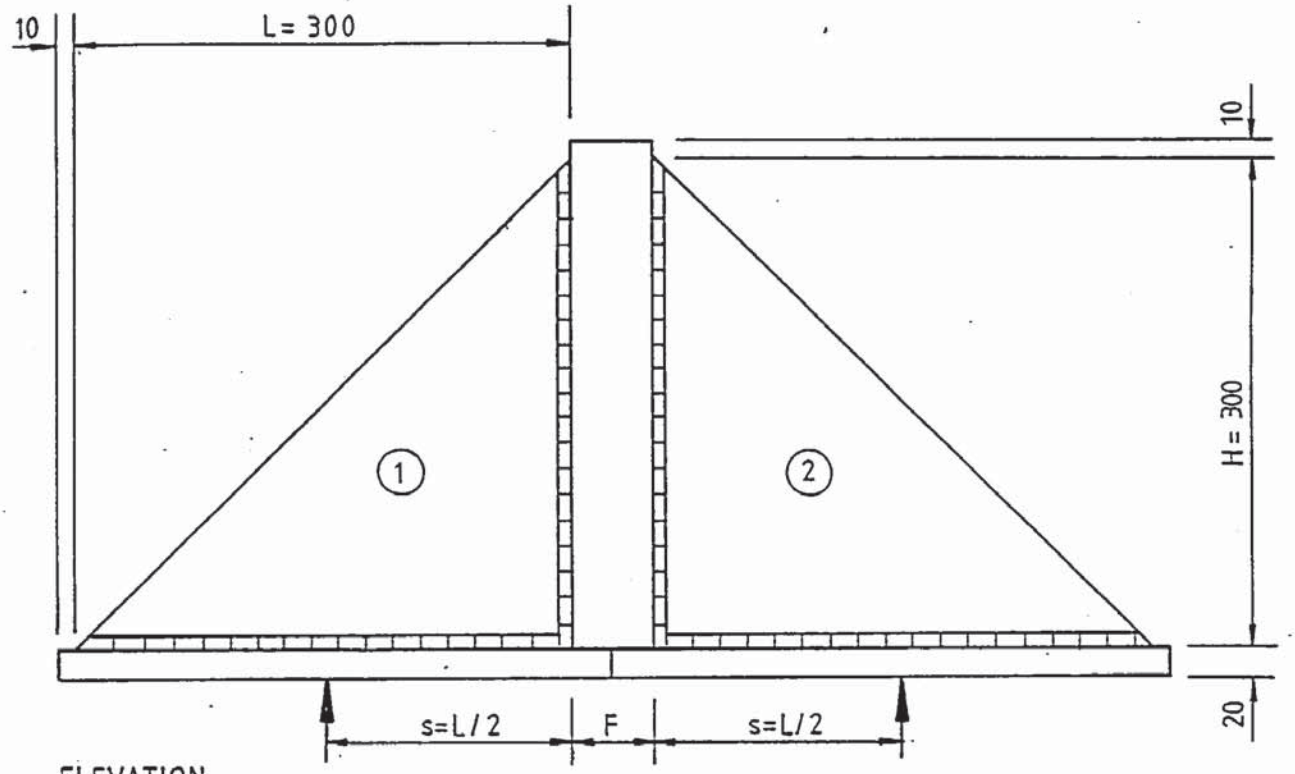

specimen	weld size mm	F mm	plate thickness t	
			side 1	side 2
1	8	50	15	13
2	6	50	11	9
3	4	20	7	5

Figure 3.29 General specimen details for series investigating the gusset plate thickness t (series 12).

3.2.7.6 Gusset plate thickness t (series 12)

This series of tests investigated the effect of varying the thickness t of the gusset plate. The values of L and H were fixed at 300mm with s=L/2=150mm. All gusset plates were machined down on one face, before welding, from the same 15mm thick mild steel plate with a yield strength of 263N/mm^2 to avoid using plates of varying yield strength. The values of t tested were 5, 7, 9, 11, 13 and 15mm with one plate of each size tested, with two adjacent sizes back to back, i.e. the 5 and 7mm plates. The loaded plates projected under the vertical support and terminated there. A fillet weld along the top edge of the loaded plate provided a lateral connection to the vertical support. The central vertical supports were made from mild steel section. The section sizes were chosen to prevent the crushing of the

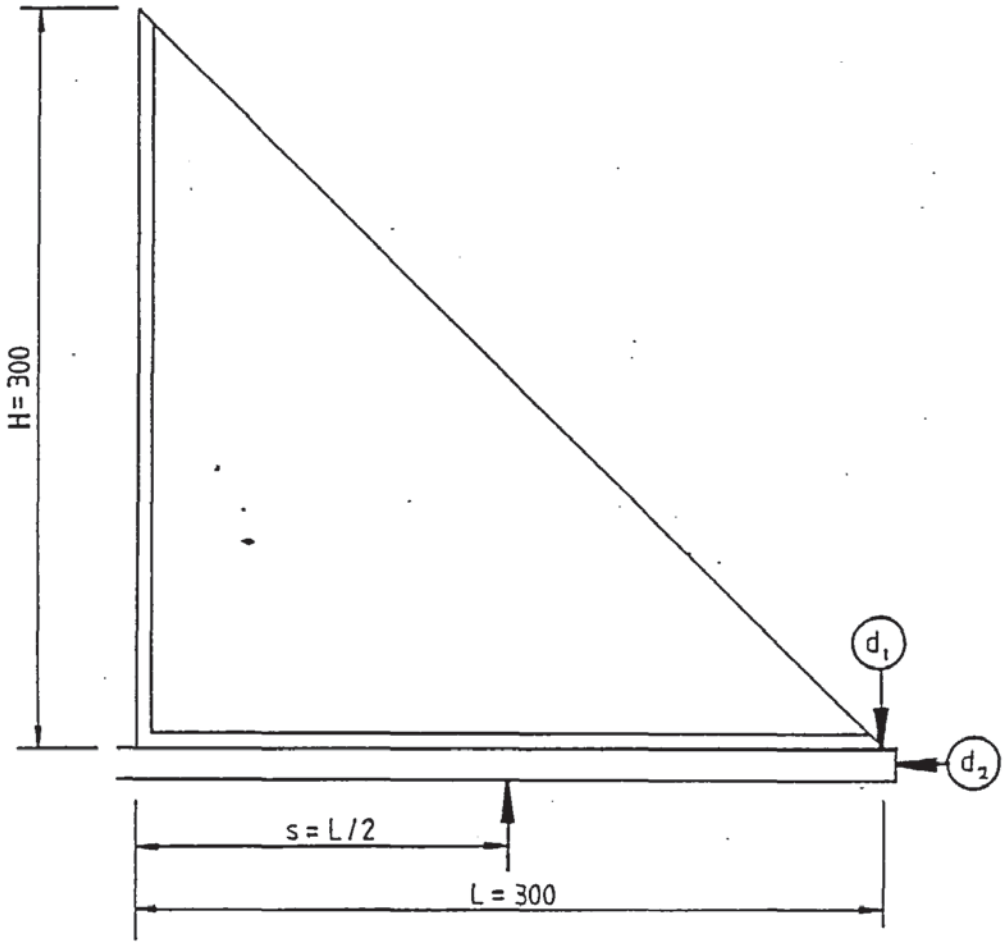

Figure 3.30 Extra dial gauge positions on specimen S12-5-1 to S12-15-1.

top of the support. All weld sizes of a specimen were the same and the weld sizes used for each specimen, together with the general specimen details, are shown in Figure 3.29. Two extra deflection guages were used as shown in Figure 3.30.

Two extra gusset plates were tested which were identical to the 13 and 15mm thick gusset plates except for the loaded plates, which were continued through at the bottom of the vertical support.

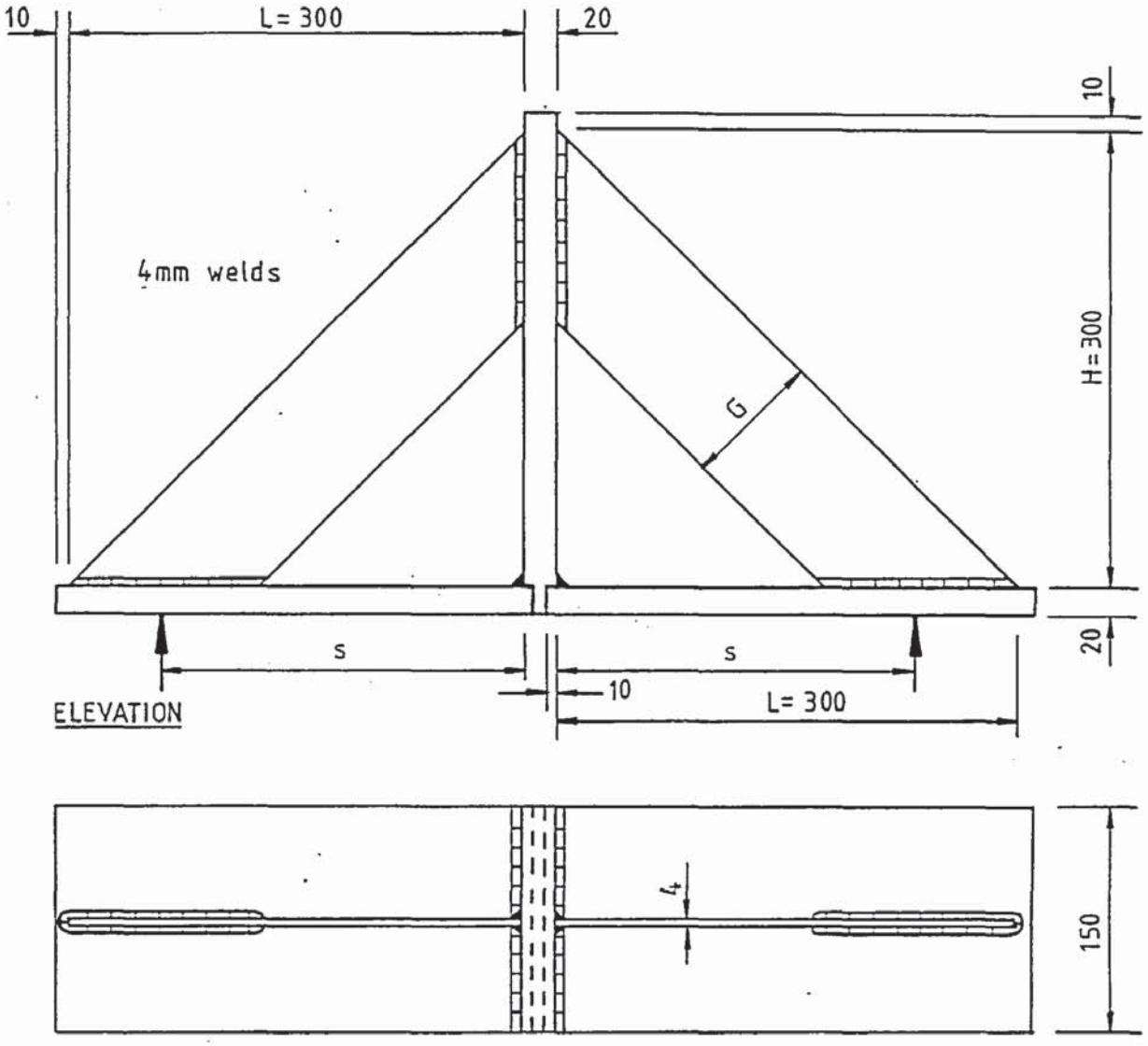

Figure 3.31 General specimen details for series investigating the removal of the inside corner of the gusset plate (series 8).

3.2.7.7 Removal of the inside corner of the gusset plate (series 8)

This series of tests investigated the effect of varying the amount of the inside corner removed from a gusset plate. As with previous tests the values of L and H were fixed at 300mm. The inside corner of each gusset plate was removed parallel to the free edge of the plate leaving a strip of plate of width G. The values of G tested were 45, 90, 135 and 180, with two plates of each. One gusset plate was tested with the load applied at the mid point of the loaded edge, s = L/2, as with previous tests, the other with the load applied at the centre of the remaining loaded edge of the gusset plate. Each specimen was made from the same batch of steel as series 3. The loaded plates projected under the vertical support and terminated there. The general specimen details are shown in Figure 3.31. Extra deflection gauges were put on specimens S8-45-2, S8-135-2 and S8-180-2 as shown in Figure 3.32.

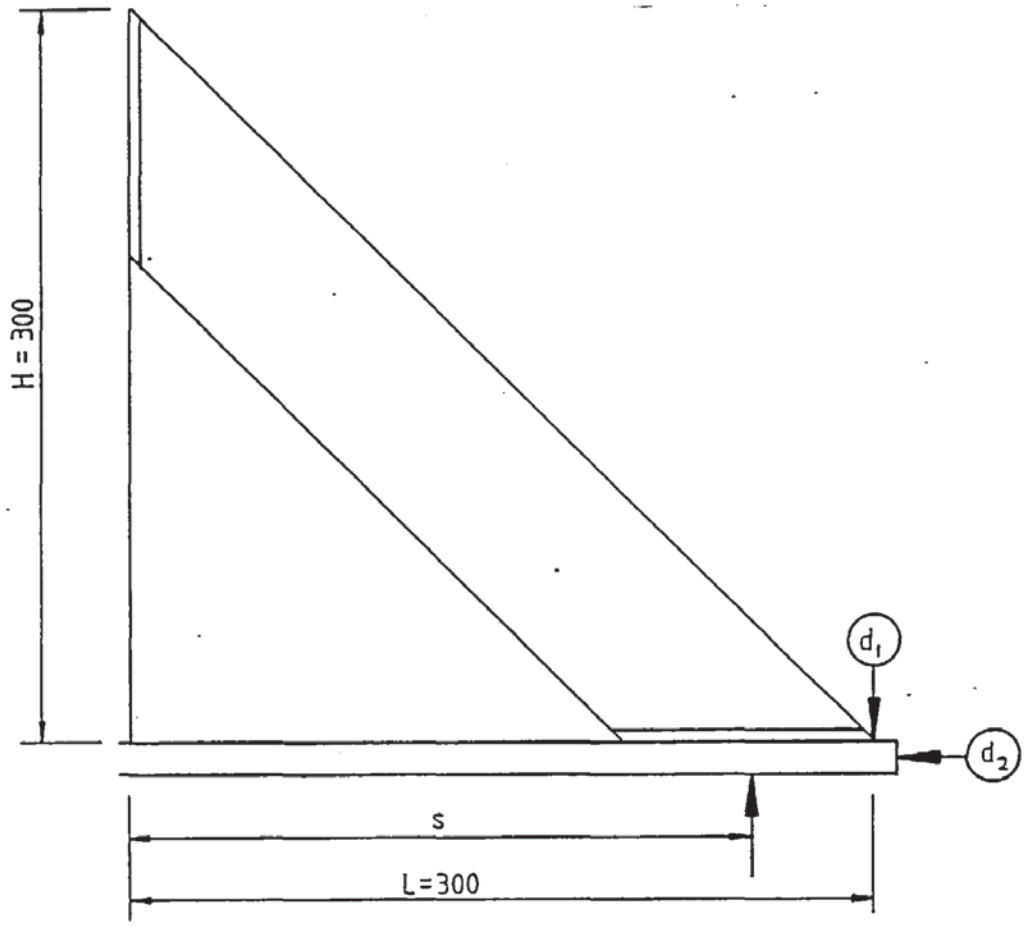

Figure 3.32 Extra dial gauge positions on specimens S8-45-2, S8-90-2, S8-135-2 and S8-180-2.

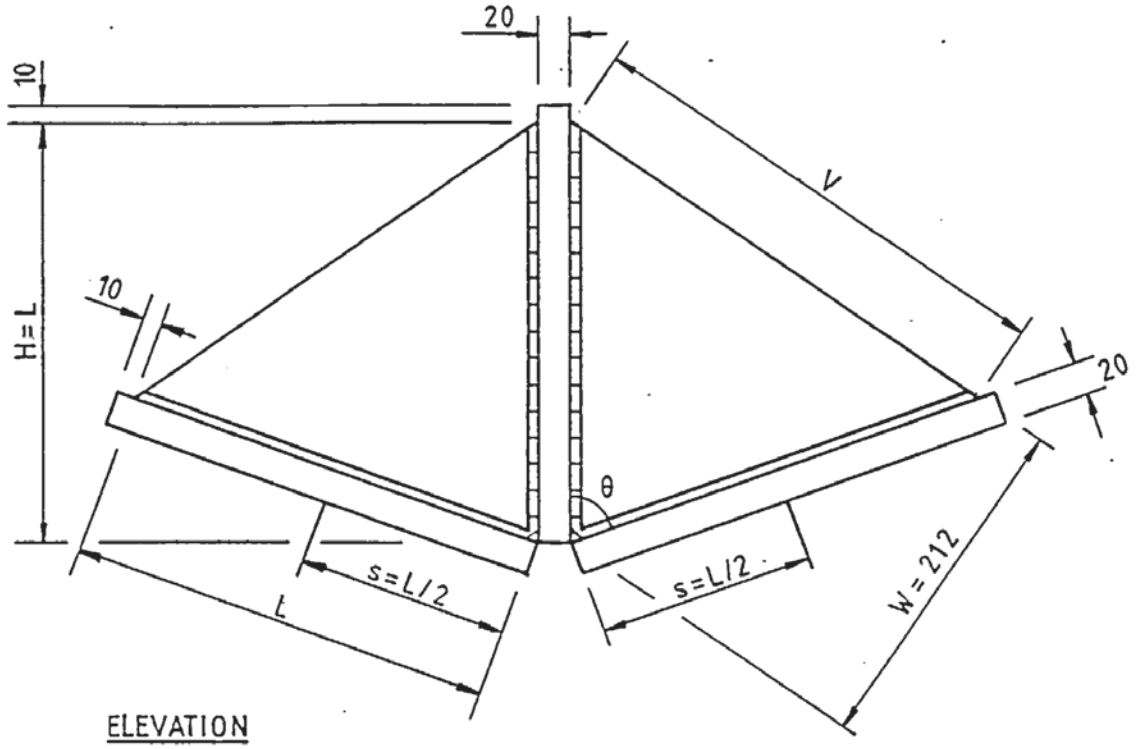

ELEVATION

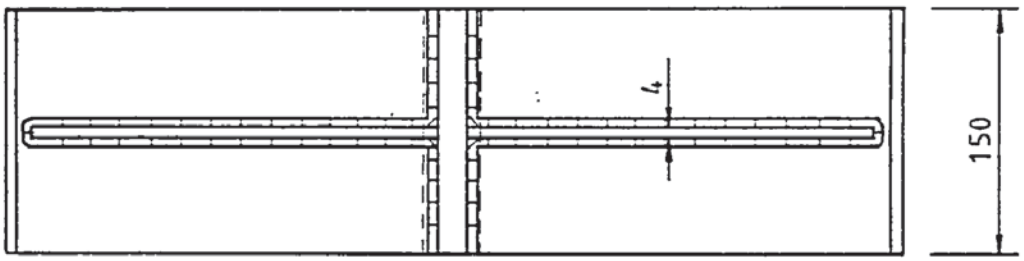

PLAN

specimen	θ°	L	V
1	30	220	114
2	50	234	198
3	70	259	297
4	90	300	424
5	110	370	606
6	130	502	909
7	140	620	1165

Figure 3.33 General specimen details for series investigating the variation of the internal angle (series 13).

3.2.7.8 Variation of the internal angle between the loaded and supported edges (series 13)

This series of tests investigated the effect of varying the internal angle between the loaded and supported edges. For comparison with previous tests the 90° specimen was made with L=H=300mm and s=L/2=150mm. So that a wide range of angles could be tested, the perpendicular from the free edge to the internal angle was fixed at 212mm, which is its dimension on the 90° specimen. Fixing L=H would have reduced the practical range of angles that could be tested. The maximum practical angle tested was 140°, the minimum considered necessary was 30°, with intermediate angles of 50, 70, 90, 110 and 130°. Two plates of each angle were tested. Other parameters and testing conditions were kept as close as possible to those of the

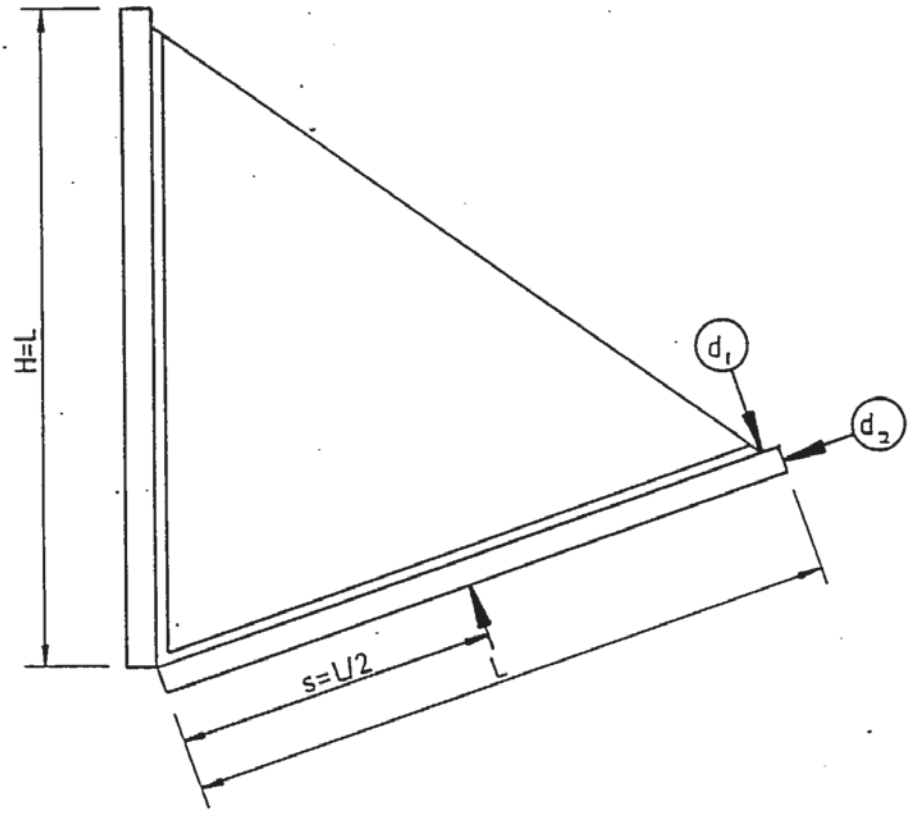

Figure 3.34 Extra dial gauge positions on specimens S13-30-1, S13-30-2, S13-50-1, S13-50-2, S13-70-1, S13-70-2, S13-90-1 and S13-90-2.

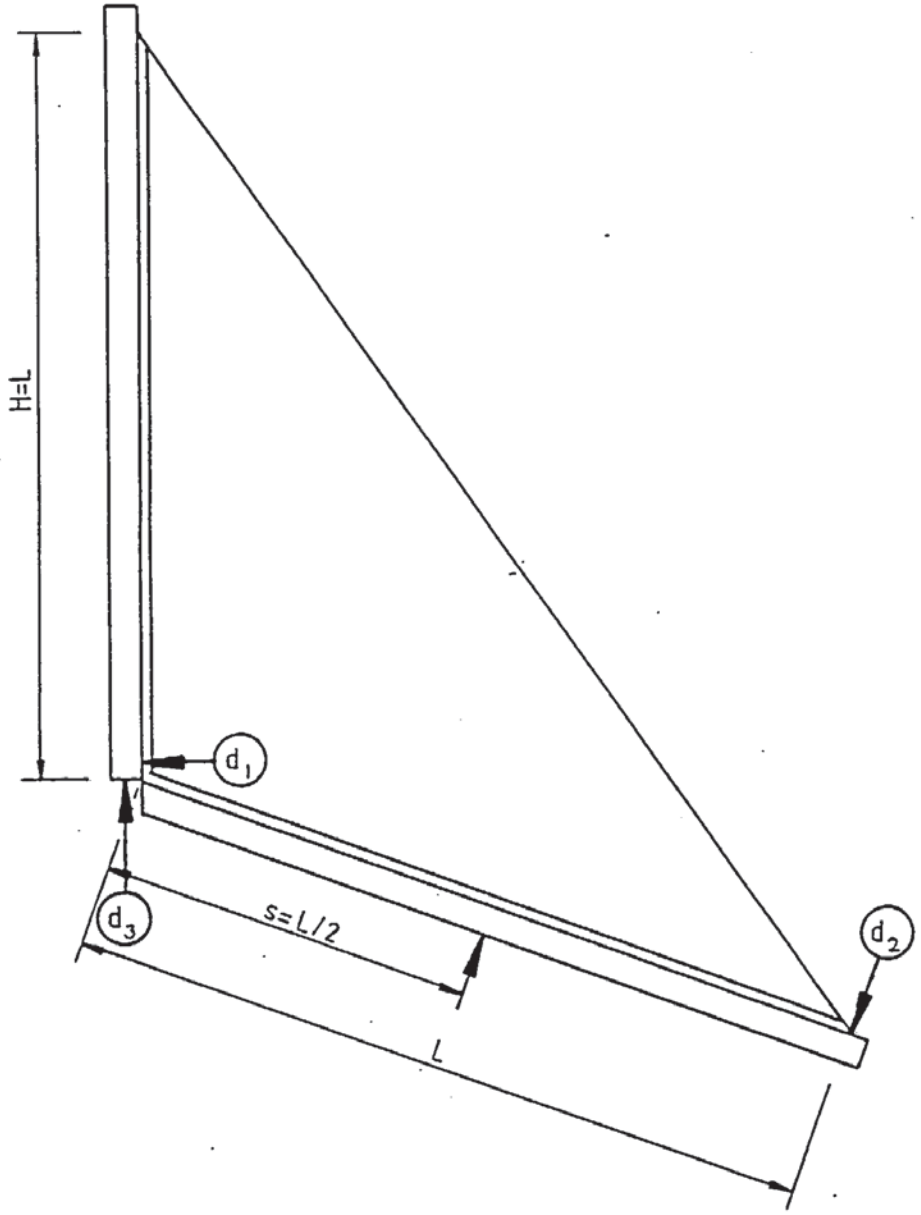

Figure 3.35 Extra dial gauge positions on specimens S13-110-1, S13-11-2, S13-130-1, S13-130-2, S13-140-1 and S13-140-2.

other test series. The load was applied perpendicular to the loaded edge, as with the other series, at a distance s = L/2 by means of a rig. The rig and testing arrangements used for this series are described in Section 3.2.2.

The gusset plates were made from the same batch of steel plate 4mm thick with a yield strength of 245 N/mm^2. The general specimen details are shown in Figure 3.33. Extra deflection gauges were put on

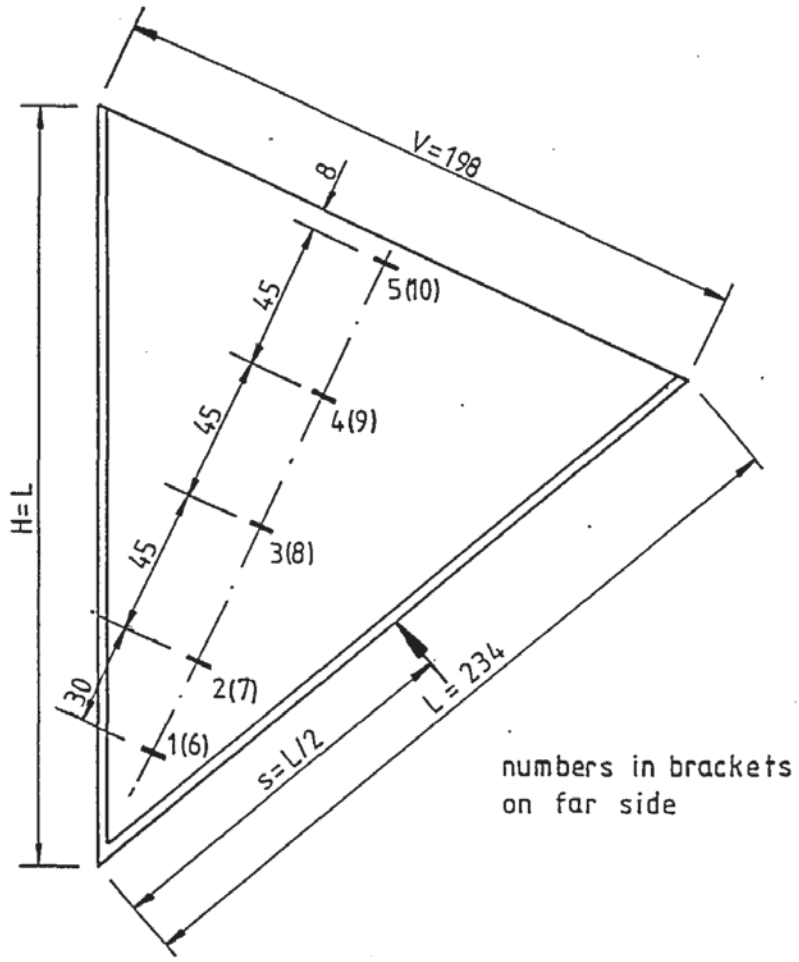

Figure 3.36 Strain gauge locations and numbers for specimen S13-50-1.

all specimens and the gauge positions referred to are as in Figure 3.34 and 3.35.

Electrical resistance strain gauges were put on specimens S13-50-1, S13-70-1, S13-110-1 and S13-130-1 as shown in Figures 3.36, 3.37, 3.38 and 3.39 respectively. Strain gauges were fixed along a line from the inside corner perpendicular to the free edge of the gusset plate, on both sides of the plate, to measure strains parallel to the free edge of these specimens. Specimens S13-70-1, S13-110-1 and S13-130-1 had gauges fixed along the free edge of the gusset plate, to measure strains along the free edge and parallel to it.

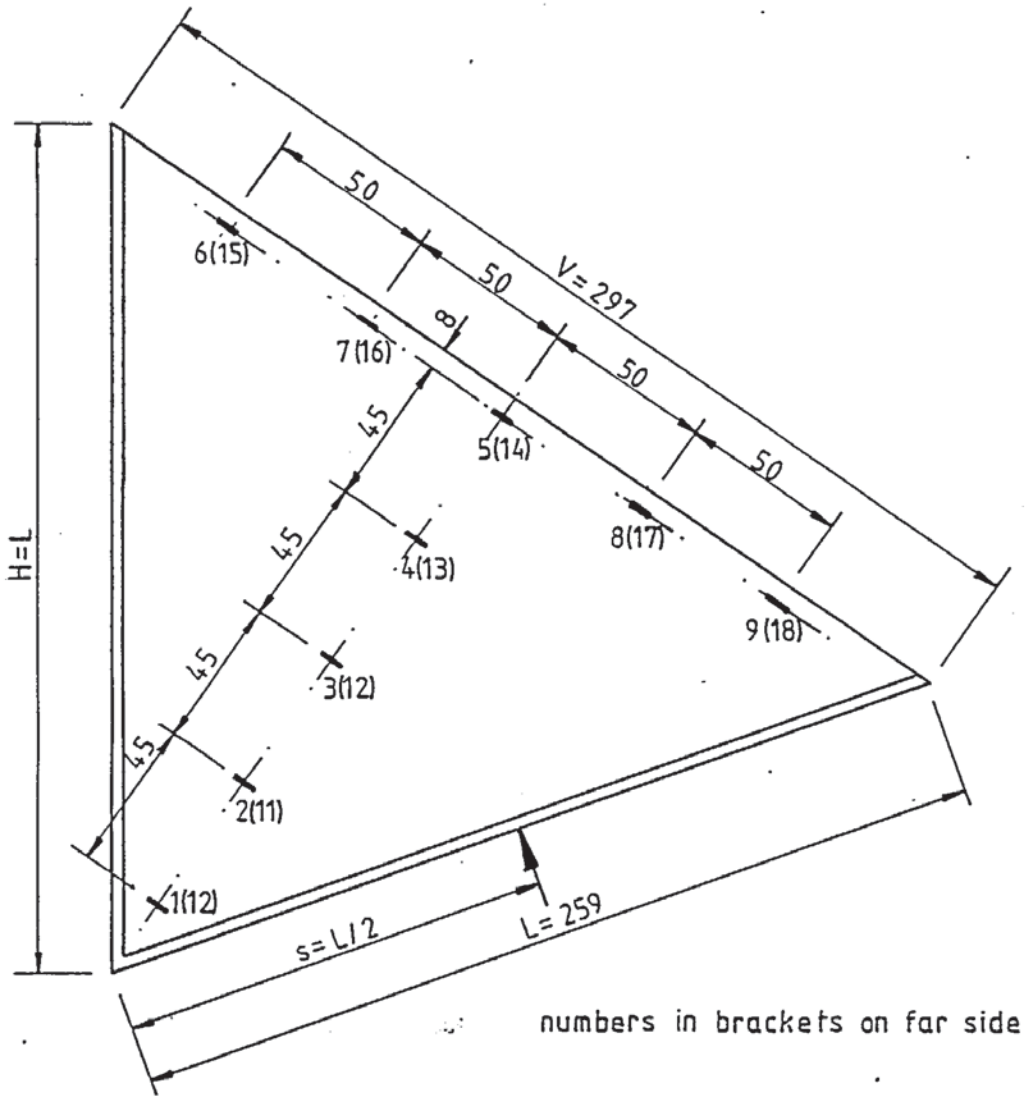

Figure 3.37 Strain gauge locations and numbers for specimen S13-70-1.

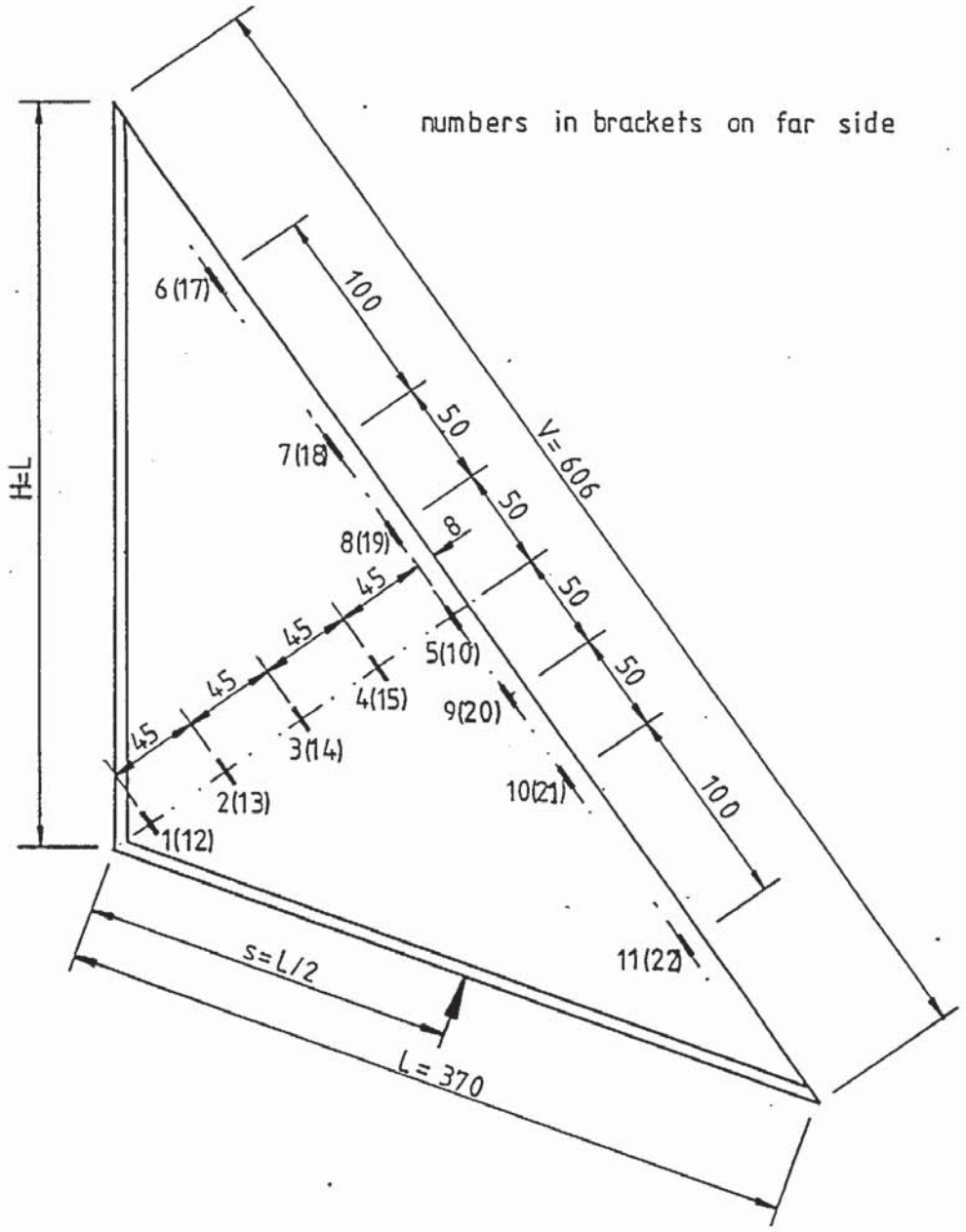

Figure 3.38 Strain gauge locations and numbers for specimen S13-110-1.

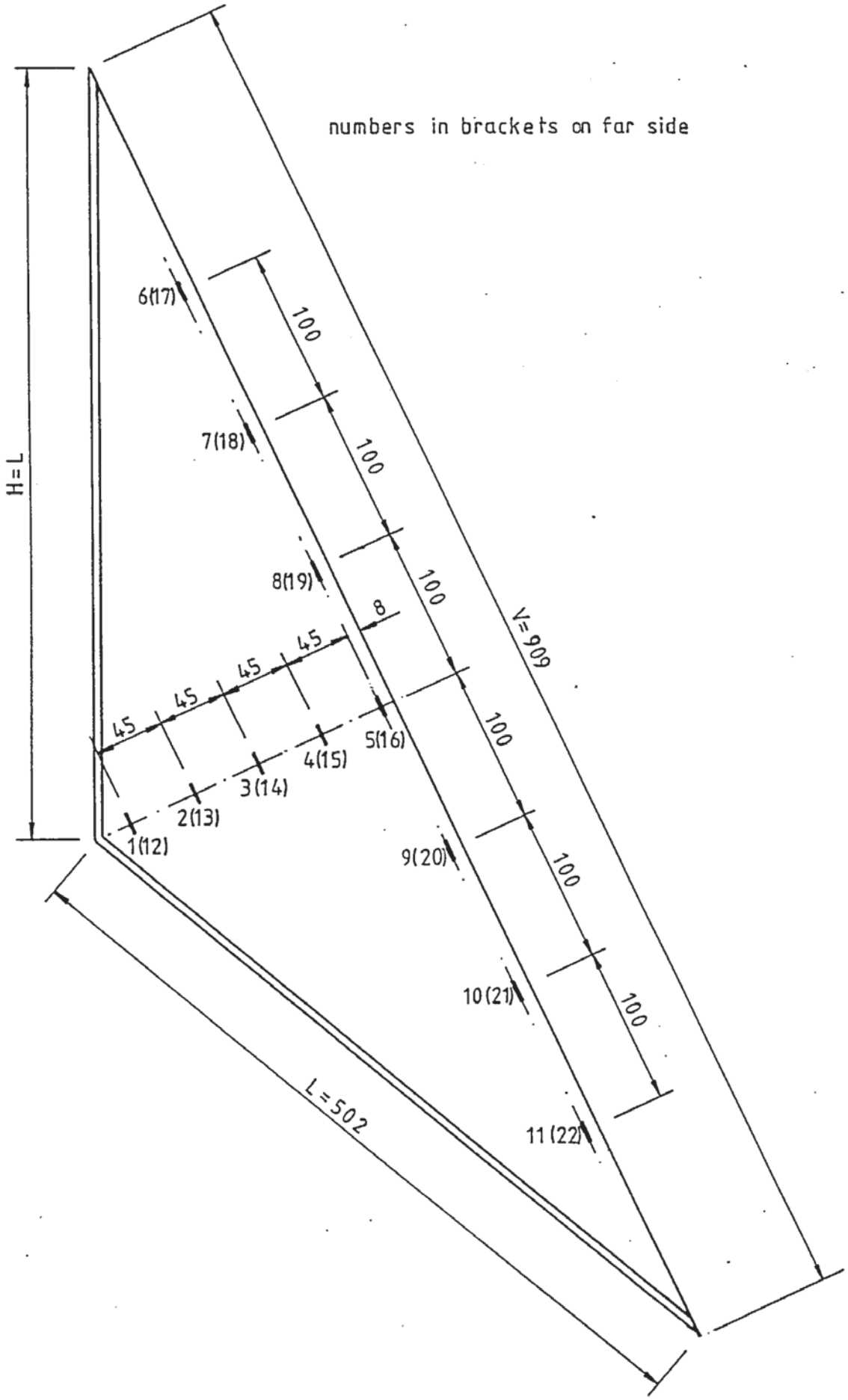

Figure 3.39 Strain gauge locations and numbers for specimen S13-130-1.

3.3 Subsidiary tests

The mode of failure of the gusset plates in the aforementioned tests suggested that the plates react in a similar way to a series of fixed ended struts running parallel to the free edge, as suggested by Martin (15), each strut taking a certain amount of the load applied to the gusset plate by the loaded plate. The maximum load taken by each strut would then be dependent upon its slenderness ratio and yield stress. It was therefore considered necessary to investigate the failure load of strips of the plate in the form of struts, both directly loaded and indirectly loaded as in the assumed gusset plate. The effect of cutting the gusset plate into strips and other special gusset plates were investigated as presented in the following section. Only those details departed from the general testing arrangement are covered.

3.3.1 Pin ended directly loaded strut tests (series 1)

This series of tests were designed to obtain the buckling stresses for the 4mm thick plate, by testing a series of directly axially loaded pin ended struts 25mm wide and 4mm thick. The lengths of the struts tested were 100, 200, 300 and 500mm. The ends of the struts were rounded off to 2mm radius to reduce the end fixity to a minimum. The struts were axially loaded between two platens of a Denison testing machine until failure. The tensile yield strength of the plate used was obtained from tensile tests and was found to be $349 N/mm^2$.

3.3.2 Fixed ended directly loaded strut tests (series 9)

This series of tests was designed to obtain the buckling stresses for a series of directly axially loaded fixed ended struts 25mm wide and 4mm thick made from 4mm steel plate with a tensile yield stress of $350 N/mm^2$.

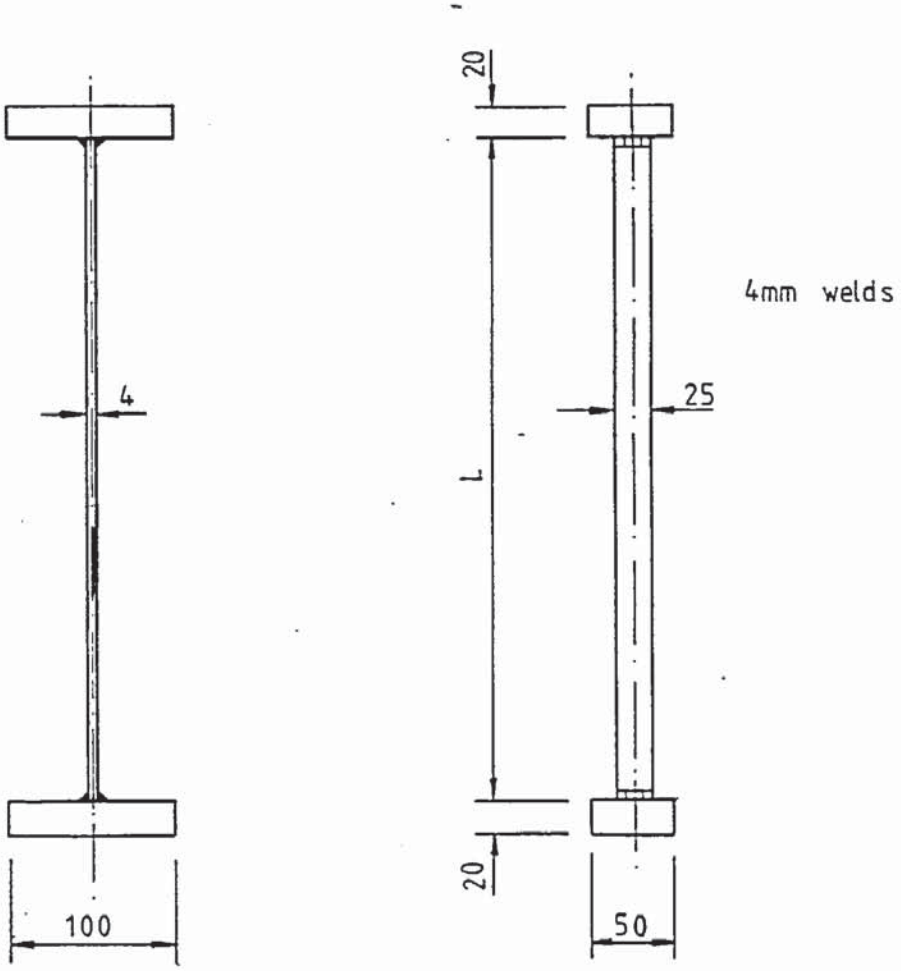

Figure 3.40 Specimen details for fixed ended directly loaded strut tests (series 9).

Blocks of steel 100x50x20mm thick were welded to each end of the struts using 4mm fillet welds to provide the end fixity. This allowed accurate placing of the struts between the platens of the testing machine so that the load was applied axially and without inducing any bending moments. This was achieved by the introduction of shims between the machine platens and the end blocks of the struts. The lengths of struts tested were 399, 348, 296.5, 246, 195, 144 and 93mm with three specimens of each tested. The lengths were chosen for comparison with the next series of tests. The general specimen details are shown in Figure 3.40. For the second and third set of each strut length tested the total axial compression of the specimen and the mid-lateral deflection of the strut were measured.

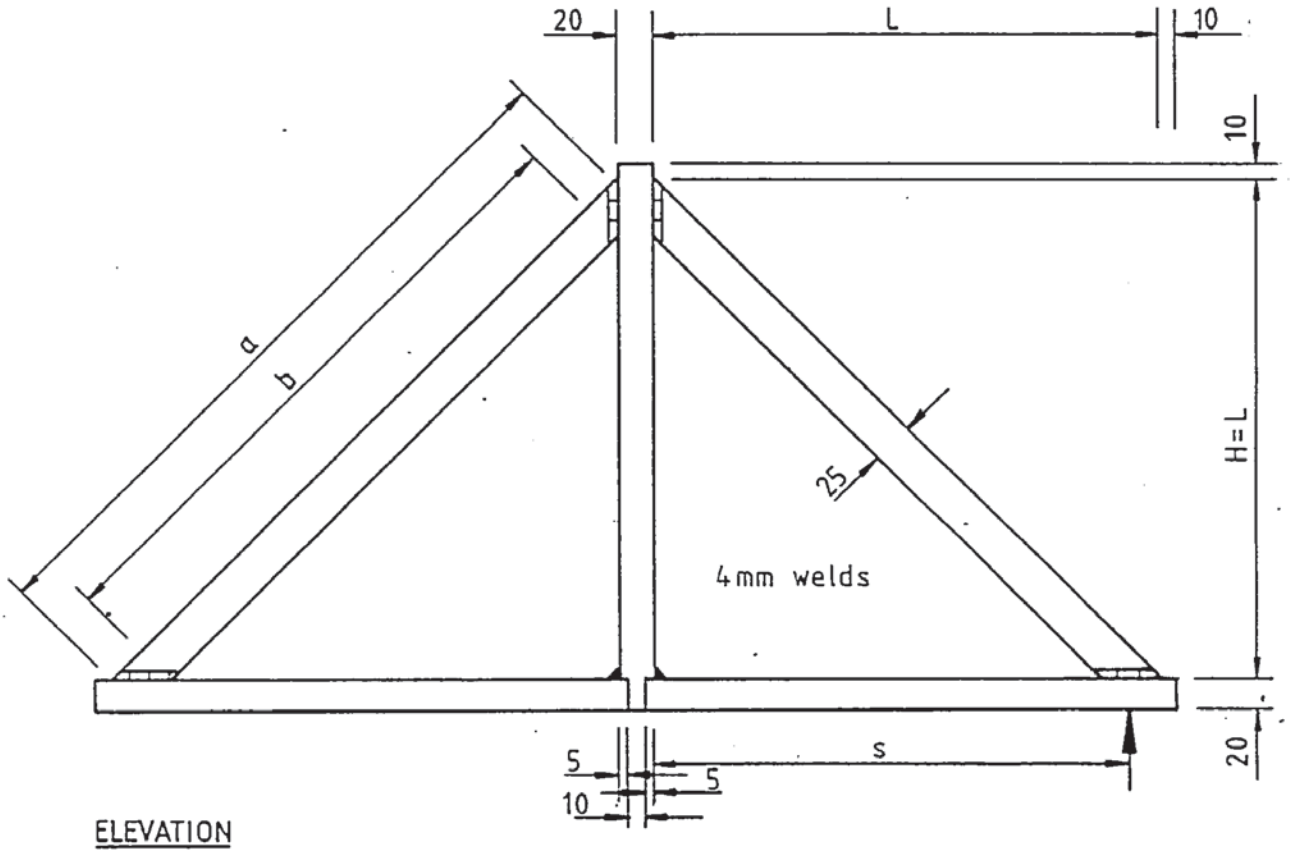

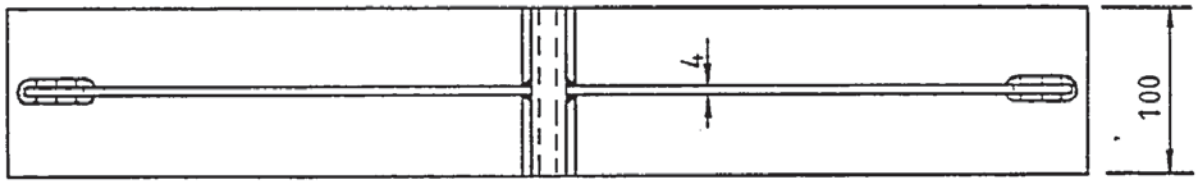

specimen	a	b	L	s
1	424	374	300	282
2	373	323	264	246
3	321	272	227	210
4	271	221	192	174
5	220	170	155·5	138
6	169	119	119·5	102
7	118	68	83·5	66

Figure 3.41 Specimen details for inclined fixed ended indirectly loaded strut tests (series 10).

3.3.3 Inclined indirectly loaded fixed ended strut tests (series 10)

This series of tests was designed to obtain the buckling stresses for a series of inclined indirectly loaded fixed ended struts 25mm wide and 4mm thick made from 4mm steel plate with a tensile yield stress of 356N/mm^2. Each strut spanned diagonally at 45^o between the loaded plate and the supported edge as shown in Figure 3.41. The centre line lengths of each strut were chosen so that if each strut was fixed to the same specimen then they would lie parallel with a 0.5mm gap between them. For comparison, the centre line lengths of these struts coincide with those of the previous tests. These lengths being 399, 348, 296.5,246, 195, 144 and 93mm with two specimens of each tested. The load in each case was applied to act at the centre of the loaded edge of the strut. The loaded plates projected under the vertical support and terminated there. The total vertical deflection of the specimen and the mid-lateral deflection of the strut were measured. The general specimen details are shown in Figure 3.41.

3.3.4 Multiple strip plate (series 11)

This series of tests was designed to investigate the effect of cutting a gusset plate into strips running parallel to the free edge. The standard plate dimensions, as used in the main series of tests, were used with L=H=300mm and s=L/2=150mm. The gusset plate was made from 4mm steel plate with a tensile yield stress of 363N/mm^2. The gusset plate was cut into strips with a 0.5mm gap between them to prevent interference between the strips. Due to the difficulty in the manufacture of such a specimen only one gusset plate was made. The loaded plates projected under the vertical support and terminated there. The total vertical deflection of the specimen and the mid lateral deflection of the end three strips were measured. Measuring the lateral deflection of the other strips was impractical due to the congestion of gauges. The general specimen details are shown in

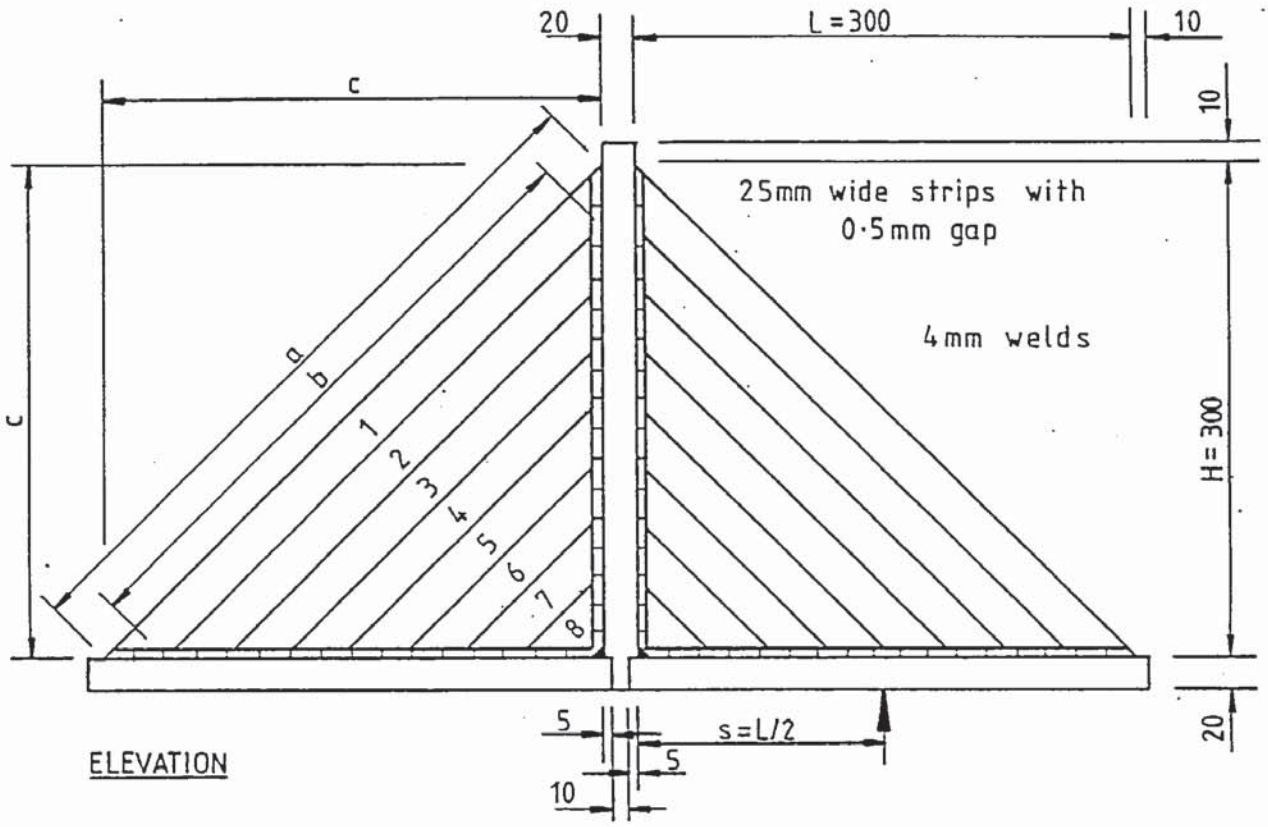

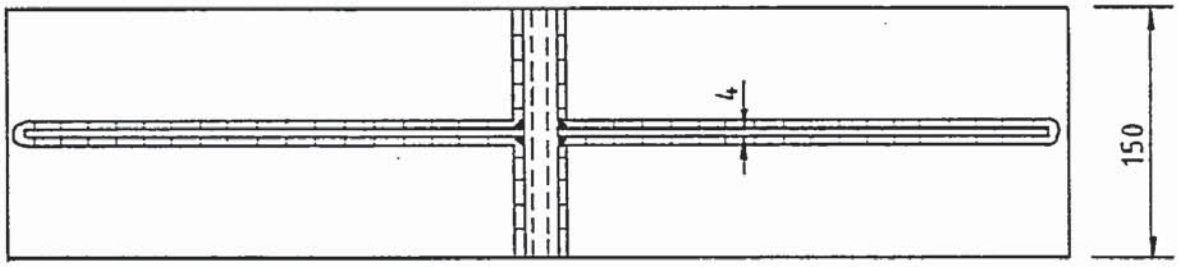

strip	a	b	c
1	424	374	300
2	373	323	264
3	321	272	227
4	271	221	192
5	220	170	155·5
6	169	119	119·5
7	118	68	83·5
8	67	0	47·5

Figure 3.42 Specimen details for multiple strip plate test (series 11)

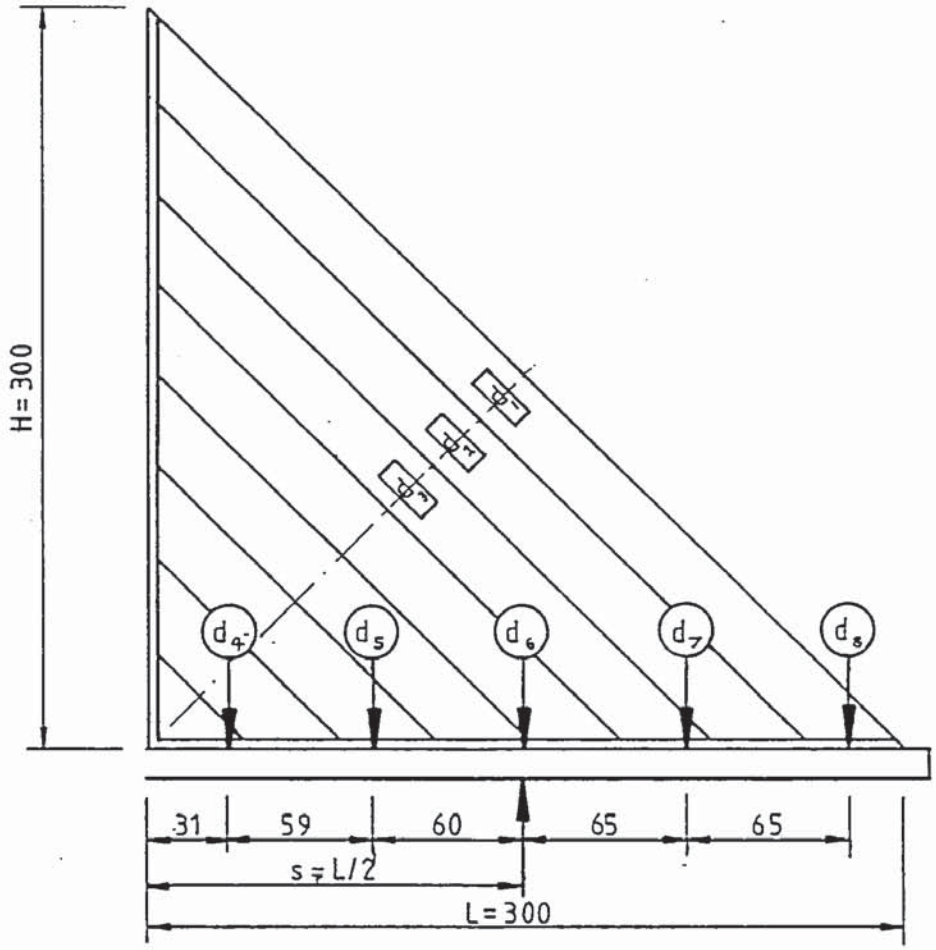

Figure 3.43 Extra dial gauge positions on specimen S11-150-1.

Figure 3.42. Extra deflection gauges were put on the loaded plate of specimen S11-150-1 as shown in Figure 3.43 to measure the deflection profile. Electrical resistance strain gauges were put on the centre line of the strips of specimen S11-150-1, as shown in Figure 3.44.

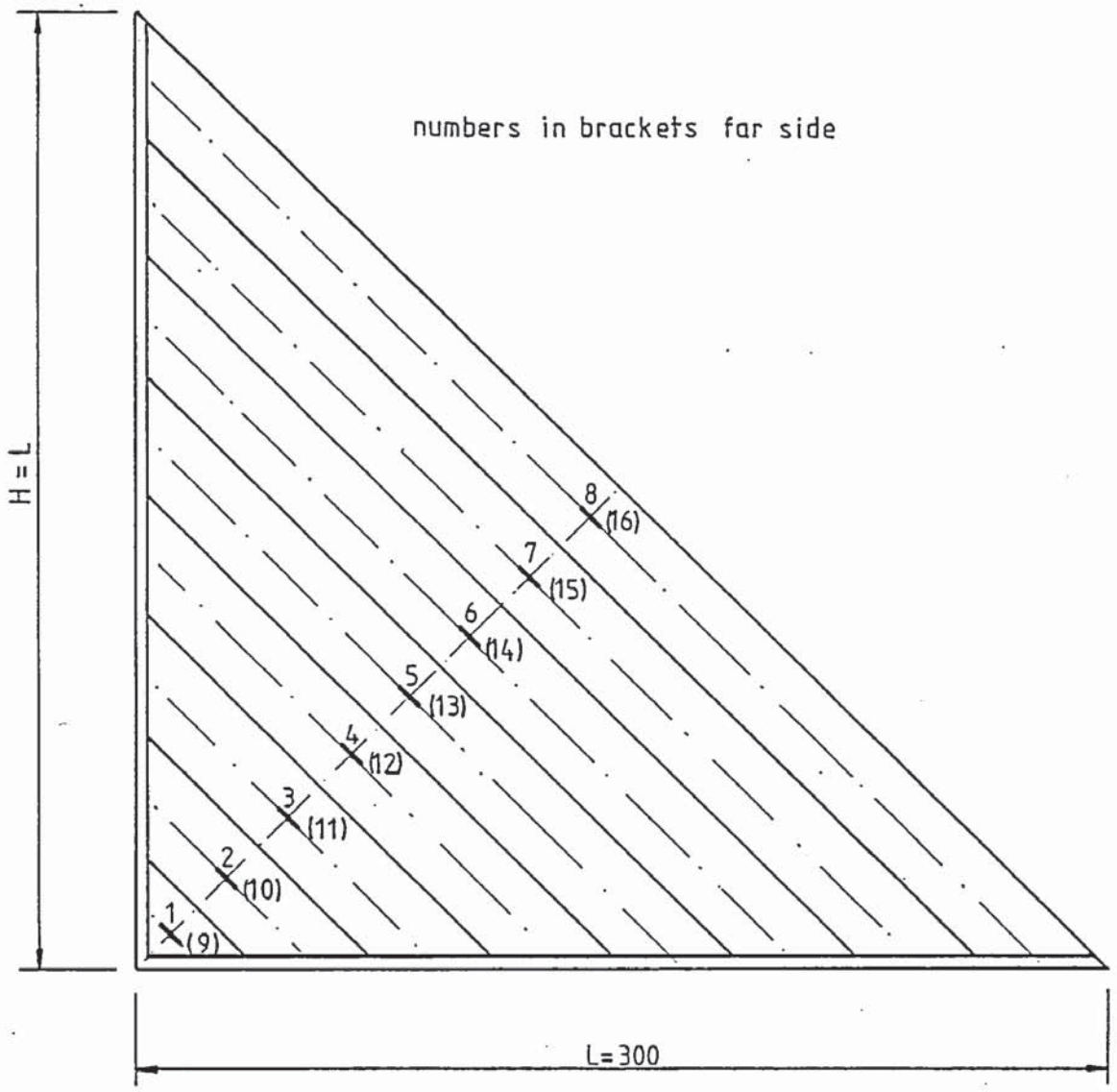

Figure 3.44 Strain gauge locations and numbers for specimen S11-150-1.

3.3.5 Loaded plate bending resistance tests (series 2)

This series of tests investigated the possible contribution of the loaded plate at its supported end to the load carrying capacity of the gusset plate. This was investigated by reducing the thickness of the loaded plate at its supported end by machining the 20mm thick loaded plate over a length of 20mm at its supported end to thicknesses of 0, 4, 8, 12, 16 and 20mm respectively. Reducing the thickness of the loaded plate at this point only, was done to avoid introducing the possible further complication of local buckling of the gusset plate at

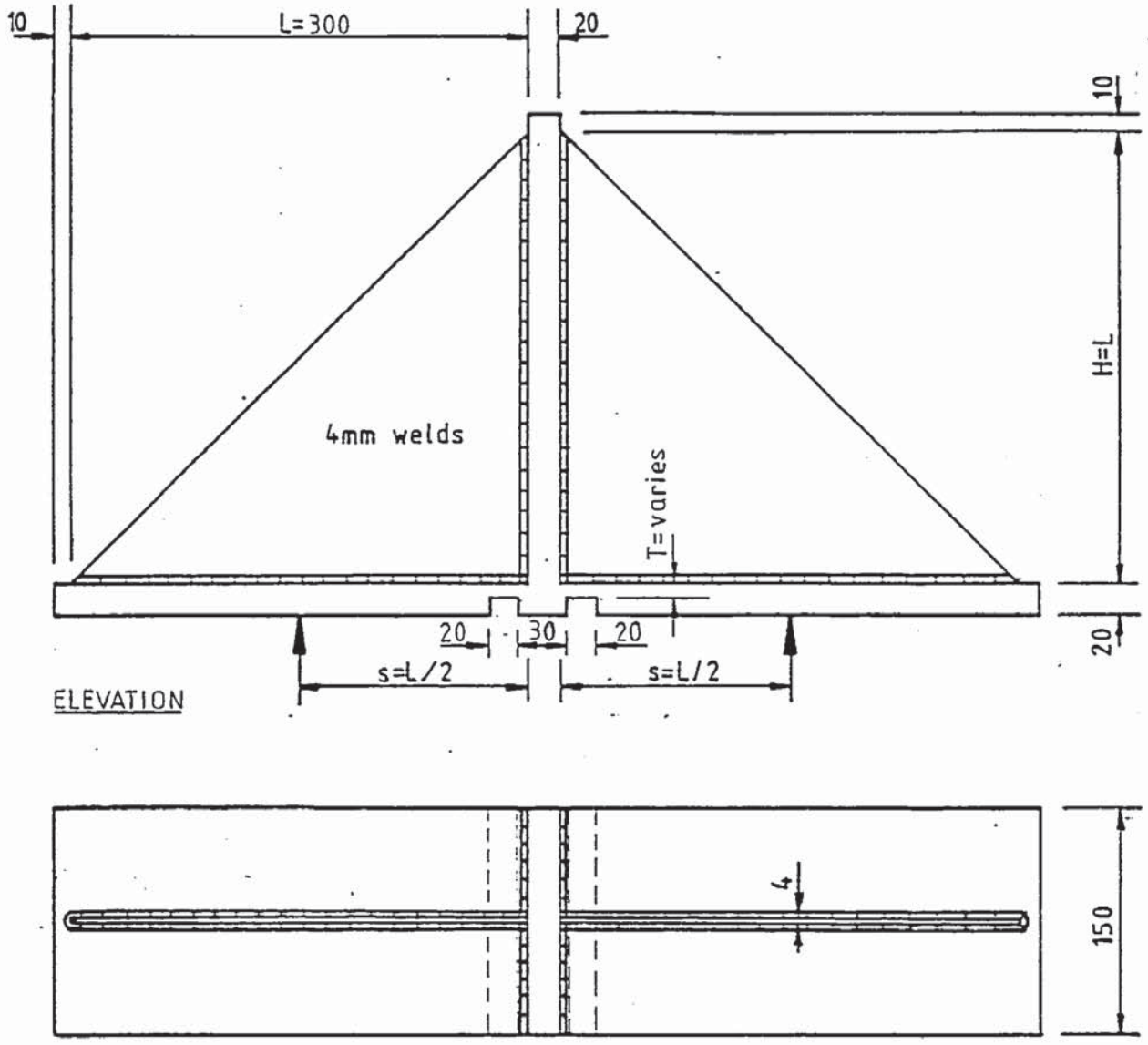

values of T= 0, 4, 8, 12, 16&20

Figure 3.45 Specimen details for loaded plate bending resistance tests (series 2).

the load point with the thinner loaded plates, which have a less distributing effect. Better control over the yield strength of the loaded plate was also obtained by machining from the same plate. The values of L and H were fixed at 300mm and the point of application of the load was fixed at s=L/2=150mm and two specimens of each were tested. Each specimen was made from the same batch of steel. The gusset plates were made from mild steel plate 4mm thick with a yield

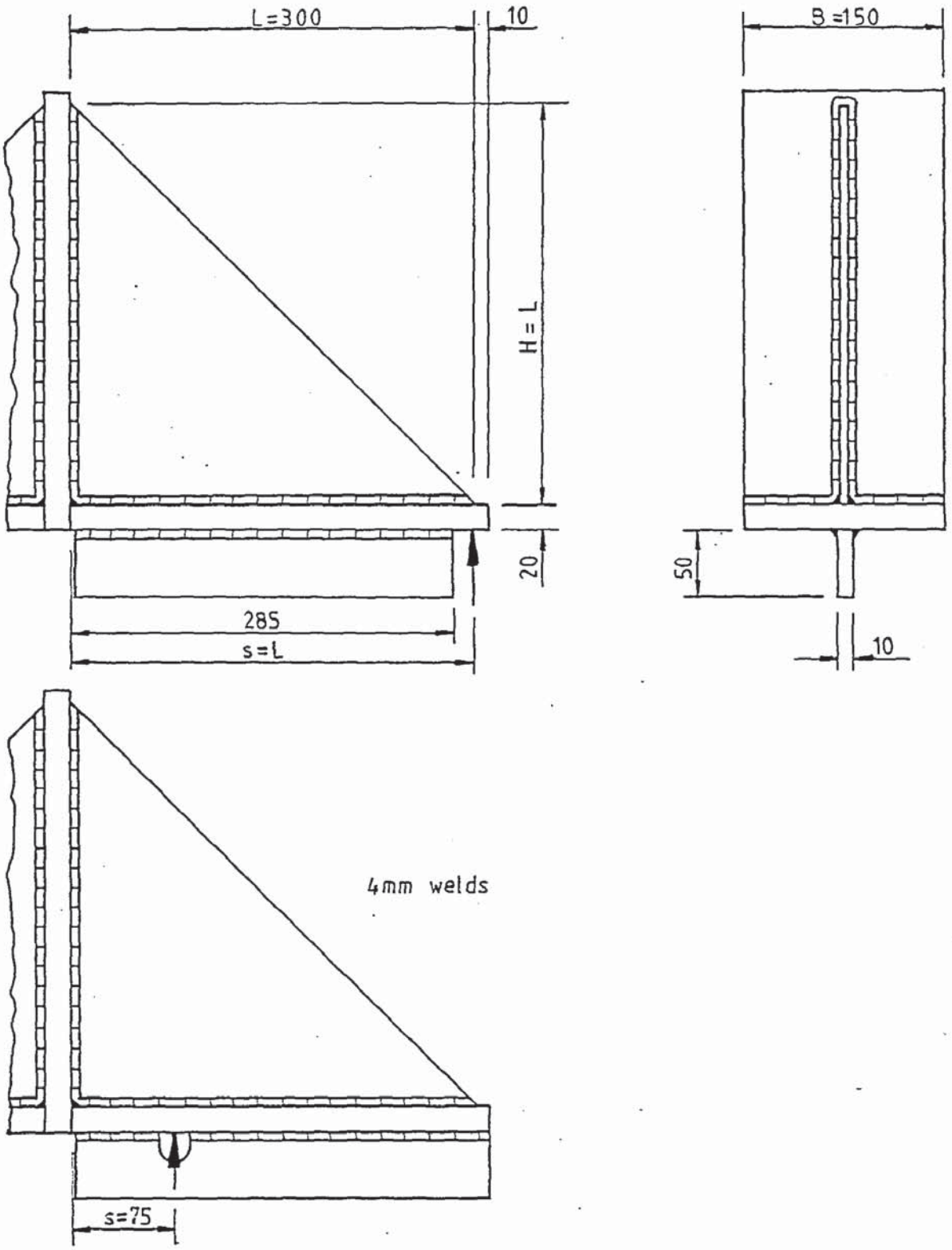

Figure 3.46 Specimen details for rigid loaded plate strain gauge tests (series 5a).

strength of 350N/mm^2. The general specimen details are shown in Figure 3.45.

3.3.6 Rigid loaded plate strain gauge tests (series 5a)

This series of tests investigated the effect of making the loaded plate as stiff as possible for two extreme points of application of the load. Two specimens were made up with L=H=300 and the point of application of the load at s=75 and s=300mm.

The loaded plates terminated at the bottom of the vertical support and were stiffened with vertical stiffeners welded to the underside. The general specimen details are shown in Figure 3.46. Electrical resistance strain gauges were put on both specimens as shown in Figure 3.47 to measure the strain across the plate parallel to the free edge.

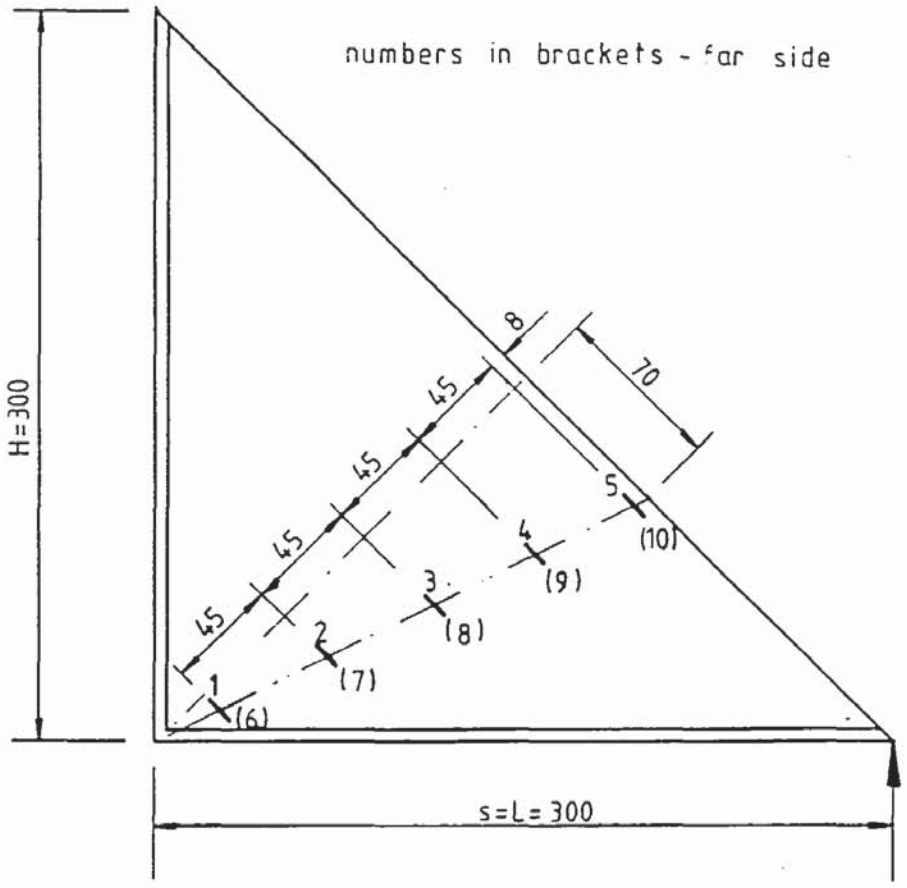

Figure 3.47 Strain gauge locations and numbers for specimen S5a-300-1.

3.4 Gusset plate weld tests

No experimental work was found on the welds connecting the gusset plate to the loaded and supported members. The methods of designing these welds as suggested by the Steel Designers Manual (13) and MacGinley (14) were not consistent and not directly related to the designing of the gusset plate. To gain some experimental information and to try and clarify the situation the following were investigated. A general account of the testing arrangement and specimen dimensions is set out in Section 3.2.2. Therefore, only variations from this are covered.

3.4.1 Variation of the loaded edge weld size (series 14)

This series of tests were designed to investigate the behaviour of the loaded edge weld and its influence on the behaviour of the gusset plate. The normal gusset plate dimensions were used with L = H = 300 mm and the load P applied at s = L/2. The gusset plate needed to be thick enough to apply a significant load on the welds and thin enough to buckle. A gusset plate that buckles is assumed to rely upon the weld to provide edge fixity. From the results of series 12, a plate thickness of 10mm was the most convenient size that fitted this category. The gusset plate material in these tests had a tensile yield strength of 281 N/mm^2. The same weld of 6 mm, as in series 12, was used on all but the loaded edge weld. The smallest practical fillet weld of 2.5 mm was used along the loaded edge of two specimens and no weld along this edge on another two specimens. To try and maintain the same contact friction between the gusset plate and the loaded plate, the two adjacent surfaces were machined. Series 16 provided two results for a 6mm weld along the loaded edge.

The loaded plates continued through at the bottom of the vertical support and the vertical supports were made from mild steel section 25 by 200 mm. This size was chosen, as in series 12, to prevent the

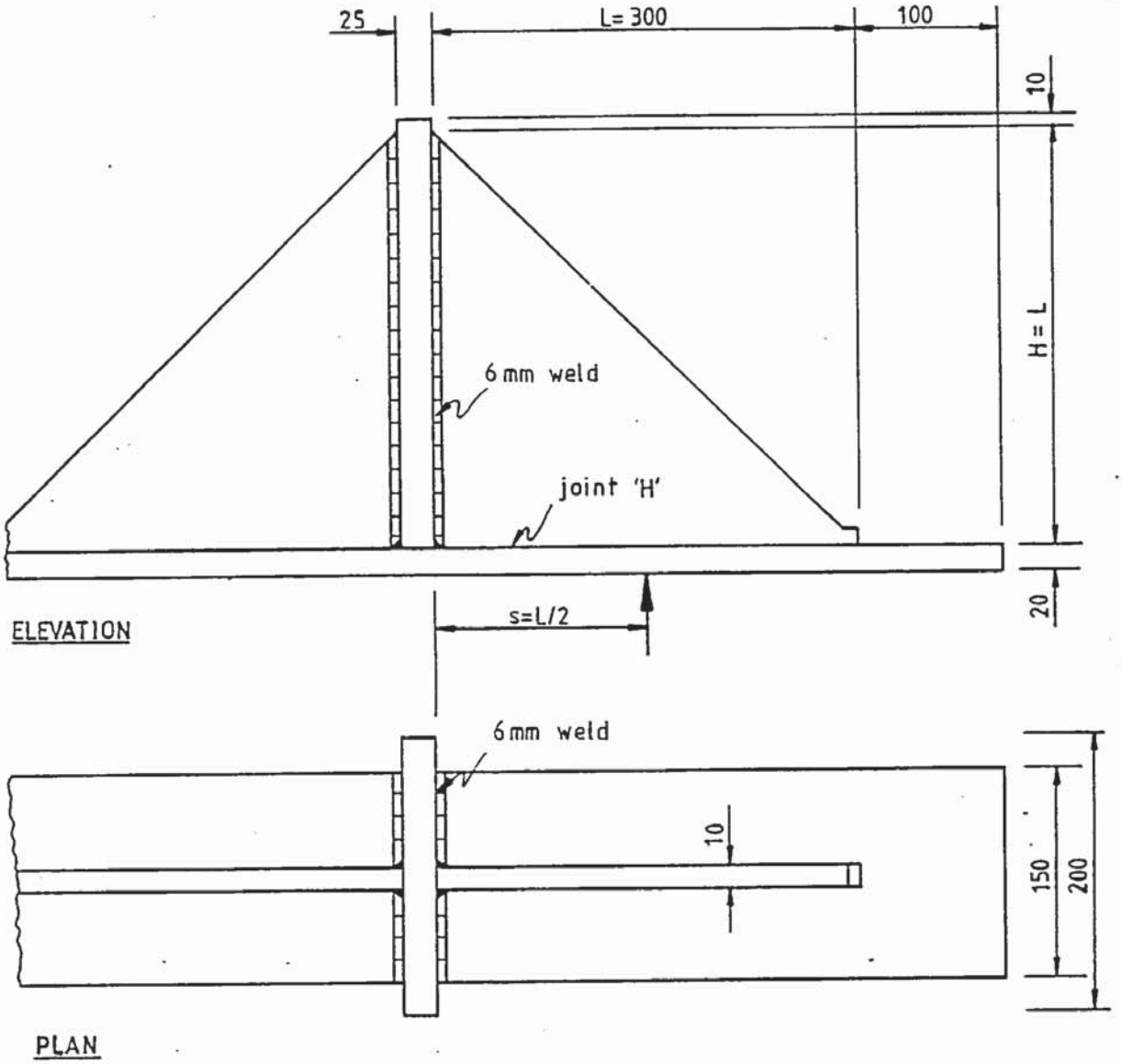

Figure 3.48 Specimen details for series investigating the size of the loaded edge weld (series 14).

failure of the central load point. At the roller supports 150 x 100 x 20mm mild steel spreader plates were used between the loaded plate and the 50mm diameter tool steel rollers to reduce high local stresses which normally do not occur. The general specimen details are shown in Figure 3.48.

Two extra deflection gauges were used to measure the horizontal

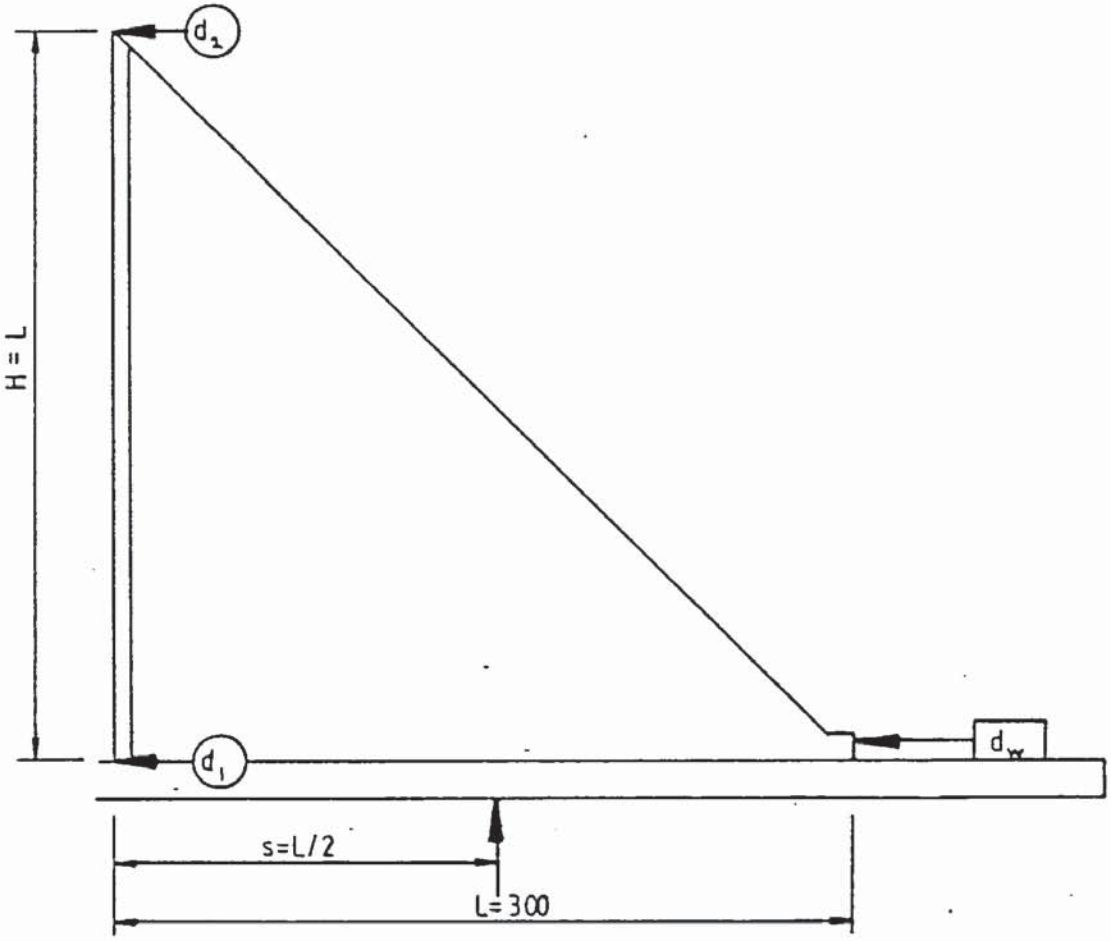

Figure 3.49 Extra dial gauge positions on series 14 specimens.

movement of the top and bottom of the vertical support ,as shown in Figure 3.49, to measure rotation. The relative slip between the loaded plate and the gusset plate was measured at the end of the horizontal weld using a 0.002 mm mechanical dial gauge.

Initially two specimens of each weld size were tested. However, the results were not considered satisfactory as problems were encountered with the testing of two of the specimens and so the series was repeated. All the results have been included.

3.4.2 Variation of the supported edge weld size (series 15)

This series of tests were designed to investigate the behaviour of the supported edge weld and its influence on the behaviour of the gusset plate. This series is very similar to the previous series investigating the loaded edge weld. The only difference is that the

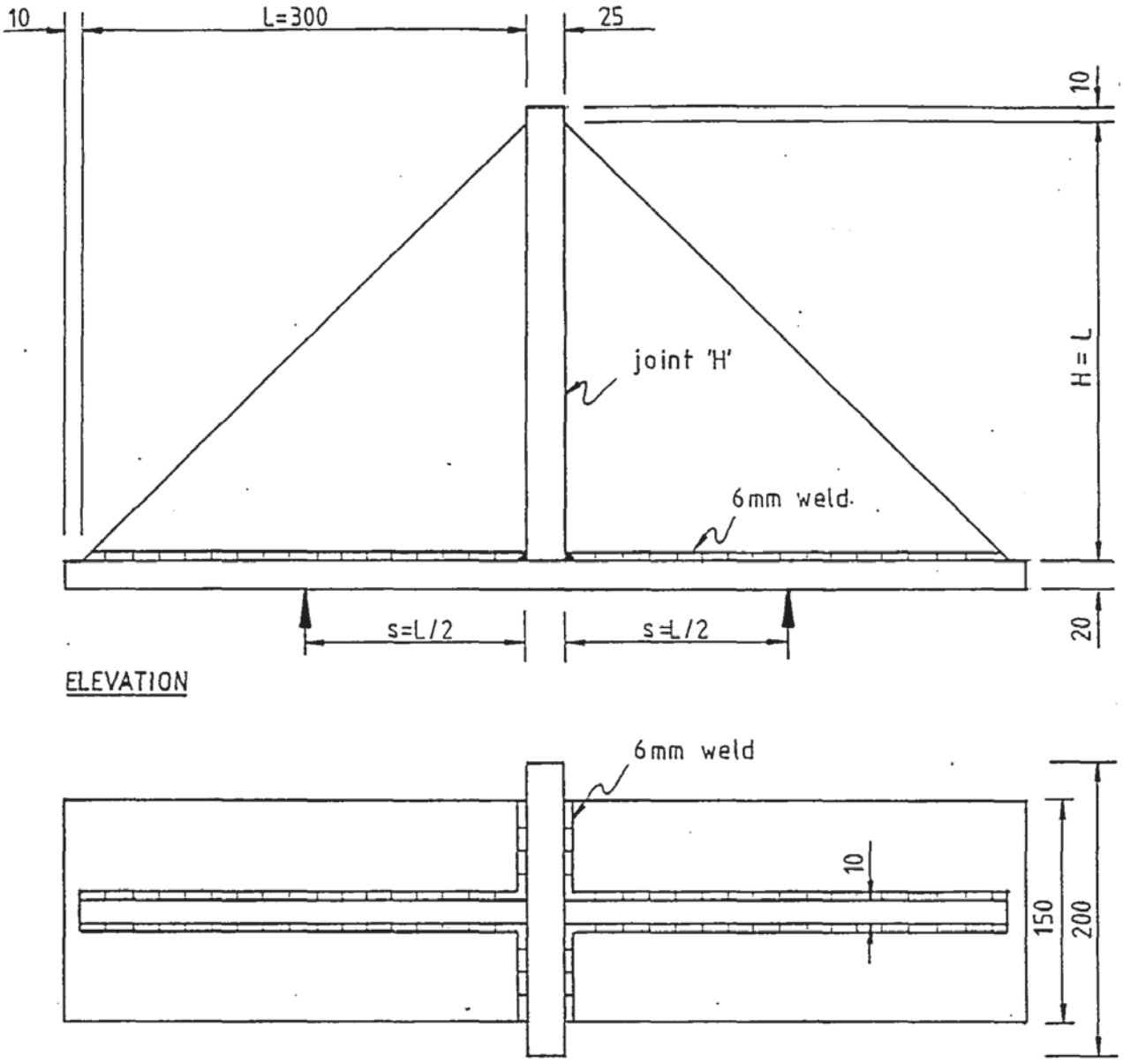

Figure 3.50 Specimen details for series investigating the size of the supported edge weld (series 15).

welding details have been reversed, i.e. two specimens used the smallest supported edge weld of 2.5 mm and another two with zero weld. These were compared with the results provided by series 16 using 6 mm welds along the supported edge. All other specimen details and testing arrangements were the same as for series 14. The general specimen details are shown in Figure 3.50.

3.4.3 Variation of both the loaded and supported edge weld sizes simultaneously (series 16)

This series of tests were designed to supplement the previous two series investigating the loaded and supported edge welds separately. In this series both the loaded and supported edge welds were varied simultaneously to see what influence they had on the behaviour of the gusset plate. The fillet weld sizes chosen were 6 mm and 2.5 mm respectively. The 6 mm fillet welds were chosen to provide a common specimen for the previous two series. The 2.5 mm fillet welds on the other specimens were the smallest practical, and provided an extreme value for comparison with the 6 mm welded specimens. The contact surfaces on both the loaded and supported edges were machined in the same manner as for the previous two series.

The relative slip between the loaded plate and the gusset plate was measured using a 0.002 mm mechanical dial gauge. All other specimen details and testing arrangements were the same as for series 14.

3.4.4 Investigation of the shear, normal and frictional forces on the welds (series 17)

This series of tests were designed to investigate the proportion of the load resisted by the welds. Short 4 mm welds were placed at the outermost edges of the loaded and supported edges in zones which were mainly subjected to shear forces even when there was slip along these edges. The problem with continuous welds is that the loaded edge weld interferes with the supported edge welds making the two difficult to isolate.

Two specimens were tested with 25 mm long 4 mm fillet welds on both sides of the plate at the outer end of both the loaded and supported edges. These were expected to fail before the gusset plate. Another two specimens had their supported edge welds increased to 75mm

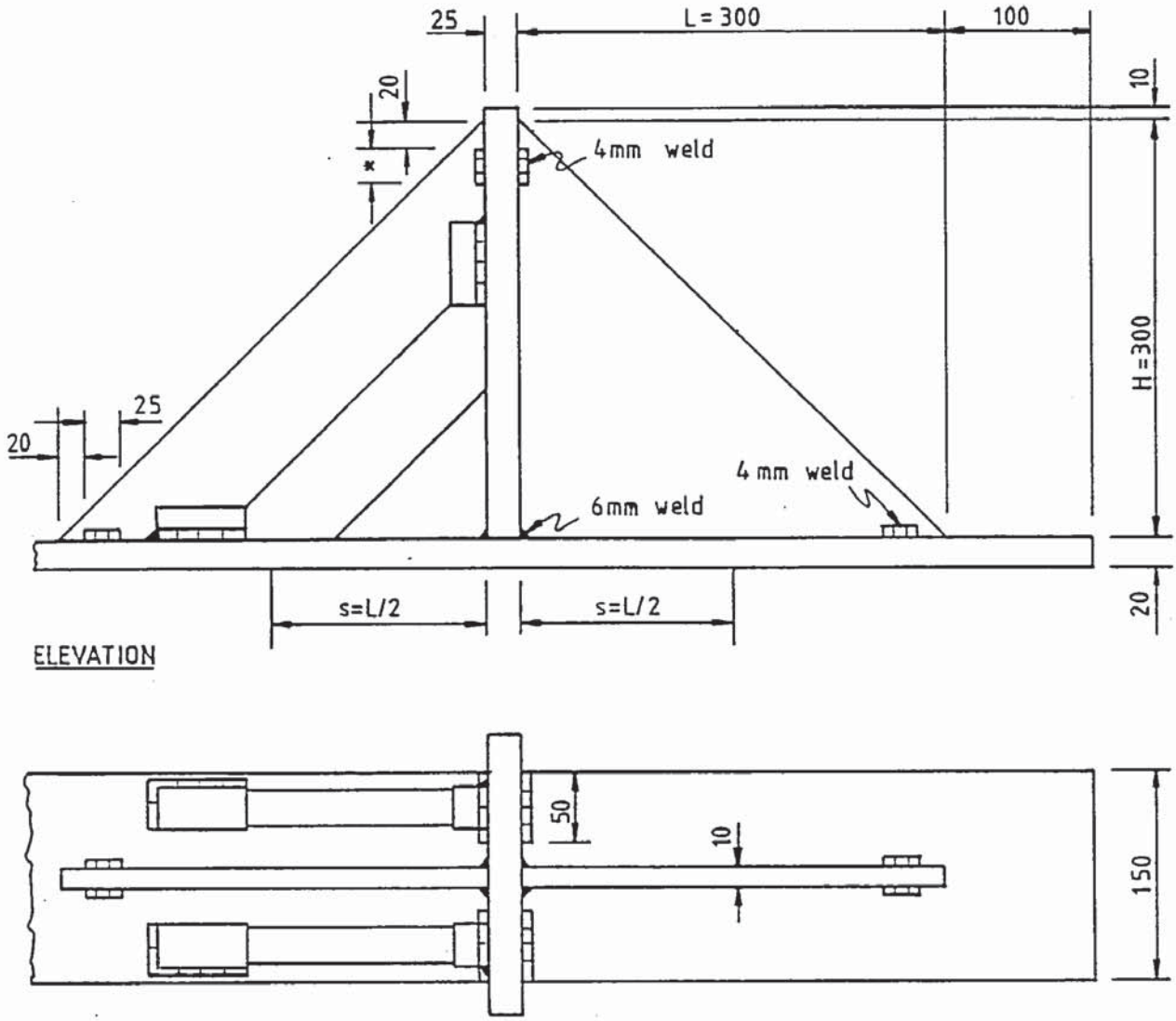

Figure 3.51 Specimen details for series investigating the shear, normal and frictional forces on the welds (series 17).

to produce failure of the loaded edge welds. The contact surfaces along the loaded and supported edges were machined as in the previous series to try and provide a consistent coefficient of friction. During the test the contact zones along these edges were monitored by the use of feeler gauges.

The relative slip along the loaded edge and supported edge welds at the ends of the gusset plates were measured using 0.002 mechanical dial guages. All other specimen details and testing arrangements were the same as for series 14. The general specimen details are shown in Figure 3.51.

To obtain the shear strength of the 4 mm fillet welds used on the gusset plate specimens three weld specimens were made with the same 10 and 25 mm thick plates. The welds were identical as far as type, size and method to those used on the gusset plate specimens. The specimen details are shown in Figure 3.52. The specimens were loaded in compression between the platens of a testing machine to shear the two sets of 4 mm fillet welds 25 mm in length. The total vertical movement of the specimen was measured using 0.002 mm mechanical dial gauges.

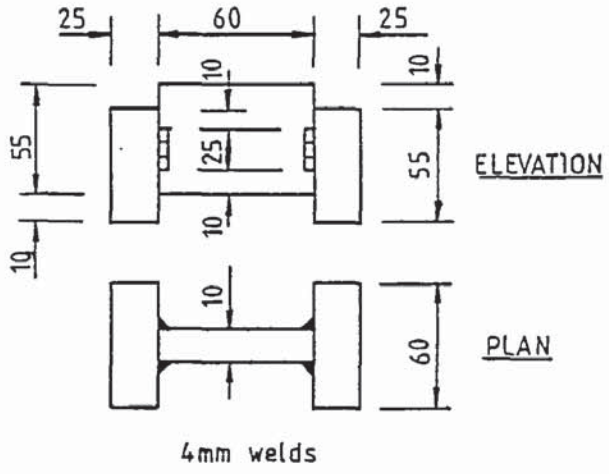

Figure 3.52 Weld test specimen details for series 17.

CHAPTER FOUR

EXPERIMENTAL RESULTS

4.1. Main test series results

This section contains the ultimate loads, deflections and strain gauge results together with the modes of failure of the main gusset plate test series as presented in Chapter 3 Section 3.2.

Presented in this section are the experimental results for the series investigating:-

(i) gusset plate size, L=H, s=L/2, H/L=1 (Series 3)

(ii) gusset plate ratio, H/L, s=L/2 (Series 4)

(iii) variation of s, i.e. the point of application of the resultant applied load P_u (Series 5)

(iv) continuation of the loaded plate (Series 6)

(v) loaded plate thickness, T (Series 7)

(vi) gusset plate thickness, t (Series 12)

(vii) removal of the inside corner of the gusset plate (Series 8)

(viii) variation of the internal angle θ between loaded and supported edges (Series 13)

4.1.1 Gusset plate size, L=H, s=L/2, H/L=1 (series 3)

4.1.1.1 Ultimate load results

The specimen dimensions and ultimate load results are given in Table A.2.1. (Appendix 2). As the same gusset plate material was used for each specimen the relationships between the ultimate load Pu and the gusset plate size L=H for s=L/2 are plotted graphically in Figure 4.1. The ultimate loads for each pair of nominally identical specimens are in good agreement with each other. The first impression from the results is that the ultimate load is approximately the same for each gusset plate size. However, the experimental curve must start at the origin because for a zero sized gusset plate there must be zero load. Also this series is an extension of one of Martin's

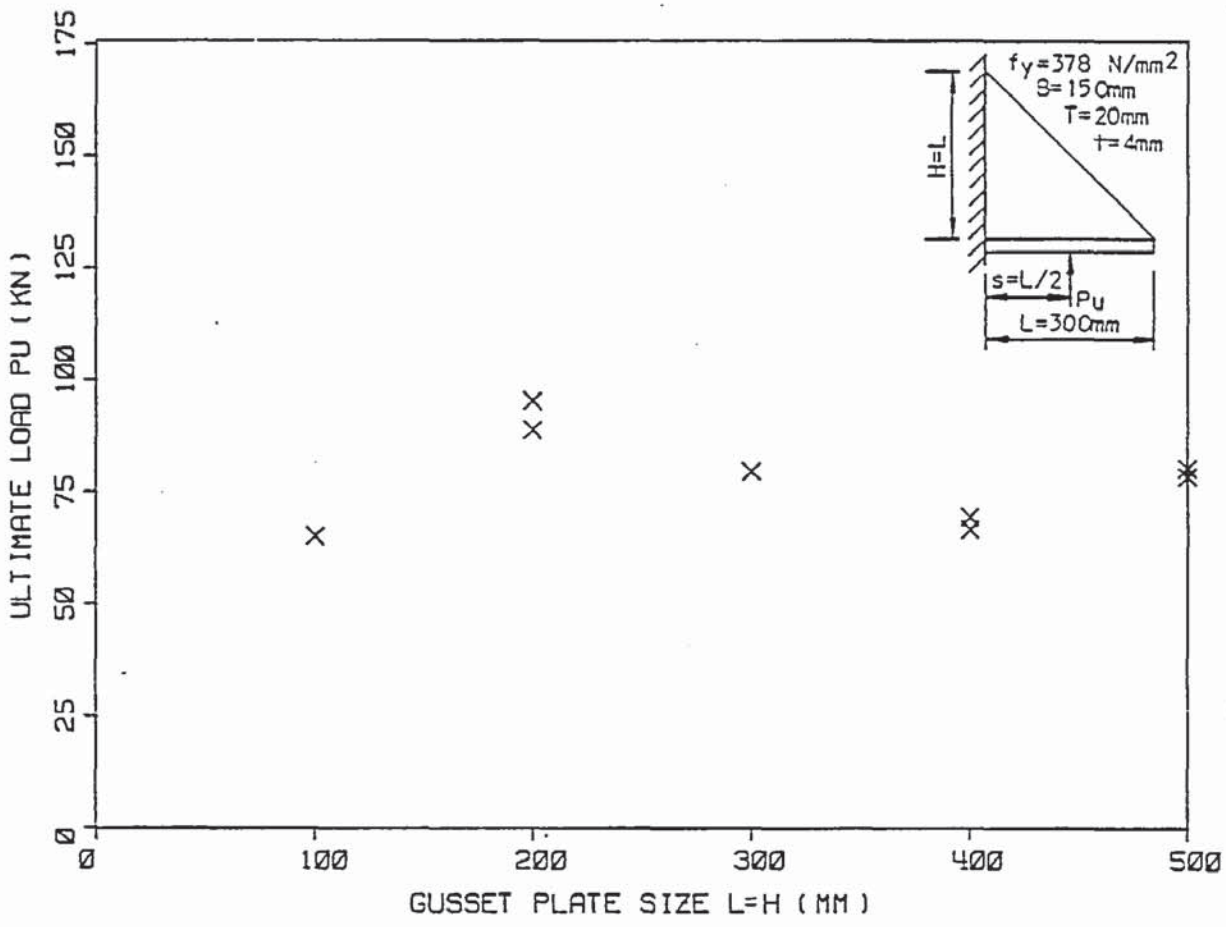

Figure 4.1 Relationship between ultimate load P_u and the gusset plate size L=H (series 3).

(15) experimental series which tested the gusset plate size. Although Martin's (15) results were for very thin gusset plates, their slenderness was equivalent to the author testing gusset plate sizes greater than L=500 mm. Martin's (15) results indicated a reduction in the ultimate load as the gusset plate size was increased. Therefore, the author's results are of the peak of the complete range, with a maximum of approximately 90kN when L=200mm. Beyond this size the failure load reduces, although the largest plate tested with L=500mm, shows an increased strength compared with the L=400mm specimen.

4.1.1.2 Deflection results

It was difficult to produce specimens with perfectly flat gusset

plates, especially with the larger plates. The effects of the welding produced distortion of the gusset plates and in the majority of the specimens there was some degree of initial lateral deflection visible along the outer free edge and possibly other out of plane deformations throughout the gusset plate. The maximum initial lateral deflections were noted and are given in Table A.3.19 (Appendix 3). The amount of initial lateral deflection varied, but generally appeared to increase with the size of the gusset plate and the maximum value was approximately at the mid-point of the free edge.

The deflection gauge results measuring the total vertical deflection of the specimen and the lateral deflection of the mid point of the gusset plate's free edge, referred to as the mid-lateral deflection, were intended to be used as an indication of the specimens' behaviour relative to each other. However, the total vertical deflection that was measured can be approximately linearly related to the vertical deflection of the load point relative to the vertical support, and also to the change in the internal angle of the gusset plate. For the most part of the tests the vertical supports remained vertical and the loaded plates remained straight. Close to failure the vertical supports moved towards the side under test as buckling commenced and the loaded plates began to bend slightly. Therefore, for the latter part of the tests the relative vertical deflection and the angle of rotation were slightly greater than the total vertical deflections indicate. The total vertical deflections and the mid-lateral deflections are given with the corresponding applied load increment in Table A.3.1. From this data, load deflection curves were produced and compared. Due to the number of graphs involved the general result is described and only representative graphs are presented in Appendix 4.

From the deflection data the deflection per unit load increment

can be determined at any point and is referred to as the deflection rate. If the deflection rate is the same for consecutive points, i.e. the load deflection curve is linear then the deflection is referred to as being linear, otherwise it is non-linear. With the non-liner deflections the deflection rates are either increasing or decreasing.

The magnitude of the total vertical deflections of the specimens were similar. There was usually some initial settlement of the specimen interpreted from the reducing deflection rate, after which the vertical deflections for the majority of the tests were steady and approximately linear for at least 80% of the ultimate load. The exceptions were for one of the specimens with L=100mm and the two with L=400mm which were linear for only 60% of the ultimate load. The vertical deflection rates for this linear section varied slightly. Two specimens, one with L=100mm and the other with L=400mm, had slightly higher deflection rates than the rest. Beyond the linear section the rate of the vertical deflection increased slowly and steadily at first and then fairly rapidly when the deformation of the gusset plate approached the ultimate load. The deflection readings were stable, i.e. they stopped increasing with the load increment, at the initial part of this non-linear section but, closer to the ultimate load the deflection readings required increasingly more time to stabilize.

The mid-lateral deflections of the free edge varied and appeared to depend on the initial deformed shape of the gusset plate and its size. Generally the plates buckled in the direction of the initial lateral deflection of the free edge, as would be expected. However, if there was more than one "kink" on the free edge the plates had a tendency to deflect in the opposite direction. In some instances the plates initially deflected in one direction and then finally buckled in the other. The initial deformed shape appeared to increase or

decrease the stability of the plate, depending on the nature of the deformation, and appeared to influence the load capacity.

The magnitude and the rate of increase of the lateral deflection along the free edge was greater for plates with a large initial lateral deflection in one direction. The maximum lateral deflection was approximately at the mid-point of the free edge. For the small plates the lateral deflection was very small for most of the loading and then suddenly increased close to the ultimate load when the deflection took longer to stabilize. With the larger plates the lateral deflection started from the initial loading and progressively increased with the load, tending to a relatively large deflection just before failure. The lateral deflection for the 400mm specimen was approximately 13mm just before failure. Although the lateral deflections were relatively large for the larger plates, they were stable with no signs of creep for the most part of the loading as were the vertical deflections.

In Appendix 4 the total vertical and mid-lateral deflections for specimens S3-100-2 and S3-500-2 are shown in Figures A.4.1. and A.4.2. respectively. These represent typical deflection results of the two extremes of the series with the others being a transition between the two. The total vertical deflection of specimen S3-100-2 has the typical initial settlement deflection that usually occurred. Specimen S3-500-2 resisted the loads immediately and shows the linear portion starting from the initial loading. The mid-lateral deflection of specimen S3-100-2 shows very little lateral deflection for most of the loading while specimen S3-500-2 shows the deflection starting from the initial loading. The small lateral deflection of specimen S3-100-2 may in fact have been due to lateral movement of the specimen as it settled down.

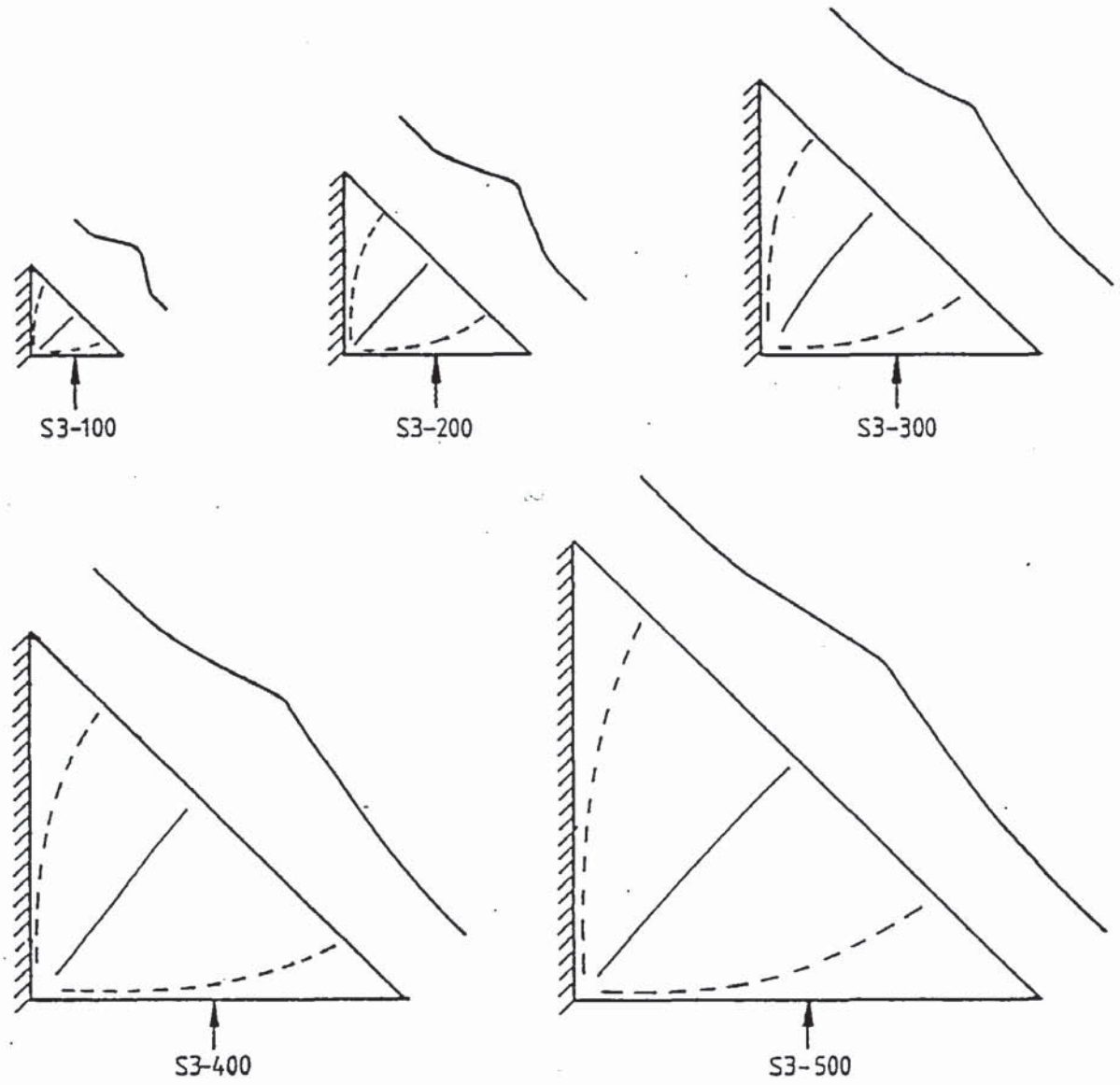

Figure 4.2 Gusset plate fold line patterns (series 3).

4.1.1.3 Failure modes

The failure modes for each specimen in this series were very similar. The specimens appeared to behave elastically for most of the loading and failed in an elastic plastic buckling manner. The buckling appeared to be progressive. The outer free edge of the gusset plate deflected laterally first but restrained by the inner part of the gusset plate. The outer free edge then buckled and the lateral buckling progressed towards the inside corner of the gusset plate. The vertical and lateral deflections showed no signs of creep

for most of the loading, but close to the ultimate load took an increasingly longer time to stabilise. A load was eventually reached where the deflection increased rapidly and the specimen gradually buckled into a less stable shape along well defined fold lines. These fold lines were very similar for each specimen, with three fold lines running from the inside corner of the gusset plates, as shown in Figure 4.2. One line ran approximately along the angle bisector to the free edge and the other two followed the loaded and supported edges so far and then curved towards the free edge to intersect it nearly perpendicularly. The actual formation of these fold lines, however, was from the free edge inwards, towards the inside corner. Prior to collapse the free edge deflection profile was a smooth transition of curves, afterwards the profile was angular. When the dial gauges were continuing to move close to the ultimate load it was possible to reduce the load until the dial gauges did not register. This load depended upon how far the buckling had progressed.

The loaded plates of the small gusset plates during loading remained relatively straight. However, with the larger gusset plates the loaded plates were concave on the surface adjacent to the rollers through which the load was applied. This suggested that as the loaded plates became longer with the larger gusset plates, they were not able to distribute the concentrated applied resultant load along the loaded edge of the gusset plate as effectively as with the smaller gusset plates. At the ultimate load of the gusset plates the loaded plates appeared to pivot about the inside corner of the gusset plate.

4.1.2 Gusset plate ratio, H/L (series 4)

4.1.2.1 Ultimate load results

Specimen dimensions and ultimate load results are given in Table A.2.2. The relationships between the ultimate load Pu and the

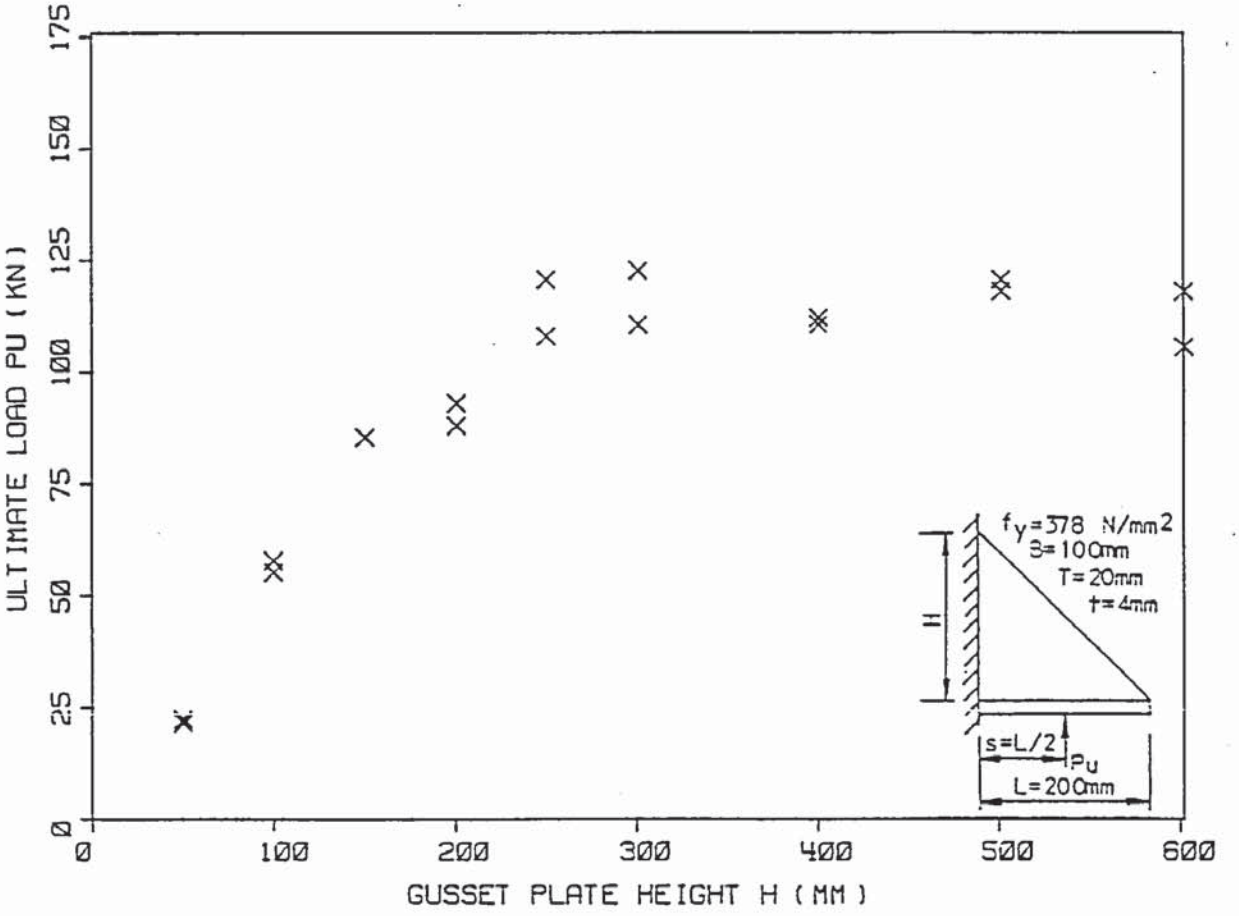

Figure 4.3 Relationship between ultimate load P_u and the gusset plate height H (series 4).

gusset plate height is plotted graphically in Figure 4.3. The ultimate loads for each pair of nominally identical specimens in most cases were in good agreement, although three pairs showed a difference of approximately 11%. The plotted results indicate a gradual increase in the ultimate load with a peak of approximately 115kN when H=250mm which corresponds to a value of H/L≃1.25. For values of H/L from 1.25 to 3.0 the failure load is approximately constant. There appears to be a slight dip in the curve at H/L=1.

4.1.2.2 Deflection results

The vertical and lateral deflections of each specimen are given in Table A.3.2. The vertical deflections were similar in nature to series 3, with an initial settlement deflection, a middle

approximately linear section and non-linear section up to the ultimate load. The vertical deflections were linear to approximately 95% of the ultimate load, with very little non-linear deflection for the majority of the specimens, and some of them failed suddenly. The exceptions were, one of the specimens with H=50mm, one with H=100mm and two with H=600mm. These exhibited noticeable non-linear deflection. Generally the vertical deflection rates of the linear section reduced as H increased up to approximately H=250mm, and then remained approximately constant with the exception of the specimens with H=600mm. These two specimens appeared to have a higher deflection rate similar to that of the specimens with H=200mm.

As with Series 3 there were some initial distortions due to welding. The initial lateral deflections were relatively small and only noticeable with the larger values of H. Generally the lateral deflections, which were measured at approximately the point of maximum lateral deflection, were very small for most of the loading but increased close to the ultimate load. The smaller plates, and where the plates were initially virtually flat, failed suddenly with little warning. The lateral deflections started to increase close to the ultimate load typically around the 80% mark. The lateral deflections were apparent before the ultimate load for the 500 and 600mm specimens, with relatively large lateral deflections approximately 6 to 9mm, just before failure. Generally the specimens deflected in the same direction as the initial deflection.

In Appendix 4 the total vertical and lateral deflections of specimens S4-150-2 and S4-500-2 are shown in Figures A.4.3 and A.4.4 respectively. Specimen S4-150-2 is representative of the smaller plates having a very small non-linear vertical deflection. The lateral deflection only started to increase very close to the ultimate load. Specimen S4-500-2 is representative of the taller plates where

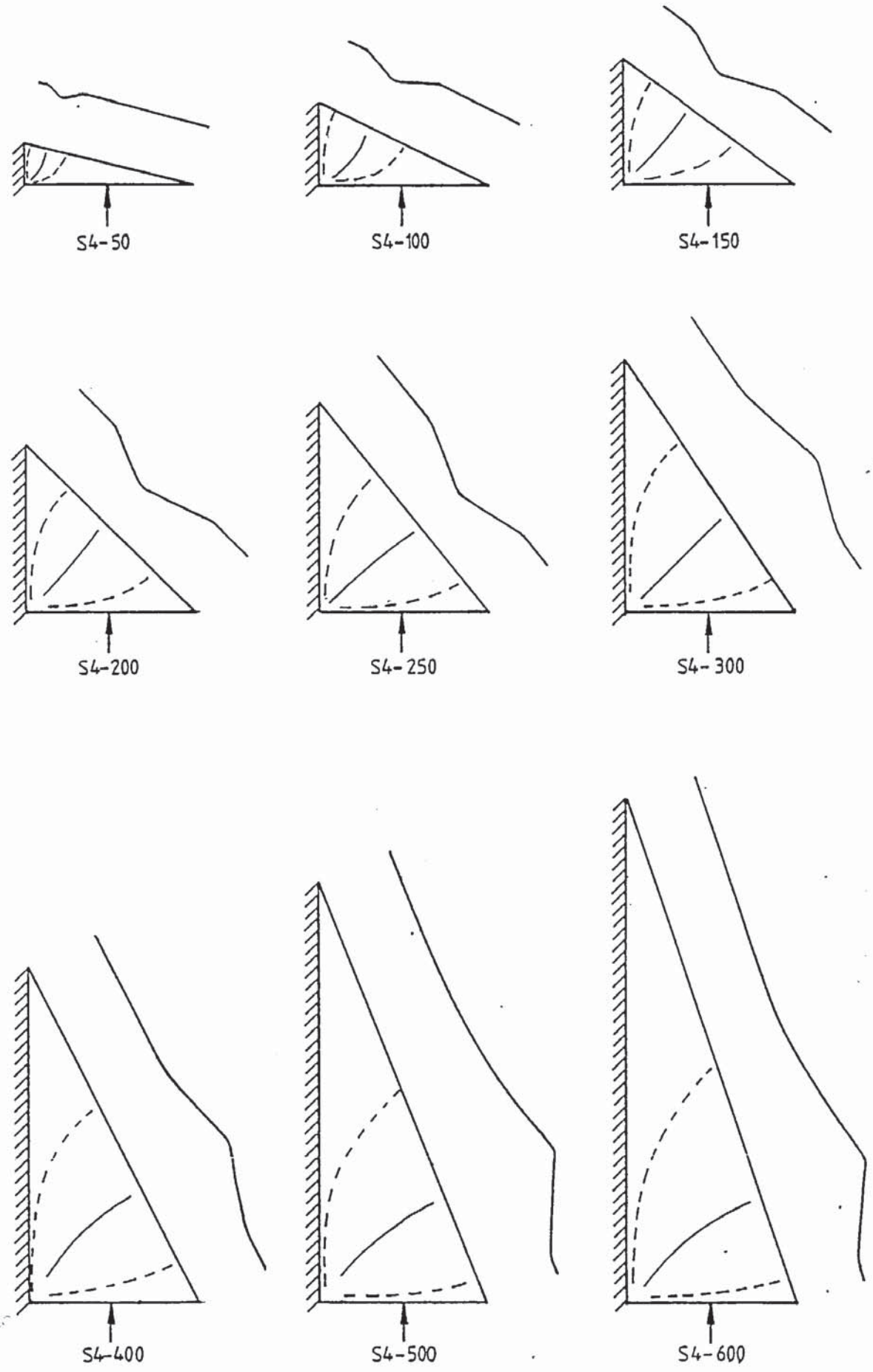

Figure 4.4 Gusset plate fold line patterns (series 4).

the lateral deflections start at a lower load. The deflection rate of the linear section is lower with the S4-500-2 than with the S4-150-2 specimen.

4.1.2.3. Failure modes

The failure modes were similar to those of series 3. With the larger values of H, the rate of collapse was slower and more apparent whereas with the smaller values of H collapse occurred relatively quickly. Although the plates were not symmetrical the fold lines still ran from the inside corner of the gusset plate. One followed the angle bisector and the other two followed the loaded and the supported edges part of their length and tended to intersect the free edge perpendicularly. The effect was a concentration of fold lines near the shortest edge of the gusset plate for $H/L \neq 1.0$ as shown in Figure 4.4.

4.1.3. Point of application of the resultant applied load P (Series 5)

4.1.3.1 Ultimate load results

The specimen dimensions and ultimate loads are given in Table A.2.3. The relationships between the ultimate load Pu and the point of application s of the applied load is shown in Figure 4.5. The ultimate load results for the whole range formed a curve and the repeated results of specimens with s=150 and 300mm were consistent. Therefore, these results were considered adequate and duplication for the other values of s was not considered necessary. The results of these were in good agreement with previous values. The plotted results indicate a non-linear relationship with a rapid increase in the ultimate load as the load is applied closer to the supported edge, i.e. as s is reduced, and conversely the load reduces as the load is applied towards the outer free edge, i.e. as s increases.

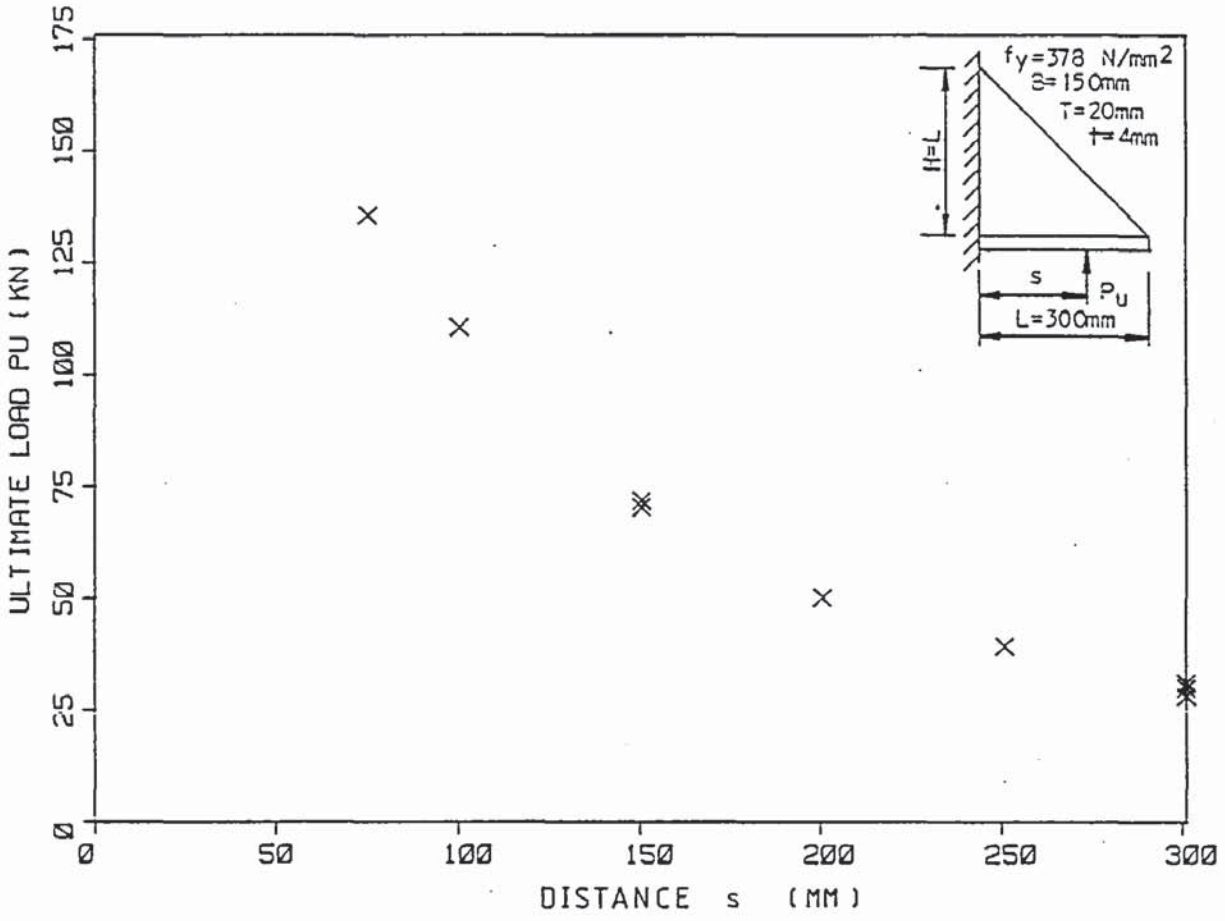

Figure 4.5 Relationship between the ultimate load P_u and the distance s of the applied load (series 5).

4.1.3.2 Deflection results

The vertical and mid-lateral deflections are given in Table A.3.3. After initial fluctuations at low load, the vertical deflections for the majority of the tests were approximately linear to at least 80% of the ultimate load, with only a small amount of non-linear vertical deflection. Although the deflection rates of the linear section varied, they generally increased as the load was moved towards the outer free edge, i.e. as s increased.

The initial lateral deflections associated with the welding were more noticeable than in the previous series. The lateral deflections again were not of a consistant nature. The mid-lateral deflections were noticeably greater at lower loads with the load applied towards

the outer free edge of the gusset plate. However, just before the ultimate load, the maximum mid-lateral deflections on the outer free edge were approximately the same for all positions.

In Appendix 4 the total vertical and mid-lateral deflections of specimen S5-75-1 and S5-300-2 are shown in Figures A.4.5 and A.4.6 respectively as examples of the two extreme types of behaviour. The two vertical deflection curves are very similar in shape, the only difference being the rate of deflection. The mid-lateral deflections are also similar in shape.

4.1.3.3 Failure modes

The failure modes were similar in nature to those of series 3 with the fold line patterns as shown in Figure 4.6. The rate of collapse was slower and more apparent with the load applied towards the outer edge.

With the load applied to the outer edge of the loaded plate, the loaded plate was convex on its underside adjacent to the roller. Deflection gauges along the loaded plate of specimen S5-300-3, measured this curvature and the deflection are given in Table A.3.3. This bending of the loaded plate was in the reverse direction to that obtained in series 3 for the largest plate. With the load applied close to the support there was a visible concave curvature to the underside of the loaded plate in the region of the applied load.

4.1.3.4. Strain gauge results

Strain gauges were placed on some of the gusset plates to measure the stresses across their width and across their supported edges. The average stress results are given in Tables A.5.1 to A.5.8. The significance of these results will be discussed later. Some strain gauge rosettes were used to measure the magnitude and direction of the major principal stress at different points in some of the gusset

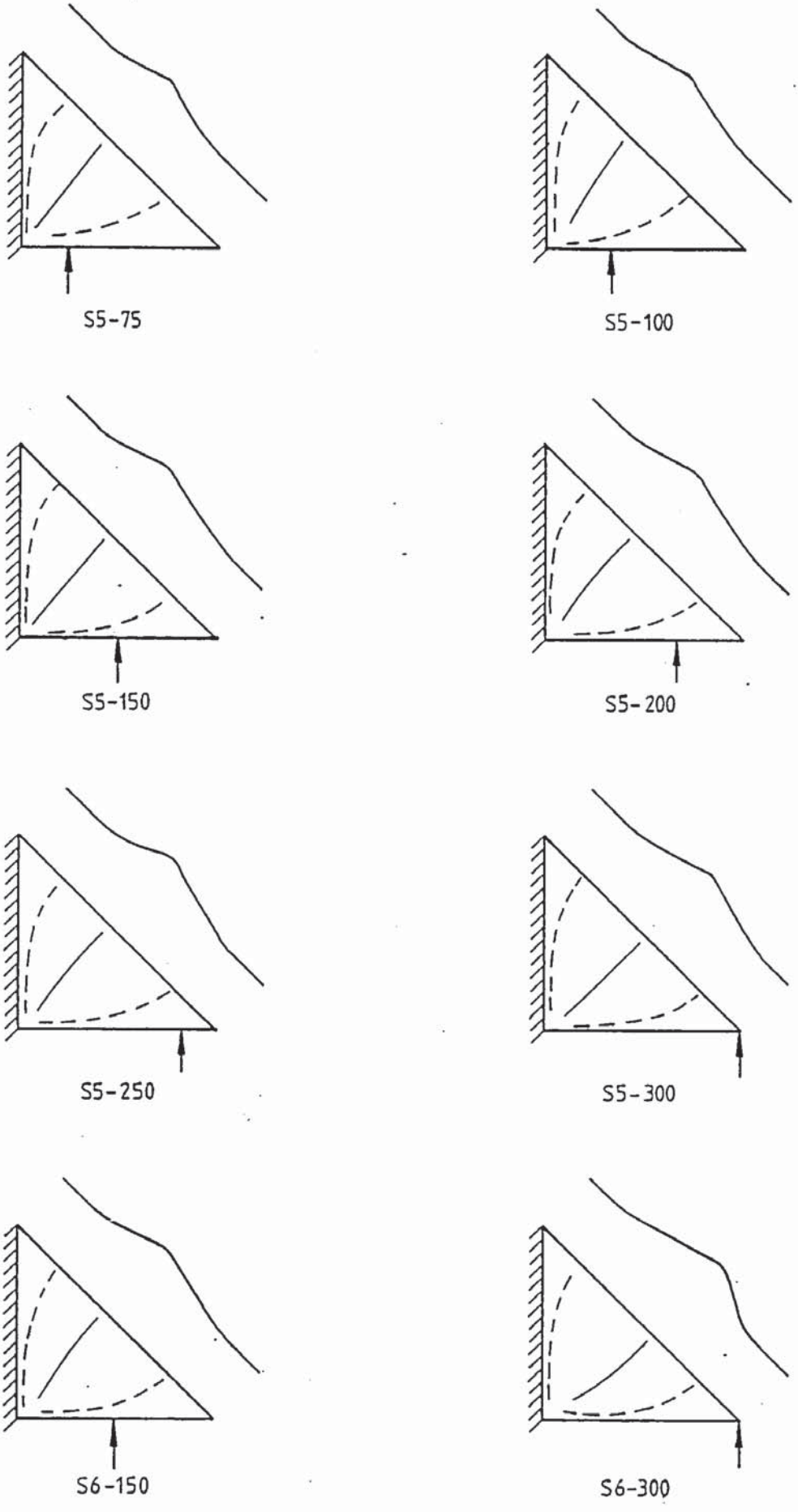

Figure 4.6 Gusset plate fold line patterns (series 5 & 6).

plates and these results are given in Tables A.5.30 to A.5.33. These results suggested that the major principal stress was roughly parallel to the free edge. The concentrated point load that was used, however, appeared to realign the direction of the major principal stress towards it, at the loaded edge of the gusset plate.

Strain gauges were also attached to the loaded plates of specimens S5-150-2 and S5-300-3 and the results are given in Tables A.5.22 and A.5.23 respectively. With specimen S5-150-2, strain gauges were placed across the width of the loaded plate at its supported end, to obtain the longitudinal stress distribution across its width. Although the loaded plate was terminated at the supported edge, readings were obtained for the gauges on the bottom face. The readings indicated that there was a net axial stress in the plate at this section, which was relatively uniform across it. There was a greater tensile stress across the top surface than across the bottom. This was expected as the lateral weld, connecting the loaded plate to its support and the gusset plate, were on its top surface. The maximum stress encountered at the ultimate load was only $91 N/mm^2$ on the top face.

The strain gauges for specimen S5-300-3 were placed at different sections along the loaded plate adjacent to the gusset plate to obtain the longitudinal stress distribution along its length. With the load at the extreme end of the loaded plate, the loaded plate was subjected to bending, which put the top face into compression and the bottom into tension towards its outer free end. However, the bending stresses at the supported end remained relatively low, and the net axial stress was tensile. This axial tensile stress progressively reduced towards its free end.

4.1.4. Continuation of the loaded plate (series 6)

4.1.4.1. Ultimate load results

The specimen dimensions and ultimate load results are given in Table A.2.4. Only two specimens were tested for comparison with the two similar specimens in the previous series. The ultimate load of the specimen with the load at s=300mm was 17% higher than the specimen with the cut loaded plate of the previous series The ultimate load of the specimen with the load at s=150mm was 32% higher than the specimen with the cut loaded plate. Because the results were different from the previous series by different amounts, the results were not considered conclusive and a separate series of tests was considered necessary to investigate the effect of the loaded plate thickness.

4.1.4.2. Deflection results

The vertical and mid-lateral deflections are given in Table A.3.4. The vertical deflections, in comparison with the two corresponding in the previous series were very similar. For the specimen with the load applied at s=L/2 the vertical deflection had a similar linear section, as with the discontinuous loaded plate, but it extended to a greater load followed by a slightly greater non-linear section. With the load applied at the end of the loaded plate (s=L) the initial vertical deflections were very similar, with the linear section extending to virtually the same load as with the discontinuous loaded plate. However, the continuous loaded plate specimen was able to tolerate even more deformation resulting in a considerably greater post-linear deflection.

The outer free edges of the gusset plates had the usual initial deflections associated with welding. The mid-lateral deflections were similar to the appropriate two in the previous series and continued to give greater lateral deflections before failure, especially with the load applied at the end of the loaded plate.

4.1.4.3. Failure mode

The failure mode of the specimen with s=L/2 was very similar to those of previous series. The loaded plate did not appear to bend at the inside corner until after the gusset plate had buckled and folded along the usual fold lines.

With the load applied at the end of the loaded plate, the loaded plate remained perpendicular to the vertical support but, it progressively deformed upwards at the outer end. As the load was increased, more of the gusset plate deflected laterally and a greater portion of the loaded plate bent upwards. This type of deformation gradually progressed inwards until the inner section of the gusset plate collapsed resulting in the collapse of the specimen itself. This mode of failure resulted in a large lateral deflection of the gusset plate's free edge and a large vertical deflection of the end of loaded plate just before failure. At the ultimate load the specimen buckled and folded along similar fold lines as described in the previous series. The loaded plate again appeared to have been bent at the inside corner after the failure of the gusset plate and it also had a convex curvature on the under side adjacent to the roller. The loaded plate deflection readings, are given in Table A.3.4.

4.1.4.4. Strain gauge results

Strain gauges were placed across the width of the gusset plates. The average stresses were calculated and are given in Tables A.5.9 and A.5.10. The significance of these results will be discussed later.

To obtain the longitudinal stress distribution across the width of the loaded plate along its length, strain gauges were also placed across various sections along its length of both specimens. The results are given in Tables A.5.24 and A.5.25. The results for specimen S6-150-1 indicate a diminishing net tensile stress from the supported end up to the load point. The bending stresses are

relatively low at the supported end. The effect of the point load at the mid-point of the loaded plate produced bending, so that there was compression on the top face towards the supported edge and compression on the bottom face towards the free edge.

The results for specimen S6-300-1 indicate a diminishing net tensile stress from the supported end towards the free end. The bending stresses along the loaded plate agree with the deflection profile, i.e. they produce a compressive stress in the top face and a tensile stress in the bottom face. The greatest bending stresses are around the mid-point which reached the yield stress just before failure. However, the bending stresses at the supported end of the loaded plate remained relatively low and only yielded after the gusset plate itself had failed, as indicated by the last set of readings.

4.1.5. Loaded plate thickness, T (series 7)

4.1.5.1. Ultimate load results

The specimen dimensions and ultimate load results are given in Table A.2.5. The relationship between the ultimate load P_u and the thickness T of the loaded plate, with the applied resultant load at positions s=L/2 and s=L, are shown in Figures 4.7 and 4.8 respectively. Except for one abnormally high load for specimen S7-16-150-1, the two sets of results for both load positions indicate that the thickness of the loaded plate has no effect on the ultimate load results of the gusset plates. All the ultimate load results for the load applied at s=L were lower than for the load applied at s=L/2 and are in agreement with the results of series 5.

4.1.5.2. Deflection results

The vertical and mid-lateral deflections are given in Table A.3.5. All the specimens with the load applied at s=L/2, the vertical

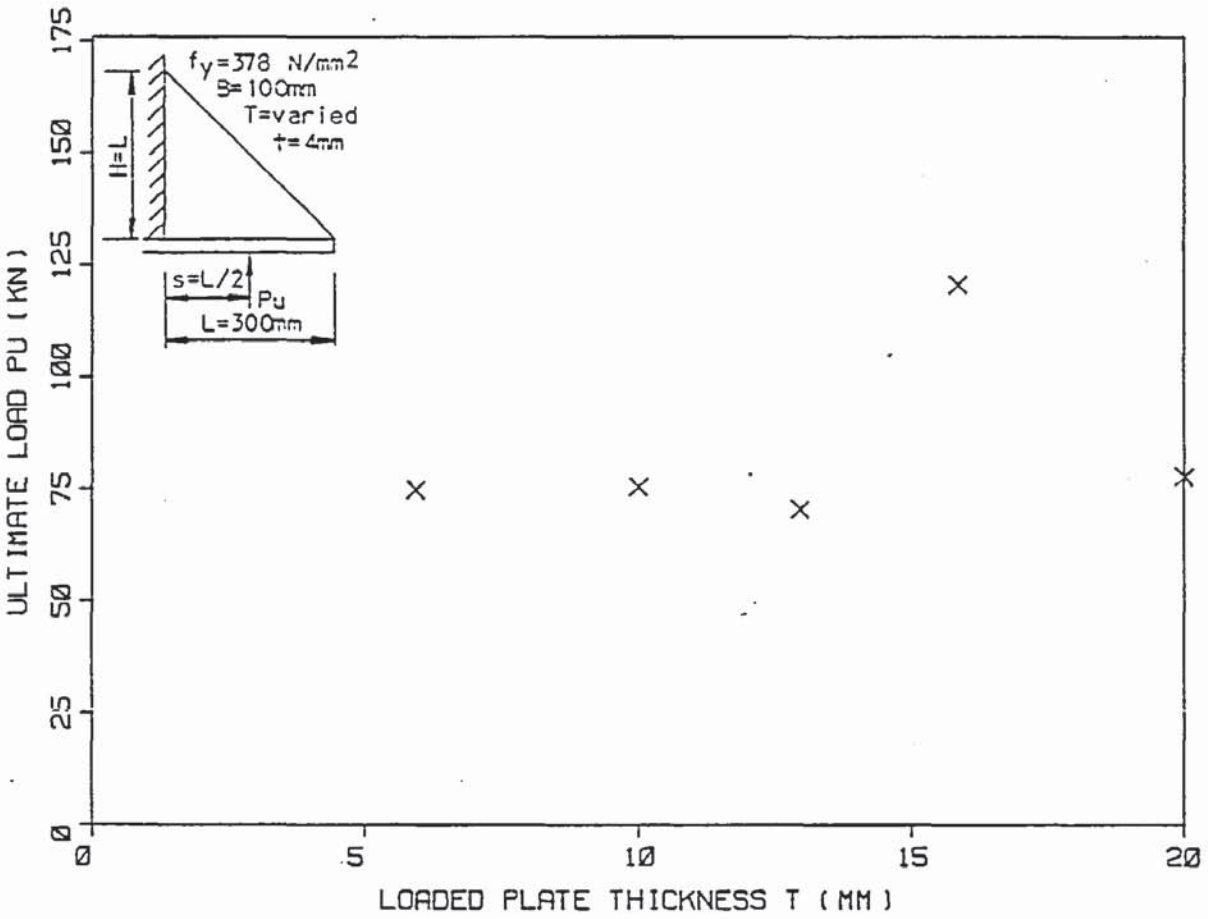

Figure 4.7 Relationship between the ultimate load P_u and the loaded plate thickness T, for s=L/2 (series 7).

deflections were of a similar nature and varied as for previously tested specimens with the same dimensions and load conditions in series 3, 5 and 6. All the specimens had small non-linear vertical deflections. The specimens with the thinnest loaded plate of 6mm did show a slightly increased rate of vertical deflection of the linear section in comparison with the others. The vertical deflections of the specimens with the load applied at the outer edge of the loaded plate were also similar to those of comparable specimens in series 5 and 6. All the specimens tested with the load applied at the end, including those in series 5 and 6, were linear to a load of 20kN. The exception was the thinnest loaded plate specimen of 6mm in this series, which was linear to 13kN. The rate of deflection of the

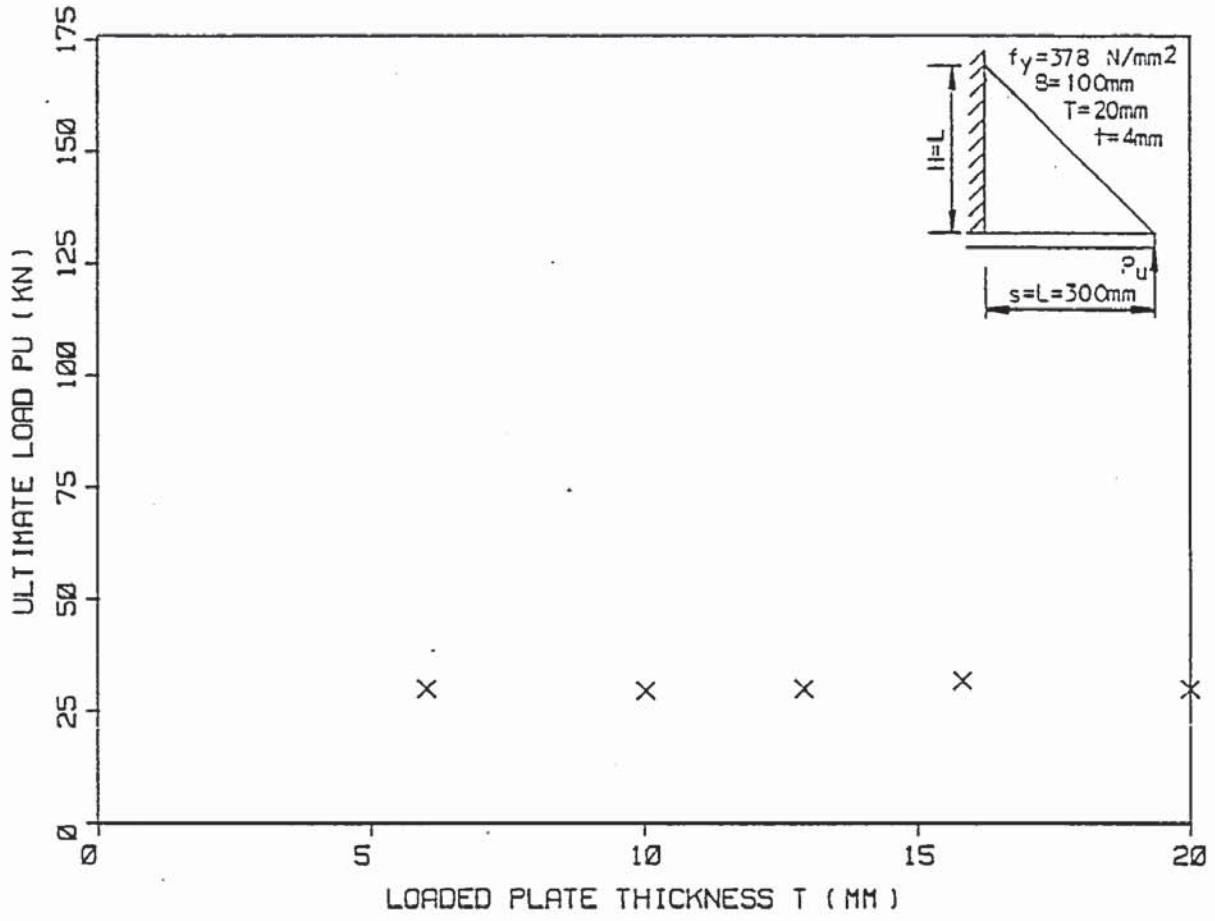

Figure 4.8 Relationship between the ultimate load P_u and the loaded plate thickness T, for s=L (series 7).

linear section for the specimens with 16 and 20mm loaded plates were the same as those tested in series 5 and 6. The deflection rates of the 13 and 10mm loaded plates were slightly greater, with the 6mm loaded plate specimen being even greater still. The non-linear deflections were virtually all the same except for the 6mm loaded plate specimen which was considerably higher. The non-linear deflection of the appropriate specimen in series 6 was greater and it supported a greater load.

The usual distortions associated with the welding were visible in these specimens with the gusset plate having a slight initial lateral deflection along the free edge. The thin loaded plates also exhibited distortion associated with the welding. The mid-lateral deflections

of the specimens with s=L/2 were as variable as with other series. Neglecting the 16mm loaded plate specimen, which appeared to be an abnormally strong specimen, it appears that the lateral deflections at the mid-point of the free edge increased with an increase in the loaded plate thickness. However, the lateral deflection results of the 20mm specimen do not agree with those of series 6. It is interesting to note that the lateral deflection of the 16mm loaded plate specimen, with the abnormally high strength, was relatively small for most of its loading and actually changed direction close to the ultimate load.

The mid-lateral deflections of the specimens with the load applied at the end of the loaded plate were not the maximum lateral deflections of the free edges, except for the 20mm thick loaded plate specimen, which was similar to those tested in series 5 and 6. As a result, the others did not show as much lateral deflection.

4.1.5.3. Failure modes

The mode of failure of the gusset plates with the load applied at s=L/2 was similar to that of previous tests. From observation and the deflection profile results of the 10mm loaded plate specimen, as given in Table A.3.5, the loaded plates deflected into a concave profile on the underside, adjacent to the applied load. This deflection was more noticeable with the thinner loaded plates and as a result the outer free edge of the gusset plates, did not deflect as much laterally. The loaded plates after failure were bent at the inside corner of the gusset plates and were concave on the underside.

The failure modes of the specimens with the load applied to the outer edge of the loaded plate failed in a different manner, as follows. The specimen with the 20mm plate failed similarly to that of the series 6, as would be expected. As the thickness of the loaded plate decreased, the length of the loaded plate which curved and the

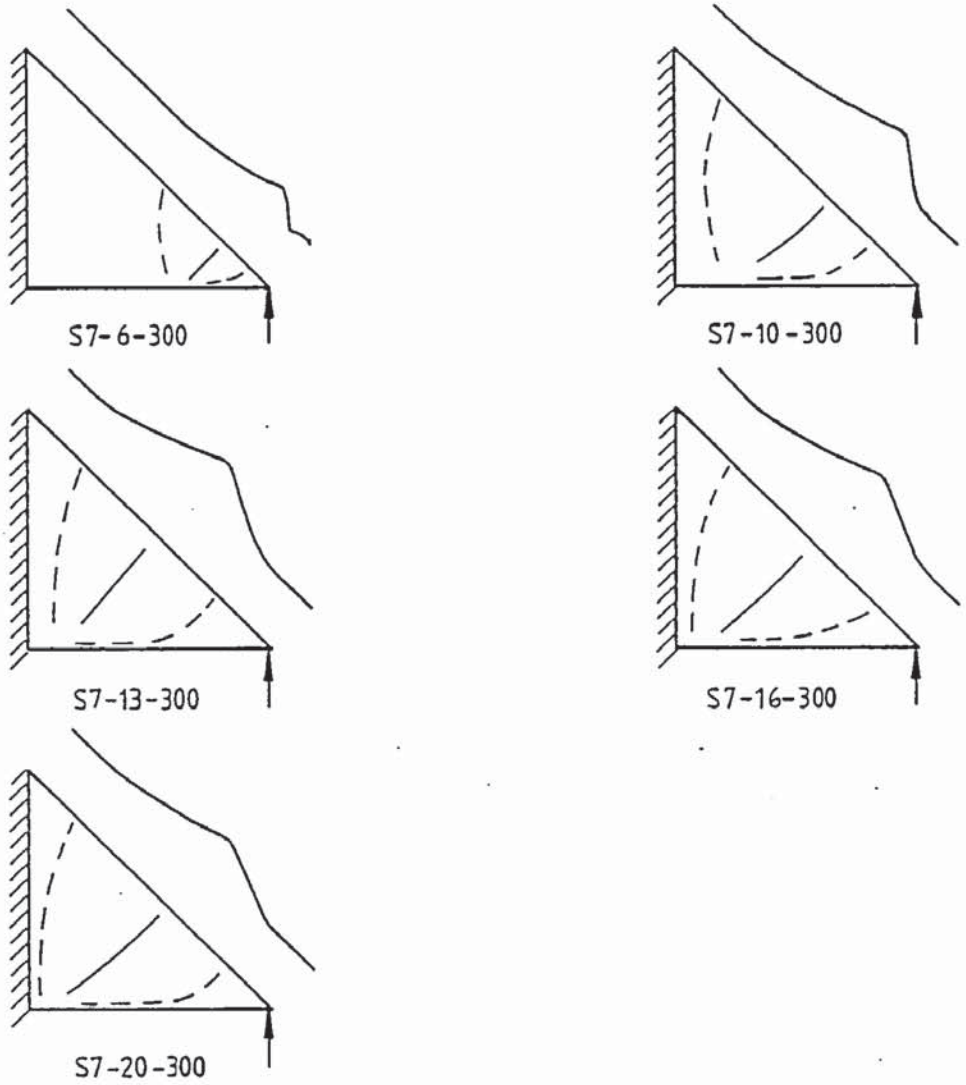

Figure 4.9 Gusset plate fold line patterns (series 7).

area of gusset plate which buckled both decreased. For a thin loaded plate only the length of the loaded plate and area of gusset plate nearest the load point were involved. That is, the loaded plate only transmitted load to a short length of the gusset plate at the end where the load was applied as shown in Figure 4.9. With the smallest gusset plate only the end 110mm was affected. As the point of maximum deflection along the free edge of the gusset plate moved towards the end of the loaded plate, the mid-lateral deflections of the gusset plates reduced with a reduction in the loaded plate thickness.

4.1.5.4. Strain gauge results

Strain gauges were placed across the width of the gusset plate of specimen S7-10-150-1. The average stresses were calculated and are given in Table A.5.11.

Strain gauges were also placed across various sections along the length of the loaded plate of specimen S7-10-150-1 and at the supported end of specimens S7-6-150-1, S7-16-150-1 and S7-13-150-1. The results are given in Tables A.5.26 to A.5.29. The results from specimen S7-10-150-1 indicated a diminishing net tensile stress up to the load point. The bending stresses for all of the tests at the supported end of the loaded plate were relatively low prior to the gusset plate failing.

4.1.6. Gusset plate thickness, t (series 12)

4.1.6.1. Ultimate load results

Initially each loaded plate was terminated at the bottom of the vertical support and connected to it by a lateral weld. However for two of the initial six specimens, these lateral welds failed before complete failure of the gusset plates had occurred. The weld failure loads are, therefore, low and the other two tests where the gusset plates failed completely are slightly higher. The specimen dimensions and the ultimate load results are given in Table A.2.6.

The relationship between the failure load P_u and the thickness of the gusset plate is shown in Figure 4.10 which shows an increase in the failure load with an increase in the gusset plate thickness. The 13mm gusset plate was the first to be tested and the lateral loaded plate weld failed before the gusset plate had failed completely. The failure of the weld may have also induced premature buckling, contributing further to a reduced ultimate load. After this loaded plate weld failure the loaded plates of the 9 and 11mm gusset plates were welded together with an 8mm butt weld and the loaded plate of the

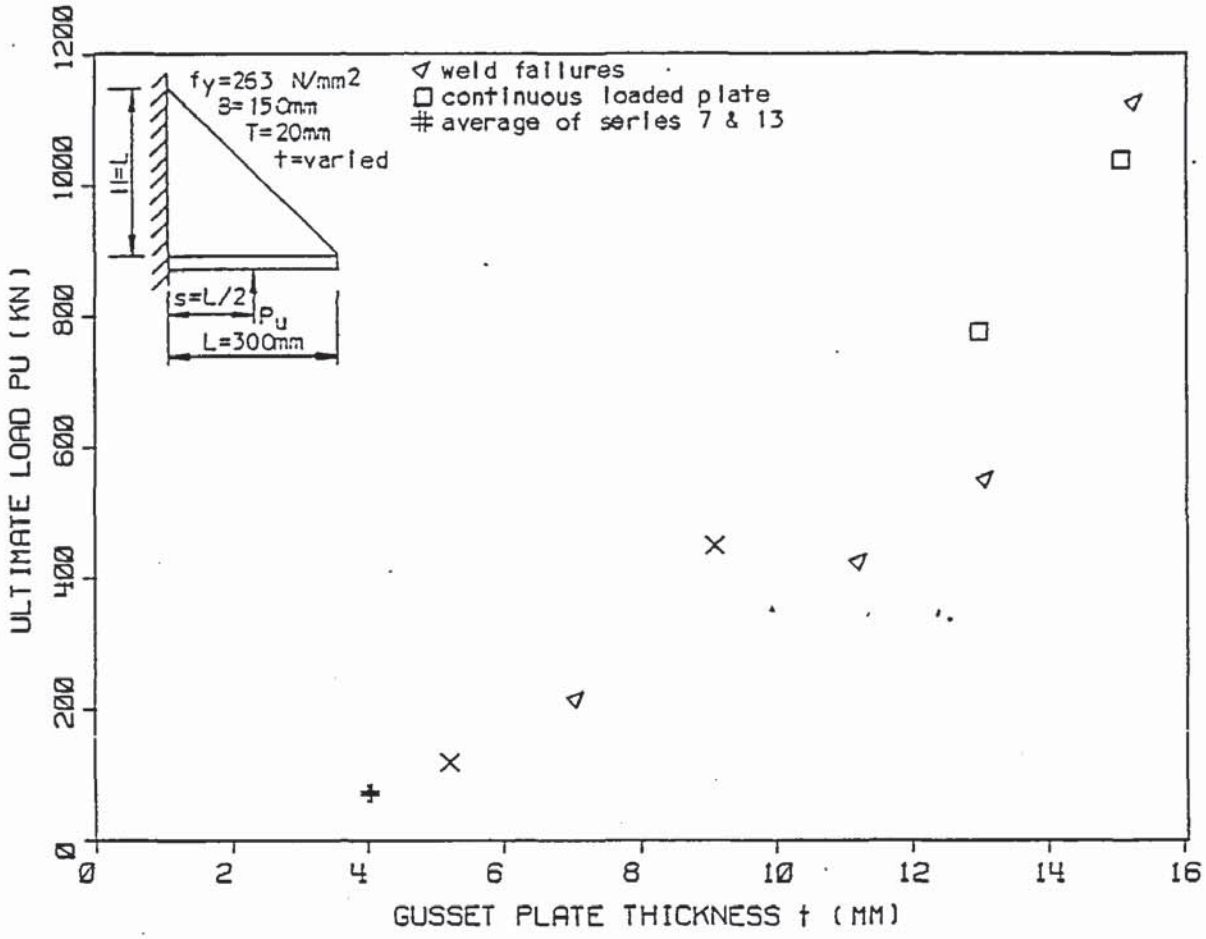

Figure 4.10 Relationship between the ultimate load P_u and the gusset plate thickness t (series 12).

15mm gusset plate with a 15mm butt weld. However, weld failure still occurred with the 11mm and 15mm gusset plates. The 9mm gusset plate appeared to fail as previously described and the 15mm gusset plate was also very close to failure when the loaded plate weld failed. The 11mm gusset plate, however, had not deflected laterally to any appreciable extent when the loaded plate weld failed, which in turn caused the gusset plate to buckle, giving a low ultimate load. The load at which the loaded plate weld of the 11mm gusset plate failed was approximately the load at which the 9mm gusset plate failed, which was the adjoining gusset plate in the testing arrangement using the same weld sizes. This suggests that the loaded plate weld of the 9mm gusset plate was also very close to failing when the gusset plate failed.

The 5mm gusset plate specimen failed in the normal manner without any weld failures. With the 7mm gusset plate, the lateral loaded plate weld of the previously tested side failed at the same time. As the same weld size was used for the loaded plate of the 7mm gusset plate, then it is quite possible that this weld was also very close to failure and had an influence on the failure of the gusset plate. This failure load, therefore, may not have been the full ultimate load of the gusset plate.

To obtain gusset plate failures as intended, rather than the loaded plate weld failures, two more gusset plates were tested, which were identical to the 13 and 15mm thick gusset plate specimens, except for the loaded plates which were continued through at the bottom of the vertical support. The results of series 7, investigating the loaded plate thickness, indicated that the bending resistance of the loaded plates had very little, if any, effect on the ultimate load. Complete gusset plate failure occurred with the 13mm gusset plate but, the supported side of the 15mm gusset plate failed before the gusset plate had completely failed. The gusset plate, however, was close to failure and the failure load was approximately that obtained for the previously tested 15mm gusset plate specimen. These two extra results have also been plotted with the other results in Figure 4.10 and show good agreement with the results which include the low weld failure results.

4.1.6.2. Deflection results

The usual distortion associated with the welding were most noticeable with the thinner gusset plates with the outer free edges showing a slight initial lateral curvature. The thicker gusset plates appeared to be less affected, with very little distortion visible.

The vertical and mid-lateral deflections are given in Table A.3.6. The vertical deflections of each specimen exhibited the usual

initial settlement deflection with an approximately linear middle section. The deflection rate of this middle section varied for each plate thickness. The thicker the gusset plate, the lower the deflection rate. However, the experimental results were not very consistent, possibly due to the weld failures. The extent of the linear portion was also not very consistent. However, it appears that the linear part extends for a smaller percentage of the ultimate load, the thicker the gusset plate. For example, with the 5mm gusset plate the linear portion extended for at least 80% of the ultimate load while for the 15mm gusset plate the linear section extended for only 60 - 70% of the ultimate load. Beyond the linear section, the rate of the vertical deflection increased slowly at first and then rapidly with the deformation of the gusset plate close to the ultimate load. For the thin gusset plates, this non-linear deflection was small before the specimen collapsed at the ultimate load. This behaviour agrees with similar 4mm thick gusset plates previously tested. With the thicker gusset plates, however, a larger amount of deflection occurred before the ultimate load.

From the readings of the mid-lateral deflection of the free edges of the gusset plates, the gusset plates generally remained virtually straight for at least the range of the linear part of the vertical deflection. The lateral deflection then increased slowly at first and then rapidly as the ultimate load approached. The lateral deflections measured were not the maximum because these points did not always coincide with the mid-point of the free edge. With specimen S12-15-1 the middle fold, where the maximum lateral deflection occurred, was in such a position that the deflection gauge was measuring the displacement of the lower fold moving in the opposite direction.

In Appendix 4, the total vertical and mid-lateral deflections of specimens S12-5-1, S12-9-1 and S4-15-2 are shown in Figures A.4.7,

A.4.8 and A.4.9, respectively. These are considered to be representative of gusset plates failing normally. The three graphs show typical vertical deflection curves with the deflection rates decreasing as the gusset plate thickness increases. The graphs also show that non-linear deflections increase as the gusset plate thickness increases and that the mid-lateral deflections are relatively small until just before the ultimate load.

4.1.6.3. Failure modes

For the thinner plates the failure modes were virtually the same as with the previous series with the plates buckling and folding soon after the plates had started to deform laterally. The thicker gusset plates on the other hand still buckled from the outer free edge inwards but they appeared to deform slowly and plastically. The thicker plates were able to tolerate considerably more deformation before failure and they did not necessarily collapse at failure. In the deformed load range, the thick gusset plates continued to deform for a short period after each increment of load had been applied. The deformation eventually stabilised giving the appearance of a re-distribution of stresses within the gusset plate. With the very thick gusset plates a load was reached where the gusset plate deformed plastically, i.e. the plate maintained the load but continued to deform slowly. Further load increments could be applied with an increased rate of creep, or the load could be reduced until the deflections stabilised. This reduction in load depended upon the deformation of the gusset plate, but generally it was only necessary to reduce the load a small amount.

The effect of the weld failures is apparent on the vertical and lateral deflections. With the 5mm and 9mm gusset plates, which failed normally, there was relatively little non-linear vertical deflection. With the 7mm gusset plate, however, the progressive failing of the

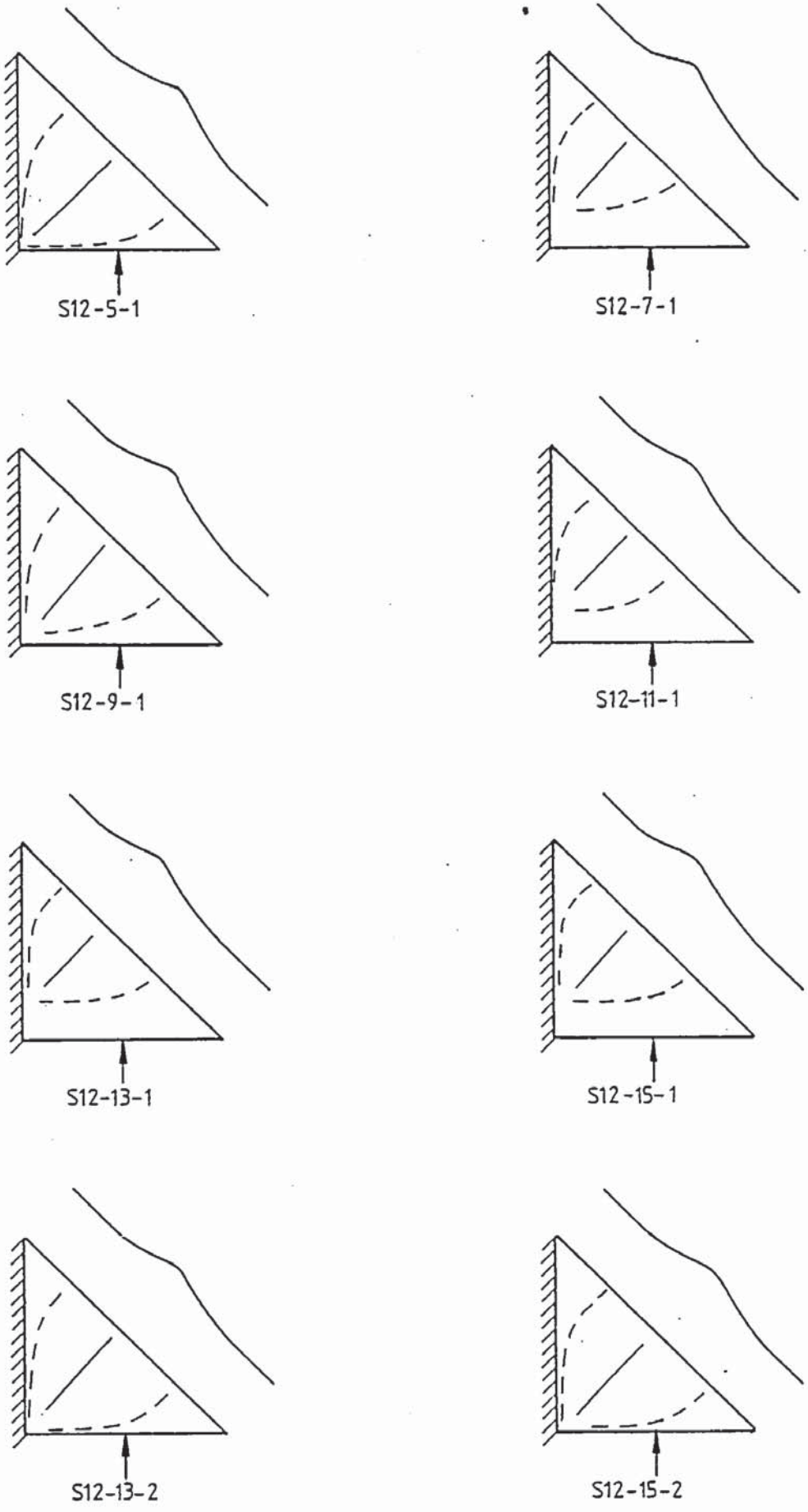

Figure 4.11 Gusset plate fold line patterns (series 12).

weld on the previously tested side showed as a larger vertical deflection with a small lateral deflection of the gusset plate. The 11mm gusset plate which had a sudden weld failure, with very little gusset plate deformation, produced a small non-linear vertical deflection and virtually no mid-lateral deflection. The non-linear vertical deflection of the 13 and 15mm thick gusset plates, which had weld failure, started at a lower load than for the 13 and 15mm thick gusset plates, which did not have weld failures. Also the non-linear vertical deflections of the 13mm gusset plate, with weld failure, progressed at a greater rate.

The fold lines at failure of the specimens were similar to the previous tests. The weld failures appeared to have influenced the position of the fold lines. The fold lines of the 5mm gusset plate and the two extra gusset plates with continuous loaded plates had the three fold lines in the normal position. However, with all of the other specimens which had failed or near failed loaded plate welds, the three fold lines were in a similar pattern but, positioned towards the top corner of the gusset plates, with the fold lines not intersecting at the inside corner of the gusset plate but, a distance along the supported edge. Approximately the bottom 50mm of the gusset plate was unaffected as shown in Figure 4.11.

4.1.7. Removal of the inside corner of the gusset plate (series 8)

4.1.7.1. Ultimate load results

The specimen dimensions and ultimate load results are given in Table A.2.7. The relationship between the ultimate load P_u and the width G of the gusset plate with the load applied at s=L/2 and at the centre of the remaining loaded edge of the gusset plate are shown in Figures 4.12 and 4.13 respectively. The experimental results with the load applied at the centre of the loaded edge (s=L/2) indicate no reduction in the strength of the gusset plate with up to 36% of the

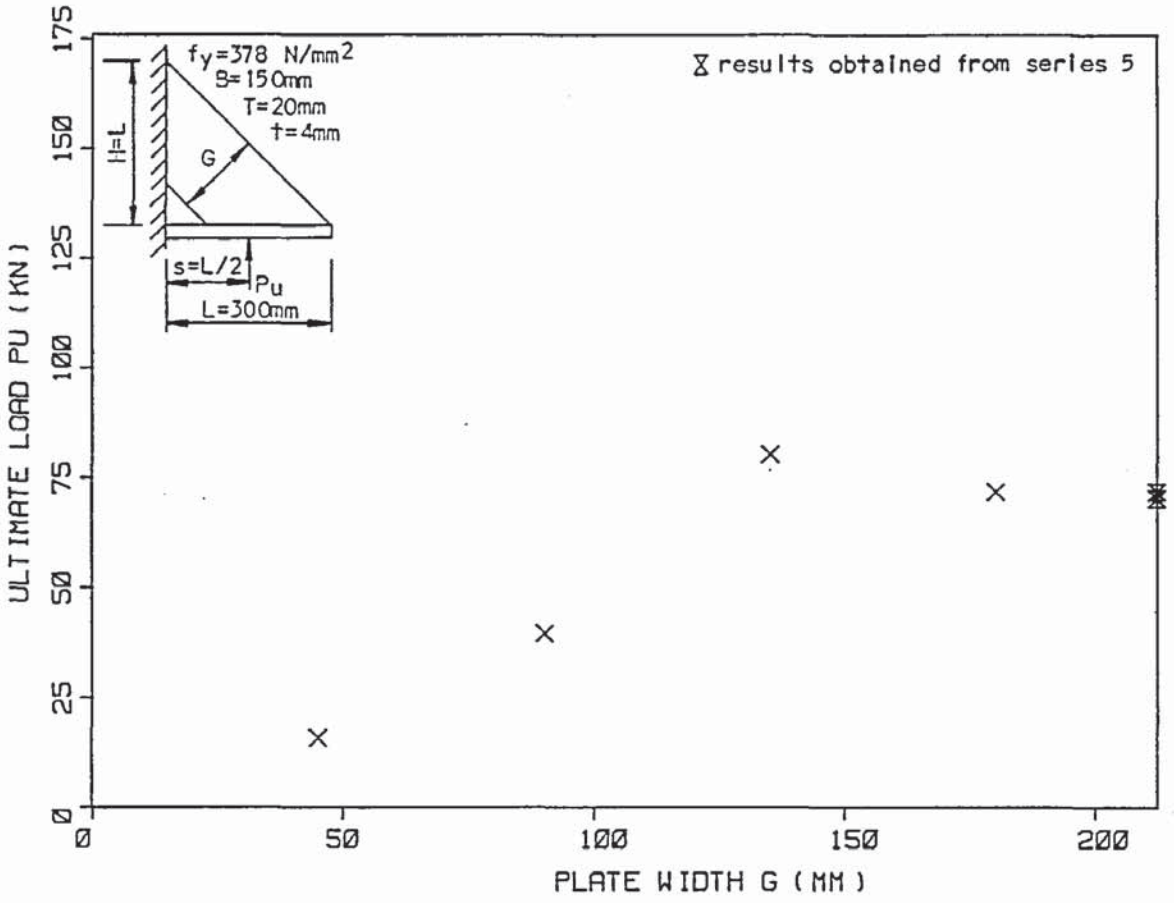

Figure 4.12 Relationship between the ultimate load P_u and the remaining gusset plate width G, for s=L/2 (series 8).

inside corner removed (i.e. G=135mm). This also corresponds to the maximum load. Beyond this amount the strength reduces with a reduction in the remaining area of gusset plate. The experimental results with the load applied at the centre of the remaining loaded edge of the gusset plate indicate a reduction in strength with a reduction in the remaining area of the gusset plate. This curve also indicates a relatively high strength for the gusset plate with up to 36% of the inside corner removed, but it should be noted that the point of application s moved out towards the free edge of the gusset plate as the remaining amount of the gusset plate G decreased.

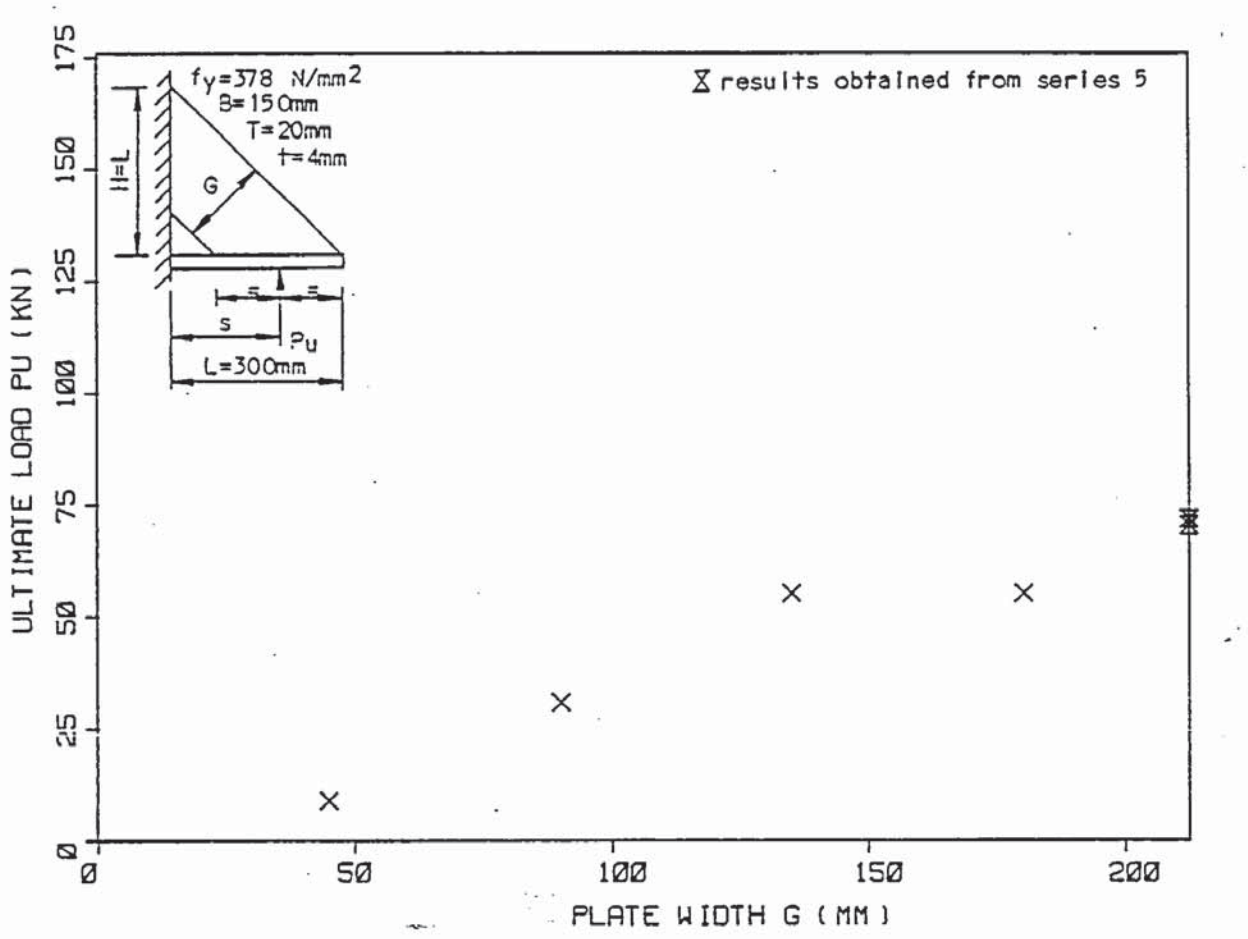

Figure 4.13 Relationship between the ultimate load P_u and the gusset plate width G, for the load applied at the mid-point of the gusset plate (series 8).

4.1.7.2. Deflection results

The vertical and mid-lateral deflections are given in Table A.3.7. The vertical deflections were characterised by an initial settlement followed by a linear section which in all but two instances continued to failure. These two instances were for the gusset plates with G=180, where there was a small amount of non-linear deflection similar to the full plates. With both loading positions the vertical deflection rate of the linear section changed with the remaining width of gusset plate. The deflection was greatest with the narrowest width of gusset plate and least with G=135mm which was the strongest plate. The larger widths of gusset plate showed a slight increase in the deflection rate. Although the load positions were different, there

was very little difference in the deflection rates of the two sets. The plates with the loading position at the mid-point of the remaining gusset plate were slightly greater than the other loading position.

The distortions associated with welding were apparent in all of the specimens producing some initial lateral deflection of the free edges which appeared to influence the amount and rate of the mid-lateral deflection during the tests. All the plates deflected in the same direction as the initial lateral deflection, and the mid-lateral deflections during testing were very similar for both loading positions. The amount of lateral deflection that occurred before failure was noticeably greater for both sets of the G=180mm gusset plates and the full gusset plates. The others had approximately the same amount of deflection before failure.

In Appendix 4 the total vertical and mid-lateral deflections of specimens S8-45-2, S8-135-2 and S8-180-2 are shown in Figures A.4.10, A.4.11 and A.4.12 respectively . These are representative of the specimens with the load at s=L/2, and are very similar to the specimens with the load at the mid-point of the remaining loaded edge. The result for the complete gusset plate is also very similar to that of specimen S8-180-2.

4.1.7.3. Failure modes

The modes of failure of the specimens were similar for both loading positions. The 45 and 90mm specimens deflected laterally across the width, with a greater deflection along the outer free edge, i.e. the strip twisted slightly. Close to failure the strip took up an elastic deformed buckled shape which finally yielded, buckled and folded up along three well defined fold lines. The other two larger plates deformed laterally from the free edge first and worked inwards similar to a complete gusset plate. Finally the specimen buckled and folded up along three well defined fold lines similar to the full

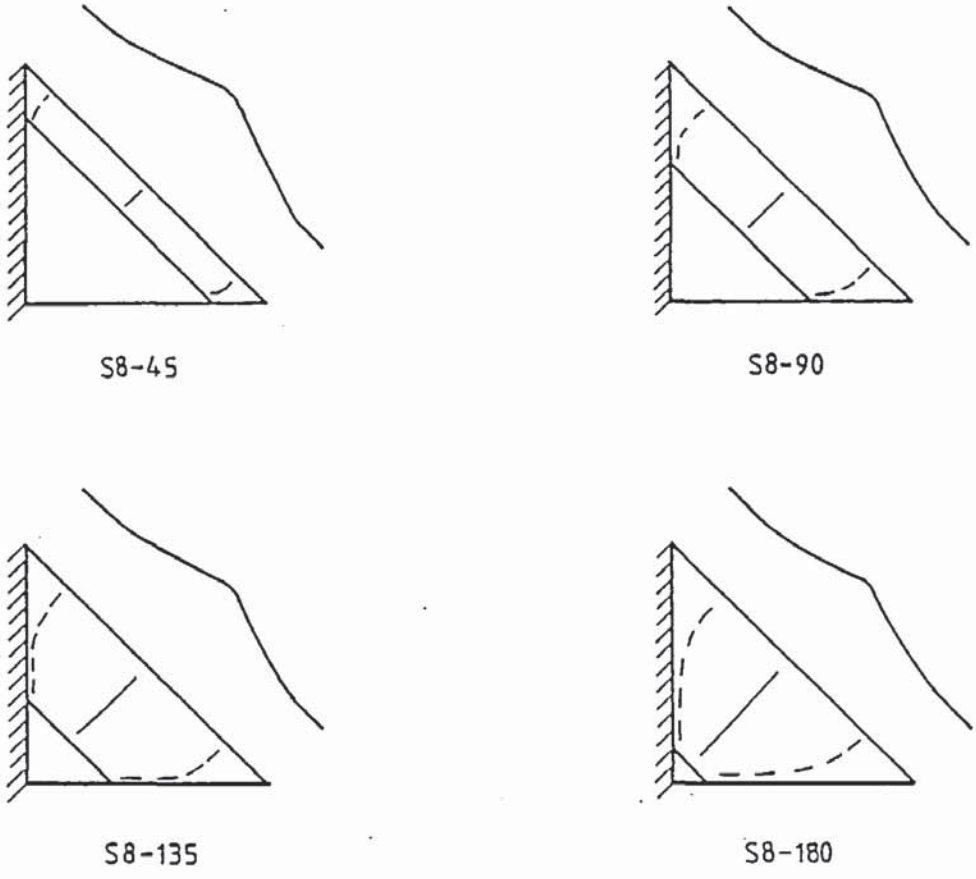

Figure 4.14 Gusset plate fold line patterns (series 8).

gusset plate.

The fold line patterns for the 135 and 180 mm specimens were similar to the corresponding area of the full gusset plate. The two smaller gusset plates of 45 and 90 mm produced loaded and supported edge fold lines further out towards the ends of the free edges. These fold lines were curved, following the fixed edges to the centre line of the strip of gusset plate and then ran perpendicular to the free edge. The fold line patterns are shown in Figure 4.14.

4.1.8. Variation of the internal angle θ between the loaded and supported edges (series 13)

4.1.8.1. Ultimate load results

The specimen dimensions and the ultimate load results are given in Table A.2.8. The relationship between the failure load P_u and the

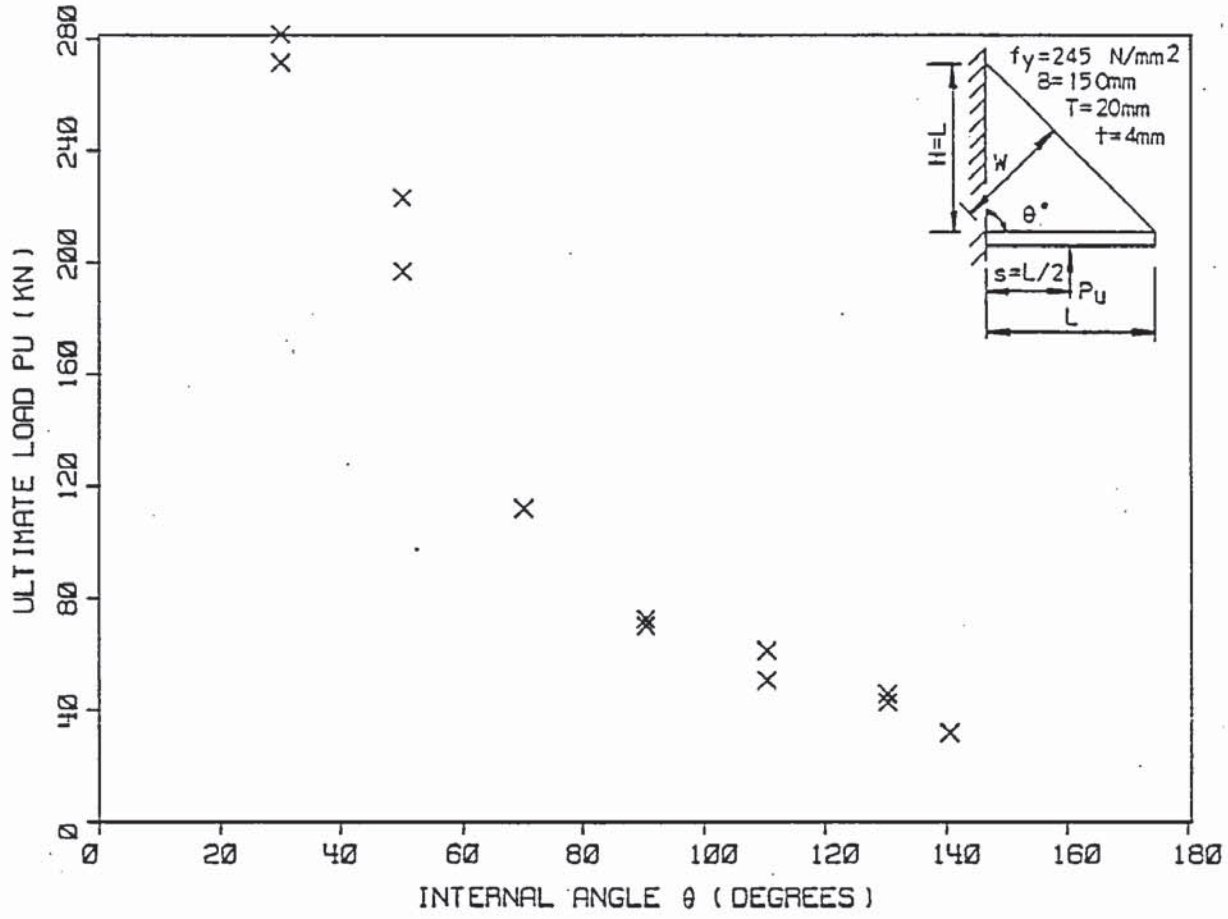

Figure 4.15 Relationship between the ultimate load P_u and the internal angle θ (series 13).

internal angle θ between the fixed edges is shown in Figure 4.15. The ultimate loads for each pair of nominally identical specimens are in good agreement with each other. The results are reasonably consistant showing a decrease in the ultimate load as the angle increases from 30° to 140°. Taking the 90° angle as reference, the failure load increases considerably as the angle reduces to 30°, with an approximate 385% increase. As the angle increases from 90° to 140° the reduction is less, the 140° specimen is 45% of the 90° specimen.

4.1.8.2 Deflection results

The vertical and mid-lateral deflections are given in Table A.3.8. The vertical deflections measured in this series were not exactly the same measurement as in the previous series because of the

varying internal angle, and this makes comparison between each angle difficult. The vertical deflections measured did show a small settlement deflection followed by an approximately linear section for the majority of the specimens. Only the first specimens of the 30° and 50° gusset plates showed any significant amount of non-linear vertical deflection. The first specimens of the 110° and 140° gusset plates had a curved characteristic which did not appear with the second specimens. All the other specimens showed virtually no non-linear vertical deflection.

The distortions associated with welding were most noticeable with the larger angled gusset plates as the size of the plate and the length of the free edge increased with the size of the internal angle. The smallest angled gusset plates exhibited very little, if any, initial lateral deflection of the free edge. From the 90° plate upwards the initial lateral deflections were noticeable, although the largest angled gusset plate of 140° did not have the largest initial lateral deflection. The initial lateral deflections of these larger plates ranged from 2 to 6mm with one of the 110° specimens having the 6mm initial lateral deflection, which was an exception. The 140° specimens had only a 2mm initial lateral deflection.

The lateral deflections during testing varied and appeared to depend on the initial deformed shape and the initial lateral deflection. The 30° and 50° gusset plates were virtually straight initially and remained so throughout the tests. The other specimens deflected laterally from the initial loading and progressively increased to give relatively large lateral deflections before failure. All of the specimens deflected in the direction of the initial lateral deflection. Generally the rate of lateral deflection increased with an increase in the internal angle.

In Appendix 4 the total vertical and mid-lateral deflection of

specimen S13-30-1, S13-70-2 and S13-140-2 are shown in Figures A.4.13, A.4.14 and A.4.15 respectively. These are chosen to represent the series, with the other results being a transition between these. Specimen S13-30-1 shows little mid-lateral deflection until just before failure, and then it is not excessive. Specimen S13-140-2 on the other hand shows the mid-lateral deflection starting from the initial loading with a much larger deflection before failure. Specimen S13-70-2 has a little more lateral deflection than specimen S13-30-1 but still not excessive before failure. The deflection rate of the linear section of the vertical deflection can be seen to increase with the internal angle and appears to be related to the ultimate load. Although specimen S13-30-1 shows a non-linear vertical deflection most of the other gusset plates have very little as shown with specimen S13-70-2. Specimen S13-140-2 also has a relatively small non-linear vertical deflection.

4.1.8.3. Failure modes

The failure modes were similar to those in previous series. There was very little deformation of the 30° and 50° angled gusset plates before failure. These specimens failed suddenly and folded along three well defined fold lines. The two 70° specimens failed in a more progressive manner with the gusset plates deforming laterally along the free edge from the initial loading. This lateral deflection was small for most of the loading and increased towards the ultimate load as more of the inner part of the gusset plate deflected. At the ultimate load the gusset plate buckled slowly from the outer free edge inwards. The 90° specimens behaved in a similar manner to the 90° specimens tested previously, and were similar to the 70° specimen but, with more lateral deflection before failure. The failure modes for the three largest angled gusset plates were similar. The rates of the lateral deflections were greater and as a result, and so were the

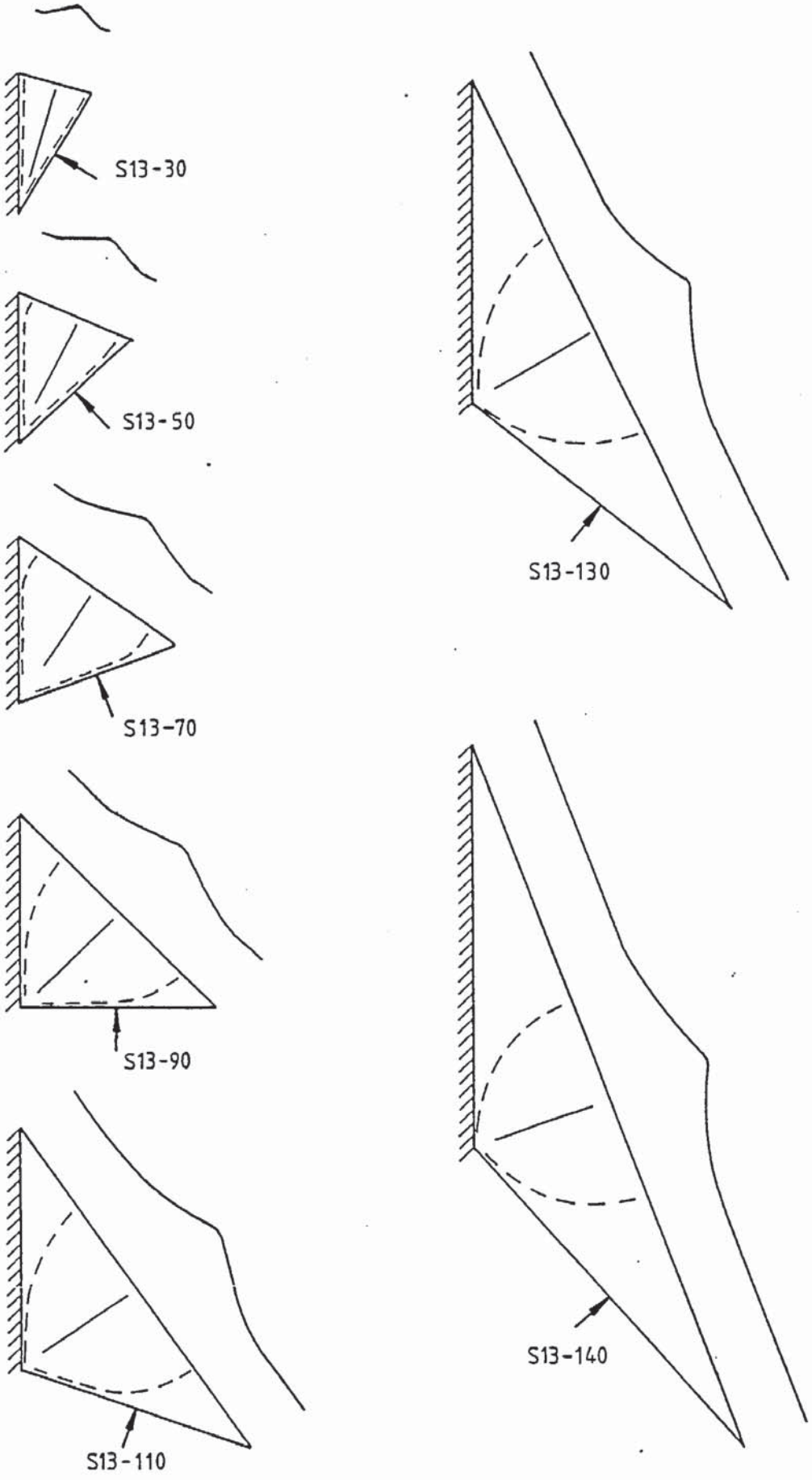

Figure 4.16 Gusset plate fold line patterns (series 13).

amount of lateral deflections before failure in comparison with the smaller angles.

At failure all the specimens had three fold lines symmetrically placed about the perpendicular bisector, as with the other series. These fold lines on the 30° plates ran along both the loaded and supported edges of the gusset plate, and the third line ran along the angle bisector. From the 50° specimens upwards the ends of the loaded and supported edge fold lines curved towards the free edge to intersect it perpendicularly. The extent of the curved section increased with the angle. The middle fold line was always approximately along the perpendicular bisector and the other two fold lines tended to intersect the free edge perpendicularly. This tendency produced failure of the central section of the gusset plate. The size and shape of the pattern of fold lines for the three largest plates greater than 90° were very similar. The extra gusset plate material towards the outer ends of the loaded and supported edges had little effect on the fold line pattern in these cases. The fold line patterns of the 70° and 90° specimens were effectively a transition from the small angled gusset plates to the larger ones, with the pattern gradually increasing. The fold line patterns are shown in Figure 4.16.

4.1.8.4 Strain gauge results

Strain gauges were placed on some of the gusset plates to measure the stresses across the width of the gusset plate and along the free edge. The average stress results are given in Tables A.5.12 to A.5.18. The significance of these results will be described later.

4.1.9 Comparison of ultimate load results between each series

In each series of tests there was usually at least one specimen that was similar to a specimen in another series. This was done to

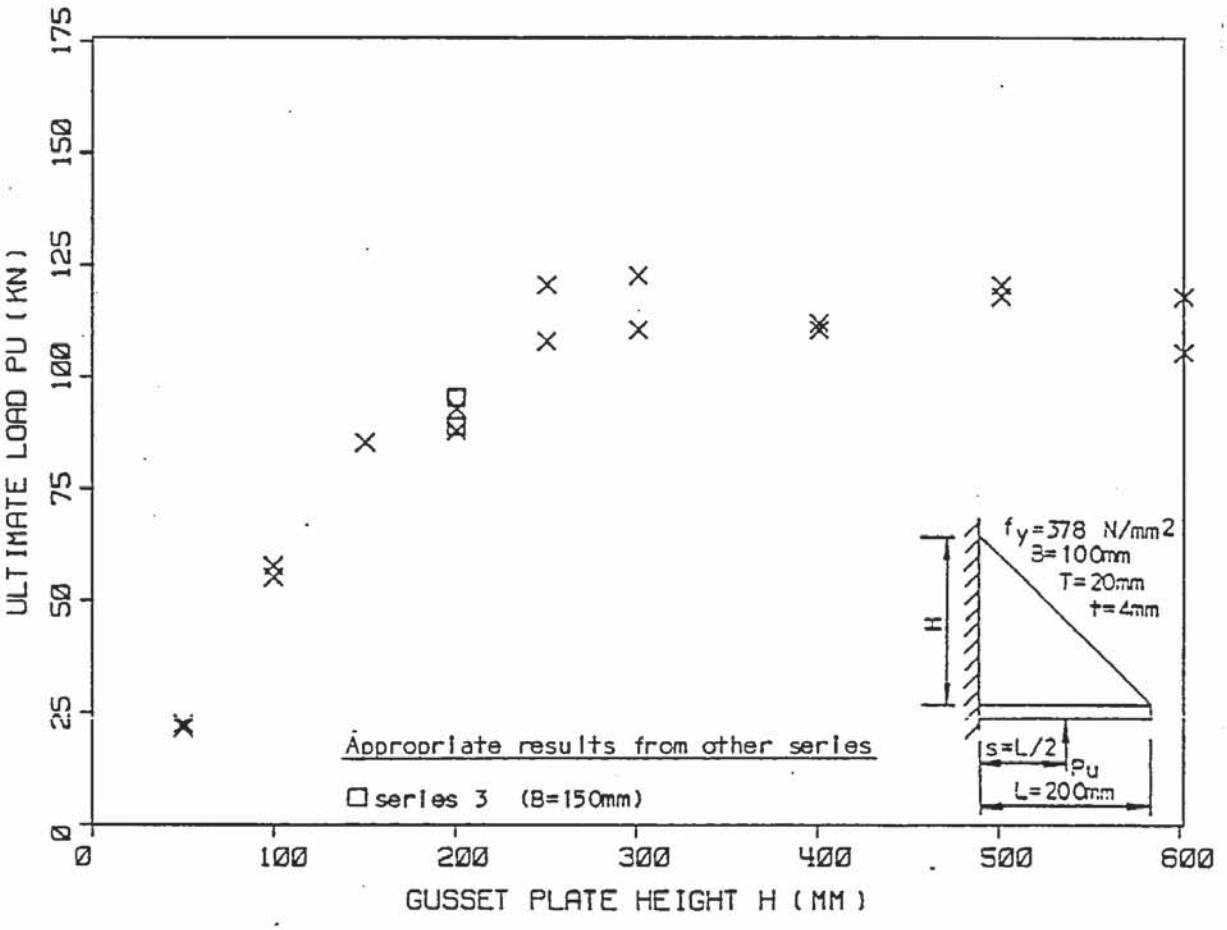

Figure 4.17 Relationship between the ultimate load P_u and the gusset plate height H for s=L/2 (series 3) with points plotted from other series.

provide some form of reference between all of the series of tests. In this section the related specimens from the different series are compared.

In series 3 (L=H varied), and series 4 (H/L varied), specimens S3-200-1/2 and S4-200-1/2 were the same except for the widths of the loaded plates, which were 150 and 100mm respectively. The series 3 results are plotted with the series 4 results in Figure 4.17, and the series 4 results are plotted with the series 3 results in Figure 4.18. The failure loads for the two sets of results are approximately the same and compare well with the rest of the results in the series. The results indicate that there is no significant difference between using 100 or 150mm wide loaded plates which terminates at the vertical

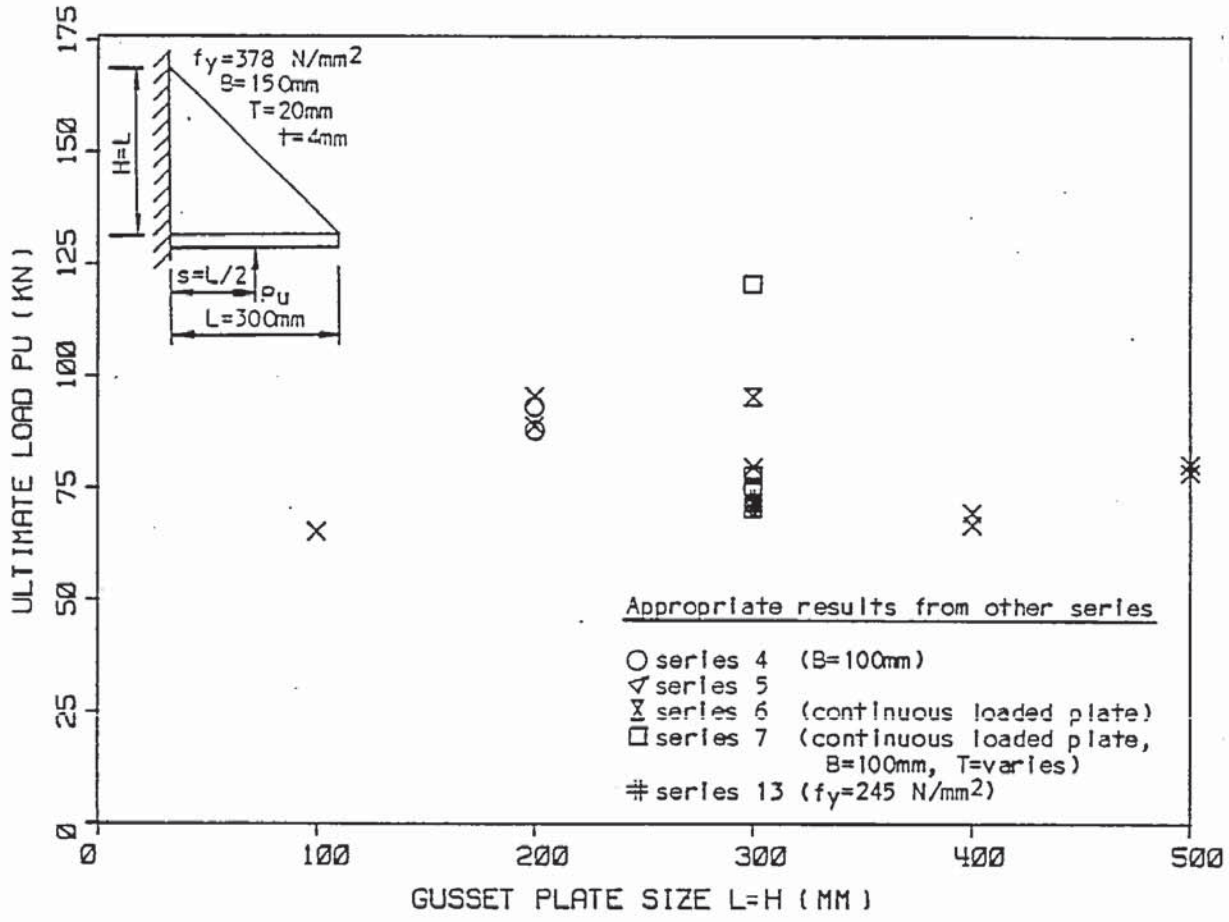

Figure 4.18 Relationship between the ultimate load P_u and the gusset plate size L=H for s=L/2 (series 4) with points plotted from other series.

support.

There were a number of specimens which were similar to the series 3 specimen with t=4mm and L=H=300mm. These specimens occurred in series 5 (s varied), series 6 (continuous loaded plate), series 7 (t varied) and series 13 (θ varied). Series 8 (G varied) included the results for a complete gusset plate from series 5. For the majority of these specimens the load was placed at s=L/2 but with some the load was placed at s=L. All the results with s=L/2 are plotted with those of series 3 in Figure 4.18.

Specimens S3-300-2 and S5-150-1/2 are identical and, therefore, directly interchangeable. The failure loads for series 5 are slightly lower, but close to that of series 3.

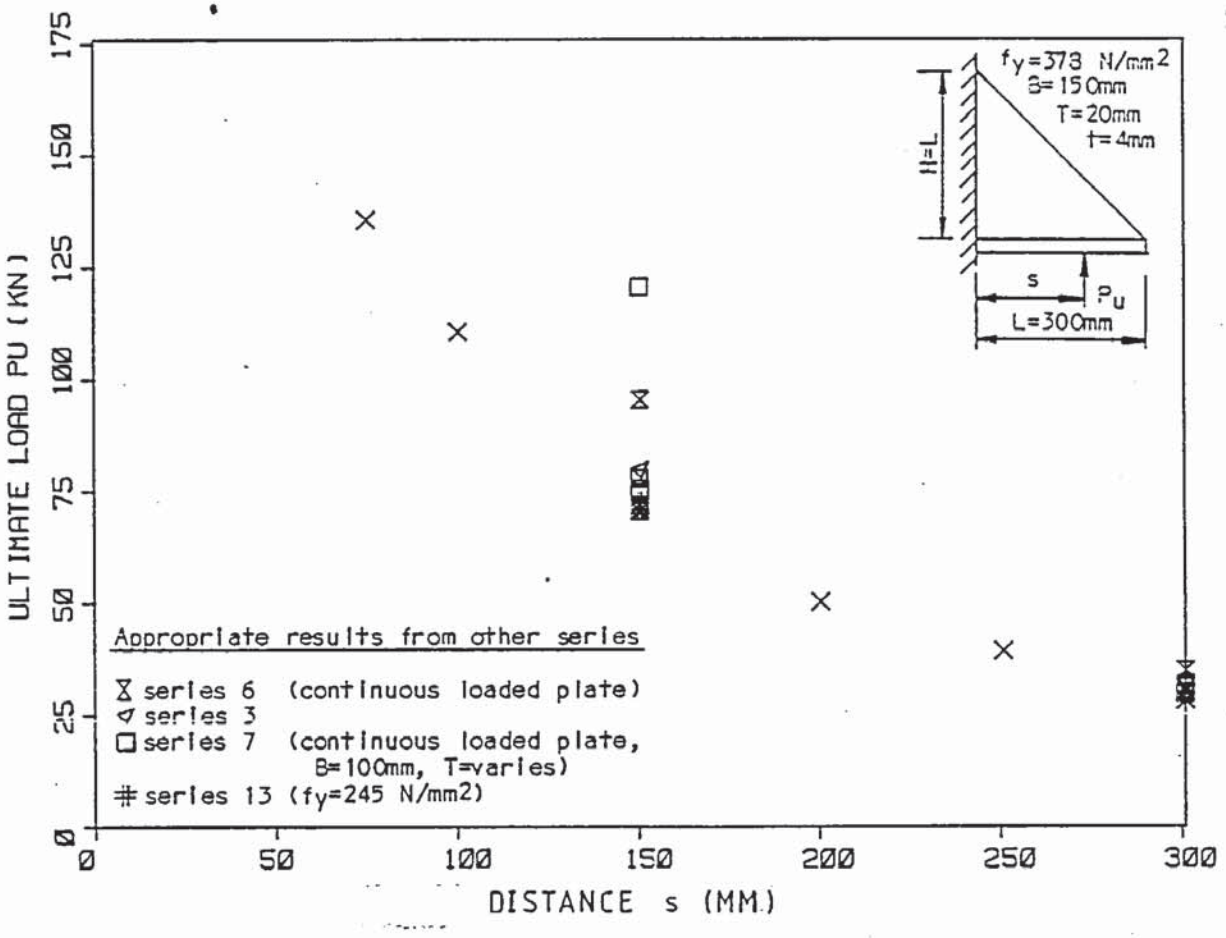

Figure 4.19 Relationship between the ultimate load P_u and the distance s of the applied load (series 5) with points plotted from other series.

Specimen S3-300-2 and S6-150-1 were similar except that the loaded plate of S6-150-1 was continuous. This result is approximately 20% higher than the series 3 result.

Specimens from series 7 with s=L/2 differed from specimen S3-300-2 by having 100mm wide loaded plates, as compared with 150mm, which were continuous and of different thicknesses. However, three of the results are approximately the same as the series 3 results, one is slightly lower and about the same as the series 5 results, and another is 50% higher than all the other results. This result is also found to be unusually high in the series 7 results as well and is, therefore, considered to be an abnormally high load.

Specimen S13-90-1/2 differed from specimen S3-300-2 by having a

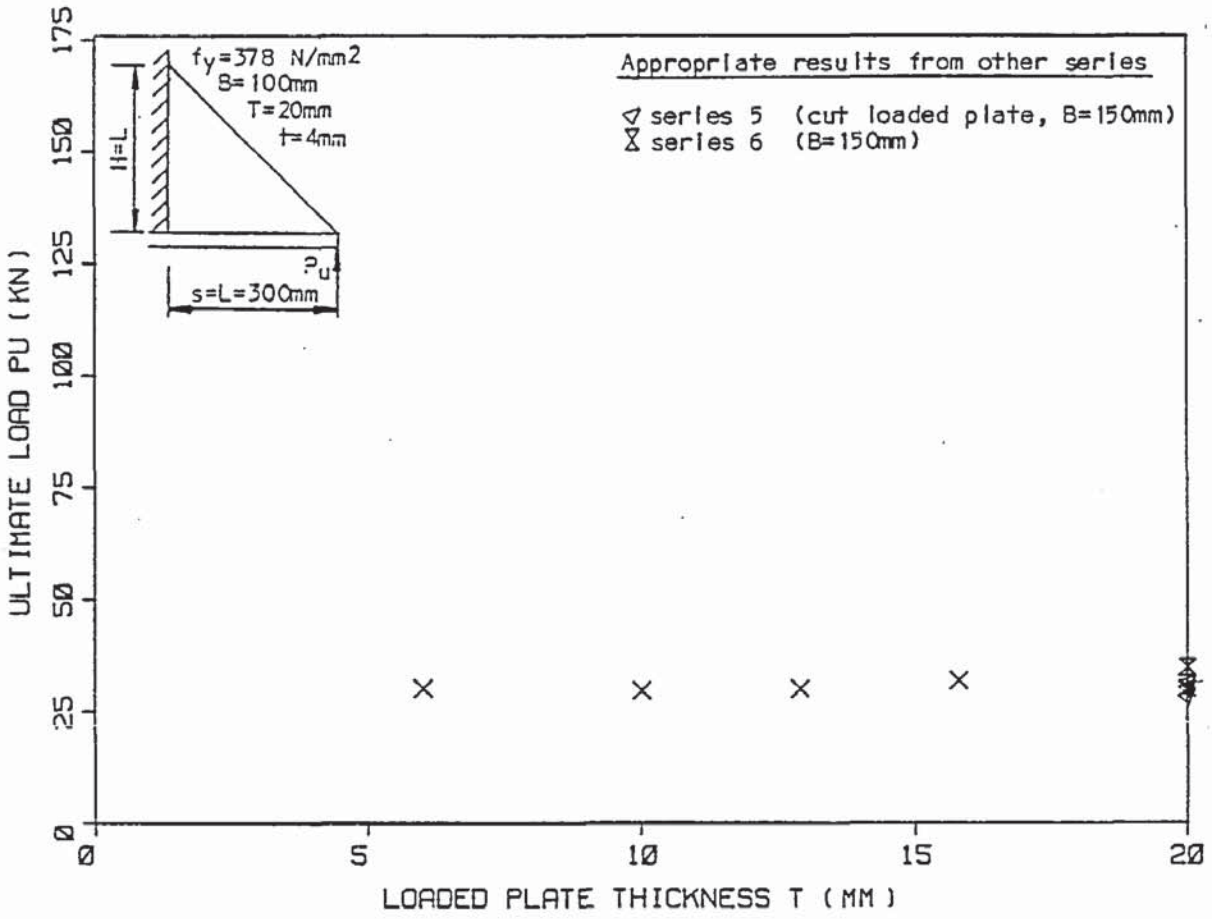

Figure 4.20 Relationship between the ultimate load P_u and the loaded plate thickness T for s=L (series 7) with points plotted from other series.

yield strength of 245N/mm^2 compared with 378N/mm^2. Despite this lower yield strength the series 13 results are only slightly lower than the series 3 results and comparable with series 5 and series 7. This suggests that for this particular plate shape, size and thickness the yield strength does not have a significant influence on the ultimate load result.

Comparing all these results with the rest of the series 3 results, suggests that the majority are similar and compare favourably with the rest of the series 3 results. The two exceptions are the unusually high results found in series 6 and 7 for specimens S6-150-1 and S7-16-150-1 respectively.

The comparable results with s=L/2 from series 3, 5, 6, 7 and 13

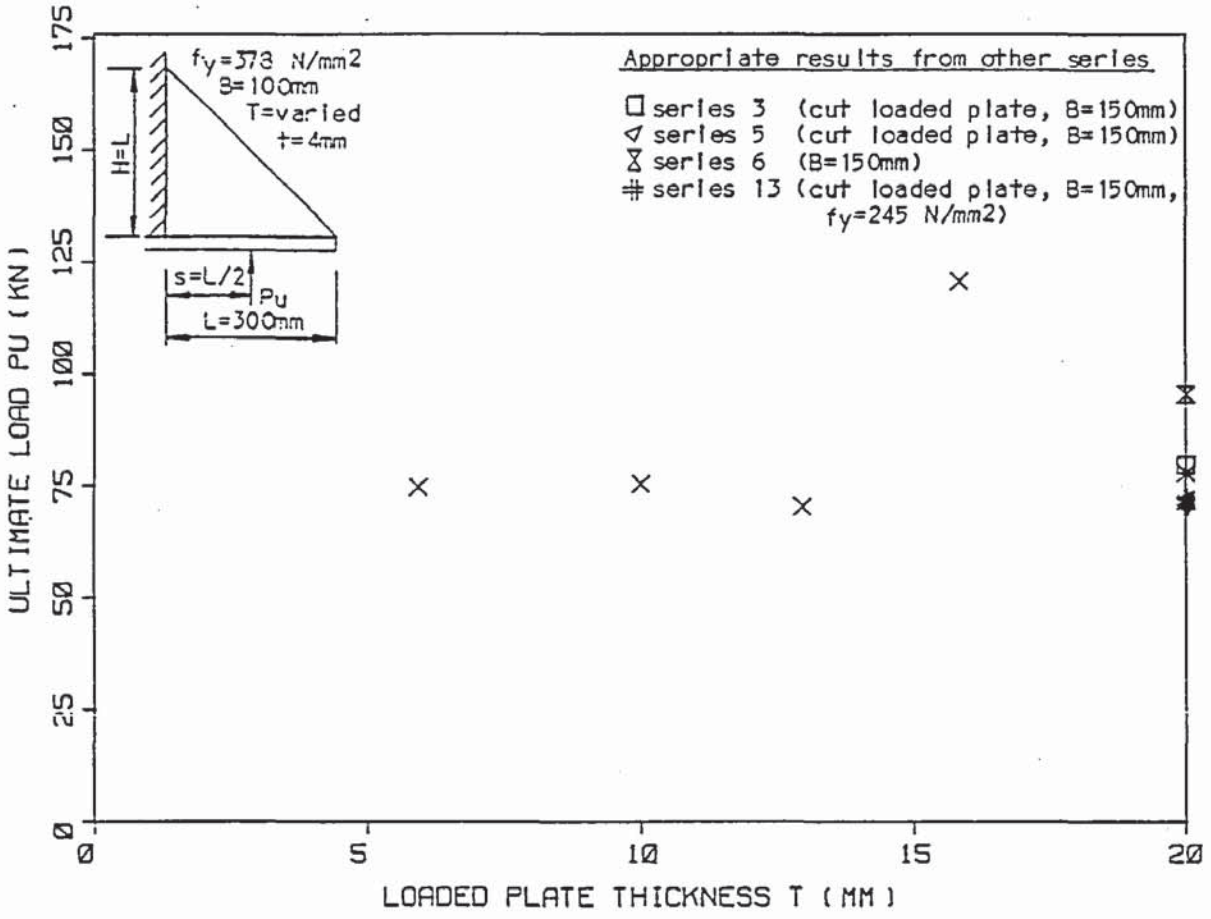

Figure 4.21 Relationship between the ultimate load P_u and the loaded plate thickness T for s=L/2 (series 7) with points plotted from other series.

have also been plotted with the results of series 5, 7, 8 and 13 in Figures 4.19, 4.20, 4.21, 4.22, 4.23 and 4.24 respectively (two graphs for series 7 & 8). The relevant specimen differences have been included with each graph. The general impression from these graphs is that the majority of the set of results with s=L/2 compare favourably for all of these series. This includes series 13 where the specimens had a different yield strength. The two unusually high results of specimens S6-150-1 and S7-16-150-1 were the exception for these series of tests.

For the set of specimens with s=L from series 5, 6 and 7 the failure loads are plotted with the series 5 and 7 results in Figures 4.19 and 4.20 respectively. The results for all of those specimens

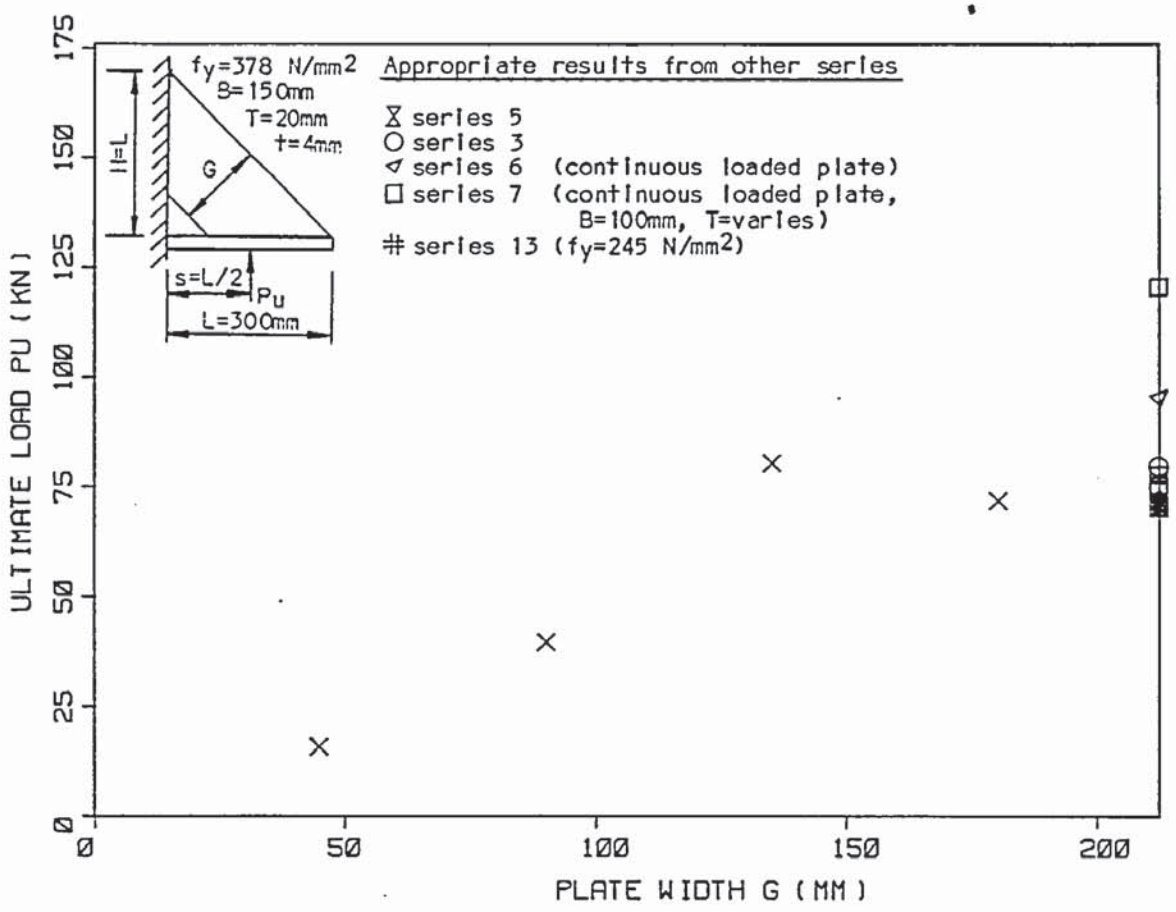

Figure 4.22 Relationship between the ultimate load P_u and the gusset plate width G for s=L/2 (series 8) with points plotted from other series.

with s=L are similar, with the results from series 6 being slightly higher than the rest. All of these results are in good agreement with those from both series 5 and 7. It is interesting to note that the results for both s=L and s=L/2 in series 5, which had cut loaded plates, and those of series 7 which had continuous loaded plates with different thicknesses, show no significant difference in their ultimate loads.

Interchanging results with series 13 suggested that the different yield strength does not have any significant influence on the failure load of the gusset plates with t=4mm and L=H=300mm. A typical failure load of 73kN for this type of plate with s=L/2, compares favourably with the results of series 12 as shown in Figure 4.24, which again

differs in yield strength.

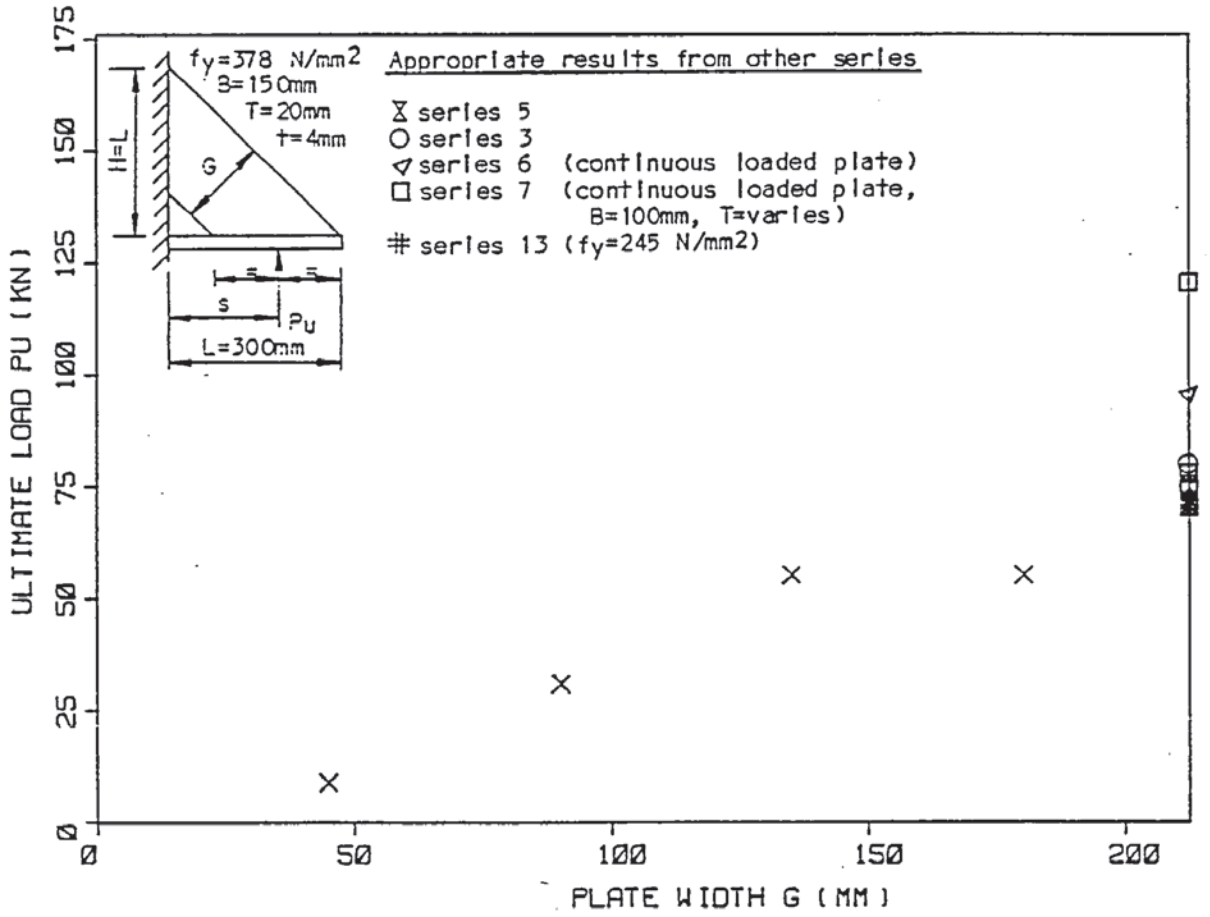

Figure 4.23 Relationship between the ultimate load P_u and the gusset plate width G for the load at the mid-point of the gusset plate (series 8) with points plotted from other series.

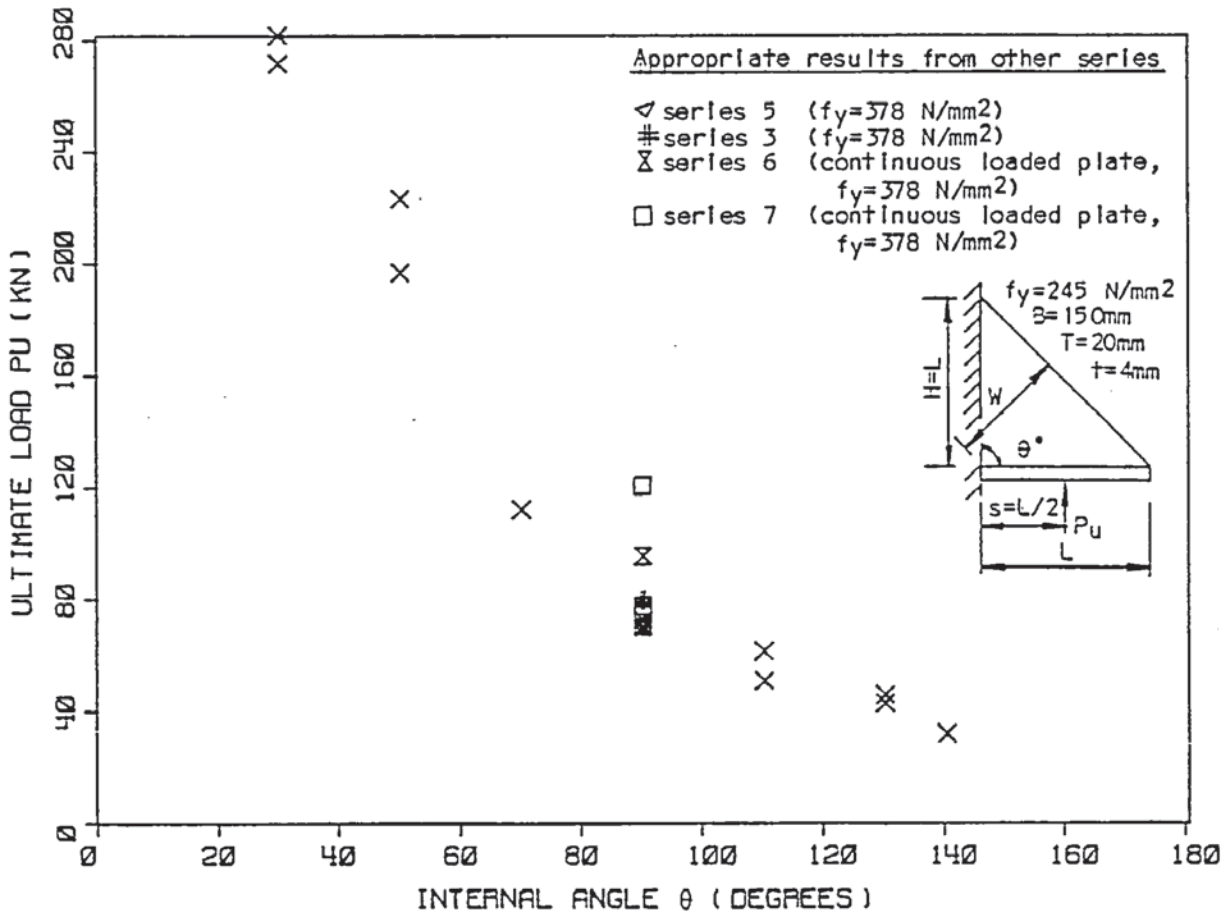

Figure 4.24 Relationship between the ultimate load P_u and the internal angle θ (series 13) with points plotted from other series.

4.2 Subsidiary test series results

This section contains the ultimate loads, deflections and strain gauge results together with the failure modes of the subsidiary test series as presented in Chapter 3 Section 3.3. Presented in this section are the experimental results for the series investigating:-

i) pin ended directly loaded strut tests (series 1)

ii) fixed ended directly loaded strut tests (series 9)

iii) inclined fixed ended indirectly loaded strut tests (series 10)

iv) multiple strip plate tests (series 11)

v) loaded plate bending resistance tests (series 2)

vi) rigid loaded plate strain gauge tests (series 5a)

The first four series were undertaken to investigate the possibility of considering the gusset plate as a series of fixed ended struts running parallel to the free edge. The first three of these were various strut tests rather than gusset plate tests. The derivations of the buckling stress equations are presented in Section 6.10.3.

4.2.1. Pin ended directly loaded strut tests (series 1)

4.2.1.1. Ultimate load results

The specimen dimensions and ultimate load results are given in Table A.2.9. Also in this Table are the theoretical buckling stresses using the equations of Euler, Rankine-Gordon and Perry Robertson, assuming an effective length l=L for a theoretically pin ended strut. With the Perry Robertson equation two values have been calculated based on two values of the Robertson constant. The experimental and theoretical buckling stresses have been plotted against the effective length in Figure 4.5. The experimental results were on or slightly higher than the Euler curve, which is the theoretical upper bound. Although the ends of the struts were rounded to a radius of 2mm, the

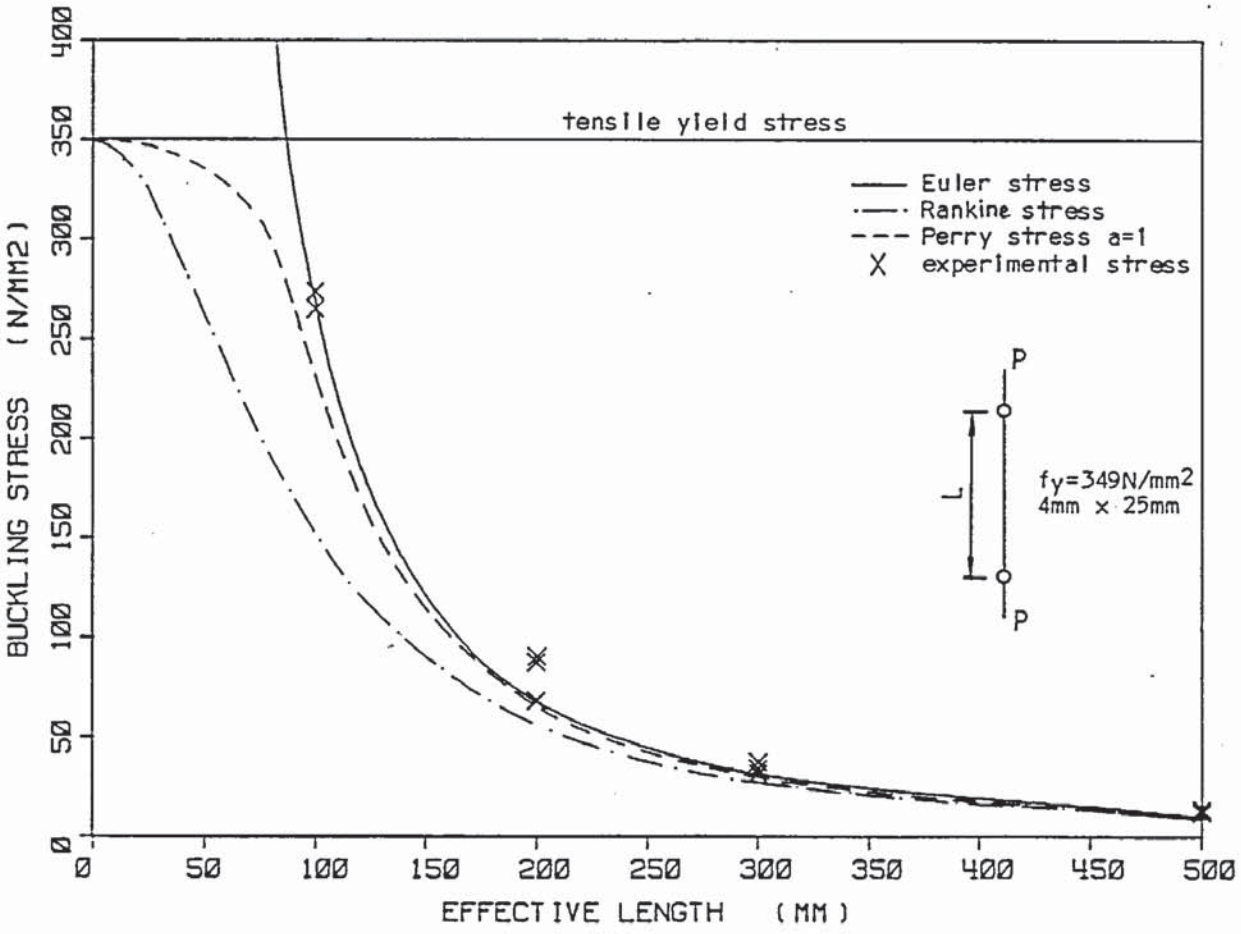

Figure 4.25 Comparison of theoretical and experimental relationship between the buckling stress f_b and the effective length l of a pin ended strut (series 1).

application of the load probably flattened the ends slightly and this may have produced sufficient restraint to rotation to reduce the effective length and increase the failure load.

4.2.2. Fixed ended directly loaded strut tests (series 9)

4.2.2.1. Ultimate load results

The specimen dimensions and ultimate load results are in Table A.2.10. Included in this Table are the theoretical buckling stresses assuming an effective length l of l=L/2 for a theoretically fixed ended strut. The experimental and theoretical buckling stresses have been plotted against the effective length in Figure 4.26. The

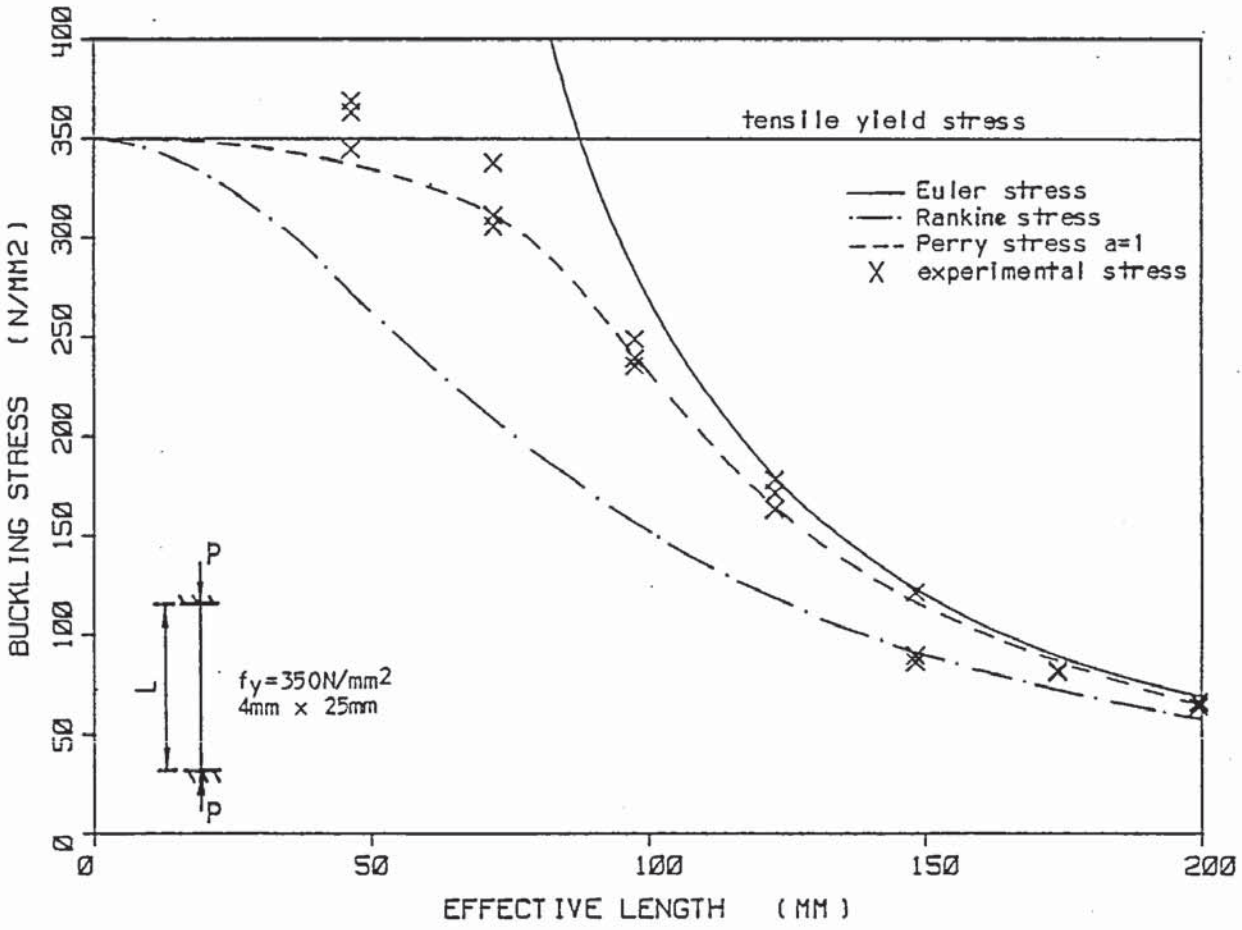

Figure 4.26 Comparison of theoretical and experimental relationship between the buckling stress f_b and the effective length l of a fixed ended strut (series 9).

experimental buckling stresses were all below the Euler curve. For effective lengths greater than 100mm the experimental results were close to the Euler value and approximate to the Perry Robertson equation with a=1. For the shorter struts some of the experimental buckling stresses were greater than the Perry-Robertson values, and with the 93mm strut, two of the specimens failed at stresses greater than the tensile yield stress. Generally, the Perry Robertson equation with a=1 agrees with the experimental results. The two low results of the specimens of length 196.5mm are most probably due to imperfections in the specimens or loading conditions, and lie close to the Rankine-Gordon curve.

4.2.2.2. Deflection results

Axial deflections and mid-lateral deflections were measured on two of each specimen sizes and the results are presented in Table A.3.9. All of the specimens were approximately straight initially, and most specimens displayed some initial settlement. After the intial settlement the deflection curves were approximately linear, with a small increase in the rate of axial deflection just before the specimens collapsed. The axial stress/strain relationships calculated from the axial loads and deflections varied but, generally they were lower than the modulus of elasticity calculated from the tensile tests, the longer struts having a lower value.

The lateral deflection for the two short struts were small for almost the complete test time with a small increase just before failure. The initial lateral deflection of the longest struts were small but then gradually increased with a relatively large deflection occuring before failure. The intermediate struts were a transition between the two extremes.

Figures A.4.16, A.4.17 and A.4.18 in Appendix 4 are examples of short, intermediate and long struts respectively. The deflections are plotted against the axial stress in the struts.

4.2.3. Inclined indirectly loaded fixed ended strut tests (series 10)

4.2.3.1. Ultimate load results

Due to the magnitude of the load, weld size and deflections, the moment resistance of the lateral weld connecting the loaded plate to the support was assumed to be negligible and the connection was assumed to be pinned. The bending moment in the strut and the moment of resistance of the strut connections in the plane of the strut were also considered to be negligible. Using these assumptions the axial compressive out of plane buckling stress was calculated for each inclined strut. The specimen dimensions and ultimate load results are

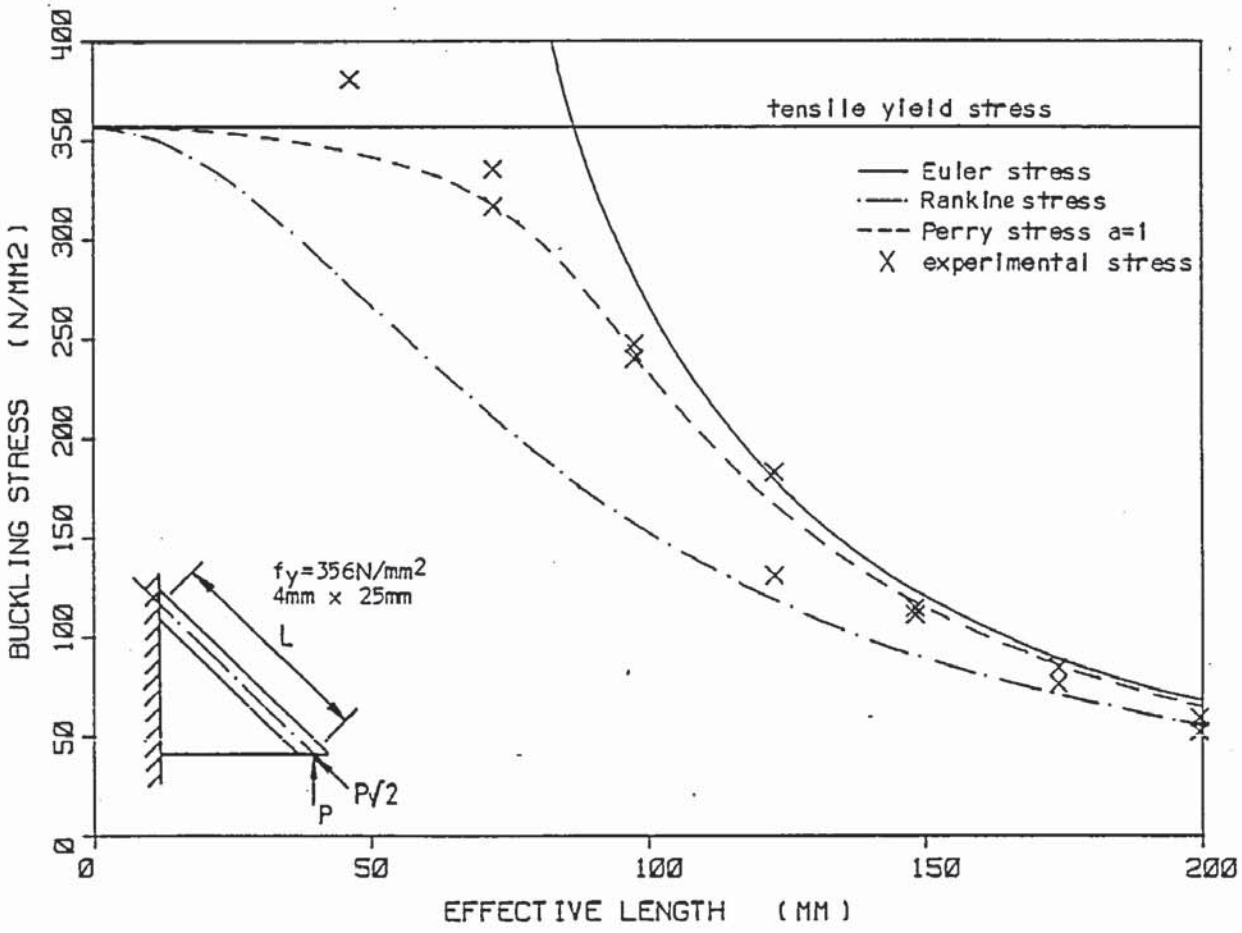

Figure 4.27 Comparison of theoretical and experimental relationship between the buckling stress f_b and the effective length of an inclined fixed ended strut (series 10).

given in Table A.2.11. Also in this Table are the theoretical out of plane buckling stresses assuming an effective length l of l=L/2 for a theoretically fixed ended strut. L in this case is the centre line length of the strut. The experimental and theoretical buckling stresses are plotted against the effective length in Figure 4.27.

The results are similar to those of the directly loaded fixed ended struts. All but one result are below the Euler curve. The buckling stresses for the longer struts appear to be slightly lower than for the directly loaded struts. This may be due to the lateral deflection before buckling for the longer struts being greater than with the directly loaded struts. The two short struts, where l = 93mm, produced buckling stresses greater than the tensile yield

stress. Generally the results are represented with reasonable accuracy by the Perry Robertson equation with a=1. The lowest stresses, as in previous tests, approximated to the Rankine Gordon equation. These tests suggest that for the 4mm plate at least, the buckling stress of an indirectly loaded inclined fixed ended strut can be approximated to the equivalent directly loaded fixed ended strut whose length is equal to its centre line length.

4.2.3.2. Deflection results

The vertical and lateral deflections were measured for both pairs of specimens and are presented in Table A.3.10. From the vertical deflections, the axial deflection of the inclined struts were calculated and within the accuracy of the measurements taken, the following was observed.

The shorter struts were approximately straight with the longer struts having a small initial lateral deflection. The axial deflections were similar to the directly loaded struts of the previous series. The axial stress/strain relationship calculated from the axial deflections and based on the centre line length of the inclined struts showed a small variation and were slightly lower than for the directly loaded struts of the previous series.

The lateral deflections were similar to those of the directly loaded struts, with the shorter struts deflecting very little, until just before failure. The lateral deflection of the longer struts, increased at a slightly greater rate than those of the directly axially loaded struts, with a resulting greater lateral deflection before failure.

Figures A.4.19, A.4.20 and A.4.21 in Appendix 4 are examples of short intermediate and long inclined struts respectively. The vertical and mid-lateral deflections are plotted against the axial stress in the struts.

4.2.4. Multiple strip plate test (series 11)

4.2.4.1. Ultimate load results

This plate was effectively all the separate inclined struts of the previous series put onto the same specimen. Irrespective of the sequence of construction of the plate the two outermost strips of plate buckled due to the effect of welding and suggested that welding stresses were relatively large for this thickness of plate. The presence of the welding stresses in the complete gusset plates were not so apparent, with only small initial lateral deflections being observed. With the gusset plate cut into strips, the lateral restraint provided by the inner part of the gusset plate was removed allowing the individual strips to buckle. The complete gusset plates were therefore stressed before the external load was applied and this may have affected their resistance to external loading. Although the outer strips had buckled due to the welding, the multi-strip gusset plate failed at a load of 55kN compared with approximately 73kN for the same complete gusset plate in the main series. The yield stress for the strip plate was 363N/mm^2 compared with 378N/mm^2 but the results of the main series suggested that for this particular plate size and thickness the yield stress had very little effect on the ultimate load. The specimen dimensions and ultimate load results are presented in Table A.2.12.

4.2.4.2. Deflection results

The load deflection results are shown in Table A.3.11 for specimen S11-150-1. The total vertical deflection is comparable with the equivalent complete gusset plate. There was an initial settlement deflection followed by a linear section which continued until failure. The deflection rate of the linear section was the same as for a complete gusset plate.

As previously mentioned the outer two struts deflected and in

opposite directions when the specimen was constructed. The initial lateral deflection at the mid-point of the outer two struts were 8 and 2.5mm respectively, while the rest of the struts remained approximately straight. During loading the lateral deflection of the outer edge and the third from the outer edge strut deflected at a similar rate to that of the outer free edge of a complete gusset plate under similar load conditions. The second strut from the outer edge deflected in the opposite direction and at a greater rate. Figure A.4.22 in Appendix 4 shows the vertical and mid-lateral deflections of specimen S11-150-1.

4.2.4.3. Failure modes

The failure mode of the multi-strip plate buckled from the outer free edge inwards as with a complete gusset plate. The outer two strips had effectively buckled before the load was applied, but the remaining strips were still able to take the applied load. As each strip deflected laterally and buckled the remaining strips were still able to take the applied load until the remaining number of strips was insufficient to maintain the load and they collapsed together. The effective fold line pattern of the multi-strip plate was different from the complete gusset plate. Where with the complete gusset plate the fold lines tended to curve inwards to intersect the free edge perpendicularly. The multi-strip plate fold lines ran along the loaded and supported edges and so effectively the strips had a longer effective length and, therefore, were weaker.

4.2.4.4. Strain gauge results

Strain gauges were attached to each strut to measure the axial stress across the width of the gusset plate. The average stresses have been calculated and tabulated in Table A.5.19. The significance of these results will be discussed later.

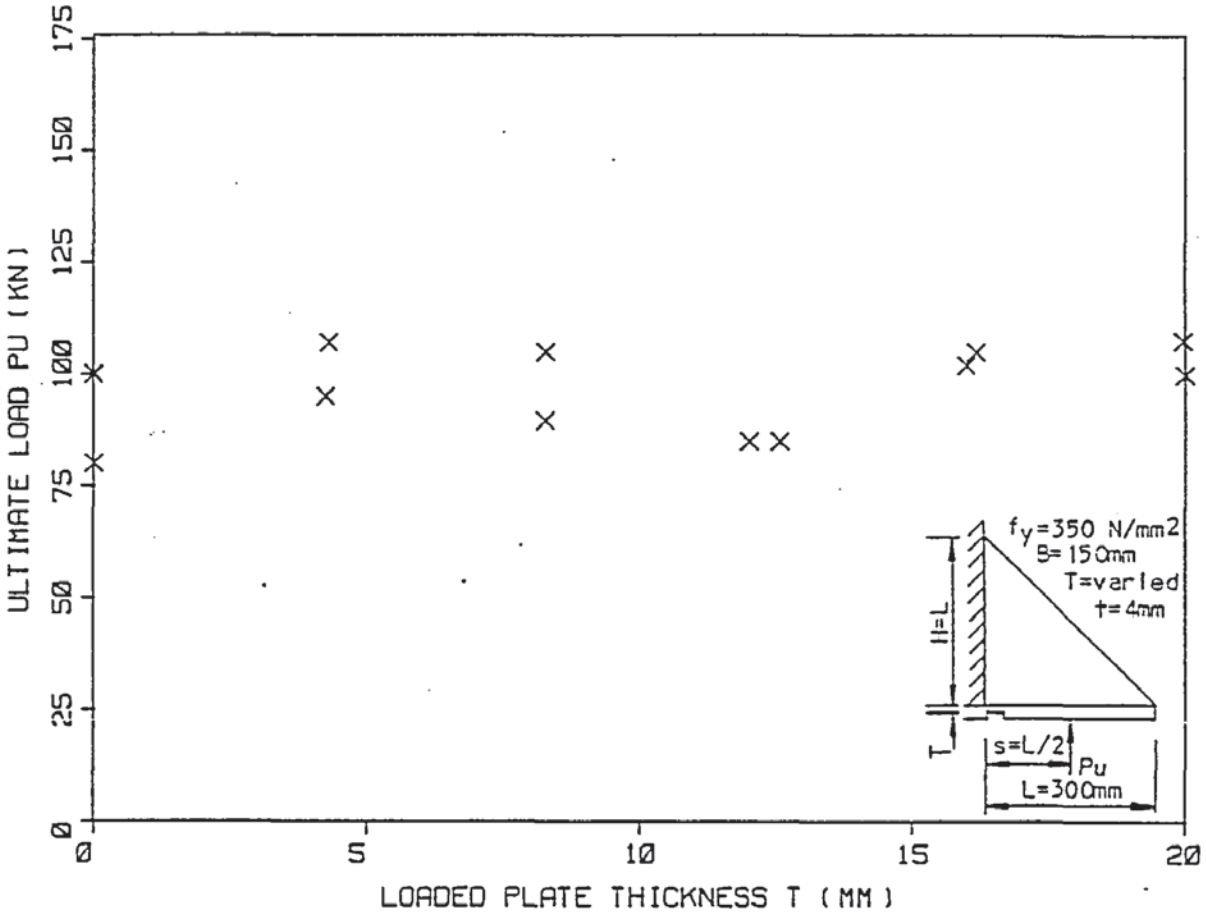

Figure 4.28 Relationship between the ultimate load P_u and the loaded plate thickness T at the vertical support (series 2).

4.2.5. Loaded plate bending resistance tests (series 2)

4.2.5.1. Ultimate load results

The specimen dimensions and ultimate load results are presented in Table A.2.13. The relationship between the experimental ultimate load Pu and the machined thickness T of the loaded plate is shown in Figure 4.28.

The results from this series of tests were not consistent and, due to the scatter it is difficult to determine whether the thickness of the loaded plate has any influence on the ultimate load. Four of the thicknesses tested produced maximum values of approximately 105kN with a fifth of 100kN for T=0. The results indicate that the loaded plate does not influence the load carrying capacity and that the

scatter may be due to the initial deformed shape of the gusset plate produced by welding as mentioned previously. The lack of influence of the loaded plate thickness on the strength in this series is in agreement with the tests in series 7.

4.2.5.2. Deflection results

The vertical and mid-lateral deflections of each specimen are given in Table A.3.12. The deflections were similar to comparable gusset plates in the main series with the load applied at s=L/2. The vertical deflections had the usual initial settlement deflection, followed by a middle approximately linear section which extended almost to the ultimate load with a very small non-linear deflection. The deflection rates of the linear sections were approximately the same as similar plates in the main series.

The mid-lateral deflections were of a similar shape to the main series but with varying rates of deflection, i.e. they were generally curved with increasing rates of deflection as the load increased. This deflection rate differed from one plate to another and was not related to the loaded plate machined thickness. However, it did appear to be related to the ultimate load, i.e. where the lateral deflection rate was high, the load was low, and vice versa.

In Appendix 4 the total vertical and mid-lateral deflections of specimens S2-0-1 and S2-0-2 are shown in Figures A.4.23 and A.4.24, respectively. The figures illustrate the two types of lateral deflection and the relation to the ultimate load, and also show that the vertical deflection rates are the same but are increased linearly. They also show that two nominally identical specimens can fail at a large difference in ultimate loads.

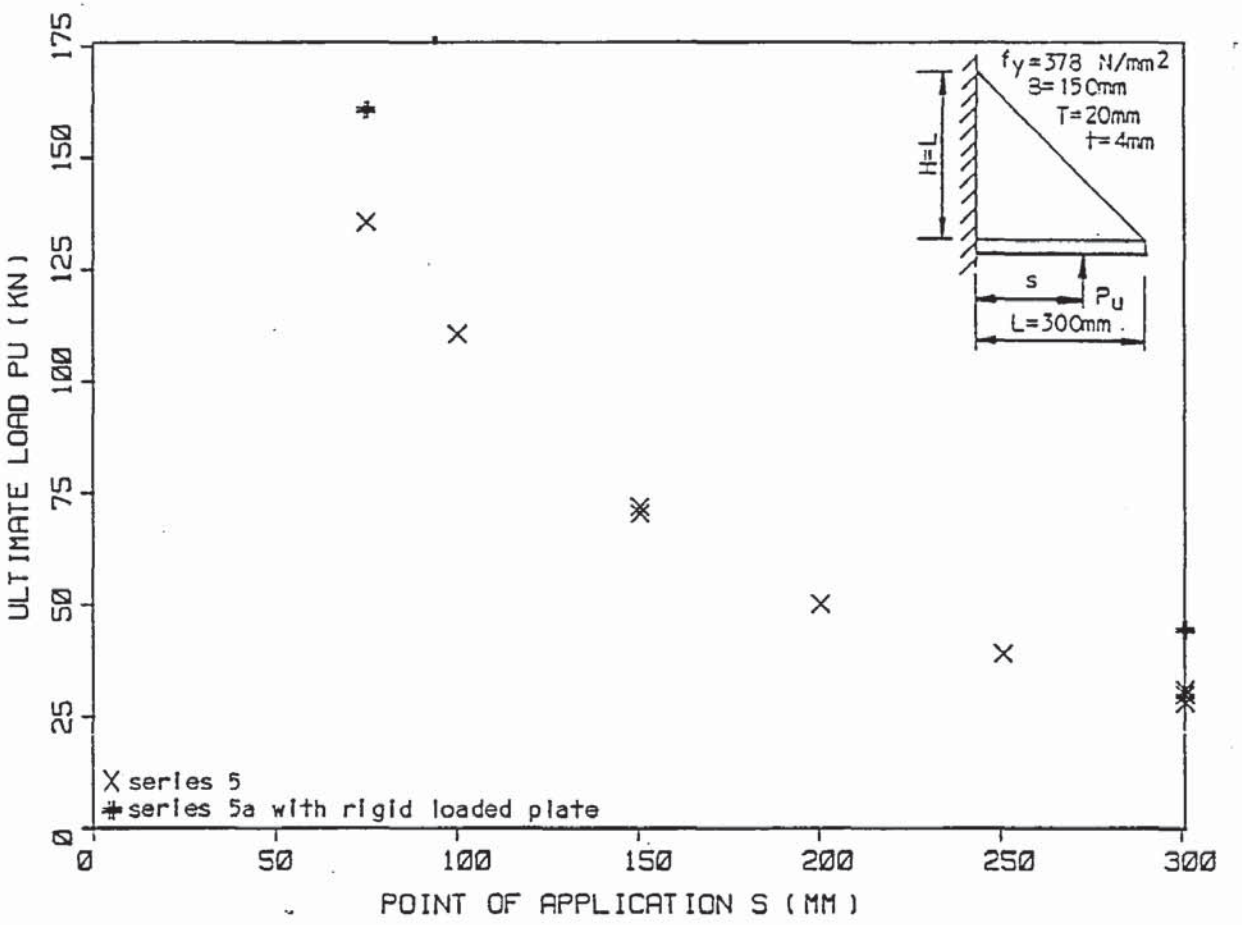

Figure 4.29 Relationship between the ultimate load P_u and the effect of the rigid loaded plate (series 5a).

4.2.6. Rigid loaded plate strain gauge tests (series 5a)

4.2.6.1. Ultimate load results

The specimen dimensions and ultimate load results are presented in Table A.2.14. Comparing with the appropriate specimens in series 5 the ultimate loads are higher as shown in Figure 4.29,

4.2.6.2. Deflection results

The vertical and mid-lateral deflections of each specimen are given in Table A.3.13. In comparison with the corresponding plate in series 5, the vertical deflections are similar in shape and there is a slight reduction in the deflection rates. The deflection rates of the lateral deflections are lower, especially at the lower loads. Figures A.4.25 and A.4.26 in Appendix 4 show the vertical and mid-lateral

deflections of specimens S5a-75-1 and S5a-300-1, respectively. These can be compared with the respective deflections of Figures A.4.5 and A.4.6 from series 5.

4.2.6.3. Strain gauge results

Strain gauges were attached across the width of both gusset plates and the average stresses have been calculated and presented in Tables A.5.20 and A.5.21. The significance of these results will be discussed later.

4.3. Weld test series results

This section contains the results and modes of failure of the experiments on the welds connecting the gusset plate to its loaded and supported plates. The full specimen descriptions are given in Chapter 3 Section 3.4. Presented in this section are the experimental results for the series investigating

i) the size of the loaded edge weld (series 14)

ii) the size of the supported edge weld (series 15)

iii) the size of both the loaded and supported edge welds simultaneously (series 16)

iv) the shear, normal and frictional forces on the welds (series 17)

The results of series 14, 15 and 16 are interrelated and are, therefore, presented together.

4.3.1. Variation of the loaded edge weld size (series 14)

4.3.1.1. Ultimate load results

The specimen dimensions and the ultimate load results are given in Table A.2.15. With the first batch of specimens tested in this series, problems were encountered with the load head of the testing machine and specimen S14-0-2 had to be re-loaded. A new load head was used and the series repeated. The results of the two series, however,

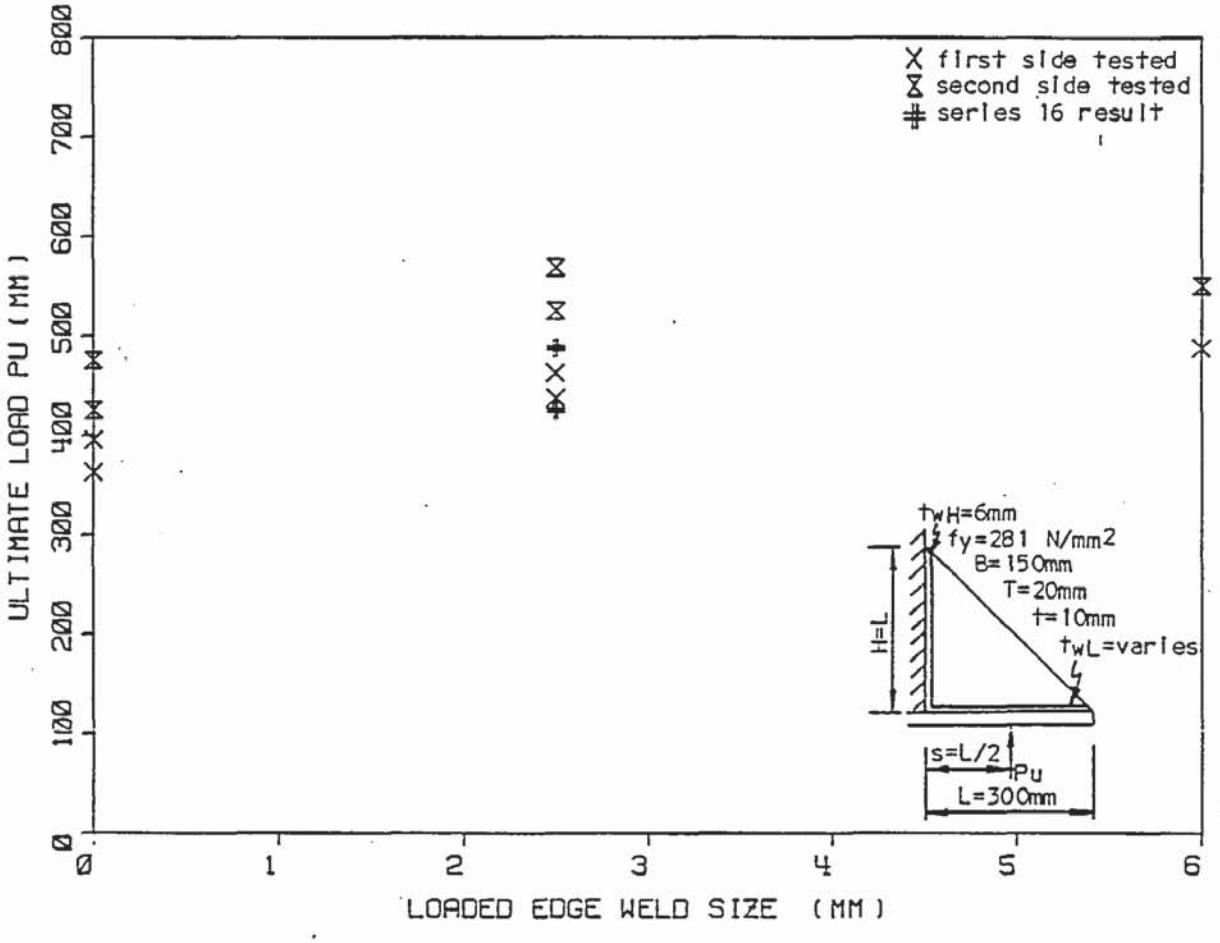

Figure 4.30 Relationship between the ultimate load P_u and the loaded edge weld size (series 14).

were in reasonable agreement with one another and all results are considered acceptable. It was noticed with this series, and with other series that followed, that the second side of each pair of specimens failed at a higher load than the first side. In the testing of the first side, the second side had plates clamped on both sides of it to prevent it from buckling. In the process of testing this did not, however, restrict the compression of this gusset plate. The vertical support plate remained vertical for most of the test and only started to move as the side under test began to deflect laterally. As the restrained side was effectively pre-loaded, it is likely that it yielded in such a way as to increase the strength, possibly by relieving stress concentrations, or by making the gusset plate

slightly thicker and so increasing the load at which it started to buckle. By comparing like sides with one another a pattern emerged, with the second side failing at approximately 20 percent higher load than the first as shown in Figure 4.30.

The most significant fact from this series is that even with no weld along the loaded edge, the gusset plates failed in the same way as a welded gusset plate. The gusset plates with a 2.5mm weld had a slightly lower failure load than the 6mm welded plate. The gusset plates with no weld failed between 15 and 20 percent lower than the 6mm welded plate.

4.3.1.2. Failure mode

The gusset plates with no weld along the loaded edge had a small amount of relative slip between the gusset plate and the loaded plate. The gusset plate moved outward with respect to the loaded plate by a very small amount, until just before failure, giving a maximum slip of only 1.964mm. Although no weld failures were apparent before failure, the presence of slip between the gusset plate and the loaded plate suggests that the supported edge weld close to the inside corner must have been resisting this slip. It must, therefore, have been resisting direct tensile forces and may have been yielding close to the ultimate load. In the delay of removing the load after the specimen had failed at the ultimate load, the supported edge weld at the inside corner fractured as the gusset plate folded. This suggests that the 6mm weld on the supported edge was close to failure and if a smaller weld had been used, it would have failed before the gusset plate had buckled. The gusset plates with welds along the loaded edge showed no slip or any signs of weld failure. This suggested that the horizontal weld resists the longitudinal shear forces, and that in its absence these forces are resisted by the tensile strength of the supported edge weld close to the inside corner. These shear forces

will also be resisted by the frictional forces between the loaded plate and the gusset plate, which were apparent as the gusset plate made noises as these forces were overcome. The loaded plate did not remain straight throughout the loading and so this will have provided some resistance to slipping along this edge.

Another effect which was noticeable just before failure, and quite apparent afterwards, was the rotation of the loaded edge of the gusset plate due to the lack of fixity. This was most noticeable at the free edge end and very quickly reduced to zero at the mid-point. It appears that the thickness of the gusset plate used has provided a certain amount of the fixity which may normally be provided by the weld. Therefore, the weld may not have to provide much bending resistance for the thicker gusset plate. Although with thin gusset plates the mechanical fixity is less, the loads are much smaller and the bending resistance will be very small. The lack of fixity caused only a small change in the fold line pattern of the gusset plate and it is most probably this lack of rotational fixity that caused the slightly lower load of these gusset plates.

4.3.1.3. Deflection results

The vertical and mid-lateral deflections are given in Table A.3.14 and did not appear to be affected by the variation in the loaded edge weld. The vertical deflections of all the specimens exhibited the usual settlement deflection followed by an approximately linear middle section which extended for most of the loading. This was followed by a slow increase in the deflection rate as the ultimate load was approached. The deflection rates for all the first sides tested were the same and agreed with those of series 12 of the main series investigating the gusset plate thickness. The second sides of some of the gusset plates demonstrated a slightly lower deflection rate than the initial side.

The mid-lateral deflections were very small for most of the loading with an increase close to the ultimate load as the gusset plate progressively buckled.

4.3.2. Variation of the supported edge weld size (series 15)

4.3.2.1. Ultimate load results

The specimen dimensions and the ultimate load results are given in Table A.2.15. As with the previous series of tests the second sides tested gave failure loads that were slightly higher than the initial side by approximately 20 percent. Therefore, in Figure 4.31 the load comparisons are made between like sides. It is interesting to note that the ultimate load results of this series are virtually the same as those for the previous series, shown in Figure 4.31. That is, even with no weld along the supported edge, the gusset plate failed in the normal way. The failure load of the gusset plates with only a 2.5mm weld failed only slightly lower than the 6mm welded plate, and the gusset plates with no weld along the supported edge failed between 15 and 20 percent lower.

4.3.2.2. Failure mode

With the gusset plates with no weld along the supported edge there was slightly more relative slip between the gusset plate and the supported plate than with the loaded edge of the previous series. The supported plate moved downwards relative to the gusset plate. This slip was not measured, but was apparent by the noise it made as it overcame the frictional forces. It was apparent that the loaded edge weld close to the inside corner was resisting this slipping. As the gusset plate was progressively buckling the loaded edge weld was visibly yielding and the loaded plate was also deforming. The vertical support plate remained straight, therefore there was less resistance to slipping as with the loaded edge weld, in the previous

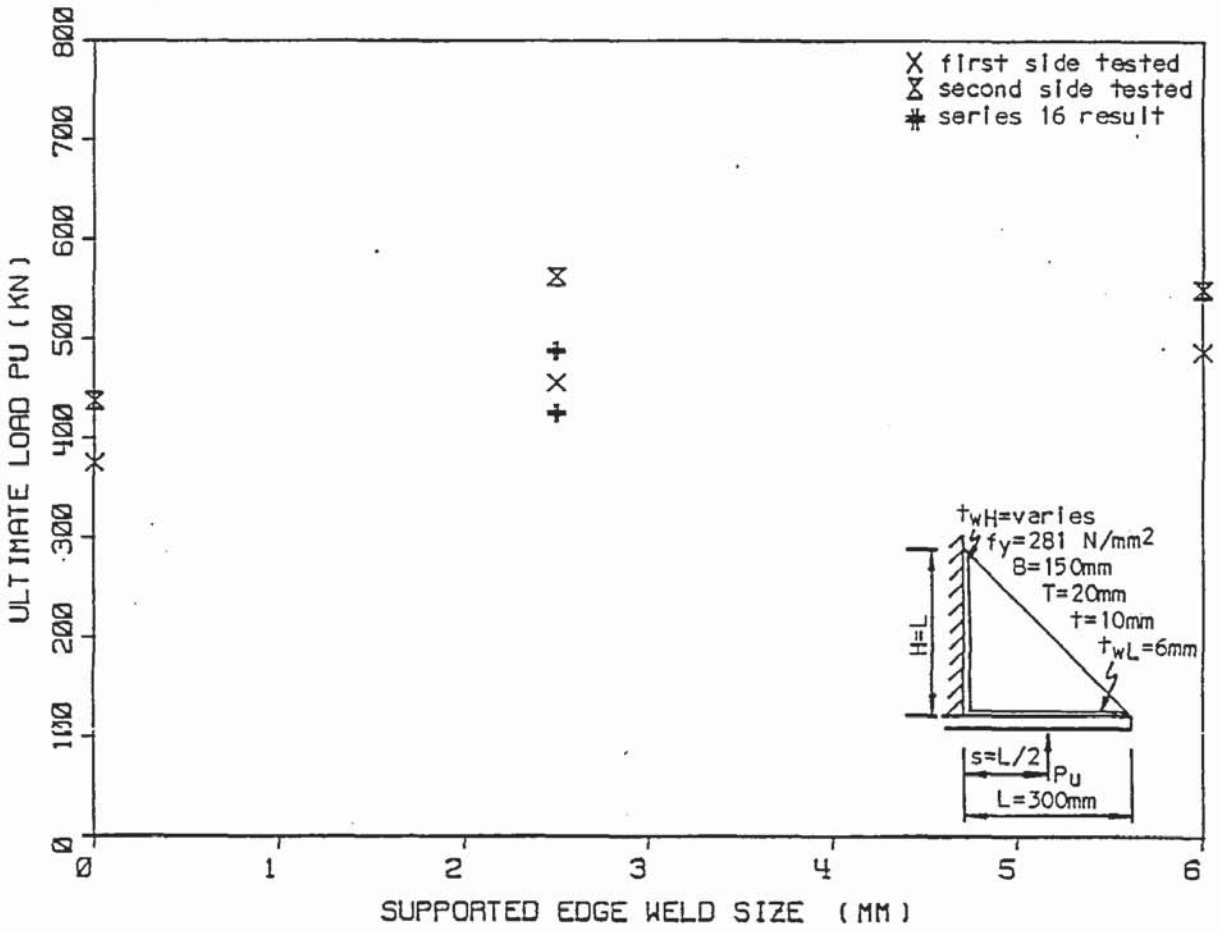

Figure 4.31 Relationship between the ultimate load P_u and the supported edge weld size (series 15).

series. Consequently the loaded edge weld was subjected to a greater tensile tearing force. As a result, this weld failed by tearing just before the gusset plate failed.

The rotational fixity of the gusset plate along the supported edge, was provided by its thickness and there was very little rotation even at the ultimate load. With a weld, along the supported edge, the gusset plates showed no signs of slip or weld failure and the gusset plates failed in the normal manner.

4.3.2.3. Deflection results

The vertical and mid-lateral deflections of the gusset plates have been tabulated in Table A.3.16 and were very similar to those of the previous series. The only noticeable difference was with the

first of the gusset plates with zero weld along the supported edge. This specimen started off normally but, the linear section was cut short as the slip along the supported edge caused the vertical deflection to increase as expected. The second side was not so noticeable, possibly due to the stiffening effect of the previously tested side.

4.3.3. Variation of both the loaded and supported edge weld sizes simultaneously (series 16)

4.3.3.1. Ultimate load results

Specimen dimensions and the ultimate load results are given in Table A.2.15. As with the previous series of tests the second sides tested produced higher failure loads than the initial sides by approximately 15 percent. The 6mm fillet welded gusset plates are used to supplement the previous two series. The gusset plates with 2.5mm fillet welds are related to the gusset plates with one of its welds 2.5mm and the other 6mm. The results of this series are plotted with those of the previous series in Figures 4.31 and 4.32. The gusset plates failed in the normal manner and without any weld failures. The failure loads of the 2.5mm welded gusset plates are approximately 15 percent lower than those with the 6mm welds. This lower load may be due to the increased effective area of the gusset plate because of the reduced size of the weld.

4.3.3.2. Deflection results

The vertical and mid-lateral deflections of the gusset plates are given in Table A.3.16 and were very similar to those of the previous two series. The only noticeable difference was between the first and the second sides to be tested.

4.3.4. Investigation of the shear, normal and frictional forces on the welds (series 17)

4.3.4.1. Ultimate load results

The specimen dimensions and the ultimate load results are given in Table A.2.16. With the specimens having 25mm fillet welds on both the loaded and supported edges, the supported edge welds failed in longitudinal shear without any deformation of the gusset plate or the loaded edge welds. The other set of specimens with the supported edge fillet welds increased to 75mm in length, the loaded edge weld failed in longitudinal shear without any deformation of the gusset plate or failure of the supported edge weld. From the ultimate load results it can be seen that a higher load was required to fail the loaded edge weld than the supported edge weld of the same length. However, it was noted that the loaded plate did deform slightly whereas the supported plate did not.

With the two specimens that failed by the supported edge welds, specimens S17-25-1 and S17-25-2, there was no slip of the loaded edge weld throughout the test. The supported edge weld, on the other hand, started to slip in the initial loading stages. The slip of the first specimen was 0.5mm before failure and the second was 1.0mm.

With the two specimens that failed by the loaded edge welds, specimens S17-75-1 and S17-75-2, the supported edge welds slipped more than the loaded edge welds, although they only slipped by a very small amount. The loaded edge welds only slipped a small distance before they failed suddenly.

4.3.4.2. Contact zone results

The contact zones were also monitored along the loaded and supported edges, and they were in agreement with the weld slips. With specimen S17-25-1, initially both edges were in contact for their full lengths and the loaded edge remained in contact for most of the

loading. Close to the failure load the loaded plate progressively parted from the gusset plate and extended the gap from the inside corner outwards, leaving approximately 200mm still in contact just before failure. The supported edge parted from the inside corner outwards soon after the initial loading, which gradually extended the gap, leaving approximately 100mm still in contact just before failure.

With specimen S17-25-2 the supported edge initially was in contact along a small length at its outermost end. The loaded edge also had a very small gap with just the outer third in contact. As the load was applied this gap along the loaded edge closed and the contact zone extended inwards past the load point. As the ultimate load approached, the loaded plate parted and the gap extended outwards, reducing the contact zone. The supported edge gap, which extended beneath the welded section, closed slowly at the outermost end and increased the contact area by a small amount as failure approached. Just before failure the loaded and supported edge contact zones were 170 and 76mm respectively.

With specimen S17-75-1 the loaded edge contact zone behaved in a similar manner as described with S17-25-2, except it did not open as much at the inside corner, ending with a contact zone of 180mm just before failure. Initially the supported edge contact zone covered over two thirds of the outermost end of the supported edge. As the supported plate parted from the gusset plate near the inside corner the contact zone was gradually reduced. Just before failure the contact zone was 85mm and terminated under the supported edge weld.

With specimen S17-75-2 the loaded edge gap initially was relatively small and did not extend to the load point. So long as the load was applied there was very little difference, with the gap closing by only a small amount, leaving a contact zone of 180mm just before failure. The supported edge was initially in contact and

gradually parted from the gusset plate from the inside corner outwards as the load was applied, until just before failure the contact zone was 85mm, which terminated under the supported edge weld.

4.3.4.3. Deflection results

The vertical and mid-lateral deflections are given in Table A.3.17. The vertical deflections, within each pair of specimens, were in agreement with each other. They were of a similar shape as previous gusset plates but, with a reduced non-linear section. With the 25mm long supported edge weld failures the vertical deflection rates were greater than the other two specimens, which had loaded edge weld failures and 75mm long supported edge welds. As these supported edge welds slipped slightly, the deflection rates were greater than for a fully welded gusset plate.

Lateral deflections were very small and their nature suggested that it was not the gusset plates deflecting laterally but, they were rotating a little due to their reduced restraint, i.e. the inside corners of the gusset plates were deflecting laterally slightly.

4.3.4.4. Weld shear tests

Three specimens were made using the same steel and 4mm fillet weld so as to measure the actual ultimate longitudinal shear strength of the welds used in this series of gusset plate tests. The welds are assumed to be in pure shear and the frictional forces are considered negligible. The ultimate stresses are given in Table A.2.17 and deflection data in Table A.3.18.

CHAPTER FIVE

COMPARISON OF EXISTING METHODS WITH EXPERIMENTAL RESULTS

5.1 Introduction

The existing theories and methods of designing triangular unstiffened steel gusset plates are outlined in the Literature Review, Chapter 2. In this chapter each of these existing methods is compared with the experimental results obtained for each gusset plate series of the main testing programme as presented in Chapter 4.

5.2 Jensen's method

In Figures 5.1 to 5.9 the critical loads calculated using Jensen's (4) method together with the variations presented in Section 2.2, are plotted with the experimental ultimate load results obtained for each of the main gusset plate series. The critical loads presented for Jensen's (4) method are the loads based on the elastic critical stress, that is elastic buckling or first yield, which is factored to give the allowable stress and in turn the allowable load.

Jensen's (4) original method is basically to apply the prism equation in the appropriate manner and to assume the critical stress to be the yield stress with no buckling occurring. In the figures, curve 1 is Jensen's (4) original method which is given by

$$P = \frac{t.L.f_y \cos^2\alpha}{(1 + 6e/L)} \qquad (5.1)$$

where $e = |s - L/2|$

However the generalised Equation 2.3 which is usually used to express Jensen's (4) method gives

$$P = \frac{t.L.f_y \cos^2\alpha}{(6s/L - 2)} \qquad (5.2)$$

which should not be used for $s<L/2$. As generally $s=L/2$ in the test series it is just applicable and gives the same results as Equation 5.1. Curve 1a in Figure 5.3 for series 5 where s was varied

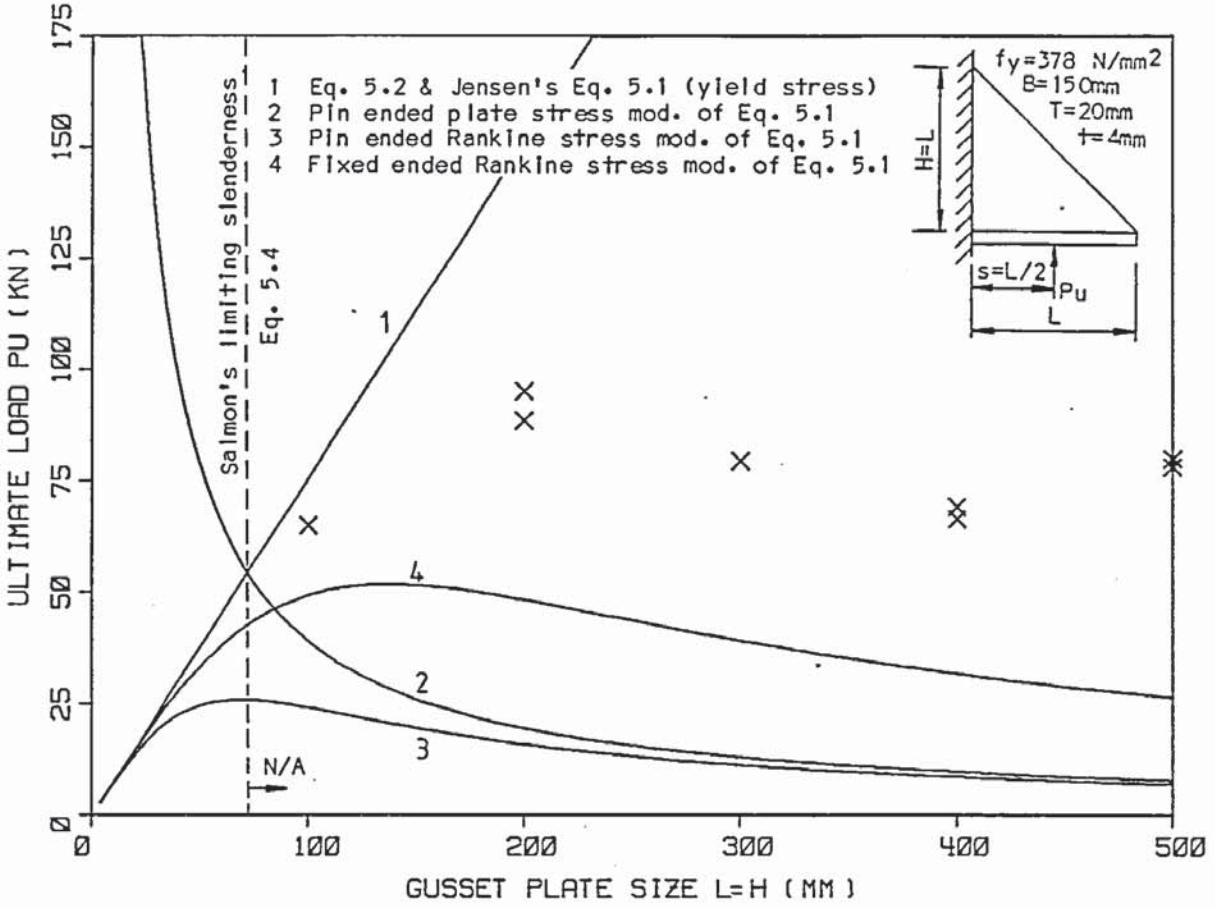

Figure 5.1 Jensen's method compared with the experimental results of series 3.

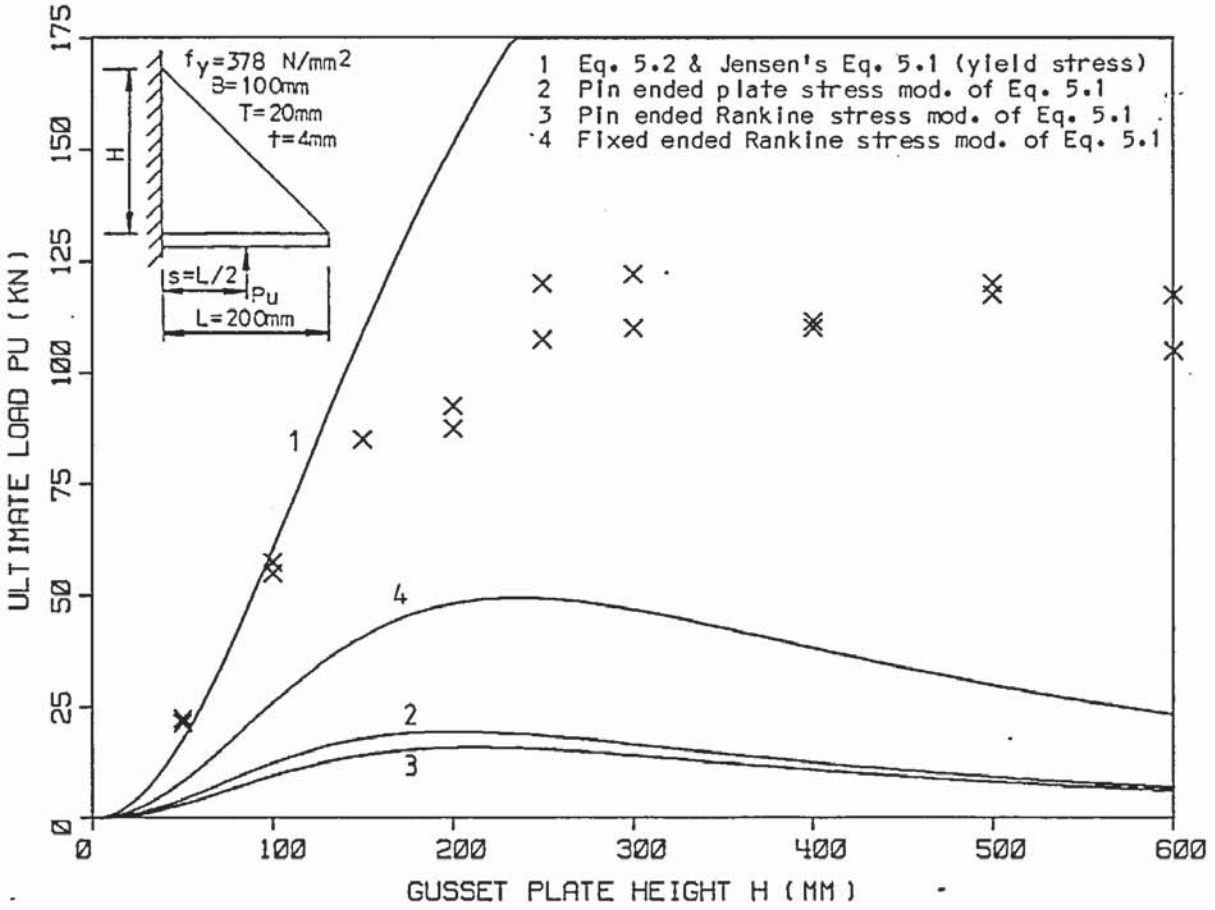

Figure 5.2 Jensen's method compared with the experimental results of series 4.

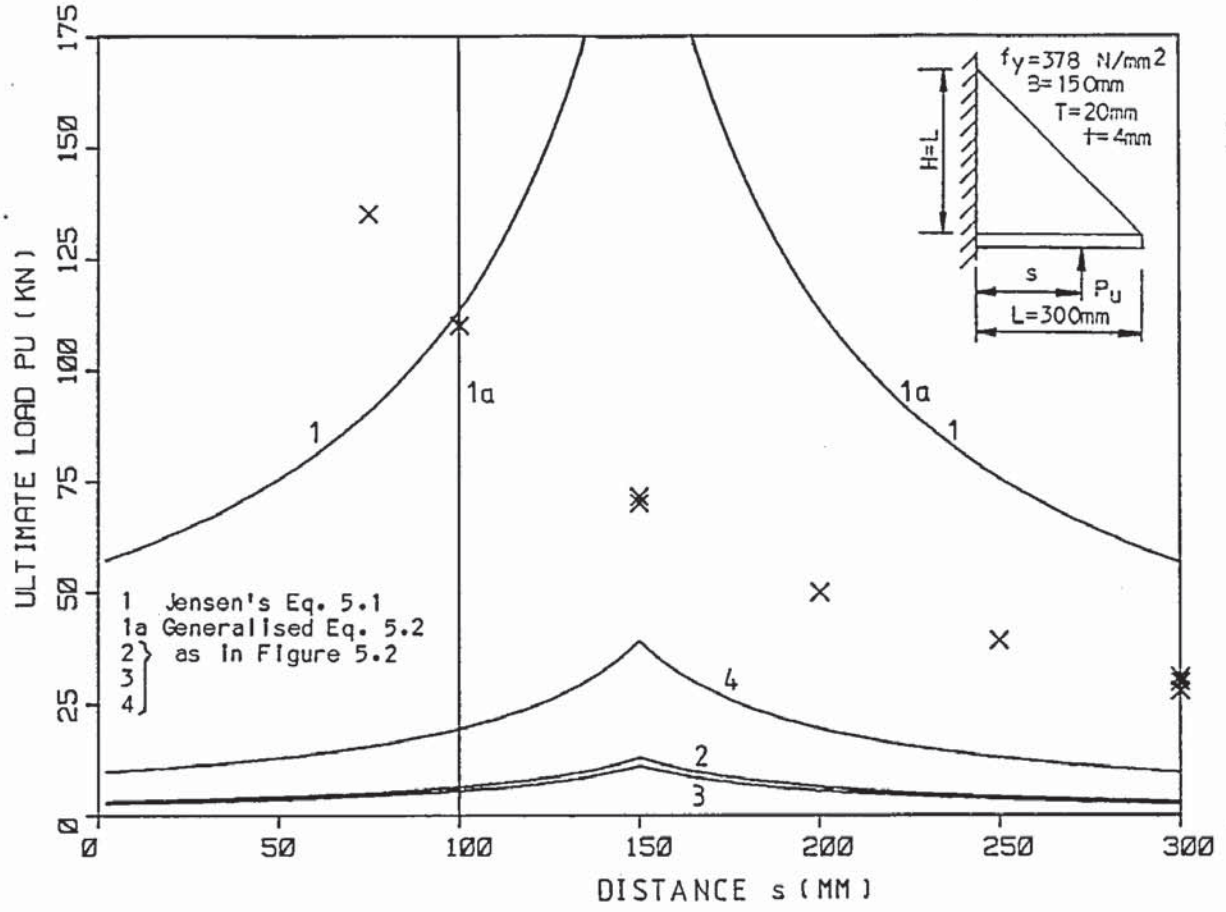

Figure 5.3 Jensen's method compared with the experimental results of series 5.

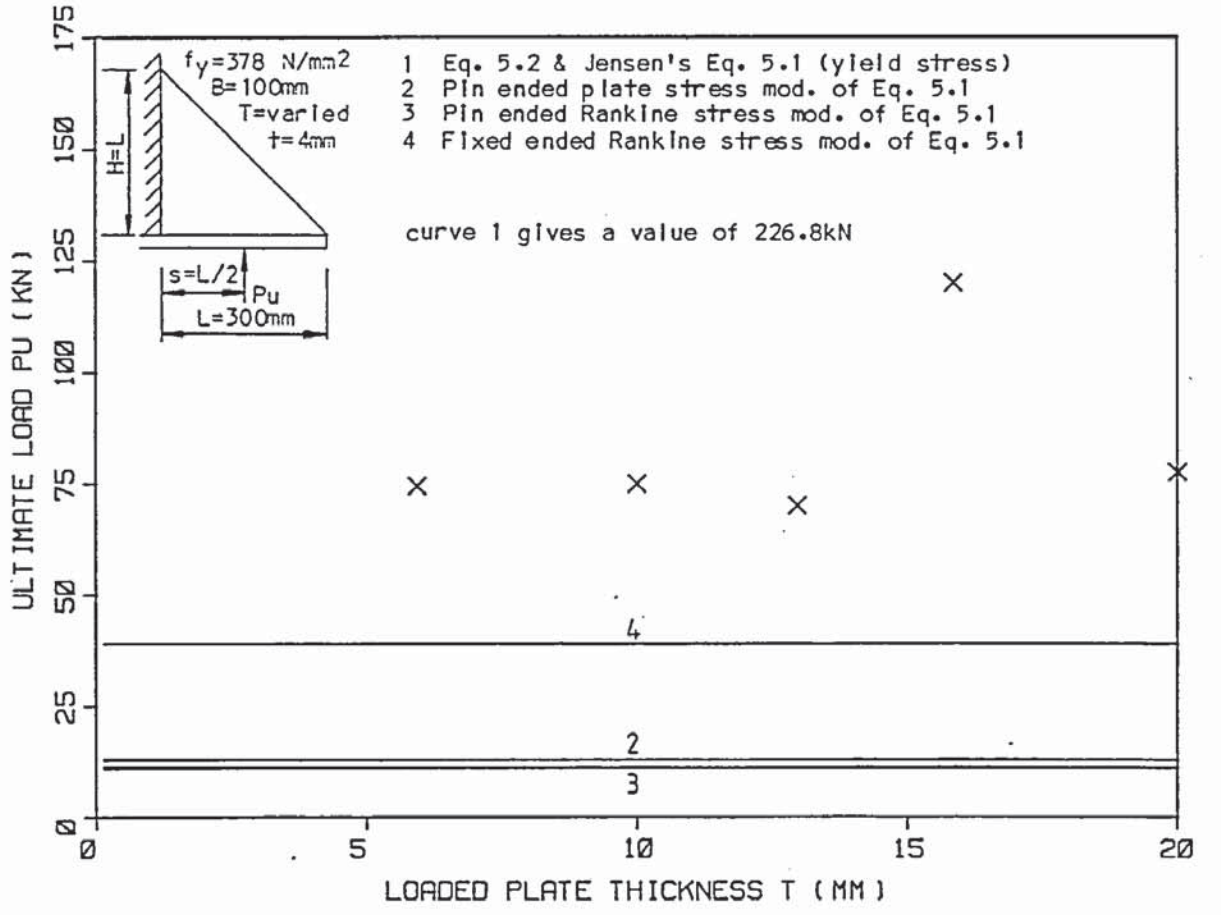

Figure 5.4 Jensen's method compared with the experimental results of series 7 (s=L/2).

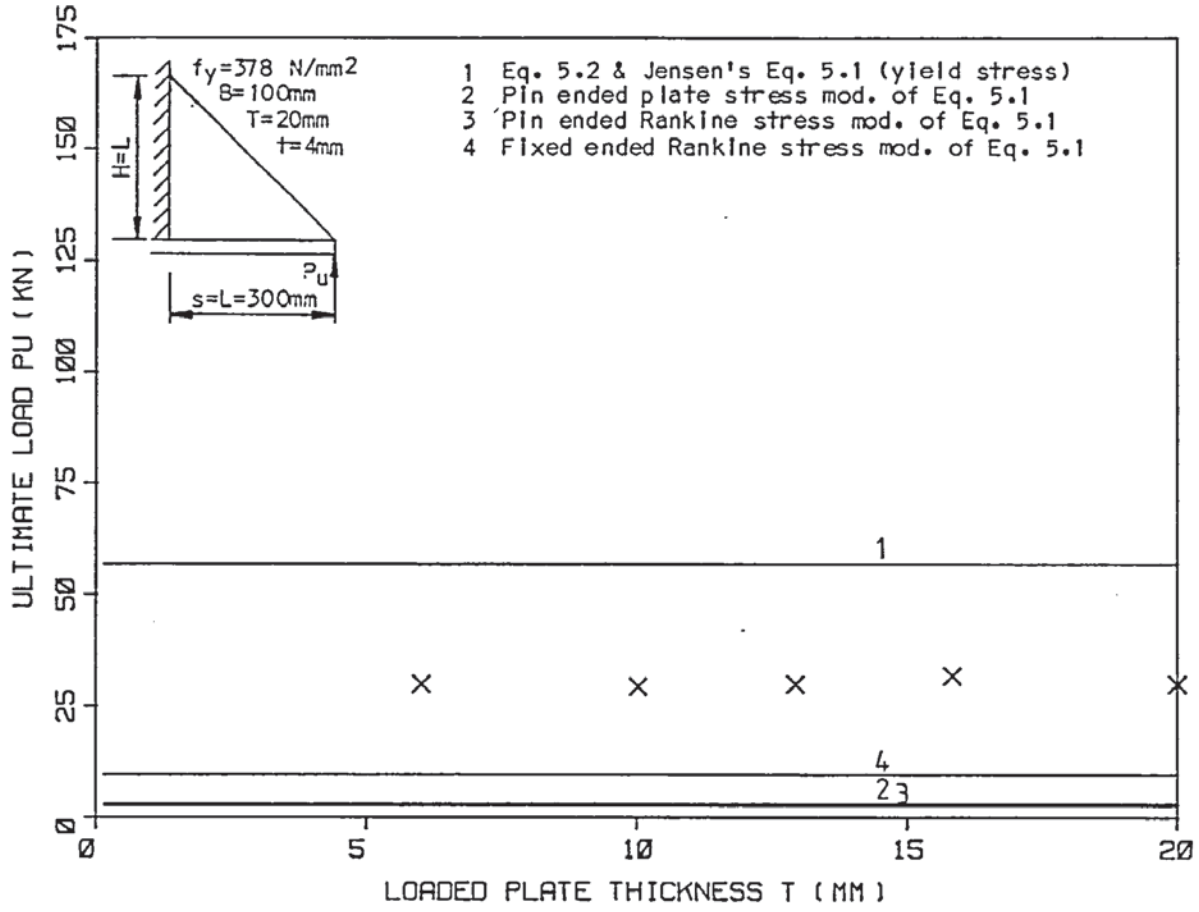

Figure 5.5 Jensen's method compared with the experimental results of series 7 (s=L).

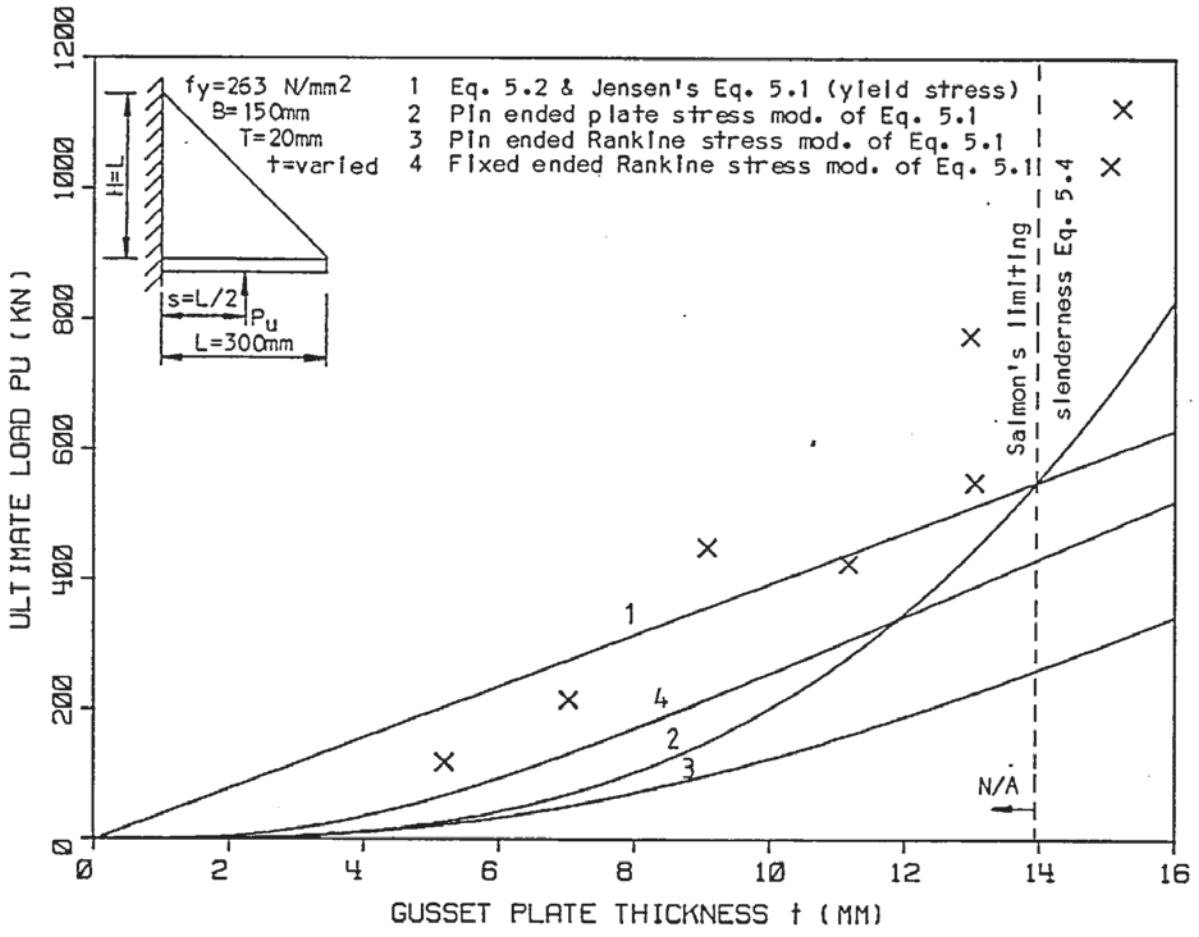

Figure 5.6 Jensen's method compared with the experimental results of series 12.

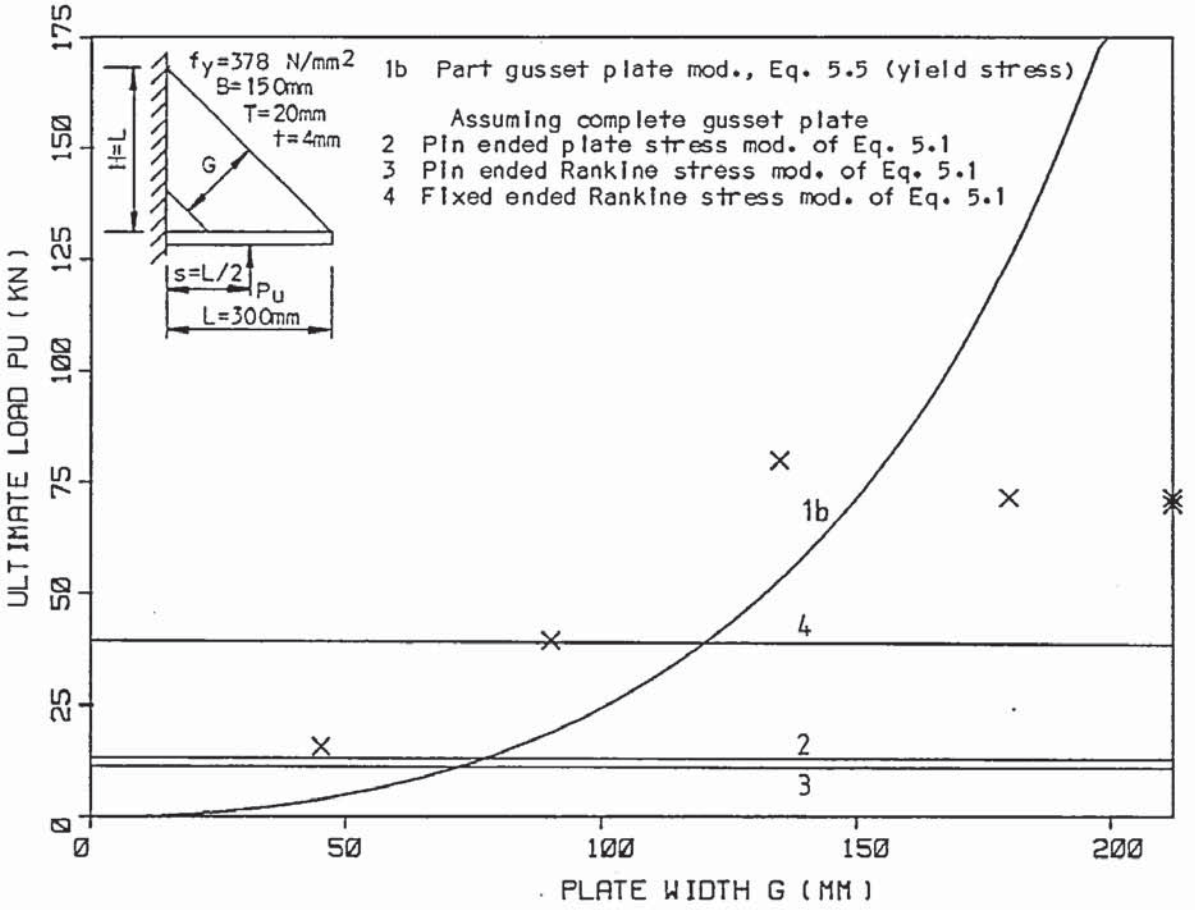

Figure 5.7 Jensen's method compared with the experimental results of series 8 (s=L/2).

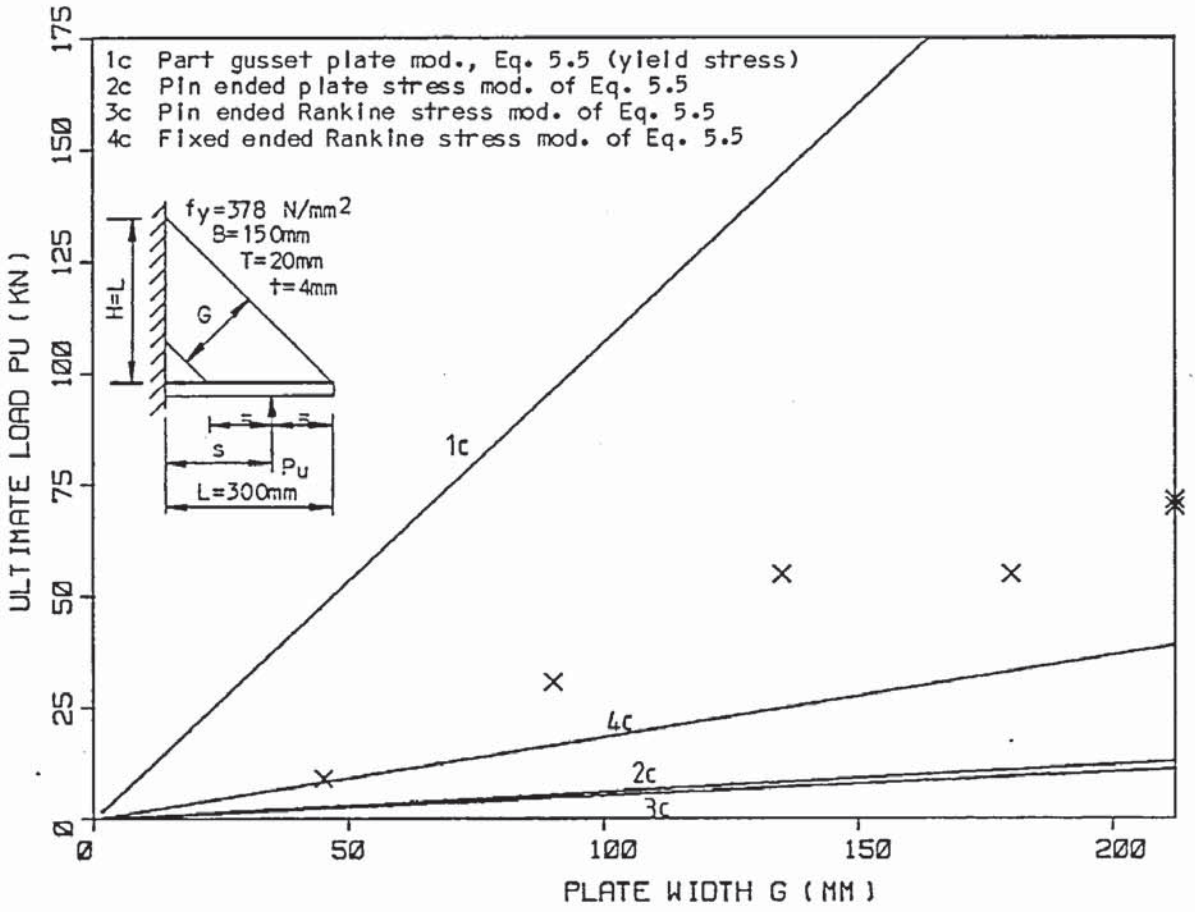

Figure 5.8 Jensen's method compared with the experimental results of series 8 (s=varies).

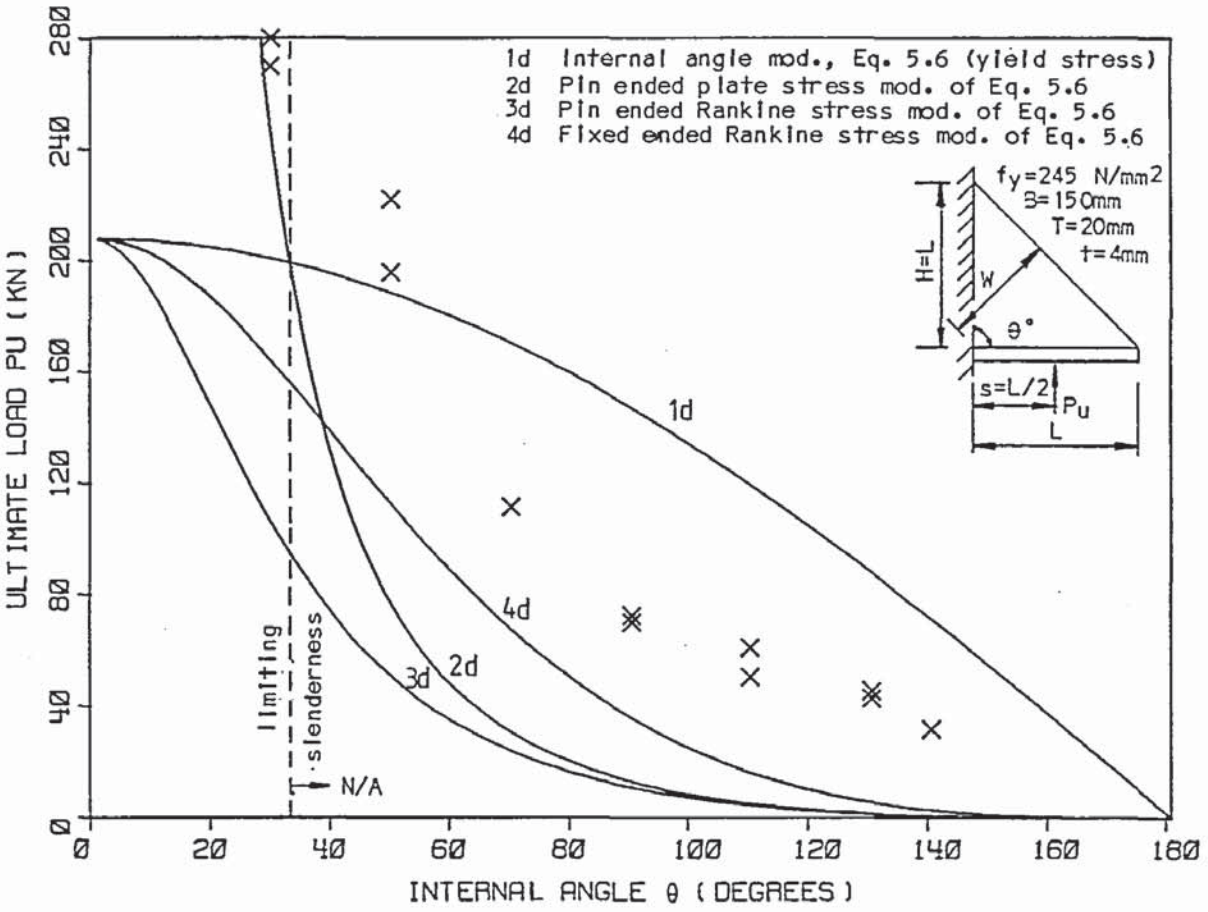

Figure 5.9 Jensen's method compared with the experimental results of series 13.

demonstrates its inaccuracy for s<L/2. The curve is assymptotic with s=L/3 and negative for values s<L/3.

Curve 1 in comparison with each series has overestimated the strength of most of the gusset plates with the exception of the non-slender gusset plates. This is because the yield stress has been used for all gusset plates.

Essentially the suggestions made by Beedle et al (7) and Salmon et al (8) to modify Jensen's (4) method to take account of buckling are the same. Taking Salmon et al's (8) suggestion of using the pin ended plate equation (Equation 2.4) gives a maximum stress to use in Jensen's (4) equation of

$$f_{max} \leqslant \frac{^{2}E.t^{2}}{12(1-\nu^{2})}\left(\frac{8}{7}\frac{\sin\alpha}{L}\right)^{2} \qquad (5.3)$$

This is represented by curve 2 in the figures, which is based on the buckling stress and therefore should be used in conjunction with curve

1, otherwise the loads will tend to infinity in certain cases as demonstrated in Figures 5.1, 5.6 and 5.9. However, this buckling stress assumption has produced an over conservative curve.

Alternatively Salmon et al (8) suggested using the plate buckling equation to give a limiting thickness to maintain the yield strength.

$$t \geqslant \frac{7}{8} \frac{L}{\sin \alpha} \sqrt{\frac{12(1 - \nu^2) f_y}{\pi^2 E}} \qquad (5.4)$$

This limiting thickness has terminated curve 1 just within the experimental results of series 3 and 12, and it has also correctly rendered the gusset plates of the other series not applicable to Jensen's (4) method. However, a limiting thickness is not always suggested.

A convenient alternative buckling stress equation which takes account of yielding is the Rankine-Gordon buckling stress equation (Equation 2.44) which is a transition curve from the elastic critical stress to the yield stress in a strut. Beedle et al's (7) intention was possibly to use a similar buckling stress equation.

A conservative assumption is for a pin ended strut, but a more appropriate assumption is for a fixed ended strut. Curves 3 and 4 are the result of such assumptions. The pin ended strut, curve 3 in Figures 5.1, 5.6 and 5.9, shows quite well the transition from the pin ended plate curve 2 to the yield curve 1. However, it is very conservative and virtually the same as the pin ended plate, curve 2, for slender gusset plates.

The fixed ended assumption, curve 4, shows a similar transition curve at a higher load. This curve shows some resemblance to the experimental results but, it is still very conservative. The fixed ended plate buckling stress equation produces a curve similar in shape to curve 2 and has a similar relationship with the fixed ended Rankine-Gordon curve 4, as curve 2 has with the pin ended Rankine-Gordon curve 3.

Comparing the shape of the curves with each series, the use of the Rankine-Gordon buckling stress equation in Jensen's (4) equation gives the best result. There is a similarity with some of the series. However, the method is inaccurate for s<L/2 as clearly shown in Figure 5.3.

Jensen (4) intended his method to be used for gusset plates with the internal corner removed parallel to the free edge, as with series 7. Effectively the remaining plate is assumed to be a prism and e, in Equation 5.1, becomes

$$e = \left| s - L + \frac{G}{2\cos\alpha} \right| \qquad (5.5)$$

also L.cosα is replaced by G, the remaining width of the gusset plate.

With the load at s=L/2, the effective eccentricity is similar to the load being applied at s<L/2 for a whole gusset plate. That is, based upon the stress on the inside edge, which is the yield stress in Jensen's (4) case. Curve 1b in Figure 5.7 is the resulting curve. As the effect is similar to s<L/2 for a complete gusset plate, similar curves cannot be plotted using the generalised equation or buckling stress modifications. Therefore only the curves for a whole gusset plate are plotted in Figure 5.7 to see if the equations can be used for small amounts of the corner removed. The experimental results suggest that possibly up to one third of the inside corner may be removed. However, this depends on how conservative the equations are.

With the load applied at the centre line of the remaining gusset plate, the eccentricity e is zero and so is equivalent to the load being applied at s=L/2 for a whole gusset plate. Therefore, all the methods are applicable to some extent. Curve 1c in Figure 5.8 uses the same equation as curve 1b in Figure 5.7. With the buckling stress modifications the buckling stress curves are calculated based on an effective length of a quarter width of a whole gusset plate despite the fact there is not one quarter width of gusset plate remaining in

some instances.

None of the existing equations presented have a factor for the variation of the internal angle and none of them can rationally be used as an approximation in their existing form. However, the basic assumption of considering an eccentrically loaded prism can be extended to include a variation of the internal angle giving

$$P = \frac{t.L.f_{max}}{(1 + 6e/L)} \left(\frac{W}{L}\right)^2 \qquad (5.6)$$

where $e = |s - L/2|$

$$W = \frac{L.H.\sin\theta}{V}$$

$$V = \sqrt{L^2 + H^2 - 2.L.H.\cos\theta}$$

This is curve 1d in Figure 5.9 and similarly the buckling stress modifications are curves 2d, 3d and 4d. These have also had an additional modification to take account of the change in the centre line length of the quarter width strip of plate with the variation in the internal angle. The limiting slenderness Equation 5.4 when modified gives the intersection point of curves 1d and 2d, which safely terminates curve 1d within the experimental results.

5.3 Salmon's method

In Figures 5.10 to 5.17 the elastic critical loads calculated using Salmon's (9) (12) method together with the associated variations presented in Section 2.3, are plotted with the experimental ultimate load results obtained for each of the main gusset plate series.

In the design methods found which use Salmon's (9) (12) work, Equation 2.9 is used as the basis for design, which when re-arranged gives

$$P = L.t.f_y.Z \qquad (5.7)$$

where Z is given by Equation 2.10.

This equation assumes yielding without buckling and is represented by curve 1 in the figures. To take account of buckling there are two

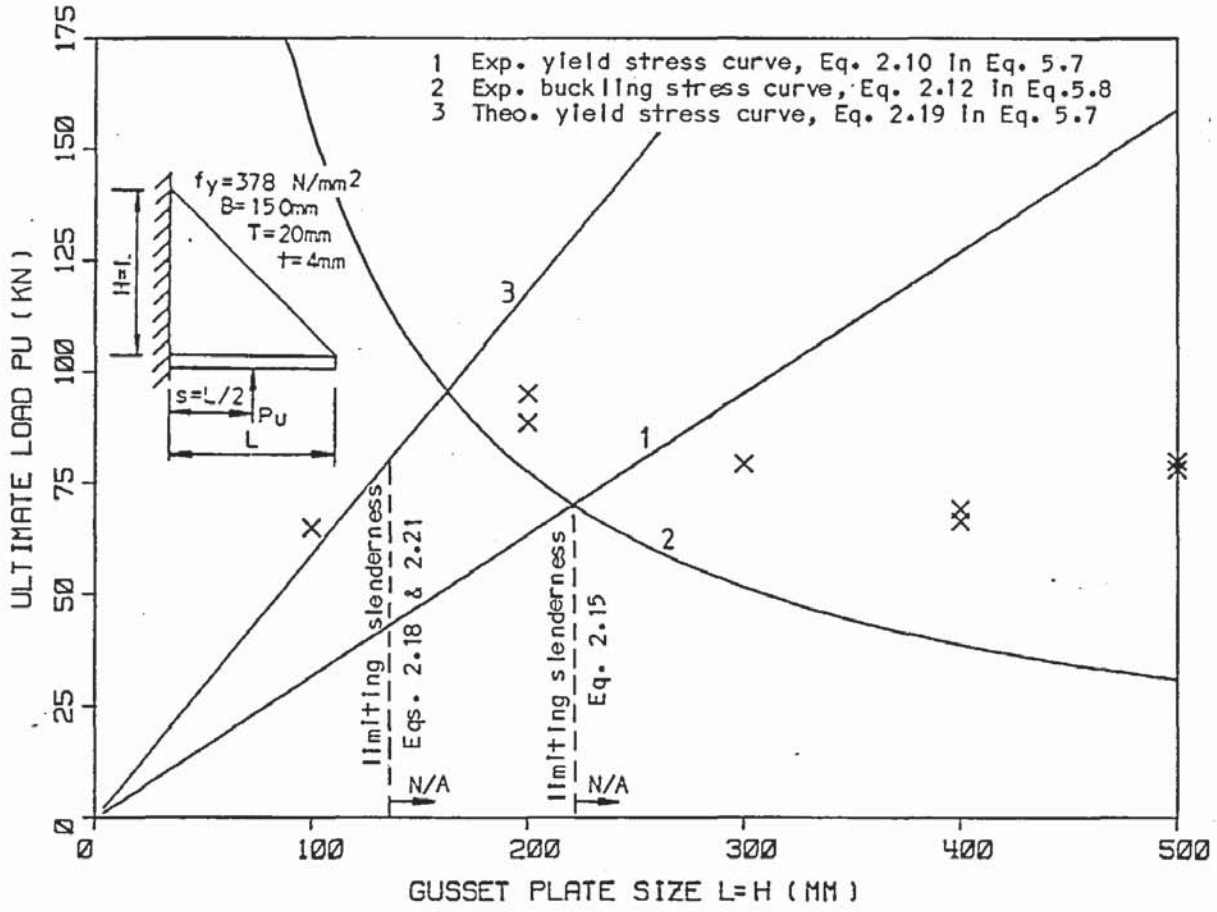

Figure 5.10 Salmon's method compared with the experimental results of series 3.

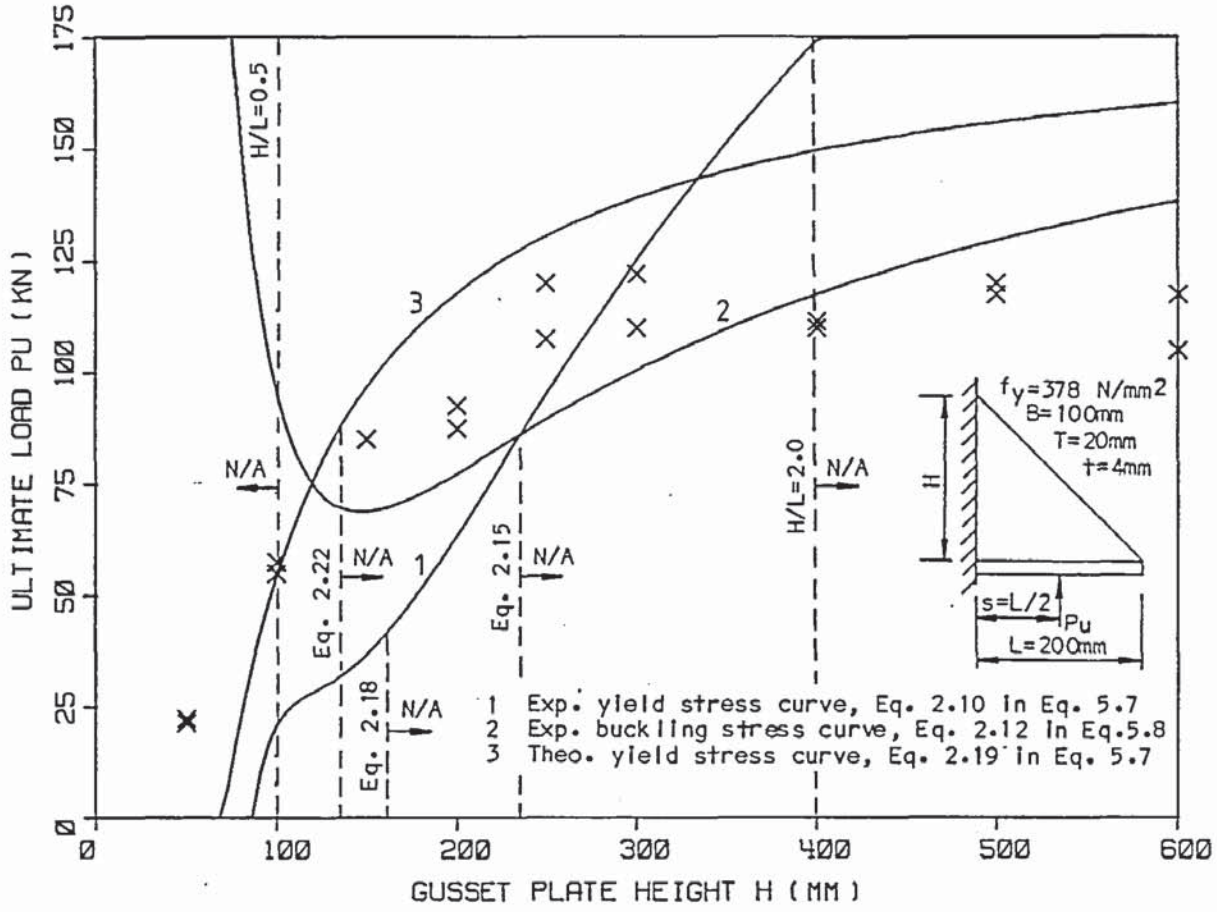

Figure 5.11 Salmon's method compared with the experimental results of series 4.

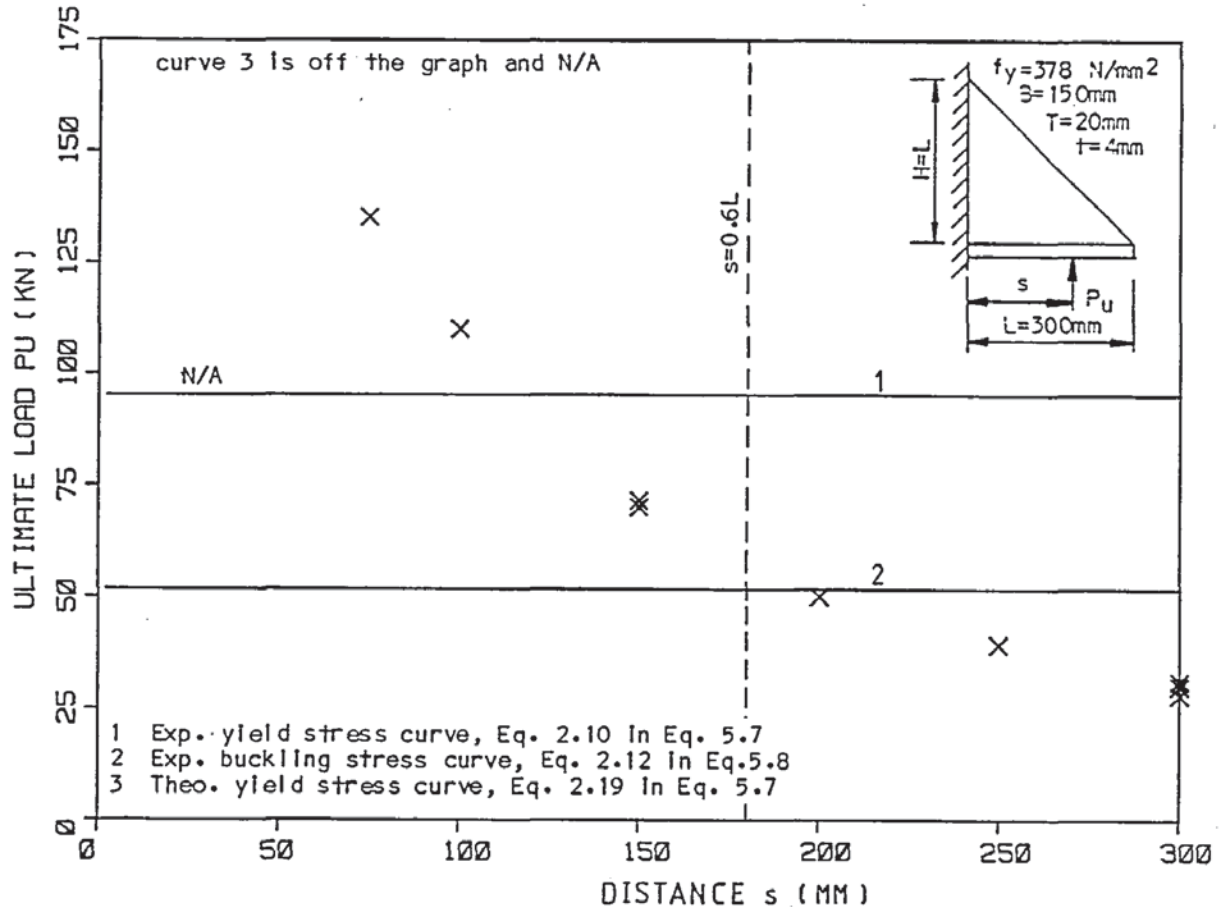

Figure 5.12 Salmon's method compared with the experimental results of series 5.

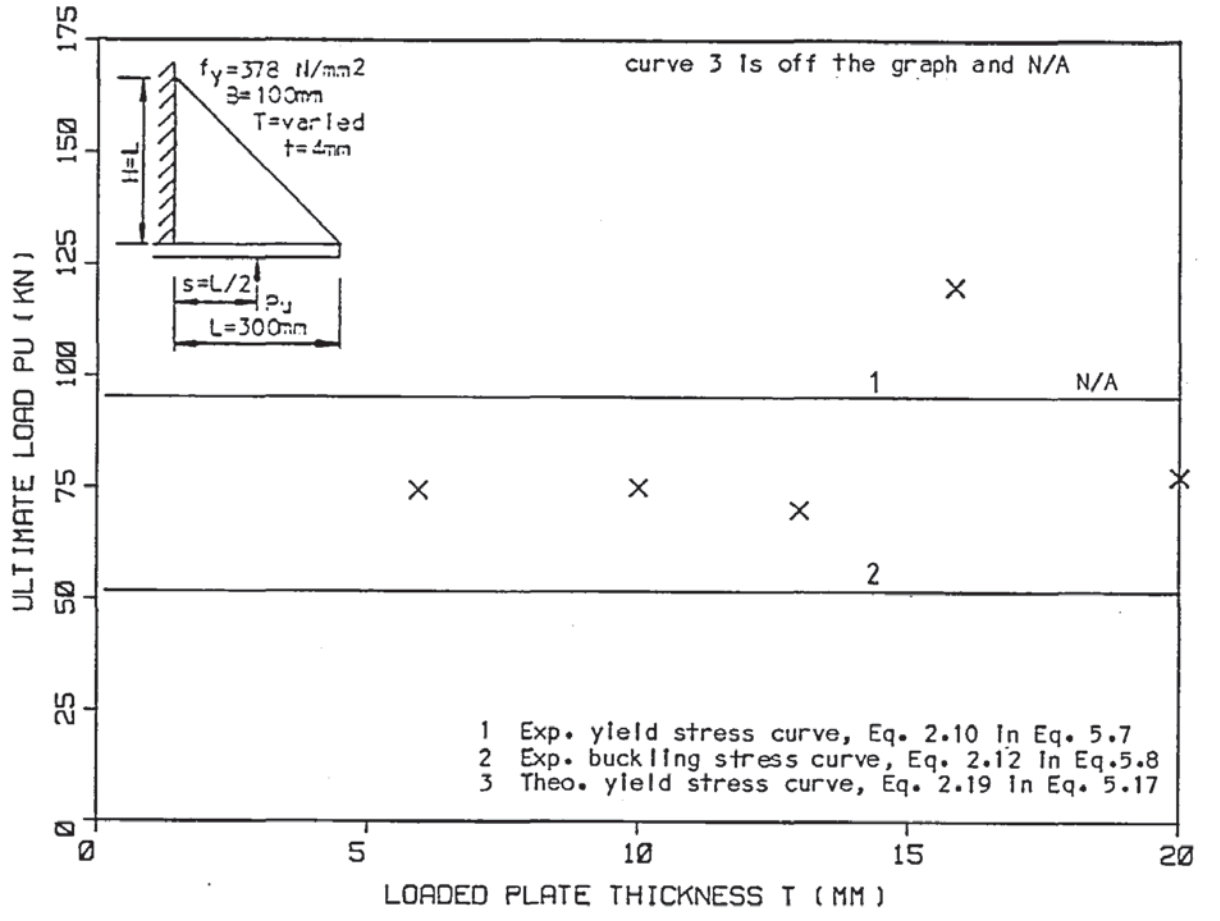

Figure 5.13 Salmon's method compared with the experimental results of series 7 (s=L/2).

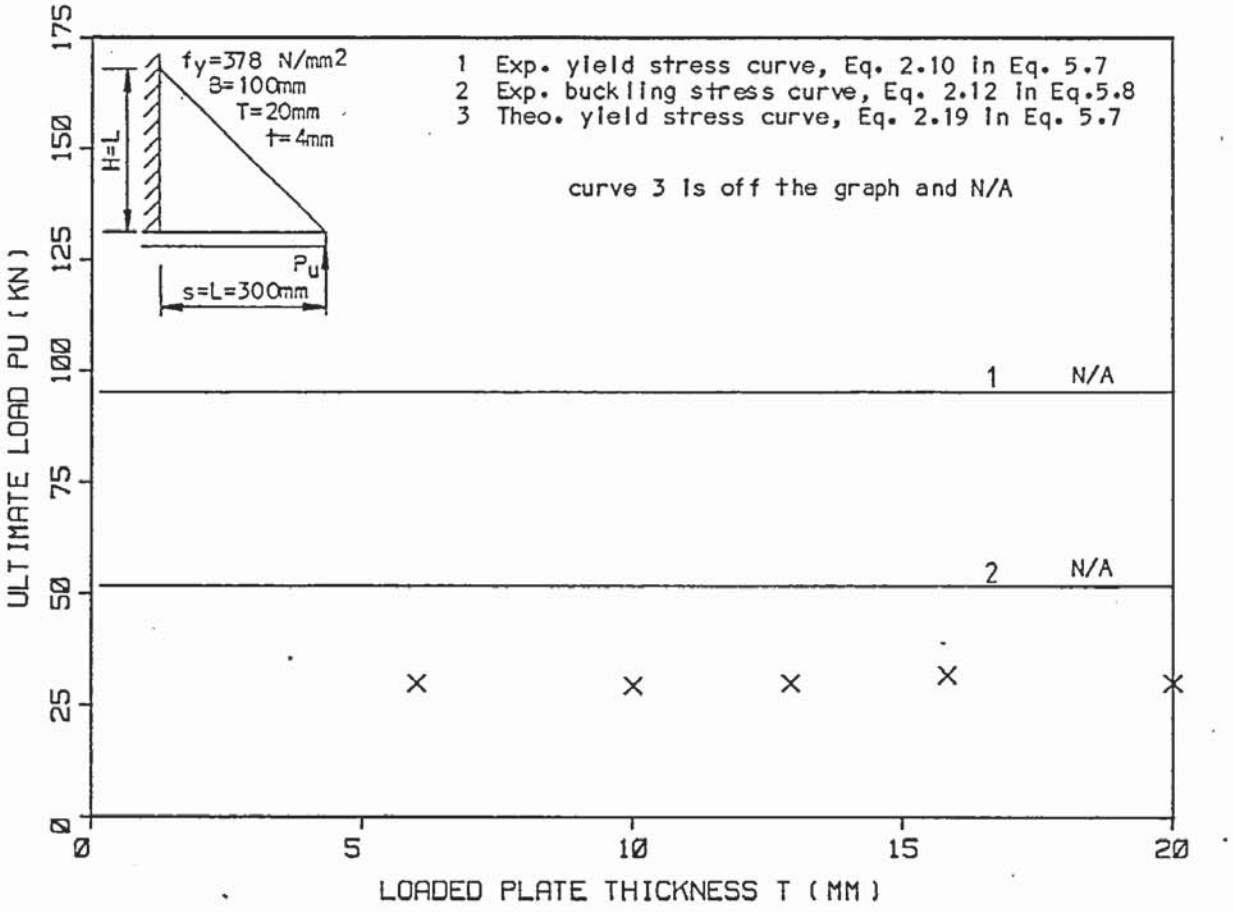

Figure 5.14 Salmon's method compared with the experimental results of series 7 (s=L).

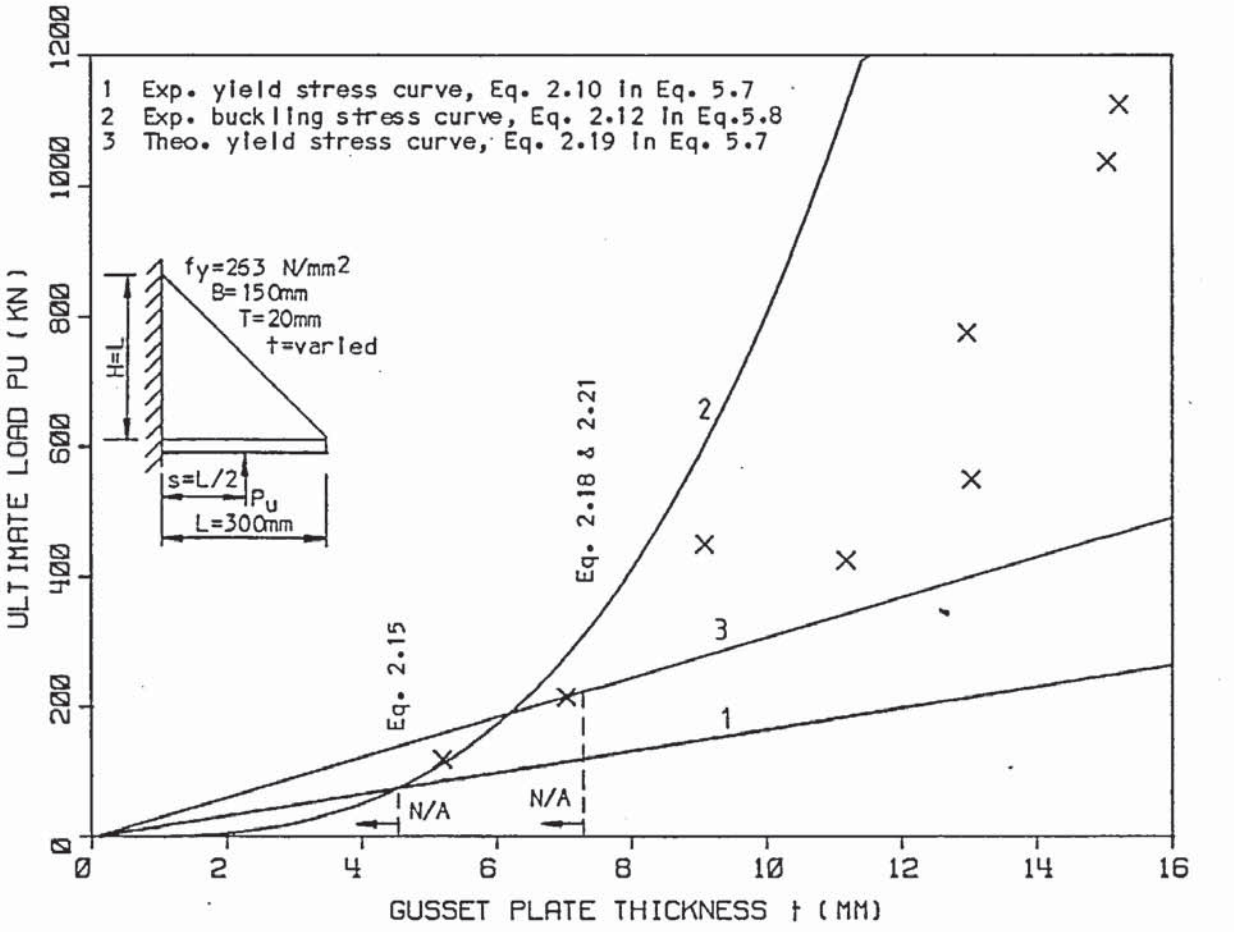

Figure 5.15 Salmon's method compared with the experimental results of series 12.

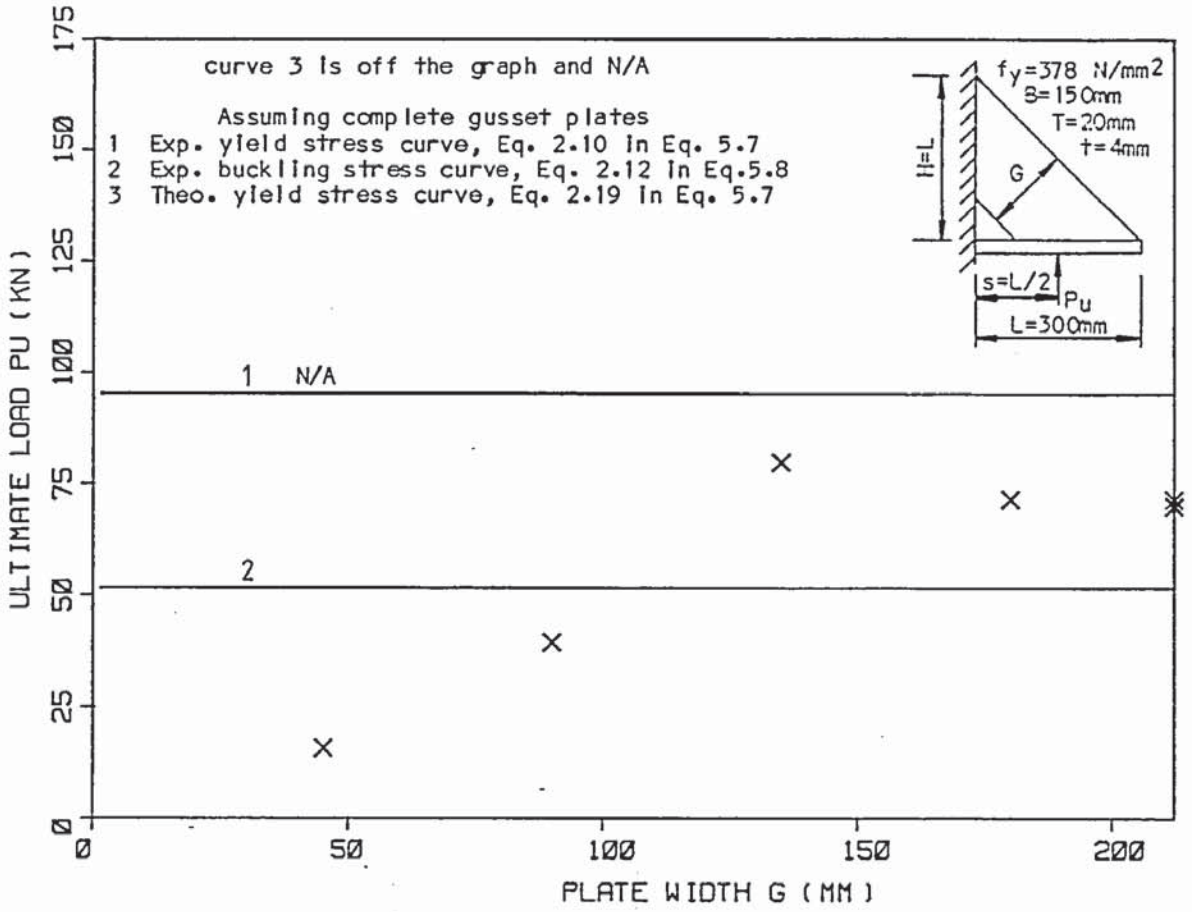

Figure 5.16 Salmon's method compared with the experimental results of series 8 (s=L/2).

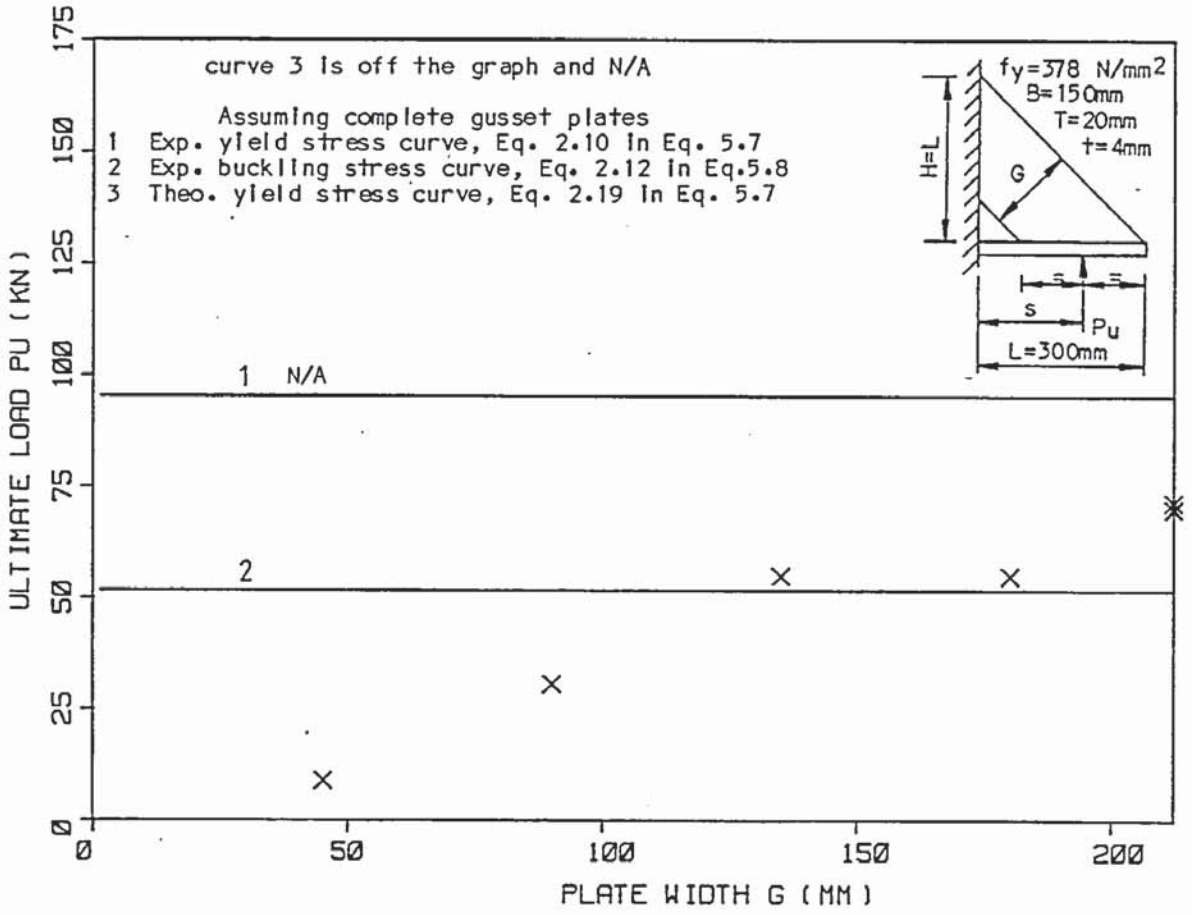

Figure 5.17 Salmon's method compared with the experimental results of series 8(L varies).

options, either the buckling stress is used in the design or it is ensured that buckling does not occur and the yield stress is used. For the elastic buckling condition Salmon (9) (12) produced Equation 2.11, which when re-arranged gives

$$P = \frac{k'\pi^2 E.t^3}{12(1-\nu^2)L} \qquad (5.8)$$

where k' is given by Equation 2.12.

This equation is represented by curve 2 in the figures and should be used in conjunction with curve 1. Alternatively one of the slenderness ratio equations presented in Section 2.3 can be used to terminate the yield curves and are included in the figures. Curve 3 is Salmon's (9) original theoretical yield curve (Equation 2.10 in Equation 5.7) which is included as it is still suggested in some references.

As the load for most of the specimens is applied at s=L/2 Salmon's (9) (12) method can be used, although it is not strictly correct. Generally the yield curves 1 and 3 are inaccurate and unsafe without the use of the buckling stress curve 2 with curve 1, or alternatively the use of the appropriate limiting thickness equation. Salmon's (9) (12) method is also restricted to $0.5 \leqslant H/L \leqslant 2.0$, the limits of which are indicated in Figure 5.11. Beyond these limits the curves are inaccurate.

As Salmon's (9) (12) method is based on a parabolic load distribution with its centroid at approximately s=0.6L it is not strictly applicable to other load conditions. However, Salmon (9) (12) stated that it could be used for approximately uniformly distributed loads. The assumed load position is indicated in Figure 5.12 and as only the buckling curve 2 is applicable in this series Salmon's assumption is correct. His method is safe to use for load positions $s \leqslant 0.6L$ although it is not very accurate and it is increasingly conservative the closer the load is applied towards the

supported edge. It is inaccurate and unsafe to use it for load positions s>0.6L, this is also reflected in Figure 5.14 where the load is applied at the end of the loaded plate.

Although Salmon's method is for complete plates the comparison with series 8 results is made to determine how much can be removed and the method remain safe. As only the buckling curve 2 is applicable it appears that up to half the inside corner of the gusset plate can be removed with the load at s=L/2 and one third removed with the load applied at the mid-side of the remaining loaded edge. However, the latter case is suspect as the load position is varied as well.

As Salmon's method is based on a 90° internal angled gusset plate it cannot be applied to or modified for gusset plates with an internal angle other than 90°.

5.4 The beam method

In Figures 5.18 to 5.23 the elastic critical loads calculated using the beam method and associated variations presented in Section 2.4, are plotted with the experimental ultimate load results obtained for each of the main gusset plates series.

This method assumes the gusset plate to act as a cantilevered beam with the critical stress being at the free edge of the critical section which is taken to be along the supported edge. The base plate is not normally included as part of the critical section and so this gives Equation 2.25 which when rearranged gives

$$P = \frac{f_{max} \cdot t \cdot H^2}{6s} \qquad (5.9)$$

Normally no allowance is made for buckling and so curve 1 in the figures shows the effect of using the yield stress. Curve 2 demonstrates the effect of using some buckling stress assumptions. With Jensen's (4) method the stress based on assuming one quarter width of the gusset plate at the free edge and using the fixed ended

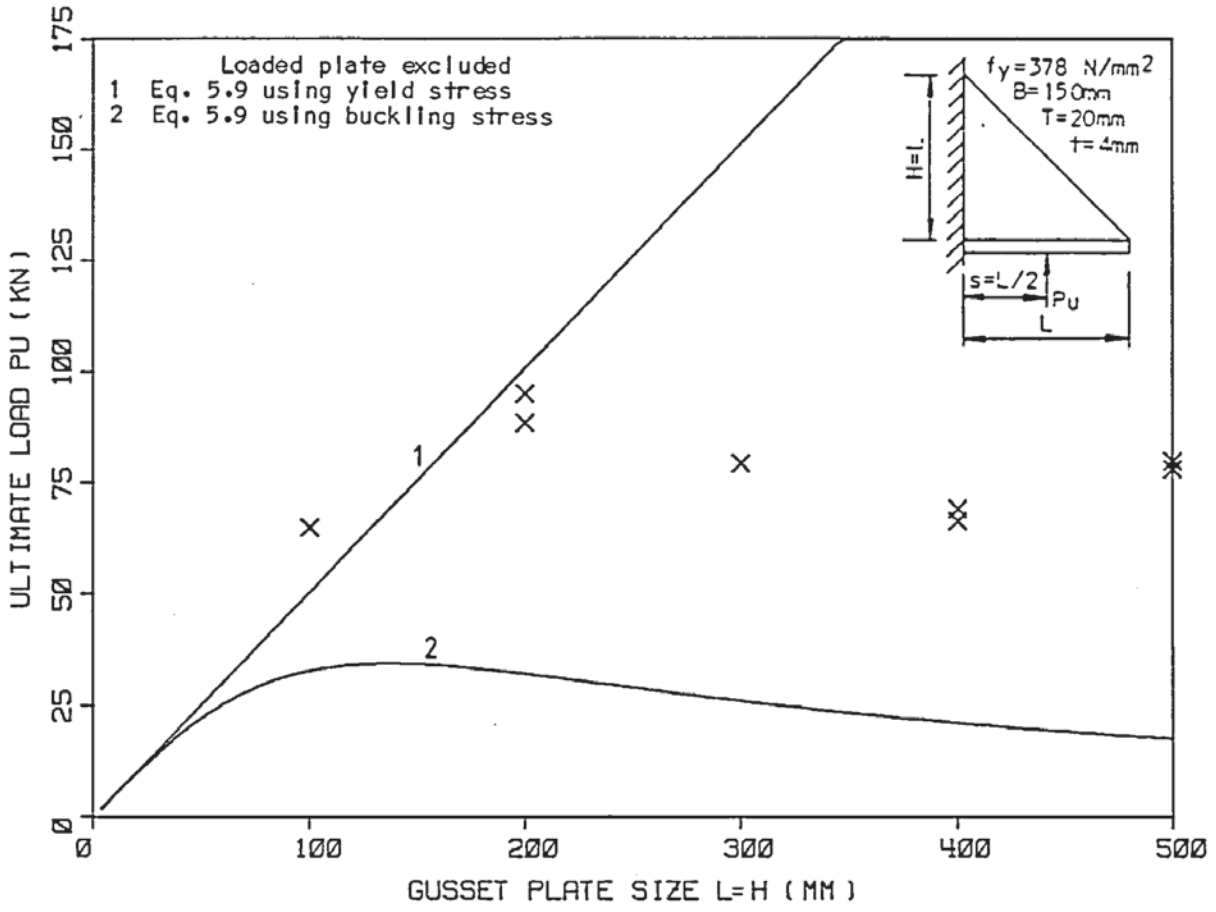

Figure 5.18 The beam method compared with the experimental results of series 3.

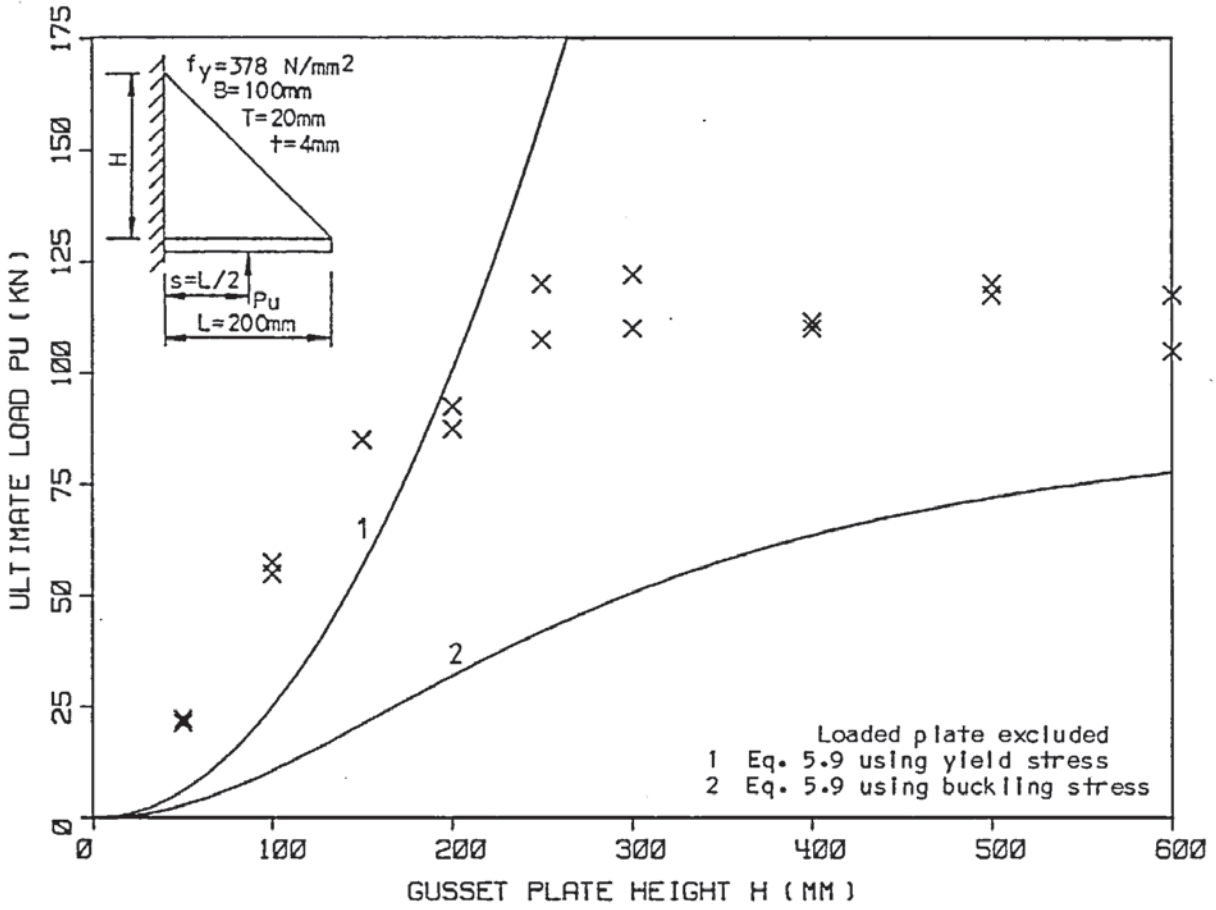

Figure 5.19 The beam method compared with the experimental results of series 4.

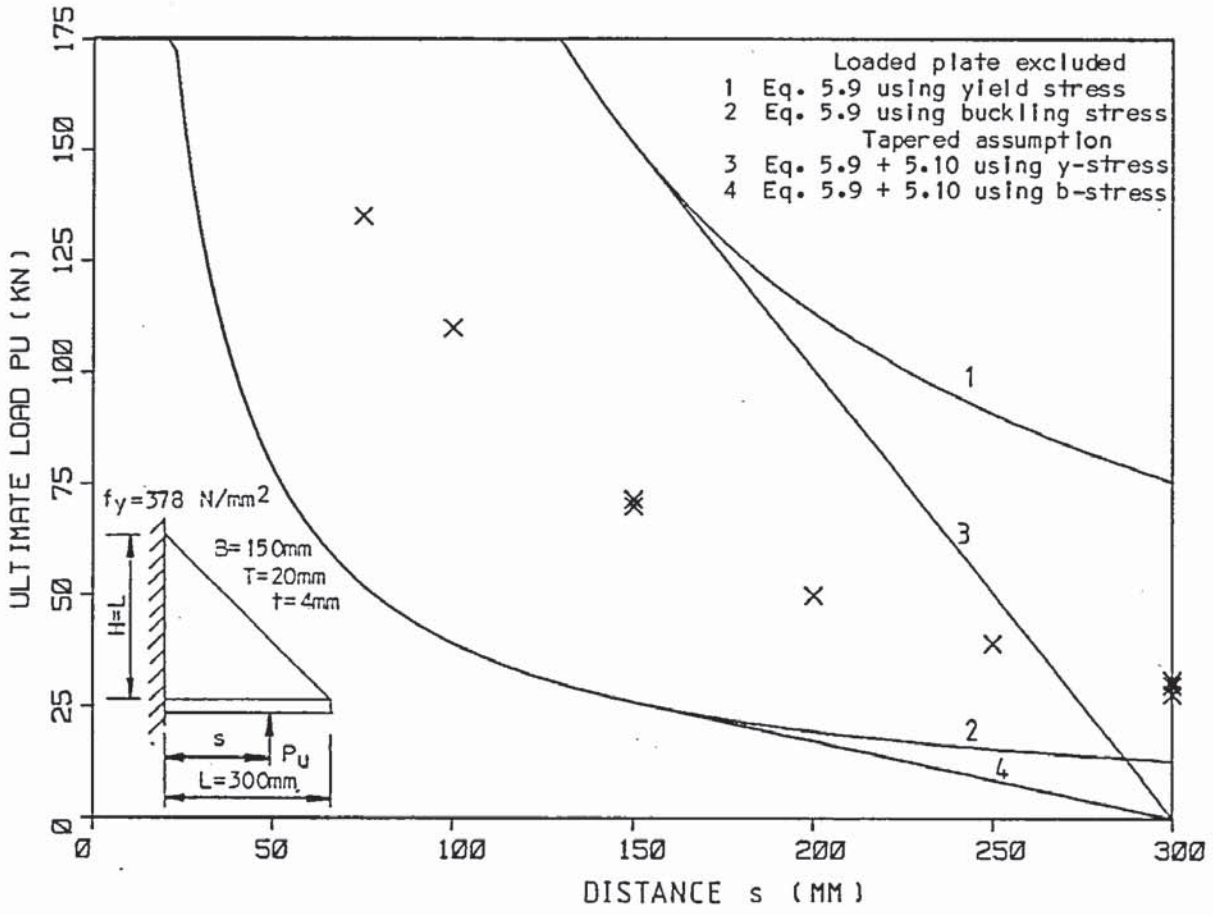

Figure 5.20 The beam method compared with the experimental results of series 5.

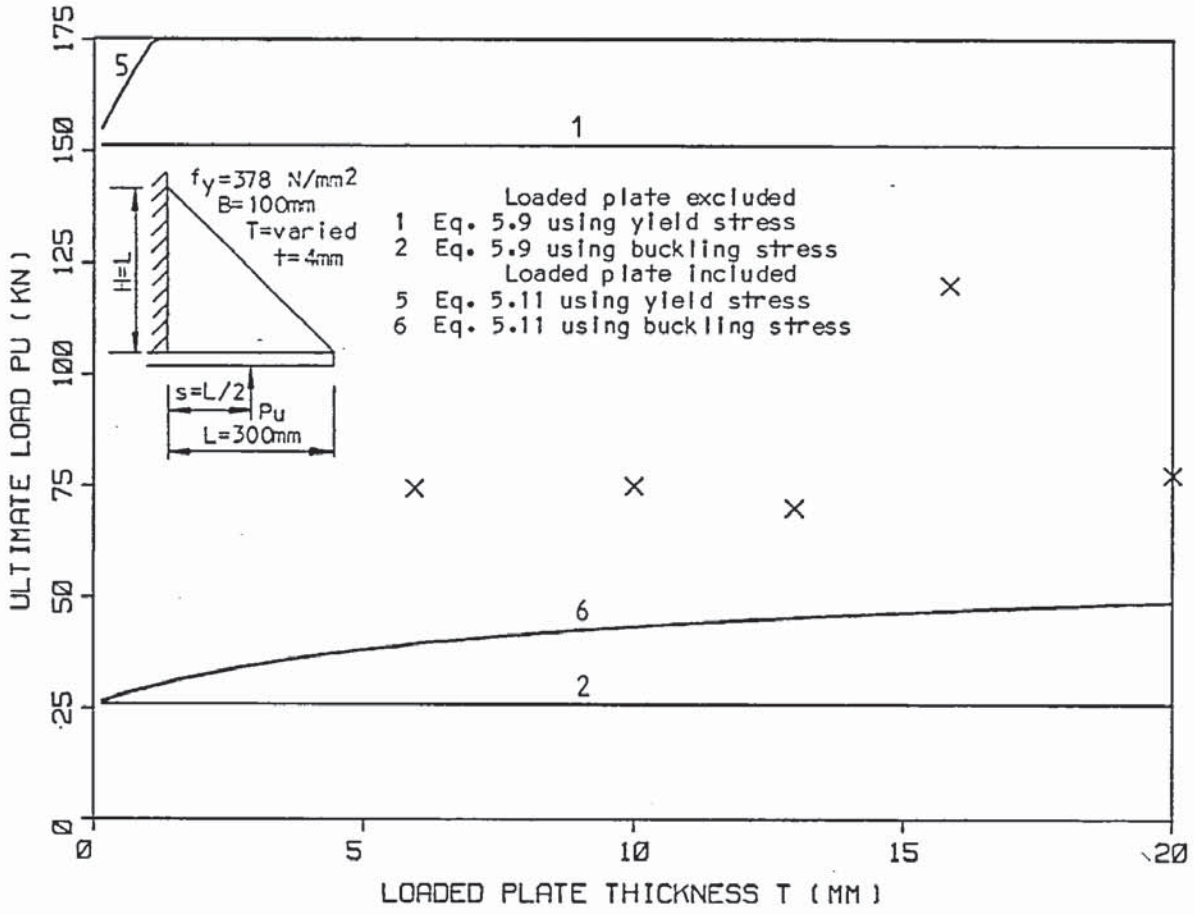

Figure 5.21 The beam method compared with the experimental results of series 7 (s=L/2).

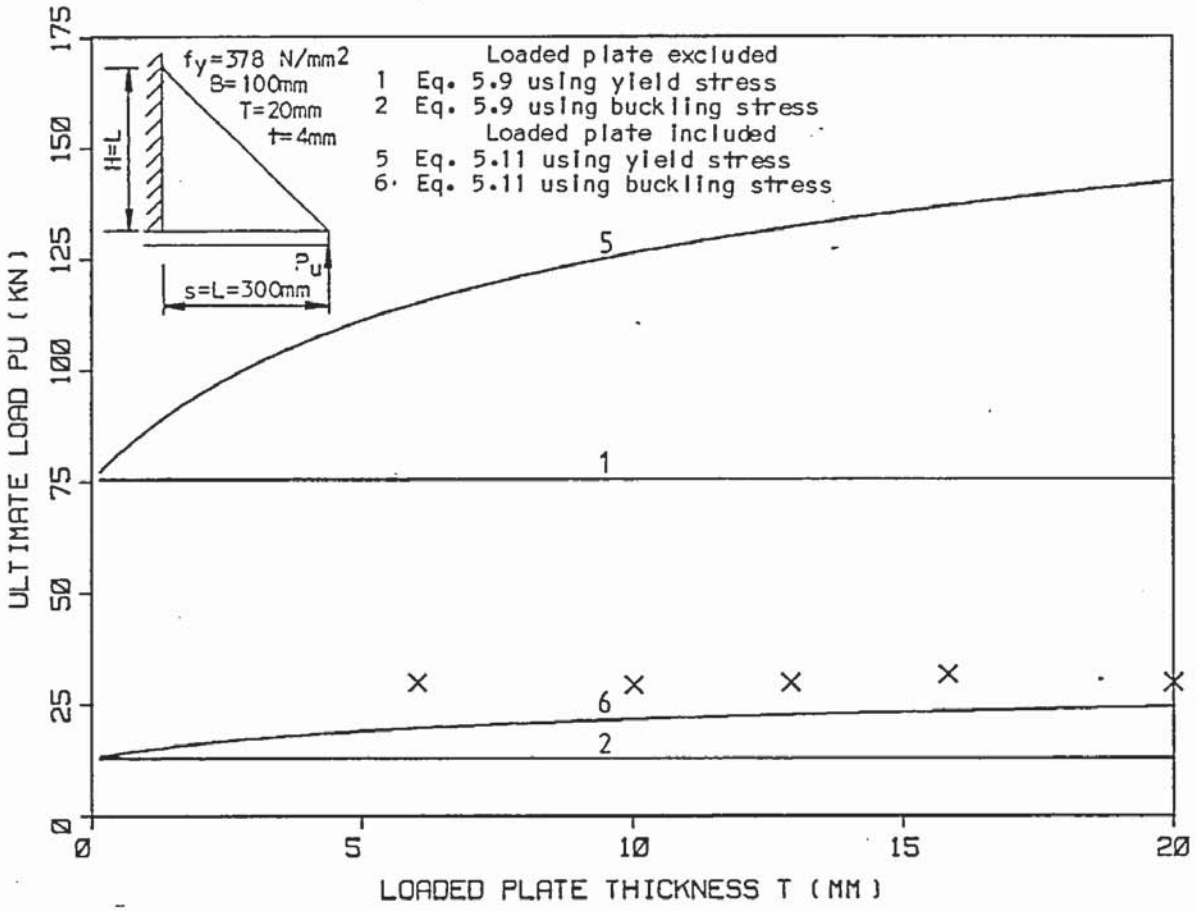

Figure 5.22 The beam method compared with the experimental results of series 7 (s=L).

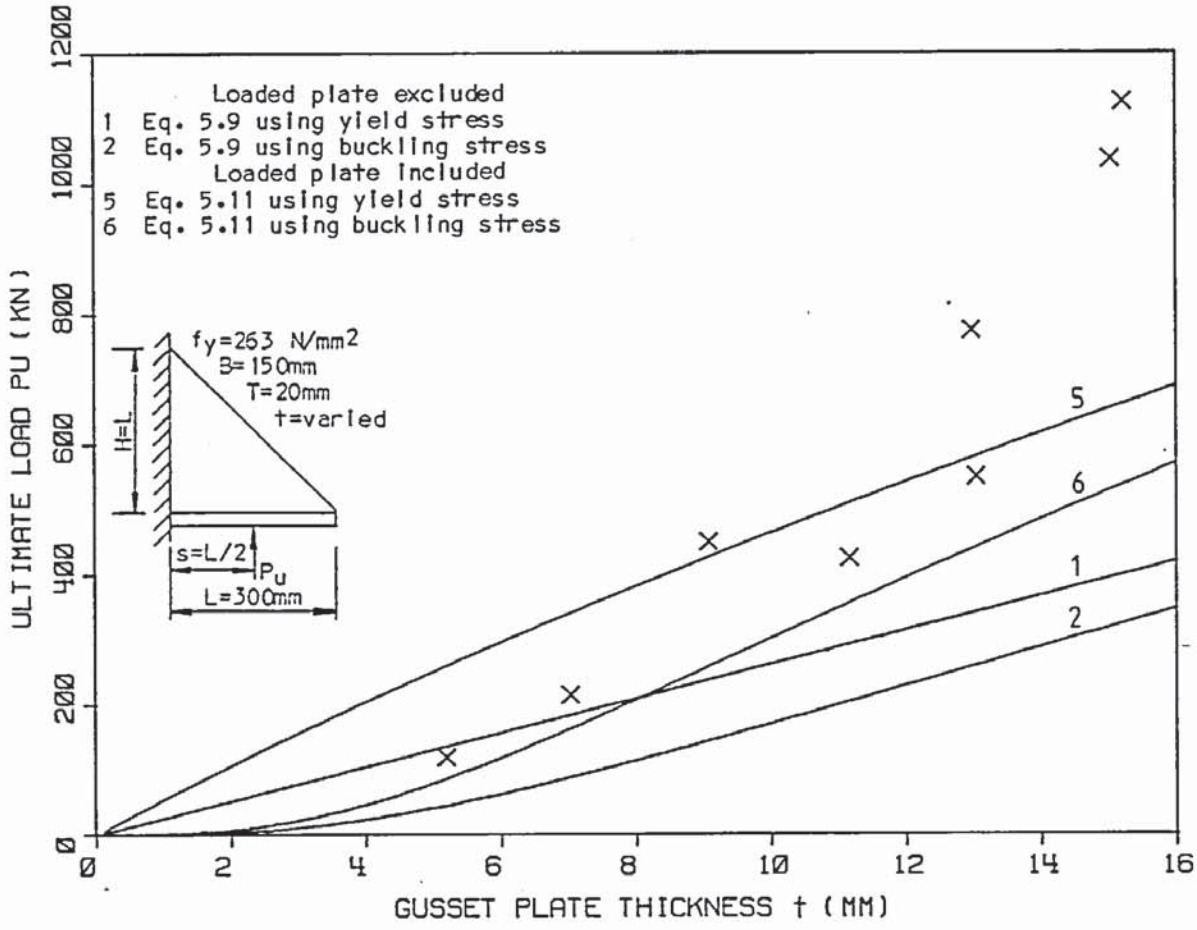

Figure 5.23 The beam method compared with the experimental results of series 12.

Rankine-Gordon buckling stress assumption was found to give the best result, therefore, this assumption is used.

From the figures it is apparent that the yield assumption curve 1 is inaccurate and very unsafe. As the curve is within the experimental results for the small plates of Figure 5.18 and 5.19 and for the thick plates of Figure 5.23, this suggests that some form of limiting thickness, to ensure yielding, may make the method safe to use in some situations. The other alternative is to use some buckling stress assumption as with curve 2. This curve resembles the experimental results, but it is very much on the conservative side.

Although the method assumes the gusset plate to act as a cantilevered beam, no account is taken that the critical section is not necessarily at the supported edge. For such a triangular profile the critical section is at

$$x = 2s - L \tag{5.10}$$

where x is measured from the supported edge. From this equation it is apparent that the critial section is only at the supported edge for $s<L/2$. Only series 5 and series 7 (s=L) shown in Figures 5.20 and 5.22, respectively, have loads at $s>L/2$. Curves 3 and 4 in Figure 5.20 are appropriate modifications to curves 1 and 2 respectively. Both curves 3 and 4 tend to zero at s=L which does not agree with the experimental results. As the load is zero at s=L, curves 3 and 4 are at zero in Figure 5.22.

If the loaded plate is taken into consideration then the combined section modulus z_{comb} of both the gusset plate and the loaded plate at the critical section is used in Equation 2.25, giving

$$P = \frac{f_{max} \cdot z_{comb}}{s} \tag{5.11}$$

Only series 7 (s=L/2), 7 (s=L) and 12 shown in Figures 5.21, 5.22 and 5.23, respectively, have continuous loaded plates. Curves 5 and 6 in these figures are appropriate modifications to curves 1 and 2

respectively. Curve 5 is very inaccurate and very unsafe. Curve 6 is conservative in each case. It is not in agreement with the variations in loaded plate thickness of series 7 but it is the best curve to fit the variation in gusset plate thickness, as shown in Figure 5.23.

The beam method cannot readily be applied to gusset plates with varying amounts of the inside corner removed or with variations in the internal angle. Therefore no comparisons are made with series 8 and 13 results.

5.5 The approximate strut method

In Figures 5.24 to 5.32 the elastic critical loads calculated using the approximate strut methods and associated variations presented in Section 2.5, are plotted with the experimental ultimate load results obtained for each of the main gusset plate series.

These methods are based on assuming a portion of the gusset plate to act as an axially loaded strut. The main problem is in determining the buckling stress. As the fixed ended Rankine-Gordon buckling stress was a reasonable choice in the previous methods, the author has chosen to use it in demonstrating the approximate strut methods.

The one quarter width method assumes that the component of the applied load parallel to the free edge, irrespective of its position along the loaded edge, acts concentrically on a quarter width strip of the gusset plate along the free edge which is assumed to act as a strut. The centre line length of the strip is taken to be the length of the strut. This gives Equation 2.31 for the stress, which when re-arranged for the load gives

$$P = \frac{1}{4} p_a L.t.\cos^2\alpha \qquad (5.12)$$

This is represented by curve 1 in the figures and is shown to be very conservative and inaccurate. The theory does not take into account the load position as demonstrated in Figure 5.26 for series 5.

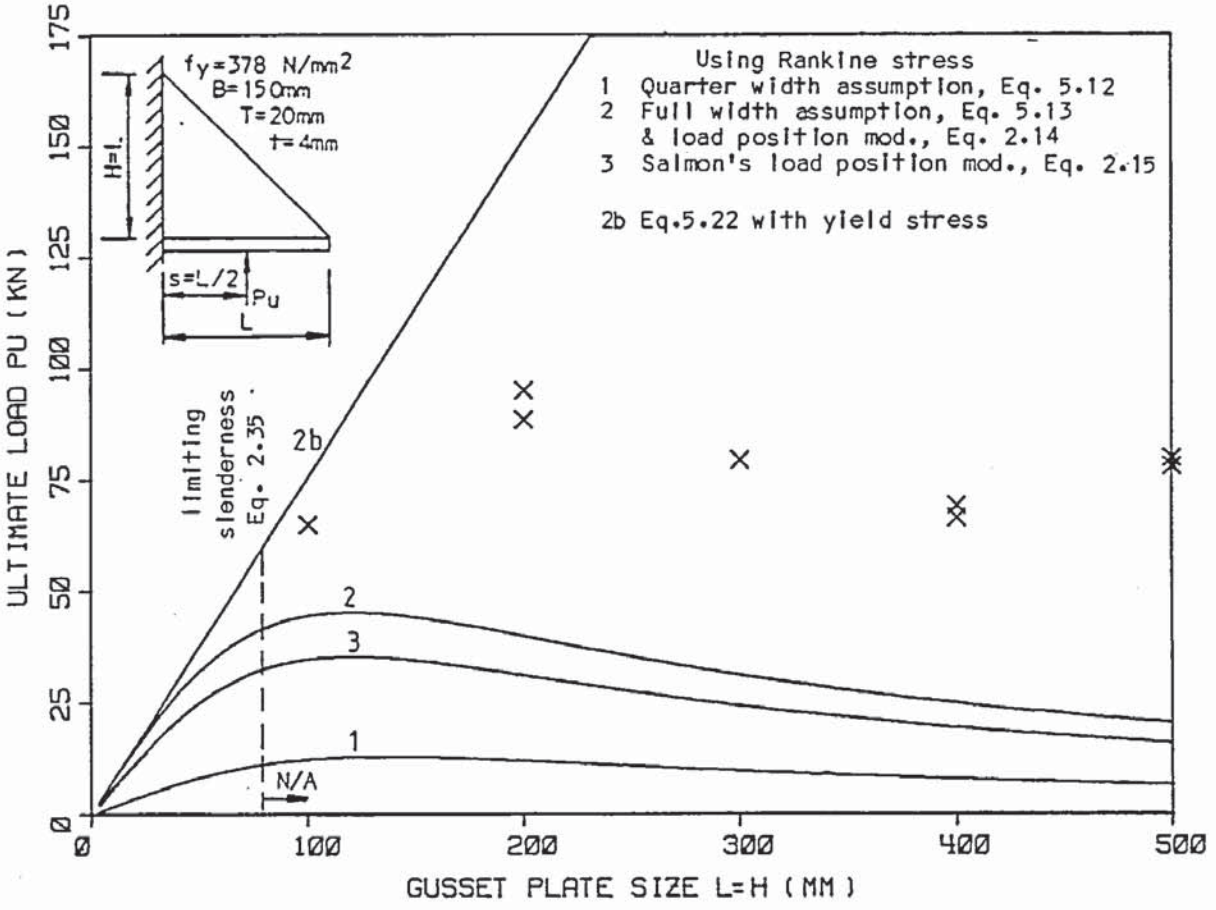

Figure 5.24 The approximate strut methods compared with the experimental results of series 3.

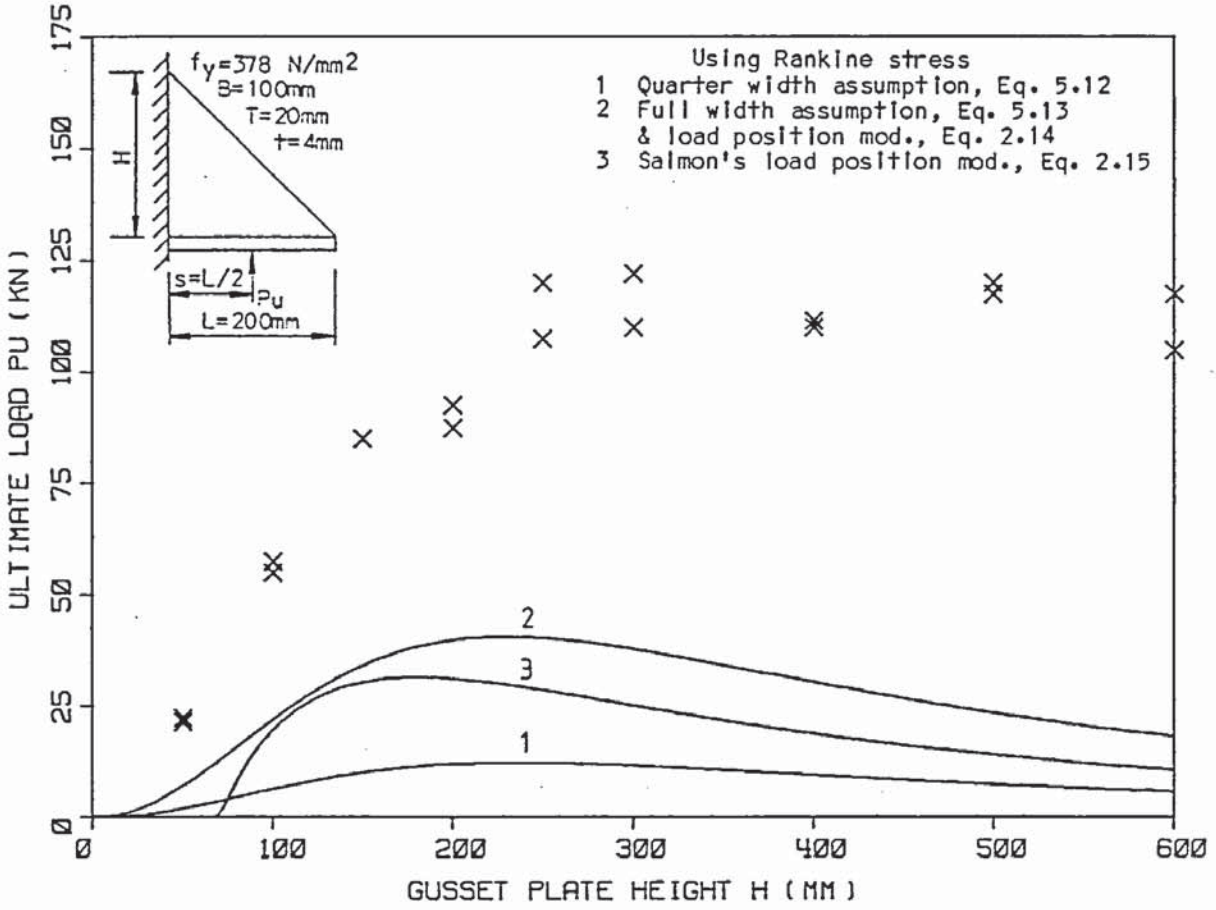

Figure 5.25 The approximate strut methods compared with the experimental results of series 4.

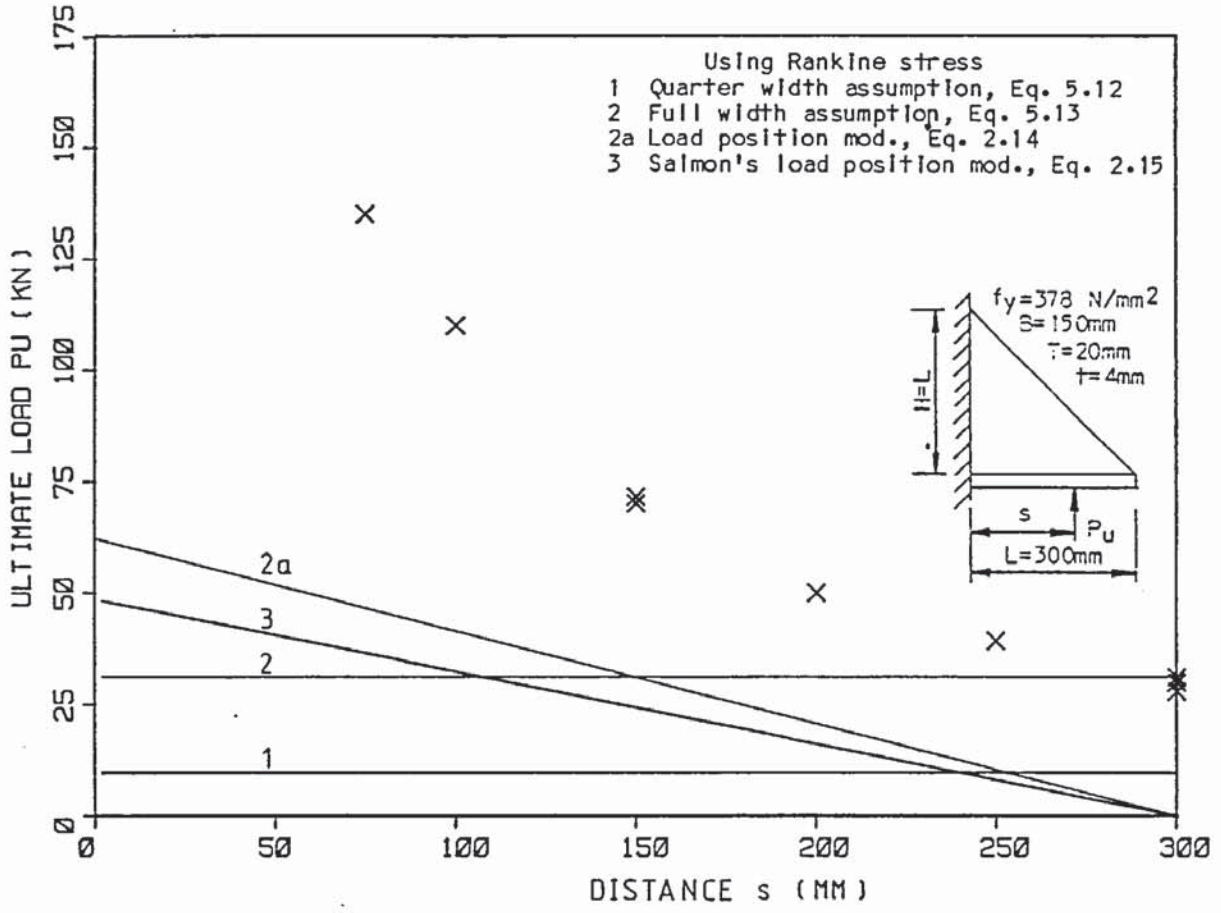

Figure 5.26 The approximate strut methods compared with the experimental results of series 5.

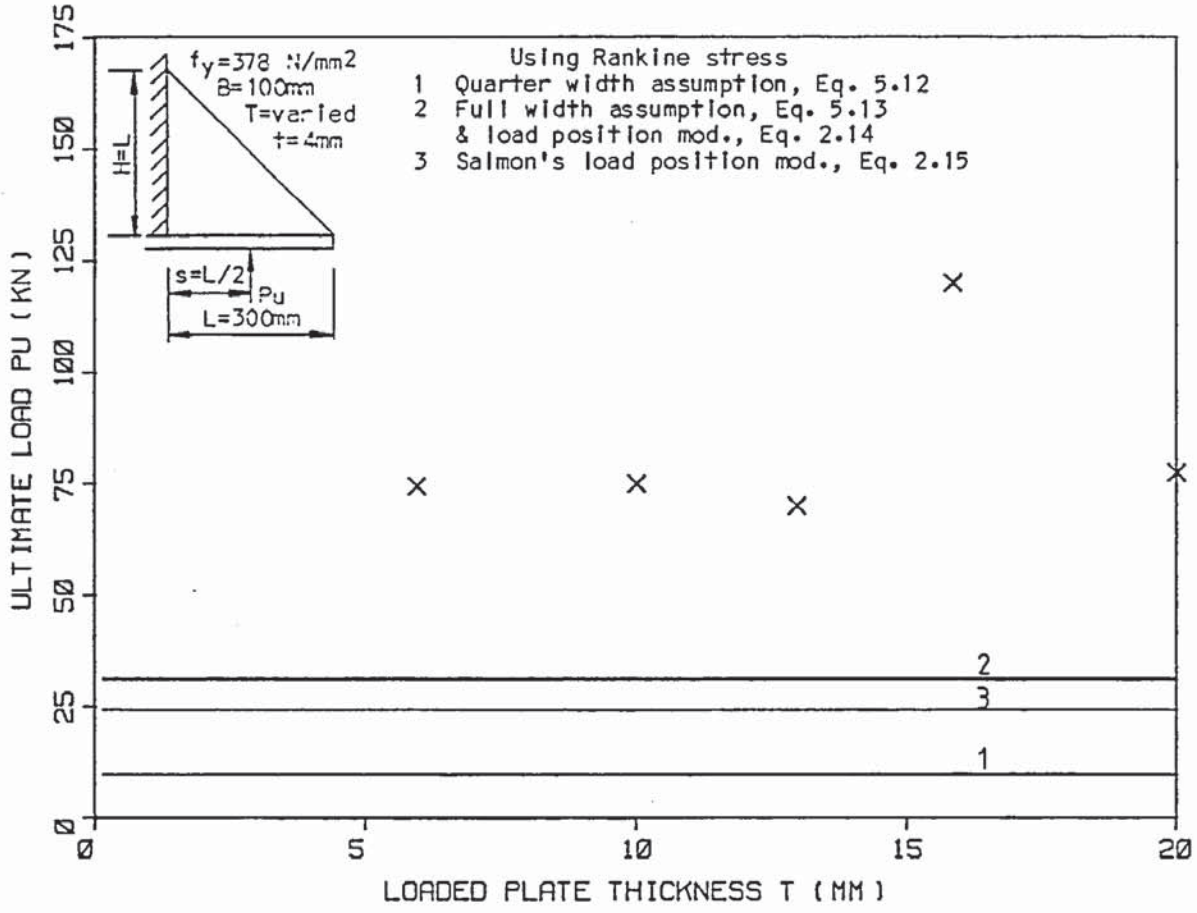

Figure 5.27 The approximate strut methods compared with the experimental results of series 7 (s=L/2).

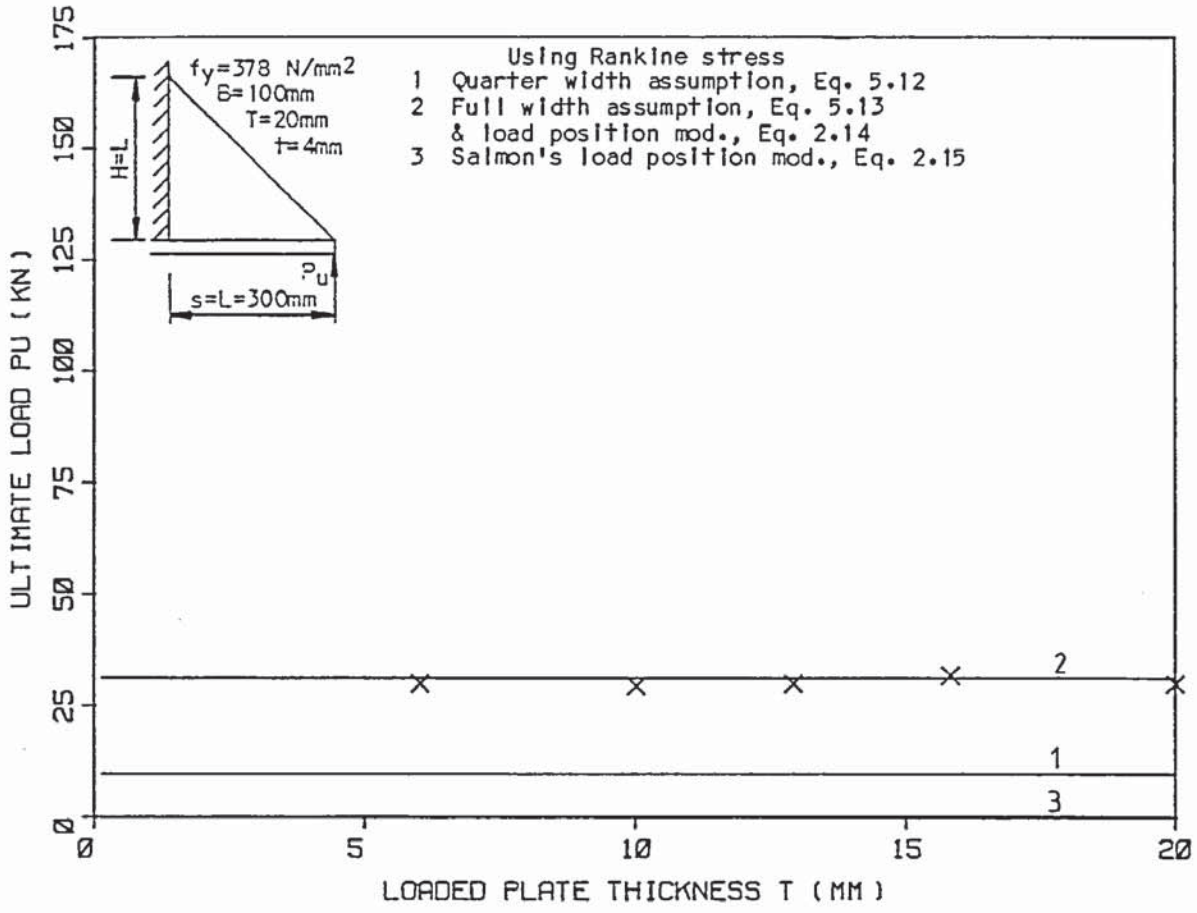

Figure 5.28 The approximate strut methods compared with the experimental results of series 7 (s=L).

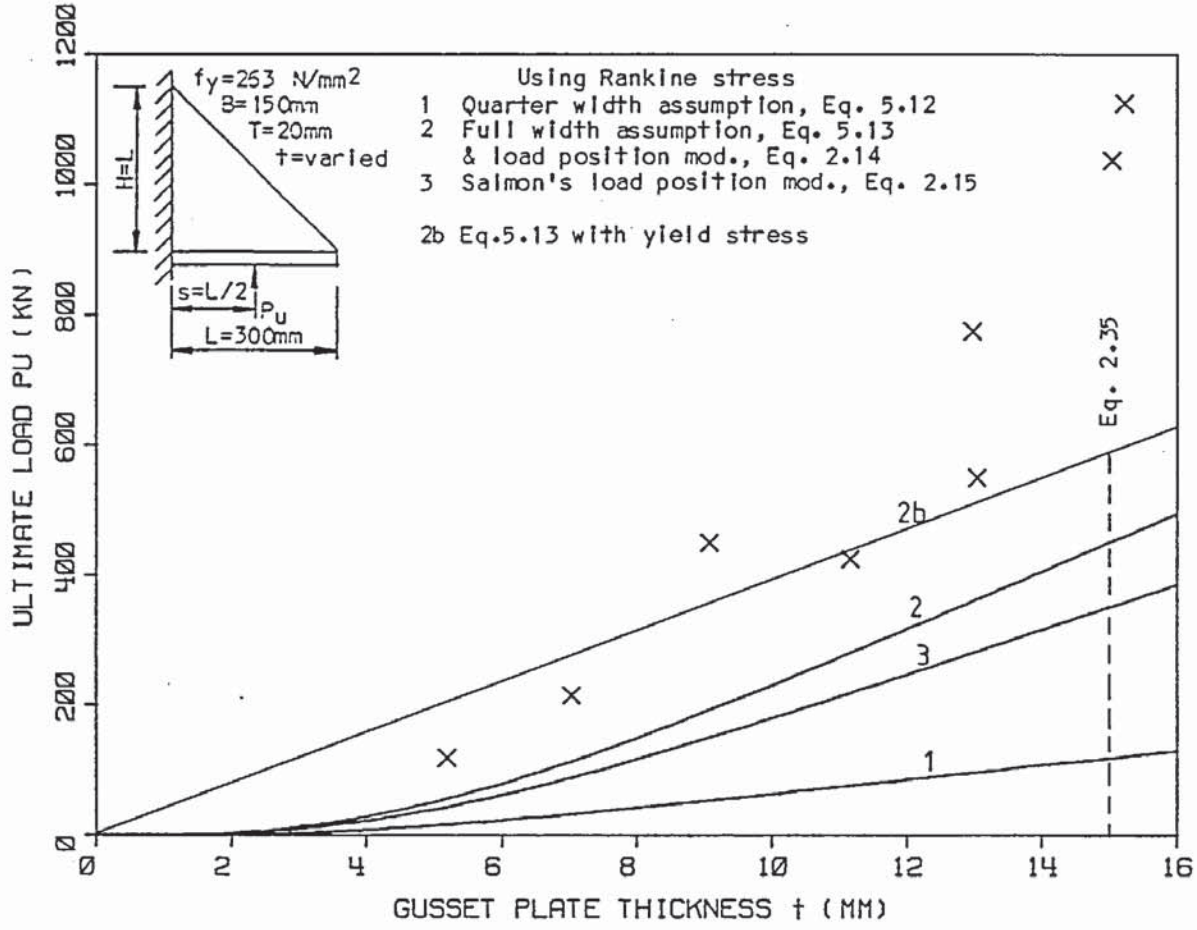

Figure 5.29 The approximate strut methods compared with the experimental results of series 12.

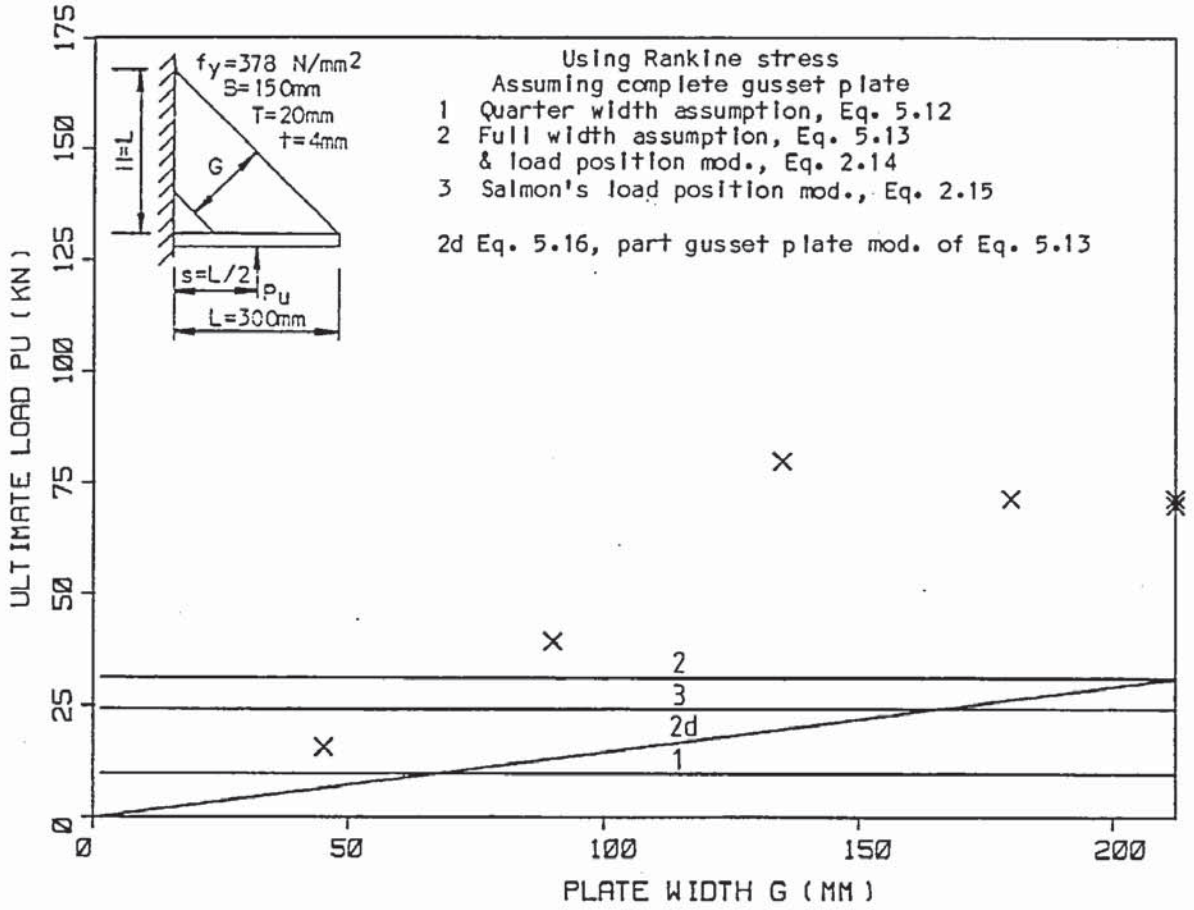

Figure 5.30 The approximate strut methods compared with the experimental results of series 8 (s=L/2).

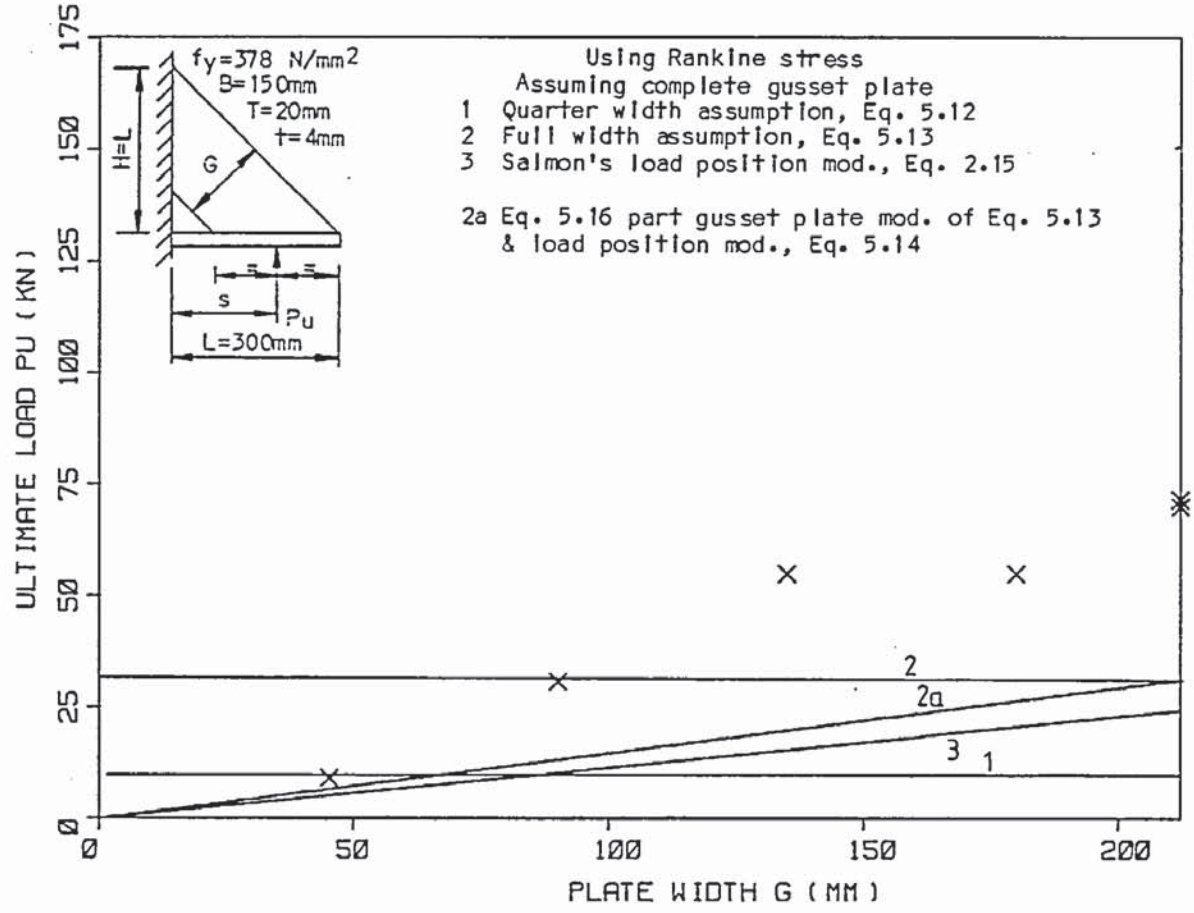

Figure 5.31 The approximate strut methods compared with the experimental results of series 8 (s=varies).

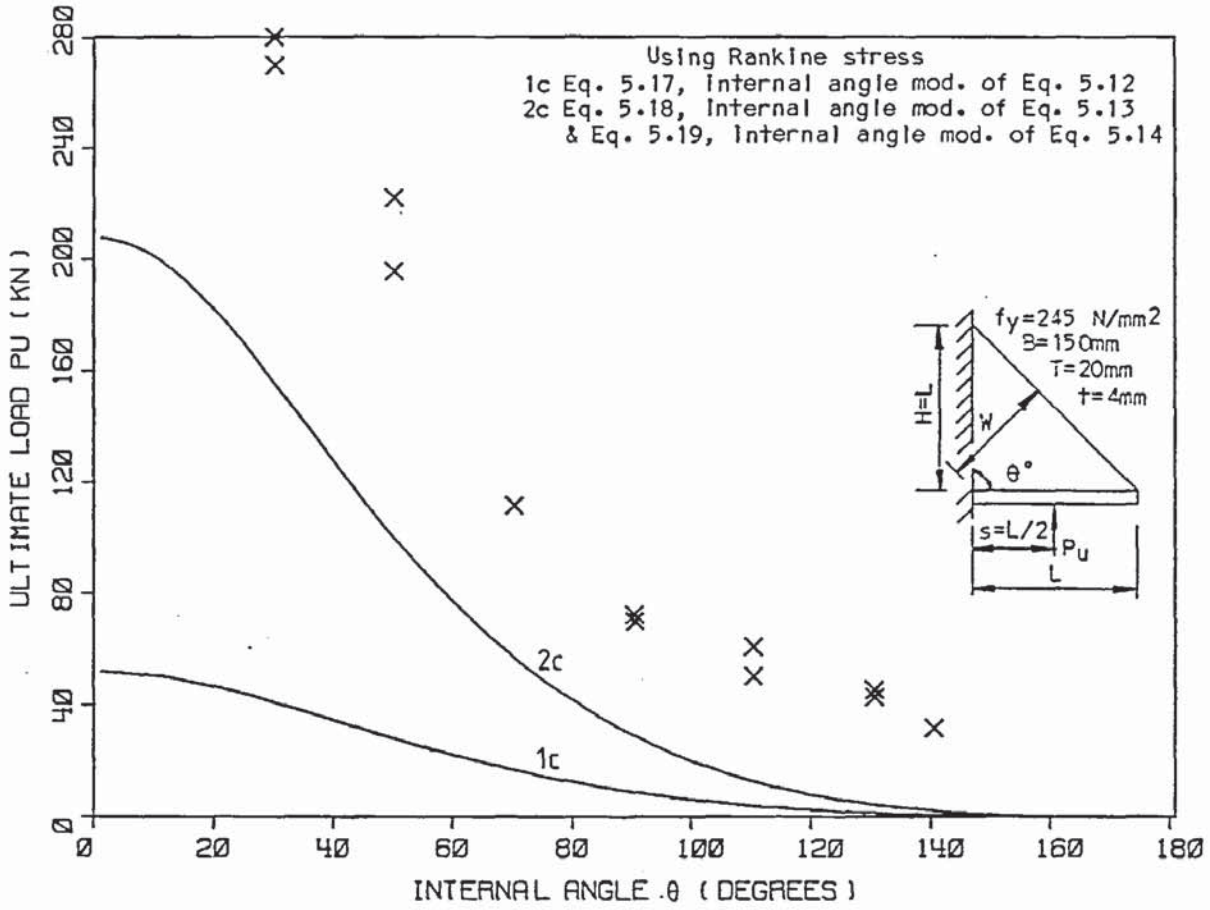

Figure 5.32 The approximate strut methods compared with the experimental results of series 13.

Assuming the free edge length for a quarter width strip instead of the centre line length will produce an even more conservative result. However, another method assumes the free edge stress applied to the whole width of the gusset plate. This then gives Equation 2.32 for the stress which when re-arranged for the load gives

$$P = f_{max} L.t.\cos^2\alpha \qquad (5.13)$$

This is represented by curve 2 in the figures and although it is approximately four times greater than curve 1, it is still very conservative and inaccurate. Likewise curve 2 does not take into account the load position.

In an attempt to take account of the load position another method assumes only the width of plate to which the load is applied concentrically. This then gives Equation 2.33 for the stress which when re-arranged for the load gives

$$P = 2(L - s)p_c t.\cos^2\alpha \qquad (5.14)$$

When s=L/2, as in the majority of the tests, Equation 5.14 gives the same value as Equation 5.13, i.e. curve 2, otherwise it gives curve 2a. The effect of this equation is demonstrated best in Figure 5.26 with the series 5 results. For s>L/2 it is more conservative than the previous method. For s<L/2 it assumes a gusset plate width greater than the actual width thus giving an increased load. Although it may appear to be safe in Figure 5.26, it is very unsafe for very thick gusset plates where the free edge stress is approaching the yield stress.

An alternative to using a buckling stress in Equation 5.14, is to use a limiting thickness equation to ensure yielding. A method of obtaining a limiting thickness is presented in Section 2.4. Only series 3 and 12 in Figures 5.24 and 5.29 have this limit marked on with the yield curve of Equation 5.14, represented by curve 2b. None of the other series were applicable. The limiting thickness has terminated curve 2b just within the experimental results.

The method based on Salmon's (9) original equation for Z and applying it to the width of the gusset plate concentric with the applied load is an attempt to extend Salmon's equation to take account of the load position. The resulting equation is Equation 2.39 for the stress, which when re-arranging for the load gives

$$P = 2(L - s)t(0.6 - 0.21L/H)f_{max} \qquad (5.15)$$

This is represented by curve 3 in the figures which gives similar but more conservative results than Equation 5.14.

Although none of the approximate strut methods have a factor for the removal of the inside corner, the methods are used assuming a complete gusset plate. As the methods are so conservative they could be used with up to half of the inside corner removed for the least conservative curve 2, for both load positions.

The slope of curves 2a and 3 representing Equations 5.14 and 5.15 in Figure 5.31 is only a result of the load position and not the

reduced width of the gusset plate. However, because the load is applied concentrically to the remaining width of gusset plate it so happens to be the width considered by the equations.

Only the full width assumption Equation 5.13 has been modified such that only the remaining width G is used. Equation 5.13 then becomes

$$P = f_{max} G.t.\cos\alpha \qquad (5.16)$$

This is represented by curve 2b in Figure 5.30 and gives the same results as curve 2a in Figure 5.31.

None of the existing methods have a factor for the variation in the internal angle and none of them can rationally be used as an approximation in their existing form. However, the basic assumption of the gusset plate acting as a form of strut with its axis parallel to the free edge can be extended to include a variation of the internal angle. The quarter width method Equation 5.12 now becomes

$$P = \frac{1}{4} p_c t \frac{W^2}{L} \qquad (5.17)$$

Also the full width assumption Equation 5.13, now becomes

$$P = p_c t \frac{W^2}{L} \qquad (5.18)$$

and the modification for the position of the applied load, Equation 5.14, now becomes

$$P = 2(L - s) f_a t (W/L)^2 \qquad (5.19)$$

where w in the above is given in Equation 5.6.

The adapted Salmon Equation 5.15, however, cannot be realistically extended to include the variation in the internal angle as it is based on a 90^o triangle.

Equation 5.17 is represented by curve 1c in Figure 5.32 and is shown to be extremely conservative. As s=L/2 Equations 5.18 and 5.19 give the same results as represented by curve 2c which is of a similar shape to the experimental results but still very conservative.

5.6 Plastic design method

In Figures 5.33 to 5.41 the loads using the plastic design method as presented in Section 2.6 are plotted with the experimental ultimate load results obtained for each of the main gusset plate series. The critical loads presented for the Plastic design method are the ultimate loads based on the plastic strength.

Basically this method is Jensen's allowable stress design extended to the plastic limit resulting in Equation 2.40 which is reproduced below.

$$P_u = f_y t.\cos^2\alpha(-2e + \sqrt{4e^2 + L^2})$$

This is represented by curve 1 in the figures.

When s=L/2 the plastic design curve produces the same result as using Jensen's (4) method when the yield strength is assumed. This method also has the same problems concerning the position of the applied load as Jensen's (4) method as demonstrated in Figure 5.35.

As this method assumes the full plastic strength then buckling must not occur. Therefore, a limiting thickness must be specified to ensure yielding. Equations 2.42 and 2.43 are such limiting thickness equations which are related to Salmon's work. These limitations are presented in Figures 5.33, 5.34 and 5.38. Equation 2.43 terminates curve 1 well within the experimental results while Equation 2.42 is on the limit. All the other results are rendered not applicable.

The plastic design equation does not have a factor for the removal of the inside corner and to apply the equation assuming complete gusset plates would result in considerably higher failure loads than the experimental results. However, the method can be modified to give

$$P_u = f_y t.\cos^2\alpha(-2e + \sqrt{4e^2 + [G/\cos\ ]^2}) \qquad (5.20)$$

This is represented by curve 1a in Figures 5.39 and 5.40. As the method is not strictly applicable to the plates thickness in the

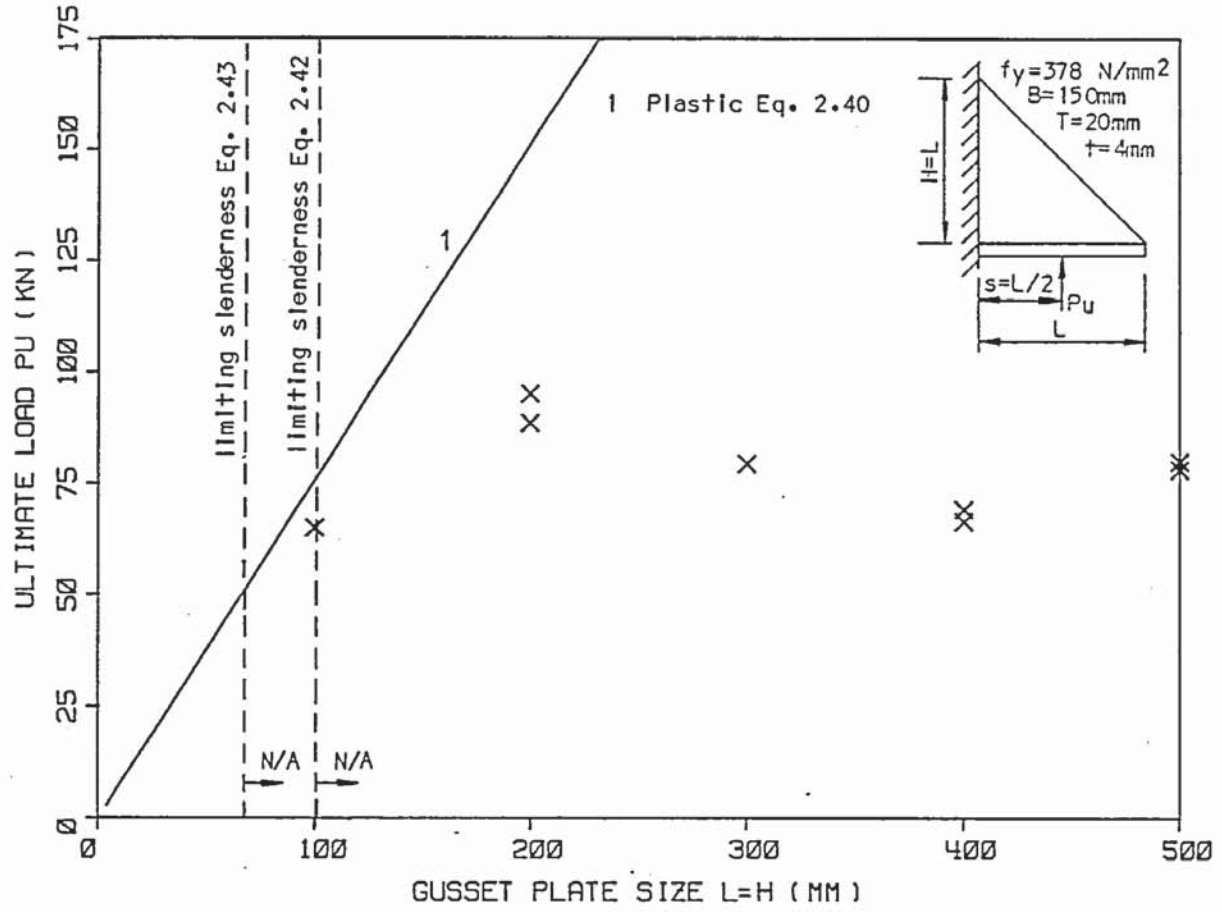

Figure 5.33 The plastic method compared with the experimental results of series 3.

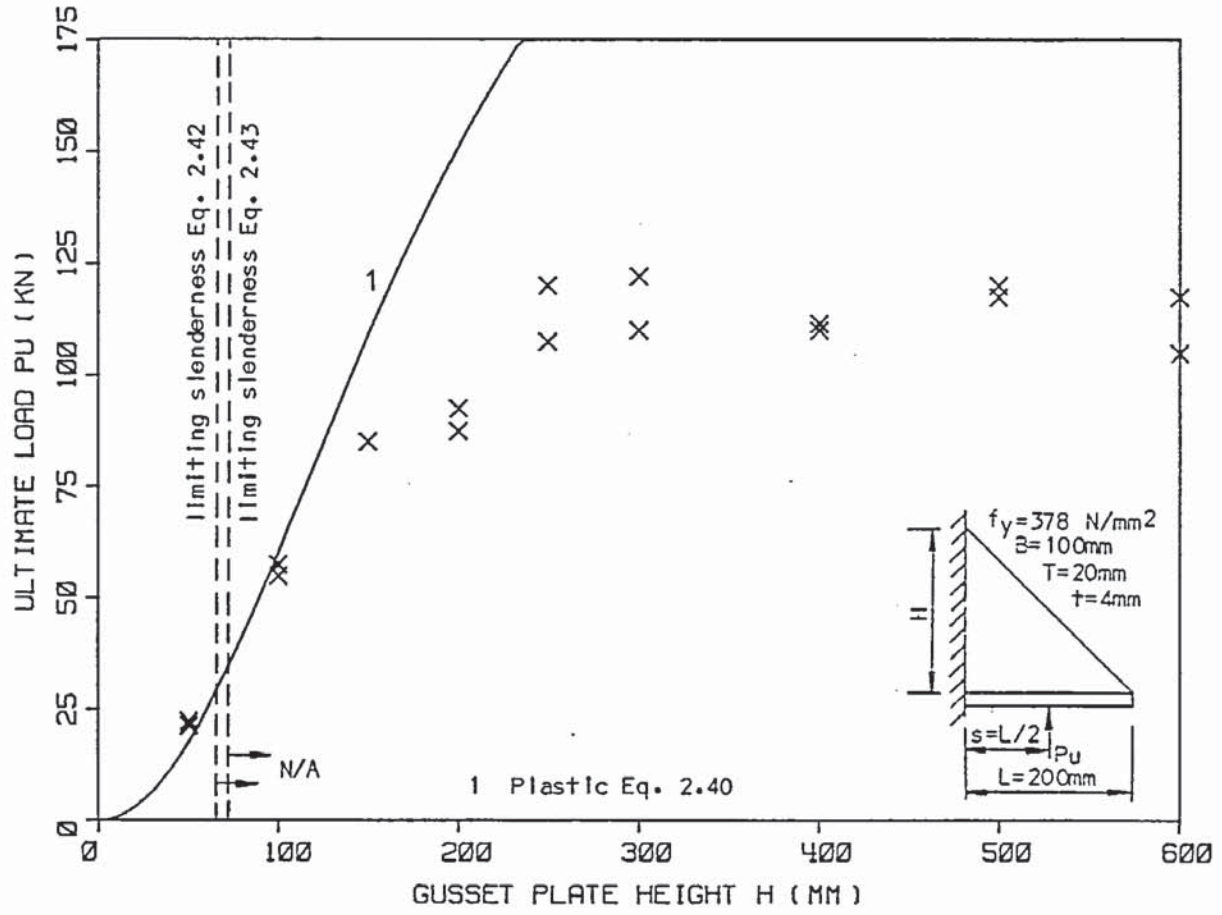

Figure 5.34 The plastic method compared with the experimental results of series 4.

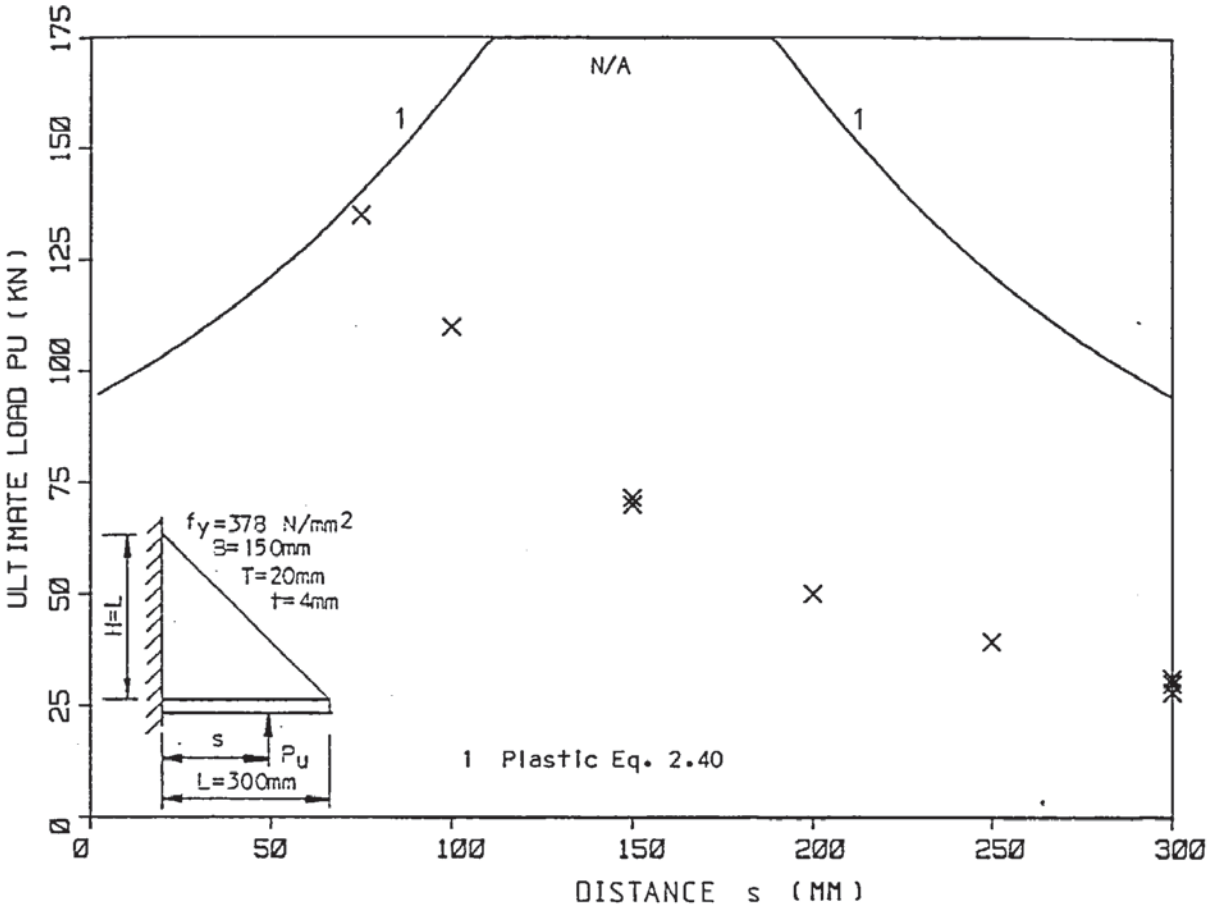

Figure 5.35 The plastic method compared with the experimental results of series 5.

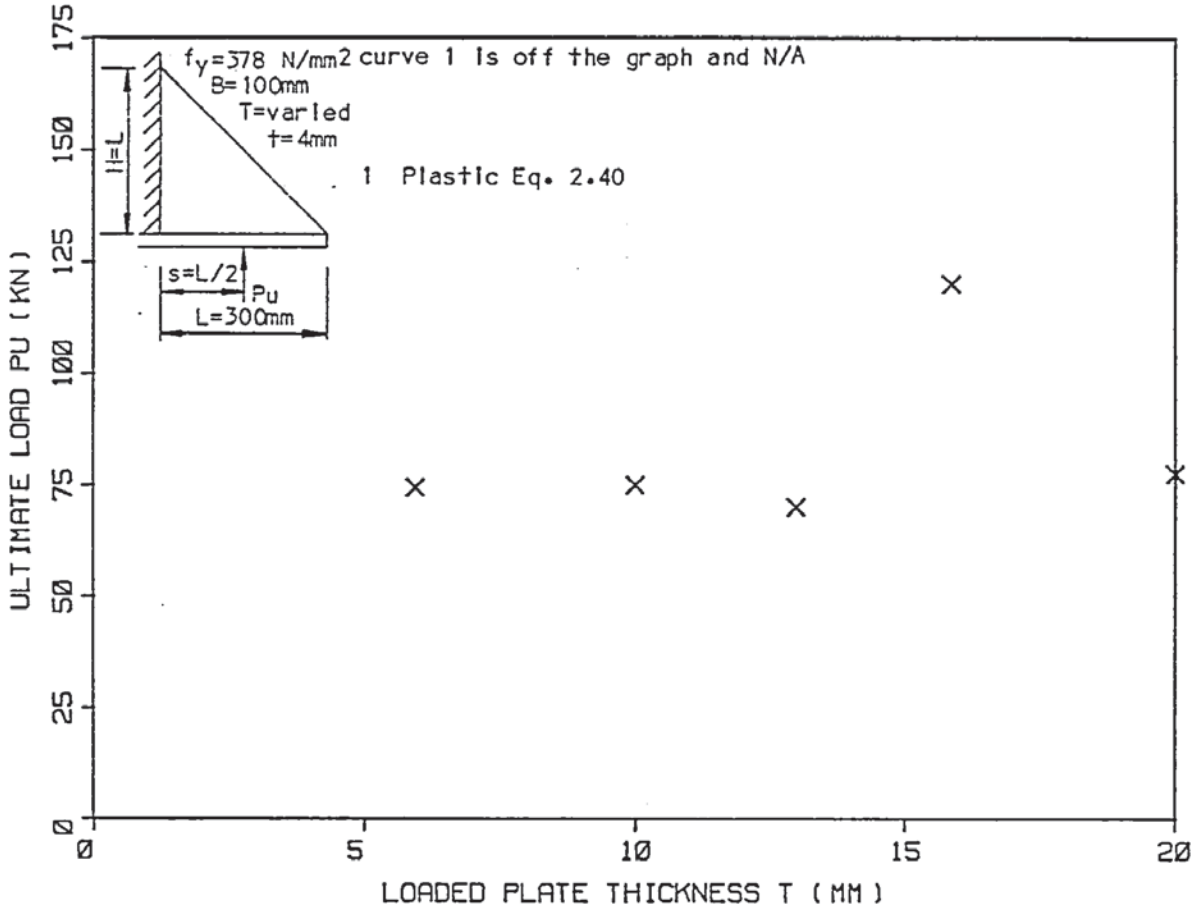

Figure 5.36 The plastic method compared with the experimental results of series 7 (s=L/2).

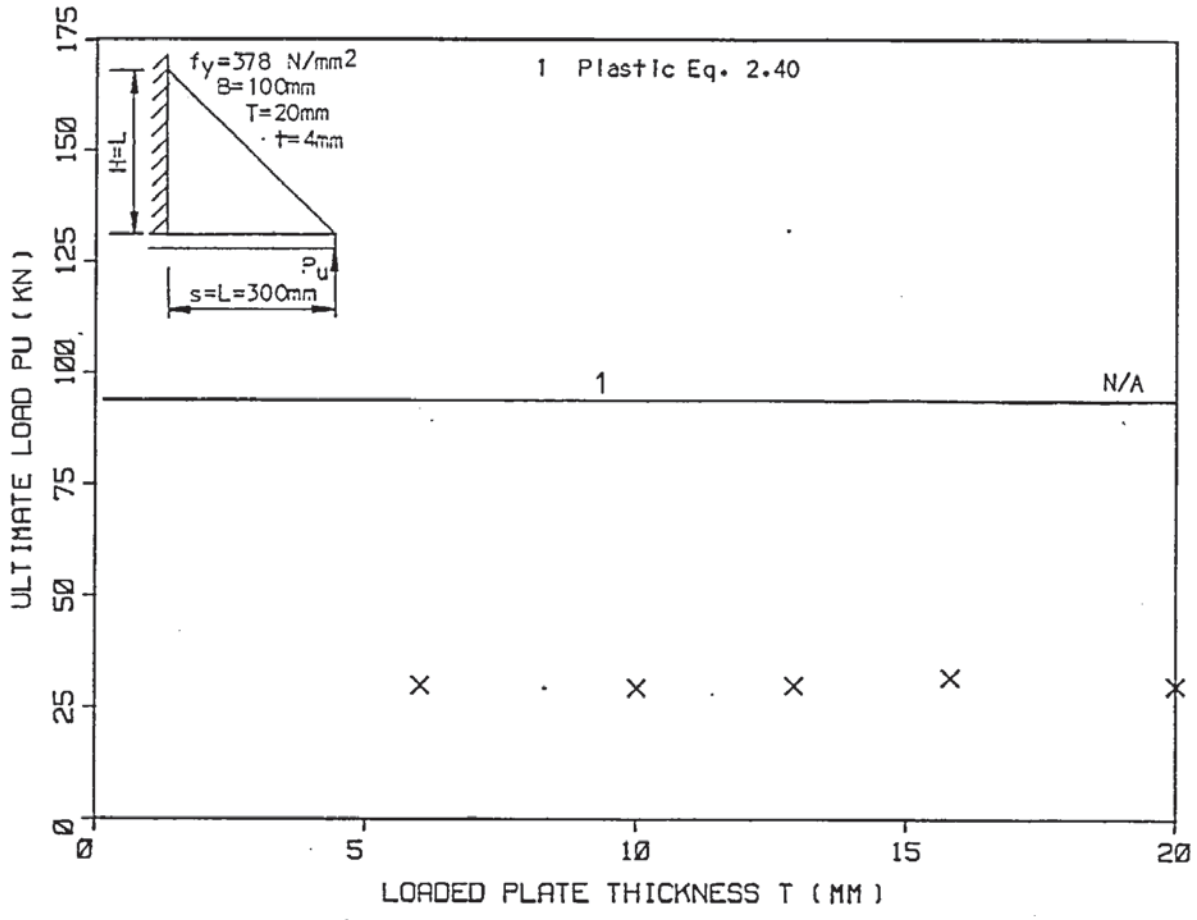

Figure 5.37 The plastic method compared with the experimental results of series 7 (s=L).

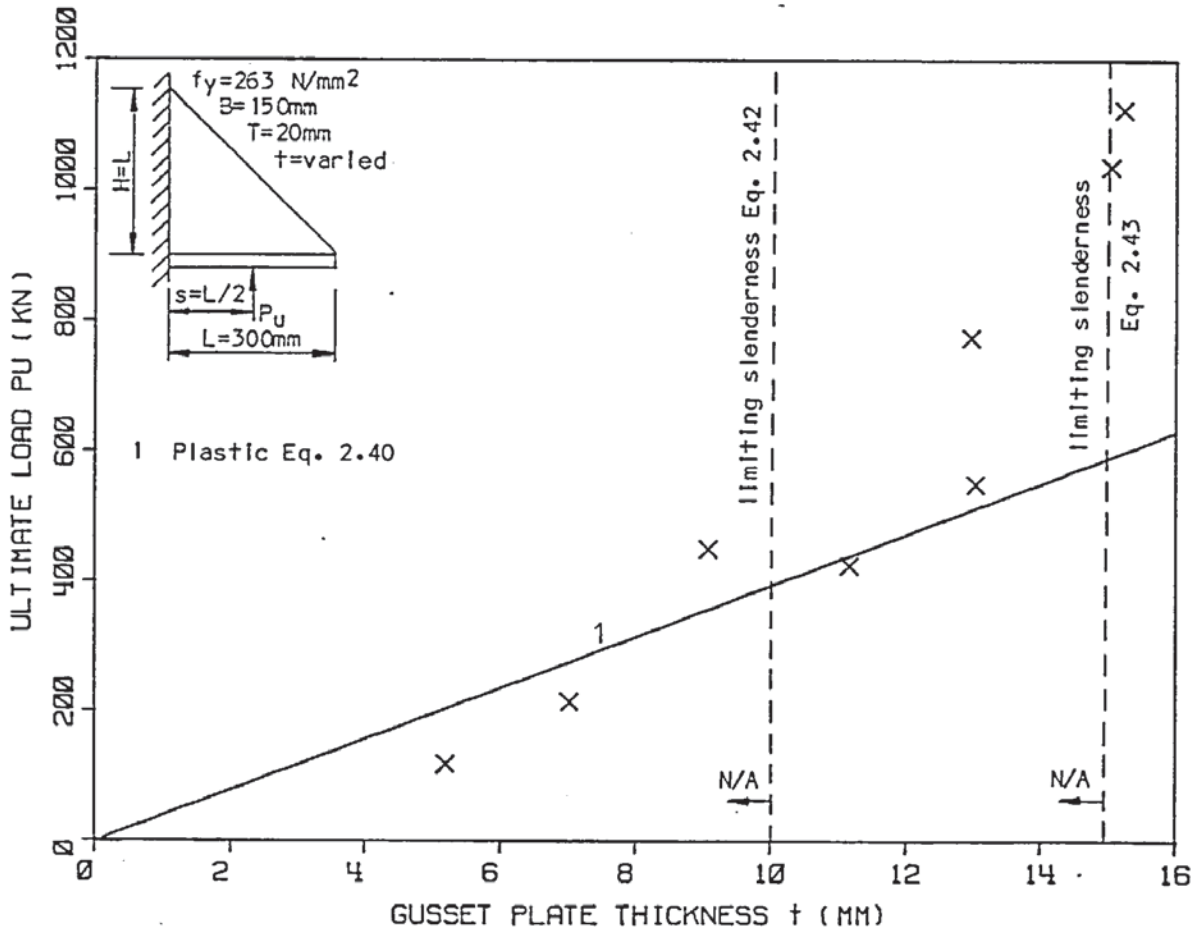

Figure 5.38 The plastic method compared with the experimental results of series 12.

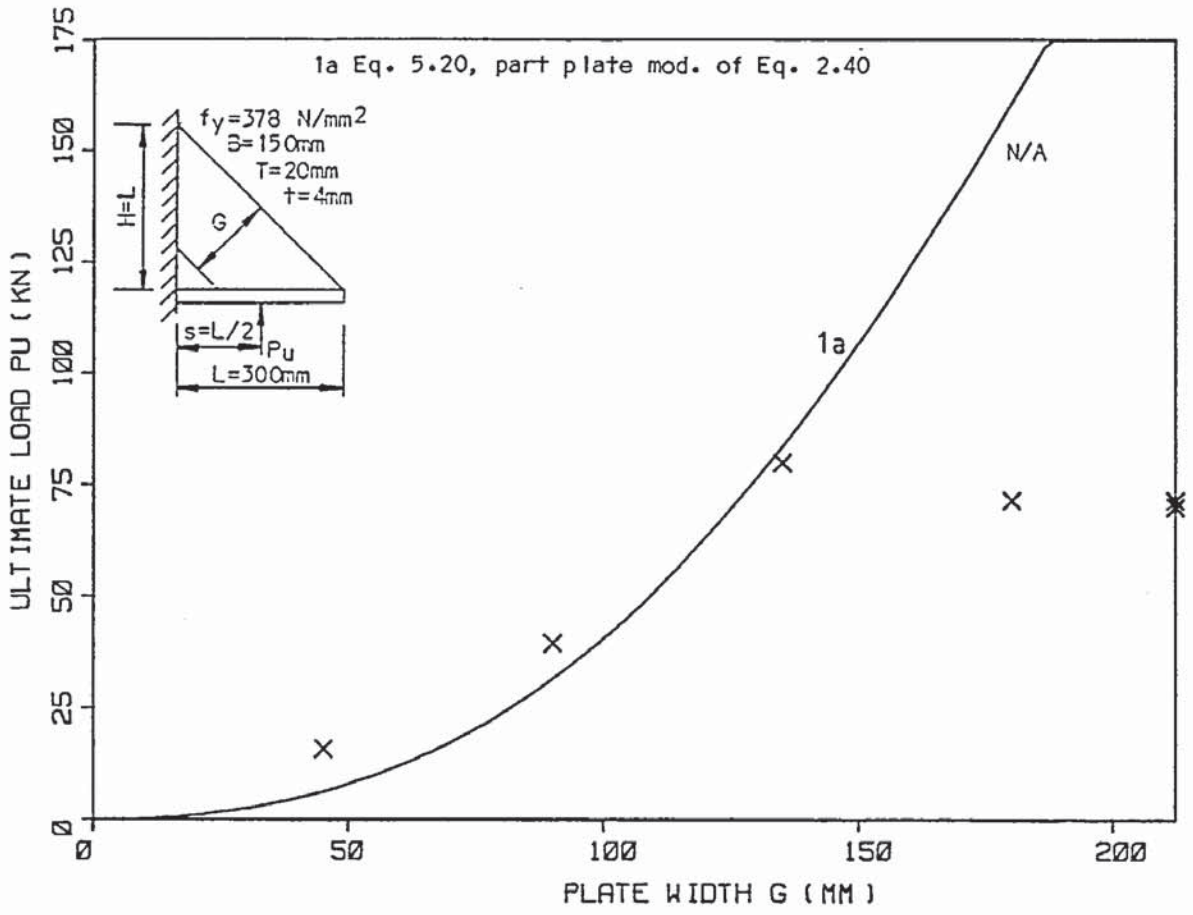

Figure 5.39 The plastic method compared with the experimental results of series 8 (s=L/2).

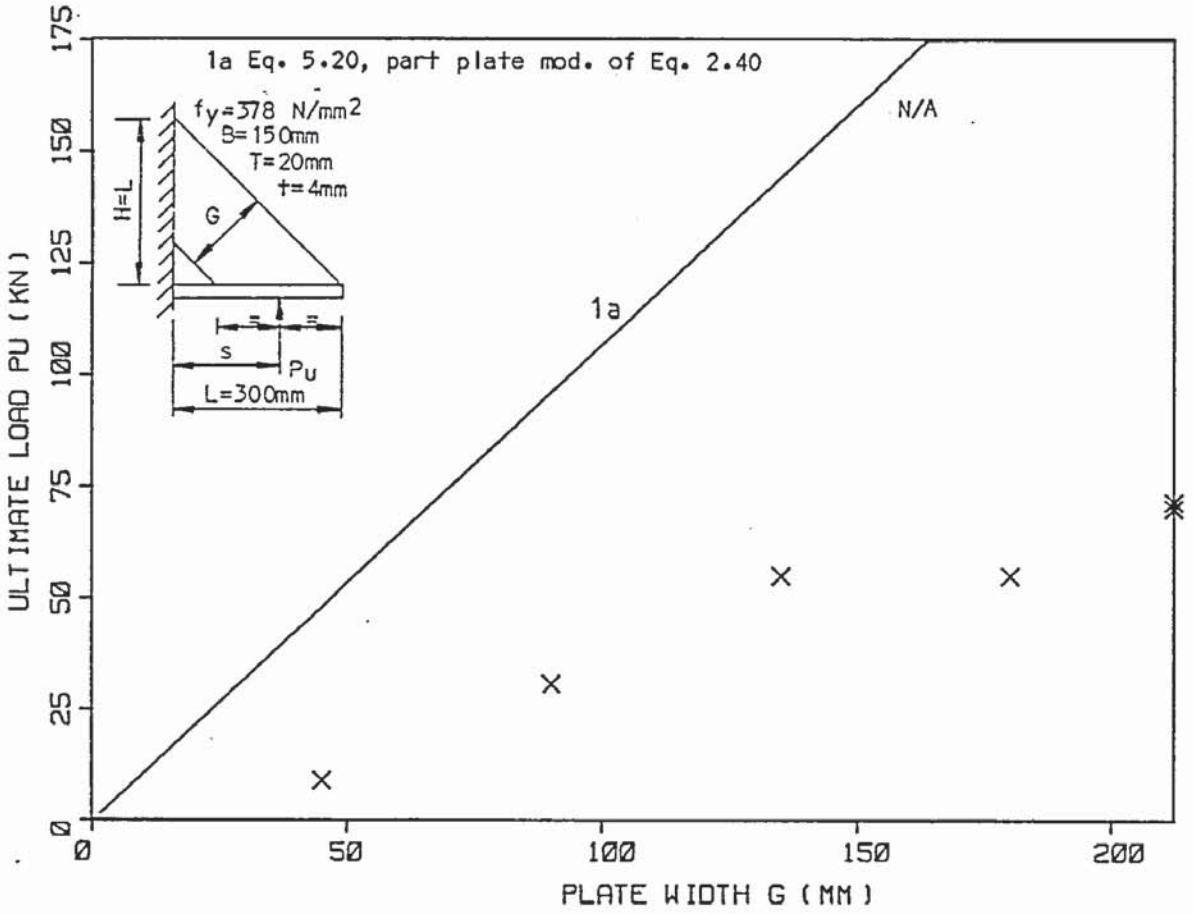

Figure 5.40 The plastic method compared with the experimental results of series 8 (s=varies).

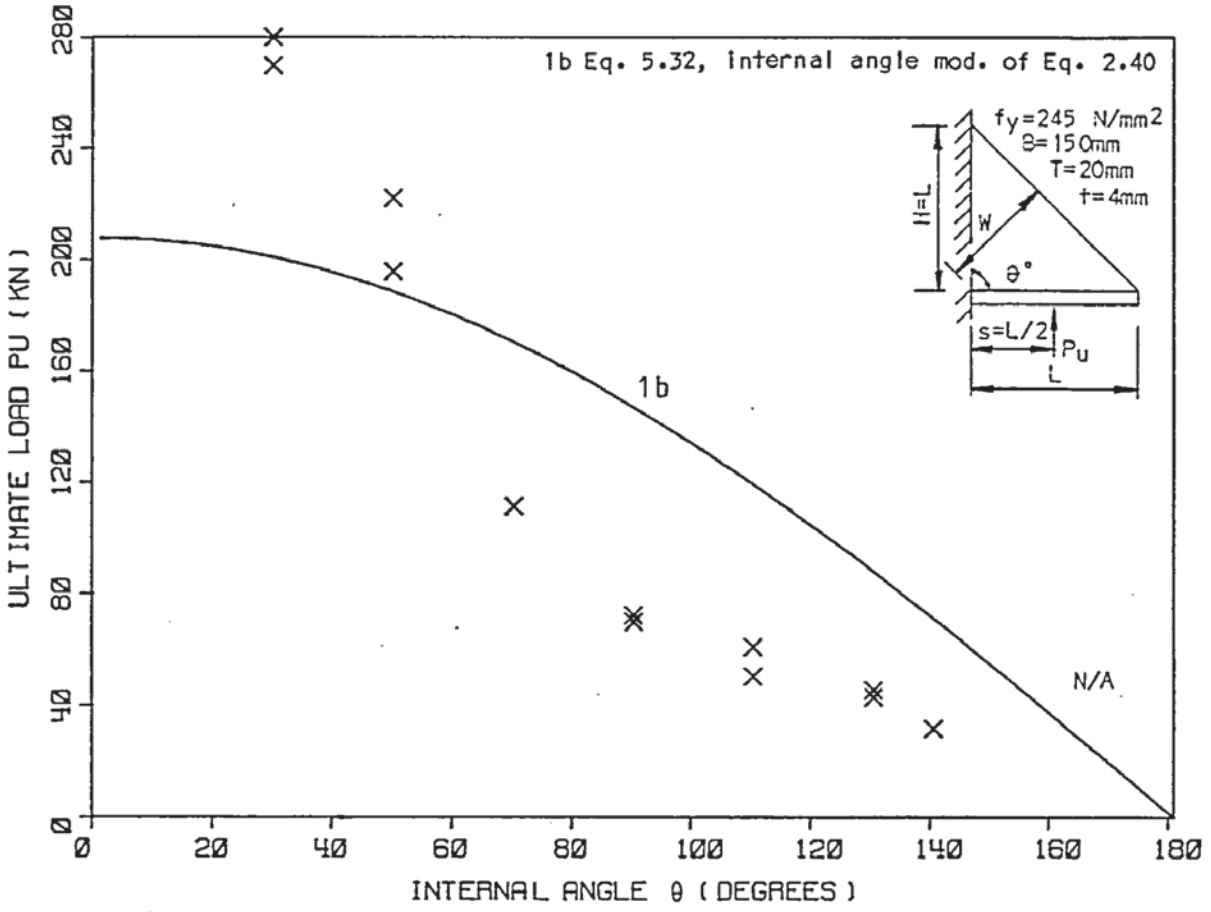

Figure 5.41 The plastic method compared with the experimental results of series 13.

experiments used it is not a fair comparison. However, as with Jensen's method the effect of the assumed eccentricity in the method causes problems. As the load is applied concentrically on the strut in Figure 5.40 it produces the same curve as for Jensen's (4) method assuming the yield stress.

The existing equation does not have a factor for the variation in the internal angle and it cannot rationally be used as an approximation in its existing form. However, as with Jensen's (4) method it can be modified to give

$$P_u = f_y t \left(\frac{H.\sin\theta}{V}\right)^2 (-2e + \sqrt{4e^2 + L^2}) \qquad (5.21)$$

where V is given in Equation 5.6.

This equation is represented by curve 1b in Figure 5.47 which is the same result as assuming the yield stress for Jensen's (4) method. This curve is higher than the majority of the results, intersecting

them at approximately the 60° angled plate. As the two limiting slenderness equations are based on Salmon's work, which was based on 90° gusset plates, they cannot be applied to these plates. However, the use of such a limitation may be effective.

5.7 Ultimate limit state design

In Figures 5.42 to 5.50 the ultimate loads calculated using Martin's (15) methods presented in Section 2.7 are plotted with the experimental ultimate load results for each of the main gusset plate series.

The method assumes the gusset plate to act as a series of fixed ended struts rather than just one, and moments of equilibrium are taken about the inside corner of the gusset plate. The loaded plate is also assumed to contribute to the moment of resistance.

The main problem with any method assuming struts is to determine the effective length and the buckling stress equation to use. Martin (15) chose to use the Rankine-Gordon (16) formula because it is conservative and easily integrated. From his experiments he chose an effective length based on the width of the gusset plate. This produced Equation 2.47 which is reproduced below.

$$P_u = \frac{\pi^2 E.t^3}{24s} \ln\left[1 + \frac{12f_y}{\pi^2 E} \frac{(L/t)^2}{[(L/H)^2 + 1]}\right] + \frac{M_p}{s}$$

This is represented by curve 1 in the figures. Because of the difficulty re-arranging this equation to give the gusset plate thickness, Martin (15) suggested an alternative approximate method for gusset plates of low slenderness ratio. The Rankine-Gordon buckling stress distribution is approximated to a triangular distribution which gives Equation 2.50, which is reproduced below

$$P_u = \frac{f_y}{(s/L)} \frac{L.t}{[(L/H)^2 + 1]} \left[\frac{1}{2} - \frac{\sqrt{3}\,(L/t)}{277.5\sqrt{(L/H)^2 + 1}}\right] + \frac{M_p}{s}$$

This is represented by curve 2 in the figures. Martin (15) defines

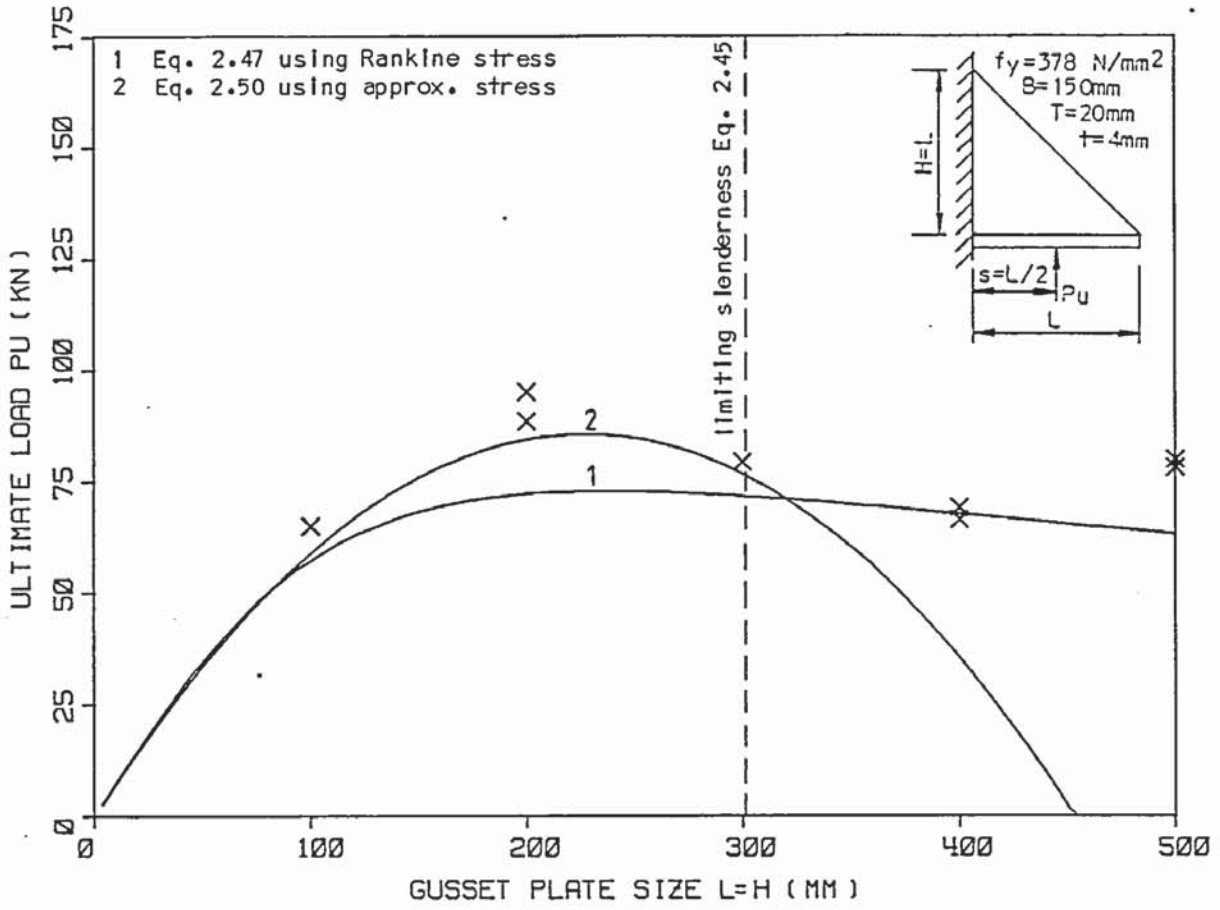

Figure 5.42 Martin's method compared with the experimental results of series 3.

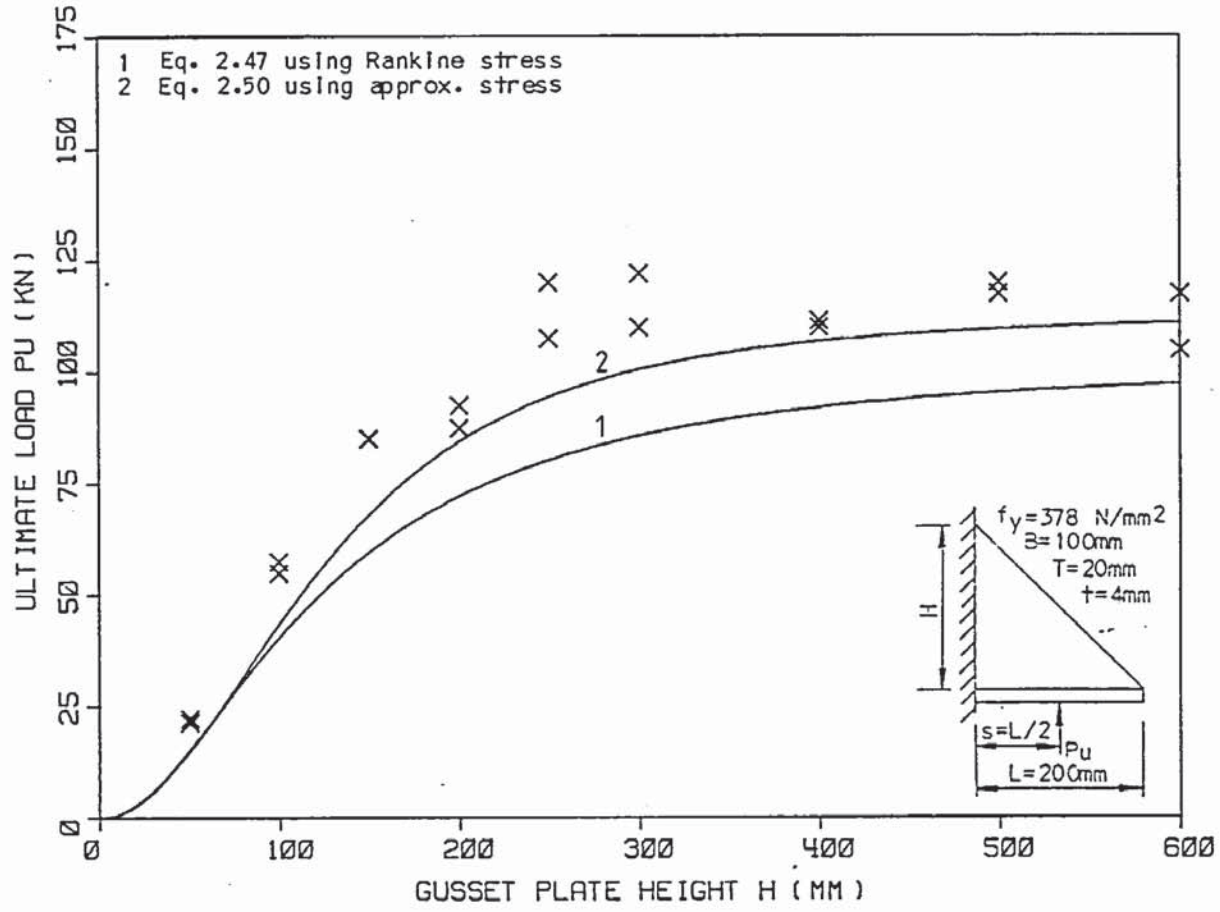

Figure 5.43 Martin's method compared with the experimental results of series 4.

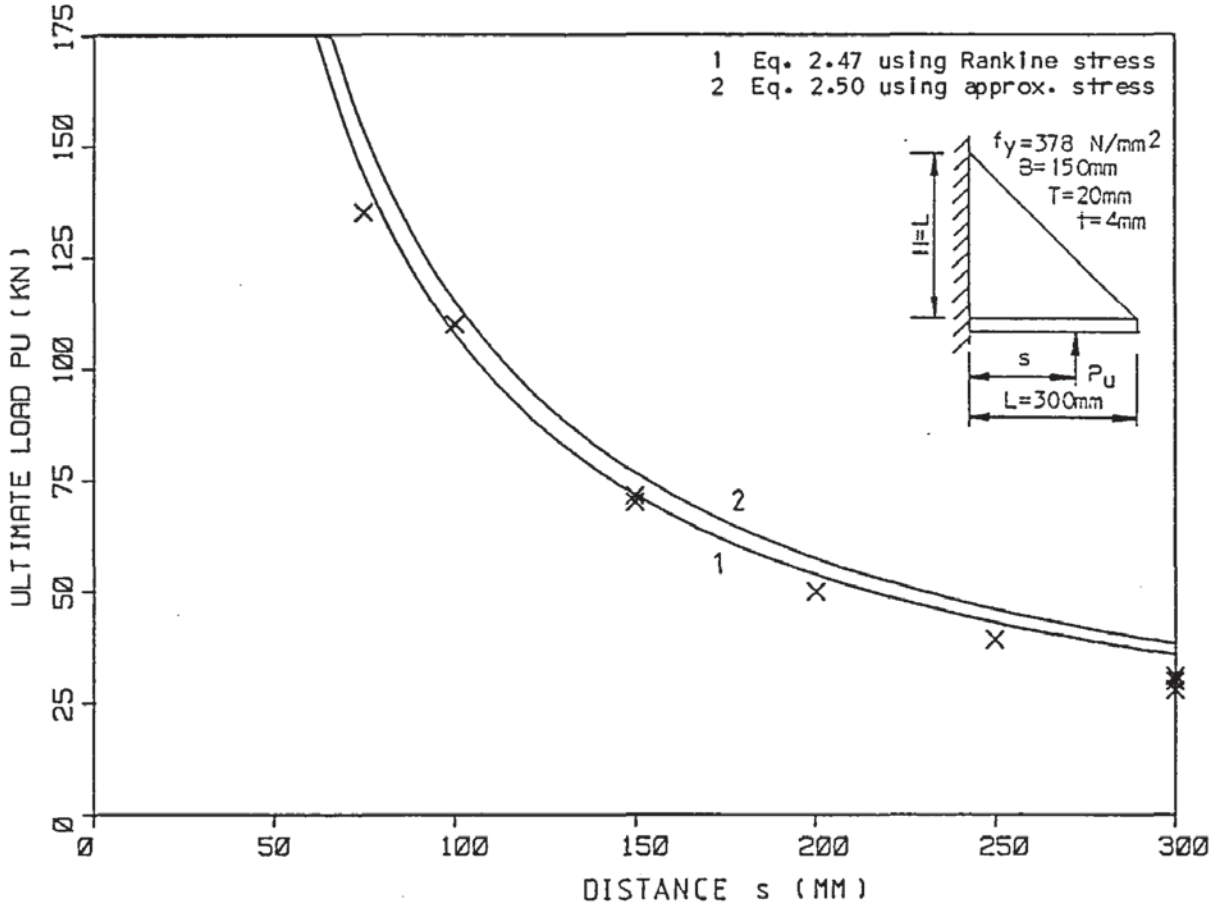

Figure 5.44 Martin's method compared with the experimental results of series 5.

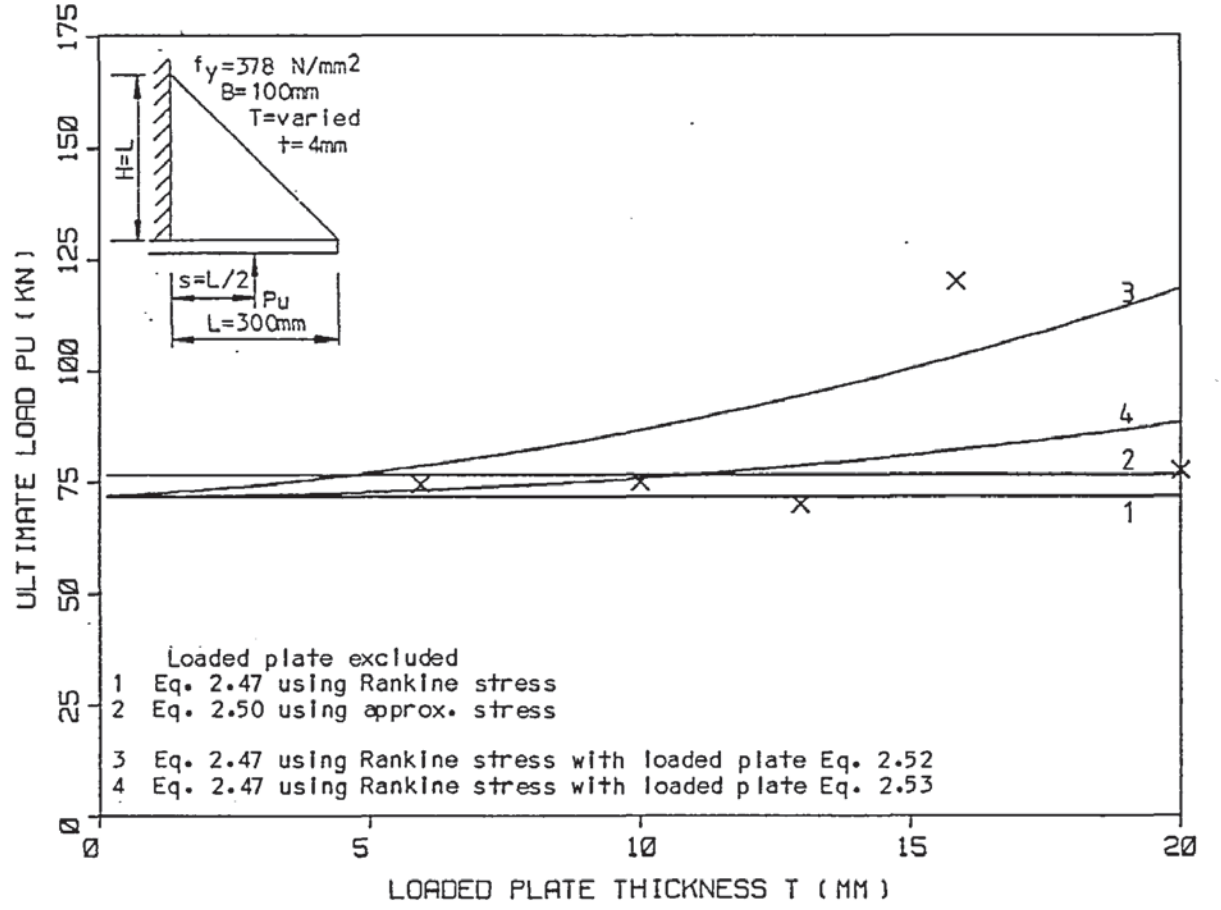

Figure 5.45 Martin's method compared with the experimental results of series 7 (s=L/2).

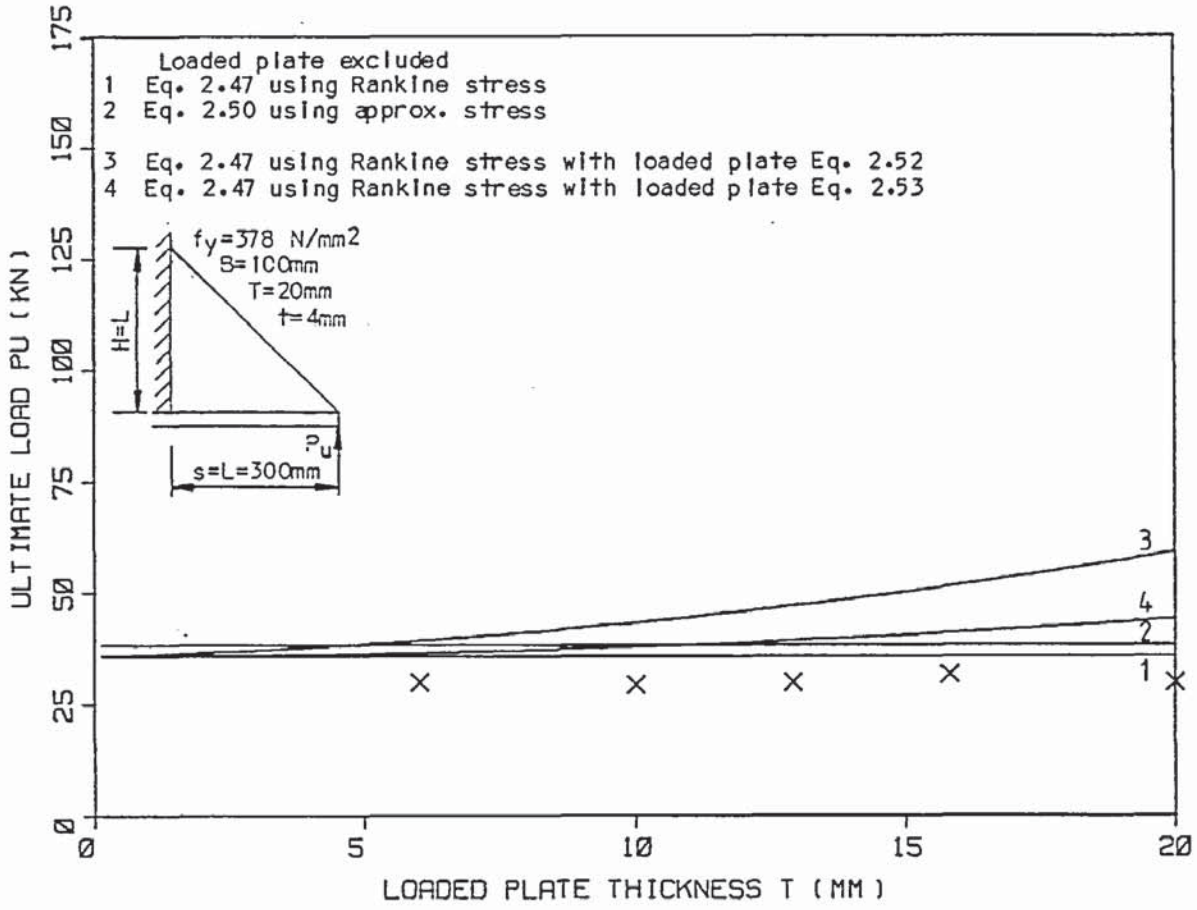

Figure 5.46 Martin's method compared with the experimental results of series 7 (s=L).

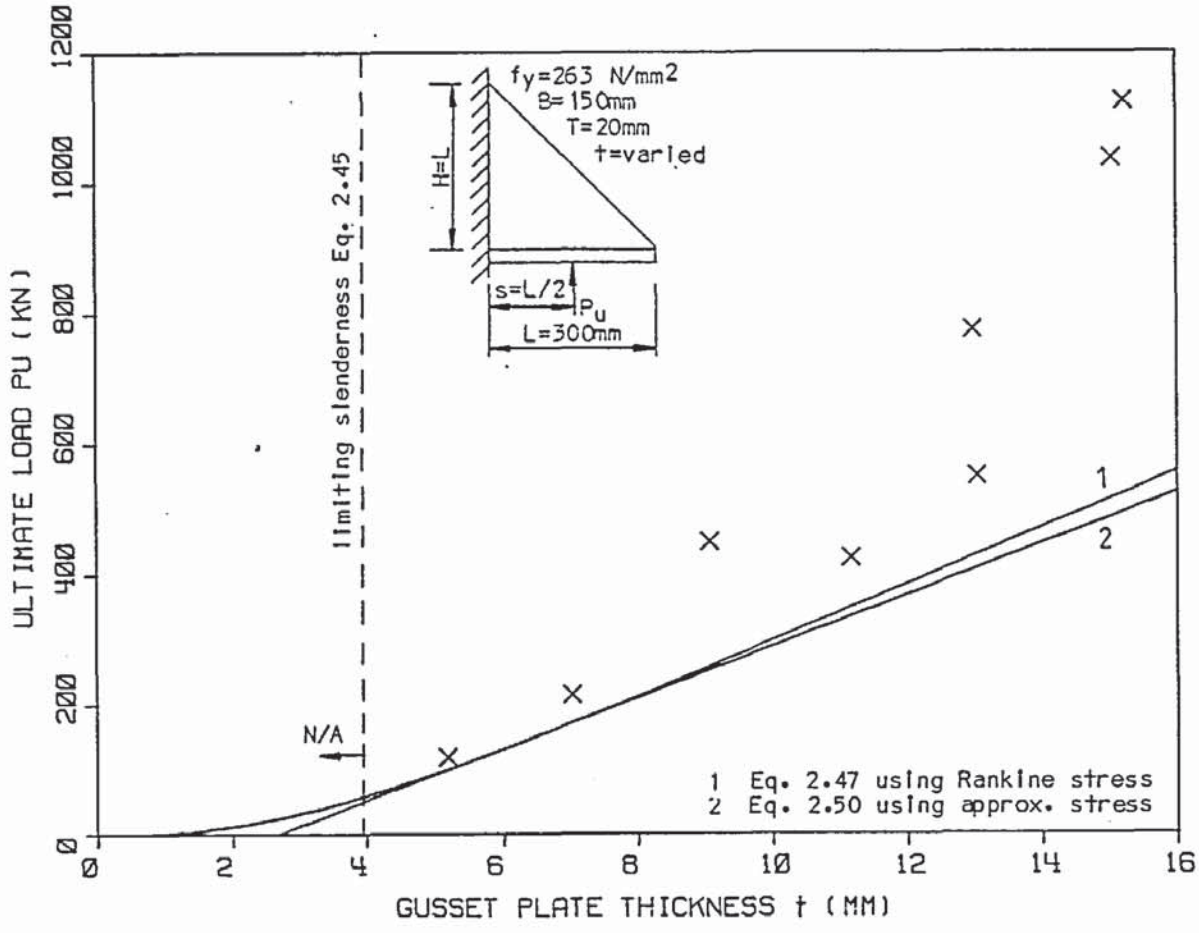

Figure 5.47 Martin's method compared with the experimental results of series 12.

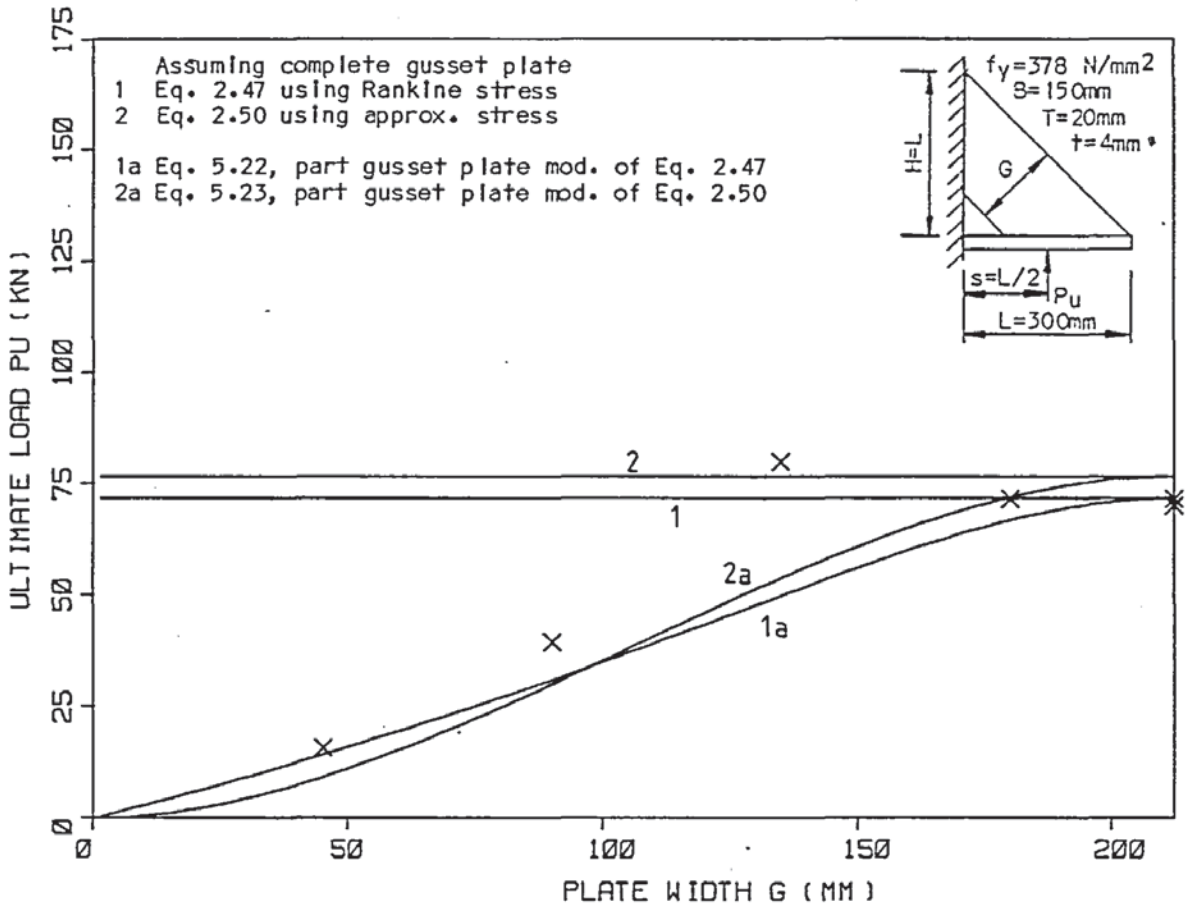

Figure 5.48 Martin's method compared with the experimental results of series 8 (s=L/2).

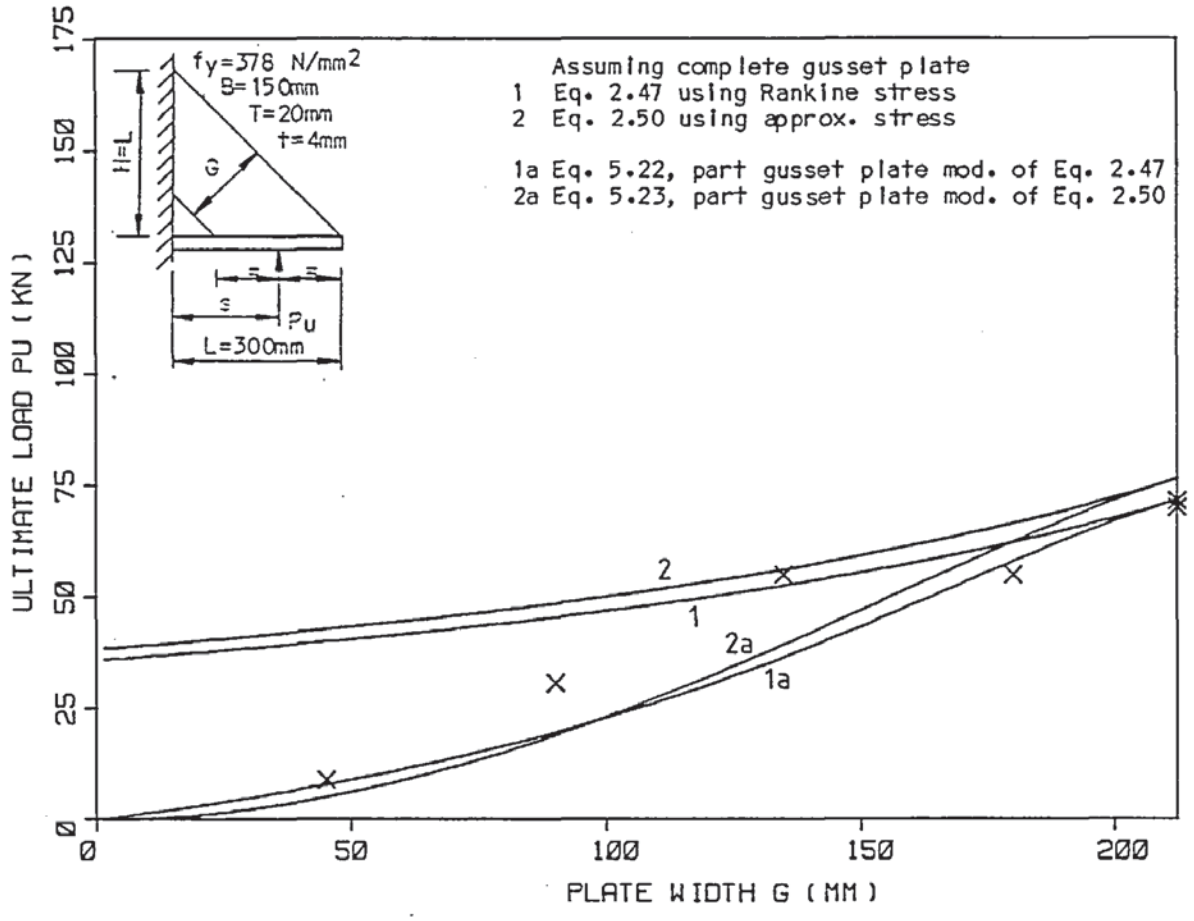

Figure 5.49 Martin's method compared with the experimental results of series 8 (s=varies).

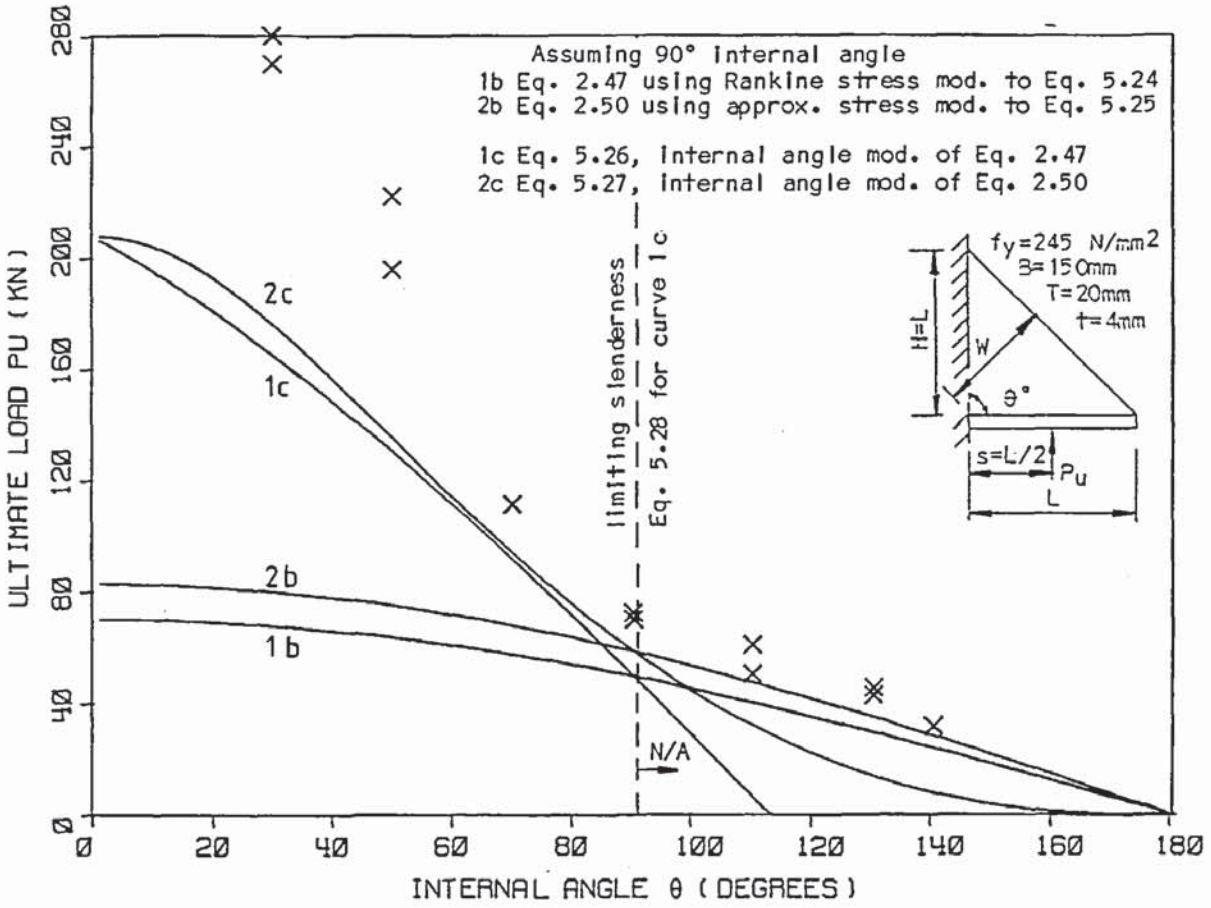

Figure 5.50 Martin's method compared with the experimental results of series 13.

the slenderness ratio of the gusset plate by Equation 2.45.

As the majority of the loaded plates were terminated at the supported edge the factor for the bending resistance M_p=0. Also, as the experimental results suggested, it is not necessary and so it is omitted from curves 1 and 2. However, Martin (15) suggested two values for M_p, Equations 2.52 and 2.53, therefore these are used in Equation 2.47 to produce curves 3 and 4 respectively in Figures 5.45 and 5.46.

Curve 1 compares well with the normal variations in the gusset plate parameters with only relatively small deviations from the experimental results. Curve 2 is very similar to curve 1 within its slenderness limitation range. Outside this range the curve tends to zero and would be safe to use but inaccurate. Virtually all the gusset plates tested were within the required range. Curves 3 and 4, which include the factor for the loaded plate, overestimate the gusset

plate strength. The curves without the factor give the best results.

Although none of Martin's (15) equations have a factor for the removal of the inside corner they are used assuming a complete gusset plate. Both curves 1 and 2 in Figures 5.48 and 5.49 may be used for up to one third of the inside corner removed. By integrating over the remaining width of the gusset plate only then can Martin's (15) method be extended to include the effect of removing the inside corner, so that Equation 2.47 becomes

$$P_u = \frac{t.f_y}{2s.k_m} [\ln(1 + k_m W^2) - \ln(1 + k_m(W - G)^2)] \qquad (5.22)$$

where $$W = \frac{L.H}{\sqrt{L^2 + H^2}}$$

$$k_m = \frac{12 f_y}{E.\pi^2 t^2}$$

which is represented by curve 1a in Figures 5.48 and 5.49

and Equation 2.50 becomes

$$P_u = \frac{t.f_y}{s} \left[\frac{(W^2 - (W - G)^2)}{2} - \frac{\sqrt{12}}{555t} (W^3 - (W - G)^3 \right] \qquad (5.23)$$

where W is given in Equation 5.22.

Both curves are very close to each other and of similar shape to the experimental results. All these gusset plates passed the limiting slenderness Equation 2.45.

Neither of the existing equations have a factor for the internal angle and cannot rationally be used in their present form, even as an approximation. This is because the width of the gusset plate assumed is based upon the width of right angled gusset plates. However, if the more general term for the width, given in Equation 5.6, is used then Equation 2.47 becomes

$$P_u = \frac{t.f_y}{2s.k_m} \ln(1 + k_m W^2) \qquad (5.24)$$

where k_m is given in Equation 5.22 and W is given in Equation 5.6.

This is represented by curve 1b in Figure 5.50.

Similarly Equation 2.50 becomes

$$P_u = \frac{t.f_y W^2}{s}\left[\frac{1}{2} - \frac{\sqrt{12}\ W}{555t}\right] \qquad (5.25)$$

where W is given in Equation 5.6.

This is represented by curve 2b in Figure 5.50. The term for the loaded plate has not been included as the loaded plates were terminated at the vertical support.

Both curves 1b and 2b are similar and compare well with the experimental results for angles greater than 90°. However, they are increasingly conservative for angles less than 90°. These curves are the result of using Martin's (15) assumption for the effective length of each strut equal to its distance from the inside corner i.e. l=w. Therefore, these curves are effectively the failure loads of equivalent 90° angled gusset plates having the same width of plate W. The effective length should be related to the critical angle so that full length fixed ended struts are assumed. Equation 2.47 then becomes

$$P_u = \frac{t.f_y}{s}\,\frac{1}{2k_m}\,\ln(1 + k_a W^2) \qquad (5.26)$$

where $$k_a = \frac{12 f_y}{E.\pi^2 t^2}\tan^2\theta/2 \ ,$$

and W is given in Equation 5.6.

This is represented by curve 1c in Figure 5.50.

Similarly Equation 2.50 becomes

$$P_u = \frac{t.f_y W^2}{s}\left[\frac{1}{2} - \frac{\sqrt{12}}{555}\,\frac{W}{t}\tan\theta/2\right] \qquad (5.27)$$

where W is given in Equation 5.6

This is represented by curve 2c in Figure 5.50.

Also the limiting slenderness ratio Equation 2.45 becomes

$$\frac{l}{r} = \frac{2\sqrt{3}\,\sin\theta.\tan\theta/2}{\sqrt{(L/H)^2 + 1 - 2(L/H)\cos\theta}} \frac{L}{t} \leqslant 185 \qquad (5.28)$$

Both curves 1c and 2c, for angles greater than 90°, are similar and of a similar shape to the experimental results. They are more conservative the smaller the angle. For angles greater than 90° curve 2c is no longer applicable and curve 1c is not of a similar shape and is conservative.

5.8 Conclusions

All the methods use the stress along the free edge at least and require some means of determining it, either directly or indirectly, to determine the limiting slenderness equations to prevent buckling. All the methods are unsafe if the yield stress is assumed for all cases. The main problem is in determining the effective length to use in some buckling equation. The method of determining the effective length should take into consideration the change in L/H ratio and the internal angle. The choice of a buckling equation is another problem in itself. Only Martin's(15) method gives any specific details as to the effective length and buckling stress equation to use, which appeared to work properly, although he did not cover all the situations tested. However, the author has modified his method to suit. Salmon's (9) method is the only other method to specify some definite guidance along these lines but, they were not very satisfactory and can not be modified to cover all the situations tested.

Another major problem is with the position of the applied load. The assumption of the gusset plate acting as an eccentrically loaded prism, as with the Jensen and Plastic design methods, does not give satisfactory results and is inaccurate for s<L/2. The approximate strut method is ineffective, as the method is so conservative, and

Salmon's (9) method does not have any means of taking it into account. Martin's (15) method handles the load position very well and the beam method is similar. The common element in both these methods is that moments are taken about the supported edge.

Only Martin's (15) method is satisfactory at handling the removal of the inside corner after modification by the author. It also gives reasonably safe results with the change in the internal angle after modification by the author. Generally speaking only Martin's (15) method could be modified by the author to handle all the situations tested and gives reasonably satisfactory results, although it requires some refinement. The method is also an ultimate limit state design, which will be required when the ultimate limit state design of steel structures is introduced for general use.

CHAPTER SIX

THEORETICAL ANALYSIS OF THE GUSSET PLATES

6.1 Introduction

There are several approaches to producing a mathematical means of designing the triangular type of steel gusset plates tested in this investigation. One approach is the purely theoretical solution using mathematical methods based on plate buckling theories, finite difference techniques and the finite element technique . These methods are related to each other and they suffer from similar problems regarding a solution for triangular gusset plates. The triangular shape and the boundary conditions at the free edge make a solution difficult. They are all limited to the elastic critical buckling load which as Jensen, Salmon and the author discovered is not the correct crtiterion for failure, as the majority of gusset plates have a considerable reserve of strength beyond this load. An important drawback is that a separate solution has to be obtained for each gusset plate size, shape and position of the load. Therefore a considerable number of solutions are required to cover the parameters associated with the gusset plates. It is then necessary to analyse all the solutions as a whole, as with experimental results, to produce a solution for design purposes. Furthermore a few experimental results are necessary to check the theoretical solution which usually requires adjusting as a result. All of these methods require a considerable amount of time and effort and the use of a high speed computer which is expensive.

Salmon's plate buckling theory produced an elastic buckling solution, using the approximate Rayleigh-Ritz energy method and large deflection theory to determine the loaded edge deformation at which elastic buckling occurs.

The solution is specifically for a complete right angled triangle with a specific load condition and was obtained from examining a considerable number of individual solutions of plates with different length to height ratios to find some limiting equation. The theoretical solution was eventually considerably modified as a result of experimental results.

Another approach is to produce a considerable number of experimental results, testing all variables, of which there are many and to statistically analyse the results to produce an empirical solution. However, experiments are expensive and time consuming.

It was decided, therefore, to develop a theoretical solution based on the simplest assumption and then make adjustments based on experimental results that systematically tested the main parameters, with the smallest number of specimens. The main assumption made is that if the method is satisfactory with two parameters varied separately, then it is reasonable to assume that the method is also satisfactory for a combination of the two parameters being varied. This method is likely to reduce the number of experimental results required in comparison with a purely empirical solution, and also to reduce the time and effort required in deriving the initial theoretical solution as compared with a more complex, entirely theoretical method. The theoretical methods may produce a more accurate initial solution but, will most probably require adjusting as a result of experimental evidence.

6.2 Basis of theory

The behaviour of gusset plates under test is the major influence for choosing this theoretical approach. All of the plates failed in the same characteristic manner. At the ultimate load the gusset plates collapsed by folding along three well defined fold lines with the loaded plate rotating about the inside corner at the supported

edge. The free edge of a gusset plate where L/H=1, viewed end on resembled the characteristic shape of a buckled fixed ended strut, and sections taken parallel to the free edge progressively towards the inside corner also resembled buckled fixed ended struts. The gusset plate at the inside corner showed signs of axial yielding as would occur in a squat fixed ended strut. The only difference with the gusset plates where L/H≠1 and with gusset plates where $\theta > 90^{o}$, was the relative area of the gusset plate that folded was less. This resulted in the free edge end-on profile still having the characterstic buckled fixed ended strut appearance, but not over the entire length of the free edge.

As a result of the experimental observations, a buckled gusset plate is assumed theoretically to be composed of a series of fixed ended struts. The loaded plates remained relatively straight for the majority of the tests and appeared to rotate about the supported edge at failure. This mode of behaviour suggested that equations of equilibrium could be formed by taking moments about the inside corner of the gusset plate, a theoretical technique that was used by Salmon (9) and Martin (15).

6.3 Theoretical approach

A gusset plate, although simple in shape, has many interacting parameters resulting in a complex behaviour, especially at the ultimate load. For design purposes a simple mathematical model is required. It is therefore necessary to simplify gusset plate behaviour as much as possible and to restrict the number of parameters to those which are important.

6.3.1 Rigid loaded plate assumption

Figure 6.1(a) shows a simple way of modelling a gusset plate by assuming individual fixed ended struts with rigid supported and loaded plates which are pinned together at the inside corner θ of the gusset

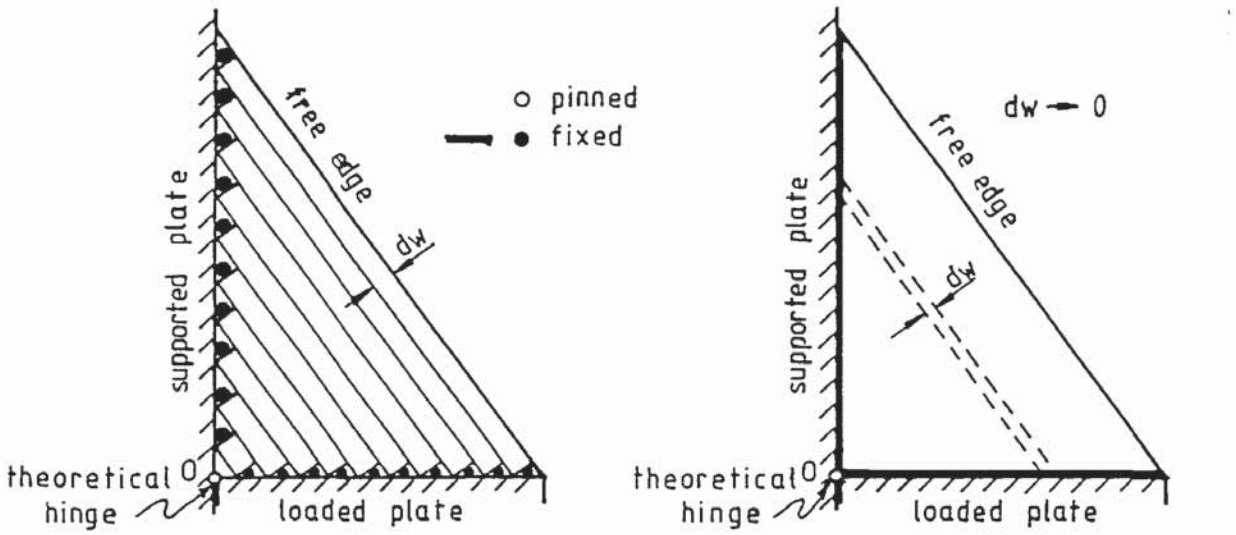

(a) finite number of fixed ended struts. (b) infinite number of fixed ended struts.

Figure 6.1 Basis of theoretical model.

plate. Figure 6.1(b) shows the model with an infinite number of elemental struts of width dw. Each elemental strut is assumed to buckle out of the plane of the gusset plate irrespective of its width.

As a load is applied to the rigid loaded plate, each elemental strut is strained axially, with the loaded plate remaining straight and rotating about the inside corner of the gusset plate as shown in Figure 6.2. As a result each elemental strut is strained axially by the same amount. Further, if the axial stress is taken to be proportional to the axial strain, then the stress in each elemental strut is the same.

Figure 6.3 shows an exploded diagram of the lower part of the gusset plate and the loaded plate, with the resulting stress distributions and reactions. The loaded plate distributes the resultant applied load P to the gusset plate as a rectangular distribution in the elastic range, with a vertical component R_y at the hinge. The resultant R of the stress distribution is supported by the horizontal component R_x in the loaded plate and the resultant axial

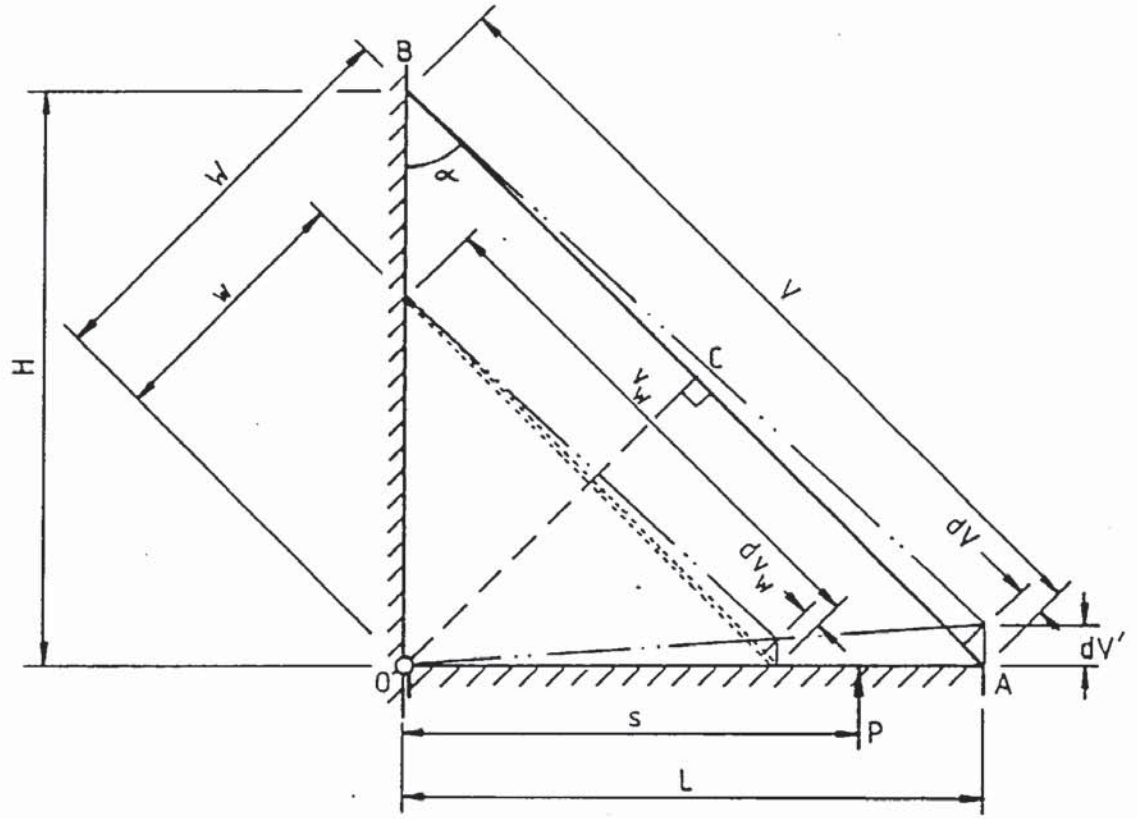

Figure 6.2 In plane deflection of theoretical model.

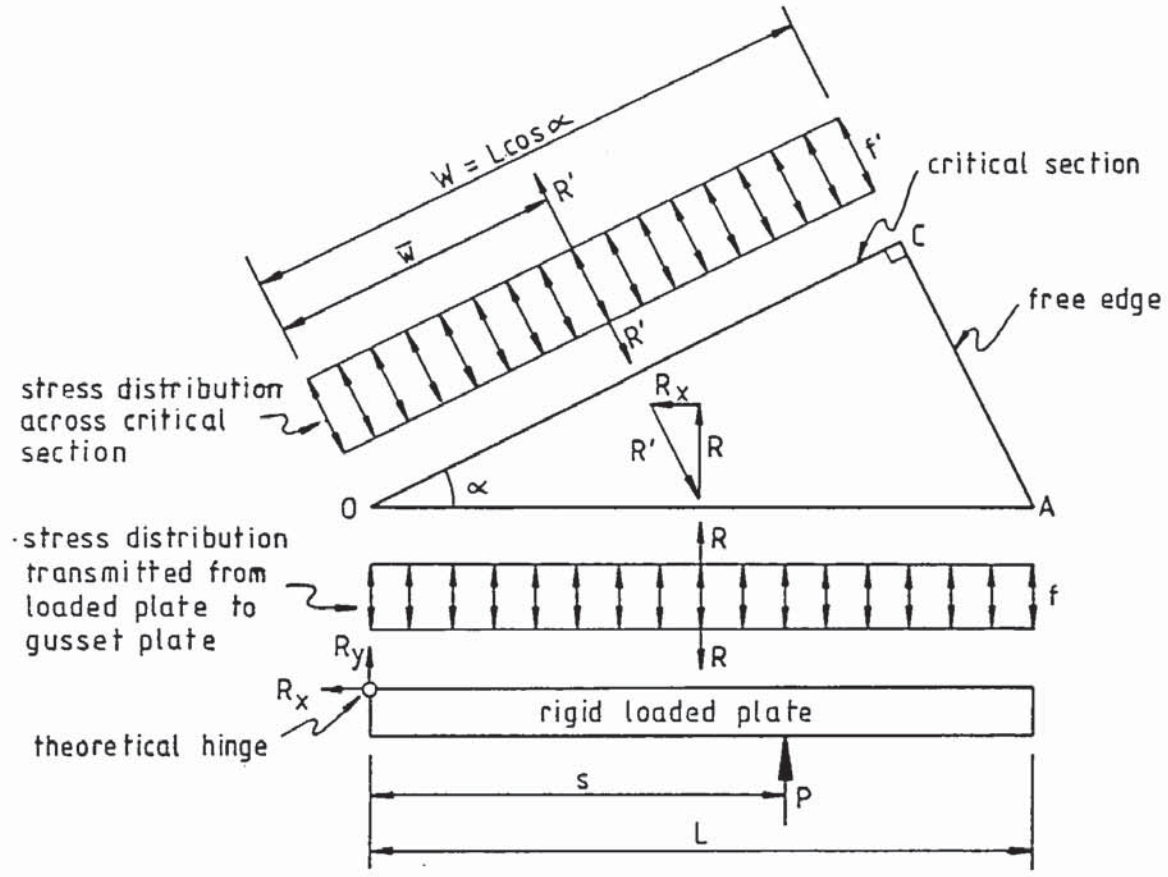

Figure 6.3 Resulting stress distribution and reactions in theoretical model.

component R' of all the assumed elemental struts which produce a rectangular stress distribution across the critical section OC.

Taking moments about the theoretical hinge for the loaded plate stress distribution gives

$$f = \frac{2.P.s}{t.L^2} \tag{6.1}$$

and taking moments about the theoretical hinge for the critical section stress distribution gives

$$f' = \frac{f}{\cos^2 \alpha} \tag{6.2}$$

Resolving vertically and horizontally gives

$$R_y = P(2.s/L - 1) \tag{6.3}$$

$$R_x = \frac{2.s.P}{H} \tag{6.4}$$

Consider a gusset plate where all the elemental struts fail by yielding and not buckling. The stress distribution across the critical section remains rectangular, and all of the elemental struts reach the yield stress and fail at the same time.

Now consider a gusset plate where the outer elemental struts fail by buckling. The failure envelope is then that of a buckling stress distribution form and not rectangular. Assuming initially that after an elemental strut has reached its buckling load its resistance falls to zero, then this produces the stress distribution as shown in Figure 6.4. As the outer elemental struts buckle, the load they sustained is distributed to the remaining elemental struts. This process gradually transfers the load towards the inner elemental struts, until eventually the resulting moment of resistance is insufficient and the gusset plate collapses.

Martin (15) in his theory assumed that all the elemental struts reached their ultimate load at the same time, even when they buckled. This assumption requires a buckling stress distribution to be

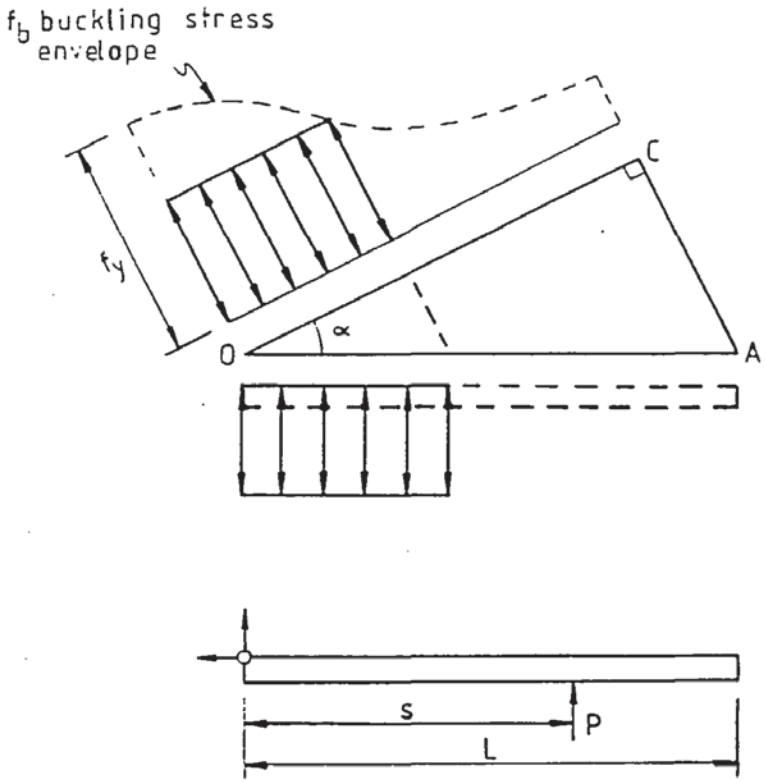

Figure 6.4 Theoretical stress distribution assuming elemental struts colapse after buckling.

transmitted from the loaded plate to the gusset plate, which cannot be achieved with a rigid loaded plate and requires a specific loaded plate deflection, which is not likely. However, the stress distribution assumed by Martin (15) does produce a solution which agrees with experimental results as shown in Section 5.

After a strut buckles it does possess a certain amount of post buckling strength, which depends on its slenderness. Therefore, its resistance after buckling does not reduce to zero. Also the elemental struts that are assumed to make up the gusset plate should not be considered independant of each other. Although the bending moments, lateral and longitudinal shear forces that may exist between each adjacent elemental strut are not easily quantifiable their effects were observed.

Each elemental strut is effectively supported laterally by the inner elemental struts, which are stronger due to their lower

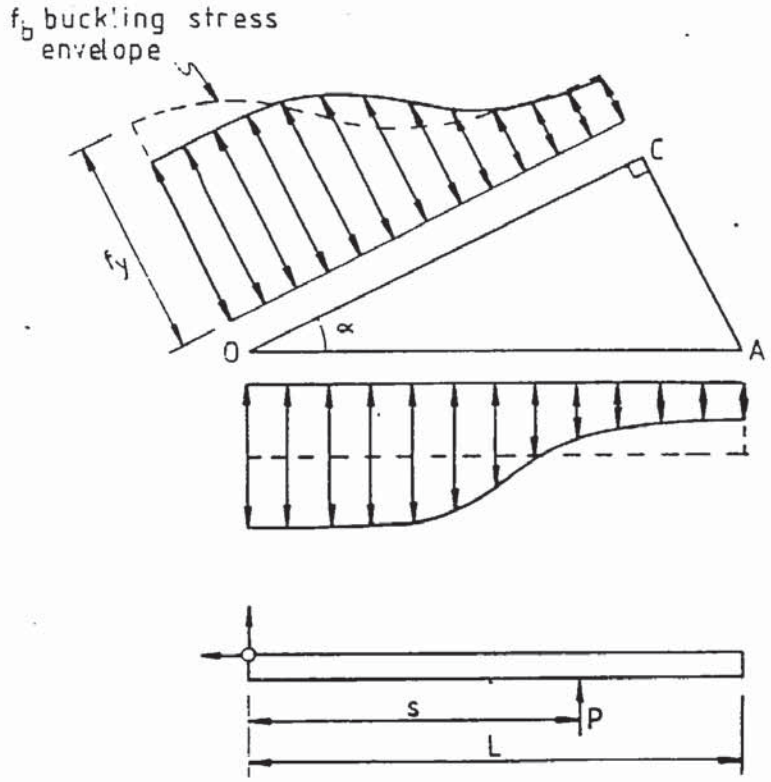

Figure 6.5 Theoretical stress distribution assuming post buckling strength and the interaction of adjacent elemental struts.

slenderness. This increases the stiffness of the outer elemental struts and increases their buckling load, but conversely it reduces the buckling load of the inner struts. As a result it is possible for the outer struts to sustain a higher stress than the buckling stress envelope suggests before they start to buckle and after buckling they may sustain a stress close to the buckling stress as shown in Figure 6.5. So at failure the stress distribution may be similar to the buckling stress distribution.

6.3.2 Flexible loaded plate assumption

In practice the loaded plate is not rigid and so it deflects into a shape depending mainly on the load position and on its thickness relative to that of the gusset plate.

The effect of the concentrated load used in the experiments is to produce a greater deflection of the loaded plate at the load point. As a result the stress distribution across the width of the gusset plate does not increase as a rectangular distribution but, with a stress

bulge at the load point. Therefore, it is not necessarily the outer free edge that reached the failure stress envelope first. With gusset plates that fail by yielding the stress bulge reaches the failure envelope first, as shown in Figure 6.6, which is at the yield stress. With further load increase more of the gusset plate reaches the yield stress until at the ultimate load, the stress distibution is rectangular.

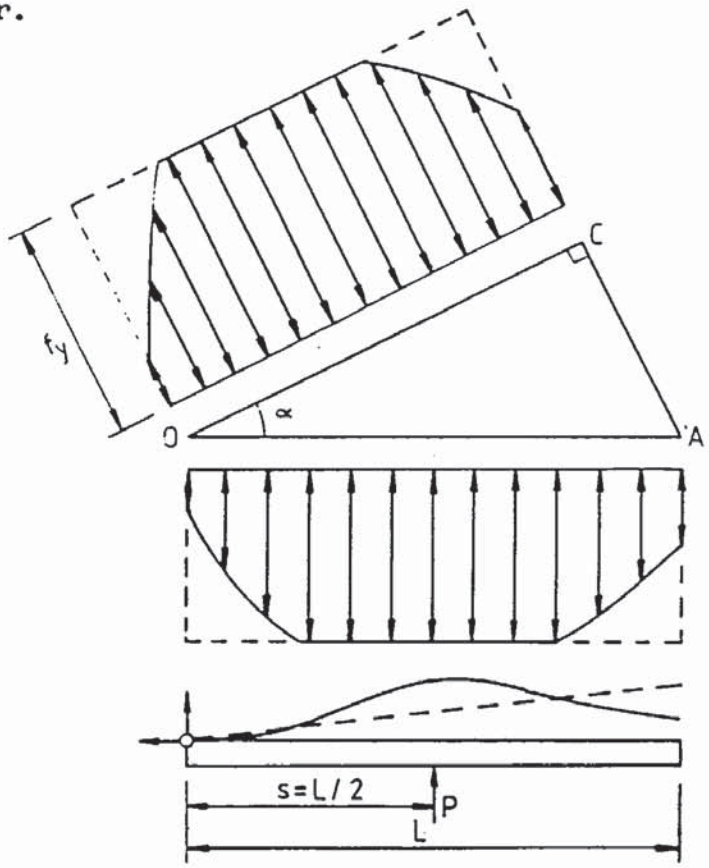

Figure 6.6 Theoretical effect of a flexible loaded plate on the stress distribution of a yielding gusset plate.

As the failure envelope for gusset plates that fail by buckling is not rectangular then the point at which the stress distribution curve reaches the failure envelope is not necessarily at the load point as shown in Figure 6.7. Also when the failure envelope is reached, then unlike the yielding condition, the stress is reduced depending on how the stress distribution curve reaches the failure envelope. The net result is, irrespective of where the stress concentration starts, it moves inwards until at the ultimate load the stress distribution is similar to the buckling stress distribution. The stress distributions leading up to failure are, however, quite

different depending on the position of the load.

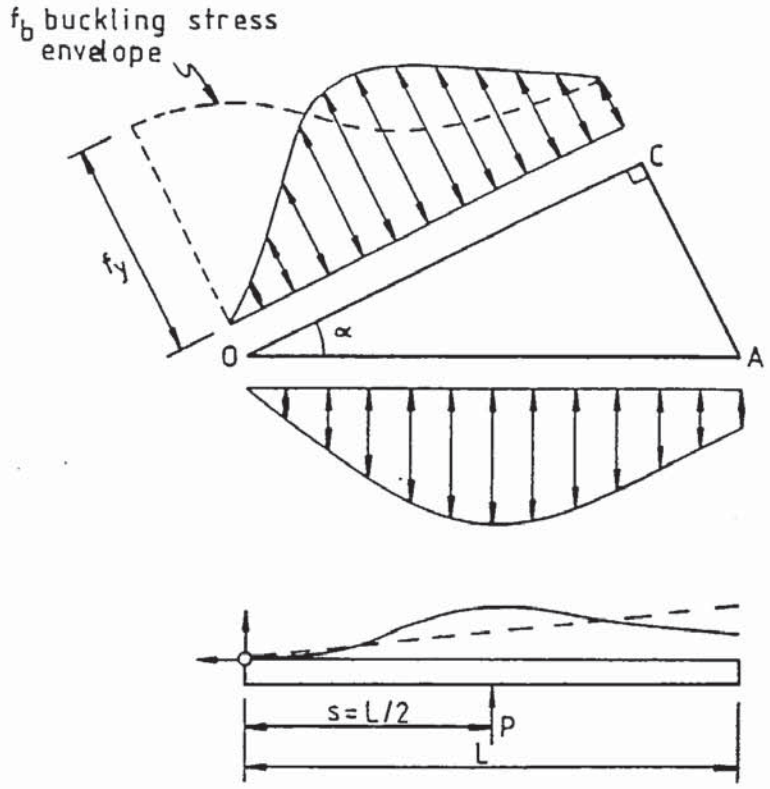

Figure 6.7 Theoretical effect of a flexible loaded plate on the stress distribution of a buckling gusset plate.

6.4. Residual stresses due to welding

As the multi-strip gusset plate was welded, the outer two strips of plate deflected laterally by a noticeable amount, which suggested that the outer strips had been pre-loaded with residual axial compressive stresses as a result of welding. Also the initial free edge lateral deflections are attributed to the effects of welding, with the continuity of the gusset plates reducing the deflections. Without specifically investigating these residual stresses it is difficult to determine exactly how they are produced and how they affect the behaviour of the gusset plates.

As the residual stresses are caused by differential contraction, then, with the gusset plates, one possibility is that the lateral contraction of the welds pull the gusset plate towards the adjacent loaded and supported plates by the same amount along both edges. For

example, consider the worst case of welding all the supported edge first. As the weld cools it contracts and pulls the gusset plate to the supported edge. This causes relative slip along the loaded edge. As the loaded edge is welded, it contracts and pulls the gusset plate to that edge. However, if at the junction of the supported and loaded plates this contraction is prevented, then the weld and the gusset plate towards the inside corner, are in tension. The loaded plate effectively pivots about its supported edge, and in the process of resisting bending it puts the outer weld and gusset plate into compression. The residual stresses increase as the weld size increases and decrease as the gusset plate thickness increases. This was evident with the thin plates showing more initial lateral deflection than the thicker plates. The complete gusset plates were welded using the step back technique to try and reduce this effect. With the multi-strip gusset plate this was not possible and so the effects were greater.

Longitudinal and lateral contraction of the welds caused the curling of the thin loaded plates, but this effect is considered to have very little effect upon the strength of the gusset plates.

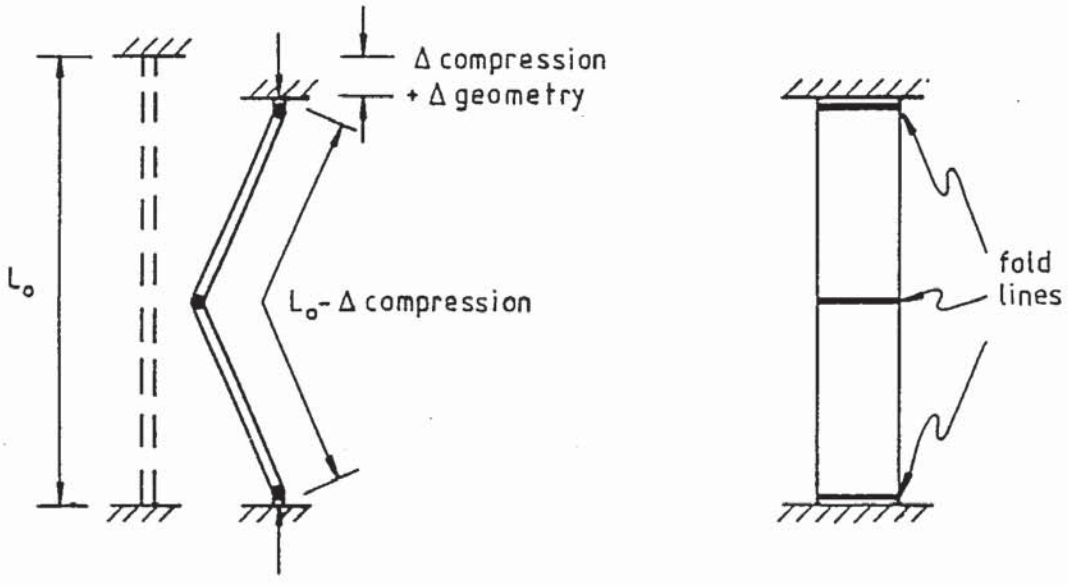

Figure 6.8 Position of plastic hinges of a fixed ended strut.

6.5 Equal sided right angled gusset plates

6.5.1 Post buckling compatibility

Consider the failure mechanism of a fixed ended strut. For the initial loading it remains straight and compresses axially until it reaches the elastic critical load, when it starts to deflect laterally. This in turn causes further axial compression. Finally plastic hinges form at either end and at the mid-point as shown in Figure 6.8, producing a mechanism and collapse occurs. With a triangular gusset plate the corresponding fold lines which produce a geometrically compatible mechanism are along the angle bisector and the two supported edges, as shown in Figure 6.9. The inclined struts

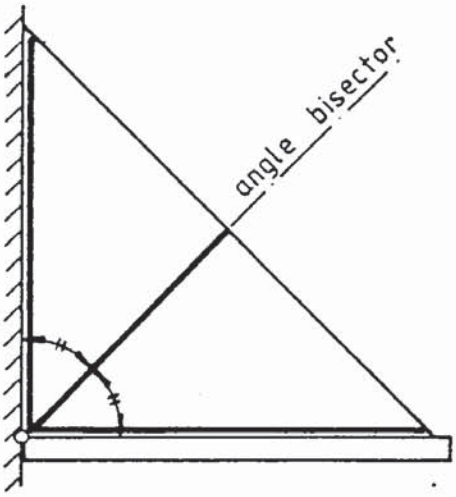

Figure 6.9 Geometrically compatible fold line pattern of a gusset plate.

tested in series 10, and the individual struts in the multi-strip gusset plates, series 11, produced fold lines as shown in Figure 6.10, which is a compromise between the two. The resulting net fold lines of the multi-strip gusset plate were in the geometrically ideal positions. However, increasing the width of the inclined strut to a full gusset plate, as in series 8, produced fold lines as given in Figure 6.11. The possible reason for the difference, is that the outer free edge is initially supported by the inner part of the

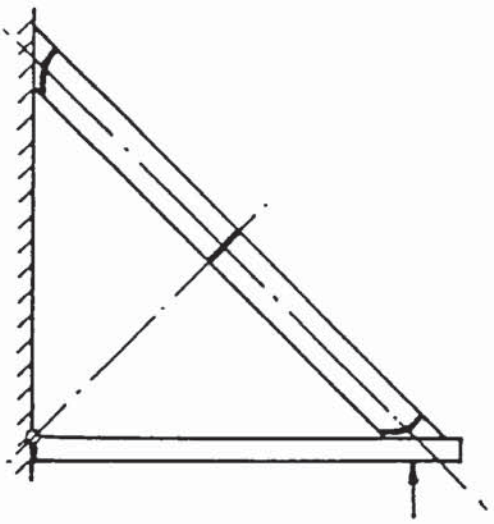

Figure 6.10 Fold line pattern of an experimental inclined strut.

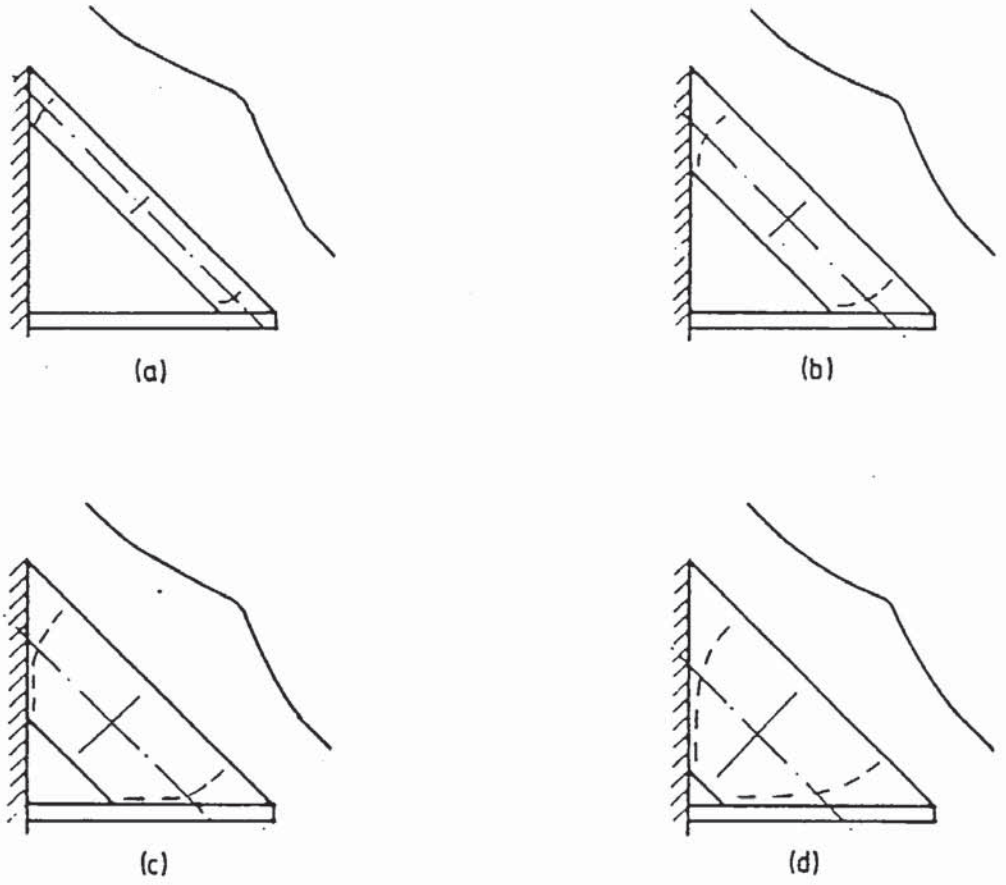

Figure 6.11 Fold line pattern as the strut width increases to the full width of a gusset plate.

inclined strut/gusset plate, to such an extent that it behaves as though it is a fixed ended strut equal to approximately the centre line length of the inclinded strut/gusset plate. As the outer free edge deflects laterally first, then it determines the start position of the fold lines along the free edge. As the buckling progresses inwards, the inner part of the gusset plate starts to buckle, but it has to buckle in a manner compatible with the geometry of the gusset plate. To do this it must modify the outer free edge which has already started to buckle in another way. This effectively requires increasing the length and the lateral deflection of the outer free edge relative to the inner gusset plate, as shown in Figure 6.12. This may induce a tensile load in the outer free edge which reduces the compressive stress already in it. As a result the outer free edge starts to support the inner part of the gusset plate by restricting its lateral deflection. Eventually this is overcome and the gusset plate collapses.

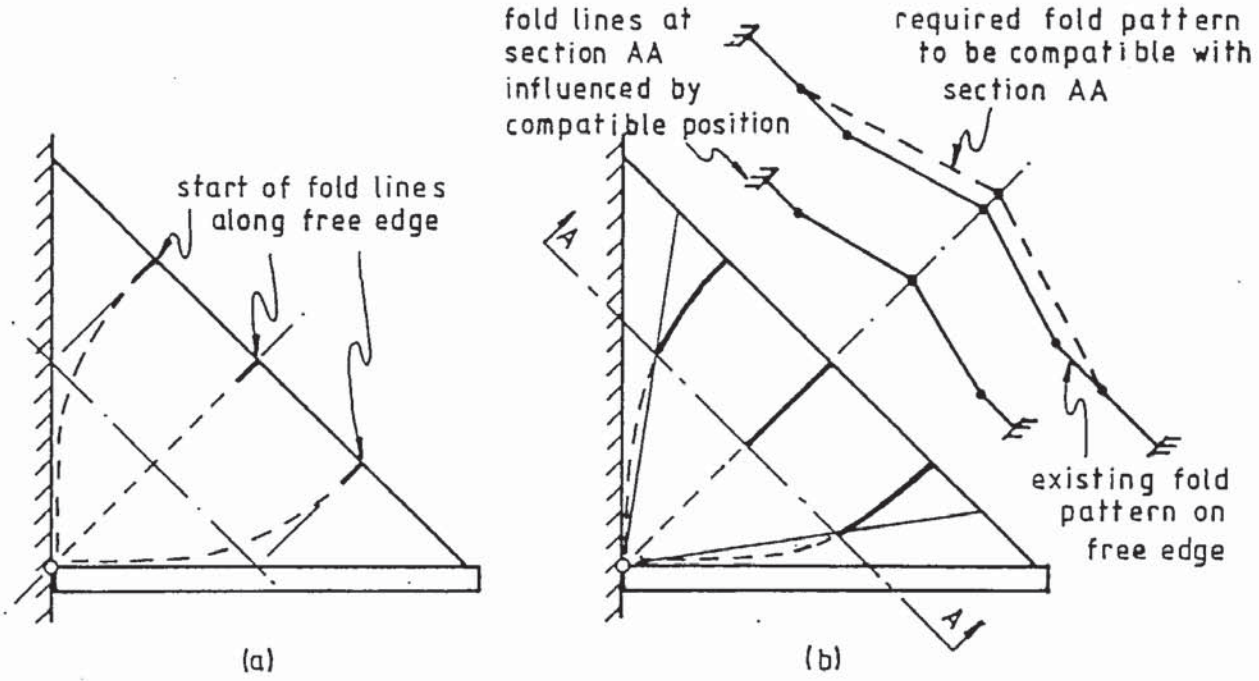

Figure 6.12 Progress of fold lines in a gusset plate to maintain compatability.

6.5.2. Experimental stress distributions

From the previous sections it can be seen that the resulting stress distribution across the width of a gusset plate is complex. It is very difficult to accurately take account of all the interacting factors so, in order to determine a simplified stress distribution which can be acceptably used at the ultimate load, a number of gusset plates had strain gauges attached across their width to measure the axial stresses parallel to the free edge. Because of the complex nature of the gusset plate, the strain gauges were not used as a means of obtaining absolute values, but as a means of trying to understand the behaviour of gusset plates during loading and at the collapse load.

6.5.2.1 Method of obtaining approximate stress distribution from strain gauges

From the raw data the average stresses across the width of the gusset plate parallel to the free edge were calculated at load increments which give a reasonable picture during the loading and are tabulated in Appendix 5. Due to the way in which the gusset plates buckled some of the strain gauges were subjected to bending strains which went beyond the yield strain close to the ultimate load. If these gauges were ignored, the resulting stress distributions revealed little about the behaviour of the gusset plates close to the ultimate load. As only an approximate indication of the plate behaviour is required, the following approximate method was used to obtain approximate axial stresses from such gauges.

As the strain gauges measured strains in excess of the yield strain for one or both faces due to bending, with one face in tension and the other face in compression, then until a plastic hinge is formed there will be a zone, in the middle of the plate section, that will still be straining elastically, as shown in Figure 6.13(a).

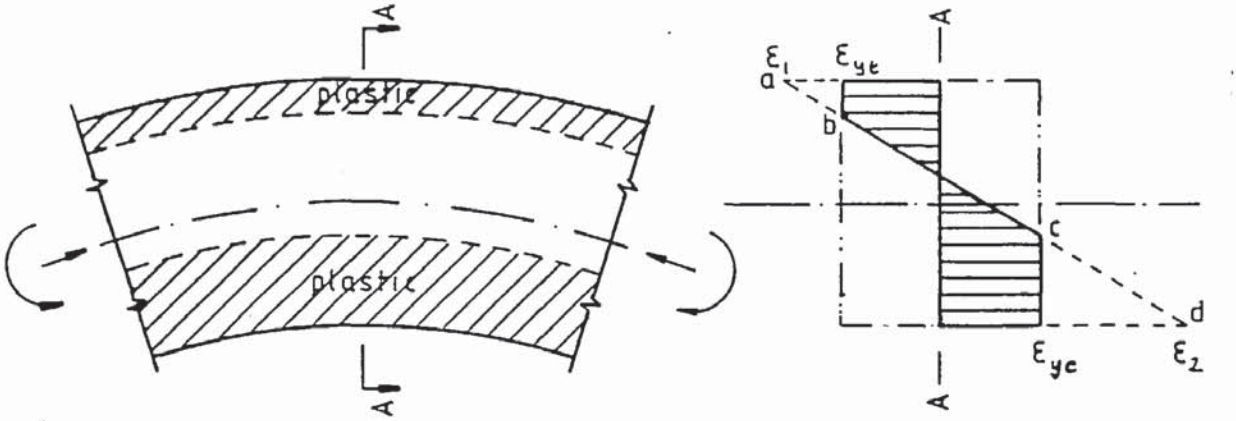

(a) section through gusset plate parallel to free edge (b) strain distribution at section AA

Figure 6.13 Stress distribution assumed across a section of plate subjected to bending strains greater than the yield strain.

Therefore, for the accuracy that is required and the thickness of plate used, it is reasonable to assume that the material is isotropic with Young's modulus being the same in tension as in compression, and the tensile yield strain is the same as the compressive yield strain. It is also reasonable to assume that the strain distribution within the elastic region is linear between bc, Figure 6.13(b), and for compatibility of strain across the section, the linear strain distribution is also carried on into the plastic zones, ba and cd, such that abcd is linear. That is, it is assumed that plane sections remain plane. The condition will exist where the outer edges have reached the yield strain and will continue to strain plastically without any additional stress. However, as they are attached to the inner layers, which are still straining elastically, they are restrained. The stress within the plastic zone will, however, only be the yield stress. Therefore, knowing the surface strains ε_1 and ε_2, the yield stress and Young's modulus of elasticity, the shaded area of the strain diagrams in Figure 6.13(b) can be summated, taking note of the signs, and converted to give an approximate axial stress in the section. As the strain gauges are actually measuring strain and not stress, then they give ε_1 and ε_2, although these will depend on the

accuracy of the gauges to measure larger strains than the yield strain. The tensile yield stress is also used for the yield stress, which is most probably lower than the compressive yield stress, which is more appropriate but is more difficult to obtain accurately.

Based on the multiple elemental strip assumption it seems reasonable to assume that, as long as the strain gauges are measuring strain parallel to the free edge they can be placed anywhere along a line parallel to the free edge and read approximately the same axial stress. Therefore, one specimen was tested with two additional lines of gauges off-set 50mm either side of the central set to test this assumption. Both sets of readings gave similar results as the middle set, although not identical. Therefore, on some specimens a line of gauges were placed running across the gusset plate from the inside corner, but off-set from the fold line onto an area of gusset plate that did not bend as much during testing. These gauges did allow strain gauge readings to be taken at higher loads, but still not close enough to the ultimate load without adjustment as previously described.

6.5.2.3 Analysis of experimental stress distribution

From the experimental stress distributions presented in Appendix 5 only the relevant specimen results are plotted and presented in the following. Those points obtained from gauges measuring strains beyond the yield strain are indicated. Tables are also presented for all the specimens, indicating the resultant force R', moment arm $\bar{w}$ and resistance moment $R'.\bar{w}$ produced by the stress distribution across the width of the gusset plate for each load increment, and compared with the applied moment M. The former were calculated from the area under each curve. R' and $\bar{w}$ are as shown in Figure 6.3.

As the model is based upon assuming a fixed ended buckling stress distribution across the width of the gusset plate, which is then

possibly modified by other factors, then such a buckling stress distribution curve is shown on the graphs. As Martin's (15) theory gives reasonable results using the Rankine-Gordon buckling stress distribution, it is used as a first approximation.

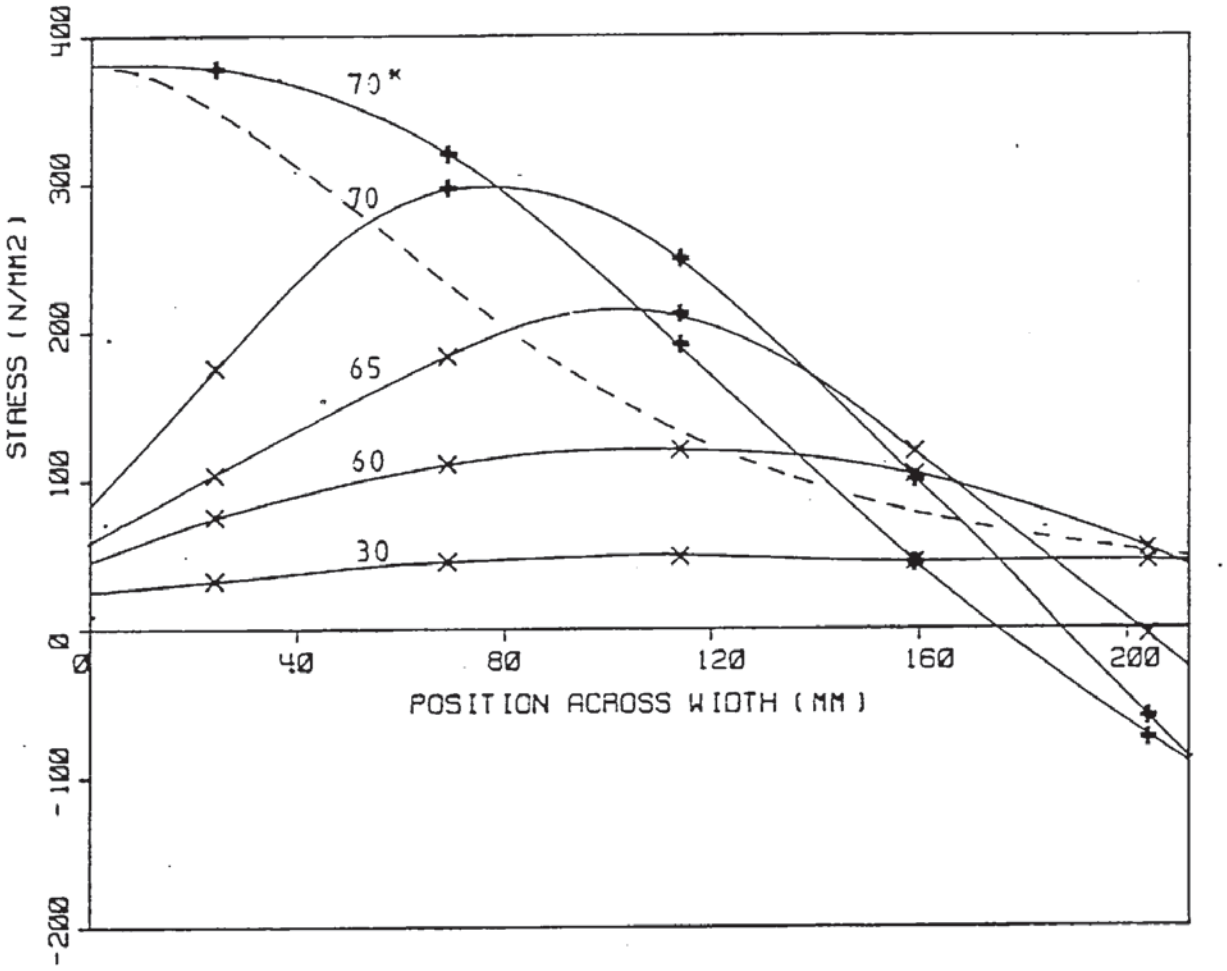

Figure 6.14 Build up of the average stress across the width of the gusset plate of specimen S5-150-1.

Figures 6.14, 6.15 and 6.16 show the stress distribution of specimens S5-150-1, S5-75-1 and S5-300-1, respectively, with the load applied in different positions. Although the terminated loaded plates were 20mm thick, they were relatively flexible and as a result, stress concentrations occurred in the stress distributions corresponding to the load positions. With the load at the mid-point and inner positions, this was in the form of a stress bulge, which became more pronounced as the load increased. This resulted in the stress distribution towards the outer half of the gusset plate reaching the buckling stress at the same time and so resulted in a low buckling

stress for the free edge. As the free edge started to deflect laterally the stresses were distributed to the inner plate, which in turn started to deflect laterally but was restrained by the incompatible lateral deflection of the outer free edge. This increased the buckling strength of the inner plate and caused the outer free edge to go gradually into tension. This lateral deflection incompatibility was accentuated with the load at the inner position as shown in Figure 6.15. The stress bulge moved inwards and increased in magnitude as it followed the buckling stress distribution curve but, at a higher stress until it reached a point where it did not produce a sufficiently large moment of resistance, and the specimen collapsed.

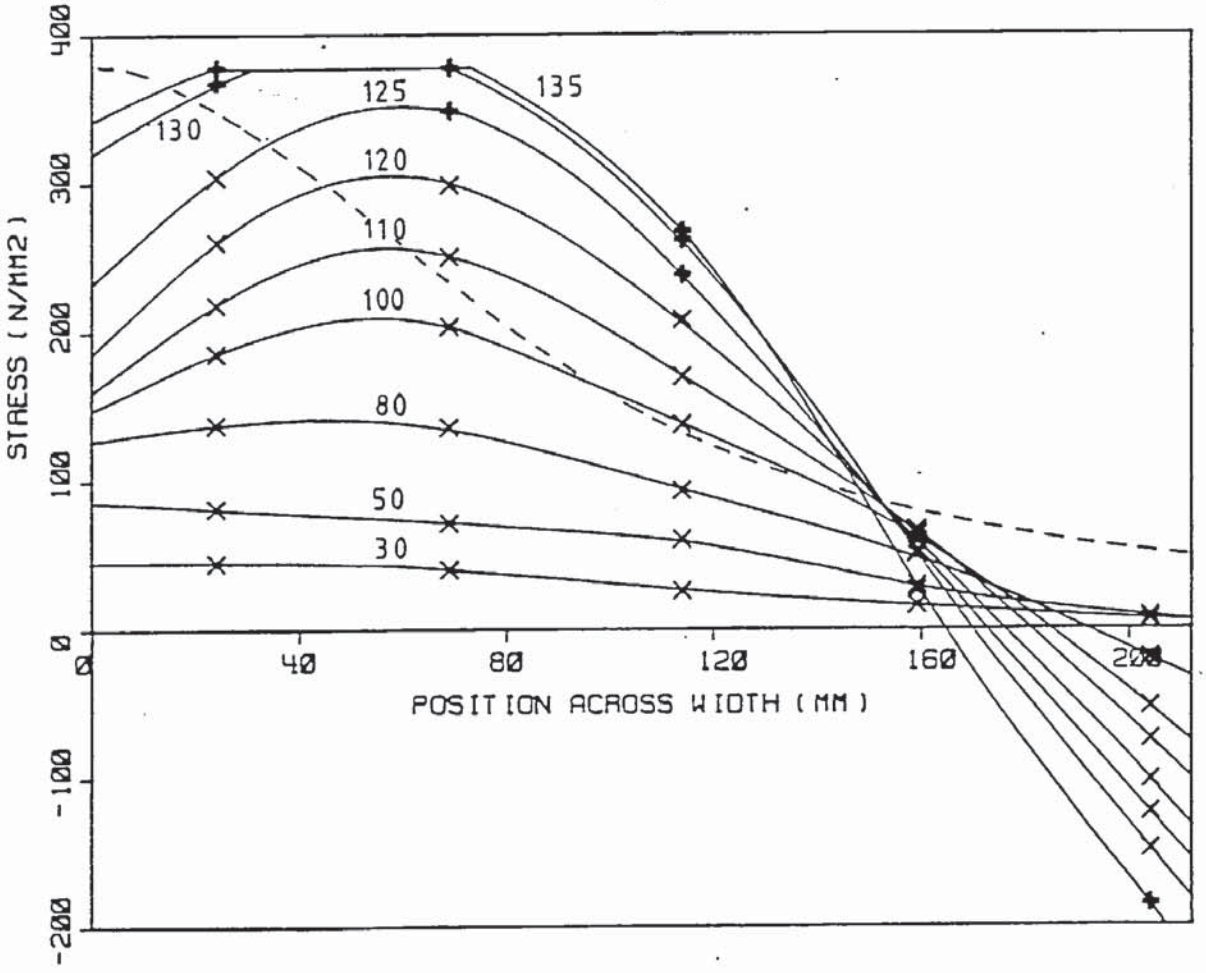

Figure 6.15 Build up of the average stress across the width of the gusset plate of specimen S5-75-1.

With the load applied at the outermost edge, the resulting initial stress distribution has a slope in the opposite direction to that of the buckling stress distribution as shown in Figure 6.16. So the inner plate supported the outer plate allowing it to reach a far

higher stress than the buckling stress curve suggests before it started to buckle. As the outer plate buckled the stress was redistributed to the inner plate, as shown by the stress bulge, moving inwards. The magnitude of this stress bulge is not as high as with the load applied further inwards, nor is there a tensile stress in the outer free edge. This is because the lateral deflection incompatiblities were reduced by the end of the loaded plate deflecting.

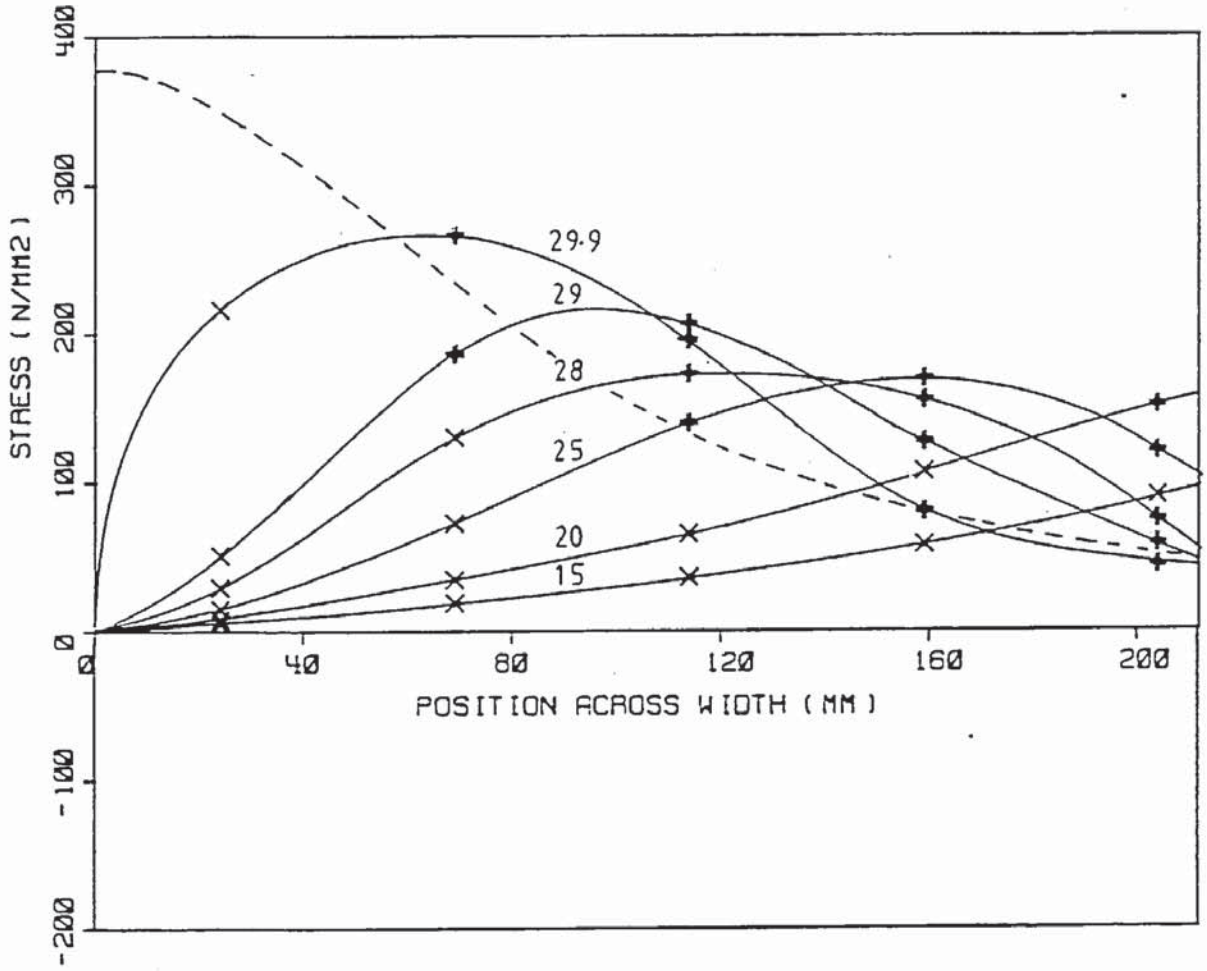

Figure 6.16 Build up of the average stress across the width of the gusset plate of specimen S5-300-1.

Specimen S5-150-2 was a repeat of specimen S5-150-1 and gave similar results. Two similar specimens to S5-300-1 were also tested, one with the same strain gauge arrangement S5-300-2 and the other, S5-300-3, with strain gauges off-set from the central fold line as previously described. Unfortunately with the former readings were not taken to the ultimate load due to data logger malfunction but those

taken were in agreement with S5-300-1. With the latter, the stress distributions were very similar to specimen S5-300-1.

The moment comparisons for specimens S5-150-1, S5-150-2, S5-75-1, S5-300-1, S5-300-2 and S5-300-3 are given in Tables 6.1 to 6.6, respectively. With each of these the applied moment and the moment of resistance of the stress distributions are shown to be within the same range. These two sets of readings are not expected to be exactly the same, firstly because the gusset plate is more complicated than the theoretical model assumes, and secondly, some of the stress readings are only approximate. With specimens S5-150-1, S5-150-2, S5-75-1 and S5-300-1, the last readings were taken very close to, or at, the failure load. Although the resultant force produced was greater than the previous load increment, its moment of resistance was less, and less than the applied moment. The moment of resistance produced by

SPECIMEN S5-150-1					
FROM APPLIED LOAD			FROM STRESS DISTRIBUTION		
Load P kN	Position s mm	Moment M=P.s kNm	Resultant force R' kN	Moment arm w mm	Resultant moment R'.w kNm
30.0	150	4.50	35.9	111	4.00
60.0	150	9.00	80.4	106	8.52
65.0#	150	9.75	111.3	95	10.56
70.0#	150	10.50	140.3	79	11.10
70.0#*	150	10.50	159.4	56	8.88

Table 6.1 Comparison of applied moment with that obtained from the experimental stress distribution of specimen S5-150-1.

SPECIMEN S5-150-2					
FROM APPLIED LOAD			FROM STRESS DISTRIBUTION		
Load P kN	Position s mm	Moment M=P.s kNm	Resultant force R' kN	Moment arm w mm	Resultant moment R'.w kNm
30.0	150	4.50	40.6	115	4.68
62.5	150	9.38	94.2	105	9.92
67.5	150	10.13	114.4	98	11.20
70.0#	150	10.50	141.3	88	12.38
71.6#*	150	10.74	159.6	54	8.56

Table 6.2 Comparison of applied moment with that obtained from the experimental stress distribution of specimen S5-150-2.

SPECIMEN S5-75-1					
FROM APPLIED LOAD			FROM STRESS DISTRIBUTION		
Load P kN	Position s mm	Moment M=P.s kNm	Resultant force R' kN	Moment arm w mm	Resultant moment R'.w kNm
30.0	75	2.24	24.7	78	1.94
50.0	75	3.75	45.7	78	3.54
80.0	75	6.00	74.6	72	5.37
100.0	75	7.50	100.6	68	6.86
110.0	75	8.25	119.7	66	7.91
120.0	75	9.00	138.7	63	8.73
125.0#	75	9.35	156.2	60	9.37
130.0#	75	9.75	172.6	55	9.56
135.0#*	75	10.13	167.9	49	8.20

Table 6.3 Comparison of applied moment with that obtained from the experimental stress distribution of specimen S5-75-1.

SPECIMEN S5-300-1					
FROM APPLIED LOAD			FROM STRESS DISTRIBUTION		
Load P kN	Position s mm	Moment M=P.s kNm	Resultant force R' kN	Moment arm w mm	Resultant moment R'.w kNm
15.0	300	4.50	32.0	149	4.78
20.0#	300	6.00	56.0	150	8.42
25.0#	300	7.50	86.4	136	11.75
28.0#	300	8.40	97.2	121	11.76
29.0#	300	8.70	109.3	109	11.90
29.9#	300	8.97	138.9	83	11.52

Table 6.4 Comparison of applied moment with that obtained from the experimental stress distribution of specimen S5-300-1.

SPECIMEN S5-300-2					
FROM APPLIED LOAD			FROM STRESS DISTRIBUTION		
Load P kN	Position s mm	Moment M=P.s kNm	Resultant force R' kN	Moment arm w mm	Resultant moment R'.w kNm
15.0	300	4.50	29.9	140	4.19
20.0	300	6.00	48.4	145	7.00
22.0#	300	6.60	60.7	145	8.80
23.0#	300	6.90	68.7	144	8.88
31.0	300	9.30			

Table 6.5 Comparison of applied moment with that obtained from the experimental stress distribution of specimen S5-300-2.

SPECIMEN S5-300-3					
FROM APPLIED LOAD			FROM STRESS DISTRIBUTION		
Load P kN	Position s mm	Moment M=P.s kNm	Resultant force R' kN	Moment arm w mm	Resultant moment R'.w kNm
15.0	300	4.50	30.4	154	4.68
22.5	300	6.75	46.5	152	7.05
28.0	300	8.40	65.6	140	9.16
30.0	300	9.00	79.2	128	10.14
31.0	300	9.30	89.4	119	10.68
32.0#	300	9.60	118.7	101	11.99

Table 6.6 Comparison of applied moment with that obtained from the experimental stress distribution of specimen S5-300-3.

assuming the Rankine-Gordon fixed ended buckling stress distribution at failure gives a similar value of 10.64kNm. Also the moment arm of the stress distribution is shown to move in towards the inside corner of the gusset plate as the load increases.

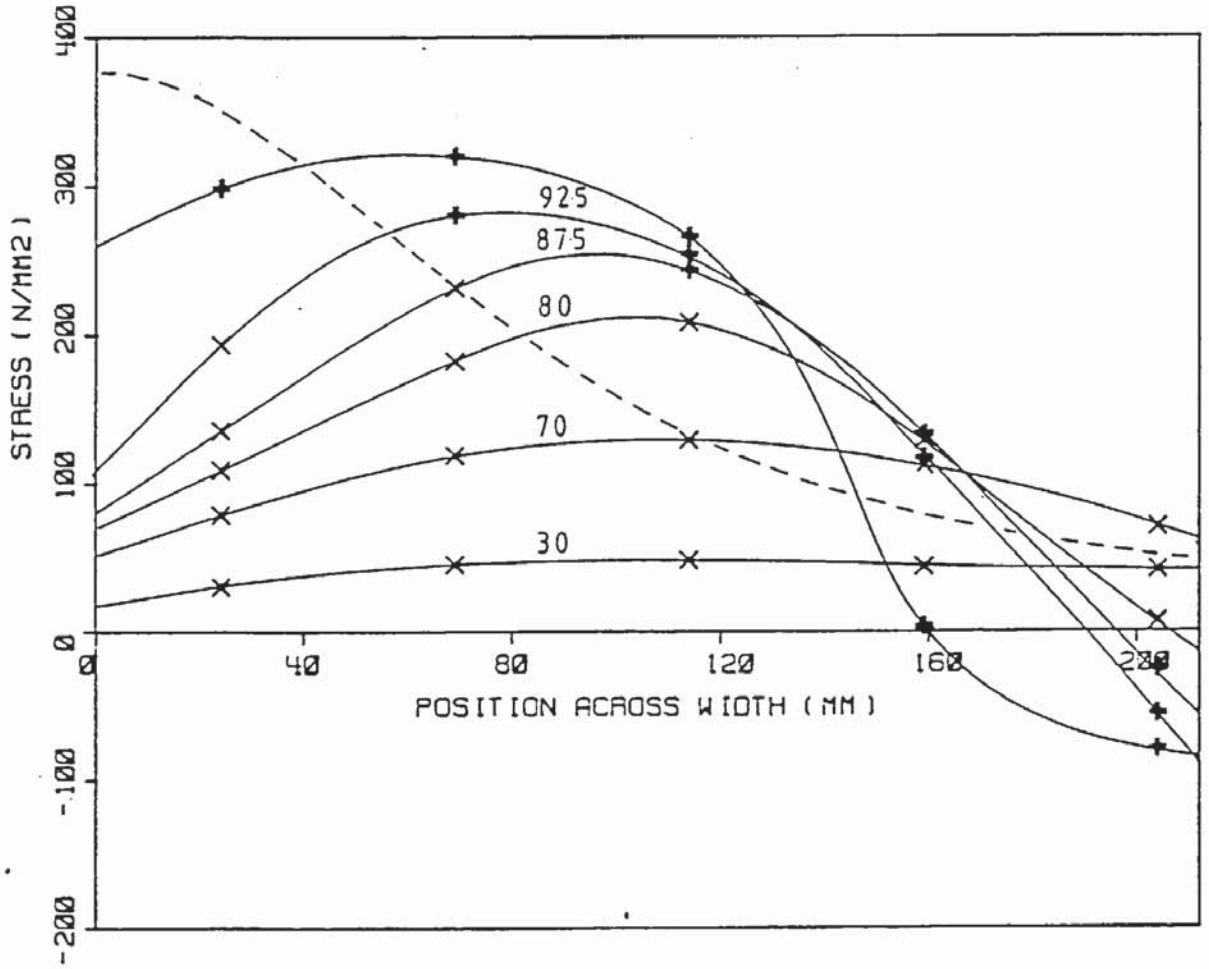

Figure 6.17 Build up of the average stress across the width of the gusset plate of specimen S6-150-1.

Strain gauges were also attached to two specimens which were similar to the previous specimens but with the loaded plate continued through at the supported edge. These were specimens S6-150-1 and S6-300-1 the stress distributions of which are shown in Figures 6.17 and 6.18 respectively. Comparison of the stress distribution of S6-150-1 with that of specimen S5-150-1 shows a similar build up of stress. The stress distribution curve at the ultimate load is different but, this was taken actually in the process of failing and the strain gauge readings may not be accurate. The loads for similar stress distributions are a little higher with the continuous loaded plate.

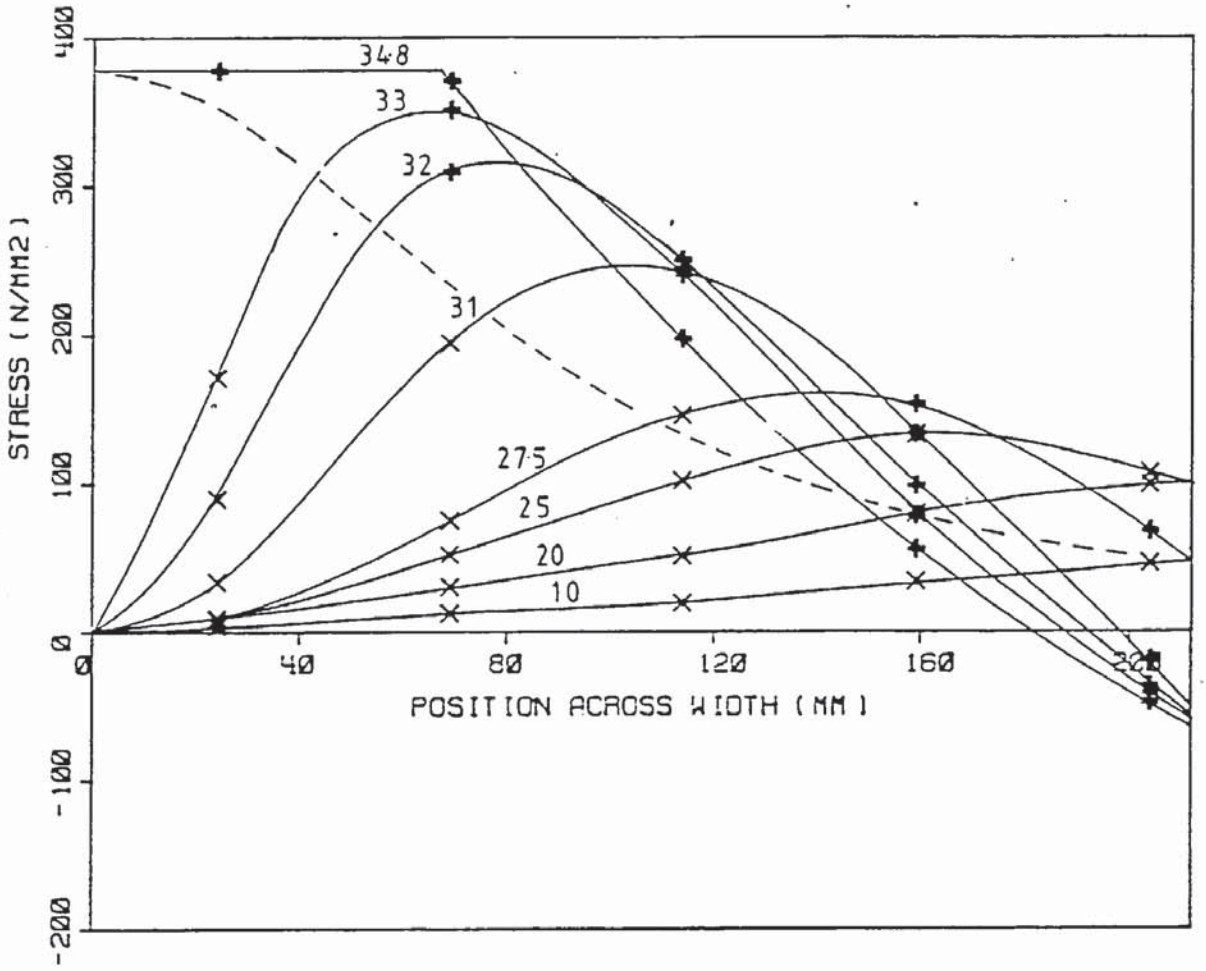

Figure 6.18 Build up of the average stress across the width of the gusset plate of specimen S6-300-1.

The stress distribution of S6-300-1 in comparison with that of specimen S5-300-1, Figure 6.16, shows a slightly different build up of stress. For the initial load increments the stress distributions are the same until the plate starts to deflect laterally. Then the

flexing of the loaded plate was such that it accentuated the lateral deflection incompatibilities rather than reducing them as with specimen S5-300-1. This produced a tensile stress in the outer free edge which did not occur with specimen S5-300-1 and it also increased the buckling stress of the inner plate. The stress bulge moved inwards following a higher stress than the buckling stress curve suggests. The last reading was taken as the specimen was in the process of failing and the yield stress was reached on the inside corner and the stress in the rest of the plate was reducing.

The moment comparisons of specimens S6-150-1 and S6-300-1 are shown in Tables 6.7 and 6.8 respectively. With both these specimens as with the others, the moment of resistance appears to agree with the applied moment reasonably well and the moment arm moves inward as the load increases. At the ultimate load the moment of resistance has dropped while the force is still increasing as in previous tests. The moment of resistance assuming the Rakine-Gordon buckling stress distribution gives a value of 10.76 KNm, which is a little lower than that obtained for the stress distribution and even lower than for the applied moment, of specimen S6-150-1. However, the ultimate load result obtained from this specimen appeared to be unusually high in comparison with other tests.

SPECIMEN S6-150-1					
FROM APPLIED LOAD			FROM STRESS DISTRIBUTION		
Load P kN	Position s mm	Moment M=P.s kNm	Resultant force R' kN	Moment arm w mm	Resultant moment R'.w kNm
30.0	150	4.50	36.6	111	4.06
70.0	150	10.50	88.3	108	9.53
80.0	150	12.00	114.2	97	11.07
87.5#	150	13.13	132.0	91	12.02
92.5#	150	13.83	147.0	82	12.06
95.0#*	150	14.25	153.6	60	9.28

Table 6.7 Comparison of applied moment with that obtained from the experimental stress distribution for specimen S6-150-1.

SPECIMEN S6-300-1					
FROM APPLIED LOAD			FROM STRESS DISTRIBUTION		
Load P kN	Position s mm	Moment M=P.s kNm	Resultant force R' kN	Moment arm w mm	Resultant moment R'.w kNm
10.0	300	3.00	18.4	146	2.70
20.0	300	6.00	42.8	144	6.15
25.0	300	7.50	67.2	139	9.35
27.5#	300	8.25	79.0	130	10.27
31.0#	300	9.30	108.1	104	11.24
32.0#	300	9.60	130.9	88	11.52
33.0#	300	9.90	146.3	79	11.56
34.8#*	300	10.44	174.5	60	10.47

Table 6.8 Comparison of applied moment with that obtained from the experimental stress distribution for specimen S6-300-1.

Two specimens were tested with effectively rigid loaded plates S5a-75-1 and S5a-300-1, which corresponded to the two load extremes, as tested with the flexible loaded plates, specimens S5-75-1 and S5-300-1, respectively. The loaded plates were terminated at the supported edge and the strain gauges were offset from the central fold

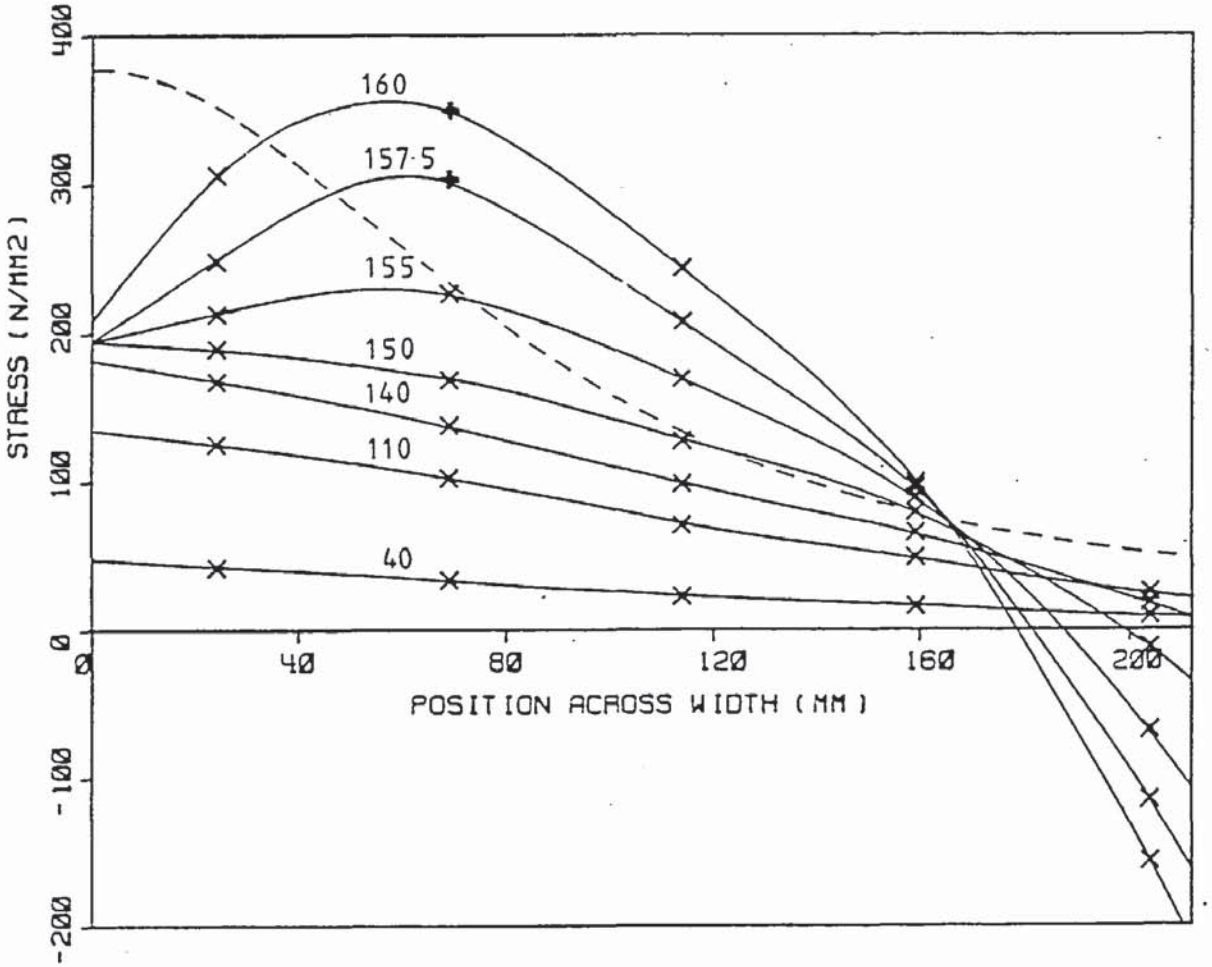

Figure 6.19 Build up of the average stress across the width of the gusset plate of specimen S5a-75-1.

line. The stress distribution obtained for specimen S5a-75-1 as shown in Figure 6.19, is similar to that of specimen S5-75-1, Figure 6.15. The stress distribution for a rigid loaded plate in the theoretical model is rectangular for the initial loading. However, the experimental stress distribution is not rectangular but it is relatively linear in comparison with specimen S5-75-1, Figure 6.15. The slope is most probably due to the compression of the supported edge, which is not assumed in the theoretical model. As the gusset plate started to deflect laterally the incompatibilities between the lateral deflection of the inner and outer plate started to take place. However, the effect was not as great as with the flexible loaded plate which accentuated this effect with the load in this position.

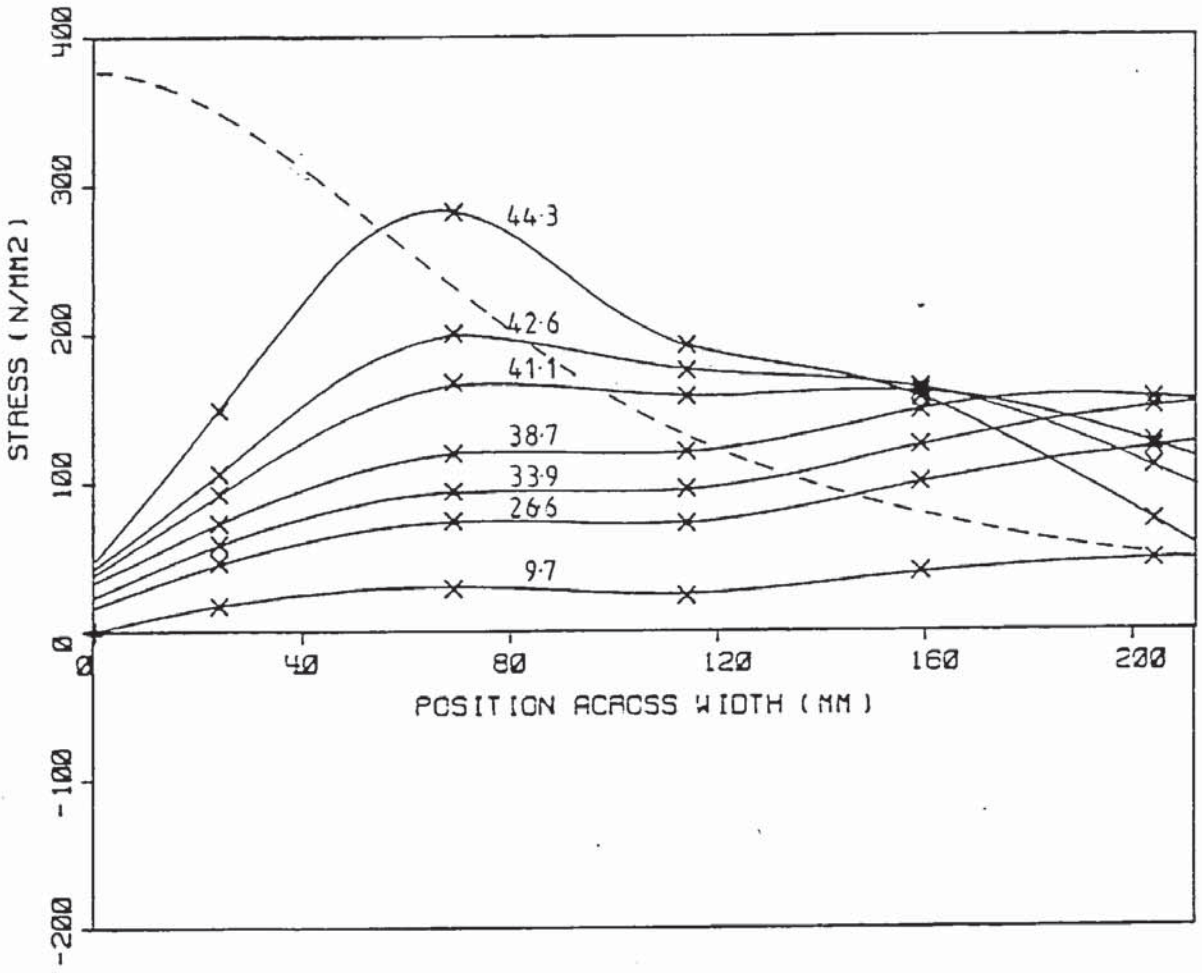

Figure 6.20 Build up of the average stress across the width of the gusset plate of specimen S5a-300-1.

The stress distribution obtained for specimen S5a-300-1, Figure 6.20, appears to be a little uneven. Whether this is correct or a

malfunction of a gauge is not known. However, the general appearance gives the impression that, although the stress distribution is not rectangular as in the theoretical model, the stress distribution is tending to be linear and sloping towards the supported edge, opposite to the previous specimens and for a similar reason. That is, the supported edge was extending which is not assumed in the theoretical model. The resulting distribution of stress increased the load at which the outer free edge started to deflect laterally. Therefore, the lateral deflections only became incompatible close to the ultimate load and so had little effect on increasing the buckling stress of the inner plate and on inducing a tensile stress in the free edge.

SPECIMEN S5a-75-1					
FROM APPLIED LOAD			FROM STRESS DISTRIBUTION		
Load P kN	Position s mm	Moment M=P.s kNm	Resultant force R' kN	Moment arm w mm	Resultant moment R'.w kNm
40.0	75	3.00	22.2	79	1.75
110.0	75	8.25	67.0	79	5.30
140.0	75	10.50	88.1	77	6.80
150.0	75	11.25	102.5	75	7.72
155.0	75	11.63	119.7	70	8.37
157.5#	75	11.81	142.5	66	9.40
160.0#	75	12.00	163.1	62	10.18

Table 6.9 Comparison of applied moment with that obtained from the experimental stress distribution of specimen S5a-75-1.

SPECIMEN S5a-300-1					
FROM APPLIED LOAD			FROM STRESS DISTRIBUTION		
Load P kN	Position s mm	Moment M=P.s kNm	Resultant force R' kN	Moment arm w mm	Resultant moment R'.w kNm
9.7	300	2.91	25.3	127	3.23
26.6	300	7.98	67.1	125	8.40
33.9	300	10.17	85.8	124	10.68
38.9	300	11.67	102.3	122	12.46
41.1	300	12.33	119.5	113	13.54
42.6	300	12.78	131.1	108	14.17
44.3	300	13.29	150.5	97	14.60

Table 6.10 Comparison of applied moment with that obtained from the experimental stress distribution for specimen S5a-300-1.

The moment comparison of specimens S5a-75-1 and S5a-300-1 are shown in Tables 6.9 and 6.10 respectively. The moments of resistance are similar to the applied moments as with other specimens and the last reading in each case was taken before the specimen actually failed and not in the process of failure, and so do not show a drop in the moment of resistance at the ultimate load. The moment of resistance calculated from the Rankine-Gordon buckling stress distribution of 10.76 kN, is similar to the S5a-75-1 specimen but lower than for the S5a-300-1 specimen.

Strain gauges were also placed at the midpoint of each strut of the multi-strip specimen S5-150-1 and so measured the equivalent stress distribution across its width, which is shown in Figure 6.21. As the gusset plate was made up of strips then there was no lateral restraint provided by adjacent struts and so all the struts buckled as individual full length fixed ended struts. There was no lateral

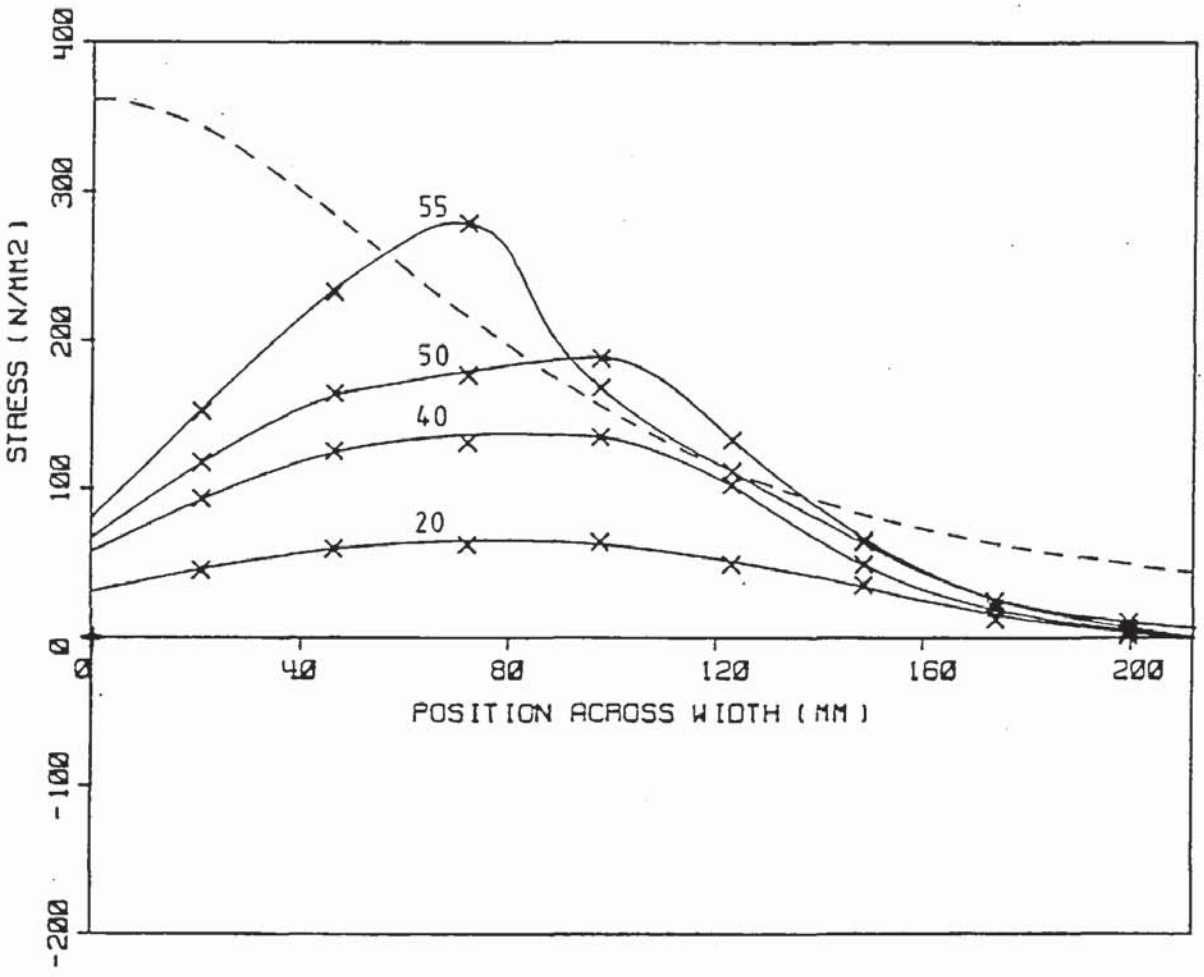

Figure 6.21 Build up of the average stress across the width of the gusset plate of specimen S11-150-1.

deflection incompatibility which increased the buckling stress of the inner plate or induced a tensile stress in the outer plate. Therefore, the buckling stress in each strut was similar to that suggested by the buckling stress distribution curve. As previously mentioned the outer two strips of plate were pre-stressed due to the effects of welding and so the strain gauges measured the additional stress due to the load being applied. Therefore, the outer two struts at least buckled at a lower stress than the buckling stress distribution curve suggests. With the buckling of the middle two struts between 50 and 55 kN the stress was redistributed to the adjacent inner struts and the process continued until all the struts had buckled. Although the outer struts had effectively buckled they still had a relatively high stress in them.

SPECIMEN S11-150-1					
FROM APPLIED LOAD			FROM STRESS DISTRIBUTION		
Load P kN	Position s mm	Moment M=P.s kNm	Resultant force R' kN	Moment arm w mm	Resultant moment R'.w kNm
20.0	150	3.00	35.3	83	2.94
40.0	150	6.00	67.7	80	5.43
50.0	150	7.50	90.1	81	7.32
55.0	150	8.25	106.8	75	8.04

Table 6.11 Comparison of applied moment with that obtained from the experimental stress distribution for specimen S11-150-1.

As with all the other specimens tested Table 6.11 shows a close agreement between the applied moment and the moment of resistance obtained from the stress distribution for this specimen. This specimen demonstrated that although each strip of plate attained the buckling stress as given by the buckling stress distribution curve, they did not do so all at the same time, but progressively from the outer strips to the inner strips. Therefore, the actual moment of resistance at the ultimate load of this specimen was less than that assuming the Rankine-Gordon buckling stress distribution.

Although the fixed ended buckling stress assumption is not entirely correct, the results of these stress distributions show that the combined effects of the flexing of the loaded plate, the load position and the lateral restraint between each elemental strut has the effect of producing a similar stress distribution at the ultimate load in each case, which has a similarity to the fixed ended buckling stress distribution. More importantly to a good approximation the stress distribution across the gusset plate obtained approximately at the ultimate load, was similar to the moment of resistance produced by the assumed buckling stress distribution.

Other points of interest were that the loaded plate did not contribute to the moment of resistance directly, but it did influence the way in which the stresses were distributed, by the way it flexed under load. Strain gauges attached across the loaded plate at the supported edge did not show high bending stresses during loading and only showed yield stresses after the gusset plate itself had collapsed.

6.6 Unequal sided right angled gusset plates

6.6.1. Post buckling compatibility

These gusset plates buckled in a very similar manner to the equal sided gusset plates. Figure 6.22 shows a few of the fold line patterns obtained from series 4. Superimposed on these are the angle bisector, and another chain line perpendicular to it and passing through the nearest corner. Examination of the fold lines within the dashed line show that they are almost symmetrical and very similar to those of the equal sided right angled gusset plates. The fold lines outside this line tend to intersect the free edge perpendicular, as though it is a strut. Because of this similarity with the equal sided right angled gusset plates, most of the discussions relating to them can be applied in this case.

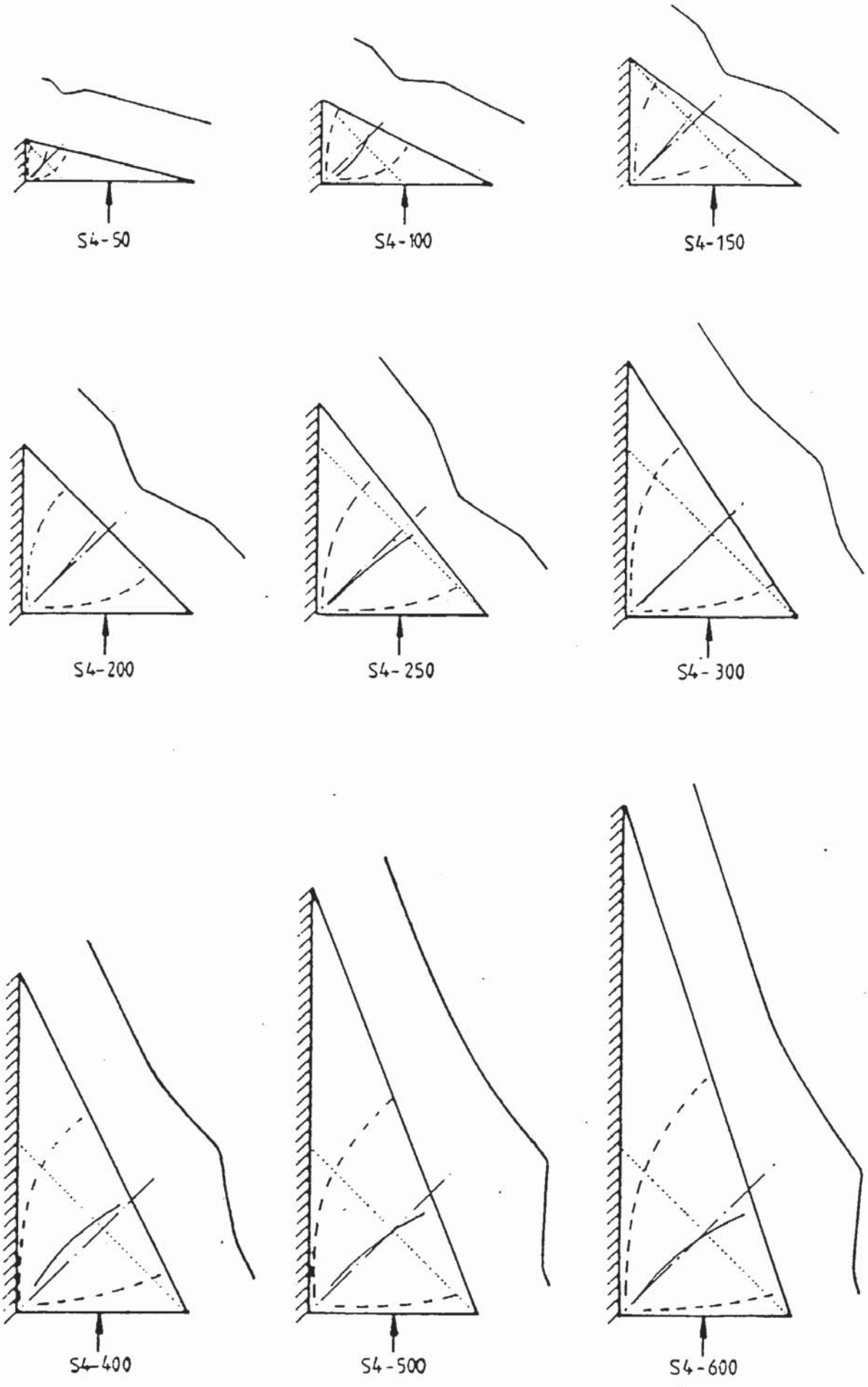

Figure 6.22 Comparison of series 4 fold line patterns with those of equal sided gusset plates.

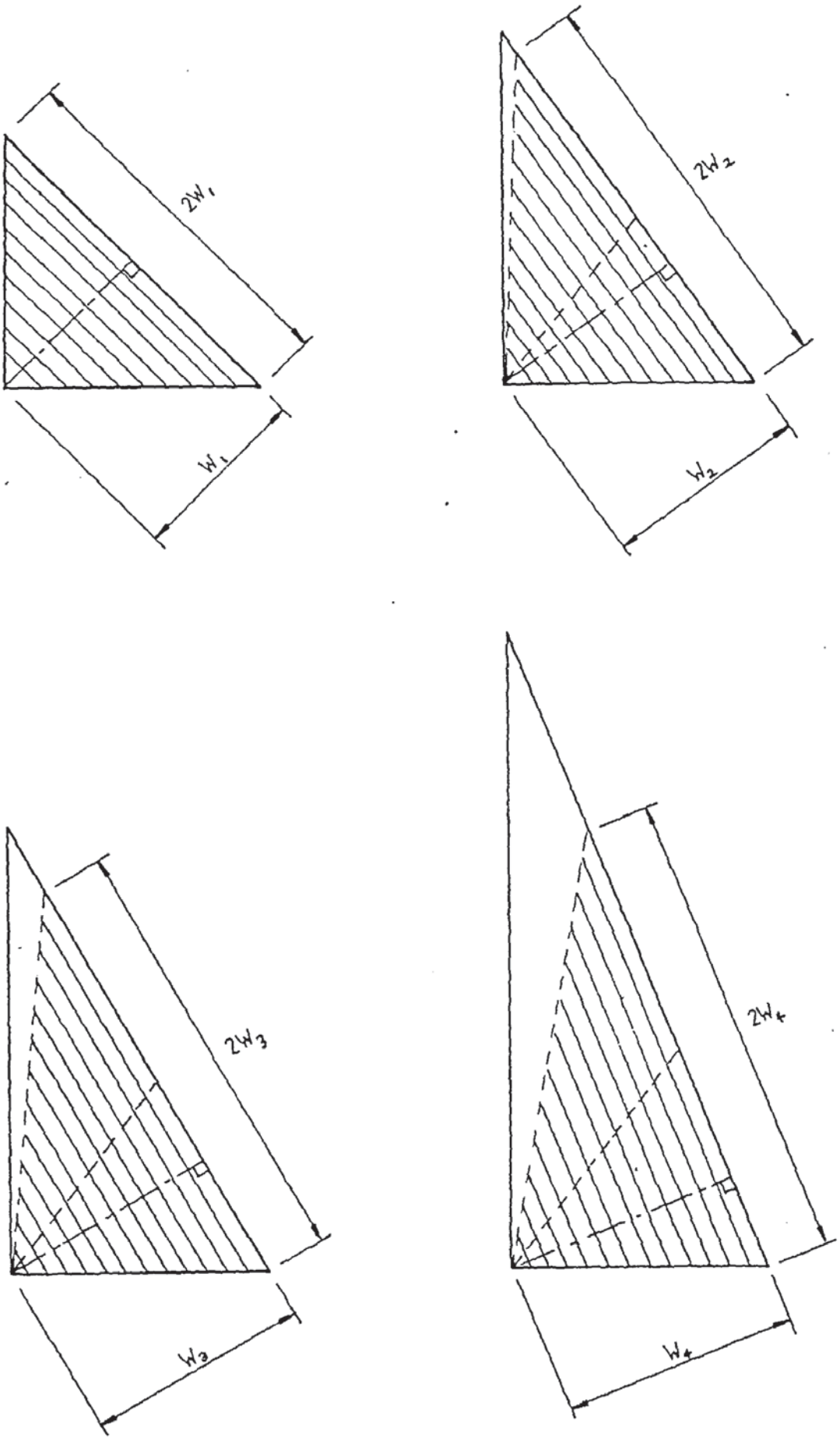

Figure 6.23 Theoretical strip model for 90° gusset plates assumed by Martin.

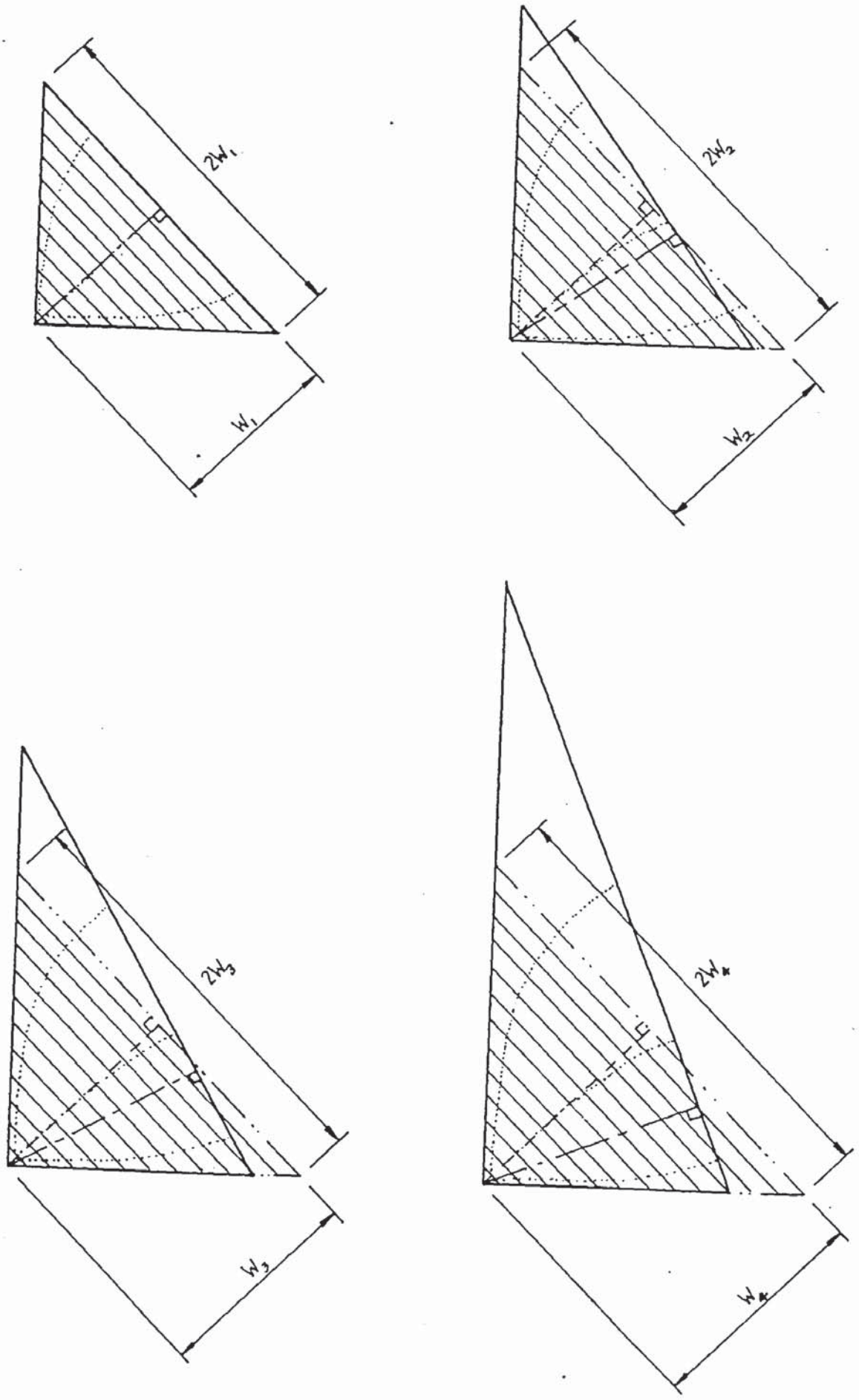

Figure 6.24 Theoretical strip model for 90° gusset plates by author.

The experimental results show that a small increase in the height beyond that of an equal sided gusset plate causes only a small increase in its strength and any further increase in height makes very little difference. Therefore, beyond a certain height a gusset plate has an equivalent strength to a gusset plate having both its fixed edges slightly greater than its shortest side. Extending the assumption of a gusset plate consisting of full length fixed ended struts running parallel to the free edge results in effective lengths of the struts of half their actual length. However, this results in a reduced moment of resistance of a gusset plate as its height increases from the equal sided gusset plate. Martin (15) used an effective length that was equal to the width of the gusset plate. This assumption is a convenient mathematical way of approximating this effect, as the increase in the width reduces, as the height increases and therefore, is virtually the same beyond a certain height. Figure 6.23 shows how this mathematical assumption can be related to the theoretical model assuming fixed ended struts parallel to the free edge. Figure 6.24 shows another fixed ended strut interpretation suggested by the buckled gusset plates, of assuming the equivalent gusset plate with both fixed edges of equal length, and using the same mathematical assumptions. From this latter model, the position of the fold lines can be approximated, based on those of equal sided gusset plates.

6.7 Equal sided gusset plates with internal angles other than 90°

6.7.1 Post buckling compatibility

These gusset plates buckled in a similar manner to the 90 degree gusset plates as shown in Figure 4.16. The inner plate tended to buckle with the fold lines in the geometric ideal position along the angle bisector and the two fixed edges. However, the outer free edge

tended to deflect laterally first, as though it was a strut running parallel to the free edge. For the gusset plates with internal angles less than 90 degrees, the fold lines were forced closer together and affected the whole of the gusset plate. With the gusset plates with internal angles greater than 90 degrees, the fold lines could have occupied a greater area of the gusset plate but, because of the greater restraining effect of the free edges as the angle increases, are concentrated about the central section, and affected roughly the same area of the gusset plate as with a 90 degree gusset plate.

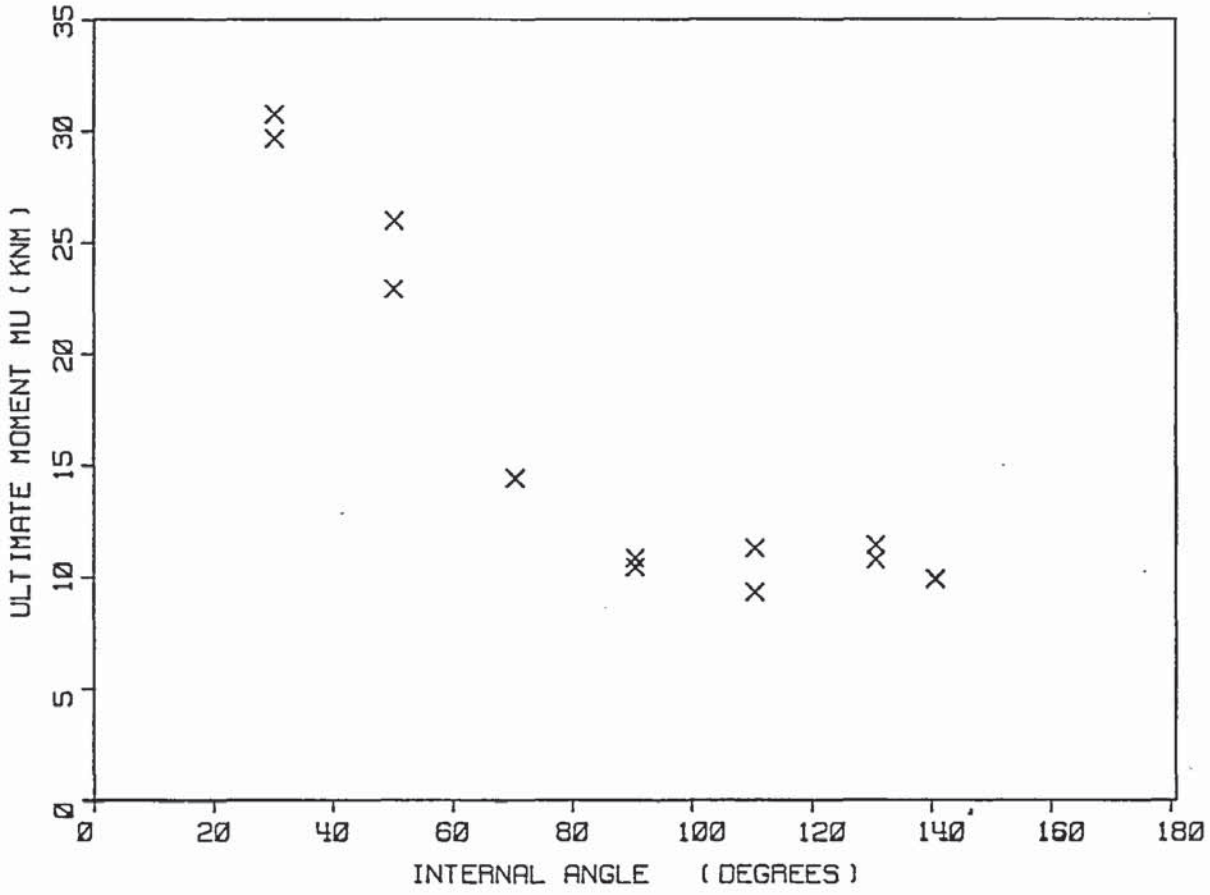

Figure 6.25 Graph of the failure moment against the internal angle.

Extending the assumption of gusset plates consisting of full length fixed ended struts running parallel to the free edge results in effective lengths of the struts half their actual lengths. This suggests, for specimens of the same width, as in series 13, that the moment of resistance increases rapidly as the internal angle decreases from 90 degrees, and it reduces rapidly as the internal angle increases from 90 degrees. In Figure 6.25 the failure moment of each

plate in series 13 was calculated based on the failure load and its lever arm distance s, and plotted against its internal angle. Figure 6.25 does show a rapid increase in the failure moment as the internal angle reduces from 90 degrees but, does not show a rapid reduction in the moment of resistance as the internal angle is increased above 90 degrees. In fact, the results suggest that gusset plates with an internal angle greater than 90 degrees have the same moment of resistance as a 90 degree gusset plate of the same width. Figure 6.26 shows how the mathematical assumption of using the effective length

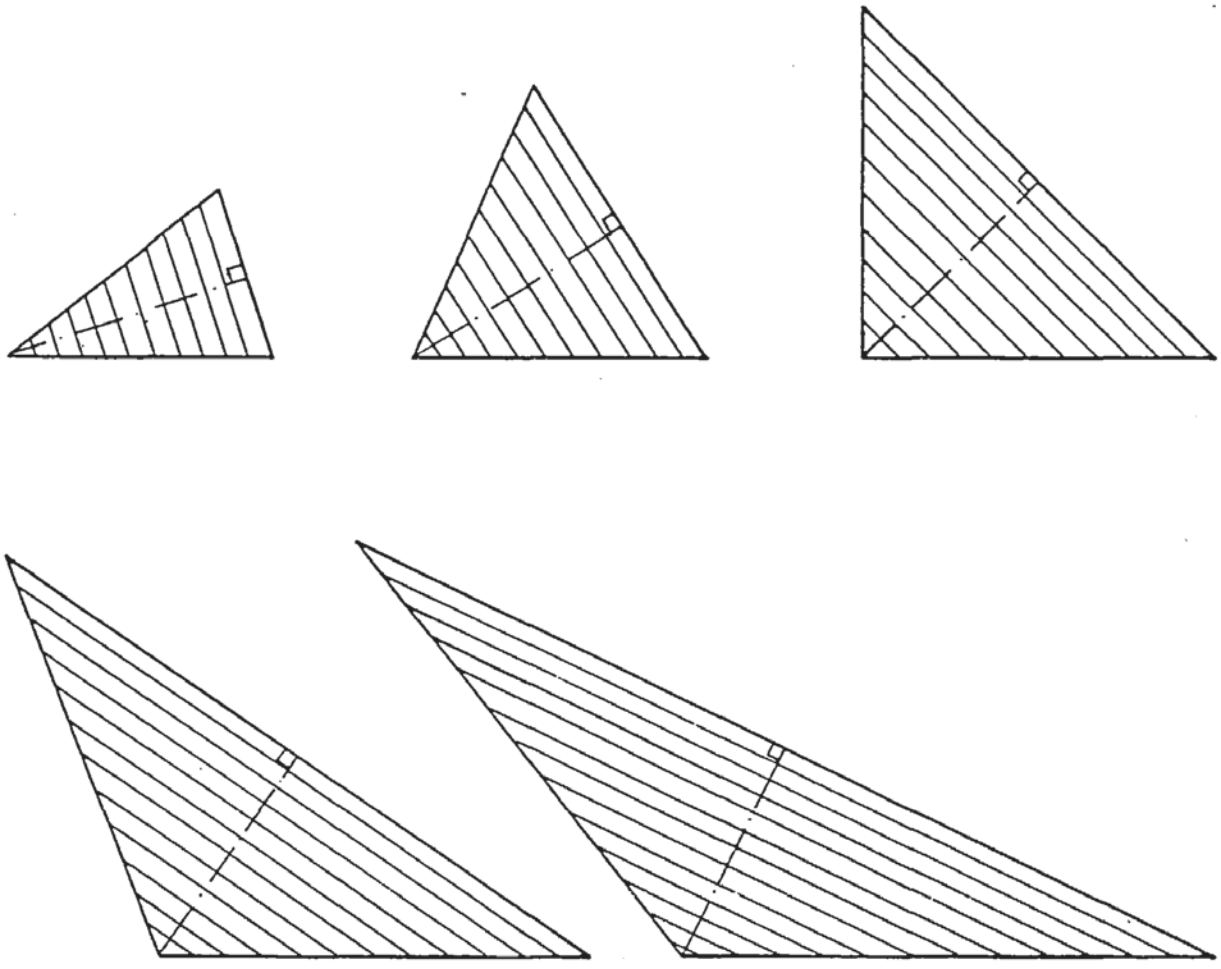

Figure 6.26 Strip model for equal sided gusset plate with varying internal angle based on full length fixed ended struts.

based on the full length of the assumed struts parallel to the free edge is represented in the theoretical model. Figure 6.27 shows how the mathematical assumption of using a maximum effective length based on the equivalent 90 degree gusset plate, is represented in the theoretical model. Comparison with the fold lines of series 13 shown in Figure 6.16 suggests that this latter model is a better representation. Again, from this latter model, the position of the fold lines can be predicted based on those of equal sided right angled gusset plates.

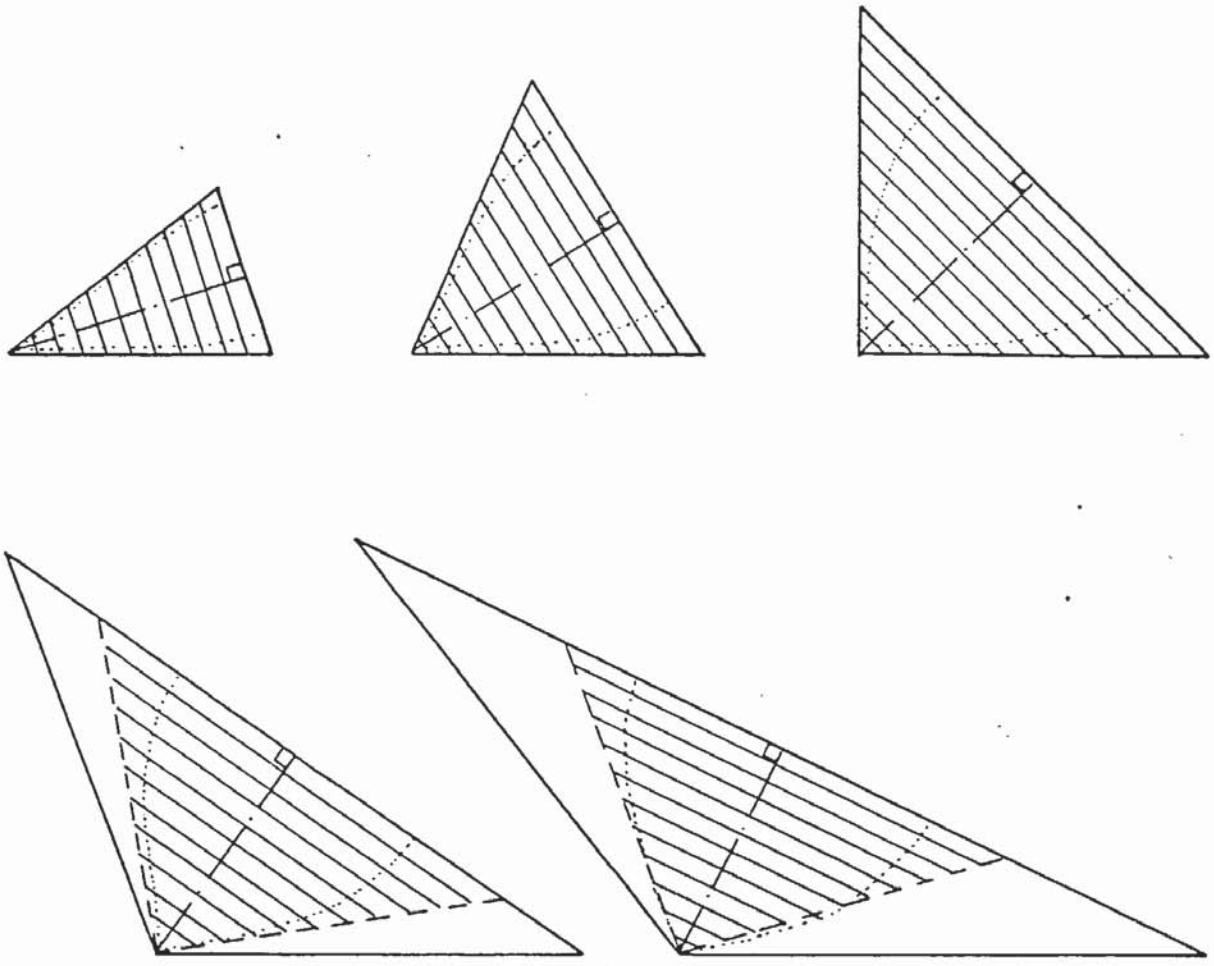

Figure 6.27 Strip model for equal sided gusset plate with varying internal angle based on reduced fixed ended strut length.

6.7.2. Analysis of experimental stress distribution

The stress distribution across the width of specimens S13-50-1, S13-70-1, S13-110-1 and S13-130-1 are presented in Figures 6.28 to 6.31 respectively. In a similar manner the Rankine-Gordon fixed ended strut buckling stress distribution has been added. With angles greater than 90 degrees this stress distribution is based upon that for a 90 degree gusset plate as suggested by the fold line patterns. Generally the stress distribution had similarities to the 90 degree gusset plates. Stress concentrations corresponding to the load position were more pronounced with the smaller angled plates, possibly due to the smaller area of gusset plate available to distribute the stress across the width. With the 50 degree gusset plate the stress concentration was such that the middle area of plate started to deflect laterally before the outer free edge. This caused the outer free edge to go into tension, while the middle section was at the

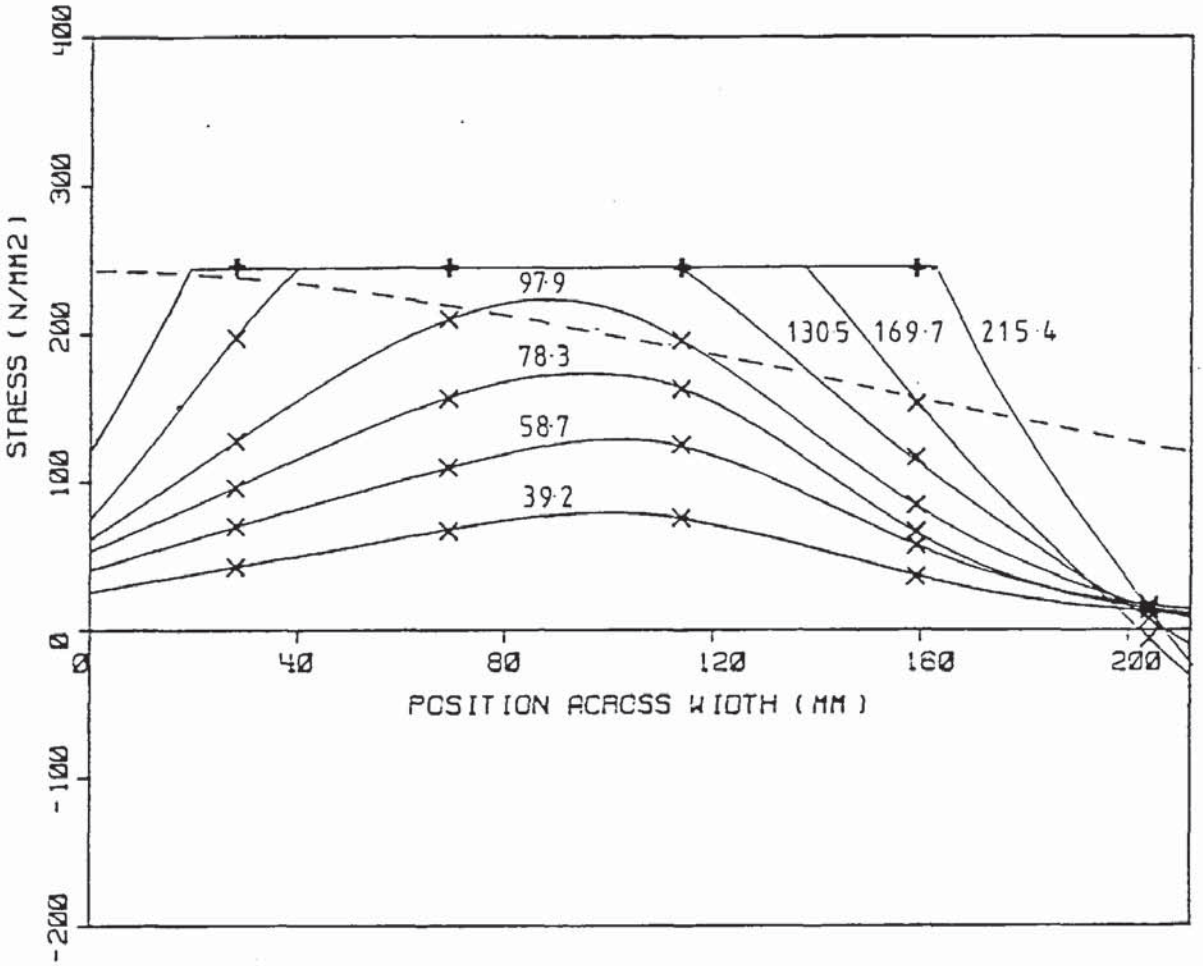

Figure 6.28 Build up of the average stress across the width of the gusset plate of specimen S13-150-1.

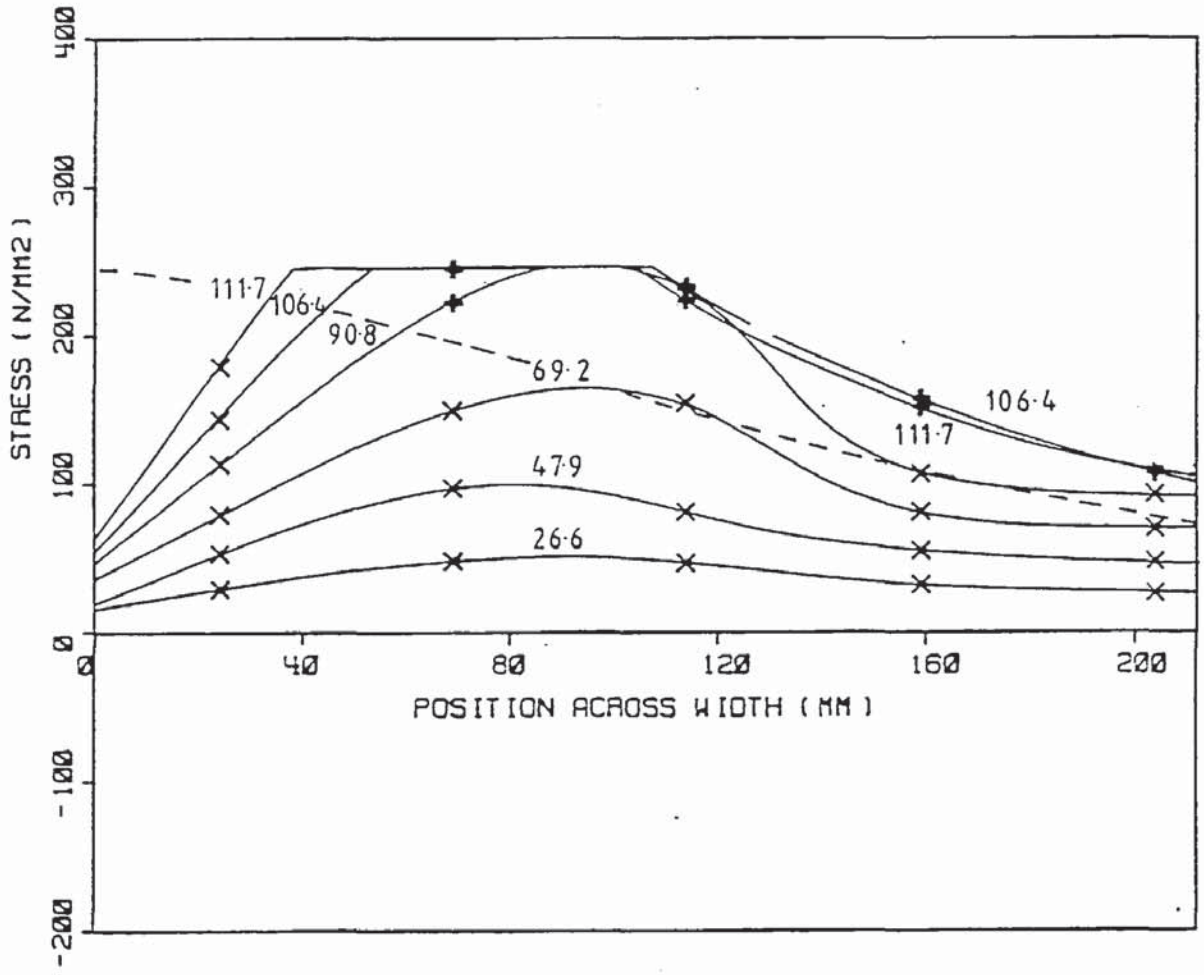

Figure 6.29 Build up of the average stress across the width of the gusset plate of specimen S13-70-1.

SPECIMEN S13-50-1					
FROM APPLIED LOAD			FROM STRESS DISTRIBUTION		
Load P kN	Position s mm	Moment M=P.s kNm	Resultant force R' kN	Moment arm w mm	Resultant moment R'.w kNm
39.2	117	4.59	41.3	97	4.00
58.7	117	6.87	66.9	96	6.39
78.3	117	9.16	88.0	92	8.10
97.9	117	11.45	111.9	91	10.15
130.5#	117	15.27	143.8	89	12.76
169.7#	117	19.85	159.0	87	13.91
215.4#	117	25.20	177.3	91	16.19
221.9	117	25.96			

Table 6.12 Comparison of applied moment with that obtained from the experimental stress distribution for specimen S13-50-1.

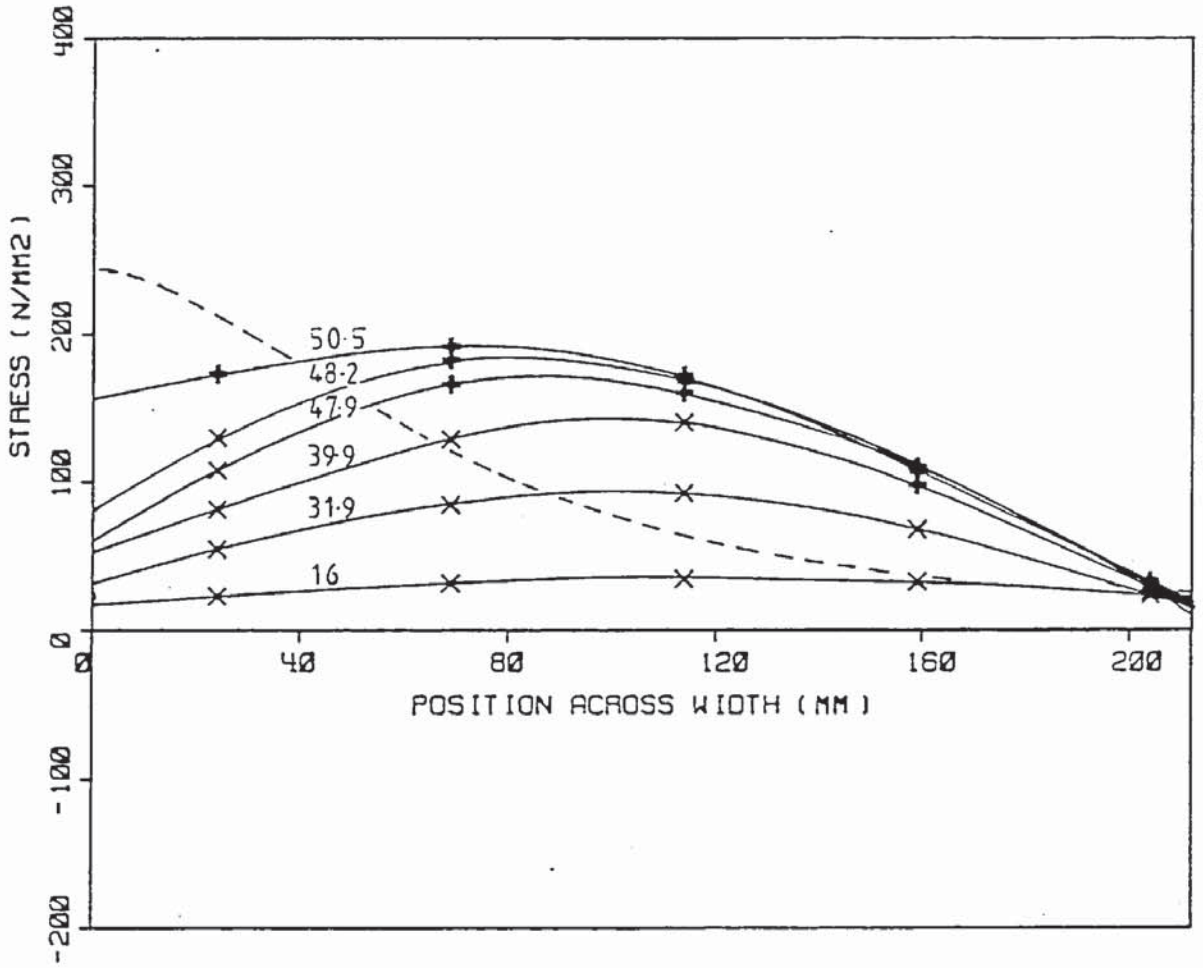

Figure 6.30 Build up of the average stress across the width of the gusset plate of specimen S13-110-1.

compressive yield stress. Eventually the specimen buckled with a sudden collapse at the ultimate load. The incompatible lateral deflections allowed most of the gusset plate to go into compressive yield. Comparison of the moments of resistance with the applied moments in Table 6.12 shows good agreement up to 97.9 kN, which corresponds to the last curve before yielding in Figure 6.28. Beyond this the applied moment has increased at a greater rate than the moment of resistance obtained from the stress distribution, which was based on the tensile yield stress being the maximum stress obtainable. However, the experimental results suggest a higher yield stress. The buckling stress distribution shows a lower stress than the yield stress and so its moment of resistance at 15.8 kNm is considerably lower than the experimental values.

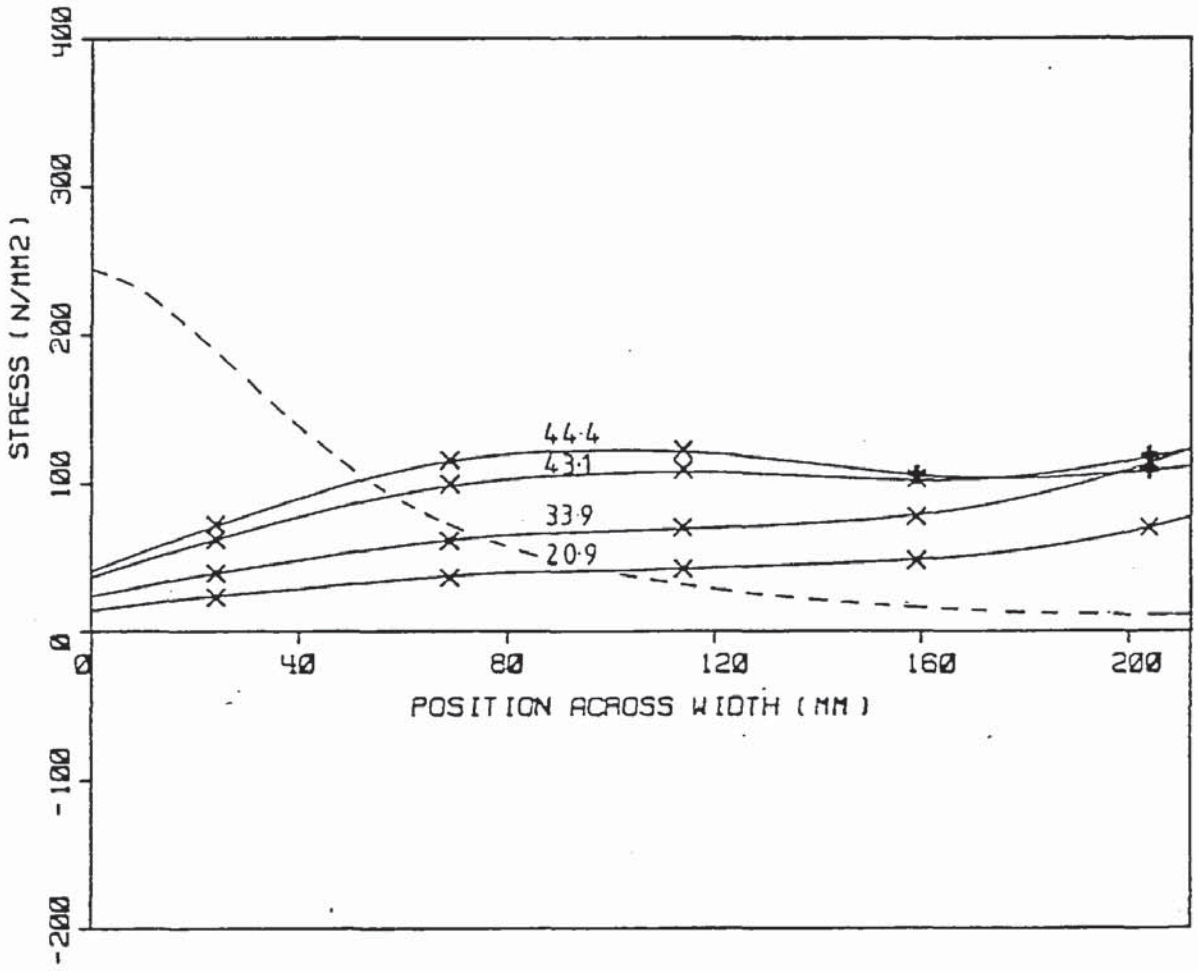

Figure 6.31 Build up of the average stress across the width of the gusset plate of specimen S13-130-1.

With the 70 and 110 degree gusset plates the stress distributions built up roughly parallel to the buckling stress distribution of the outer half of the gusset plate which buckled approximately at the same time. With the 110 degree gusset plate more stress was distributed to the outer free edge, and with the inner plate not so highly stressed it allowed the outer plate to sustain a greater stress than the buckling stress distribution indicates before it buckled.

In Tables 6.13 to 6.15 the applied moments and the moments of resistance of the stress distribution of specimens S13-70-1, S13-110-1 and S13-130-1 are shown to be in reasonable agreement. The moment of resistance obtained using the buckling stress distribution is slightly lower at 12.13 kNm than the experimental moments for specimen S13-70-1 and similar to the other two at 8.79 kNm.

SPECIMEN S13-70-1					
FROM APPLIED LOAD			FROM STRESS DISTRIBUTION		
Load P kN	Position s mm	Moment M=P.s kNm	Resultant force R' kN	Moment arm w mm	Resultant moment R'.w kNm
26.6	129	3.43	32.4	103	3.35
47.9	129	6.18	57.8	102	5.89
69.2	129	8.93	91.5	102	9.37
90.8#	129	11.71	132.3	101	13.39
106.4#	129	13.73	153.1	102	15.62
111.7#	129	14.41	157.6	98	15.52

Table 6.13 Comparison of applied moment with that obtained from the experimental stress distribution for S13-70-1.

SPECIMEN S13-110-1					
FROM APPLIED LOAD			FROM STRESS DISTRIBUTION		
Load P kN	Position s mm	Moment M=P.s kNm	Resultant force R' kN	Moment arm w mm	Resultant moment R'.w kNm
16.0	185	2.96	25.7	108	2.78
31.9	185	5.90	57.3	102	5.83
39.9#	185	7.38	84.7	100	8.47
45.2#	185	8.36	101.9	97	9.85
47.9#	185	8.86	110.9	93	10.35
50.5#	185	9.34	121.5	88	10.66

Table 6.14 Comparison of applied moment with that obtained from the experimental stress distribution for S13-110-1.

SPECIMEN S13-130-1					
FROM APPLIED LOAD			FROM STRESS DISTRIBUTION		
Load P kN	Position s mm	Moment M=P.s kNm	Resultant force R' kN	Moment arm w mm	Resultant moment R'.w kNm
20.9	251	5.25	35.1	125	4.40
33.9	251	8.51	58.0	125	7.27
43.1#	251	10.82	81.3	117	9.53
44.4#	251	11.14	88.4	113	9.95
45.7	251	11.47			

Table 6.15 Comparison of applied moment with that obtained from the experimental stress distribution for S13-130-1.

6.8 Unequal sided gusset plates with internal angles other than 90°

6.8.1 Post buckling compatibility

No experimental gusset plates were tested of this nature. However, from an understanding of the behaviour of gusset plates with the two variables independantly varied, a theoretical model is developed as follows.

With all the gusset plates tested there was a tendency for the inner gusset plate to buckle in the geometric compatible manner. That is, with the fold lines symmetrically about the angle bisector. This had the effect of the gusset plates tending to fail in as similar a manner as possible to a gusset plate having both fixed edges the same length. Therefore, when considering a gusset plate with an internal angle greater than 90 degrees with its fixed edges of different lengths, it is expected to buckle in a similar manner to a 90 degree gusset plate with its fixed edges the same length. It is also expected to buckle symmetrically about the angle bisector.

Assuming full length fixed ended struts running parallel to the free edge with their effective lengths based mathematically upon the plate width and internal angle, gives a good simulation for equal sided plates with varying internal angles, and a reasonable simulation for unequal sided, 90 degree plates. However, using this assumption with the unequal sided, varying angled plates does not give such a satisfactory model simulation, as shown in Figure 6.32. It is difficult to fit this model in with the fold line requirements. Figure 6.33 shows the same mathematical assumption modelled in a slightly different way, to fill the requirements of the gusset plates tending to buckle symmetrically and in a similar manner to an equal sided 90 degree gusset plate. This is an extension of the model expressed in Figures 6.24 and 6.27 for the other types of plate. This model appears to comply better with the fold line requirements, and the position of the fold lines can be estimated more easily, as

before, based on those for equal sided gusset plates.

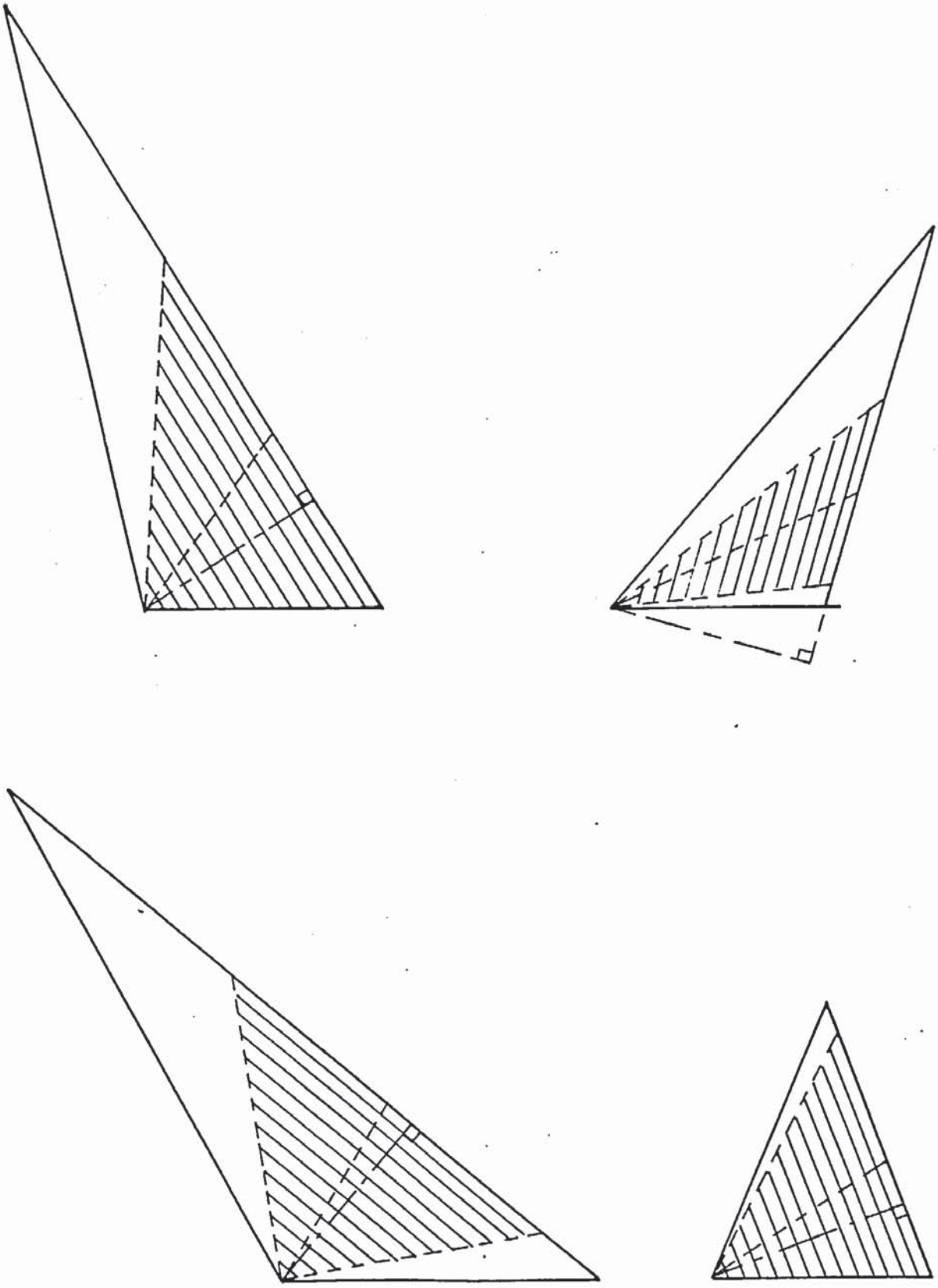

Figure 6.32 Strip model for unequal sided varying angled gusset plates assuming fixed ended struts running parallel to free edge.

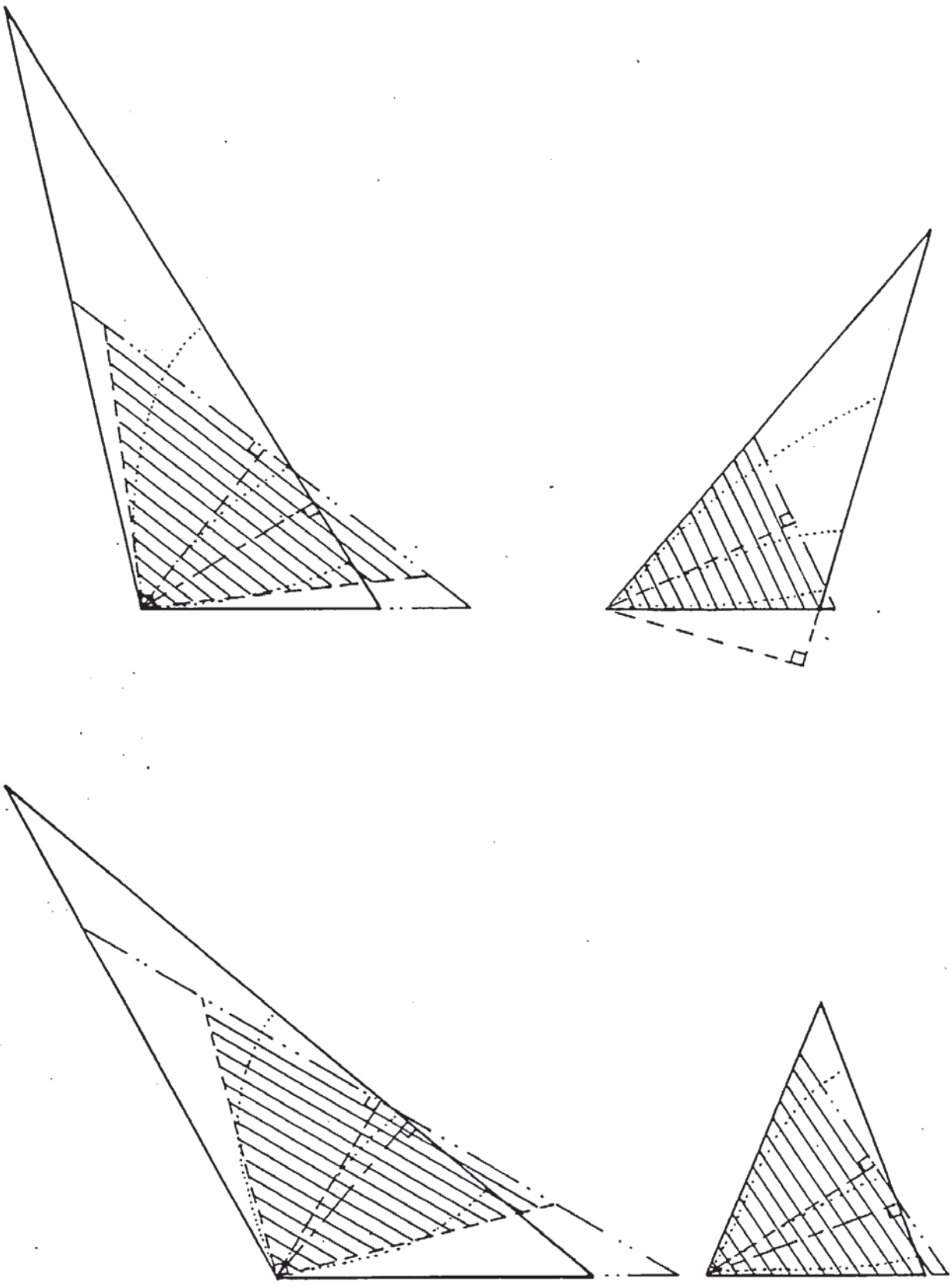

Figure 6.33 Strip model for unequal sided varying angled gusset plates assuming fixed ended struts of an equivalent equal sided gusset plate.

6.9 Gusset plates with the internal angle removed parallel to the free edge

6.9.1 Post buckling compatibility

So far only complete gusset plates are considered, however, incomplete gusset plates are sometimes used in various situations in practice. In developing the mode of failure of the equal sided 90 degree gusset plates, reference is made to gusset plates with varying amounts of the inside corner removed. With only small amounts removed, the behaviour is similar to a complete gusset plate. With large amounts removed, the gusset plates were gradually reduced to just strips of plate spanning between the loaded and supported plates. Also a series of tests were performed on different lengths of strips of plate inclined at 45 degrees. These narrow strips of plate behaved in a similar manner to fixed ended struts equal to approximately their centre line lengths. That is, their effective length was equal to half their centre line length, the same as the equivalent strip of plate in an equal sided gusset plate. Therefore, for an equal sided gusset plate the load capacity of a strip of gusset plate can be calculated irrespective of its size, by deducting the load capacity of the gusset plate that is removed from the load capacity of a complete gusset plate.

A similar narrow strip of plate inclined at an angle other than 45 degrees, also behaves in a similar manner to a fixed ended strut with its effective length equal to approximately half its centre line length. The equivalent strip of plate in a gusset plate with its free edge inclined at the same angle carries a higher load, because it has an effective length less than $\frac{1}{2}$ its centre line length, as previously discussed. Therefore the method discussed for the equal sided gusset plate cannot be used for unequal sided gusset plates with the inside corner removed parallel to the free edge. The error will be greater the greater the amount of gusset plate removed. A gusset plate with a

small amount removed behaves very much like a complete gusset plate, whereas a gusset plate that has had so much removed that there is only a narrow strip of plate left, behaves as though it is a strut. Therefore, the effective lengths of the struts in the model have to change from the shorter lengths calculated for a complete gusset plate to the longer length calculated for a strut. The controlling factor is the proportion of the original gusset plate that is left or more conveniently, that which is removed.

As the calculation of the effective lengths is based on the plate width, it is convenient to use the ratio of the amount of plate width removed C to the original width W. For a complete gusset plate this ratio is 0 and for the absolute limit of an infinitesimally wide strip of plate, this ratio is 1. Therefore, it is convenient to relate the effective lengths calculated for each strip to this ratio such that when a complete plate is used then the effective lengths are calculated based upon that for a complete gusset plate, and when an infinitesimally wide strip of plate is used, then the effective lengths are calculated based upon the full centre line length of each strut. Further, for mathematical convenience it is assumd that the relationship is linear between these two extremes. Calculation of the load capacity of a particular remaining strip of gusset plate then involves the calculation of the load capacity of the gusset plate removed, using the appropriate ratio, and then deducting it from the load capacity calculated for the complete gusset plate, again using the appropriate ratio.

6.10 Mathematical Model

Having developed the theoretical model it now requires expressing mathematically.

6.10.1 Complete gusset plates

Consider the general complete gusset plate as shown in Figure

6.34. Basically the mathematical model converts the gusset plate into

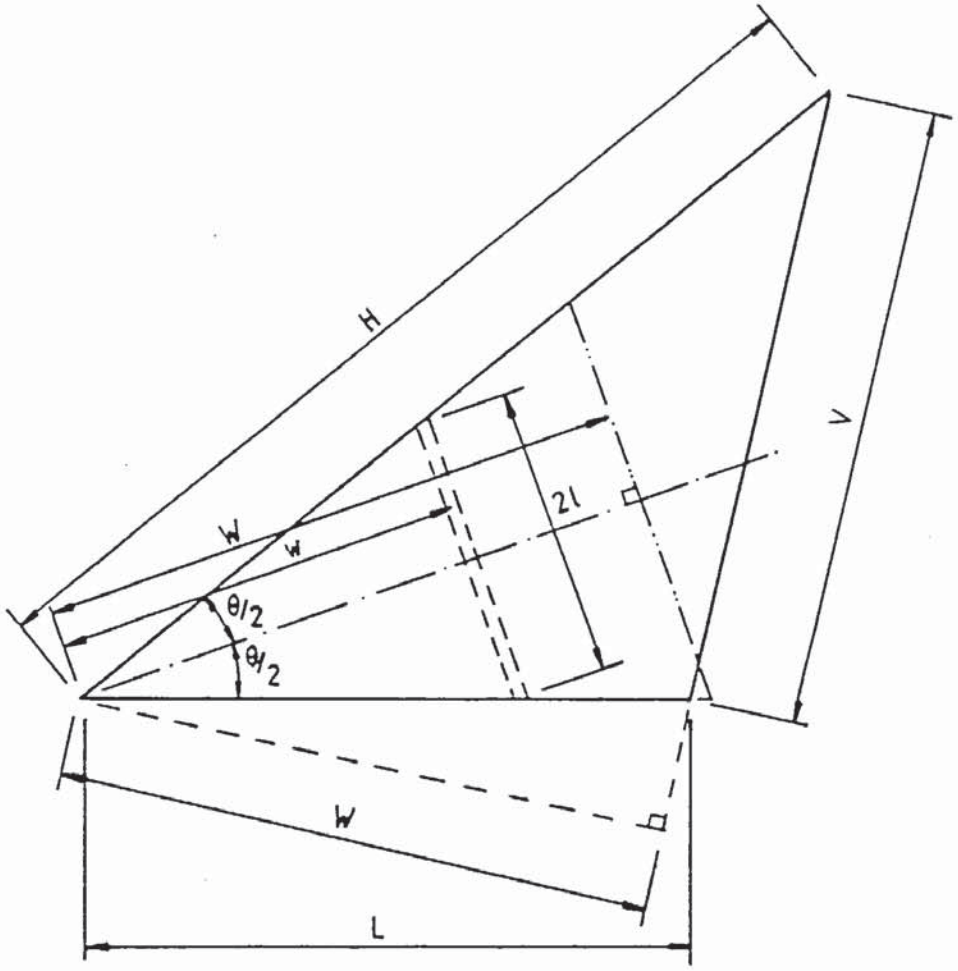

(a) internal angle $\theta < 90^{\circ}$

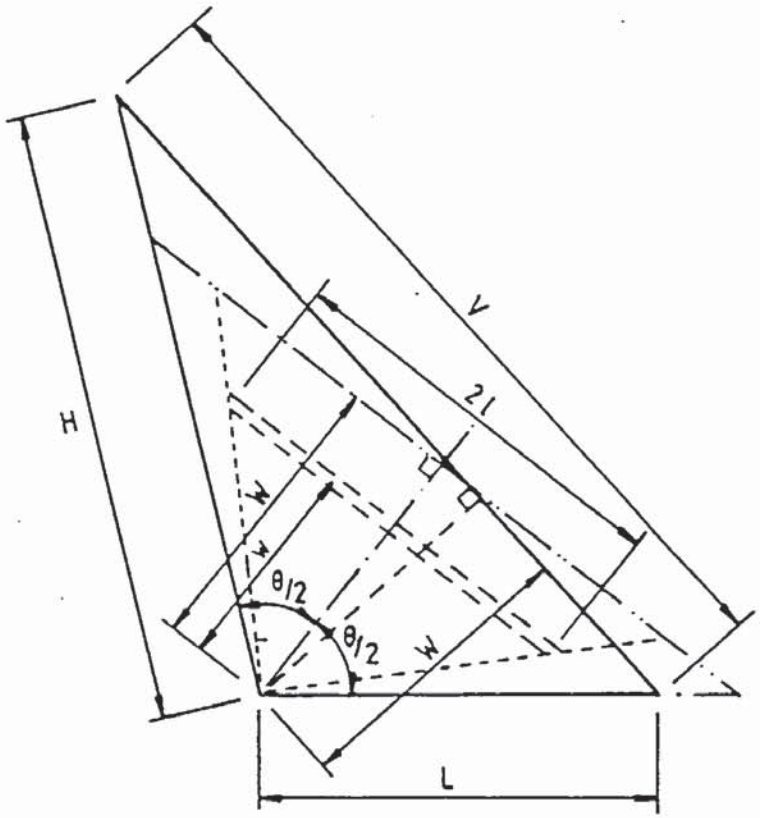

(b) internal angle $\theta > 90^{\circ}$

Figure 6.34 Mathematical model of a complete gusset plate.

an equal sided gusset plate having the same width and internal angle up to a maximum of 90 degrees. The moment of resistance is then calculated for this gusset plate based upon assuming it consists of a series of full length fixed ended struts running parallel to its free edge. Therefore, the effective length of any given elemental strut is given by

$$l_w = w.\tan\ \theta/2, \text{ where } \theta \not> 90^\circ \qquad (6.5)$$

where w varies from θ to W.

Special case when $\theta = 90^\circ$, Equation 6.5 gives

$$l_w = w$$

this is the value used by Martin (15).

Also where $\theta > 90^\circ$ as in Figure 6.34(b), Equation 6.5 gives

$$l_w = w$$

6.10.2 Incomplete gusset plates

Now consider the incomplete gusset plate taken almost to the extreme with only a thin strip remaining. Figures 6.35(a) and (b) show such plates correspond to the full plates as shown in Figures 6.34 (a) and (b) respectively. The fixed ended strut length used for the outermost elemental strut, in such a narrow remaining strip of gusset plate approaches the free edge length as C tends towards W, and each corresponding elemental strut approaches v where

$$v = w.V/W \qquad (6.6)$$

Therefore, the effective lengths of an elemental strut, at the two limits are:

for a complete plate C/W = 0

$$l_w = zw\tan\theta/2 = w.\tan\ \theta/2, \quad \theta \not> 90^\circ$$

therefore z = 1

and for a strip of plate C/W = 1

$$l_w = z.w.\tan\theta/2 = v/2 = w.V/2W\ , \ \theta \not> 90^\circ$$

therefore $z = V/(2W.\tan\theta/2)$

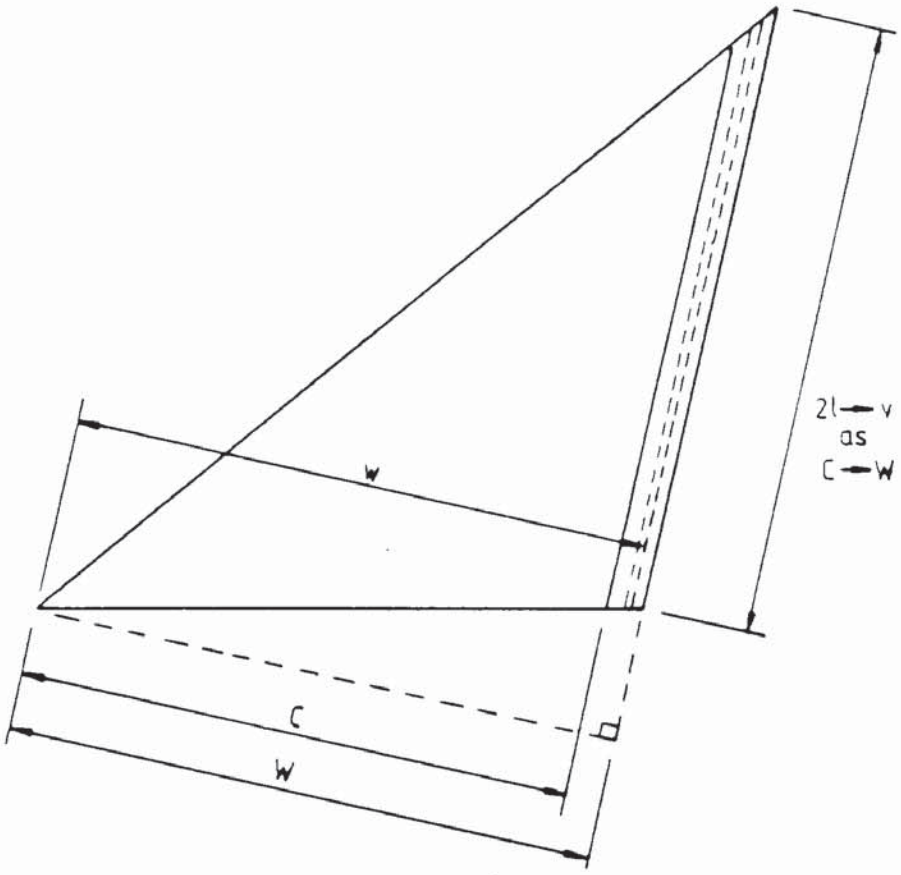

(a) internal angle $\theta < 90^{\circ}$

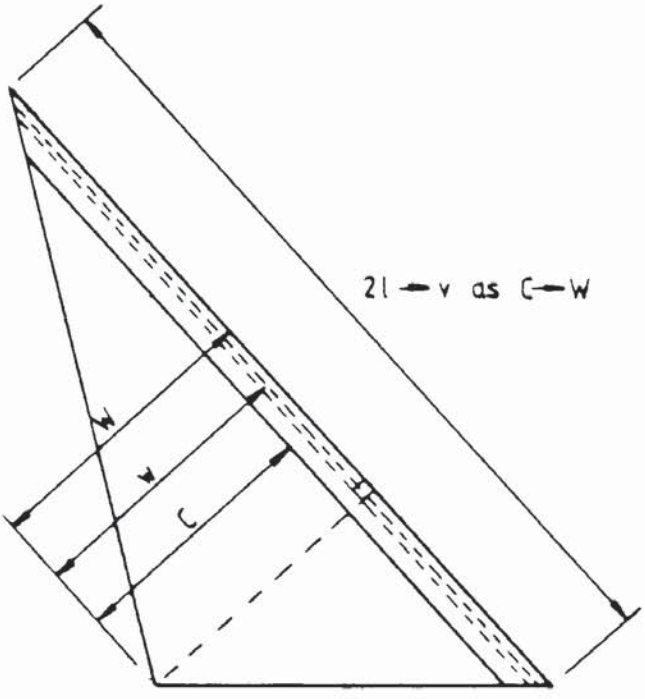

(b) internal angle $\theta > 90^{\circ}$

Figure 6.35 Mathematical model of an incomplete gusset plate.

Assuming a linear relationship i.e. $y = m.x + c$

$$z = [V/(2.W.\tan\theta/2) - 1]C/W + 1$$

Therefore the general expression for the effective length of all gusset plates becomes

$$l_w = \{[V/(2.W.\tan\theta/2) - 1]C/W + 1\}w.\tan\theta/2 \quad , \quad \text{where } \theta \geq 90^\circ \qquad (6.7)$$

where $V = \sqrt{L^2 + H^2 - 2.L.H.\cos\theta}$

and $W = (L.H.\sin\theta)/V$

Note the $\theta \geq 90^\circ$ does not apply to the calculation of V and W.

6.10.3 Buckling stress formula used in the mathematical model

Now that the effective lengths for the elemental struts used in the mathematical model are established, the next step is to determine which buckling stress equation to use. Martin chose the empirical Rankine buckling equation because of the ease by which it is integrated. Derivation of this equation is based upon the elastic Euler buckling stress and the yield stress as follows.

6.10.3.1 Rankine-Gordon buckling stress formula

The theoretical elastic critical stress of an axially loaded straight strut is referred to as the Euler buckling stress f_e curve ABC Figure 6.36, and is related to the slenderness ration l/r by

$$f_e = \pi^2 E/(l/r)^2 \qquad (6.8)$$

where f_e is the elastic critical stress, E is Youngs modulus, l is the effective length and r is the radius of gyration. The strut cannot theoretically sustain a mean stress greater than the yield stress f_y. The line DB, Figure 6.36, therefore, represents an absolute upper limit to the load-carrying capacity of the strut.

Tests on real struts show that the ultimate stress lies somewhat below the composite curve DBC in the region of B, the corner at B is rounded off. A rough estimate of the ultimate stress may be obtained from the interaction formula

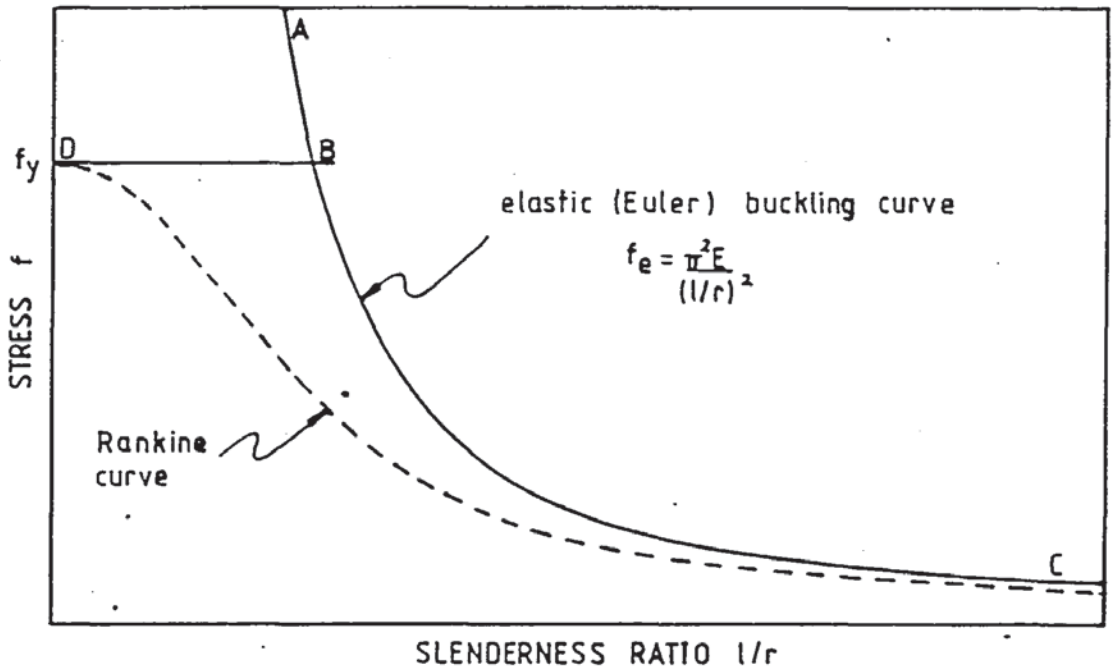

Figure 6.36 Theoretical buckling stress curves.

$$\frac{1}{f_b} = \frac{1}{f_e} + \frac{1}{f_y} \qquad (6.9)$$

This provides an arbitrary transition curve between the two extreme cases. If Equation 6.8 is used to eliminate f_e from Equation 6.9 the latter can be written as

$$f_b = f_y/(1 + k(l/r)^2) \qquad (6.10)$$

where $k = f_y/(\pi^2.E)$

This relationship between f_b and l/r appears as the broken line in Figure 6.36 and is the Rankine formula. It has been customary to alter the value of k in Equation 6.10, and even the value of f_y, in order to adjust the position of the curve to match the results of tests. Martin(15) chose not to alter these values and from the comparison of his method with the experimental results, it gives reasonable results where applicable.

6.10.3.2 Perry-Robertson buckling stress formula

Martin(15) also used a linear approximation to the Rankine formula, which also gave reasonable results, within its limits of use. However, to put the method into context with other buckling problems, and make it more acceptable, the method is developed using the Perry-

Robertson buckling equation which is presently in use and accepted in this country. In a similar way other buckling equations used in other parts of the world can be adapted to suit the requirements of other buckling codes.

The Perry-Roberston formula is obtained by considering the initial bow or crookedness of a strut. It can be shown that if an unloaded elastic pin-ended strut has the initial deflected shape

$$z_o = a_1 \sin(\pi . x/l) \tag{6.11}$$

then the transverse displacement of the loaded strut is

$$z = \bar{a}_1 \sin(\pi . x/l) \tag{6.12}$$

where $\bar{a}_1 = a_1/(1 - (P/P_E))$

(z and z_o are measured from the load axis)

The bending moment at the midpoint of the loaded strut is $P.\bar{a}$, and the maximum stress in the strut is the sum of the axial and bending stresses

$$f_{max} = P/A + P.\bar{a}_1.h/I \tag{6.13}$$

where h is the distance from the centroid of the section to the extreme fibre on the concave side. Equation 6.13 can be simplified by writing $I = Ar^2$

$$f_{max} = f_b[1 + \eta/(1 - f/f_e)] \tag{6.14}$$

where $\eta = a_1.h/r^2 = \text{constant}$

As the mean stress f_b is increased, the maximum stress increases at a progressively greater rate until, eventually, it reaches the yield stress. If the mean stress is increased still further, a plastic zone forms on the concave side of the strut, the stiffness of the strut deteriorates and collapse follows. The load at which f_{max} reached f_y may therefore be taken as a lower bound to the collapse load. If f_{max} is replaced by f_y in Equation 6.14, the result is a quadratic equation to be solved for the unknown mean stress f_b. The solution is

$$f_b = f_2 - \sqrt{[f_2^2 - f_y f_e]} \tag{6.15}$$

where $f_2 = [f_y + (\eta + 1)f_e]/2$

Equation 6.15 was derived by Perry and defines the mean stress f_b, at which yielding begins, in terms of the slenderness ratio l/r. (f_y is a property of the material, η can be determined in principle from measurements of real struts, and f_e is a function of l/r).

If it is assumed that the initial lack of straightness a_1 is proportional to the length of the strut, then $a_1 = k_1 l$ and $h = k_2 r$, where k_1 and k_2 are constants. Hence

$$\eta = a_1 h/r^2 = k_1 k_2 l/r = \text{constant} \times (l/r)$$

Robertson suggested that $\eta = 0.001(l/r)$ corresponds to the average of points obtained from tests, while that $\eta = 0.003(l/r)$ gives a lower bound to test results. The value $\eta = 0.003(l/r)$ was used in BS 449(1) until 1969, when it was replaced by an expression proposed by Godfrey.(1) The expression is

$$\eta = 0.3(l/r)^2 \times 10^{-4} \qquad (6.16)$$

The new British draft Steel code (2) now suggests

$$\eta = 0.001a(\lambda - \lambda_o), \quad \text{but} \not< 0 \qquad (6.17)$$

which is referred to as the Perry factor, where a is the Robertson constant, which is obtained from a table relating it to various sections, λ is the slenderness ratio (l/r), and λ_o is the limiting slenderness given by

$$\lambda_o = 0.2\sqrt{\pi^2 E/f_y} \qquad (6.18)$$

By altering the assumptions made about the nature of the coefficient η, the shape and position of the curve can be adjusted to obtain the best agreement with experimental results. The Perry-Robertson formula, Equation 6.15, is therefore regarded as an empirical formula despite the logic by which it was derived.

6.10.4 Development of the mathematical model using the Perry-Robertson strut formula

Using the effective lengths selected and the latest version of the Perry-Robertson strut formula as given in the British draft steel

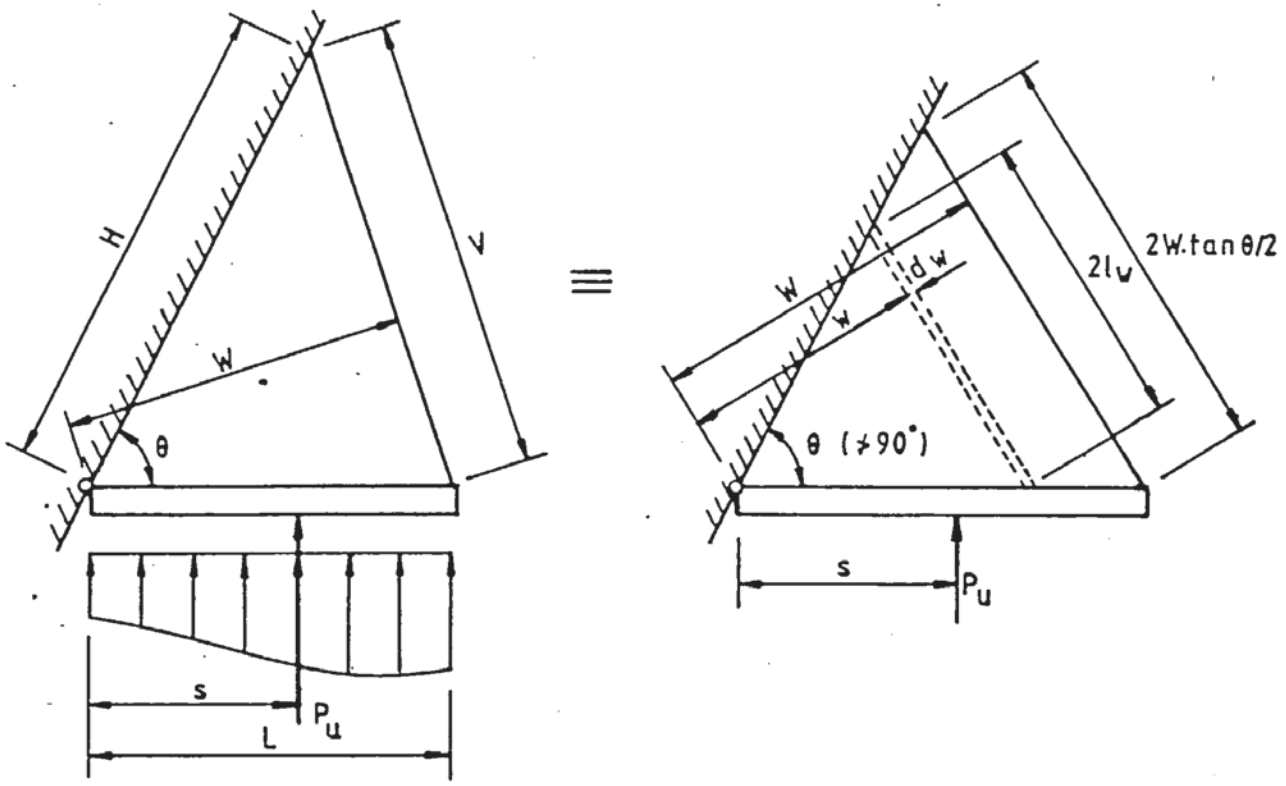

(a) general gusset plate (b) theoretical model

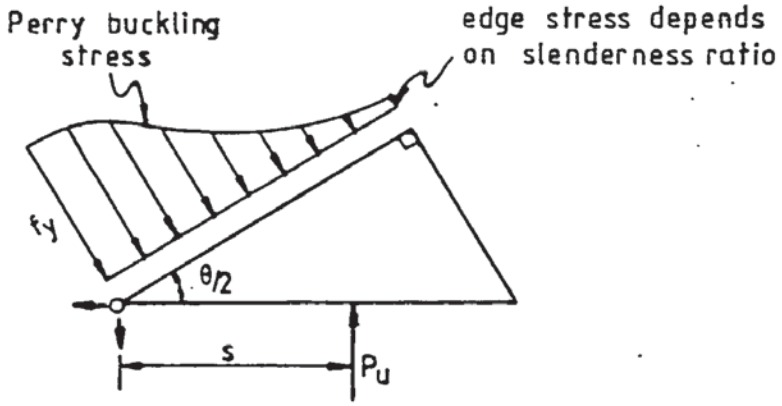

(c) theoretical loading

Figure 6.37 General theoretical model of a complete gusset plate.

code B20 (1977) (2) the model is as shown in Figure 6.37. Taking moments about the inside corner of the model gusset plate shown in Figure 6.37(b) gives

$$P_u s = \int_o^W f_{bw} t.w:dw \qquad (6.19)$$

where f_{bw} is the buckling stress of the elemental strut of width d_w at a distance w from the inside corner of the gusset plate of width W. As the Perry-Robertson equation is used, f_w is given by Equation 6.15

with the new value of η Equation 6.17 giving

$$f_{bw} = f_{2w} - \sqrt{[f_{2w}^2 - f_y f_{ew}]} \qquad (6.20)$$

where $f_{2w} = [f_y + (\eta_w + 1)f_{ew}]$

$f_{ew} = \pi^2 E/(l_w/r)^2$

$\eta_w = 0.001a(\lambda_w - \lambda_o)$, but $\neq \theta$

$\lambda_w = l_w/r$

$\lambda_o = 0.2\sqrt{\pi^2 E/f_y}$

Combining Equations 6.19 and 6.20 gives

$$P_u s = t\int_o^W \{f_{2w} - \sqrt{[f_{2w}^2 - f_y f_{ew}]}\} w\,dw \qquad (6.21)$$

For complete gusset plates the effective length l_w of the elemental strut at a distance w from the internal corner is given by Equation 6.15 which is reproduced below.

$$l_w = w.\tan\theta/2 \ , \quad \text{where} \quad \theta \neq 90^o$$

Unlike the Rankine strut formula, the Perry-Robertson strut formula, Equation 6.20 is not easily integrated and so a numerical solution is as follows.

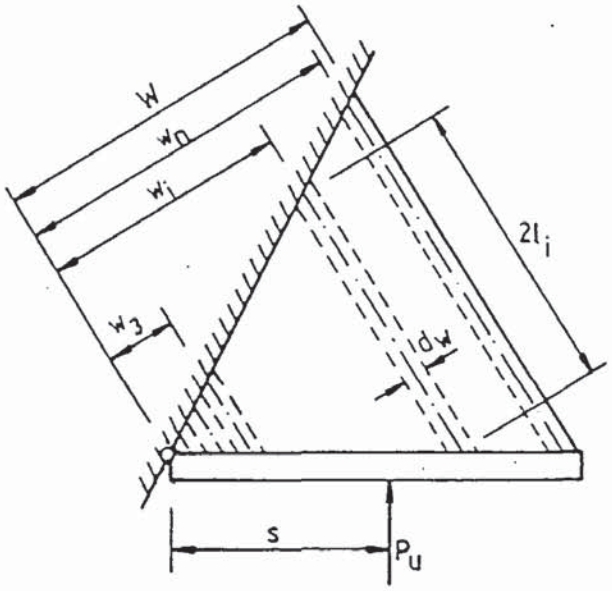

Figure 6.38 Numerical version of theoretical model.

The moment of resistance M_{ui} produced by strip i at failure, as shown in Figure 6.38, is

$$M_{ui} = f_{bi} t . w_i dw \qquad (6.22)$$

where f_{bi} = Perry buckling stress for strip i

$$= f_{2i} - \sqrt{[f_{2i}^2 - f_y f_{ei}]} \qquad (6.23a)$$

f_{ei} = Euler buckling stress for strip i

$$= \pi^2 E/(l_i/r)^2 = \pi^2 E.t^2/(12.l_i^2) \qquad (6.23b)$$

f_y = yield stress

$$= [f_y + (\eta_i + 1)f_{ei}]/2 \qquad (6.23c)$$

η_i = Perry factor for strip i

$$= 0.001a(\lambda_i - \lambda_o) \text{ , but } \neq 0 \qquad (6.23d)$$

a = Robertson constant

λ_i = slenderness of strip i

$$= l_i/r = l_i\sqrt{12}/t \qquad (6.23e)$$

λ_o = limiting slenderness

$$= 0.2\sqrt{[\pi^2 E/f_y]} \qquad (6.23f)$$

l_i = effective length of strip i

w_i = moment arm distance of strip i

Now

w_i for 1st strip, $w_1 = dw/2$

w_i for 2nd strip, $w_2 = dw/2 + dw$

w_i for 3rd strip, $w_3 = dw/2 + dw + dw = dw(1/2 + 2)$

w_i for ith strip, $w_i = dw(1/2 + (i - 1))$

Therefore

$$w_i = dw(1/2 + (i - 1)) \qquad (6.24)$$

Also from Equation 6.10, the effective length of strip i is

$$l_i = w_i \tan\theta/2 \text{ , where } \theta \neq 90^o \qquad (6.25)$$

If there are n strips and W is the total width of all strips then

$$dw = W/n \qquad (6.26)$$

Therefore the total ultimate moment produced by n strips is given by

$$M_u = \sum_{i=1}^{n} M_{ui} = \sum_{i=1}^{n} f_{bi} t . w_i dw \qquad (6.27)$$

If this is equated to the externally applied moment then

$$P_{us} = \sum_{i=1}^{n} f_{bi}t.w_i dw \qquad (6.28)$$

Which is Equation 6.19 expressed as a numerical summation instead of an integration.

For the model to be used with gusset plates with varying amounts of the internal corner removed then the more generalised equation for calculating the effective lengths, Equation 6.7, can be used instead of Equation 6.5. Therefore,

$$l_i = \{[V/(2.W.\tan\theta/2) - 1]c/w + 1\}w_i\tan\theta/2 \qquad (6.29)$$

where $\theta \not> 90^{\circ}$.

also Equation 6.24 becomes

$$w_i = C + dw(1/2 + (i - 1)) \qquad (6.30)$$

and Equation 6.26 becomes

$$dw = (W - C)/n \qquad (6.31)$$

6.11 Comparison of mathematical model with experimental results

In the following, the mathematical model, (Equation 6.28), using the Perry buckling stress equation, (Equation 6.2), for the stress distribution and the generalised equation, (Equation 6.29), for the effective lengths, are compared with the experimental ultimate load results in a similar manner as with the other theories presented in Chapter 5.

6.11.1 Choice of Robertson constant

In using the Perry buckling equation, as presented in Section 6.10.3.2, by altering the assumptions made about the nature of the Perry factor η, the shape and position of the buckling stress curve can be adjusted to obtain the best agreement with experimental results. The Perry factor used in the mathematical model is that which is recommended in the British draft steel code of practice, (Equation 6.17). This equation has another factor, a, which is referred to as the Robertson constant and is obtained from a table in

the code relating it to various sections. The greater the value of the Robertson constant, the more conservative the buckling stress is. The largest value used is a=8 The nearest category in which the gusset plates may be placed would be for welded plate I or H-section up to 40mm thick which gives a value of a=3.5 for the x-x axis and a=5.5 for the y-y axis. A value of a=0 corresponds to the upper limit and gives the combined Euler and yield stress curves. The experimental buckling stresses obtained from the strut tests, were very close to the Perry curve with a=1. Therefore, in the comparison with the experimental results, the two extreme values of the Robertson constant are used, with a=1 corresponding to an upper bound and a=8 corresponding to a lower bound.

6.11.2 Number of strips used

As a numerical solution is given using the Perry buckling stress equation it requires the plate to be considered as a finite number of strips. The number of strips required to produce an accurate solution depends mainly on how quickly the slenderness changes across the width of the gusset plate. Therefore, it is not possible to choose a specific gusset plate to determine the number of strips. As it is considered impractical to relate the number of strips to the change in slenderness across the gusset plate, theoretical curves are calculated using different numbers of strips for both values of a and all the experimental series. It is found that the accuracy of the solution increases very quickly as the number of strips are increased. The use of one strip is noticeably inaccurate. The use of two strips is reasonably close with all except the series investigating the gusset plate size. The use of three strips is slightly inaccurate with the series investigating the gusset plate size and the series investigating the gusset plate height. With the other series and other number of strips, the results are very close to the solution.

Convergence is found with ten strips for all but the series investigating the gusset plate size, which is found to have converged with 15 strips. However, a reasonably accurate solution can be obtained with as few as four strips. In the following examples 15 strips are used, which is taken to give an accurate solution for all gusset plates.

6.11.3 Comparison of ultimate loads

In Figures 6.39 to 6.47 the ultimate loads calculated using the Perry buckling stress equation in the mathematical model using 15 strips and for a=1 and 8 are plotted with the experimental ultimate load results obtained for each of the main gusset plate series.

With the variation in the gusset plate size, Figure 6.39, the two theoretical curves are in reasonable agreement with the experimental results which lie between the two curves. The theoretical and experimental peaks coincide at L=H=200mm.

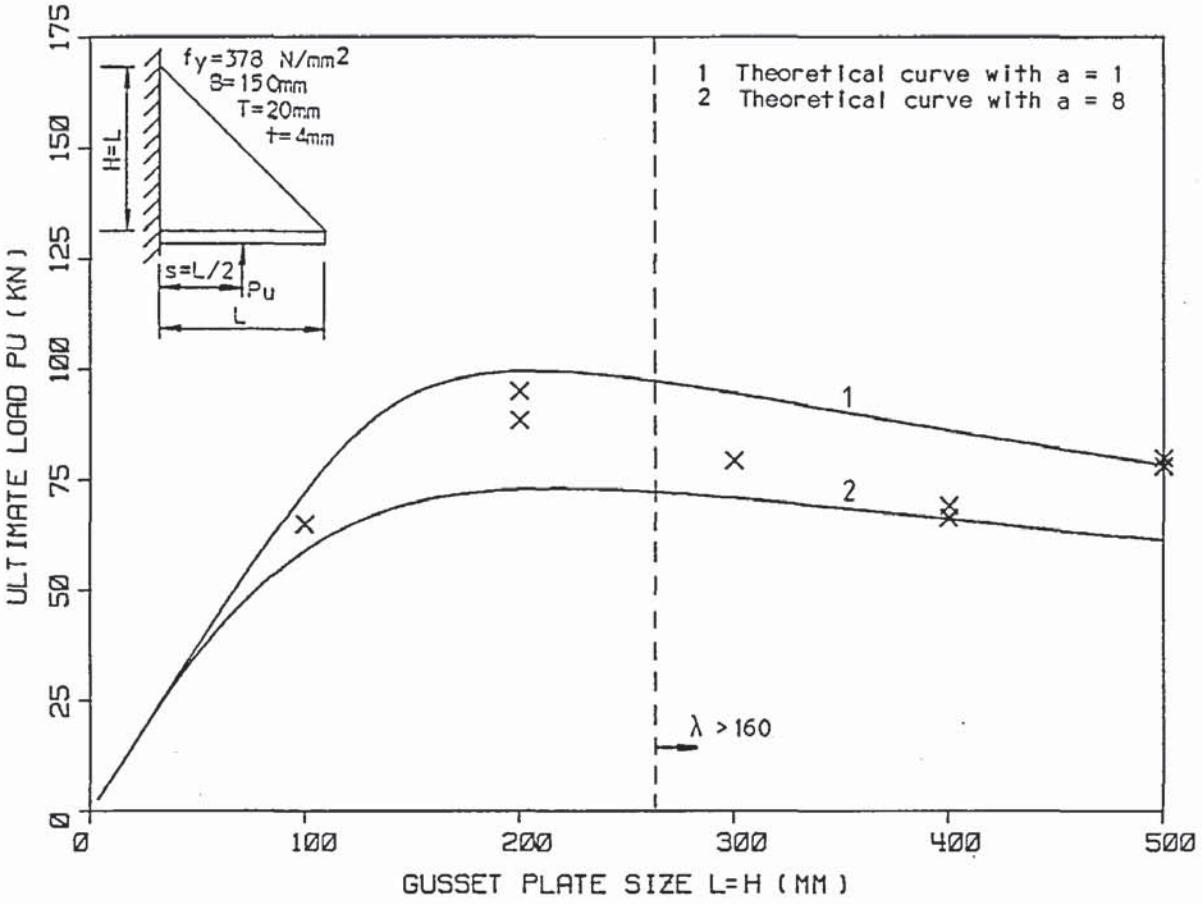

Figure 6.39 Comparison of theoretical with experimental ultimate loads for series 3.

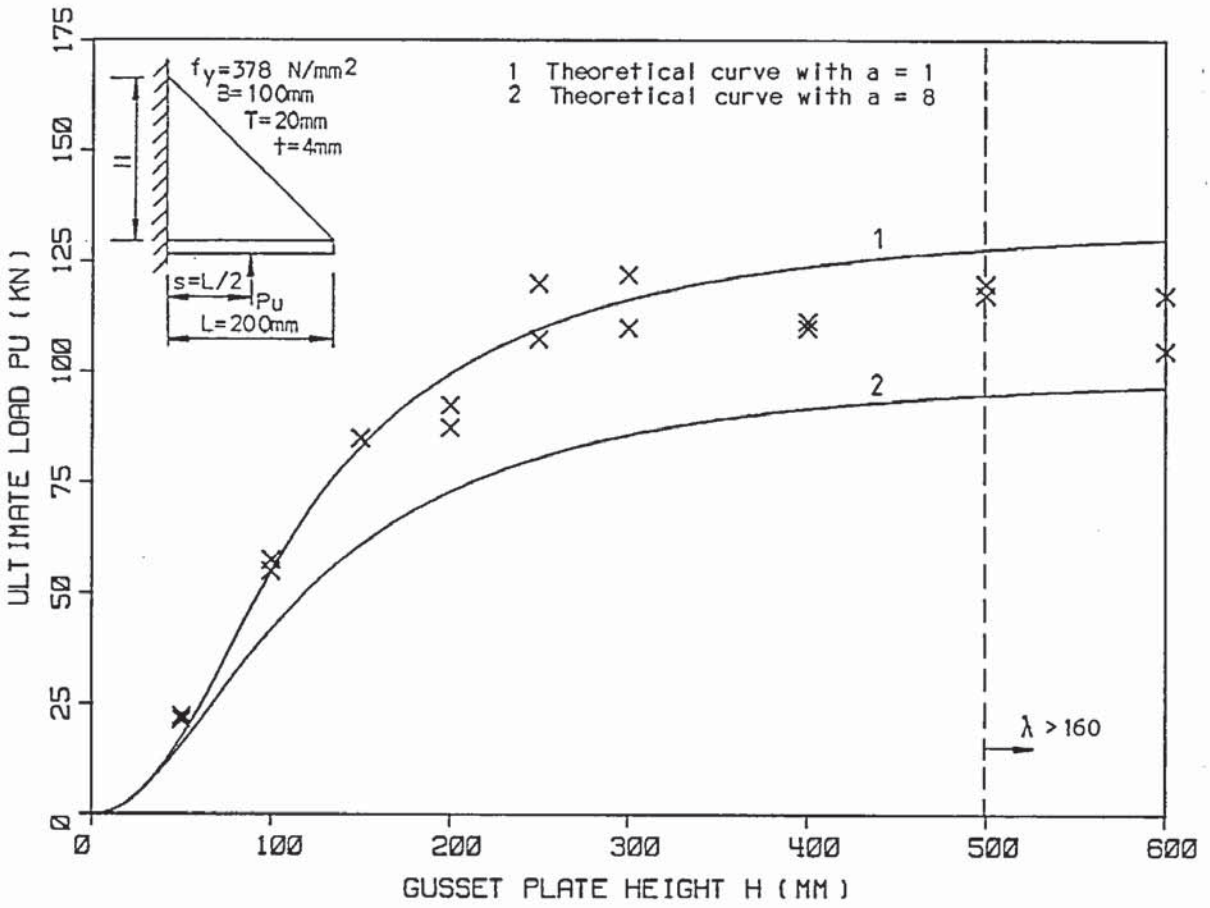

Figure 6.40 Comparison of theoretical with experimental ultimate loads for series 4.

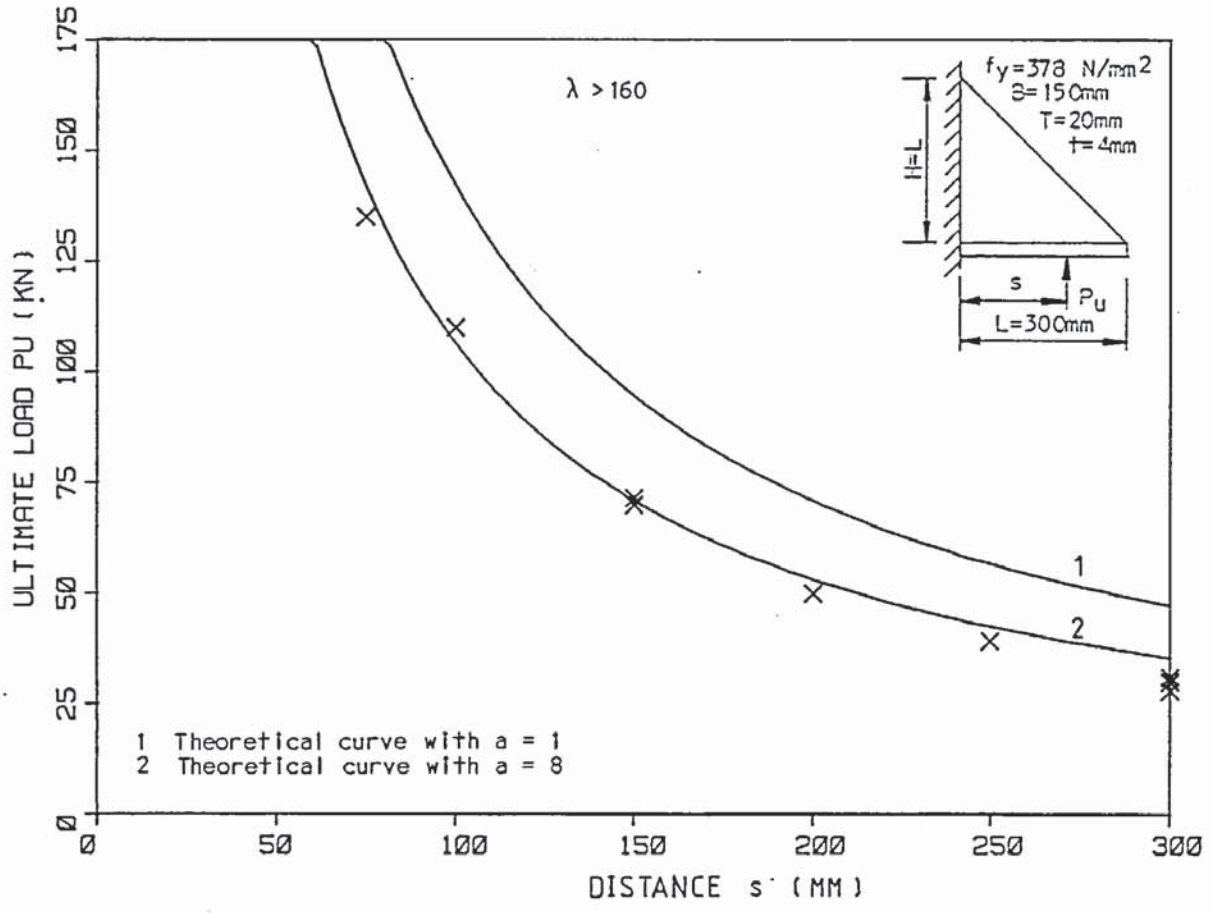

Figure 6.41 Comparison of theoretical with experimental ultimate loads for series 5.

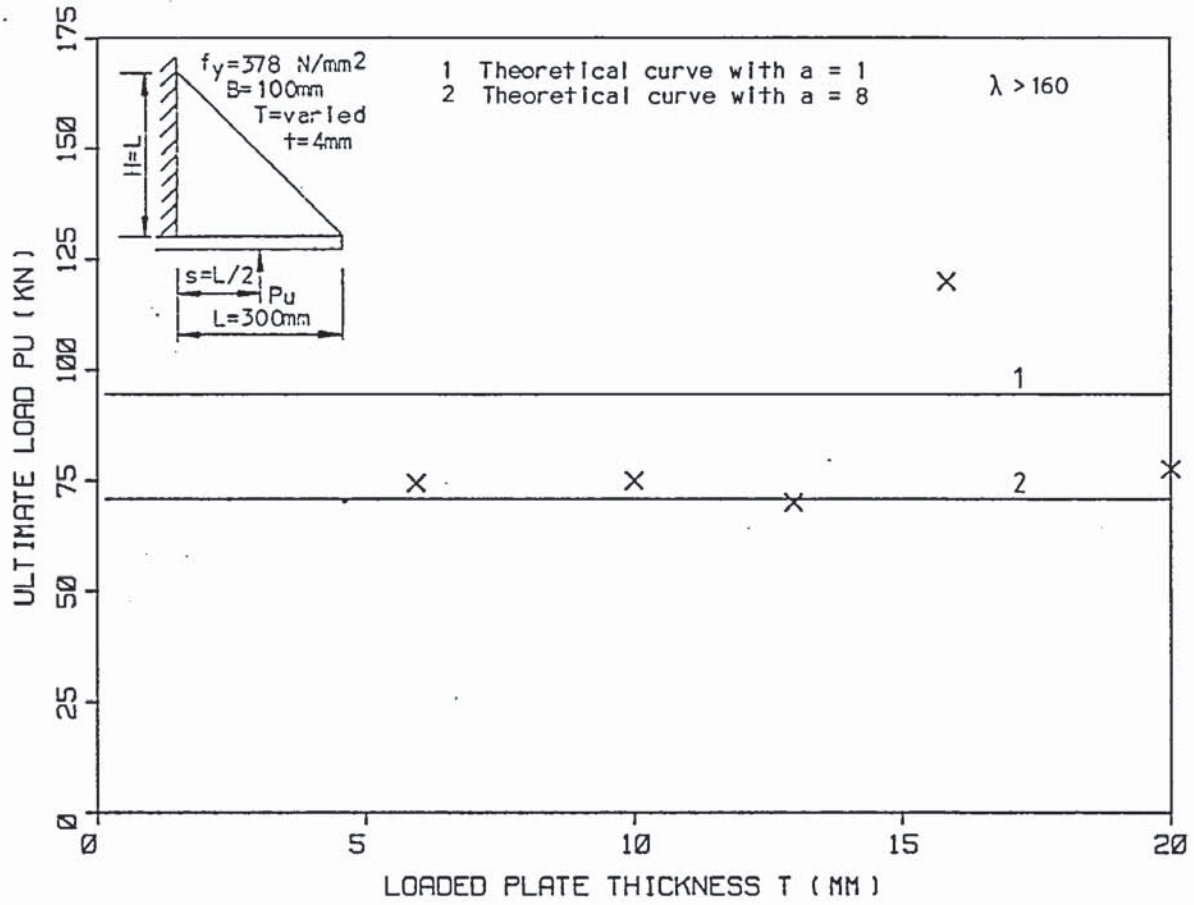

Figure 6.42 Comparison of theoretical with experimental ultimate loads for series 7, (s = L/2).

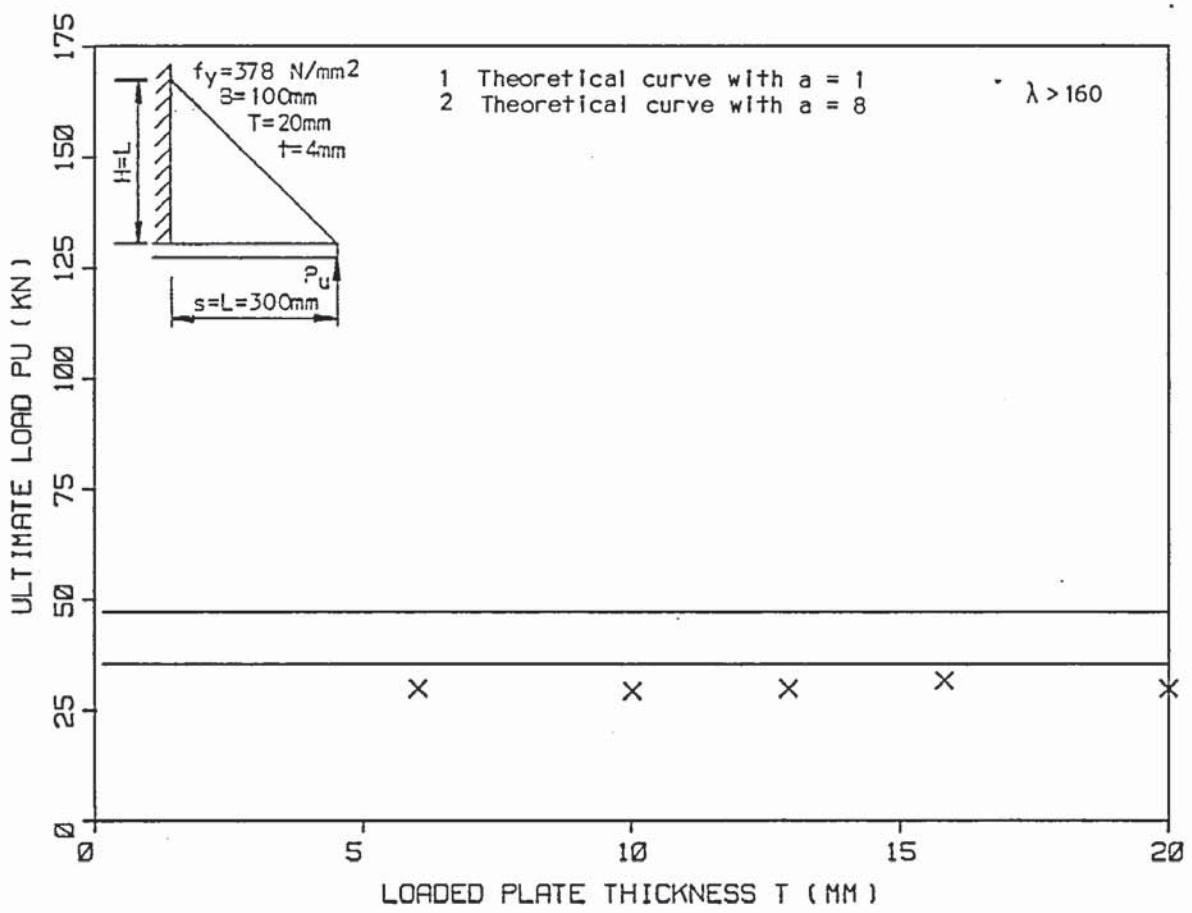

Figure 6.43 Comparison of theoretical with experimental ultimate loads for series 7, (s = L).

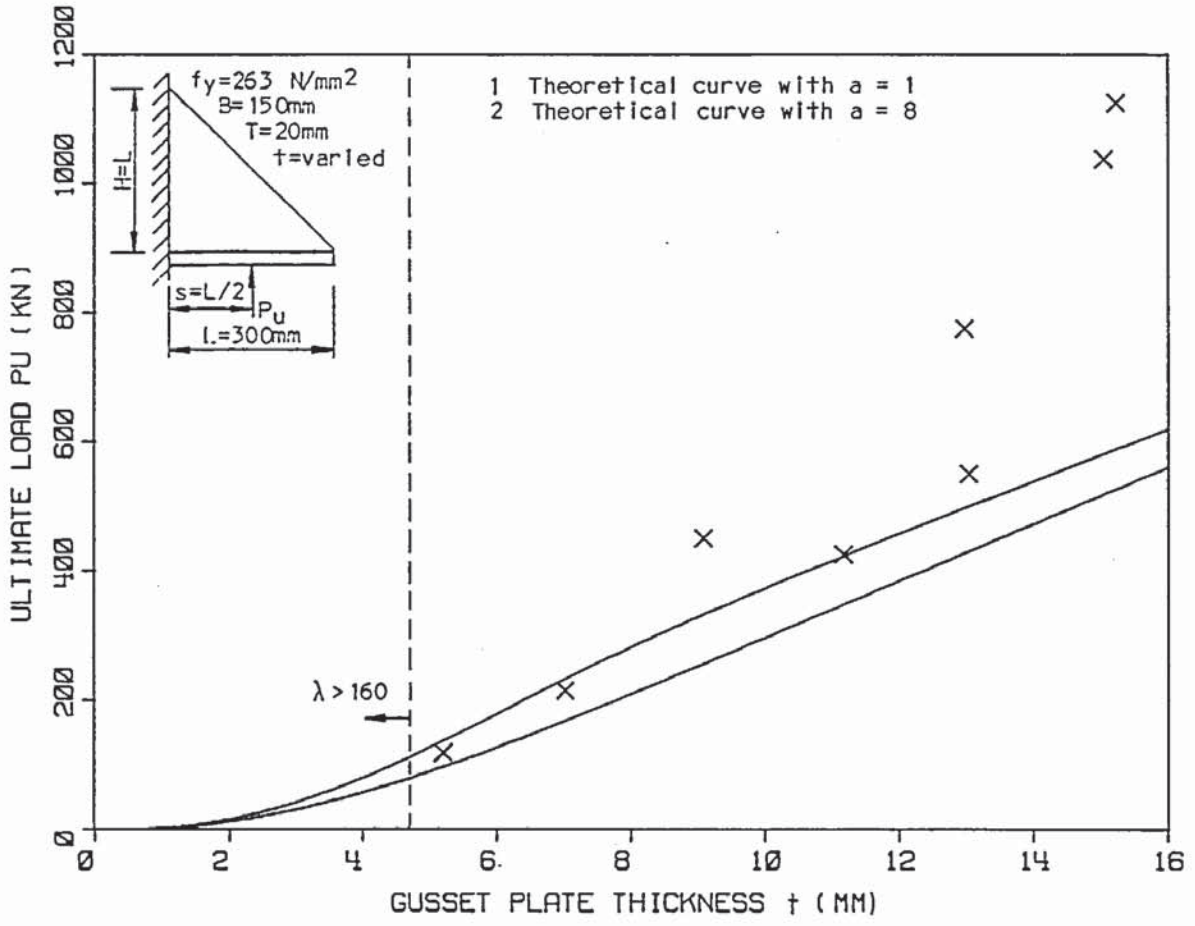

Figure 6.44 Comparison of theoretical with experimental ultimate loads for series 12.

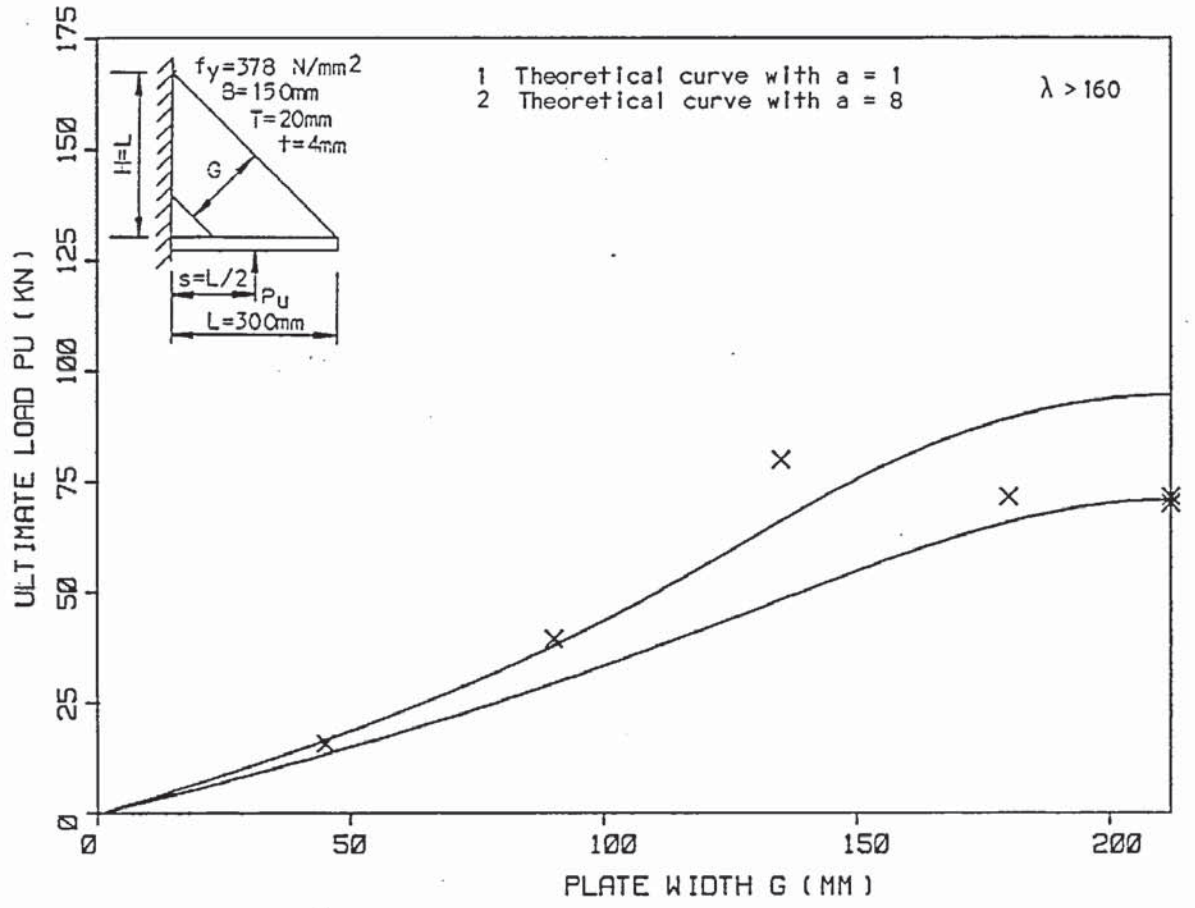

Figure 6.45 Comparison of theoretical with experimental ultimate loads for series 8, (s = L/2).

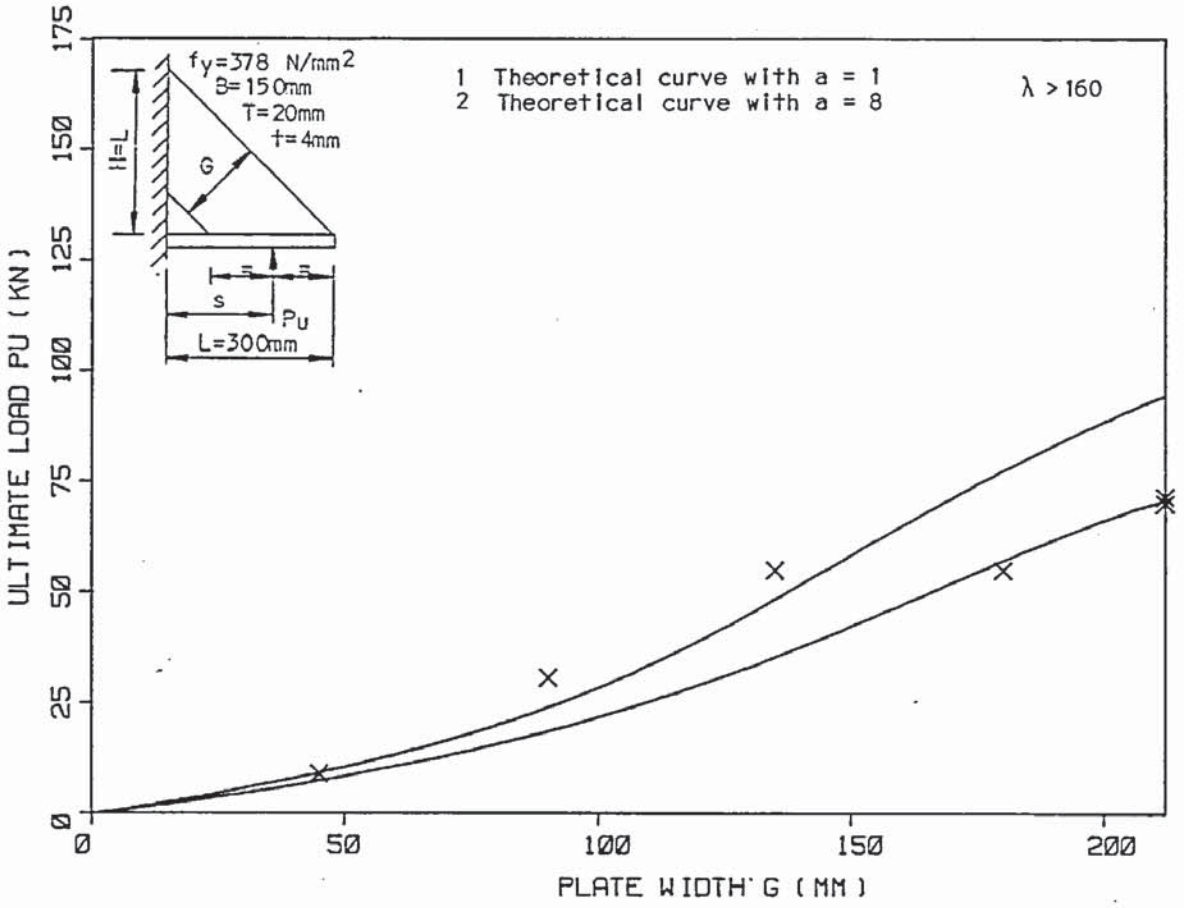

Figure 6.46 Comparison of theoretical with experimental ultimate loads for series 8, (s varies).

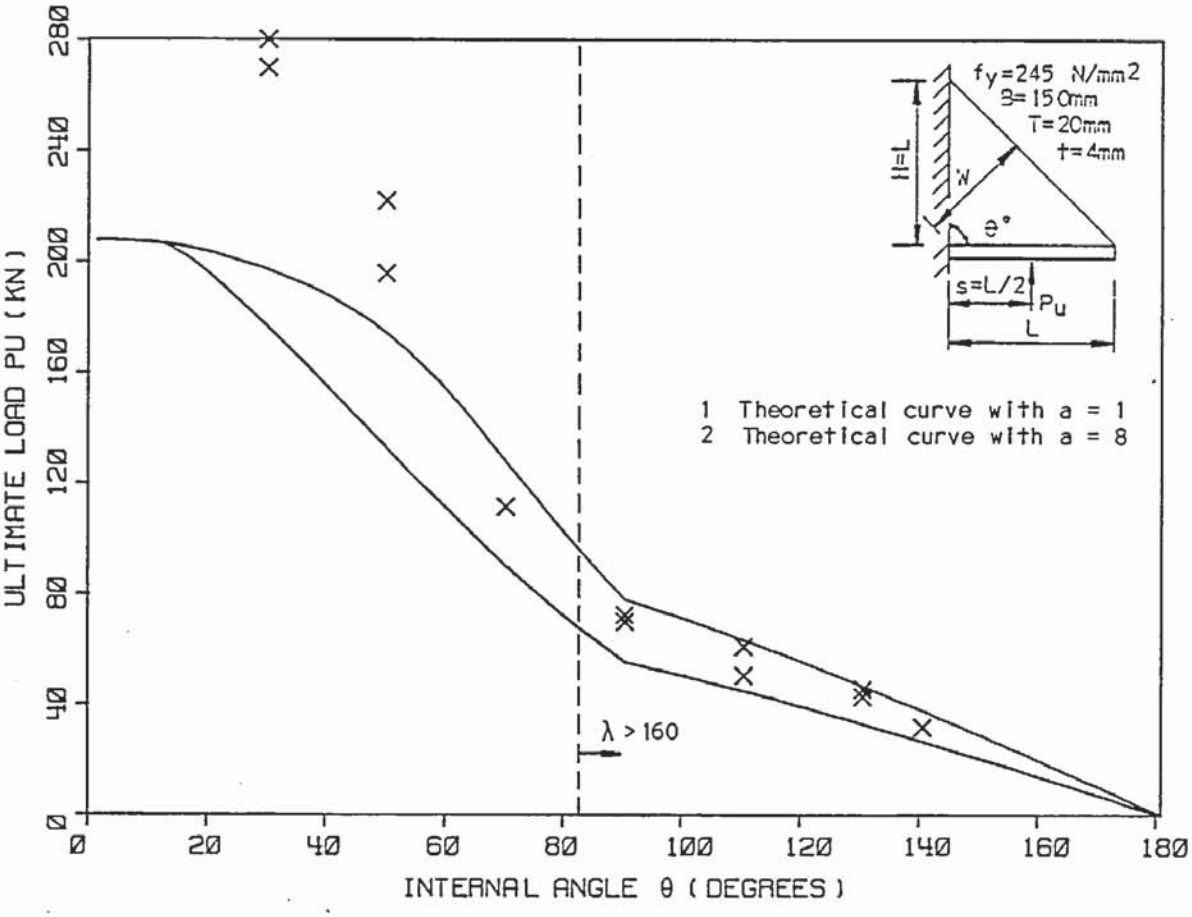

Figure 6.47 Comparison of theoretical with experimental ultimate loads for series 13.

With the unequal sided gusset plates, Figure 6.40 the effect of considering the mathematical equivalent sided gusset plate having the same width gives satisfactory results. This assumption is not expected to give the same curve, because the plate width slowly increases as the height increases beyond the equal sided plate and then remains approximately the same. None of the experimental results lie below the lower limit curve and most of them are between the two curves.

With the variation in the load position, Figure 6.41, the theoretical curves are very similar in shape to the experimental results which are very close to the lower curve. The experimental results fall slightly lower as the load moves towards the outer edge of the plate. This is attributed to the deflection of the loaded plate reducing the post buckling incompatibility as the load position moves out towards the free edge and so reduces the restraining effect and in turn the load capacity of the gusset plate.

With the variation of the loaded plate thickness, Figures 6.42 and 6.43, the theoretical curves do not include a term for the resistance of the loaded plate, as suggested by Martin (15). However, the experimental evidence does not support the necessity of including such a factor, with the lower limit curve closely following the experimental results. The experimental failure loads for s=L/2 lie slightly higher than this curve, and for s=L they lie slightly lower, which is in agreement with the previous results.

With the variation of the gusset plate thickness, Figure 6.44. for small thicknesses the experimental results lie between the two theoretical curves, which is in agreement with the other series. As the plate thickness is increased the experimental failure loads increase at a greater rate than the theoretical curves and so are conservative for the thicker gusset plates. With the theoretical curves, the tensile yield strength is used. From observations in the

tests and the separate strut tests, this value may be low and a crushing strength should perhaps be substituted.

Despite the experimental peaks with the two thirds remaining width of gusset plate, Figures 6.45 and 6.46, the smooth theoretical curves fit satisfactorily. The two extremes of remaining gusset plate width are very close to the lower limit curve, and the mid range remaining widths are slightly higher than the upper limit curve.

For internal angles greater than and equal to 90 degrees the experimental results (Figure 6.47), lie between the two theoretical curves satisfactorily. As the angle is reduced from 90 degrees, the experimental results gradually increase far more rapidly, resulting in higher failure loads for the very small angles than the theoretical curves predict. As with series 12 investigating the gusset plate thickness, this may be due to the tensile yield strength being used instead of the crushing strength.

6.11.4. Summary of comparisons of mathematical model with the experimental results

Considering the complex behaviour of the gusset plates and the scatter of results that normally accompany most buckling tests, the theory compares well with all the parameters tested. The theoretical curves follow the same pattern as the experimental results. The majority of the experimental results have fallen within or close to the theoretical band denoted by the upper and lower curves, with a=1 and 8 respectively. The only departure from this is with the thick gusset plates of series 12 and those with small internal angles of series 13, which are greater than the theoretical upper curve. This is most likely due to the tensile yield strength being used instead of a crushing strength. Furthermore, for very low slenderness ratios, the effects of strain hardening may be quite significant. Therefore,

this makes the theoretical curves conservative and safe for non-slender gusset plates.

6.12 Deflections

6.12.1. In plane deflections and moment rotations

Examination of all the vertical deflection data related to the gusset plates tested reveals a characteristic vertical deflection curve. The curve usually consists of a small initial settlement deflection followed by a linear main section and finally a non-linear section as it approached failure. With the testing arrangement, it was inevitable that some gusset plates would show some initial settlement deflection and others not. With a very small number of the gusset plates the linear section is not quite apparent, with a curve taking its place. However, with repeated results it is evident that it was masked by other interfering deflections. The gradient of the linear section varies, and despite some scatter, it is evident that there is some relationship with some of the parameters tested. There is also a similar relationship with the extent of the linear section. With some gusset plates there was virtually no non-linear deflection, whereas with others there was quite a large amount.

Because of the nature of the vertical deflection curves it is only considered possible to obtain some estimate of the gradient of the linear section. Attempts were made to obtain some theoretically derived equation for the moment rotation characteristics of the gusset plates, from which the vertical deflection gradient at the load point could be calculated. Unfortunately, due to the complex behaviour of the gusset plates no simple theoreticaly derived equation was obtained that matched the experimental results. However, when considering the deflection perpendicular to the loaded plate and at the load point, that the graphs of the load deflection gradients $P/d\bar{v}$ plotted against the respective variables for each series of gusset plates, has a

similar shape to the ultimate load curves. That is

$$\frac{P}{dv} \alpha P_u$$

Therefore

$$\frac{P}{dv} = \frac{P_u}{k} \qquad (6.32)$$

furthermore, with P and P_u in kN, and d in mm

$$k \simeq 1\text{mm} \qquad (6.33)$$

Using Equation 6.28 to calculate P_u with a=8, the gradients are calculated and plotted with the deflection graphs. It is found that the gradients are in the same range as the experimental gradients, allowing for the scatter in the experimental results and for the effects of the thin loaded plate tests. The only series in which the results are not satisfactory is the series in which the inside corner was removed. The results are in agreement with the complete and near complete gusset plates but, they underestimated the load deflection gradients of the narrow strips of plates. That is the predicted deflections are greater than the experimental deflections for these plates. Therefore, for a complete gusset plate the deflection d of a point load P perpendicular to the loaded plate is given by Equation 6.32. Furthermore, the moment rotation relationship of the gusset plate $M/d\theta$ can be related to P/dv by considering similar triangles to give

$$\frac{M}{d\theta} = \frac{P.s.L}{dv}$$

Therefore

$$\frac{M}{d\theta} = \frac{P_u s.L}{k} \qquad (6.34)$$

where $d\theta$ is in radians.

The implication of using Equation 6.33 in Equations 6.32 and 6.34 is that the ultimate load is attained after the load P moves a perpendicular distance dv, to the loaded plate by 1 mm. Also the predicted values of P/dv and $M/d\theta$ are dependant on the value of P_u used

and as to how close it is to the actual value. Therefore, the more conservative the estimated value of P_u used, the greater the estimated value of the deflections and rotations. The theoretical vertical deflection curves for a=8 are plotted with the experimental curves in Appendix 3.

6.12.2 Out of plane deflections

Examination of all the lateral deflection data related to the gusset plates tested reveals a range of different types and amounts of out of plane deflections. However, they can be split into two groups. The first group consists of relatively small lateral deflections for most of the loading, typically less than 1 mm for 90% of the ultimate load, with virtually no deflection at 50% of the ultimate load. The second group consists of relatively large deflections, in some cases starting from the initial loading. The curves in this latter group vary considerably and appear to be influenced by the initial lateral deflection, the load position and loaded plate thickness. Other gusset plates that are related to those belonging to the second group, start to buckle in one direction and then fail in the other.

With the series having both types of gusset plates it is possible to select two gusset plates between which the transition occurs. In series 3, in which the size of the gusset plate was varied, the transition is between the gusset plates with L=H=200 and 300 mm. The smaller gusset plates are of the first group, and the larger are of the second. In series 4, in which the height of the gusset plate was varied, there appears to be a transition between H=500 and 600 mm, the lower values of H belonging to the first group. Series 13, in which the internal angle was varied, the transition is between the gusset plates with θ =70 and 90 degrees, with the smaller angles belonging to the first group. Also in series 12, in which the thickness of the

gusset plate was varied, for values of $t \geq 5$mm they belonged to the first group. All the other series belong to the second group.

The group to which each gusset plate belongs appears to be related to the slenderness of the gusset plate, i.e. those in the first group were of a lower slenderness than those of the second. Therefore, the slenderness ratio of each gusset plate is calculated based on Equation 6.7 in which w is replaced by W, to give the effective length l of the free edge, which in turn gives the slenderness ratio λ when divided by the radius of gyration r giving

$$\lambda = \frac{l}{r} = \sqrt{12}.z.W.\tan\theta/2; \quad \theta \neq 90^{o} \qquad (6.35)$$

where $z = [V/(2.W.\tan\theta/2) - 1]C/W + 1$

(=1 for complete gusset plates)

The results are as given in Table 6.16.

Series	Variable	Slenderness ratio of gusset plate	
		Group 1	Group 2
3	L = H	$\leq$ 122.5	$\geq$ 183.7
4	H	$\leq$ 160.8	$\geq$ 164.3
5	S		183.7
7	T		183.7
12	t	$\leq$ 146.9	> 146.9
8	G		183.7
13	θ	$\leq$ 128.6	$\geq$ 183.7

Table 6.16 Slenderness ratios of gusset plates in the two out of plane deflection groups for each series of tests

Therefore, the transition is between λ =160.8 and 164.3. Examination of the associated deflections suggests that the former would be in the second group. Therefore, a value of λ = 160 is taken to be an upper limit of the first group.

CHAPTER SEVEN

THEORETICAL ANALYSIS OF THE WELDS

7.1 Introduction

In the following a theory for the failure of welds along the loaded and supported edges is developed with the aid of the experimental results obtained from the weld series. The theory is related to the theory for the gusset plates and is developed in a similar manner.

7.2 Development of the weld theory

Consider the simplest gusset plate with the loaded and supported edges of the same length and the internal angle 90°. The loaded and support plates are assumed to be rigid, in the sense that they are straight, and are free to rotate about the inside corner of the gusset plate, as shown in Figure 7.1(a). As the load P is applied the loaded and supported edges close together on the gusset plate and reduce the internal angle as shown in Figure 7.1(b). However, with no shear resistance between the adjacent surfaces the gusset plate effectively moves outwards from between the two closing surfaces under wedge action as shown in Figure 7.1(c) thus preventing any load being applied to it. With shear resistance this movement is resisted and a load is applied to the gusset plate. The magnitude of the load depends upon the shear resistance along the loaded and supported edges.

With the shear resistance along the loaded and supported edges sufficiently high to prevent any movement along these edges then the gusset plate is loaded with full contact as shown in Figure 7.1(b). However with slip along these edges the gusset plate is loaded towards the free edge of the loaded and supported edges. This concentration of loading deforms these edges, either elastically, or if the load is high enough, plastically, to produce contact zones as shown in Figure

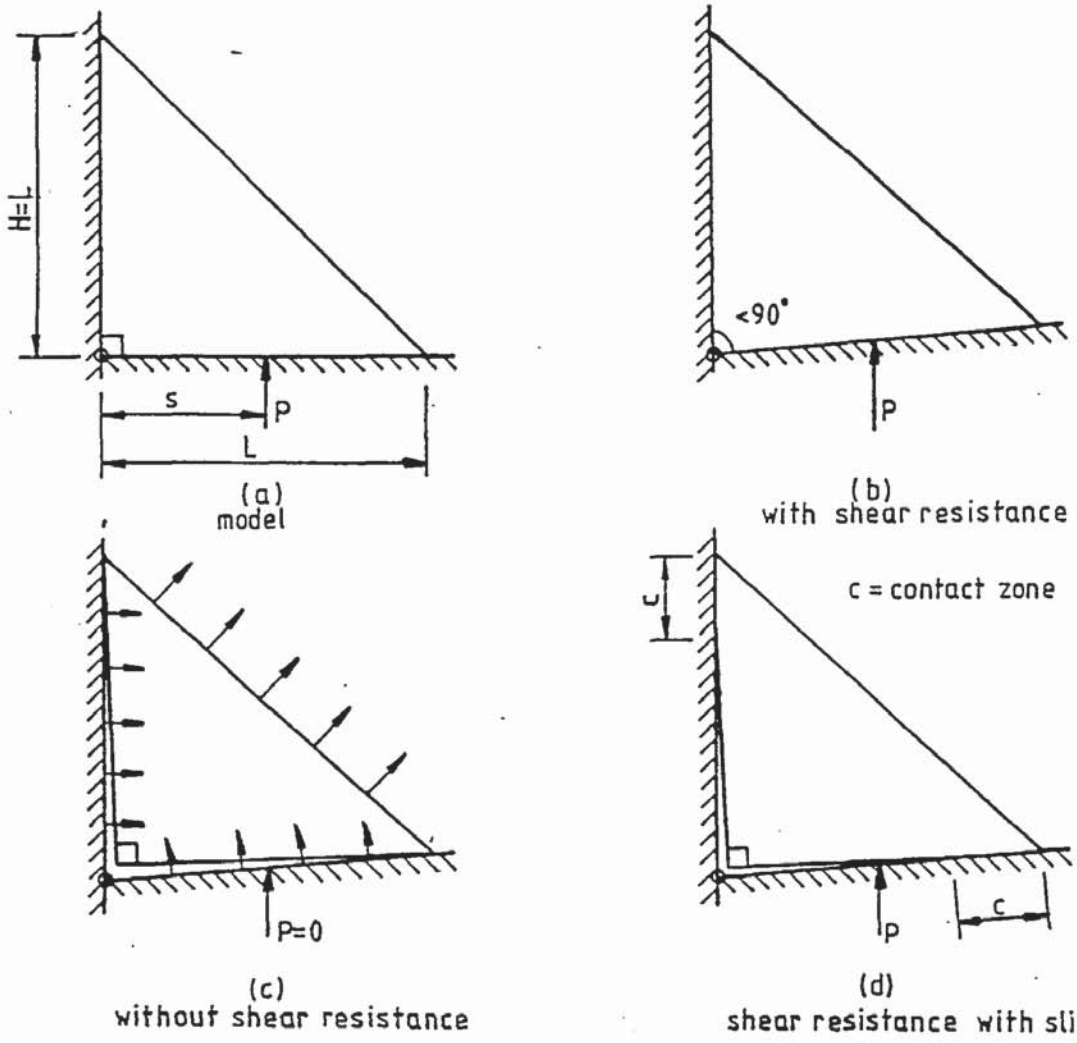

Figure 7.1 Theoretical model showing effects of with and without shear resistance along the loaded and supported edges.

7.1(d).

With the full contact zone along both the loaded and supported edges, the applied resultant load P, is transmited to the gusset plate with a resultant reaction P" at the point s", and from the gusset plate to the vertical support, with a resultant reaction P' at point s', as shown in Figure 7.2(a).

In the development of the gusset plate theory it is shown that such a model, with gusset plates that are still in the elastic range, or in the fully plastic range without buckling, then the gusset plate reactions P" and P' are at the mid points of their respective sides. That is s"=L/2 and s'=H/2. For plates with post buckling the values of s" and s' are more complicated and are not considered at present in the development of the weld theory.

As slip occurs, the contact zones are reduced and move out

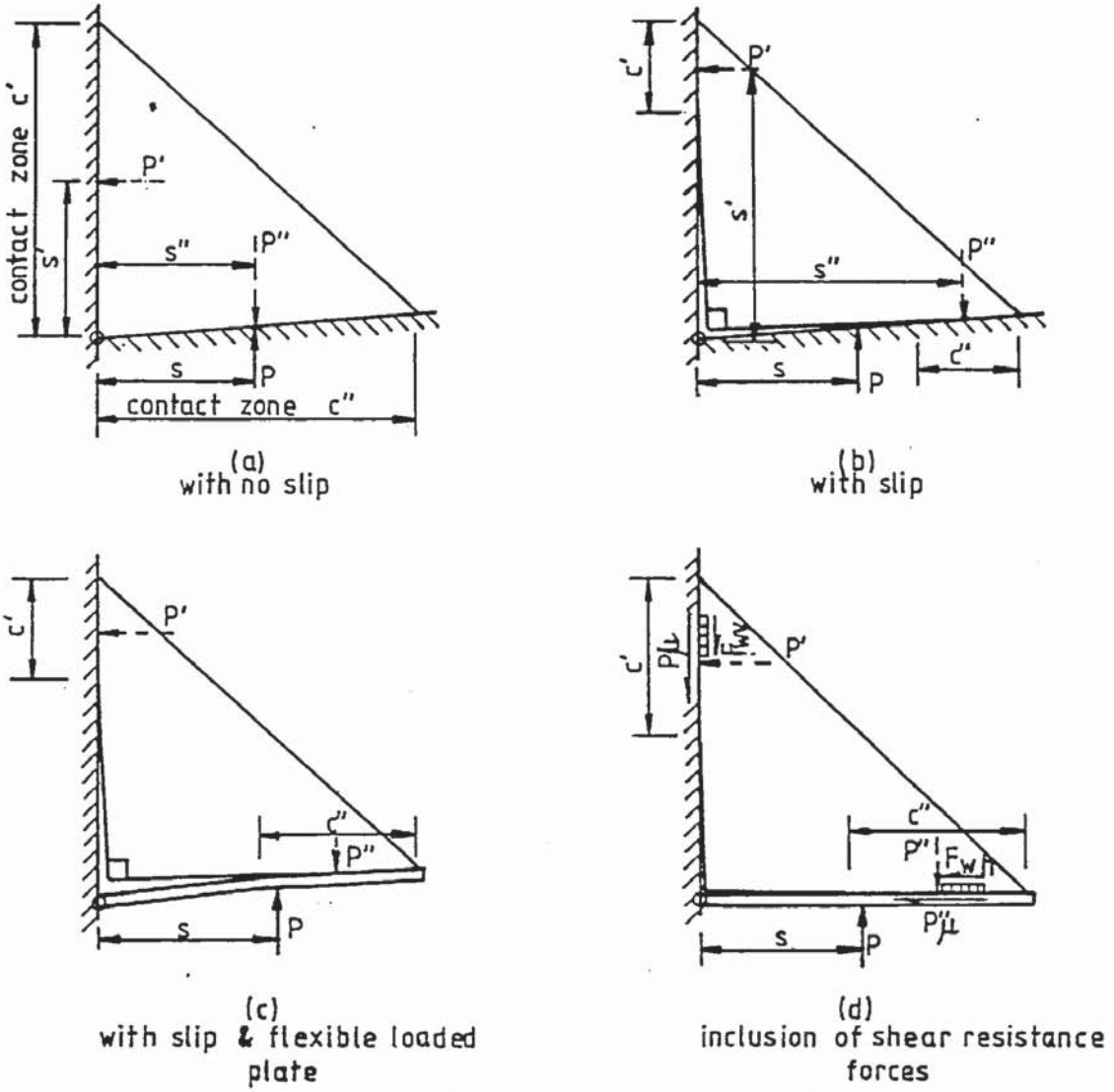

Figure 7.2 Resultant contact reaction points and contact zones along the loaded and supported edges.

towards the free edges, the resultant reactions P' and P" on the gusset plates must be within these contact zones and therefore move with them, as shown in Figure 7.2(b). The positions s' and s" of the resultant reaction P' and P" within the contact zones c' and c", respectively, depend upon the way the gusset, loaded and support plates deform. However, for a first approximation it can be taken as half of the contact zone. With the resultant applied load used in the experiments, the deflecton of the loaded plate alters the contact zone similar to that shown in Figure 7.2(c). The initial effect is to move the contact zone outwards. Also in this case, the more flexible the loaded plate, the closer the resultant reaction P" is to the applied load P, i.e. s" tends to s. As the actual amount of bending of the

loaded plate is very small the bending resistance is considered negligible.

7.2.1 Welds along both edges subjected to shear forces only

At this stage it is assumed that slip is prevented along the loaded edge solely by the shear resistance along the loaded edge itself and not by normal forces along the supported edge. Similarly with the shear resistance of the supported edge. This form of shear resistance can be provided by friction alone. If welds are placed only within the contact zones then the supported edge weld does not interfere with the shear resistance of the loaded edge and similarly the other way round. This then gives the arrangement as shown in Figure 7.2(d), which was the arrangement of series 17.

Referring to Figure 7.2(d) consider the equilibrium of the gusset plate alone.

Resolving vertically we have

$$P'' = P'\mu + F_{wv} \qquad (7.1)$$

Resolving horizontally we have

$$P' = P''\mu + F_{wh} \qquad (7.2)$$

Considering the loaded plate alone and taking moments about O and neglecting the bending resistance of the loaded plate, as deflections are small, then

$$P''s'' = P.s$$

therefore $$P'' = P.s/s'' \qquad (7.3)$$

Similarly for the equilibrium of the specimen as a whole then

$$P's' = P.s$$

therefore $$P' = P.s/s' \qquad (7.4)$$

Eliminating P' and P'' from Equation 7.1 using Equations 7.3 and 7.4 gives

$$\frac{P.s}{s''} = \frac{P.s.\mu}{s'} + F_{wv}$$

therefore $$F_{wv} = P.s(1/s'' - \mu/s') \qquad (7.5)$$

Similarly by eliminating P' and P" from Equation 7.2 gives

$$F_{wh} = P.s(1/s' - \mu/s") \qquad (7.6)$$

Equations 7.5 and 7.6 give the required weld strength for a given loading Ps knowing the coefficient of friction μ and the position, s' and s", of the resultant reaction, P' and P", along the supported and loaded edges respectively.

The main problem is in determining the values of s' and s". In the elastic range of the gusset plate with full contact zones on both the loaded and supported edges the values of s' and s" are H/2 and L/2 respectively for a rigid loaded plate. With a flexible loaded plate P" is expected to move towards the position of the applied load P. When considering the ultimate strength of the welds, slip occurs before the welds fail. Therefore the slipped condition exists with the reduced contact zones. So the resultant reactions move further than the mid-point position on both the loaded and supported edges for a rigid loaded plate. But, with a flexible loaded plate the loaded edge resultant reaction P" may be anywhere between the applied load and the rigid condition, depending on the amount of slip and the flexibility of the loaded plate. The possible extreme ranges of resultant reaction contact positions for varying degrees of weld slip and loaded plate flexibility are shown in Figure 7.3.

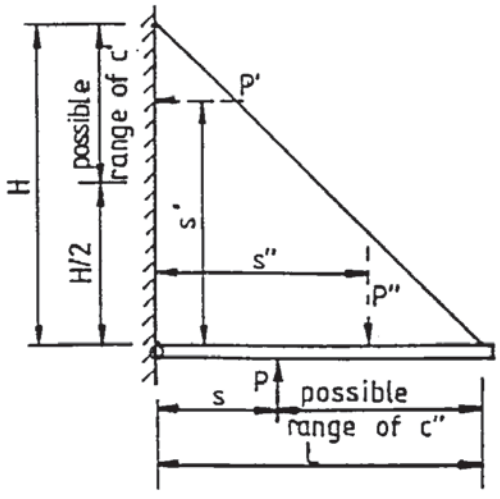

Figure 7.3 Possible extreme ranges of resultant reaction contact positions.

Specimen	ult. load Pu (kN)	SUPPORTED EDGE							LOADED EDGE						
		Contact zone (mm)	Reaction positon S' (mm)	WELD Lnth. (mm)	ult. load Fwh (kN)	(1) Theo. Fwh μ=0.45 (kN)	(2) Theo. μ	(3) Theo. Fwh μ=0.395 (kN)	Contact zone (mm)	Reaction positon S' (mm)	WELD Lnth. (mm)	ult. load Fwl (kN)	(1) Theo. Fwl μ=0.45 (kN)	(2) Theo. μ	(3) Theo. Fwl μ=0.395 (kN)
S17-25-1	100.0	100	250	48	61.0*	48.0+	0.233	51.3+	200	200	50	63.5	26.3	-	30.4
S17-25-2	100.0	76	262	51	64.8*	60.5+	0.395	64.8+	170	215	50	63.5	35.6	-	40.8
S17-75-1	220.0	85	258	150	190.5	99.6	-	106.6	180	210	51	65.8*	57.2+	0.395	65.8
S17-75-2	225.0	85	258	156	198.1	101.8	-	109.0	180	210	53	67.3*	58.5+	0.395	67.3

(1) Theoretical strength of weld based on equation 7.5 or 7.6 using experimental data and a coefficient of friction μ=0.45.
(2) Theoretical coefficient of friction based on equation 7.5 or 7.6 using experimental data for the weld that failed.
(3) Theoretical strength of weld based on equation 7.5 of 7.6 using experimental data and a value of μ=0.395 as a result of (2).
* Experimental weld failure.
\+ Theoretical weld failure.

Table 7.1 Comparison of theoretical and experimental weld failures for series 17.

7.2.1.1 Comparison with experimental results

Series 17 specimens were tested with only short lengths of fillet weld in the contact zones of the loaded and supported edges. In Table 7.1 the experimental ultimate loads and contact zones are used in Equations 7.5 and 7.6 to calculate the theoretical shear loads in the welds. These are compared with the strength of the weld based on separate ultimate shear stress tests as described in Section 3.4.4.

The theoretical loads in the welds based on a friction coefficient of 0.45 indicated the correct weld failures. The theoretical coefficient of friction based on these welds failing is the same for three of the tests i.e. μ =0.395. When this value is used to calculate the loads in the weld, they still indicate the same weld failures.

The accuracy of this theory is based on knowing the contact zones or more accurately the position of the resultant reaction on the two edges of the gusset plate. For specimen S17-25-1 the theory gives a higher ultimate applied load P given the actual weld strength. This specimen however was in full contact all the way across the loaded edge for most of the test, while the other three specimens started off with a gap which closed when loading. This suggests that with the latter three the resultant contact point started towards the free edge and moved inwards as the loaded plate deformed to close the gap. This left the resultant contact point somewhere in the middle of the contact zone on the loaded edge, as assumed. However with specimen S17-25-1 the plate was already in contact and on loading, the resultant contact point was at the point of loading i.e. at s=l/2. It then moved only slightly out towards the free edge as the load was applied, but not necessarily to the centre of the contact zone. To verify this assumption the theory was used to determine the position of the contact point s" that would produce the required weld failure. The theory gave s"=177mm which is approximately midway between the

middle of the contact zone and the load point, which is in the area expected.

7.2.2 Continuous weld along loaded edge only

Consider the same gusset plate in the elastic range of behaviour and a rigid loaded plate with a weld along the full length of the loaded edge, as shown in Figure 7.4(a). The weld along the loaded edge not only provides resistance against slip along the loaded edge, but also provides resistance against slip along the supported edge by its tensile strength adjacent to the supported edge. Effectively the shear resistance that would be provided by the missing supported edge weld is replaced by the tensile resistance of a section of the loaded edge weld. The tensile stress distribution will be the highest, adjacent to the supported edge and gradually reduce away from it.

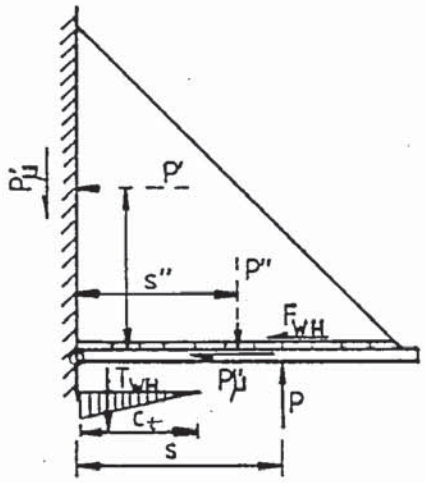

Figure 7.4 Effects of only a loaded edge weld.

Equation 7.5 for the shear force in the supported edge weld F_{wv} now becomes the equation for the tensile force T_{wh} in the loaded edge weld. With Equation 7.6 for the shear force F_{wh} in the loaded edge weld remaining the same.

$$T_{wh} = P.s(1/s'' - \mu/s') \qquad (7.7)$$

The tensile force T_{wh} produced by the loaded edge weld is given by

$$T_{wh} = \frac{f_t c_t t}{\sqrt{2}}$$

therefore the maximum tensile stress f_t in the weld becomes

$$f_t = \frac{T_{wh}\sqrt{2}}{c_t t} \tag{7.8}$$

The shear force F_{wh} produced from the loaded edge weld is given by

$$F_{wh} = \frac{2.f_q.L.t}{\sqrt{2}}$$

Therefore, the maximum shear stress f_q in the weld becomes

$$f_q = \frac{F_{wh}.\sqrt{2}}{2.L.t} \tag{7.9}$$

With f_t=1.3 f_q the simplest equation combining these stresses is given by

$$Q = \sqrt{(f_t/1.3)^2 + f_q^2} \tag{7.10}$$

Where Q is a constant and equal to the shear strength of the welds. Substituting Equations 7.8 and 7.9 into Equation 7.10 gives

$$Q = \sqrt{\left(\frac{T_{wh}\sqrt{2}}{1.3c_t t}\right)^2 + \left(\frac{F_{wh}\sqrt{2}}{2.L.t}\right)^2} \tag{7.11}$$

Substituting Equations 7.6 and 7.7 into Equation 7.11 gives

$$Q = \left[\frac{P.s\sqrt{2}}{1.3c_t t}\left(\frac{1}{s''} - \frac{\mu}{s'}\right)\right]^2 + \left[\frac{P.s\sqrt{2}}{2.L.t}\left(\frac{1}{s'} - \frac{\mu}{s''}\right)\right]^2$$

and re-arranging for the load applied to the gusset plate P gives

$$P = \frac{Q.t}{\sqrt{2}.s} \quad \frac{1}{\left[\frac{1}{1.3c_t t}\left(\frac{1}{s''} - \frac{\mu}{s'}\right)\right]^2 + \left[\frac{1}{2.L}\left(\frac{1}{s'} - \frac{\mu}{s''}\right)\right]^2} \tag{7.12}$$

The main problem with Equation 7.12 is in determining the values of s', s'' and c_t. s' and s'' will vary as described in Section 7.2.1. With a full weld along the loaded edge, which will prevent longitudinal slip, the value of s' will be approximately H/2. With a little slip it will move outwards, and with the buckling of the gusset plate it will move inwards.

The length of the tensile zone will vary depending upon the deformation of the gusset plate and the loaded plate. For example,

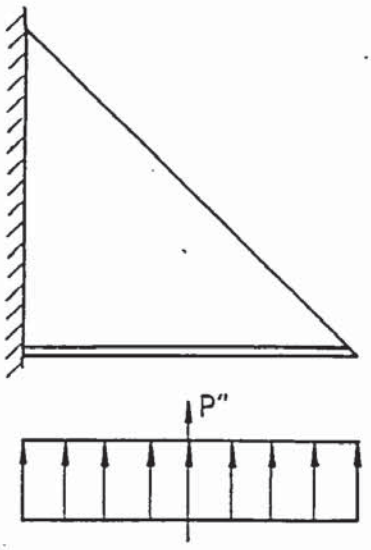

(a) no slip along supported edge, rigid loaded plate

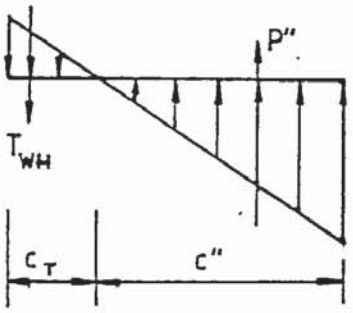

(b) slip along supported edge, rigid loaded plate

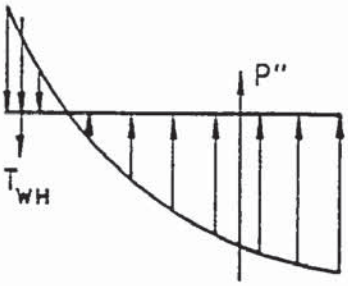

(c) slip along supported edge, flexible loaded plate

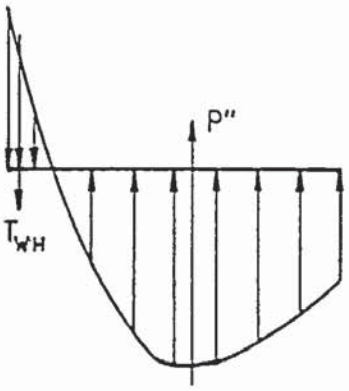

(d) slip along supported edge, flexible loaded plate, buckling gusset plate

Figure 7.5 The effects of supported edge slip on the distribution of the load transmitted from the loaded plate to the gusset plate.

with a rigid loaded plate and an elastic gusset plate the direct load distribution from the loaded plate to the gusset plate before any slip, that is before friction is overcome, is rectangular as shown in Figure 7.5(a). As the friction is overcome and slip occurs along the supported edge, a bending moment is applied to the gusset plate. This increases the compressive load towards the outer end of the gusset plate, pushing the reaction P'' outwards. Eventually a tensile load T_{wh} is produced at the inner end as shown in Figure 7.5(b).

In practice, the loaded plates are flexible and redistribution of the load takes place depending upon the load position as described with the short weld in Section 7.2.1. With the load at the mid point, the load distribution is as in Figure 7.5(c). The tensile zone moves towards the supported edge and the resultant compressive reaction P'' moves inwards again. Further, with gusset plates that buckle, it is shown in Section 6.5.2.3 that their resultant reactions move inwards as the ultimate load is approached. Therefore, it can be expected that the compressive reaction P'' moves even further inwards as shown in Figure 7.5(d).

7.2.2.1. Comparison with experimental results

Of the weld series, specimens S15-0-1 and S15-0-2 were tested with only fillet welds along the loaded edges. These specimens failed by the loaded edge weld failing in tension adjacent to the supported edge just before the gusset plates themselves failed by buckling. The failure loads were 375 and 437 kN for the first and second sides, respectively. The first side result is considered to be the most realistic value as discussed in the experimental results Section 4.3.1.1.

From Series 17 with only small welds, the remaining gaps along the loaded edge were approximately 100 to 120mm in length. Taking into account that for the gaps to extend so far, the slip was

relatively greater than with the weld running its full length. Then, a tension zone of 90mm was estimated. The ultimate shear strength of the welds was found by experiment to be 449N/mm^2 and from series 17 the coefficient of friction was shown to be approximately 0.395.

Initially the values of s' and s" started off at the mid point and then moved outwards as slip occurred. s' moved, say to 180mm and s" to 220mm. Substituting these values into Equation 7.12 for the failure load based on the weld strength gives a value of 603 kN, greater than the failure load of 375 kN. As the load was further increased the loaded plate deflected and the gusset plate started to buckle. s' moved inwards say to 170mm and s" to 190mm. Substituting these values into Equation 7.12 gives a failure load of 490 kN, still greater than the ultimate load. Further deformation and buckling brought both s' and s" further in, and if at the ultimate load, s'=140mm and s"=150mm then Equation 7.12 gives a failure load of 377kN, which is approximately the experimental failure load.

It is interesting to note that if the section of the loaded edge weld which is subjected to the tensile force is considered to only be subjected to this force and not the shear force, then the failure load would be 386kN. Therefore the failure load of the loaded edge weld is effectively dependent upon the tensile resistance of this section of the weld.

7.2.3 Continuous weld along supported edge only

Consider the same gusset plate in the elastic range of behaviour with a rigid loaded plate, and with a weld along the full length of its supported edge, as shown in Figure 7.6. This gusset plate and weld arrangement will effectively behave in the same manner as a loaded edge weld. The only difference is that all the factors are interchanged in Equation 7.12 giving

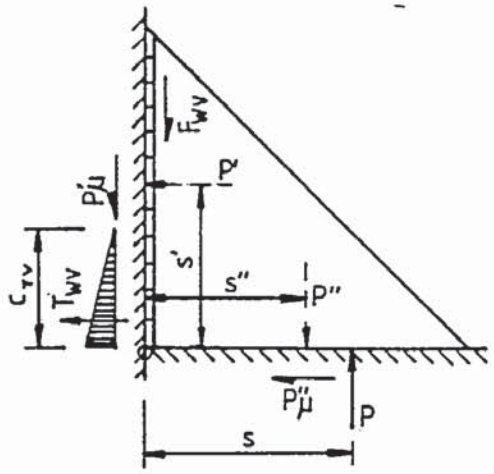

Figure 7.6 Effects of only a supported edge weld.

$$P = \frac{Q.t}{\sqrt{2}.s} \quad \frac{1}{\left[\frac{1}{1.3c_t t}\left(\frac{1}{s''} - \frac{\mu}{s'}\right)\right]^2 + \left[\frac{1}{2.H}\left(\frac{1}{s''} - \frac{\mu}{s'}\right)\right]^2} \qquad (7.13)$$

The difference lies in the values of s', s" and c_{tv}. With a full weld along the supported edge which prevents longitudinal slip, the distance s" is located close to the mid point of the loaded edge. With a little slip it may move outwards but, because of the flexibility of the loaded plate, this movement is dependent upon the load point. With the load at the mid point this movement is unlikely to be great. As the gusset plate starts to buckle it moves inwards again and the reaction P" is located approximately at the load point. The supporting plate remains effectively rigid, and with the initial slip along the loaded edge the load distribution along the supported edge is closer to that shown in Figure 7.5(b) than that in Figure 7.5(c). The supported edge reaction P' is expected to move further outwards from its mid point as more slip takes place, compared with its counterpart P" which occured with the loaded edge weld. Also, the tensile zone is spread over a greater length of the supported edge weld. As the gusset plate begins to buckle, the supported edge reaction P' moves inwards a little. The experimental results suggest that there is a resistance to slip along the loaded edge provided by the deflection of the loaded plate which effectively reduces the

amount of tensile force applied to the supported edge weld.

7.2.3.1 Comparison with experimental results

In series 14 four specimens were tested with only welds along the supported edges. In each case the gusset plates failed before the welds failed in tension at the inside corner of the supported edge weld. Some welds, however, did fail as the gusset plates folded after they had failed. The failure loads were 362 and 395 kN for the first sides tested, and 425 and 475 kN for the second sides tested. The tensile zone will most likely be greater than with the loaded edge and a value of 120mm seems reasonable. The ultimate shear strength of the welds was 449 N/mm^2 and the coefficient of friction was approximately 0.395.

The values of s' and s" initiated at the mid points and then moved outwards as slip occurred. s" moved little because of the flexible loaded plate and remained roughly at the mid point throughout the loading. s' moved out considerably as slip occurred and then moved back in as the gusset plate began to buckle. s'=225mm, which is a little less than that measured for series 17, to take account of the weld extending the full length of the supported edge. Substituting these values into Equation 7.13 gives a weld failure load of 894 kN. As s' reduced to say 180mm with a reduction of the tensile zone to 100mm due to the buckling of the gusset plate at failure, the weld failure becomes 536kN which is higher than the failure load of the gusset plate. Further folding moved s' further in and reduced the tensile zone and consequently reduced the failure load of the weld.

As with the loaded edge weld, if the section of the supported edge weld that is subjected to the tensile force is considered to be subjected solely to the tensile force, then the failure load based upon this weld failure in tension only, would be 564 kN. Therefore, the failure load of the supported edge weld is effectively dependent

upon the tensile resistance of this section of weld.

7.2.4 Continuous welds along supported and loaded edges

It was shown with the equal sided 90 degree gusset plates that with slip the reactions P' and P" move towards the free edge. The effect of this was to unevenly load the gusset plate and so reduce its failure load. The effect upon the welds was to reduce the load applied to them. With no slip, the gusset plate is loaded evenly and its full capacity is reached. With an equal sided yielding gusset plate the reactions P' and P" remain at the centre of their respective edges. With a buckling gusset plate the reactions P' and P" start to move in as the failure load is approached and are relatively greater than if they remained in the middle. The positions and magnitudes of these reactions are determined by the stress distribution across the gusset plate.

In the development of the theory for the gusset plates, it was found that all complete gusset plates at the ultimate load behaved in a similar manner irrespective of their shape, and can be represented by an equivalent equal sided gusset plate of the width and internal angle up to a maximum of 90 degrees. Figure 7.7(a) shows such a gusset plate together with its equivalent equal sided gusset plate and its stress distribution at the ultimate load. The resultant reaction of the stress distribution R' is taken to run parallel to the free edge of the equivalent equal sided gusset plate for complete gusset plates and not parallel to the free edge of the actual gusset plate. This assumption is based upon the way in which the gusset plates failed under test. This resultant reaction is taken to be resisted by direct forces, P" and P', and shear forces, F_l and F_h along the loaded and supported edges respectively. The direct forces P" and P' are assumed to be transmitted directly from the gusset plate to the adjacent loaded and supported plates. The shear forces F_l and F_h are

assumed to be resisted by both the frictional forces F_{fl} and F_{fh}, and the longitudinal shear resistance forces F_{wl} and F_{wh} of the welds. It is considered that if all the shear forces are resisted by shear resistance along the respective edges then there will be no tensile force in the other weld.

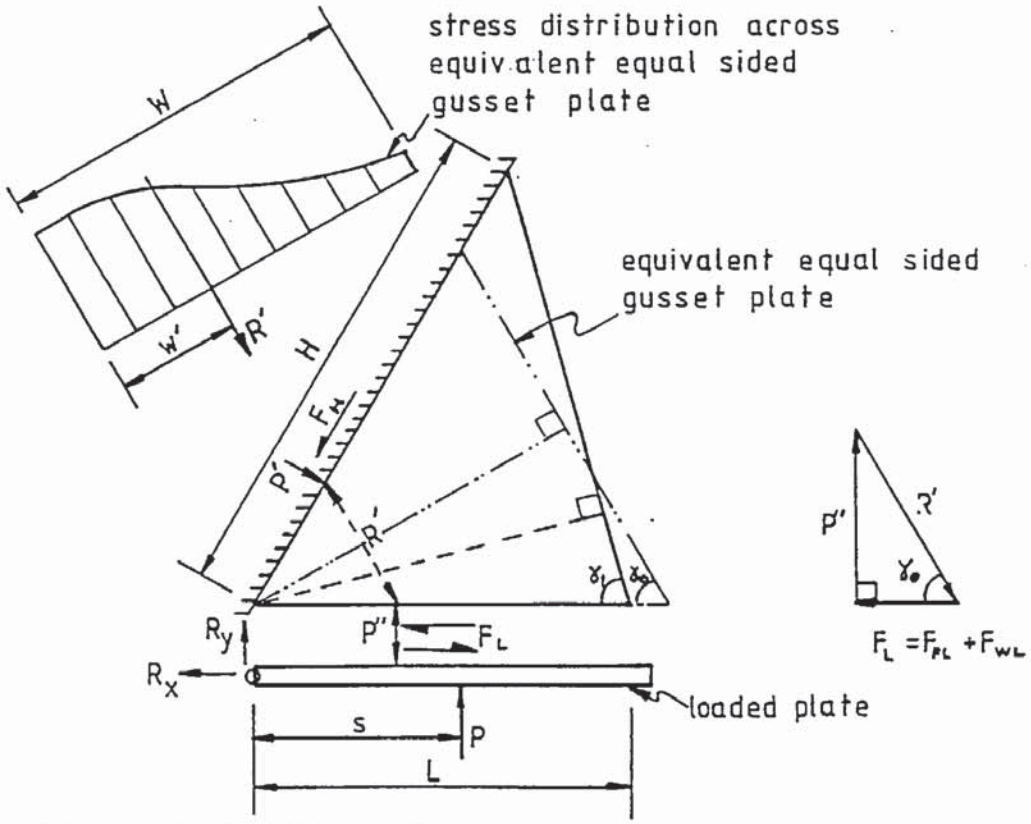

Figure 7.7 General weld model.

Only the loaded edge is considered, as the supported edge is derived in a similar manner. Figure 7.7(b) shows the triangle of forces along the loaded edge. Taking the frictional force F_{fl} to be

$$F_{fl} = \mu.P'' \tag{7.14}$$

then

$$F_{wl} = R'(\cos\gamma_o - \mu.\sin\gamma_o) \tag{7.15}$$

With complete gusset plates the above equivalent equal sided assumption gives the same value of F_{wh} as F_{wl}. However, with the incomplete gusset plates, their failure modes changed as more of the inside corner was removed, which prompted the modification in the gusset plate design with the incorporation of the factor z, which increased the effective lengths in relation to the amount of the inside corner removed. The same experimental behaviour suggested that the removal of the inside corner reduced the tendency of the gusset

plate to fail in a similar manner to an equal sided gusset plate, and more towards an inclined strut. The result is a change in the angle of incidence of the reaction R' to the loaded edge from the equivalent equal sided free edge angle γ_o for a complete gusset plate i.e. C/W=0 to the actual free edge angle γ_1 for an extremely narrow strip of plate, i.e. as C/W→1. Therefore

for C/W = 0 $\qquad \gamma_1 = \gamma_o = (90 - \theta/2)$ (7.16)

and for C/W = 1 $\qquad \gamma_1 = \gamma_1 = \sin^{-1}(W/L)$ (7.17)

assuming a linear transition gives

$$\gamma_1' = [\sin^{-1}(W/L) - 90 + \theta/2]C/W + 90 - \theta/2 \qquad (7.18)$$

Equation 7.15 then becomes

$$F_{wl} = R'(\cos\gamma_1' - \mu.\sin\gamma_1') \qquad (7.19)$$

Replacing L with H in Equation 7.18, Equation 7.19 then gives the shear force in the supported edge weld, F_{wh}.

With two full length fillet welds either side of the gusset plate, the fillet weld size required along the loaded edge is given by

$$t_{wl} = \frac{F_{wl}}{\sqrt{2}.f_t} \frac{1}{L(1 - C/W)} \qquad (7.20)$$

where f_t is the ultimate shear strength of the weld.

Similarly for the size of the supported edge weld.

7.2.4.1 Comparison with experimental results

The accuracy of the theory is compared preferably with experimental results where the welds failed. There were no weld failures with fully welded gusset plates, however, even when using the smallest practical weld on a relatively thick gusset plate. An approximate method is to compare the theoretical loads in the welds, based on the experimental gusset plate ultimate loads, with the theoretical strengths of the welds. As the welds did not fail the theory should give lower loads in the welds than their actual strength.

The only series with any significant shear forces in the welds was series 12 and the comparison is presented in Table 7.2 as an example. In the theory, the shear force in the weld is related to the resultant reaction in the gusset plate which is in turn related to the gusset plate's ultimate load. As the experimental gusset plate ultimate load was generally higher than the theoretical ultimate load, the theoretical loads in the welds are adjusted by the same ratio as the gusset plate theoretical ultimate loads, to arrive at the experimental value. In all cases the theoretical load in the welds were much lower than the ultimate weld strengths and even lower than the yield strengths.

Specimen	P_u exp. (kN)	P_u theo. (a=1) (kN)	T_{wl} theo. = T_{wh} theo. (a=1) μ=0 (kN)	T_{wl} theo. factored (kN)	T_{wl} exp. ult. from welds (kN)	T_{wl} exp. yield from welds (kN)
S12-5-1	119.5	137.6	161.7	140.4	762.0	586.1
S12-7-1	215.0	234.4	250.4	229.7	762.0	586.2
S12-9-1	450.0	333.3	342.3	462.1	1143.0	879.2
S12-11-1	425.0	423.3	429.5	431.2	1143.0	879.2
S12-13-1	550.0	500.5	505.6	555.6	1524.0	1172.3
S12-15-1	1125.0	589.2	593.4	1133.0	1524.0	1172.3

Table 7.2 Comparison of theoretical loads in the gusset plate welds with their theoretical strength for series 12 specimens.

7.3 Summary

From the analysis of the experimental weld tests the welds along the loaded and supported edges are mainly there to prevent the gusset plate from sliding out from between the loaded and supported plates. The actual shear forces along these welds are resisted in several ways. There is the frictional resistance that exists between the adjacent surfaces which are pushed together by the compressive load applied to the gusset plate, there is the shear resistance of the welds along these edges, and there is also the tensile resistance

provided by the adjacent section of the weld running along the other edge of the gusset plate. The experiments show that the shear forces along these edges are relatively low and can be resisted by a relatively small weld. The experiments also show that the shear resistance provided by a weld along one edge can be replaced by the tensile resistance of a weld along the inside corner of the other edge. However, with no weld along one edge, the full capacity of the gusset plate is not obtained as the loads are not transmitted to the gusset plate in the desired manner. Also with no weld along one edge there is a reduction in the amount of lateral rotational restraint and so the gusset plate will buckle at a slightly lower load. From the experiments, it appears that most of the lateral rotational restraint is provided by the physical thickness of the gusset plate, and the welds only supplement this by a small amount.

Slip along either edge influences the way in which the load is transmitted to the gusset plate and so influences the way in which it fails, and the load at which it fails. The flexibility of the loaded and supporting plates influences the sensitivity of the gusset plate to slip. Slip along one edge may change the way in which the load is transmitted and in turn cause another part of the gusset plate as a whole to actually fail. Therefore, for the full strength of the gusset plate to be developed, the welds have to be designed to produce the minimal amount of slip along the loaded and supported edges. If the welds are designed to prevent slip, then no tensile load will be applied to the other weld and the tensile load can be ignored.

7.4 Development of loaded plate theory

The function of the loaded plate is to ensure that the gusset plate is restrained and loaded in the correct manner so that its full capacity can be obtained. To do this it is required to distribute the load over the whole of the loaded edge of the gusset plate. It is

also required to restrain the gusset plate from moving away from its support by the shear forces between it and the loaded edge.

Consider the way in which the loaded plate distributes the load to the gusset plate. For it to distribute any load to the gusset plate it has to deflect. If it deflects then it must provide a moment of resistance to the applied load. However, the experimental deflections were measured on a few specimens and were found to be negligible. Furthermore the width and thickness of the loaded plates did not have any apparent influence on the ultimate loads.

The experiments did show that the thickness of the loaded plate determined the area of the gusset plate to which the load was distributed. With the load applied at the end of the loaded edge it was found that as the thickness was reduced so was the area of the gusset plate that buckled. The whole of the gusset plate buckled with the 20mm thick loaded plate.

With the load applied at the mid point of the loaded plate, irrespective of its thickness, all the gusset plates failed in the normal way. Problems therefore only appear to occur with the load applied towards the free edge.

On the whole the experimental results suggest that there is some relationship between the position of the applied load, the thickness of the loaded plate and the thickness of the gusset plate, which determines whether the loaded plate distributes the load to the whole of the gusset plate. The results were too few to determine any definite relationship and this is one area that requires further investigation.

For the loaded plate to distribute the load to the gusset plate with the applied load anywhere along the loaded edge, then there must be a lateral reaction at the supported end of the loaded plate, which is shown as R_y in Figure 7.7.

Therefore, resolving perpendicular to the loaded plate at the ultimate load

$$P_u + R_y + P'' = 0$$

now from Figure 7.7 $P'' = R' \sin \gamma_1'$

Therefore $R_y = R' \sin \gamma_1' - P_u$ (7.21)

The loaded plate is also required to restrain the gusset plate from moving away from the supported plate. Therefore, the shear force transmitted to the loaded plate will be resisted by the reaction Rx at the supported end of the loaded plate as shown in Figure 7.7(a). Therefore resolving parallel to the loaded plate

$$F_1 - R_x = 0$$

now from Figure 7.7 $F_1 = R' \cos \gamma_1'$

therefore $R_x = R' \cos \gamma_1'$ (7.22)

For a continuous loaded plate R_y is the maximum shear force in the loaded plate at the ultimate load, and R_x is the maximum tensile force in the loaded plate at the ultimate load. For a loaded plate welded to the support, then these will also be the forces in the weld at the ultimate load.

7.4.1 Comparison with experimental results

To check the theory for the loaded plate thickness and weld size it is best compared with experimental results where the welds actually failed. Series 12 investigating the gusset plate thickness was the only series where this type of failure occurred and so the comparison is made with the results of this series. In the theory the weld size is related to the resultant reaction in the gusset plate which is in turn related to the ultimate load. In order to make a comparison it is necessary to compare like with like, therefore the theoretical loads in the welds based upon the experimental ultimate loads are obtained in a similar manner as with the gusset plate welds. Also as the welds actually failed, then the ultimate strength of the welds is

used and not just the yield strength. In some cases the loaded plate weld consisted of a fillet weld connecting it to the vertical support plate, and a butt weld connecting the ends of the loaded plates of the back to back specimens. Although the weld metal was stronger than the parent metal, the fillet welds themselves failed across the throat as the effective cross sectional strength was lower than for the parent metal interface. With the butt welds it was the parent metal that failed along the interface as its cross sectional area strength was lower. So the corresponding strengths are used. Table 7.3 compares the ultimate tensile force in the loaded plate based upon the theory with that calculated from the weld sizes and strengths. Also included are the calculated tensile yield forces based upon the weld sizes and strengths. With the load applied at the mid point the theoretical shear stresses at the supported end of the loaded plate were relatively small and as the loaded plate is welded to the gusset plate its actual presence was considered negligible.

Specimen	P_u exp. (kN)	P_u theo. (a=1) (kN)	R_x theo. ult. (a=1) (kN)	R_x theo. ult. factored (kN)	R_x exp. ult. from welds (kN)	R_x exp. yield from welds (kN)
S12-5-1	119.5	137.6	161.7	140.4	247.6 *	190.5
S12-7-1	215.0	234.4	250.4	229.7	247.6 +	190.5
S12-9-1	450.0	333.3	342.3	462.1	761.4 *	585.7
S12-11-1	425.0	423.3	429.5	431.2	761.4 #	585.7
S12-13-1	550.0	500.5	505.6	555.6	495.3 #	381.0
S12-15-1	1125.0	589.2	593.4	1133.0	1226.5 #	943.5

* no weld failure
\+ failure of previous side weld
\# weld failure

Table 7.3 Comparison of theoretical load in loaded plate welds with theoretical strength for series 12 specimens.

Table 7.3 shows that the theoretical ultimate loads in the welds of the two specimens that did not fail, specimens S12-5-1 and S12-9-1,

were lower than both their ultimate and yield strengths. Both of these specimens were the first sides of a pair tested, together with specimen S12-13-1. With the latter specimen the weld failed and its theoretical ultimate load in the weld is higher than its theoretical strength and so is safe.

With the testing of the second sides these particular welds will most likely have been weakened with the failing of the first side. So the calculated loads based upon the weld sizes and strengths can be expected to be higher than the actual values. With specimen S12-7-1 it was the weld of the previously tested side that actually failed but it was the same as that tested. As a result the theoretical ultimate load in the weld was a little lower than that based upon the calculated ultimate strength of the welds, and higher than the yield strength. With specimen S12-11-1 the theoretical ultimate load was 43 percent lower than the calculated ultimate strength of the weld and 26 percent lower than the yield load. With this gusset plate the loaded plate butt weld was considered to have been badly damaged in the process of the initial side folding up after failing. The loaded plate would have been under bending and direct tensile stresses above those calculated during loading. Therefore its strength will most probably have been reduced considerably below that estimated. This is supported by the fact that the failure load of this gusset plate was lower than the previously tested side.

With specimen S12-15-1 the fillet weld will most probably have been damaged from the testing of the initial side. However, the butt weld connecting the loaded plates was put in after the testing of the initial side and therefore was a full strength weld. As a result the theoretical ultimate load in the weld is only a little lower than its ultimate strength above its yield strength.

From the results of this series, giving more weighting to the

initial side results, it appears that the theoretical ultimate loads are reasonably accurate. Further support is given by the fact that the calculated ultimate loads of the loaded plate welds for all other series are lower than the actual weld strengths and no weld failures occurred.

In the above weld comparison with series 12 the theoretical shear force in the weld was calculated to be very small as the load was applied at the mid point. As this shear force is based upon the position of the applied load relative to the reaction produced by the gusset plate, then the largest values will be obtained with the applied load at either end of the loaded plate. It is therefore considered only necessary to check shear forces in the loaded plate weld or the loaded plate itself when the applied load is towards either end of the loaded plate. Generally speaking the tensile force is dominant. If the shear forces are relatively high then it may be necessary to combine the shear and tensile stress in the weld connecting the loaded plate to the support.

In a similar manner the loaded plate thickness can be checked as for the weld. The theoretical loaded plate thicknesses were governed by the tensile stress and even when the yield stress was used with all but series 12 the loaded plates were found to be more than adequate, even the 6mm used in series 7. Series 12 was the only series where the loaded plate stresses were above the yield stress and that was because the gusset plate itself failed at a greater load than the theoretical load.

CHAPTER EIGHT

DESIGN

8.1 Introduction

This chapter demonstrates how the theoretical work can be used in the design of gusset plates. Each part of the gusset plate is dealt with in turn. A design summary and examples are given in Appendix 6.

8.2 Design considerations

In designing gusset plates using the limit state design method, two limit states are considered, the ultimate limit state and the serviceability limit state. The theoretical model is developed to predict the ultimate limit state i.e. the load at which the gusset plates collapse.

The serviceability limit state is concerned with the conditions at service loads, such as deflections, vibrations, etc. With the gusset plates the deflections are of a major concern. The in plane deflections are related to the moment rotational characteristics, which are important in the design of the members connected by the gusset plates. The out of plane deflections are also important, especially with the gusset plates. Although the gusset plates can sustain the required load, in some cases the out of plane deflections are relatively high and may cause some alarm or damage to its surroundings. Therefore, they should be kept small enough not to be visible, and not to cause any damage.

8.3 Designing the gusset plate

8.3.1 Choice of theoretical curve for design purposes

As with any experiment, especially buckling tests, the experimental results can fall within a range of values and the theory can be adjusted to give an average or a range of theoretical values to

suit the experimental results. However, when considering a method for designing the gusset plates it is necessary to provide a safe value without being too conservative. For the ultimate limit state, the method can be applied to all gusset plates with the appropriate value of 'a'. The lowest range of 'a' used in the British draft steel code (2) is 8, and from the experimental results this is safe for virtually all the gusset plates, except those with the load applied towards the outermost end of the loaded plate. However, in this case, it must be taken into consideration that the results are of the worst possible loading condition of a concentrated point load applied in the worst possible position along the loaded edge of a relatively slender gusset plate. Even then the experimental values are only slightly lower. This type of loading condition is considered to be far worse than any encountered in practice and so a value of a=8 is considered to be safe under practical conditions.

It is found in Section 6.12.2 that the out of plane deflections become unacceptable for gusset plates with slenderness ratios greater than 160. That is, to satisfy the serviceability requirements the slenderness ratio of the gusset plate given by Equation 6.35 should be limited to 160. Therefore

$$\lambda < 160 \qquad (8.1)$$

As it is usual for the serviceability limit state to be used as well as the ultimate limit state, then the slenderness ratio can be applied to the ultimate limit state requirement. In this case, a value of a can be chosen based upon the experimental results satisfying this requirement. From such experimental results a value of a = 3.5 produces safe results. As mentioned in Section 6.11.1 the nearest category in which the gusset plates may be placed, as presented in Table 6.2.1 of the British draft steel code (2), is for welded plate, I or H-section up to 40 mm thick, giving a value of a = 3.5 for bending about the x-x axis and a = 5.5 for bending about the

y-y axis. Therefore, the value of a obtained for the non-slender gusset plates, fits into this category on the safe side. As to which axis category the buckling is considered to be, is debatable. To be conservative the latter case is taken with a value of a = 5.5 for gusset plates up to 40 mm thick. There is no reason for the method not being applicable for gusset plates over 40 mm, and so the code value of a = 8 can be used. Note 3 of Table 6.2.1 of the draft code suggests that if it is guaranteed that the edges of the flanges are only flame-cut, then a = 3.5 may be used for buckling about the y-y axis for flanges up to 40 mm thick, and a = 5.5 for flanges over 40 mm thick. The reference to the flanges may be applied to the gusset plate.

8.3.2 Design strength

For the different grades of steel the characteristic yield strengths are given. These strengths refer to the strength of the material. However, the variation of strength in the actual structure may be greater than that of the material, due to conditions such as corrosion and variation of cross section. So those effects are allowed for in design by dividing the characteristic strength by a partial safety factor for strength γ_m to obtain the design strength. The value adopted depends on the design code in use. With the British draft steel code (2) the design strengths are given in Table 5.7.1 for the appropriate material, thickness and grade of steel. Alternatively, in Section 5.7.1 of the code, the design strengths can be calculated based on 0.93Ys but $\geq$ 0.73Us, where Ys and Us are, respectively, the minimum yield stress and the minimum value of the ultimate tensile strength specified in BS4360, which is the basis for Table 5.7.1 of the code.

When buckling occurs, the strength of the member is no longer based upon the yield strength but upon the buckling strength.

However, the buckling strength is a function of the yield strength and the critical buckling strength based either on elastic stability theory or on inelastic buckling. The buckling strength is generally below both the yield strength and the critical strength due to imperfections present, including residual stresses, small variations in material properties, initial curvature and other minor variations in the geometry. There are two alternative methods of calculation for design purposes : either the materials factor is applied to the buckling stress after its calculation or to the characteristic yield strength before the buckling stress is calculated. The reasoning for the former is to ensure that the effect of the materials factor will always be present. The reasoning for the latter method is whereas the yield strength is a material property, the buckling strength is a mechanical property related to the dimensions of the structural element which uses the design strength obtained from the factored yield strength. Also the buckling stress equation used is based upon experimental results and already takes into account all the expected imperfections related to buckling. The British draft steel code (2) adopts the latter reasoning which will also be adopted by the author.

In addition to the application of a form of materials factor to obtain the design strength, the British draft steel (2) code requires the design strength for sections fabricated from plates by welding to be reduced by $20 N/mm^2$, as given in Section 6.2.3 and note 2 of Table 6.4.1 of the draft code. Therefore, the design stress that is used for fy is that given by Section 5.7.1 and Table 5.7.1 of the code less $20\ N/mm^2$.

8.3.3 Design load

The characteristic load is determined from the normal variation in load. In practice the design load may be larger than the characteristic load for the following reasons.

a) there is no pretence that the characteristic load is an absolute maximum, with 5% probable values greater than the characteristic load.

b) the effect of some limit states can be more disastrous than others.

c) the lack of dimensional accuracy of construction can lead to larger or smaller loads.

d) there may be inaccuracies in the assessment of the loading and stress redistribution within the structure.

e) there may be unusual increases in load beyond those envisaged when determining the characteristic load.

Each characteristic load (dead, imposed or wind) is therefore multiplied by a partial safety factor and the loads are added to produce a design load. Therefore, for any limit state, the design load is given by the sum of the characteristic loads each multiplied by its own partial safety factor.

$$\text{i.e } P = \gamma_{fy}G_k + \gamma_{fq}Q_k + \gamma_{fw}W_k \qquad (8.2)$$

where

G_k is the characteristic dead load

Q_k is the characteristic imposed load

W_k is the characteristic wind load

and the appropriate γ_f factors.

At the ultimate limit state the partial safety factors for load are much greater than 1.0, with the exception of dead and wind loading condition where the dead load factor is less than 1.0. At this limit state the important consideration is one of strength. At the serviceability limit states the partial safety factors will be equal to 1.0. Values of the design loads will be given in the appropriate design code.

8.3.4 Design tables

As Equation 6.28 is a numerical solution involving the summation of adjacent strips of gusset plate, it is best presented in tabular form. It can be used by hand using 4 strips to give an approximate solution, but this would be tedious. Alternatively, a programmable calculator can quite easily be programmed. However, in practical design situations it is usually the gusset plate thickness t that is required, the other factors being known from other considerations. Unfortunately, Equation 6.28 is not in a suitable form to obtain t directly. A solution may be obtained by tedious iteration but, the best method is to use design tables or graphs.

The main problem with design tables or graphs is that there are many parameters to be considered. The best way to overcome this problem is to non-dimensionalise the design Equation 6.28 thus reducing the number of variables that have to be tabulated. In the following the general form of the equation will be non-dimensionalised, which includes incomplete gusset plates.

Consider the general gusset plate as shown in Figure 8.1. The ultimate load P_u is given by Equation 6.28 which is reproduced below

$$P_u s = \sum_{i=1}^{n} f_{bi} t . w_i dw$$

Divide both sides by $1.W^2E$ to non dimensionalise gives

$$\frac{P_u s}{1.W^2E} = \sum_{i=1}^{n} \frac{f_{bi}}{E} \cdot \frac{t}{1} \cdot \frac{w_i}{W} \cdot \frac{dw}{W} \qquad (8.3)$$

Consider $\frac{dw}{W}$

now from Equation 6.31

$$dw = (W - C)/n$$

therefore

$$\frac{dw}{W} = \frac{1}{n}(1 - C/W) \qquad (8.4)$$

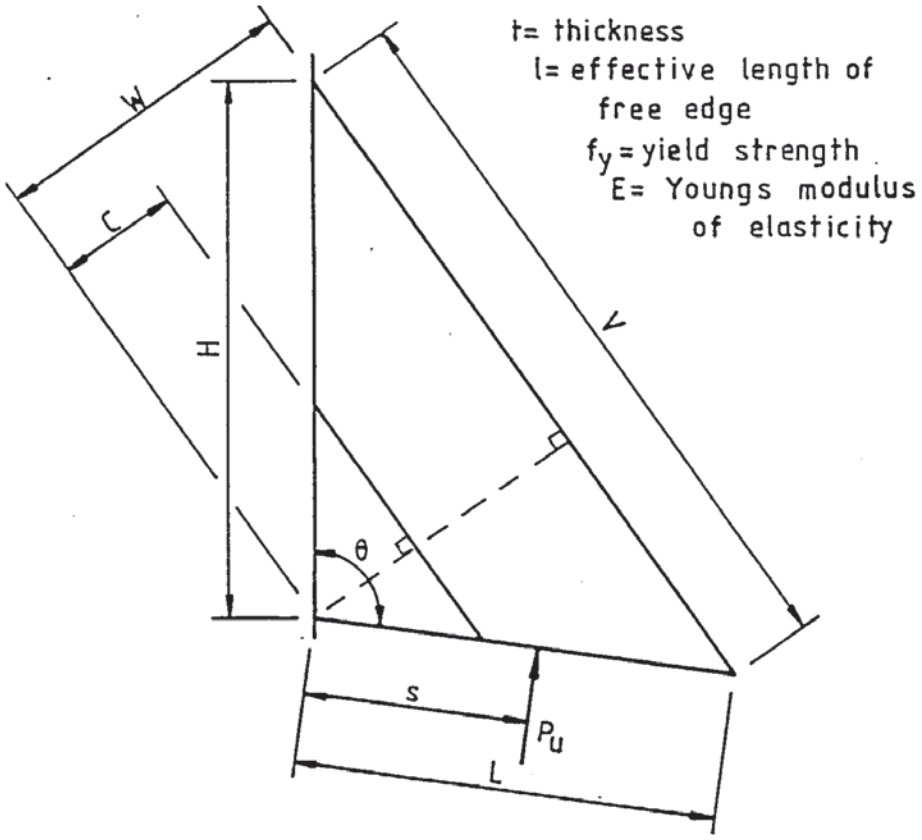

Figure 8.1 General gusset plate.

Consider $\frac{w_i}{W}$

now from Equation 6.30

$$w_i = C + dw(1/2 + (i - 1))$$

therefore

$$\frac{w_i}{W} = \frac{C}{W} + \frac{dw}{W}(1/2 + (i - 1)) \qquad (8.5)$$

Consider $\frac{f_{bi}}{E}$

now from Equation 6.23(a)

$$f_{bi} = f_{2i} - \sqrt{f_{2i}^2 - f_y f_{ei}}$$

therefore

$$\frac{f_{bi}}{E} = \frac{f_{2i}}{E} - \sqrt{\left(\frac{f_{2i}}{E}\right)^2 - \frac{f_y}{E}\frac{f_{ei}}{E}} \qquad (8.6)$$

Consider $\frac{f_{ei}}{E}$

now from Equation 6.23(b)

$$f_{ei} = \frac{\pi^2}{12} E\left(\frac{t}{l_i}\right)^2$$

therefore

$$\frac{f_{ei}}{E} = \frac{\pi^2}{12}\left(\frac{t}{l_i}\right)^2 \qquad (8.7)$$

Consider $\frac{t}{l_i}$

now from Equation 6.29

$$l_i = Z.w_i \tan\theta/2 \ , \quad \theta > 90^o$$

where

$$Z = [V/(2.W.\tan\theta/2) - 1)C/W + 1$$

also from this equation

$$l = Z.W.\tan\theta/2 \ , \quad \theta > 90^o$$

therefore

$$l_i = l\frac{w_i}{W}$$

therefore

$$\frac{t}{l_i} = \frac{t}{l}\left(\frac{W}{w_i}\right) \qquad (8.8)$$

Consider $\frac{f_{2i}}{E}$

now from Equation 6.23(c)

$$f_{2i} = [f_y + (\eta_i + 1)f_{ei}]/2$$

therefore

$$\frac{f_{2i}}{E} = \left[\frac{f_y}{E} + (\eta_i + 1)\frac{f_{ei}}{E}\right]\frac{1}{2} \qquad (8.9)$$

Consider η_i

now from Equation 6.23(d)

$$\eta_i = 0.001a(\lambda_i - \lambda_o) \quad \text{but} < 0$$

Consider λ_i

now from Equation 6.23(e)

$$\lambda_i = \left(\frac{l_i}{t}\right)\sqrt{12}$$

Consider λ_o

now from Equation 6.23(f)

$$\lambda_o = 0.2\pi\sqrt{\left(\frac{E}{f_y}\right)}$$

From the above equation it can be seen that the ratio $P_u.s/l.W^2.E$ on the left hand side is related to the ratio f_y/E, C/W and t/l on the right hand side. Further examination shows that if Equation 6.28 is divided through by $l.W^2fy$ instead of $l.W^2E$, then $P_u.s/l.w^2.fy$ can be related to f_y/E, C/W and t/l. Now only a total of three variables can be presented on one table or graph. Therefore, if only complete gusset plates are required, then $P_u.s/l.W^2.E$ or $P_u.s/l.W^2.fy$ can be related to f_y/E for values of t/l. Alternatively, as f_y/E is a materials factor, a table can be produced for a specific material relating $P_u.s/l.W^2.E$ or $P_u.s/l.W^2.f_y$ to C/W for values of t/l. As E is taken to be constant for steel with different yield strengths, then f_y/E can be replaced with f_y in the appropriate units. If a table is produced for a specific system of units then the E or f_y on the left hand side can be replaced by actual values so that the non-dimensional value $P_u.s/l.W^2E$ or $P_u.s/l.W^2.E$ can be replaced by the dimensional value $P_u.s/l.W^2$.

For example, consider a general gusset plate as shown in Figure 8.1. The thickness t of the gusset plate is required and θ,H,L,C,s,f_y,E and P_u are known from other considerations. V,W and l are required and are obtained using the following equation

$$V = \sqrt{L^2 + H^2 - 2.L.H.\cos\theta}$$

$$W = \frac{L.H.\sin\theta}{V}$$

$$l = \{[V/(2.W.\tan\theta/2) - 1]C/W + 1\}W.\tan\theta/2, \text{ but } \theta > 90^o \qquad (8.10)$$

With these the non-dimensional values $P_u.s/l.W^2.E$ or $P_u.s/l.W^2.f_y$, f_y/E, C/W can be calculated and used with the appropriate table to give t/l.

Table 8.1 is a non-dimensional table relating $P_u.s/l.W^2.E$ to C/W

$\frac{P_u.s}{l.W^2.E}$ (x 10^{-6})	t/l values (x 10^{-3}) C/W ratio										$\frac{P_u.s}{l.W^2.}$ (N/mm^2)
	0.0	0.1	0.2	0.3	0.4	0.5	0.6	0.7	0.8	0.9	
0.25	5.53	5.75	6.22	6.76	7.36	8.06	9.92	10.08	11.86	15.49	0.052
0.50	7.35	7.56	8.06	8.70	9.45	10.34	11.44	12.94	15.27	20.12	0.103
0.75	8.71	8.91	9.43	10.13	10.98	12.00	13.28	15.04	17.78	23.63	0.154
1.00	9.85	10.05	10.57	11.32	12.24	13.37	14.80	16.77	19.88	26.65	0.206
2.00	13.38	13.59	14.14	14.99	16.11	17.55	19.43	22.10	26.48	36.92	0.412
3.00	16.17	16.37	16.96	17.89	19.15	20.82	23.08	26.36	31.97	46.43	0.618
4.00	18.59	18.81	19.43	20.43	21.83	23.71	26.32	30.20	37.10	55.93	0.824
6.00	22.91	23.14	23.84	24.99	26.64	28.96	32.27	37.43	47.12	75.17	1.236
8.00	26.85	27.11	27.89	29.20	31.14	33.90	37.97	44.51	57.18	94.59	1.648
10.00	30.63	30.91	31.78	33.27	35.50	38.74	43.61	51.61	67.34	114.06	2.060
12.00	34.32	34.63	35.60	37.28	39.83	43.57	49.27	58.75	77.56	133.53	2.472
14.00	37.99	38.33	39.39	41.28	44.15	48.42	54.97	65.94	87.81	152.98	2.884
16.00	41.65	42.02	43.19	45.27	48.48	53.28	60.68	73.15	98.08	173.47	3.296
20.00	48.99	49.44	50.82	53.30	57.19	63.05	72.18	87.63	118.64	216.84	4.120
25.00	58.25	58.78	60.43	63.41	68.13	75.34	86.60	105.76	144.38	271.05	5.150
30.00	67.58	68.20	70.14	73.62	79.14	87.65	101.05	123.90	171.67	325.26	6.180
40.00	86.43	87.24	89.75	94.28	101.48	112.62	130.39	161.70	228.89	433.68	8.240
50.00	105.54	106.53	109.64	115.27	124.25	138.27	161.05	201.96	286.11	542.11	10.300
60.00	124.93	126.12	129.86	136.66	147.58	164.84	193.13	242.35	343.33	650.53	12.360
80.00	164.82	166.47	171.67	181.10	196.19	219.73	257.50	323.14	457.78	867.38	16.480
100.00	206.00	208.08	214.58	226.37	245.24	274.67	321.87	403.92	572.22	1084.23	20.600
120.00	247.20	249.70	257.50	271.65	294.29	329.60	386.25	484.71	686.67	1301.05	24.720
140.00	288.40	291.31	300.42	316.92	343.33	384.53	450.62	565.49	801.12	1517.92	28.840
160.00	329.60	332.93	343.33	362.20	392.38	439.47	515.00	646.28	915.55	1734.79	32.960

Table 8.1 Relating $P_u.s/l.W^2.E$ and $P_u.s/l.W^2$ to C/W for values of t/l for a value of f_y/E = 0.9709×10^{-3}, which corresponds to a steel of f_y = 200N/mm^2 and E = 206kN/mm^2. Robertson constant a = 5.5.

$\frac{P_u.s}{l.W^2.E}$ ($\times 10^{-6}$)	t/l values ($\times 10^{-3}$) yield stress (N/mm^2)												$\frac{P_u.s}{l.W^2}$ (N/mm^2)
	180.0	200.0	220.0	240.0	260.0	280.0	300.0	320.0	340.0	360.0	380.0	400.0	
0.25	5.62	5.53	5.46	5.39	5.34	5.29	5.25	5.20	5.17	5.13	5.10	5.08	0.052
0.50	7.48	7.35	7.23	7.14	7.05	6.98	6.91	6.85	6.80	6.75	6.70	6.66	0.103
0.75	8.88	8.71	8.56	8.44	8.33	8.25	8.15	8.07	8.00	7.94	7.88	7.83	0.154
1.00	10.06	9.85	9.67	9.52	9.39	9.28	9.17	9.08	9.00	8.92	8.85	8.79	0.206
2.00	13.73	13.38	13.09	12.85	12.63	12.45	12.29	12.14	12.01	11.89	11.79	11.69	0.412
3.00	16.66	16.17	15.76	15.42	15.14	14.89	14.67	14.47	14.30	14.14	14.00	13.87	0.618
4.00	19.23	18.59	18.08	17.64	17.28	16.96	16.69	16.45	16.23	16.04	15.86	15.70	0.824
6.00	23.85	22.91	22.15	21.52	21.00	20.55	20.16	19.82	19.52	19.25	19.01	18.80	1.236
8.00	28.14	26.85	25.83	24.99	24.30	23.71	23.20	22.76	22.37	22.03	21.72	21.45	1.648
10.00	32.29	30.63	29.31	28.25	27.37	26.63	25.99	25.45	24.97	24.55	24.17	23.83	2.060
12.00	36.38	34.32	32.70	31.38	30.30	29.40	28.63	27.97	27.40	26.89	26.45	26.05	2.472
14.00	40.45	37.99	36.03	34.46	33.16	32.08	31.17	30.39	29.72	29.13	28.60	28.14	2.884
16.00	44.54	41.65	39.35	37.50	35.98	34.71	33.65	32.74	31.96	31.27	30.67	30.14	3.296
20.00	52.74	48.99	46.00	43.56	41.57	39.91	38.51	37.32	36.30	35.41	34.64	33.96	4.120
25.00	63.06	58.25	54.36	51.19	48.56	46.37	44.52	42.95	41.60	40.44	39.42	38.53	5.150
30.00	73.47	67.58	62.81	58.89	55.62	52.88	50.56	48.58	46.88	45.41	44.13	43.00	6.180
40.00	94.52	86.43	79.88	74.48	69.94	66.10	62.81	59.99	57.54	55.41	53.55	51.92	8.240
50.00	115.92	105.54	97.17	90.26	84.45	79.53	75.28	71.62	68.41	65.61	63.14	60.96	10.300
60.00	137.77	124.93	114.64	106.19	99.11	93.09	87.90	83.39	79.45	75.98	72.90	70.17	12.360
80.00	183.11	164.82	150.31	138.58	128.82	120.55	113.44	107.25	101.84	97.05	92.79	88.98	16.480
100.00	228.89	206.00	187.27	171.80	159.11	148.45	139.34	131.44	124.52	118.41	112.97	108.10	20.600
120.00	274.67	247.20	224.73	206.00	190.15	176.89	165.63	155.93	147.46	140.00	133.35	127.42	24.720
140.00	320.44	288.40	262.18	240.34	221.85	206.00	192.40	180.76	170.67	161.79	153.94	146.90	28.840
160.00	366.22	329.60	299.65	274.67	253.54	235.43	219.73	206.05	194.21	183.86	174.72	166.55	32.960
	0.8738	0.9709	1.0680	1.1651	1.2621	1.3592	1.4563	1.5534	1.6505	1.7476	1.8447	1.9418	
	fy/E values ($\times 10^{-3}$)												

Table 8.2 Relating $P_u.s/l.W^2.E$ and $P_u.s/l.W^2$ to f_y/E and f_y for values of t/l for complete gusset plates. E = 206kN/mm^2 for dimensioned values. Robertson constant a = 5.5.

for values of t/l for one value of $f_y/E = 970.87 \times 10^{-6}$, which corresponds to a steel of $f_y = 200$ N/mm^2 and $E = 206$ kN/mm^2. This table is also dimensionalised by multiplying all the $P_u.s/l.W^2.E$ values by E giving $P_u.s/l.W^2$ values in N/mm^2. A separate table is required for each value of f_y/E.

If only complete gusset plates are considered then l is simplified to

$$l = W.\tan\theta/2 \quad \text{but } \theta \geqslant 90^o \qquad (8.11)$$

Table 8.2 is a non-dimensional table relating $P_u.s/l.W^2.E$ to f_y/E for values of t/l. Also included in Table 8.2 are the dimensional values relating $P_u.s/l.W^2$ to f_y for $E = 206$ kN/mm^2.

Both Tables 8.1 and 8.2 are produced using a value of the Robertson constant a=5.5 which is in agreement with that given for welded plate or I section up to 40 mm as given in Table 6.2.1 of the British draft steel code (2). Also the value of $f_y = 200$ N/mm^2, used for Table 8.1, is the design stress for grade 43A welded plate up to and including 40 mm thickness, $p_y = (220 - 20)$ N/mm^2. 220 N/mm^2 from Table 5.7.1 of the code and 20 N/mm^2 from Section 6.2.1 of the code and note 2 Table 6.2.1 of the code.

As a Robertson constant of a = 5.5 is used, then the slenderness of a gusset plate as defined by Equation 6.35 is limited to 160, which when rearranged gives

$$t/l \geqslant 21.65 \times 10^{-3} \qquad (8.12)$$

The limit is indicated on both Tables 8.1 and 8.2. Any value less than this will not satisfy the author's serviceability requirements concerning out of plane deflections.

As for the in plane deflections, the ultimate load used to obtain the gusset plate thickness can be used in Equations 6.32 and 6.34 together with Equation 6.33 to give the deflection rates at the load points or the moment rotation rate, respectively as required. If the selected gusset plate thickness is different from that obtained from

the table, then the table should be used in reverse to obtain a value of P_u to be used in Equations 6.32 and 6.34.

8.4 Designing the loaded and supported edge welds

8.4.1 Design considerations

From the analysis of the experimental results it is apparent that the function of the loaded and supported edge welds is to prevent the gusset plate slipping from between the two edges. Therefore, they are mainly subjected to longitudinal shear forces, which are relatively low. Usually in design the frictional forces are not taken into account as they are not easily determined, and so they are used as reserve strengths. However, with the gusset plates in compression they are of an appreciable amount so they may be taken into account.

The experimental results indicated that it is not necessary to consider the direct load as it can be assumed to be transmitted directly through edge contact. It is also not necessary to design the welds for rotational restraint of the gusset plate.

A gusset plate and its welds can be designed with no weld or part welds along one edge.

The theory for the welds is related to that of the gusset plates which is based upon the ultimate load. From the analysis of the welds this is the worst possible condition.

8.4.2 Design tables

For the design of the welds it is necessary to obtain a value for the resultant reaction R'. Now $P_u.s=R'w$, therefore R' can be treated in exactly the same way as for P_u. The equivalent equation to Equation 6.28 is

$$R' = \sum_{i=1}^{n} f_{bi} t.dw \qquad (8.13)$$

Similarly a non-dimensional form can be obtained by dividing both sides by 1.W.E to give

R'/l.W.E (x 10^{-6})	t/l values (x 10^{-3}) C/W ratio 0.0	0.1	0.2	0.3	0.4	0.5	0.6	0.7	0.8	0.9	R'/l.W (N/mm^2)
1.00	4.96	6.33	7.65	8.93	10.25	11.70	13.42	15.66	19.03	26.06	0.206
2.00	7.17	8.64	10.16	11.72	13.39	15.26	17.53	20.53	25.23	35.94	0.412
3.00	8.94	10.49	12.13	13.89	15.81	18.00	20.70	24.37	30.31	45.00	0.618
4.00	10.48	12.10	13.86	15.77	17.89	20.37	23.47	27.77	35.00	54.01	0.824
6.00	13.17	14.93	16.90	19.09	21.58	24.58	28.45	34.06	44.05	72.25	1.236
8.00	15.57	17.46	19.63	22.08	24.93	28.44	33.11	40.10	53.08	90.68	1.648
10.00	17.78	19.82	22.19	24.90	28.12	32.16	37.65	46.11	62.18	109.17	2.060
12.00	19.90	22.06	24.64	27.62	31.21	35.80	42.17	52.15	71.36	127.67	2.472
16.00	23.90	26.38	29.35	32.91	37.30	43.06	51.24	64.34	89.80	164.96	3.292
20.00	27.74	30.55	33.96	38.12	43.36	50.34	60.38	76.61	108.30	206.00	4.120
30.00	37.14	40.86	45.42	51.17	58.61	68.70	83.42	107.42	154.97	309.00	6.180
40.00	46.53	51.23	57.02	64.37	73.98	87.16	106.54	138.56	206.00	412.00	8.240
50.00	56.01	61.73	68.80	77.77	89.58	105.89	130.20	171.67	257.50	515.00	10.300
60.00	65.57	72.33	80.70	91.36	105.44	125.06	154.74	206.00	309.00	618.00	12.360
80.00	84.90	93.80	104.86	119.04	137.97	164.83	206.00	274.67	412.00	824.00	16.480
100.00	104.51	115.61	129.49	147.43	171.67	206.00	257.50	343.33	515.00	1030.00	20.600
120.00	124.36	137.76	154.62	176.57	206.00	247.20	309.00	412.00	618.00	1236.00	24.720
140.00	144.44	160.27	180.25	206.00	240.33	288.40	360.50	480.67	721.01	1442.02	28.840
160.00	164.81	183.11	206.00	235.43	274.67	329.60	412.00	549.33	824.00	1648.05	32.960
180.00	185.40	206.00	231.75	264.86	309.00	370.80	463.50	618.00	927.00	1854.01	37.080
200.00	206.00	228.89	257.50	294.29	343.33	412.00	515.00	686.67	1030.01	2060.07	41.200
220.00	226.63	251.78	283.25	323.71	377.67	453.20	566.50	755.33	1133.03	2266.07	45.320
260.00	267.77	297.56	334.75	382.57	446.33	535.60	669.50	892.68	1339.02	2677.91	53.560
300.00	309.04	343.34	386.25	441.43	515.00	618.00	772.50	1030.02	1545.05	3090.10	61.800

Table 8.3 Relating R'/l.W.E and R'/l.W to C/W for values of t/l for a value of $f_y/E = 0.9709 \times 10^{-3}$, which corresponds to a steel of $f_y = 200 N/mm^2$ and $E = 206 kN/mm^2$. Robertson constant a = 5.5.

$\frac{R'}{1.W.E}$ ($\times 10^{-6}$)	t/l values ($\times 10^{-3}$) yield stress (N/mm^2)												$\frac{R'}{1.W}$ (N/mm^2)
	180.0	200.0	220.0	240.0	260.0	280.0	300.0	320.0	340.0	360.0	380.0	400.0	
1.00	5.13	4.96	4.81	4.68	4.56	4.45	4.36	4.27	4.20	4.12	4.06	3.99	0.206
2.00	7.45	7.17	6.94	6.73	6.54	6.39	6.25	6.12	6.00	5.89	5.79	5.70	0.412
3.00	9.30	8.94	8.64	8.37	8.14	7.93	7.74	7.57	7.42	7.28	7.15	7.04	0.618
4.00	10.92	10.48	10.11	9.79	9.51	9.26	9.04	8.83	8.65	8.48	8.33	8.19	0.824
6.00	13.77	13.17	12.68	12.25	11.88	11.55	11.26	11.00	10.77	10.55	10.35	10.17	1.236
8.00	16.31	15.57	14.95	14.42	13.96	13.56	13.21	12.89	12.60	12.34	12.10	11.88	1.648
10.00	18.70	17.78	17.03	16.40	15.86	15.39	14.97	14.60	14.26	13.96	13.68	13.42	2.060
12.00	20.98	19.90	19.01	18.27	17.64	17.09	16.61	16.18	15.80	15.45	15.13	14.85	2.472
16.00	25.33	23.90	22.74	21.78	20.96	20.25	19.65	19.11	18.63	18.19	17.80	17.44	3.296
20.00	29.55	27.74	26.29	25.10	24.09	23.22	22.47	21.81	21.23	20.72	20.25	19.82	4.120
30.00	39.98	37.14	34.87	33.01	31.46	30.17	29.05	28.09	27.24	26.48	25.81	25.20	6.180
40.00	50.46	46.53	43.36	40.78	38.64	36.84	35.30	33.99	32.85	31.84	30.95	30.15	8.240
50.00	61.05	56.01	51.93	48.60	45.81	43.48	41.50	39.79	38.31	37.02	35.88	34.87	10.300
60.00	71.72	65.57	60.59	56.47	53.05	50.16	47.69	45.58	43.75	42.15	40.74	39.49	12.360
80.00	93.33	84.90	78.07	72.44	67.71	63.70	60.26	57.30	54.71	52.45	50.46	48.71	16.480
100.00	115.28	104.51	95.80	88.61	82.57	77.43	73.02	69.20	65.85	62.91	60.32	58.01	20.600
120.00	137.57	124.36	113.69	104.93	97.57	91.31	85.93	81.24	77.14	73.53	70.31	67.46	24.720
140.00	160.22	144.44	131.80	121.40	112.70	105.31	98.94	93.39	88.55	84.25	80.44	77.03	28.840
160.00	183.11	164.81	150.08	138.04	127.96	119.40	112.04	105.64	100.03	95.06	90.65	86.68	32.960
180.00	203.00	185.40	168.59	154.80	143.33	133.59	125.23	117.96	111.57	105.95	100.92	96.43	37.080
200.00	228.90	206.00	187.27	171.73	158.81	147.89	138.49	130.34	123.20	116.87	111.26	106.21	41.200
220.00	251.78	226.63	206.00	188.83	174.42	162.25	151.84	142.79	134.87	127.86	121.64	116.05	45.320
260.00	297.65	267.77	243.45	223.18	206.00	191.32	178.75	167.89	158.38	149.99	142.53	135.84	53.560
300.00	343.25	309.04	280.91	257.53	237.68	220.73	205.99	193.23	182.11	172.30	163.58	155.78	61.800
	0.8738	0.9709	1.0680	1.1651	1.2621	1.3592	1.4563	1.5534	1.6505	1.7476	1.8447	1.9418	
	fy/E values ($\times 10^{-3}$)												

Table 8.4 Relating R'/1.W.E and R'/1.W to fy/E and fy for values of t/l for complete gusset plates. E = 206kN/mm^2 for dimensioned values. Robertson constant a = 5.5.

$$\frac{R'}{l.W.E} = \sum_{i=1}^{n} \frac{f_{bi}}{E} \frac{t}{l} \frac{dw}{W} \qquad (8.14)$$

This equation can be treated in the same way as Equation 8.3, with $R'/l.W.E$ or $R'/l.W.f_y$ being related to f_y/E or f_y, C/W and t/l. Similar tables as described in Section 8.3.4 for P_u, can be obtained to give R' for designing the welds. Tables 8.3 and 8.4 are such tables which are equivalent to Tables 8.1 and 8.2 for P_u.

The shear force in the loaded edge is given by Equation 7.19. The factor 'γ_1' is obtained from Equation 7.18 which for complete gusset plates reduces to Equation 7.16. The loaded edge weld size is then given by Equation 7.20. The supported edge weld size is given by similar equations. The ultimate shear strength of the welds is given in BS 5400 Part 3 (16).

8.5 Designing the loaded plates

8.5.1 Design considerations

Where the loaded plate is continuous as in the base plate of a column then its thickness will also be governed by other considerations. Therefore its thickness will only require checking concerning the shear and tensile forces induced in it by the gusset plate. The shear force is likely to be negligible in relation to the tensile force especially with a distributed load.

Where the loaded plate is part of a bracket which is welded to a column, then its thickness and the weld connecting it to the column will have to be checked. If the load is close in or at the end of the loaded plate then the shear may have to be considered if the applied load is high. However, under distributed loading this may not be necessary and only the tensile forces need be considered. Preferably the weld should be applied on the loaded side of the bracket loaded plate. The loaded plate thickness obtained from the theory should be used as a check, the thickness of the loaded plate is usually

determined by other practical consideratons. Where the load is applied towards the outer end of the loaded plate then the thickness should be increased so that it is relatively stiff in relation to the gusset plate thickness. Further work is required to determine a theoretical way of determining this.

8.5.2 Design loads

The shear and axial forces in the loaded plate and its weld at the supported edge are given by Equations 7.21 and 7.23 respectively. These equations are based on the ultimate load and the gusset plate resultant reaction R' as obtained in Section 8.4.2 and given in Tables 8.3 and 8.4.

CHAPTER NINE

CONCLUSIONS AND RECOMMENDATIONS FOR FUTURE WORK

9.1 General

The conclusions presented below are drawn from the main test programme of 82 triangular steel gusset plates and numerous subsidiary tests. The subsidiary tests included 47 strut tests to investigate the buckling characteristics, 15 special gusset plates to test the assumptions made in the theoretical work and a series of 22 similar gusset plates with varying welds connecting the gusset plate to the adjacent loaded and supported plates.

9.2 Gusset plate tests

The following conclusions are based on the gusset plate tests.

1. Gusset plates fail in an elastic-plastic buckling manner. The buckling progresses from the outer free edge towards the inside corner. The ultimate load is considerably higher than the load at which the free edge starts to buckle.

2. Provided the loaded plate is adequately fixed to the supported plate and it is stiff enough to distribute the load to the gusset plate, then the gusset plate has a specific moment of resistance capacity about its inside corner.

3. The effect of increasing the size of a gusset plate for a given thickness, is to increase its moment capacity until an optimum point is reached.

4. The moment capacity of a gusset plate increases as H/L increases until an optimum is reached when $H/L \simeq 1.25$.

5. For a given gusset plate the ultimate load, applied as either distributed or point load perpendicular to the loaded plate, is dependent upon the position of its resultant from the supported edge.

6. The loaded plate does not provide any significant moment of resistance to the applied load at failure. It is important, however, in distributing the load and providing lateral, longitudinal and rotational fixity of the loaded edge.

7. The moment capacity of a gusset plate increases as its thickness increases, but the relationship is not linear as it is related to the slenderness of a gusset plate.

8. The removal of small portions of the inside corner of a gusset plate parallel to the free edge has little effect upon its moment capacity. For large portions the moment capacity decreases significantly, especially with slender gusset plates.

9. For a constant width and thickness, the moment capacity of a slender gusset plate increases as its internal angle decreases from 90 degrees. The amount of increase is dependent upon its slenderness. Any increase in the internal angle from 90 degrees produces little change in moment capacity.

10. The main function of the loaded and supported edge welds is to prevent the gusset plate slipping from between the respective plates. The frictional forces along these edges are very high.

11. The lateral deflection characteristics of the free edge of a gusset plate are related to its slenderness ratio. With non-slender gusset plates the deflections are consistent and relatively small for most of the loading. With slender gusset plates the deflections vary considerably and are influenced by the initial lateral deflections, the load position and the loaded plate thickness. In some cases the deflections start from the initial loading, in others they change direction.

9.2.1 Existing methods

The following conclusions are based on comparing the existing design methods with the experimental gusset plate results.

1. None of the existing methods can be used for gusset plates with the inside corner removed nor for gusset plates with an internal angle other than 90 degrees.

2. Jensen's method discussed in Section 5.2, does not take account of the effects of buckling and is therefore unsafe. The use of the limiting slenderness equation however, appears to safely restrict the use of the method. Generally the method is inaccurate especially with the variation in the load position.

3. Salmon's method discussed in Section 5.3, does take into account the effects of buckling. The method is discontinuous using two equations, one for yielding and the other for buckling. The various limiting slenderness equations which supersede the use of the buckling equation appear to safely restrict the use of the method. The method is not particularly accurate and does not take account of a variation in the load position, nor should it be used for $0.5 > H/L > 2.0$.

4. The beam method discussed in Section 5.4, assumes bending and not buckling and so is inaccurate and unsafe. The loaded plate is not usually considered, but when it is, it does not improve the accuracy of the method.

5. The four variations of the approximate strut method discussed in Section 5.5, do consider buckling but are inaccurate. Two variations do not take the load position into account and are very conservative, the other two do, but are unsafe for use with non-slender gusset plates.

6. The plastic design method discussed in Section 5.6, is only for use with gusset plates that fail plastically. The slenderness limitations appear to safely restrict the use of this method. The method is inaccurate especially with variations in the load position.

7. Martin's methods discussed in Section 5.7, do consider buckling. One method is used for all gusset plates, the other has a slenderness limitation. Martin included a term for the loaded plate, which if used renders the equations inaccurate and unsafe. However, if the term is excluded both equations are accurate and conservative within the limits of their use.

9.3 Proposed design methods

9.3.1 Gusset plate design

1. The proposed method assumes for analytical purposes a gusset plate consists of a series of fixed ended struts and moments of equilibrium are taken about the inside corner. (See Section 6.10).

2. The method is developed to incorporate any combination of the variables tested.

3. The Perry strut formula is used to determine the buckling stress of each strut, although any buckling equations could be adopted. (See Section 6.10.4).

4. With a value of the Robertson constant a =8 in the Perry strut formula the method safely predicts the ultimate load for all practical gusset plates. (See Section 6.11.3).

5. To satisfy the serviceability requirements regarding lateral deflections the slenderness ratio of a gusset plate, given

by equation 6.35, should be limited to 160. (See Section 6.12.2).

6. When the serviceability limit state is used then a value of a= 3.5 can be used to give a more accurate value for the ultimate load. For design purposes a value of a = 5.5 is in better agreement with values used in the British draft steel code (2). (See Section 8.3.1).

7. The nature of the Perry strut formula necessitated splitting a gusset plate into a finite number of strips and numerically summing their load carrying capacity. A reasonably accurate solution is obtained with as few as 4 strips and an accurate solution with 15 strips. (See Section 6.11.2.).

8. The solution, equation 6.2.8, expresses the ultimate load of a gusset plate in terms of its dimensions and material strength. In practice it is usually the gusset plate thickness that is required, the other parameters being known from other considerations.

9. The thickness of a gusset plate can be obtained from non-dimensional design tables or graphs. (See Section 8.3.4).

10. For complete gusset plates one design table or graph covers all the other parameters for various material strengths. (Table 8.1).

11. To cover all gusset plate parameters, a separate design table or graph is required for each material strength. (Table 8.2).

12. An approximate indication of the load deflection rate of the load point, or the moment rotation rate of the load point can be obtained using equations 6.32 to 6.34. (See Section 6.11.4).

9.3.2 Gusset plate weld design

1. The loaded and supported edge welds are subjected to shear forces from the gusset plate as given by equation 7.19 for the loaded edge and a similar equation for the supported edge.

2. The design of the loaded and supported edge welds are based on the strength, slenderness and completeness of the gusset plate. (See section 7.2.4).

3. The strength and slenderness of a gusset plate are represented by R', which is obtained fron non-dimensional design tables or graphs in a similar way to the gusset plate thickness. (See Section 8.4.4).

4. To account for the removal of the inside corner, the completeness of a gusset plate is represented by γ' given by equation 7.18 for the loaded edge and a similar equation for the supported edge. (See Section 7.2.4).

5. The frictional forces along the loaded and supported edges can be taken into account in design.

6. Discontinuous welds can be used along the loaded and supported edges.

9.3.3 Loaded plate design

1. Normally the thickness of the loaded plate is determined by other considerations and only requires checking for shear and axial load at its supported end using equations 7.2.1 and 7.2.3 respectively.

2. When the load is applied towards the free end of the loaded plate, then to prevent local deformation its thickness should be chosen so that it is relatively stiff in relation to the gusset plate thickness. Further work is necessary to accurately determine the correct thickness.

9.3.4 Loaded plate support weld design

1. Where the loaded plate is welded to the support, then the loaded plate support weld is designed to carry the same shear and axial loads as the loaded plate. (See Section 8.5.2).

9.4 Recommendations for future work

1. The behaviour of the loaded plates requires further investigation to determine the correct thickness to use in order to prevent its deformation when the load is applied towards its free end.

2. The effects of a load applied eccentrically from the plane of the gusset plate requires investigation. Out-of-plane moments may be applied to the loaded edge of the gusset plate, the magnitude of which may be related to the loaded plate stiffness.

3. The fatigue life of gusset plates requires investigation as they are used in fatigue loading situations such as in crane gantries.

4. The effect of lateral impact on a loaded gusset plate requires investigation as it may induce premature buckling.

5. The addition of stiffeners along the free edge requires investigation.

6. The use of rolled sections as an alternative to gusset plates for column bases and support brackets has received little attention.

7. The use of different materials such as aluminium requires investigation.

8. To cost when to use gussets on foundation bases.

NOTATION

a = Robertson constant

A = area of section

B = width of loaded plate

c = contact zone

c_t = tensile contact zone

c' = contact zone between supported edge and support plate

c'' = contact zone between loaded edge and loaded plate

C = width of gusset plate removed

d = lateral deflection of the free edge of a gusset plate

dv = total vertical deflection

dV = change in length of the free edge of a gusset plate

dV' = component of dV perpendicular to the loaded plate

dv_w = change in length of an element strut at a distance w from the inside corner of a gusset plate

dw = width of an elemental strut

D = depth of a column

e = eccentricity of applied load

e' = component of eccentricity of applied load

E = Young's modulus of elasticity

f_{avg} = average stress

f_b = buckling stress

f_{bc} = allowable bending stress

f_{bi} = buckling stress for strip i

f_{bw} = direct buckling stress acting on as elemental strut of width dw at a distance w from the inside corner of a gusset plate

f_{cr} = elastic critical stress

f_e = Euler buckling stress

f_{ei} = Euler buckling stress of strip i

f_{ew} = Euler buckling stress acting on an elemental strut of width dw at a distance w from the inside corner of a gusset plate

f_{max} = maximum stress

f_q = shear stress

f_y = yield stress

F_{fb} = frictional force along the supported edge of a gusset plate

F_{fl} = frictional force along the loaded edge of a gusset plate

F_h = shear force between the supported plate and the supported edge of a gusset plate

F_l = shear force between the loaded plate and the loaded edge of a gusset plate

F_{wh} = shear resistance of loaded edge weld

F_{wv} = shear resistance of supported edge weld

G = remaining width of a gusset plate after the inside corner removed

H = supported edge length of a gusset plate

k = elastic buckling constant

k' = an elastic buckling constant defined by Salmon

K = an elastic buckling constant defined by Salmon

l = effective length of a strut

li = effective length of strip i

lw = effective length of a strut at a perpendicular distance w from the inside corner of a gusset plate

L = loaded edge length of a gusset plate

M = bending moment

M_p = moment of resistance of loaded plate at its supported end

M_u = total ultimate moment of resistance

M_{ui} = ultimate moment of resistance produced by strip i

n = number of strips

p_c = allowable stress

p_y = ultimate limit state design stress

P = applied load

P_u = ultimate load applied to a gusset plate

P_u' = additional ultimate load to produce buckling failure when material is added to the free edge of a gusset plate

P' = perpendicular resultant reaction from the gusset plate to the support plate

P'' = perpendicular resultant reaction from the gusset plate to the loaded plate

Q = constant equal to the shear strength of a weld

r = radius of gyration

R = component of R' perpendicular to loaded plate

R_x = axial force in loaded plate at its supported end

R_y = shear force in loaded plate at its supported end

R' = resultant reaction of stress distribution assumed across critical section of a gusset plate

s = distance of resultant load Pu from the supported edge measured along the loaded edge

s' = distance of P' from inside corner

s'' = distance of P'' from inside corner

t = gusset plate thickness

t_w = leg length of a fillet weld

T = thickness of a loaded plate

v_w = length of an elemental strut at a distance w from the inside corner of a gusset plate

V = length of the free edge of a gusset plate

w = perpendicular distance from an elemental strut to the inside corner of a gusset plate

w_i = perpendicular distance from strip i to the inside corner of a gusset plate

$\overline{w}$ = perpendicular distance from R' to inside corner pf a gusset plate

W = width of a gusset plate measured perpendicular to the free edge of the gusset plate to the inside corner of a gusset plate

W' = width of aditional material added to the free edge, measured perpendicular to the free edge of a gusset plate

z = gusset plate completeness factor

z' = elastic section modulus

Z = ratio of average stress loaded edge to maximum stress free edge

α = angle between supported edge and free edge of a gusset plate

γ_1 = angle between the free edge and loaded edge of an equal sided gusset plate

γ_o = angle between the free edge and loaded edge

γ'_1 = transition angle between γ_o and γ_1 to take account of the removal of the inside corner of a gusset plate

ε_1 = surface strain

ε_2 = surface strain

ε_{yt} = surface strain at which tensile stress is reached

ε_{yc} = surface strain at which compressive yield stress is reached

η = Perry factor

η_i = Perry factor for strip i

θ = angle between supported edge and loaded edge of a gusset plate

λ = slenderness ratio

λ_i = slenderness ratio of strip i

λ_o = limiting slenderness ratio

μ = coefficient of friction

ν = Poisson's ratio

APPENDIX 1

During the course of the testing programme a new data logger was purchased and the author was required to write a suitable strain gauge acquisition and logging program for general use. In the process the author encountered numerous hardware and software faults which had to be overcome.

The data logger used is an Intercole Systems Limited Compulog Four. This machine is a computer controlled data acquisition and control system which may incorporate facilities for processing and evaluation of analogue and digital signals, status and data storage/retrieval. The system comprises of a main cabinet housing the central processing unit, two floppy disc drives and a digital volt meter. The computer is operated via the use of a visual display unit and a printer. A graph plotter is also available. The strain gauges are connected to the system via four remote connection boxes with 100 channels each.

The strain gauge reading part of the system is effectively a Wheatstone Bridge with a choice of quarter, half or full bridge configurations. The system is set up for half bridge configuration. That is the logger acts as one half, and the other half consists of the strain gauge to be read and a dummy gauge of a similar electrical resistance. The logger provides an energising constant current through both the dummy and the strain gauges. The logger measures the voltage difference between the two, which is a result of their different resistances. As the current is kept constant then the change in voltage is proportional to the change in resistance of the strain gauge. Now the rate of change in resistance of a strain gauge is proportional to the amount by which it has strained. Therefore the

change in voltage measured by the logger is proportional to the change in strain of the gauge.

i.e. $\Delta\varepsilon = \frac{\Delta V}{I.G.R.}$

where $\Delta\varepsilon$ = change in strain

ΔV = change in voltage

I = energising constant current

G = gauge factor

R = gauge resistance before straining.

For convenience a system of programs were developed for:

1. Preparation of strain gauge information relating to a specific test.
2. Experimental data acquisition during test.
3. Output data manipulation for plotting purposes.
4. Plotting of experimental data.

The first program is used to prepare a data file containing the following information about the test:

1. Data file number for retrieval purposes.
2. Title of experiment for identification.
3. The number of strain gauge types and deflation gauges. Any batch of consecutive strain gauges having the same gauge resistance, gauge factor and multiplying factor constitutes a type.
4. For each strain gauge type the first and last channel numbers, gauge resistance, gauge factor and Youngs modulus of elasticity.
5. For each deflection gauge the channel number and gauge factor.

6. The number of channels and channel numbers to be checked during the running of the test.

The second program is the main program which is run while the test is in progress. A general flow diagram of the program is given in Figure A.1.1. and a more detailed flow diagram in Figure A.1.2.

The user has the option of selecting a manual mode which allows the inspection of individual channels. The gauge information has to be entered at the terminal. This facility allows the continuous scan of a gauge, which is useful when there is a suspect gauge.

On auto control the information concerning the channels to be read is obtained from the appropriate pre-written channel data file. All channels are initially zeroed before the test commences. This process also acts as a form of gauge test . Faulty gauges can be inspected individually using the manual facility.

At each load increment, each channel is read and the data is stored on a pre-selected data file. The pre-selected channels for checking purposes can be inspected or any other specific channel not included in the selection. At the end of the test the recorded data is converted into stress, strain or defection whichever is appropriate for each load increment and output in tabular form. This information can be retrieved at any time from the data file.

The third program is used to extract from the experimental data specific information for plotting purposes. This allows the plotting of load increment against stress, strain or defection as required for

any selection of gauges. The program produces a data file which can be read by the graph plotting program.

The fourth program is a general purpose graph plotting program that is used to plot graphs given the x-y co-ordinates on a data file. Most of the graphs presented in this thesis are drawn using this program.

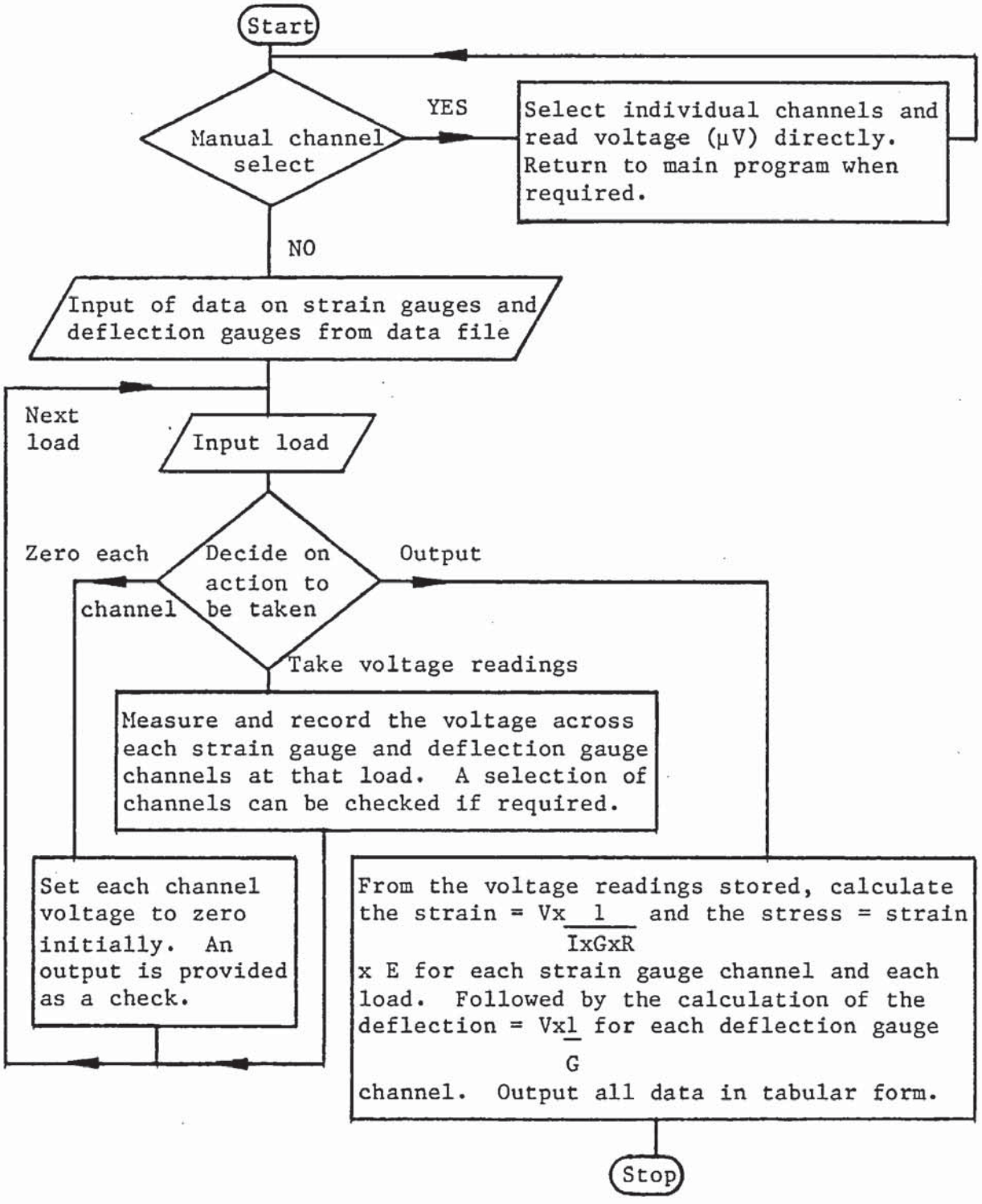

Figure A.1.1 General flow diagram of strain gauge acquisition and logging program

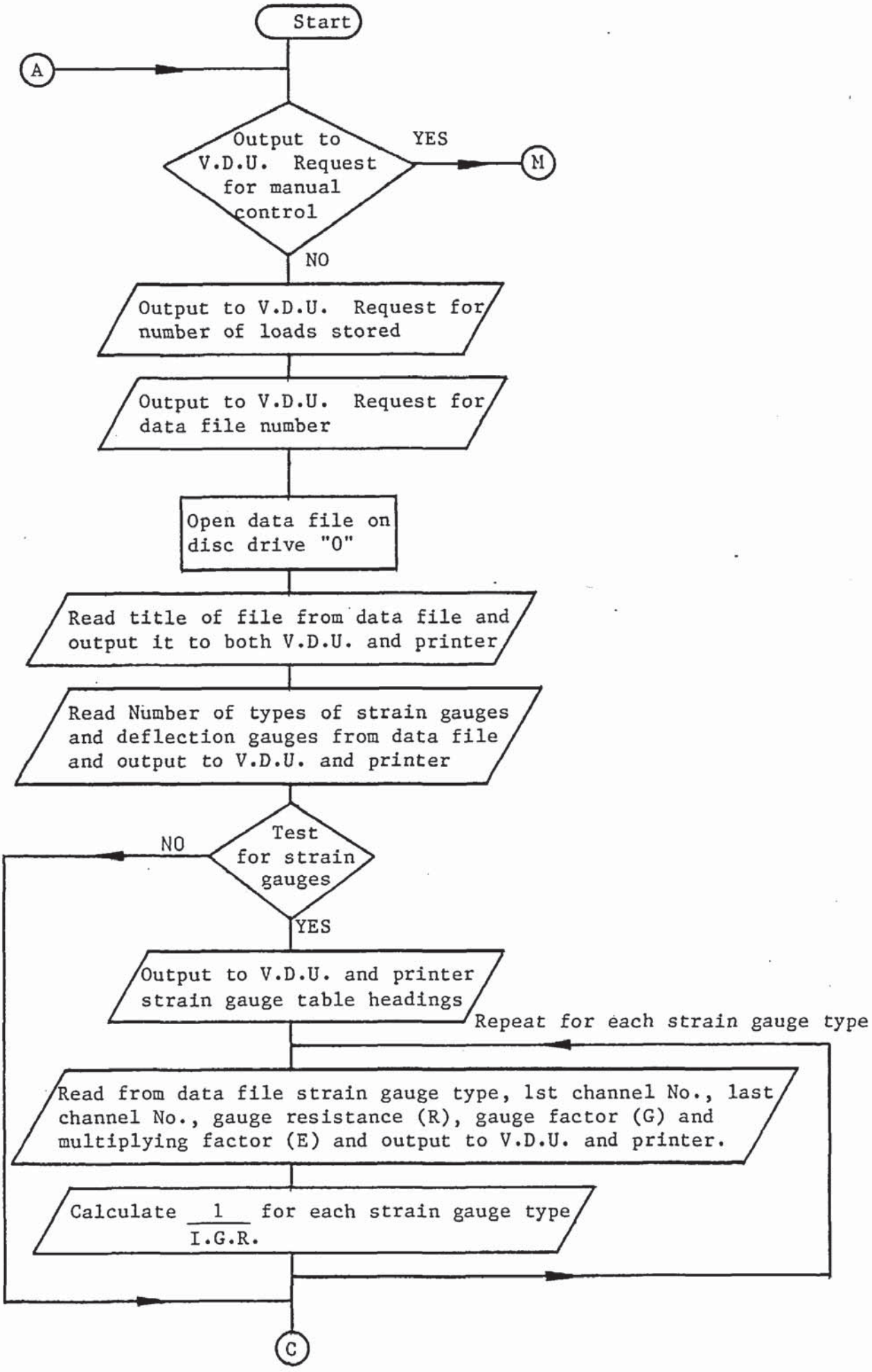

Figure A.1.2 Detailed flow diagram of strain gauge acquisition and logging program

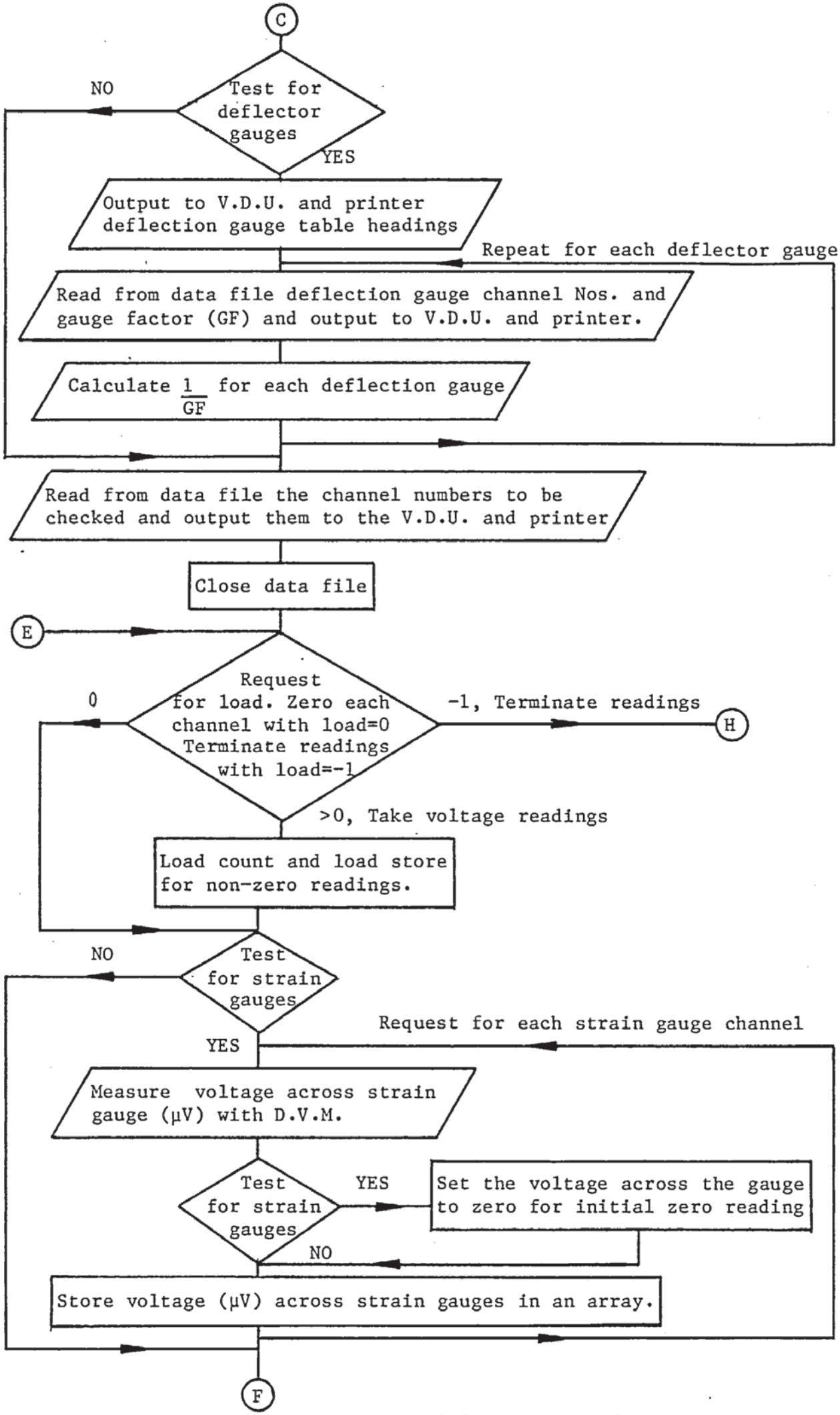

Figure A.1.2 Continued

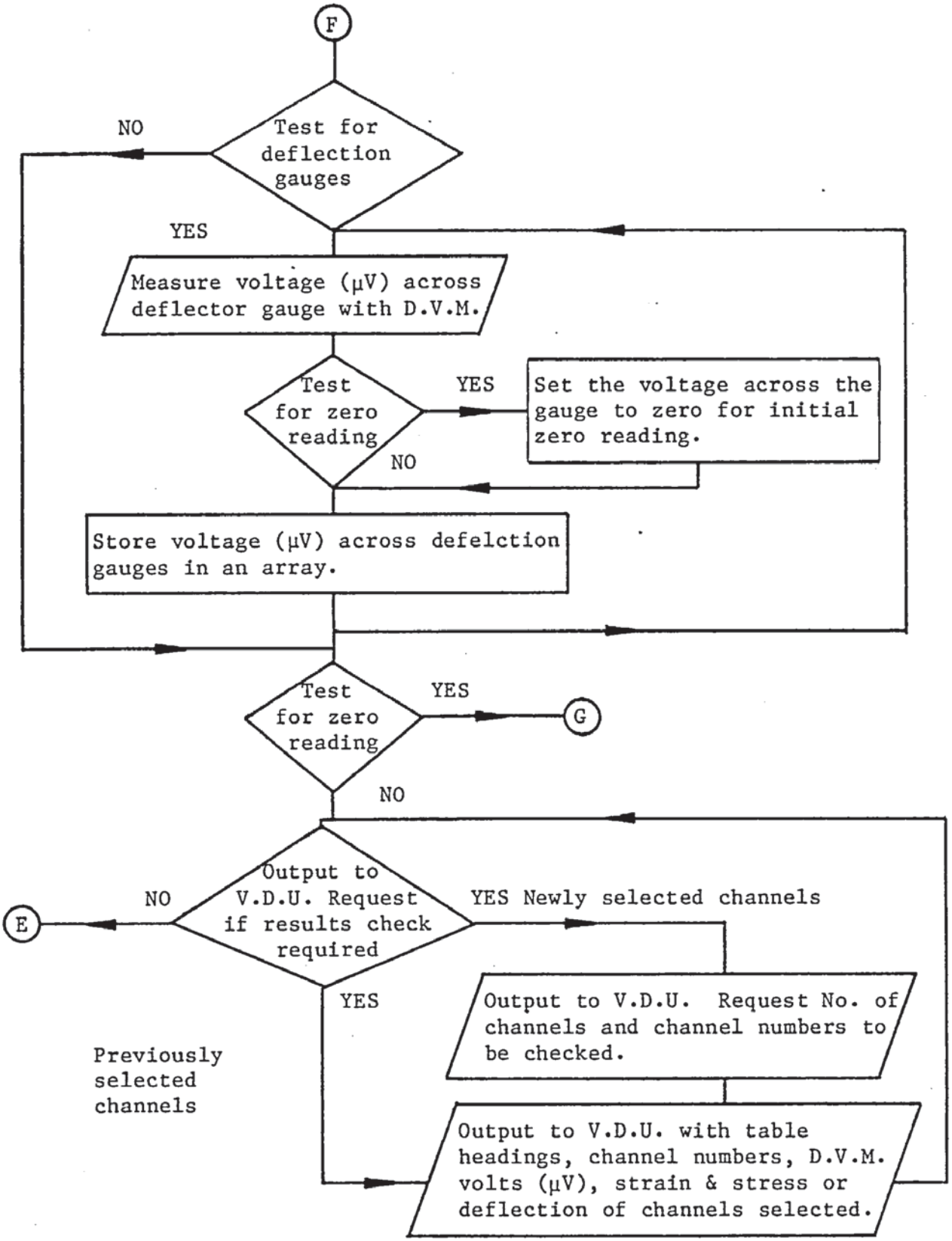

Figure A.1.2 Continued

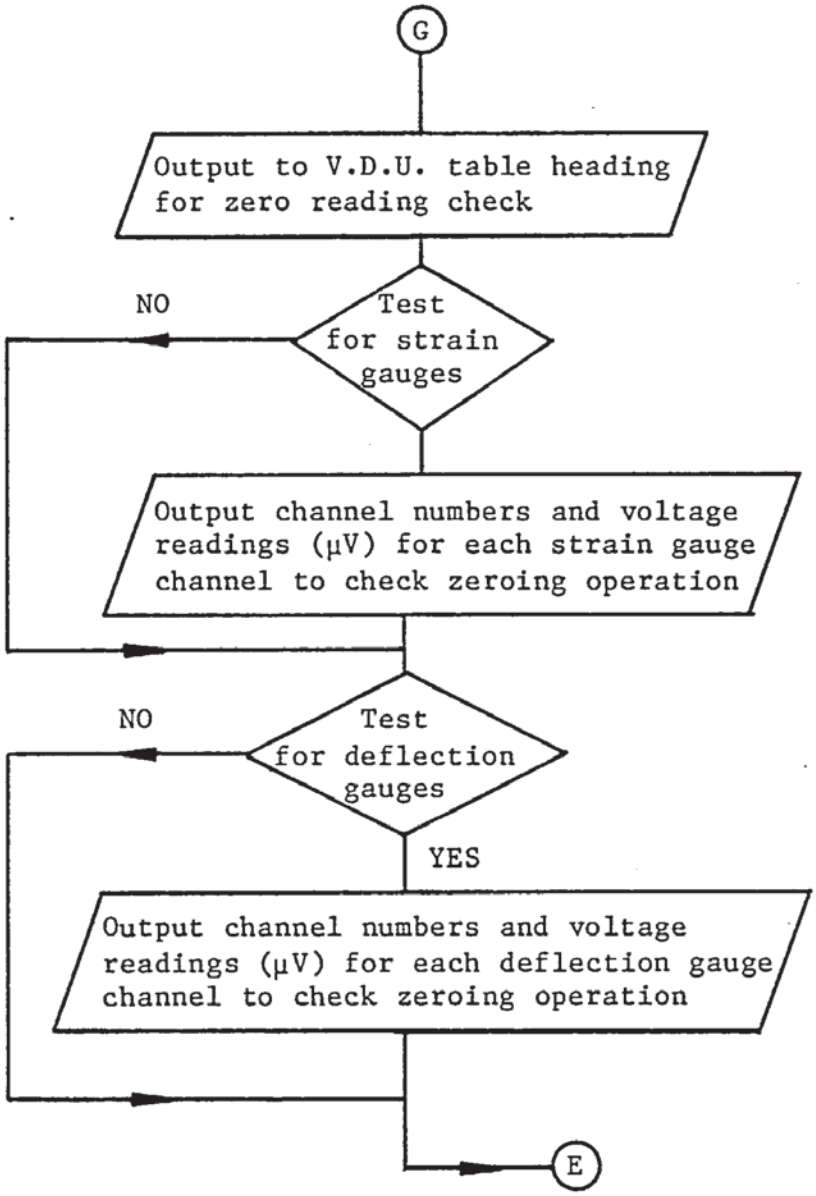

Figure A.1.2 Continued

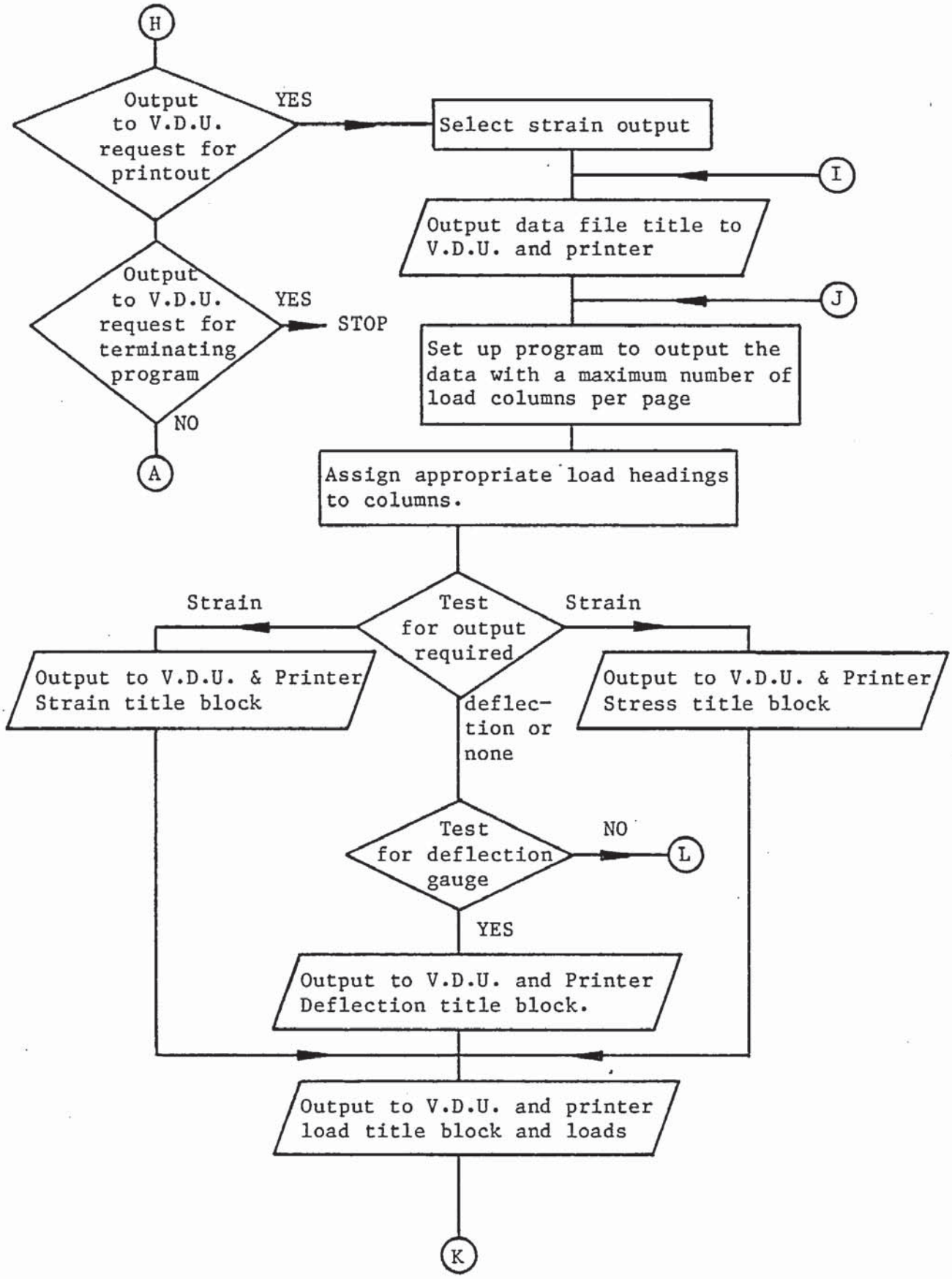

Figure A.1.2 Continued

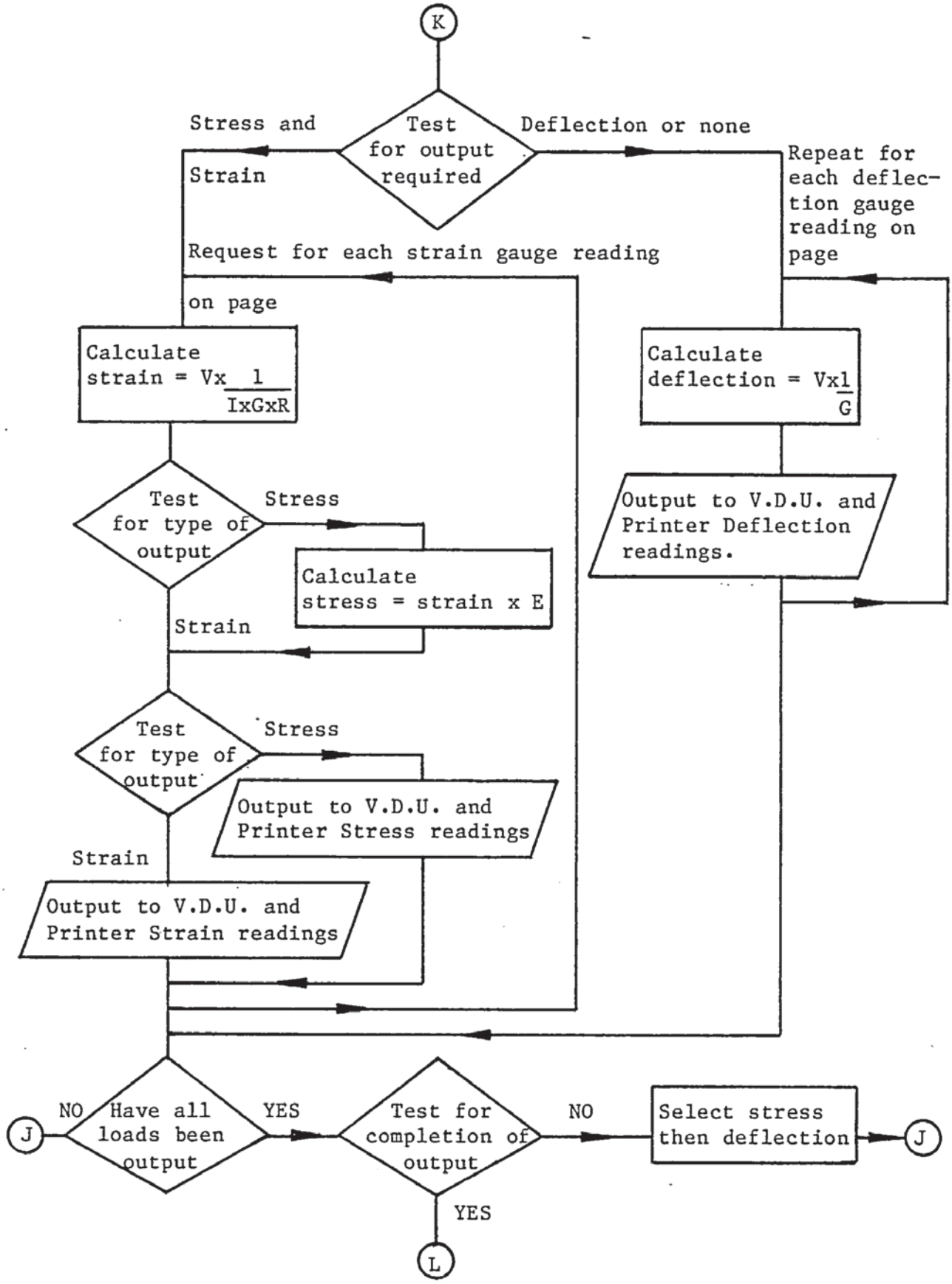

Figure A.1.2 Continued

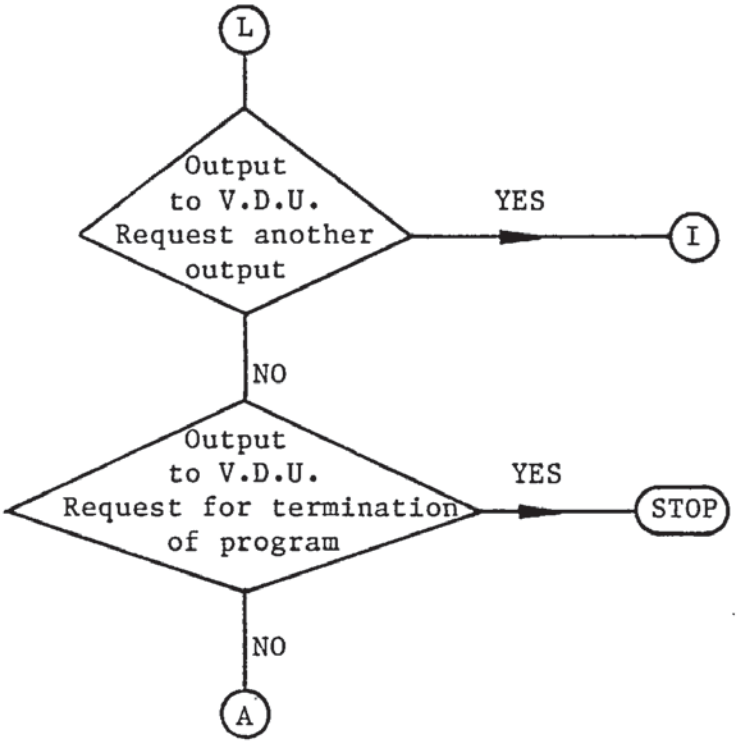

Figure A.1.2 Continued

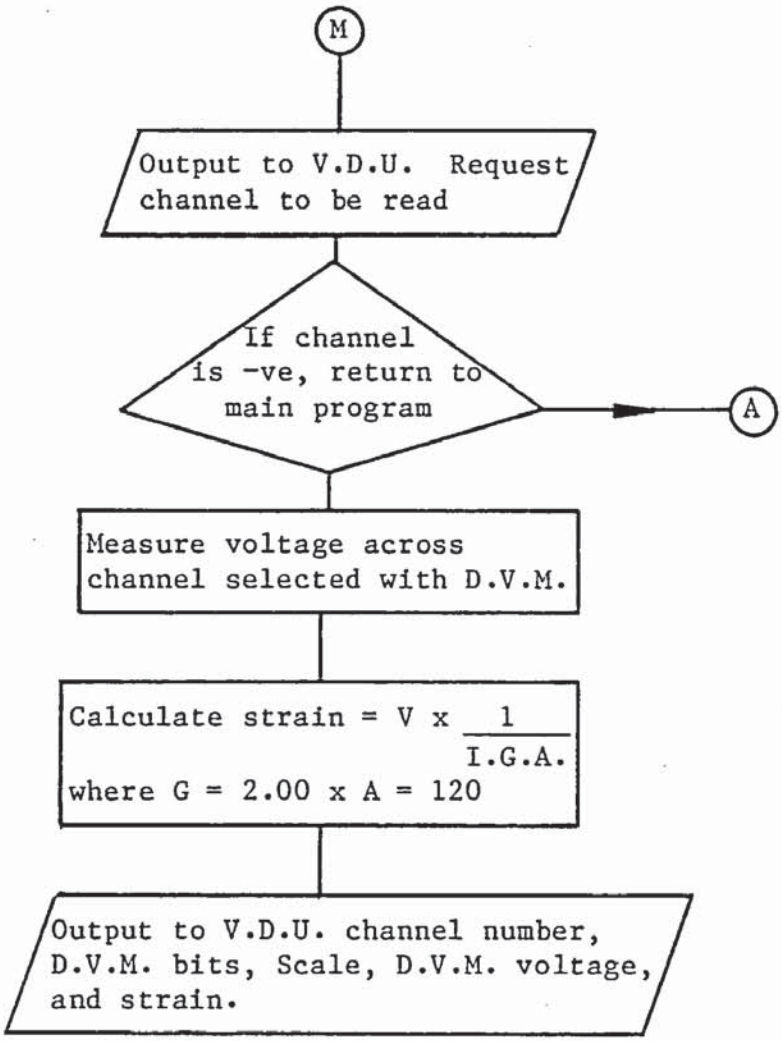

Figure A.1.2 Continued

APPENDIX 2

This appendix contains the tables of the specimen dimensions and ultimate load results for the main series, subsidiary series and the weld series respectively.

The dimensions presented in the tables refer to the appropriate dimensions for that series as given in Chapter 3.

SPECIMEN NUMBER	GUSSET PLATE								LOADED PLATE					Pu kN
	L mm	H mm	s mm	t mm	G mm	θ degs.	fy N/mm2	tw mm	T mm	B mm	fy N/mm2	tw mm	cut	
S3-100-1	100	100	50	3.91	70	90	378	4	20.00	150	-	4	yes	65.0
S3-100-2	"	"	"	3.97	"	"	"	"	"	"	"	"	"	65.0
S3-200-1	200	200	100	3.97	141	"	"	"	"	"	"	"	"	88.5
S3-200-2	"	"	"	3.96	"	"	"	"	"	"	"	"	"	95.0
S3-300-1	300	300	150	4.00	212	"	"	"	"	"	"	"	"	-
S3-300-2	"	"	"	4.00	"	"	"	"	"	"	"	"	"	79.3
S3-400-1	400	400	200	3.96	282	"	"	"	"	"	"	"	"	66.4
S3-400-2	"	"	"	3.97	"	"	"	"	"	"	"	"	"	69.2
S3-500-1	500	500	250	3.96	353	"	"	"	"	"	"	"	"	80.0
S3-500-2	"	"	"	3.95	"	"	"	"	"	"	"	"	"	78.2

Table A.2.1. Specimen dimensions and ultimate load results of series 3.

SPECIMEN NUMBER	GUSSET PLATE								LOADED PLATE					Pu kN
	L mm	H mm	s mm	t mm	G mm	θ degs.	fy N/mm2	tw mm	T mm	B mm	fy N/mm2	tw mm	cut	
S4-50-1	200	50	100	3.93	48	90	378	4	20.00	100	-	4	yes	21.5
S4-50-2	"	"	"	3.99	"	"	"	"	"	"	"	"	"	22.4
S4-100-1	"	100	"	4.01	89	"	"	"	"	"	"	"	"	57.5
S4-100-2	"	"	"	3.96	"	"	"	"	"	"	"	"	"	55.0
S4-150-1	"	150	"	3.97	119	"	"	"	"	"	"	"	"	85.0
S4-150-2	"	"	"	3.97	"	"	"	"	"	"	"	"	"	85.0
S4-200-1	"	200	"	3.94	141	"	"	"	"	"	"	"	"	92.5
S4-200-2	"	"	"	3.92	"	"	"	"	"	"	"	"	"	87.5
S4-250-1	"	250	"	3.97	156	"	"	"	"	"	"	"	"	120.0
S4-250-2	"	"	"	4.00	"	"	"	"	"	"	"	"	"	107.5
S4-300-1	"	300	"	3.99	166	"	"	"	"	"	"	"	"	110.0
S4-300-2	"	"	"	3.95	"	"	"	"	"	"	"	"	"	122.0
S4-400-1	"	400	"	3.97	178	"	"	"	"	"	"	"	"	111.5
S4-400-2	"	"	"	3.98	"	"	"	"	"	"	"	"	"	110.0
S4-500-1	"	500	"	3.99	185	"	"	"	"	"	"	"	"	117.5
S4-500-2	"	"	"	3.98	"	"	"	"	"	"	"	"	"	120.0
S4-600-1	"	600	"	3.97	189	"	"	"	"	"	"	"	"	105.0
S4-600-2	"	"	"	3.99	"	"	"	"	"	"	"	"	"	117.5

Table A.2.2. Specimen dimensions and ultimate load results of series 4.

SPECIMEN NUMBER	GUSSET PLATE								LOADED PLATE					Pu kN
	L mm	H mm	s mm	t mm	G mm	θ degs.	fy N/mm2	tw mm	T mm	B mm	fy N/mm2	tw mm	cut	
S5-75-1	300	300	75	3.98	212	90	378	4	20.00	150	-	4	yes	135.0
S5-100-1	"	"	100	3.96	"	"	"	"	"	"	"	"	"	110.0
S5-150-1	"	"	150	3.97	"	"	"	"	"	"	"	"	"	70.0
S5-150-2	"	"	"	3.97	"	"	"	"	"	"	"	"	"	71.6
S5-200-1	"	"	200	3.98	"	"	"	"	"	"	"	"	"	50.0
S5-250-1	"	"	250	3.99	"	"	"	"	"	"	"	"	"	39.2
S5-300-1	"	"	300	3.97	"	"	"	"	"	"	"	"	"	29.9
S5-300-2	"	"	"	4.00	"	"	"	"	"	"	"	"	"	28.0
S5-300-3	"	"	"	4.00	"	"	"	"	"	"	"	"	"	31.0

Table A.2.3. Specimen dimensions and ultimate load results of series 5.

SPECIMEN NUMBER	GUSSET PLATE								LOADED PLATE					Pu kN
	L mm	H mm	s mm	t mm	G mm	θ degs.	fy N/mm2	tw mm	T mm	B mm	fy N/mm2	tw mm	cut	
S6-150-1	300	300	150	4.00	212	90	378	4	20.00	150	250	4	no	95.0
S6-300-1	"	"	300	4.00	"	"	"	"	"	"	"	"	"	34.8

Table A.2.4. Specimen dimensions and ultimate load results of series 6.

SPECIMEN NUMBER	GUSSET PLATE								LOADED PLATE					Pu kN
	L mm	H mm	s mm	t mm	G mm	θ degs.	fy N/mm2	tw mm	T mm	B mm	fy N/mm2	tw mm	cut	
S7-6-150-1	300	300	150	3.99	212	90	378	4	5.95	100	252	4	no	74.4
S7-10-150-1	"	"	"	3.99	"	"	"	"	10.01	"	"	"	"	75.0
S7-13-150-1	"	"	"	3.99	"	"	"	"	12.97	"	"	"	"	70.0
S7-16-150-1	"	"	"	4.00	"	"	"	"	15.86	"	"	"	"	120.0
S7-20-150-1	"	"	"	3.98	"	"	"	"	20.01	"	"	"	"	77.5
S7-6-300-1	"	"	300	4.00	"	"	"	"	6.02	"	"	"	"	30.0
S7-10-300-1	"	"	"	4.00	"	"	"	"	10.02	"	"	"	"	29.5
S7-13-300-1	"	"	"	3.99	"	"	"	"	12.93	"	"	"	"	30.0
S7-16-300-1	"	"	"	4.00	"	"	"	"	15.82	"	"	"	"	31.8
S7-20-300-1	"	"	"	4.00	"	"	"	"	20.24	"	"	"	"	30.0

Table A.2.5. Specimen dimensions and ultimate load results of series 7.

SPECIMEN NUMBER	GUSSET PLATE								LOADED PLATE					Pu kN
	L mm	H mm	s mm	t mm	G mm	θ degs.	fy N/mm2	tw mm	T mm	B mm	fy N/mm2	tw mm	cut	
S12-5-1	300	300	150	5.19	212	90	263	4	20.00	150	250	4	yes	119.5
S12-7-1	"	"	"	7.03	"	"	"	4	"	"	"	4	yes	215.0§
S12-9-1	"	"	"	9.08	"	"	"	6	"	"	"	6	8mm*	450.0
S12-11-1	"	"	"	11.17	"	"	"	6	"	"	"	6	8mm*	425.0†
S12-13-1	"	"	"	13.04	"	"	"	8	"	"	"	8	yes	500.0†
S12-15-1	"	"	"	15.22	"	"	"	8	"	"	"	8	15mm*	1125.0†
S12-13-2	"	"	"	12.96	"	"	"	8	"	"	"	8	no	775.0
S12-15-2	"	"	"	15.04	"	"	"	8	"	"	"	8	no	1037.5¶

§ The loaded plate weld on the previously tested side also failed.
† The loaded plate weld failed causing the gusset plate to fail.
* The butt weld used to weld size the loaded plates together under the vertical support.
¶ The previous tested side failed first.

Table A.2.6. Specimen dimensions and ultimate load results of series 12.

SPECIMEN NUMBER	GUSSET PLATE								LOADED PLATE					Pu kN
	L mm	H mm	s mm	t mm	G mm	θ degs.	fy N/mm2	tw mm	T mm	B mm	fy N/mm2	tw mm	cut	
S8-45-1	300	300	268	4.00	45	90	378	4	20.00	150	-	4	yes	8.94
S8-45-2	"	"	150	4.00	"	"	"	"	"	"	"	"	"	15.75
S8-90-1	"	"	236	3.99	90	"	"	"	"	"	"	"	"	30.80
S8-90-2	"	"	150	4.00	"	"	"	"	"	"	"	"	"	39.50
S8-135-1	"	"	205	3.99	135	"	"	"	"	"	"	"	"	55.00
S8-135-2	"	"	150	3.99	"	"	"	"	"	"	"	"	"	80.00
S8-180-1	"	"	173	3.95	180	"	"	"	"	"	"	"	"	55.00
S8-180-2	"	"	150	3.99	"	"	"	"	"	"	"	"	"	71.00

Table A.2.7. Specimen dimensions and ultimate load results of series 8.

SPECIMEN NUMBER	GUSSET PLATE								LOADED PLATE					Pu kN
	L mm	H mm	s mm	t mm	G mm	θ degs.	fy N/mm2	tw mm	T mm	B mm	fy N/mm2	tw mm	cut	
S13-30-1	220	220	110	4.04	212	30	245	4	20.00	150	-	4	yes	280.0
S13-30-2	"	"	"	4.03	"	"	"	"	"	"	"	"	"	270.0
S13-50-1	234	234	117	4.01	"	50	"	"	"	"	"	"	"	222.0
S13-50-2	"	"	"	4.02	"	"	"	"	"	"	"	"	"	195.8
S13-70-1	259	259	129	4.00	"	70	"	"	"	"	"	"	"	111.7
S13-70-2	"	"	"	4.00	"	"	"	"	"	"	"	"	"	111.7
S13-90-1	300	300	150	4.02	"	90	"	"	"	"	"	"	"	70.0
S13-90-2	"	"	"	3.91	"	"	"	"	"	"	"	"	"	72.5
S13-110-1	370	370	185	4.01	"	110	"	"	"	"	"	"	"	50.5
S13-110-2	"	"	"	3.90	"	"	"	"	"	"	"	"	"	61.2
S13-130-1	502	502	251	4.02	"	130	"	"	"	"	"	"	"	45.7
S13-130-2	"	"	"	4.02	"	"	"	"	"	"	"	"	"	43.0
S13-140-1	620	620	310	4.03	"	140	"	"	"	"	"	"	"	32.0
S13-140-2	"	"	"	4.04	"	"	"	"	"	"	"	"	"	32.0

Table A.2.8. Specimen dimensions and ultimate load results of series 13.

SPECIMEN NUMBER	EXPERIMENTAL						THEORETICAL				
	MEASURED				CALCULATED			Buckling stresses			
	Lnth. L mm	Width mm	Thick-ness t mm	Ult. load Pu kN	Buckling stress Ind. N/mm2	Buckling stress avg. N/mm2	Efctv. ln. l=L/2 mm	Euler N/mm2	Rankin N/mm2	Perry a=8 N/mm2	Perry a=1 N/mm2
S1a-100-1	100	25.00	4.00	26.50	265.0	269.5	100	271.1	152.8	152.7	232.7
S1a-100-2	"	"	"	27.40	274.0						
S1a-100-3	"	"	"	-	-						
S1a-200-1	200	"	"	9.07	90.7	82.3	200	67.8	56.8	52.6	65.3
S1a-200-2	"	"	"	6.86	68.6						
S1a-200-3	"	"	"	8.77	87.7						
S1a-300-1	300	"	"	3.79	37.9	34.7	300	30.1	27.7	25.5	29.4
S1a-300-2	"	"	"	3.19	31.9						
S1a-300-3	"	"	"	3.43	34.3						
S1a-500-1	500	"	"	1.32	13.2	13.2	500	10.8	10.5	9.8	10.7
S1a-500-2	"	"	"	1.41	14.1						
S1a-500-3	"	"	"	1.22	12.2						

Table A.2.9. Specimen dimensions, ultimate load results and theoretical buckling stresses of series 1 .

SPECIMEN NUMBER	EXPERIMENTAL						THEORETICAL				
	MEASURED				CALCULATED						
	Lnth. L mm	Width mm	Thick-ness t mm	Ult. load P_u kN	Buckling stress Ind. N/mm2	Buckling stress avg. N/mm2	Efctv. ln. l=L/2 mm	Buckling stresses Euler N/mm2	Rankin N/mm2	Perry a=8 N/mm2	Perry a=1 N/mm2
S9-1-1	93	25.08	3.99	34.48	344.5	358.9	46.5	1253.8	273.6	278.4	338.4
S9-1-2	"	25.06	3.99	36.32	363.2						
S9-1-3	"	25.04	3.99	36.87	369.0						
S9-2-1	144	25.01	3.99	30.49	305.5	318.2	72.0	522.9	209.7	213.7	313.2
S9-2-2	"	24.88	3.99	30.89	311.2						
S9-2-3	"	24.77	4.00	33.48	337.9						
S9-3-1	195	24.98	4.00	23.91	239.3	241.2	97.5	285.2	157.1	156.9	241.3
S9-3-2	"	25.00	3.97	24.71	248.9						
S9-3-3	"	25.06	4.01	23.66	235.5						
S9-4-1	246	24.89	3.99	17.04	171.6	170.9	123.0	179.2	118.5	115.1	164.7
S9-4-2	"	24.89	3.94	15.98	163.0						
S9-4-3	"	24.88	4.00	17.74	178.2						
S9-5-1	296.5	24.94	3.95	8.53	86.6	99.2	148.3	123.3	91.2	86.6	116.4
S9-5-2	"	24.92	3.94	8.60	89.6						
S9-5-3	"	24.96	4.00	12.12	121.4						
S9-6-1	348	24.65	3.95	8.01	82.3	81.6	174.0	89.5	71.3	66.7	85.6
S9-6-2	"	24.89	4.00	8.08	81.2						
S9-6-3	"	25.02	4.00	8.14	81.3						
S9-7-1	399	25.09	3.96	6.37	64.1	65.6	199.5	68.1	57.0	62.8	65.6
S9-7-2	"	25.09	4.01	6.69	66.5						
S9-7-3	"	25.07	3.95	6.66	66.2						

Table A.2.10. Specimen dimensions, ultimate load results and theoretical buckling stresses of series 9.

SPEC. NUMBER	EXPERIMENTAL									THEORETICAL				
	MEASURED							CALCULATED						
	Ln. L mm	Wdth. mm	Thick-ness t mm	L=H mm	s mm	Ult. load P_u kN	Axial ult. load kN	Buckling stress Ind. N/mm2	Buckling stress avg. N/mm2	Efct. ln. l=L/2 mm	Buckling stresses Euler N/mm2	Rank. N/mm2	Perry a=8 N/mm2	Perry a=1 N/mm2
S10-7-1	95	25.10	3.98	83.5	66	26.90	38.05	380.9	380.8	46.5	1253.7	277.3	282.6	344.1
S10-7-2	"	25.05	3.99	"	"	26.90	38.05	380.7						
S10-6-1	144	25.03	4.00	119.5	102	22.42	31.71	316.7	326.2	72.0	522.9	211.8	216.4	317.7
S10-6-2	"	25.09	3.99	"	"	23.76	33.61	335.7						
S10-5-1	195	25.08	3.97	155.5	133	17.44	24.66	247.7	244.0	97.5	285.2	158.3	158.4	242.8
S10-5-2	"	24.98	3.99	"	"	16.94	23.96	240.3						
S10-4-1	246	24.92	3.95	192.0	174	12.75	18.04	183.2	157.1	123.0	197.2	119.2	115.9	165.0
S10-4-2	"	25.07	3.98	"	"	9.24	13.07	131.0						
S10-3-1	296	25.08	3.97	227.0	210	8.09	11.44	144.9	113.3	148.3	123.3	91.6	87.1	116.5
S10-3-2	"	24.99	3.99	"	"	7.89	11.13	111.6						
S10-2-1	348	24.90	3.94	264.0	246	5.31	7.51	76.6	80.6	174.0	89.5	71.5	67.0	85.7
S10-2-2	"	25.02	3.98	"	"	5.96	8.42	84.6						
S10-1-1	399	25.00	4.00	300.0	282	4.23	5.99	59.9	56.4	199.5	68.1	57.2	53.1	65.7
S10-1-2	"	25.03	3.99	"	"	3.74	5.28	52.9						

Table A.2.11. Specimen dimensions, ultimate load results and theoretical buckling stresses of series 10.

SPECIMEN NUMBER	GUSSET PLATE								LOADED PLATE					Pu kN
	L mm	H mm	s mm	t mm	G mm	θ degs.	fy N/mm2	tw mm	T mm	B mm	fy N/mm2	tw mm	cut	
S11-150-1	300	300	150	4.00	212	90	363	4	20.00	150	-	4	yes	55.0

Table A.2.12. Specimen dimensions and ultimate load results of series 11.

SPECIMEN NUMBER	GUSSET PLATE								LOADED PLATE					Pu kN
	L mm	H mm	s mm	t mm	G mm	θ degs.	fy N/mm2	tw mm	T* mm	B mm	fy N/mm2	tw mm	cut	
S2-0-1	300	300	150	3.95	212	90	350	4	0.00	150	251	4	no	79.7
S2-0-2	"	"	"	4.00	"	"	"	"	0.00	"	"	"	"	99.6
S2-4-1	"	"	"	4.01	"	"	"	"	4.25	"	"	"	"	94.6
S2-4-2	"	"	"	4.01	"	"	"	"	4.32	"	"	"	"	106.6
S2-8-1	"	"	"	3.69	"	"	"	"	8.27	"	"	"	"	89.2
S2-8-2	"	"	"	4.01	"	"	"	"	8.29	"	"	"	"	104.6
S2-12-1	"	"	"	3.96	"	"	"	"	12.57	"	"	"	"	84.7
S2-12-2	"	"	"	3.95	"	"	"	"	12.03	"	"	"	"	84.7
S2-16-1	"	"	"	4.00	"	"	"	"	15.99	"	"	"	"	101.6
S2-16-2	"	"	"	4.00	"	"	"	"	16.18	"	"	"	"	104.6
S2-20-1	"	"	"	4.01	"	"	"	"	20.10	"	"	"	"	99.6
S2-20-2	"	"	"	3.95	"	"	"	"	19.98	"	"	"	"	107.1

*Machined to this thickness over a 20mm length of the loaded plate at the bottom of the vetical support.

Table A.2.13. Specimen dimensions and ultimate load results of series 2.

SPECIMEN NUMBER	GUSSET PLATE								LOADED PLATE					Pu kN
	L mm	H mm	s mm	t mm	G mm	θ degs.	fy N/mm2	tw mm	T* mm	B mm	fy N/mm2	tw mm	cut	
S5a-75-1	300	300	75	4.00	212	90	378	4	-	150	-	4	yes	160.0
S5a-300-1	"	"	300	4.00	"	"	"	"	"	"	"	"	"	44.3

*The loaded plate was stiffened to approximate a rigid loaded plate.

Table A.2.14. Specimen dimensions and ultimate load results of series 5a.

SPECIMEN NUMBER	GUSSET PLATE									LOADED PLATE					Pu kN
	L mm	H mm	s mm	t mm	G mm	θ deg.	fy N/mm2	tw* mm		T mm	B mm	fy N/mm2	tw mm	cut	
S14-0-1	300	300	150	10.19	212	90	281	6	0	20.00	150	250	6	no	362.5
S14-0-2	"	"	"	10.17	"	"	"	6	0	"	"	"	6	"	425.0
S14-0-3	"	"	"	10.20	"	"	"	6	0	"	"	"	6	"	395.0
S14-0-4	"	"	"	10.21	"	"	"	6	0	"	"	"	6	"	475.0
S14-2-1	"	"	"	10.17	"	"	"	6	2.5	"	"	"	6	"	437.5
S14-2-2	"	"	"	10.18	"	"	"	6	2.5	"	"	"	6	"	525.0
S14-2-3	"	"	"	10.24	"	"	"	6	2.5	"	"	"	6	"	462.5
S14-2-4	"	"	"	10.23	"	"	"	6	2.5	"	"	"	6	"	568.8
S15-0-1	"	"	"	10.19	"	"	"	0	6	"	"	"	6	"	375.0
S15-0-2	"	"	"	10.17	"	"	"	0	6	"	"	"	6	"	437.5
S15-2-1	"	"	"	10.19	"	"	"	2.5	6	"	"	"	6	"	456.5
S15-2-2	"	"	"	10.18	"	"	"	2.5	6	"	"	"	6	"	562.5
S16-2-1	"	"	"	10.22	"	"	"	2.5	2.5	"	"	"	2.5	"	425.0
S16-2-2	"	"	"	10.22	"	"	"	2.5	2.5	"	"	"	2.5	"	487.5
S16-6-1	"	"	"	10.20	"	"	"	6	6	"	"	"	6	"	487.5
S16-6-2	"	"	"	10.21	"	"	"	6	6	"	"	"	6	"	550.0

*The measurments given are the sizes of the fillet welds used along the supported and loaded edges respectively.

Table A.2.15. Specimen dimensions and ultimate load results of series 14,15 & 16.

SPECIMEN NUMBER	GUSSET PLATE									LOADED PLATE					Pu kN
	L mm	H mm	s mm	t mm	G mm	θ deg.	fy N/mm2	weld* mm	mm	T mm	B mm	fy N/mm2	tw mm	cut	
S17-25-1	300	300	150	10.15	212	92	281	25	25	20.00	150	250	6	no	100.0
S17-25-2	"	"	"	10.15	"	"	"	"	"	"	"	"	"	"	137.5
S17-75-1	"	"	"	10.15	"	"	"	75	"	"	"	"	"	"	220.0
S17-75-2	"	"	"	10.15	"	"	"	"	"	"	"	"	"	"	225.0

*The measurments given are the lengths of the 4mm fillet welds used along the supported and loaded edges respectively.

Table A.2.16. Specimen dimensions and ultimate load results of series 17.

SPECIMEN NUMBER	WELD LENGTHS					Weld size mm	Ult. load kN	Ult. indv. N/mm2	Stress ave. N/mm2
	1 mm	2 mm	3 mm	4 mm	Total mm				
1	27	24	26	27	104	4	130	442	449
2	22	25	22	26	95	4	124	461	
3	26	24	19	22	91	4	114	443	

Table A.2.17. Ultimate load and stress results of the weld tests for series 17.

APPENDIX 3

This appendix contains the tables of load deflection data for the main series, subsidiary series and the weld series respectively. With the strut tests in the secondary series the experimental and theoretical axial stresses have also been included.

The deflections presented in the tables refer to the appropriate deflections for that series as given in Chapter 3.

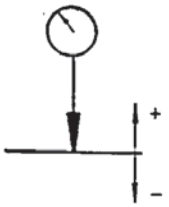

Deflection gauge notation.

Initial lateral deflections are presented in Table A.3.19.

SPECIMEN												
S3-100-1			S3-100-2			S3-200-1			S3-200-2		
LOAD	DEFLECTION		LOAD	DEFLECTION		LOAD	DEFLECTION		LOAD	DEFLECTION	
P	vert.	lat.	P	vert.	lat.	P	vert.	lat.	P	vert.	lat.
kN	mm	mm	kN	mm	mm	kN	mm	mm	kN	mm	mm
0.0	0.00	0.00	0.0	0.00	0.00	0.0	0.00	0.00	0.0	0.00	0.00
10.0	0.06	0.08	5.0	0.31	0.04	10.0	0.29	0.10	10.0	0.18	-0.09
20.0	0.23	0.12	20.0	0.45	0.06	20.0	0.46	0.17	20.0	0.34	-0.13
30.0	0.37	0.14	30.0	0.57	0.06	30.0	0.62	0.22	40.0	0.58	-0.15
40.0	0.53	0.16	40.0	0.68	0.06	40.0	0.74	0.31	60.0	0.79	-0.12
45.0	0.62	0.16	45.0	0.74	0.06	50.0	0.86	0.45	70.0	0.91	-0.06
50.0	0.72	0.16	50.0	0.79	0.06	60.0	0.97	0.71	80.0	1.03	0.07
55:0	0.84	0.17	55.0	0.95	0.06	70.0	1.09	1.11	85.0	1.11	0.21
60.0	1.01	0.18	60.0	0.94	0.06	80.0	1.24	1.97	90.0	1.20	0.60
65.0	1.47	0.33	65.0	1.35	0.16	85.0	1.35	3.42	92.5	1.26	1.20
65.0	2.09	1.93	67.5	-	-	88.5	-	-	95.0	-	-

SPECIMEN											
S3-300-1			S3-300-2			S3-400-1			S3-400-2		
LOAD	DEFLECTION		LOAD	DEFLECTION		LOAD	DEFLECTION		LOAD	DEFLECTION	
P	vert.	lat.	P	vert.	lat.	P	vert.	lat.	P	vert.	lat.
kN	mm	mm	kN	mm	mm	kN	mm	mm	kN	mm	mm
			0.0	0.00	0.00	0.0	0.00	0.00	0.0	0.00	0.00
			10.0	0.06	0.19	10.0	0.23	0.58	10.0	0.08	0.33
			20.0	0.29	0.40	20.0	0.37	2.07	20.0	0.21	0.93
			30.0	0.56	0.55	30.0	0.55	6.18	30.0	0.32	2.01
			50.0	1.57	0.80	40.0	0.75	9.13	40.0	0.45	5.27
			60.0	3.05	0.92	50.0	0.96	11.57	50.0	0.60	7.47
			65.0	4.00	0.99	60.0	1.27	13.78	55.0	0.67	8.77
			70.0	5.20	1.07	65.0	1.70	-	60.0	0.76	10.47
			75.0	7.00	1.18	66.4	-	-	65.0	0.92	13.05
			77.5	9.05	1.30				69.2	-	-
			79.3	-	-						

SPECIMEN					
S3-500-1			S3-500-2		
LOAD	DEFLECTION		LOAD	DEFLECTION	
P	vert.	lat.	P	vert.	lat.
kN	mm	mm	kN	mm	mm
0.0	0.00	0.00	0.0	0.00	0.00
10.0	0.11	-0.04	10.0	0.11	0.20
20.0	0.29	-0.03	20.0	0.24	0.48
30.0	0.43	-0.03	30.0	0.37	0.92
50.0	0.64	-0.11	40.0	0.49	1.95
55.0	0.69	-0.11	50.0	0.61	4.33
60.0	0.74	0.80	60.0	0.74	7.49
65.0	0.80	2.79	65.0	0.81	9.20
70.0	0.86	5.50	70.0	0.90	11.28
75.0	0.94	8.09	75.0	1.06	15.28
80.0	1.14	-	78.2	-	-

Table A.3.1. Load deflection data for series 3.

SPECIMEN											
S4-50-1			S4-50-2			S4-100-1			S4-100-2		
LOAD	DEFLECTION		LOAD	DEFLECTION		LOAD	DEFLECTION		LOAD	DEFLECTION	
P	vert.	lat.	P	vert.	lat.	P	vert.	lat.	P	vert.	lat.
kN	mm	mm	kN	mm	mm	kN	mm	mm	kN	mm	mm
0.0	0.00	0.00	0.0	0.00	0.00	0.0	0.00	0.00	0.0	0.00	0.00
2.5	0.21	0.01	2.5	0.19	0.00	10.0	0.27	0.08	10.0	0.22	-0.10
7.5	0.50	0.05	5.0	0.23	0.00	20.0	0.48	0.11	20.0	0.43	-0.12
10.0	0.66	0.07	7.5	0.32	0.00	30.0	0.63	0.13	30.0	0.63	-0.12
12.5	0.86	0.08	10.0	0.42	0.01	40.0	0.90	0.13	40.0	0.83	-0.12
15.0	1.31	0.12	12.5	0.51	0.02	45.0	1.31	0.14	45.0	0.94	-0.13
17.0	2.01	0.17	15.0	0.61	0.02	50.0	1.63	0.15	50.0	0.99	-0.13
18.0	2.50	0.22	17.5	0.73	0.03	52.5	2.18	0.17	55.0	-	+ve
19.0	3.13	0.27	20.0	0.91	0.03	55.0	2.78	0.20			
20.0	3.95	0.36	22.0	1.63	0.03	55.0	2.86	0.22			
21.5	-	-	22.4	-	-	57.5	-	-			

Table A.3.2. Load deflection data for series 4.

SPECIMEN												
S4-150-1			S4-150-2			S4-200-1			S4-200-2		
LOAD	DEFLECTION		LOAD	DEFLECTION		LOAD	DEFLECTION		LOAD	DEFLECTION	
P	vert.	lat.	P	vert.	lat.	P	vert.	lat.	P	vert.	lat.
kN	mm	mm	kN	mm	mm	kN	mm	mm	kN	mm	mm
0.0	0.00	0.00	0.0	0.00	0.00	0.0	0.00	0.00	0.0	0.00	0.00
5.0	0.12	0.03	5.0	0.11	-0.01	10.0	0.52	0.00	10.0	0.09	-0.13
10.0	0.23	0.07	10.0	0.22	-0.02	20.0	0.69	0.04	20.0	0.26	-0.11
20.0	0.41	0.11	20.0	0.41	-0.02	30.0	0.86	0.07	30.0	0.40	-0.06
40.0	0.71	0.17	40.0	0.69	0.01	50.0	1.16	0.14	40.0	0.53	0.00
60.0	1.04	0.24	60.0	0.97	0.03	60.0	1.32	0.20	50.0	0.67	0.07
65.0	1.13	0.27	70.0	1.12	0.06	70.0	1.47	0.28	60.0	0.81	0.15
70.0	1.23	0.33	75.0	1.22	0.13	80.0	1.53	0.43	70.0	0.94	0.25
75.0	1.33	0.43	80.0	1.34	0.40	85.0	1.63	0.63	80.0	1.06	0.46
80.0	1.40	0.69	82.5	1.41	0.75	90.0	1.73	1.35	85.0	1.14	0.87
85.0	-	-	85.0	-	-	92.5	1.73	-	87.5	1.22	2.02

SPECIMEN												
S4-250-1			S4-250-2			S4-300-1			S4-300-2		
LOAD	DEFLECTION		LOAD	DEFLECTION		LOAD	DEFLECTION		LOAD	DEFLECTION	
P	vert.	lat.	P	vert.	lat.	P	vert.	lat.	P	vert.	lat.
kN	mm	mm	kN	mm	mm	kN	mm	mm	kN	mm	mm
0.0	0.00	0.00	0.0	0.00	0.00	0.0	0.00	0.00	0.0	0.00	0.00
10.0	0.10	-0.03	10.0	0.14	0.04	20.0	0.41	0.12	20.0	0.38	0.16
20.0	0.26	-0.03	30.0	0.48	0.07	40.0	0.63	0.21	40.0	0.56	0.22
40.0	0.53	-0.03	50.0	0.74	0.11	60.0	0.81	0.35	60.0	0.72	0.28
60.0	0.81	-0.03	60.0	0.84	0.14	70.0	0.90	0.44	80.0	0.88	0.36
70.0	0.96	-0.03	70.0	0.94	0.17	80.0	0.99	0.56	100.0	1.05	0.43
80.0	1.11	-0.02	80.0	1.03	0.22	90.0	1.08	0.72	105.0	1.09	0.45
90.0	1.24	-0.01	90.0	1.11	0.28	100.0	1.19	0.93	110.0	1.15	0.50
100.0	1.37	0.04	100.0	1.22	0.44	105.0	1.24	1.32	115.0	1.20	0.61
110.0	1.50	0.23	105.0	1.28	1.04	110.0	1.36	2.12	120.0	1.31	1.88
120.0	-	-	107.5	-	-				122.0	-	-

SPECIMEN												
S4-400-1			S4-400-2			S4-500-1			S4-500-2		
LOAD	DEFLECTION		LOAD	DEFLECTION		LOAD	DEFLECTION		LOAD	DEFLECTION	
P	vert.	lat.	P	vert.	lat.	P	vert.	lat.	P	vert.	lat.
kN	mm	mm	kN	mm	mm	kN	mm	mm	kN	mm	mm
0.0	0.00	0.00	0.0	0.00	0.00	0.0	0.00	0.00	0.0	0.00	0.00
20.0	0.34	-0.05	20.0	0.38	-0.04	10.0	0.18	0.09	20.0	0.38	0.30
40.0	0.57	-0.04	40.0	0.57	-0.02	30.0	0.49	0.21	40.0	0.61	0.48
60.0	0.75	-0.03	60.0	0.73	0.03	40.0	0.59	0.25	60.0	0.80	0.73
70.0	0.84	-0.02	70.0	0.81	0.07	60.0	0.74	0.34	80.0	0.98	1.09
80.0	0.94	0.01	80.0	0.88	0.12	80.0	0.89	0.46	100.0	1.16	2.02
90.0	1.04	0.10	90.0	0.96	0.20	90.0	0.97	0.61	110.0	1.26	3.35
100.0	1.14	0.44	100.0	1.05	0.58	100.0	1.06	1.36	115.0	1.32	4.38
105.0	1.21	1.09	105.0	1.11	1.66	110.0	1.20	2.46	117.5	1.36	5.18
110.0	1.35	-	110.0	1.26	6.48	115.0	1.39	4.16	120.0	1.44	7.33
111.5	-	-	110.0	-	-	117.5	-	-	120.0	-	-

SPECIMEN					
S4-600-1			S4-600-2		
LOAD	DEFLECTION		LOAD	DEFLECTION	
P	vert.	lat.	P	vert.	lat.
kN	mm	mm	kN	mm	mm
0.0	0.00	0.00	0.0	0.00	0.00
10.0	0.46	0.05	10.0	0.38	-0.06
30.0	0.86	0.03	30.0	0.80	-0.10
50.0	1.16	0.12	50.0	1.11	0.01
70.0	1.46	0.76	70.0	1.35	0.17
80.0	1.63	2.88	80.0	1.49	0.33
90.0	1.81	5.38	90.0	1.64	0.60
100.0	2.13	9.28	100.0	1.82	1.23
105.0	-	-	110.0	2.05	3.93
			115.0	2.22	6.53
			117.5	3.53	9.13

Table A.3.2. Load deflection data for series 4 (continued).

SPECIMEN												
S5-75-1			S5-100-1			S5-150-1			S5-150-2		
LOAD	DEFLECTION		LOAD	DEFLECTION		LOAD	DEFLECTION		LOAD	DEFLECTION	
P	vert.	lat.	P	vert.	lat.	P	vert.	lat.	P	vert.	lat.
kN	mm	mm	kN	mm	mm	kN	mm	mm	kN	mm	mm
0.0	0.00	0.00	0.0	0.00	0.00	0.0	0.00	0.00	0.0	0.00	0.00
5.0	0.11	0.00	10.0	0.22	0.00	10.0	0.12	0.02	10.0	0.21	0.16
20.0	0.33	0.09	20.0	0.37	0.03	20.0	0.19	0.05	20.0	0.37	0.32
40.0	0.55	0.28	40.0	0.58	0.12	30.0	0.33	0.13	30.0	0.50	0.51
60.0	0.73	0.81	60.0	0.74	0.25	40.0	0.44	0.26	40.0	0.64	0.80
80.0	0.88	1.79	80.0	0.90	0.50	50.0	0.56	0.61	50.0	0.75	1.30
100.0	1.06	3.17	90.0	1.01	2.65	60.0	0.89	3.64	60.0	0.83	2.84
110.0	1.17	4.03	100.0	1.16	5.45	65.0	1.01	5.99	65.0	0.91	4.50
120.0	1.29	5.04	105.0	1.26	7.05	70.0	-	-	67.5	0.98	5.71
130.0	1.47	7.19	107.5	1.36	7.25				70.0	1.12	8.45
135.0	1.63	-	110.0	-	-				71.6	-	-

SPECIMEN												
S5-200-1			S5-250-1			S5-300-1			S5-300-2		
LOAD	DEFLECTION		LOAD	DEFLECTION		LOAD	DEFLECTION		LOAD	DEFLECTION	
P	vert.	lat.	P	vert.	lat.	P	vert.	lat.	P	vert.	lat.
kN	mm	mm	kN	mm	mm	kN	mm	mm	kN	mm	mm
0.0	0.00	0.00	0.0	0.00	0.00	0.0	0.00	0.00	0.0	0.00	0.00
5.0	0.13	0.00	2.5	0.22	0.02	2.5	0.12	0.00	2.5	0.07	0.00
10.0	0.25	0.00	5.0	0.31	0.08	5.0	0.21	0.08	5.0	0.16	0.03
20.0	0.41	0.01	10.0	0.44	0.21	10.0	0.39	0.33	10.0	0.34	0.25
25.0	0.48	0.07	15.0	0.53	0.41	15.0	0.55	0.99	16.0	0.48	0.56
30.0	0.55	0.22	20.0	0.62	0.91	20.0	0.73	2.82	20.0	0.64	1.72
35.0	0.66	3.43	25.0	0.73	2.39	25.0	1.00	5.87	24.0	0.83	4.46
40.0	0.77	5.83	30.0	0.88	4.74	27.0	1.11	7.57	27.0	1.00	6.20
45.0	0.92	8.13	35.0	1.09	7.49	28.0	1.29	9.77	28.0	1.07	7.03
47.5	1.04	9.88	37.5	1.32	9.84	29.0	1.52	11.07	30.0	1.34	9.75
50.0	-	-	39.2	-	-	29.9	-	-	31.0	-	-

SPECIMEN							
S5-300-3							
LOAD	DEFLECTION						
P	vert.	lat.	d1	d2	d3	d4	d5
kN	mm	mm	mm	mm	mm	mm	mm
0.0	0.00	0.00	0.00	0.00	0.00	0.00	0.00
5.0	0.28	0.09	0.11	0.11	0.10	0.08	0.05
10.0	0.43	0.21	0.21	0.21	0.19	0.15	0.09
15.0	0.57	0.40	0.32	0.31	0.27	0.21	0.12
20.0	0.71	0.82	0.43	0.40	0.36	0.28	0.15
25.0	0.87	2.24	0.57	0.53	0.47	0.36	0.18
26.0	0.92	2.79	0.60	0.57	0.50	0.38	0.19
28.0	1.03	4.43	0.72	0.67	0.58	0.38	0.21
29.0	1.10	5.47	0.79	0.74	0.64	0.37	0.23
30.0	1.21	6.70	0.88	0.83	0.71	0.42	0.24
31.0	1.36	-	1.03	0.97	0.83	0.59	0.27

Table A.3.3. Load deflection data for series 5.

SPECIMEN										
S6-150-1			S6-300-1							
LOAD	DEFLECTION		LOAD	DEFLECTION						
P	vert.	lat.	P	vert.	lat.	d1	d2	d3	d4	d5
kN	mm	mm	kN	mm	mm	mm	mm	mm	mm	mm
0.0	0.00	0.00	0.0	0.00	0.00	0.00	0.00	0.00	0.00	0.00
5.0	0.13	0.08	5.0	0.23	0.34	0.18	0.17	0.14	0.13	0.10
15.0	0.30	0.13	10.0	0.43	0.63	0.30	0.28	0.26	0.21	0.15
40.0	0.59	0.25	15.0	0.56	1.12	0.42	0.40	0.36	0.29	0.19
60.0	0.78	0.51	20.0	0.73	2.36	0.56	0.53	0.48	0.39	0.24
70.0	0.88	2.12	25.0	1.00	5.16	0.80	0.79	0.71	0.55	0.30
80.0	1.04	6.05	27.5	1.19	6.98	1.10	0.99	0.90	0.68	0.35
85.0	1.11	7.22	30.0	1.57	9.98	1.40	1.40	1.29	0.93	0.43
90.0	1.22	8.82	32.0	2.68	16.13	2.56	2.64	2.33	1.59	0.68
92.5	1.33	10.52	34.0	4.67	23.87	-	4.72	3.95	3.55	1.05
95.0	-	-	34.8	-	-	-	-	-	-	-

Table A.3.4. Load deflection data for series 6.

SPECIMEN											
S7-6-150-1			S7-10-150-1								
LOAD	DEFLECTION		LOAD	DEFLECTION							
P	vert.	lat.	P	vert.	lat.	d1	d2	d3	d4	d5	
kN	mm	mm	kN	mm	mm	mm	mm	mm	mm	mm	
0.0	0.00	0.00	0.0	0.00	0.00	0.00	0.00	0.00	0.00	0.00	
5.0	0.18	0.03	5.0	0.11	0.05	0.06	0.06	0.05	0.06	0.06	
10.0	0.30	0.06	15.0	0.24	0.15	0.16	0.14	0.11	0.12	0.13	
20.0	0.45	0.17	30.0	0.41	0.40	0.28	0.23	0.16	0.18	0.19	
30.0	0.63	0.31	45.0	0.56	0.91	0.40	0.31	0.19	0.23	0.24	
40.0	0.77	0.50	55.0	0.67	1.63	0.47	0.35	0.20	0.26	0.26	
50.0	0.92	0.80	65.0	0.79	3.29	0.55	0.41	0.21	0.27	0.27	
60.0	1.05	1.28	70.0	0.88	5.02	0.62	0.45	0.22	0.27	0.26	
65.0	1.13	1.64	75.0	-	-	-	-	-	-	-	
70.0	1.22	2.44									
74.4	-	-									

SPECIMEN								
S7-13-150-1			S7-16-150-1			S7-20-150-1		
LOAD	DEFLECTION		LOAD	DEFLECTION		LOAD	DEFLECTION	
P	vert.	lat.	P	vert.	lat.	P	vert.	lat.
kN	mm	mm	kN	mm	mm	kN	mm	mm
0.0	0.00	0.00	0.0	0.00	0.00	0.0	0.00	0.00
5.0	0.15	0.00	5.0	0.11	0.05	5.0	0.13	0.07
10.0	0.23	0.01	10.0	0.19	0.09	10.0	0.22	0.24
20.0	0.35	0.11	30.0	0.42	0.15	20.0	0.35	0.75
30.0	0.46	0.34	50.0	0.61	0.20	30.0	0.46	1.79
40.0	0.56	1.62	70.0	0.79	0.22	40.0	0.57	3.27
50.0	0.70	4.57	90.0	0.96	0.22	50.0	0.70	5.09
55.0	0.79	5.92	100.0	1.06	0.19	60.0	0.83	6.99
60.0	0.91	7.87	110.0	1.14	0.03	70.0	1.04	9.69
65.0	1.13	10.87	115.0	1.19	-0.16	75.0	1.24	12.29
70.0	-	-	120.0	-	-	77.5	-	-

SPECIMEN											
S7-6-300-1									S7-10-300-1		
LOAD	DEFLECTION								LOAD	DEFLECTION	
P	vert.	lat.	d1	d2	d3	d4	d5	d6	P	vert.	lat.
kN	mm	mm	mm	mm	mm	mm	mm	mm	kN	mm	mm
0.0	0.00	0.00	0.00	0.00	0.00	0.00	0.00	0.00	0.0	0.00	0.00
2.5	0.22	0.02	0.15	0.12	0.09	0.05	0.01	0.08	5.0	0.30	0.15
5.0	0.35	0.06	0.24	0.21	0.17	0.12	0.06	0.09	10.0	0.52	0.31
10.0	0.61	0.12	0.45	0.42	0.37	0.30	0.16	0.13	15.0	0.71	0.52
15.0	0.97	0.21	0.76	0.74	0.69	0.62	0.41	0.15	20.0	0.92	0.83
20.0	1.54	0.33	1.31	1.31	1.27	1.22	0.87	0.17	25.0	1.19	1.54
24.0	2.24	0.48	1.99	2.00	1.98	1.90	1.41	0.17	27.5	1.39	2.97
26.0	2.72	0.56	2.47	2.50	2.49	2.47	1.82	0.11	29.3	-	-
28.0	3.39	0.67	3.15	3.22	3.22	3.20	2.42	0.02			
29.0	3.80	0.67	3.56	3.65	3.65	3.66	2.80	0.03			
30.0	-	-	-	-	-	-	-	-			

SPECIMEN								
S7-13-300-1								
LOAD	DEFLECTION							
P	vert.	lat.	d1	d2	d3	d4	d5	d6
kN	mm	mm	mm	mm	mm	mm	mm	mm
0.0	0.00	0.00	0.00	0.00	0.00	0.00	0.00	0.00
2.5	0.14	0.02	0.07	0.06	0.09	0.02	0.01	0.02
5.0	0.22	0.07	0.13	0.11	0.09	0.02	0.03	0.04
10.0	0.40	0.17	0.26	0.24	0.20	0.11	0.09	0.05
15.0	0.58	0.32	0.40	0.38	0.33	0.26	0.16	0.06
20.0	0.78	0.60	0.57	0.54	0.48	0.42	0.24	0.07
22.5	0.88	1.07	0.66	0.63	0.57	0.49	0.29	0.07
25.0	1.00	2.22	0.78	0.75	0.69	0.55	0.35	0.07
27.5	1.25	5.37	1.03	1.02	0.92	0.77	0.46	0.07
29.0	1.50	8.17	1.33	1.22	1.18	0.93	0.54	0.06
30.0	-	-	-	-	-	-	-	-

Table A.3.5. Load deflection data for series 7.

SPECIMEN					
S7-16-300-1			S7-20-300-1		
LOAD	DEFLECTION		LOAD	DEFLECTION	
P	vert.	lat.	P	vert.	lat.
kN	mm	mm	kN	mm	mm
0.0	0.00	0.00	0.0	0.00	0.00
5.0	0.19	0.08	2.5	0.11	0.16
10.0	0.37	0.20	5.0	0.20	0.29
20.0	0.68	0.67	10.0	0.37	0.62
30.0	1.22	5.70	15.0	0.52	1.21
31.8	-	-	20.0	0.69	2.47
			22.5	0.81	3.42
			25.0	0.94	4.62
			27.5	1.13	6.42
			30.0	-	-

Table A.3.5. Load deflection data for series 7 (continued).

SPECIMEN									
S12-5-1					S12-7-1				
LOAD	DEFLECTION				LOAD	DEFLECTION			
P	vert.	lat.	d_1	d_2	P	vert.	lat.	d_1	d_2
kN	mm	mm	mm	mm	kN	mm	mm	mm	mm
0.0	0.00	0.00	0.00	0.00	0.0	0.00	0.00	0.00	0.00
10.0	0.30	-0.03	0.00	0.36	5.0	0.21	0.01	0.08	0.20
20.0	0.43	-0.05	-0.05	0.37	25.0	0.50	0.06	0.06	0.29
40.0	0.63	-0.06	-0.12	0.35	70.0	0.86	0.12	0.03	0.37
60.0	0.79	-0.06	-0.17	0.33	115.0	1.20	0.16	0.01	0.48
80.0	0.95	-0.06	-0.21	0.29	145.0	1.47	0.22	0.02	0.60
90.0	1.04	0.31	-0.22	0.26	170.0	1.85	0.31	0.07	0.74
100.0	1.14	1.26	-0.22	0.22	190.0	3.30	0.40	0.22	1.01
105.0	1.21	1.98	-0.22	0.19	205.0	5.62	0.55	0.44	1.35
115.0	1.38	4.91	-0.17	0.10	210.0	6.64	0.68	0.57	1.55
119.5	-	-	-	-	215.0	-	-	-	-
SPECIMEN									
S12-9-1					S12-11-1				
LOAD	DEFLECTION				LOAD	DEFLECTION			
P	vert.	lat.	d_1	d_2	P	vert.	lat.	d_1	d_2
kN	mm	mm	mm	mm	kN	mm	mm	mm	mm
0.0	0.00	0.00	0.00	0.00	0.0	0.00	0.00	0.00	0.00
25.0	0.14	0.02	-0.12	0.70	50.0	0.18	0.01	-0.13	-0.36
50.0	0.29	0.04	-0.18	0.80	100.0	0.31	0.02	-0.20	-0.52
100.0	0.51	0.07	-0.30	0.96	150.0	0.42	0.03	-0.25	-0.62
200.0	0.89	0.17	-0.38	1.20	225.0	0.56	0.05	-0.32	-0.77
300.0	1.28	0.30	-0.38	1.32	300.0	0.70	0.05	-0.37	-0.88
375.0	1.78	0.47	-0.39	1.33	325.0	0.74	0.05	-0.39	-0.91
400.0	2.04	0.62	-0.43	1.27	350.0	0.78	0.05	-0.41	-0.94
425.0	2.47	1.26	-0.44	1.19	375.0	0.94	0.05	-0.44	-0.96
437.5	2.82	2.66	-0.33	1.06	400.0	1.13	-0.05	-0.43	-1.02
450.0	-	-	-	-	425.0	-	-	-	-
SPECIMEN									
S12-13-1					S12-15-1				
LOAD	DEFLECTION				LOAD	DEFLECTION			
P	vert.	lat.	d_1	d_2	P	vert.	lat.	d_1	d_2
kN	mm	mm	mm	mm	kN	mm	mm	mm	mm
0.0	0.00	0.00	0.00	0.00	0.0	0.00	0.00	0.00	0.00
50.0	0.27	0.05	-0.19	-0.27	100.0	0.34	0.04	-0.23	-0.39
100.0	0.44	0.04	-0.27	-0.30	250.0	0.67	0.10	-0.43	-0.43
200.0	0.76	0.03	-0.39	-0.33	450.0	1.02	0.18	-0.65	-0.47
300.0	1.06	0.03	-0.50	-0.35	650.0	1.37	0.28	-0.90	-0.52
350.0	1.32	0.03	-0.61	-0.40	800.0	1.84	0.29	-1.41	-0.64
450.0	2.87	0.20	-1.08	-0.54	900.0	2.83	0.22	-2.19	-0.90
475.0	3.72	0.31	-1.05	-0.52	1025.0	5.04	0.54	-3.96	-1.68
500.0	4.48	0.48	-0.94	-0.36	1075.0	6.26	1.13	-5.10	-2.01
537.5	6.15	1.12	-0.69	-0.12	1100.0	7.14	3.03	-5.84	-2.23
550.0	-	-	-	-	1125.0	-	-	-	-

Table A.3.6. Load deflection data for series 12.

SPECIMEN									
S12-13-2					S12-15-2				
LOAD	DEFLECTION				LOAD	DEFLECTION			
P	vert.	lat.	d1	d2	P	vert.	lat.	d1	d2
kN	mm	mm	mm	mm	kN	mm	mm	mm	mm
0.0	0.00	0.00	0.00	0.00	0.0	0.00	0.00	0.00	0.00
50.0	0.36	0.08	-0.14	-0.11	100.0	0.50	-0.10	-0.20	-0.24
150.0	0.76	-0.12	-0.24	0.20	200.0	0.77	-0.11	-0.30	-0.24
350.0	1.29	-0.08	-0.38	0.53	400.0	1.19	-0.11	-0.45	-0.19
450.0	1.77	-0.04	-0.50	0.65	600.0	1.59	-0.08	-0.59	-0.09
550.0	3.30	0.11	-0.71	0.81	700.0	1.80	-0.04	-0.67	-0.03
600.0	4.38	0.44	-0.77	0.93	800.0	2.05	0.02	-0.78	-0.02
675.0	6.35	2.32	-0.72	1.12	900.0	2.74	0.37	-1.14	-0.01
700.0	7.25	3.85	-0.65	1.15	950.0	3.49	1.08	-1.42	-0.07
762.5	10.35	13.92	-0.18	0.70	1000.0	5.45	3.38	-1.70	-0.13
775.0	-	-	-	-	1037.5	-	-	-	-

Table A.3.6. Load deflection data for series 12 (continued).

SPECIMEN												
S8-45-1			S8-90-1			S8-135-1			S8-180-1		
LOAD	DEFLECTION		LOAD	DEFLECTION		LOAD	DEFLECTION		LOAD	DEFLECTION	
P	vert.	lat.	P	vert.	lat.	P	vert.	lat.	P	vert.	lat.
kN	mm	mm	kN	mm	mm	kN	mm	mm	kN	mm	mm
0.0	0.00	0.00	0.0	0.00	0.00	0.0	0.00	0.00	0.0	0.00	0.00
1.0	0.12	0.02	2.5	0.17	0.00	5.0	0.12	0.02	5.0	0.11	0.04
2.0	0.18	0.07	5.0	0.23	0.00	10.0	0.18	0.03	15.0	0.28	0.35
3.0	0.23	0.15	10.0	0.34	0.06	20.0	0.31	0.13	25.0	0.41	1.10
4.0	0.28	0.24	15.	0.44	0.15	30.0	0.42	0.26	35.0	0.55	2.93
5.0	0.32	0.37	20.0	0.53	0.30	35.0	0.48	0.35	45.0	0.72	5.77
6.0	0.37	0.58	24.0	0.60	0.51	40.0	0.53	0.47	50.0	0.83	7.49
7.0	0.42	0.90	26.0	0.65	0.71	45.0	0.59	0.69	55.0	-	-
8.0	0.47	1.53	28.0	0.69	1.04	50.0	0.64	1.15			
8.5	0.50	2.19	30.0	0.73	1.93	52.5	0.67	1.65			
8.9	-	-	30.8	-	-	55.0	-	-			

SPECIMEN									
S8-45-2					S8-90-2				
LOAD	DEFLECTION				LOAD	DEFLECTION			
P	vert.	lat.	d1	d2	P	vert.	lat.	d1	d2
kN	mm	mm	mm	mm	kN	mm	mm	mm	mm
0.0	0.00	0.00	0.00	0.00	0.0	0.00	0.00	0.00	0.00
1.0	0.15	0.08	0.05	0.07	2.5	0.46	-0.04	0.10	0.11
4.0	0.29	0.27	0.06	0.06	5.0	0.57	-0.04	0.10	0.10
7.0	0.41	0.58	0.06	0.06	10.0	0.82	-0.03	0.16	0.07
9.0	0.49	0.90	0.06	0.05	15.0	1.02	0.02	0.16	0.04
11.0	0.58	1.37	0.06	0.03	20.0	1.13	0.12	0.16	0.04
12.0	0.62	1.67	0.05	0.02	25.0	1.23	0.30	0.16	0.02
13.0	0.67	2.16	0.05	0.02	30.0	1.33	0.62	0.16	0.01
14.0	0.72	2.78	0.05	-0.01	35.0	1.43	1.29	0.16	-0.02
15.0	0.79	4.01	0.05	-0.06	37.5	1.49	2.03	0.16	-0.04
15.8	-	-	-	-	39.5	-	-	-	-

SPECIMEN									
S8-135-2					S8-180-2				
LOAD	DEFLECTION				LOAD	DEFLECTION			
P	vert.	lat.	d1	d2	P	vert.	lat.	d1	d2
kN	mm	mm	mm	mm	kN	mm	mm	mm	mm
0.0	0.00	0.00	0.00	0.00	0.0	0.00	0.00	0.00	0.00
5.0	0.19	-0.03	0.05	0.09	5.0	0.39	0.05	0.10	0.10
15.0	0.38	-0.03	0.06	0.10	15.0	0.54	0.12	0.11	0.12
25.0	0.50	0.03	0.06	0.13	30.0	0.71	0.40	0.14	0.18
35.0	0.62	0.11	0.08	0.16	35.0	0.77	0.53	0.15	0.19
50.0	0.77	0.26	0.11	0.22	45.0	0.88	0.85	0.18	0.23
60.0	0.87	0.43	0.12	0.25	55.0	0.98	2.03	0.20	0.25
67.5	0.95	0.67	0.12	0.26	60.0	1.06	3.70	0.21	0.21
72.5	1.01	0.97	0.12	0.26	65.0	1.14	5.20	0.24	0.16
77.5	1.07	1.52	0.12	0.26	70.0	1.28	7.65	0.32	0.08
80.0	1.11	2.97	0.12	0.26	71.5	-	-	-	-

Table A.3.7. Load deflection data for series 8.

SPECIMEN							
S13-30-1				S13-30-2			
LOAD	DEFLECTION			LOAD	DEFLECTION		
P	vert.	lat.	d_1	P	vert.	lat.	d_1
kN	mm	mm	mm	kN	mm	mm	mm
0.0	0.00	0.00	0.00	0.0	0.00	0.00	0.00
10.0	0.16	0.00	-0.01	10.0	0.16	0.03	-0.06
30.0	0.38	0.04	-0.05	30.0	0.39	0.07	-0.01
50.0	0.58	0.12	-0.25	70.0	0.76	0.14	0.05
100.0	1.03	0.14	-0.70	100.0	0.98	0.14	0.09
160.0	1.62	0.14	-0.94	140.0	1.29	0.15	0.02
200.0	2.14	0.15	-1.18	180.0	1.58	0.15	-0.27
240.0	2.89	0.27	-1.70	220.0	1.87	0.15	-0.41
260.0	3.43	0.41	-2.05	240.0	2.06	0.15	-0.50
270.0	3.77	0.64	-2.29	260.0	2.49	0.02	-0.57
280.0	-	-	-	270.0	-	-ve	-

SPECIMEN							
S13-50-1				S13-50-2			
LOAD	DEFLECTION			LOAD	DEFLECTION		
P	vert.	lat.		P	vert.	lat.	d_1	d_2
kN	mm	mm		kN	mm	mm	mm	mm
0.0	0.00	0.00		0.0	0.00	0.00	0.00	0.00
13.1	0.23	0.00		6.5	0.14	0.00	0.00	-0.02
39.2	0.48	0.05		26.1	0.41	0.00	0.00	-0.07
78.3	0.80	0.05		52.2	0.61	0.00	-0.04	-0.12
117.5	1.15	0.05		78.3	0.87	0.00	-0.07	-0.16
143.6	1.39	0.05		104.4	1.08	0.00	-0.09	-0.21
169.7	1.70	0.05		130.5	1.28	0.00	-0.11	-0.26
195.8	2.29	0.05		156.6	1.47	0.00	-0.11	-0.30
208.9	2.81	0.05		169.7	1.59	0.00	-0.11	-0.32
215.4	3.16	0.05		182.8	1.72	0.04	-0.09	-0.34
221.9	-	-ve		195.8	-	-	-	-

SPECIMEN								
S13-70-1				S13-70-2				
LOAD	DEFLECTION			LOAD	DEFLECTION			
P	vert.	lat.	d_1	P	vert.	lat.	d_1	d_2
kN	mm	mm	mm	kN	mm	mm	mm	mm
0.0	0.00	0.00	0.00	0.0	0.00	0.00	0.00	0.00
5.3	0.12	0.04	-0.03	5.3	0.10	0.00	0.00	-0.01
16.0	0.24	0.16	-0.10	16.0	0.23	0.02	0.00	-0.04
37.2	0.47	0.31	-0.23	26.6	0.34	0.05	0.00	-0.05
58.5	0.69	0.48	-0.28	42.6	0.50	0.12	0.00	-0.08
69.2	0.80	0.60	-0.28	63.9	0.68	0.26	-0.05	-0.10
90.5	1.02	0.97	-0.28	85.1	0.87	0.51	-0.08	-0.13
95.8	1.07	1.17	-0.28	95.8	0.97	0.72	-0.09	-0.15
101.1	1.14	1.65	-0.28	101.1	1.04	1.09	-0.10	-0.16
106.4	1.21	2.85	-0.28	106.4	1.10	1.79	-0.10	-0.17
111.7	-	-	-	111.7	-	-	-	-

SPECIMEN									
S13-90-1					S13-90-2				
LOAD	DEFLECTION				LOAD	DEFLECTION			
P	vert.	lat.	d_1	d_2	P	vert.	lat.	d_1	d_2
kN	mm	mm	mm	mm	kN	mm	mm	mm	mm
0.0	0.00	0.00	0.00	0.00	0.0	0.00	0.00	0.00	0.00
2.5	0.06	0.00	-0.02	0.00	2.5	0.09	0.00	0.00	-0.01
5.0	0.10	0.00	-0.04	0.01	5.0	0.13	0.00	0.00	-0.01
10.0	0.20	0.00	-0.09	0.03	10.0	0.21	0.04	-0.04	-0.02
25.0	0.44	0.07	-0.17	0.06	25.0	0.42	0.29	-0.12	-0.02
40.0	0.64	0.35	-0.24	0.09	40.0	0.59	0.68	-0.16	-0.01
55.0	0.85	1.61	-0.29	0.12	55.0	0.76	1.66	-0.19	-0.01
65.0	1.00	3.66	-0.30	0.13	65.0	0.88	3.06	-0.19	-0.01
67.5	1.04	4.46	-0.28	0.14	70.0	0.97	5.47	-0.17	-0.01
70.0	1.10	-	-0.24	0.15	72.5	-	-	-	-

Table A.3.8. Load deflection data for series 13.

SPECIMEN									
S13-110-1					S13-110-2				
LOAD	DEFLECTION				LOAD	DEFLECTION			
P	vert.	lat.	d1	d2	P	vert.	lat.	d1	d2
kN	mm	mm	mm	mm	kN	mm	mm	mm	mm
0.0	0.00	0.00	0.00	0.00	0.0	0.00	0.00	0.00	0.00
10.6	0.08	0.62	0.00	-0.22	10.6	0.15	0.08	-0.04	-0.21
21.3	0.18	1.52	-0.02	-0.31	21.3	0.30	0.19	-0.04	-0.27
26.6	0.27	2.22	0.00	-0.33	31.9	0.40	0.32	-0.05	-0.29
31.9	0.34	3.21	0.02	-0.34	42.6	0.51	0.61	-0.08	-0.30
37.2	0.42	4.42	0.06	-0.34	47.9	0.58	1.09	-0.09	-0.31
39.9	0.46	5.01	0.09	-0.34	50.5	0.62	1.55	-0.10	-0.31
42.6	0.52	5.71	0.11	-0.31	53.2	0.66	2.40	-0.11	-0.31
45.2	0.57	6.61	0.15	-0.28	55.9	0.72	3.95	-0.13	-0.30
47.9	0.67	8.07	0.20	-0.20	58.5	0.81	5.95	-0.17	-0.22
50.5	-	-	-	-	61.2	-	-	-	-

SPECIMEN								
S13-130-1				S13-130-2				
LOAD	DEFLECTION			LOAD	DEFLECTION			
P	vert.	lat.	d1	P	vert.	lat.	d1	d2
kN	mm	mm	mm	kN	mm	mm	mm	mm
0.0	0.00	0.00	0.00	0.0	0.00	0.00	0.00	0.00
3.3	0.09	0.00	-0.04	3.3	0.22	0.10	-0.03	-0.01
5.2	0.17	0.02	-0.08	6.5	0.35	0.21	-0.06	-0.02
13.1	0.55	0.29	-0.16	13.1	0.50	0.38	-0.11	-0.02
23.5	0.84	1.00	-0.20	19.6	0.77	0.79	-0.16	0.01
28.7	1.01	1.62	-0.12	26.1	1.01	1.45	-0.23	0.06
33.9	1.18	2.50	0.00	32.6	1.22	2.43	-0.33	0.16
40.5	1.39	4.12	0.15	35.9	1.32	3.33	-0.40	0.24
43.1	1.53	5.80	0.19	39.2	1.46	5.03	-0.49	0.36
44.4	1.63	5.92	0.13	42.4	1.81	9.03	-0.81	0.69
45.7	-	-	-	43.1	-	-	-	-

SPECIMEN										
S13-140-1						S13-140-2				
LOAD	DEFLECTION					LOAD	DEFLECTION			
P	vert.	lat.	d1	d2	d3	P	vert.	lat.	d1	d2	d3
kN	mm	mm	mm	mm	mm	kN	mm	mm	mm	mm	mm
0.0	0.00	0.00	0.00	0.00	0.00	0.0	0.00	0.00	0.00	0.00	0.00
3.9	0.07	0.14	0.05	-0.02	0.03	1.5	0.00	0.02	-0.06	0.02	0.00
9.3	0.14	0.56	0.20	-0.19	0.20	3.1	0.04	0.05	-0.11	0.06	0.00
12.4	0.20	0.87	0.26	-0.28	0.30	9.3	0.27	0.27	-0.18	0.13	0.20
15.6	0.29	1.19	0.29	-0.37	0.40	15.6	0.47	0.56	-0.22	0.25	0.39
18.7	0.37	1.65	0.37	-0.44	0.50	18.7	0.56	0.78	-0.27	0.30	0.48
21.8	0.46	2.16	0.43	-0.46	0.61	21.8	0.68	1.00	-0.30	0.37	0.58
24.9	0.61	2.91	0.42	-0.42	0.72	24.9	0.84	1.29	-0.31	0.42	0.68
28.0	0.82	4.76	0.40	-0.34	1.03	28.0	0.99	2.27	-0.33	0.48	0.80
31.1	1.15	8.08	0.28	-0.09	1.21	31.1	1.23	5.77	-0.35	0.63	1.10
32.7	-	-	-	-	-	32.7	-	-	-	-	-

Table A.3.8. Load deflection data for series 13 (continued).

SPECIMEN											
S9-1-2				S9-1-3				S9-2-2			
LOAD	STRESS	DEFLECTION		LOAD	STRESS	DEFLECTION		LOAD	STRESS	DEFLECTION	
P	f	vert.	lat.	P	f	vert.	lat.	P	f	vert.	lat.
kN	N/mm2	mm	mm	kN	N/mm2	mm	mm	kN	N/mm2	mm	mm
0.0	0.0	0.00	0.00	0.0	0.0	0.00	0.00	0.0	0.0	0.00	0.00
2.0	20.0	0.22	0.09	2.0	20.0	0.04	0.00	2.0	20.0	0.16	0.06
5.0	49.9	0.30	0.10	5.0	50.0	0.07	0.00	4.0	40.1	0.21	0.07
10.0	99.8	0.35	0.11	10.0	100.0	0.12	0.00	10.0	100.3	0.32	0.10
15.0	149.6	0.39	0.13	15.0	150.0	0.16	0.00	15.0	150.4	0.40	0.14
20.0	199.5	0.43	0.15	20.0	200.0	0.19	0.00	20.0	200.5	0.46	0.20
25.0	249.4	0.48	0.19	25.0	250.2	0.23	0.04	25.0	250.7	0.53	0.26
30.0	299.3	0.53	0.22	30.0	300.3	0.26	0.07	27.0	270.7	0.55	0.28
35.0	349.1	0.60	0.26	35.0	350.3	0.30	0.10	29.0	290.8	0.58	0.32
36.0	359.1	0.62	0.25	36.5	365.3	0.32	0.10	30.0	300.8	0.60	0.35
36.9	368.7	-	-	36.9	369.3	-	-	30.9	309.8	-	-

Table A.3.9. Load deflection data for series 9.

SPECIMEN											
S9-2-3				S9-3-2				S9-3-3			
LOAD	STRESS	DEFLECTION		LOAD	STRESS	DEFLECTION		LOAD	STRESS	DEFLECTION	
P	f	vert.	lat.	P	f	vert.	lat.	P	f	vert.	lat.
kN	N/mm2	mm	mm	kN	N/mm2	mm	mm	kN	N/mm2	mm	mm
0.0	0.0	0.00	0.00	0.0	0.0	0.00	0.00	0.0	0.0	0.00	0.00
2.0	20.1	0.10	0.01	1.0	10.0	0.03	0.00	1.0	9.9	0.03	0.00
4.0	40.4	0.14	0.01	4.0	40.1	0.13	0.01	2.0	19.8	0.06	0.00
8.0	80.7	0.20	0.01	8.0	80.2	0.21	0.02	4.0	39.7	0.11	0.02
12.0	121.1	0.24	0.01	12.0	120.4	0.26	0.05	8.0	79.3	0.17	0.06
20.0	201.9	0.31	0.01	16.0	160.5	0.31	0.09	12.0	119.0	0.23	0.10
24.0	242.2	0.35	0.01	20.0	200.6	0.36	0.17	16.0	158.6	0.28	0.15
28.0	282.6	0.39	0.02	22.0	220.7	0.39	0.25	20.0	198.3	0.33	0.26
31.5	317.9	0.42	0.05	23.0	230.7	0.41	0.32	22.0	218.1	0.36	0.40
33.0	333.1	0.43	0.07	24.0	240.7	0.42	0.44	23.0	228.0	0.37	0.55
33.5	338.1	0.44	0.10	24.8	248.8	-	-	23.7	235.0	-	-

SPECIMEN											
S9-4-2				S9-4-3				S9-5-2			
LOAD	STRESS	DEFLECTION		LOAD	STRESS	DEFLECTION		LOAD	STRESS	DEFLECTION	
P	f	vert.	lat.	P	f	vert.	lat.	P	f	vert.	lat.
kN	N/mm2	mm	mm	kN	N/mm2	mm	mm	kN	N/mm2	mm	mm
0.0	0.0	0.00	0.00	0.0	0.0	0.00	0.00	0.0	0.0	0.00	0.00
1.0	10.2	0.22	0.07	1.0	10.0	0.03	0.00	0.5	5.1	0.37	0.33
3.0	30.5	0.32	0.09	2.0	20.0	0.05	0.01	1.0	10.2	0.44	0.34
5.0	50.8	0.40	0.10	4.0	40.1	0.09	0.02	2.0	20.3	0.49	0.35
9.0	91.4	0.48	0.16	6.0	60.1	0.12	0.02	4.0	40.6	0.54	0.37
11.0	111.7	0.51	0.22	8.0	80.1	0.14	0.03	6.0	60.9	0.58	0.39
13.0	132.0	0.55	0.34	12.0	120.2	0.19	0.04	7.0	71.1	0.60	0.41
14.0	142.1	0.56	0.44	15.0	150.2	0.22	0.07	8.0	81.3	0.63	0.44
15.0	152.3	0.58	0.62	16.5	165.2	0.24	0.19	8.6	87.4	0.69	0.93
16.0	162.4	0.61	1.45	17.5	175.2	0.25	0.50	8.8	89.4	0.72	1.88
16.0	162.8	-	-	17.8	178.2	-	-	8.8	89.7	-	-

SPECIMEN											
S9-5-3				S9-6-2				S9-6-3			
LOAD	STRESS	DEFLECTION		LOAD	STRESS	DENLECTION		LOAD	STRESS	DEFLECTION	
P	f	vert.	lat.	P	f	vert.	lat.	P	f	vert.	lat.
kN	N/mm2	mm	mm	kN	N/mm2	mm	mm	kN	N/mm2	mm	mm
0.0	0.0	0.00	0.00	0.0	0.0	0.00	0.00	0.0	0.0	0.00	0.00
1.0	10.0	0.07	0.00	0.5	5.0	0.43	0.18	0.5	5.0	0.09	0.08
2.0	20.0	0.11	0.00	1.0	10.0	0.48	0.18	1.0	10.0	0.11	0.08
4.0	39.9	0.17	0.01	2.0	20.0	0.52	0.18	2.0	19.9	0.15	0.08
6.0	59.9	0.21	0.04	3.0	30.0	0.55	0.18	4.0	39.8	0.19	0.05
8.0	79.8	0.25	0.12	5.0	50.0	0.59	0.12	5.0	49.8	0.22	0.01
9.5	94.8	0.28	0.26	6.0	60.0	0.61	0.05	6.0	59.7	0.24	-0.06
10.5	104.8	0.30	0.43	7.0	70.0	0.63	-0.06	7.0	69.7	0.26	-0.19
11.4	113.8	0.32	0.75	7.8	78.1	0.65	-0.27	7.5	74.7	0.27	-0.33
12.0	119.8	0.35	1.51	8.0	80.1	0.66	-0.44	8.0	79.6	0.28	-0.65
12.2	121.4	-	-	8.2	82.2	-	-	8.2	81.3	-	-

SPECIMEN											
S9-7-1				S9-7-2				S9-7-3			
LOAD	STRESS	DEFLECTION		LOAD	STRESS	DEFLECTION		LOAD	STRESS	DEFLECTION	
P	f	vert.	lat.	P	f	vert.	lat.	P	f	vert.	lat.
kN	N/mm2	mm	mm	kN	N/mm2	mm	mm	kN	N/mm2	mm	mm
0.0	0.0	0.00	0.00	0.0	0.0	0.00	0.00	0.0	0.0	0.00	0.00
0.5	5.0	0.20	0.11	0.5	5.0	0.20	0.11	0.5	5.0	0.06	-0.02
1.0	9.9	0.25	0.11	1.0	9.9	0.25	0.11	1.0	10.1	0.10	-0.02
2.0	19.8	0.29	0.11	2.0	19.8	0.29	0.11	2.0	20.1	0.17	-0.01
3.0	29.7	0.31	0.15	3.0	29.7	0.31	0.15	3.0	30.2	0.22	0.02
4.0	39.6	0.34	0.22	4.0	39.6	0.34	0.22	4.0	40.2	0.25	0.07
5.0	49.5	0.36	0.36	5.0	49.6	0.36	0.36	5.0	50.3	0.27	0.17
6.0	59.4	0.39	0.82	6.2	61.4	0.40	1.05	6.0	60.4	0.29	0.56
6.2	61.4	0.40	1.05	6.4	63.4	0.41	1.44	6.4	64.4	0.31	1.36
6.6	65.4	0.44	2.41	6.6	65.4	0.44	2.41	6.5	65.4	0.34	2.17
6.7	66.5	-	-	6.7	66.5	-	-	6.6	66.2	-	-

Table A.3.9. Load deflection data for series 9 (continued).

SPECIMEN									
S10-7-1					S10-7-2				
LOAD	STRESS	DEFLECTION			LOAD	STRESS	DEFLECTION		
P	f	vert.	axial	lat.	P	f	vert.	axial	lat.
kN	N/mm2	mm	mm	mm	kN	N/mm2	mm	mm	mm
0.0	0.0	0.00	0.00	0.00	0.0	0.0	0.00	0.00	0.00
2.5	35.3	0.09	0.06	0.00	2.5	35.3	0.11	0.08	0.01
7.5	105.8	0.19	0.13	0.00	7.5	105.8	0.22	0.16	0.02
12.5	176.4	0.28	0.20	0.00	12.5	176.4	0.32	0.23	0.03
17.5	246.9	0.38	0.27	0.00	17.5	246.9	0.43	0.30	0.05
22.0	310.4	0.48	0.34	0.00	22.5	317.5	0.55	0.39	0.06
23.5	331.5	0.52	0.37	0.00	24.0	338.6	0.60	0.42	0.07
25.0	352.7	0.57	0.40	0.00	25.0	352.8	0.63	0.45	0.07
26.0	366.8	0.61	0.43	0.01	26.0	366.9	0.66	0.47	0.07
26.5	373.9	0.66	0.47	0.03	26.5	373.9	0.69	0.49	0.09
27.0	380.9	0.81	0.57	0.13	27.0	381.0	0.72	0.51	0.10

SPECIMEN									
S10-6-1					S10-6-2				
LOAD	STRESS	DEFLECTION			LOAD	STRESS	DEFLECTION		
P	f	vert.	axial	lat.	P	f	vert.	axial	lat.
kN	N/mm2	mm	mm	mm	kN	N/mm2	mm	mm	mm
0.0	0.0	0.00	0.00	0.00	0.0	0.0	0.00	0.00	0.00
2.5	35.2	0.16	0.11	0.00	2.5	35.2	0.24	0.10	0.10
5.0	70.4	0.24	0.17	-0.02	5.0	70.5	0.35	0.25	0.16
7.5	105.6	0.31	0.22	-0.04	7.5	105.7	0.45	0.32	0.21
10.0	140.7	0.38	0.27	-0.04	12.5	176.1	0.60	0.42	0.24
12.5	175.9	0.44	0.31	-0.04	17.5	246.6	0.73	0.52	0.27
17.5	246.3	0.58	0.41	-0.03	20.0	281.8	0.82	0.58	0.27
20.0	281.5	0.65	0.46	-0.01	21.5	303.0	0.88	0.62	0.28
21.5	302.6	0.70	0.49	0.01	23.0	324.1	0.92	0.65	0.28
22.0	309.6	0.72	0.51	0.06	23.5	331.1	0.94	0.66	0.29
22.5	316.7	-	-	-	23.9	336.1	-	-	-

SPECIMEN									
S10-5-1					S10-5-2				
LOAD	STRESS	DEFLECTION			LOAD	STRESS	DEFLECTION		
P	f	vert.	axial	lat.	P	f	vert.	axial	lat.
kN	N/mm2	mm	mm	mm	kN	N/mm2	mm	mm	mm
0.0	0.0	0.00	0.00	0.00	0.0	0.0	0.00	0.00	0.00
2.5	35.4	0.34	0.24	0.04	2.5	35.4	0.16	0.11	0.05
5.0	70.8	0.42	0.30	0.06	5.0	70.7	0.26	0.18	0.06
7.5	106.2	0.49	0.35	0.08	7.5	106.1	0.36	0.25	0.08
10.0	141.7	0.56	0.40	0.11	10.0	141.5	0.44	0.31	0.11
12.5	177.1	0.64	0.45	0.17	12.5	176.9	0.52	0.37	0.16
14.0	198.3	0.68	0.48	0.22	14.0	198.1	0.57	0.40	0.20
16.0	226.7	0.75	0.53	0.34	15.0	212.2	0.60	0.42	0.25
16.5	233.7	0.77	0.54	0.38	17.0	240.5	-	-	-
17.0	240.8	0.78	0.55	0.43					
17.5	247.9	-	-	-					

SPECIMEN									
S10-4-1					S10-4-2				
LOAD	STRESS	DEFLECTION			LOAD	STRESS	DEFLECTION		
P	f	vert.	axial	lat.	P	f	vert.	axial	lat.
kN	N/mm2	mm	mm	mm	kN	N/mm2	mm	mm	mm
0.0	0.0	0.00	0.00	0.00	0.0	0.0	0.00	0.00	0.00
1.0	14.3	0.12	0.08	0.06	1.0	14.1	0.10	0.07	0.11
2.0	28.6	0.18	0.13	0.08	2.0	28.2	0.15	0.11	0.18
4.0	57.3	0.27	0.19	0.11	3.0	42.3	0.18	0.13	0.26
6.0	85.9	0.35	0.25	0.16	4.0	56.4	0.22	0.16	0.33
8.0	114.5	0.44	0.31	0.23	5.0	70.6	0.25	0.18	0.44
9.0	128.8	0.48	0.34	0.28	6.0	84.7	0.29	0.21	0.58
10.0	143.2	0.52	0.37	0.35	7.0	98.8	0.33	0.23	0.74
11.0	157.5	0.56	0.40	0.46	8.0	112.9	0.33	0.26	0.97
12.0	171.8	0.60	0.42	0.70	9.0	127.0	0.42	0.30	1.51
12.8	183.2	-	-	-	9.3	130.9	-	-	-

Table A.3.10. Load deflection data for series 10.

SPECIMEN									
S10-3-1					S10-3-2				
LOAD	STRESS	DEFLECTION			LOAD	STRESS	DEFLECTION		
P	f	vert.	axial	lat.	P	f	vert.	axial	lat.
kN	N/mm2	mm	mm	mm	kN	N/mm2	mm	mm	mm
0.0	0.0	0.00	0.00	0.00	0.0	0.0	0.00	0.00	0.00
1.0	14.2	0.16	0.11	0.08	1.0	14.1	0.13	0.09	0.10
2.0	28.3	0.23	0.16	0.12	2.0	28.3	0.19	0.13	0.17
3.0	42.5	0.28	0.20	0.17	3.0	42.4	0.24	0.17	0.26
4.0	56.6	0.33	0.23	0.23	4.0	56.6	0.29	0.21	0.38
5.0	70.8	0.37	0.26	0.34	5.0	70.7	0.34	0.24	0.55
6.0	84.9	0.42	0.30	0.51	6.0	84.9	0.40	0.28	0.82
7.0	99.1	0.47	0.33	0.83	6.5	92.0	0.43	0.30	1.02
7.5	106.1	0.50	0.35	1.14	7.0	99.0	0.46	0.33	1.31
8.0	113.2	0.54	0.38	1.96	7.5	106.1	0.49	0.35	1.80
8.1	114.6	-	-	-	7.9	111.8	-	-	-
SPECIMEN									
S10-2-1					S10-2-2				
LOAD	STRESS	DEFLECTION			LOAD	STRESS	DEFLECTION		
P	f	vert.	axial	lat.	P	f	vert.	axial	lat.
kN	N/mm2	mm	mm	mm	kN	N/mm2	mm	mm	mm
0.0	0.0	0.00	0.00	0.00	0.0	0.0	0.00	0.00	0.00
0.5	7.2	0.10	0.07	0.04	0.5	7.1	0.07	0.05	0.02
1.0	14.4	0.15	0.11	0.10	1.5	21.2	0.16	0.11	0.05
2.0	28.8	0.21	0.15	0.22	2.0	28.3	0.19	0.13	0.06
3.0	43.1	0.27	0.19	0.41	3.0	42.4	0.24	0.17	0.11
3.5	50.3	0.30	0.21	0.57	4.0	56.6	0.28	0.20	0.22
4.0	57.5	0.32	0.23	0.82	4.5	63.6	0.31	0.22	0.33
4.5	64.7	0.35	0.25	1.31	5.0	70.7	0.33	0.23	0.54
5.0	71.9	0.39	0.28	2.28	5.5	77.8	0.36	0.25	1.03
5.2	75.5	0.43	0.30	3.48	5.8	81.3	0.38	0.27	1.58
5.3	76.6	-	-	-	6.0	84.6	-	-	-
SPECIMEN									
S10-1-1					S10-1-2				
LOAD	STRESS	DEFLECTION			LOAD	STRESS	DEFLECTION		
P	f	vert.	axial	lat.	P	f	vert.	axial	lat.
kN	N/mm2	mm	mm	mm	kN	N/mm2	mm	mm	mm
0.0	0.0	0.00	0.00	0.00	0.0	0.0	0.00	0.00	0.00
0.5	7.0	0.22	0.16	-0.05	0.5	7.1	0.10	0.07	0.15
1.0	14.1	0.27	0.19	0.01	1.0	14.1	0.18	0.13	0.34
1.5	21.1	0.30	0.21	0.10	1.5	21.2	0.22	0.16	0.59
2.0	28.2	0.32	0.23	0.24	2.0	28.2	0.26	0.18	0.93
2.5	35.2	0.35	0.25	0.47	2.5	35.3	0.31	0.22	1.50
3.0	42.3	0.38	0.27	0.86	3.0	42.4	0.36	0.25	2.43
3.5	49.3	0.41	0.29	1.69	3.3	45.9	0.40	0.28	3.24
3.8	52.8	0.44	0.31	2.57	3.5	49.4	0.45	0.32	4.22
4.0	56.4	0.49	0.35	4.03	3.8	53.0	-	-	-
4.3	59.9	-	-	-					

Table A.3.10. Load deflection data for series 10 (continued).

S11-150-1									
LOAD	DEFLECTION								
P	vert.	dH1	dH2	dH3	d4	d5	d6	d7	d8
kN	mm	mm	mm	mm	mm	mm	mm	mm	mm
0.0	0.00	0.00	0.00	0.00	0.00	0.00	0.00	0.00	0.00
10.0	0.29	0.10	0.43	0.07	0.12	0.09	0.04	0.04	0.04
15.0	0.37	0.19	0.65	0.16	-	-	-	-	-
20.0	0.45	0.29	0.89	0.28	0.21	0.14	0.08	0.07	0.09
25.0	0.52	0.40	1.16	0.44	-	-	-	-	-
30.0	0.59	0.53	1.44	0.63	0.29	0.19	0.11	0.09	0.12
35.0	0.66	0.69	1.74	0.91	-	-	-	-	-
40.0	0.72	0.89	2.13	1.29	0.36	0.22	0.13	0.10	0.14
45.0	0.79	1.23	2.65	1.87	-	-	-	-	-
50.0	0.87	1.91	3.53	2.78	0.43	0.27	0.14	0.09	0.12
55.0	-	-	-	-	-	-	-	-	-

Table A.3.11. Load deflection data for series 11.

SPECIMEN												
S2-0-1			S2-4-1			S2-8-1			S2-12-1		
LOAD	DEFLECTION		LOAD	DEFLECTION		LOAD	DEFLECTION		LOAD	DEFLECTION	
P	vert.	lat.	P	vert.	lat.	P	vert.	lat.	P	vert.	lat.
kN	mm	mm	kN	mm	mm	kN	mm	mm	kN	mm	mm
0.0	0.00	0.00	0.0	0.00	0.00	0.0	0.00	0.00	0.0	0.00	0.00
10.0	0.27	0.05	10.0	0.30	0.03	10.0	0.31	0.14	10.0	0.47	0.08
20.0	0.40	0.14	20.0	0.44	0.04	20.0	0.44	0.27	20.0	0.62	0.17
30.0	0.51	0.27	30.0	0.54	0.10	30.0	0.55	0.47	30.0	0.72	0.26
40.0	0.61	0.44	40.0	0.63	0.15	40.0	0.64	0.79	40.0	0.81	0.39
50.0	0.70	0.67	50.0	0.71	0.23	50.0	0.73	1.26	50.0	0.88	0.60
60.0	0.79	1.08	65.0	0.84	0.50	60.0	0.83	1.97	60.0	0.96	1.07
65.0	0.84	1.39	75.0	0.92	0.93	70.0	0.92	3.00	70.0	1.04	2.48
70.0	0.89	1.82	80.0	0.97	1.51	80.0	1.03	4.76	75.0	1.11	4.38
75.0	0.94	2.59	85.0	1.02	2.71	85.0	1.14	6.36	80.0	1.28	-
80.0	1.04	8.09	90.0	1.09	4.71	89.2	1.33	-			

SPECIMEN												
S2-16-1			S2-20-1			S2-0-2			S2-4-2		
LOAD	DEFLECTION		LOAD	DEFLECTION		LOAD	DEFLECTION		LOAD	DEFLECTION	
P	vert.	lat.	P	vert.	lat.	P	vert.	lat.	P	vert.	lat.
kN	mm	mm	kN	mm	mm	kN	mm	mm	kN	mm	mm
0.0	0.00	0.00	0.0	0.00	0.00	0.0	0.00	0.00	0.0	0.00	0.00
10.0	0.34	0.03	10.0	0.72	0.07	10.0	0.30	0.03	10.0	0.26	0.00
20.0	0.42	0.10	20.0	0.89	0.16	20.0	0.44	0.05	20.0	0.39	0.04
40.0	0.58	0.21	30.0	0.98	0.28	30.0	0.55	0.08	40.0	0.55	0.12
60.0	0.75	0.35	40.0	1.10	0.43	50.0	0.71	0.16	60.0	0.68	0.23
70.0	0.82	0.46	50.0	1.17	0.63	65.0	0.83	0.25	75.0	0.78	0.35
80.0	0.90	0.63	60.0	1.24	0.90	80.0	0.96	0.40	85.0	0.86	0.48
90.0	0.98	0.93	70.0	1.32	1.22	90.0	1.05	0.51	95.0	0.93	0.74
95.0	1.02	1.23	75.0	1.41	1.73	95.0	1.10	0.66	100.0	0.98	1.09
100.0	1.06	1.94	80.0	1.51	2.66	100.0	1.16	2.17	105.0	1.04	3.44
101.7	1.09	-	85.0	1.70	-	105.0	-	-	106.7	-	-

SPECIMEN												
S2-8-2			S2-12-2			S2-16-2			S2-20-2		
LOAD	DEFLECTION		LOAD	DEFLECTION		LOAD	DEFLECTION		LOAD	DEFLECTION	
P	vert.	lat.	P	vert.	lat.	P	vert.	lat.	P	vert.	lat.
kN	mm	mm	kN	mm	mm	kN	mm	mm	kN	mm	mm
0.0	0.00	0.00	0.0	0.00	0.00	0.0	0.00	0.00	0.0	0.00	0.00
10.0	0.32	0.04	10.0	0.35	0.11	10.0	0.50	0.03	10.0	0.23	0.01
30.0	0.59	0.05	20.0	0.48	0.21	30.0	0.72	0.03	20.0	0.36	0.01
50.0	0.81	0.01	30.0	0.58	0.34	50.0	0.90	0.05	30.0	0.46	0.03
60.0	0.88	-0.02	40.0	0.67	0.51	70.0	1.07	0.23	50.0	0.64	0.06
70.0	0.98	-0.08	50.0	0.75	0.75	80.0	1.13	0.45	60.0	0.72	0.09
80.0	1.05	-0.15	60.0	0.83	1.22	85.0	1.17	0.59	70.0	1.80	0.13
85.0	1.10	-0.23	70.0	0.92	2.21	90.0	1.21	0.80	80.0	1.95	0.29
90.0	1.14	-0.34	75.0	0.98	3.24	95.0	1.26	1.11	85.0	2.04	0.61
95.0	1.18	-0.55	80.0	1.05	4.64	100.0	1.32	1.71	90.0	2.11	1.49
100.0	1.23	-1.14	85.0	-	-	105.0	-	-	107.1	-	-
105.0	1.33	-									

Table A.3.12. Load deflection data for series 2.

SPECIMEN							
S5a-75-1							
LOAD	DEFLECTION						
P	vert.	lat.	d1	d2	d3	d4	d5
kN	mm	mm	mm	mm	mm	mm	mm
0.0	0.00	0.00	0.00	0.00	0.00	0.00	0.00
10.0	0.22	0.05	0.11	0.10	0.09	0.08	0.06
30.0	0.41	0.10	0.22	0.21	0.20	0.19	0.17
70.0	0.66	0.28	0.36	0.31	0.30	0.29	0.25
110.0	0.93	0.70	0.45	0.38	0.36	0.33	0.29
130.0	1.27	1.13	0.49	0.41	0.38	0.34	0.29
145.0	1.74	2.26	0.53	0.43	0.39	0.33	0.26
150.0	1.92	3.44	0.55	0.43	0.38	0.31	0.23
155.0	2.18	5.91	0.58	0.43	0.34	0.24	0.12
157.5	2.37	8.11	0.61	0.42	0.30	0.15	0.01

Table A.3.13. Load deflection data for series 5a.

SPECIMEN							
S5a-300-1							
LOAD	DEFLECTION						
P	vert.	lat.	d_1	d_2	d_3	d_4	d_5
kN	mm	mm	mm	mm	mm	mm	mm
0.0	0.00	0.00	0.00	0.00	0.00	0.00	0.00
4.8	0.24	0.10	0.16	0.14	0.12	0.11	0.08
14.5	0.51	0.24	0.37	0.34	0.28	0.24	0.17
24.2	0.77	0.44	0.58	0.52	0.44	0.37	0.24
31.5	0.95	0.76	0.74	0.66	0.55	0.46	0.28
36.3	1.10	1.47	0.77	0.76	0.63	0.52	0.32
38.7	1.19	2.49	0.95	0.83	0.69	0.55	0.34
39.7	1.25	3.39	1.00	0.88	0.72	0.58	0.35
41.1	1.35	4.67	1.08	0.95	0.78	0.61	0.36
42.6	1.48	6.32	1.20	1.05	0.84	0.65	0.38
44.3	-	-	-	-	-	-	-

Table A.3.13. Load deflection data for series 5a (continued).

SPECIMEN									
S14-0-1					S14-0-2				
LOAD	DEFLECTION				LOAD	DEFLECTION			
P	vert.	lat.	d_w	d_1	P	vert.	lat.	d_w	d_1
kN	mm	mm	mm	mm	kN	mm	mm	mm	mm
0.0	0.00	0.00	0.000	0.00	0.0	0.00	0.00	0.000	0.00
25.0	0.15	0.04	0.000	0.04	50.0	0.23	0.04	0.004	-0.10
50.0	0.25	0.04	0.010	0.06	100.0	0.46	0.13	0.008	-0.16
100.0	0.40	0.04	0.026	0.06	175.0	0.68	0.32	0.012	-0.21
150.0	0.54	0.04	0.038	0.06	275.0	0.99	0.58	0.028	-0.30
200.0	0.68	0.09	0.064	0.06	325.0	1.17	0.73	0.048	-0.33
250.0	0.85	0.06	0.096	0.04	350.0	1.32	0.90	0.060	-0.34
275.0	0.93	0.02	0.114	0.03	387.5	1.69	1.64	0.096	-0.28
300.0	1.09	-0.02	0.170	0.03	400.0	2.00	2.59	0.170	-0.14
325.0	1.77	-0.51	0.718	0.25	412.5	2.34	4.02	0.324	0.07
337.5	-	-	-	-	425.0	-	-	-	-

SPECIMEN											
S14-0-3						S14-0-4					
LOAD	DEFLECTION					LOAD	DEFLECTION				
P	vert.	lat.	d_w	d_1	d_2	P	vert.	lat.	dw	d_1	d_2
kN	mm	mm	mm	mm	mm	kN	mm	mm	mm	mm	mm
0.0	0.00	0.00	0.000	0.00	0.00	0.0	0.00	0.00	0.000	0.00	0.00
50.0	0.27	0.04	0.000	-0.06	-0.03	25.0	0.24	0.09	0.008	0.91	1.55
75.0	0.40	0.04	0.000	-0.06	-0.02	50.0	0.42	0.13	0.009	1.01	1.81
150.0	0.63	0.07	0.005	-0.06	-0.01	75.0	0.56	0.15	0.009	1.08	2.01
225.0	0.87	0.08	0.022	-0.15	-0.07	150.0	0.79	0.16	0.000	1.25	2.32
275.0	1.08	0.09	0.053	-0.19	-0.09	225.0	0.96	0.17	0.000	1.35	2.48
300.0	1.25	0.13	0.074	-0.19	-0.10	300.0	1.12	0.17	0.000	1.46	2.59
325.0	2.29	0.40	0.690	-0.20	0.01	375.0	1.29	0.19	-0.004	1.51	2.69
350.0	3.09	0.85	0.996	-0.25	0.00	425.0	1.45	0.19	0.000	1.51	2.79
387.5	5.28	6.93	1.964	-0.44	-0.04	450.0	1.70	0.29	-0.623	1.42	3.01
395.0	-	-	-	-	-	475.0	-	-	-	-	-

SPECIMEN									
S14-2-1					S14-2-2				
LOAD	DEFLECTION				LOAD	DEFLECTION			
P	vert.	lat.	d_w	d_1	P	vert.	lat.	dw	d_1
kN	mm	mm	mm	mm	kN	mm	mm	mm	mm
0.0	0.00	0.00	0.000	0.00	0.0	0.00	0.00	0.000	0.00
25.0	0.12	0.04	0.000	0.08	50.0	0.20	0.07	0.000	0.31
100.0	0.41	0.07	0.000	-0.20	125.0	0.37	0.11	0.000	0.25
175.0	0.64	0.12	0.000	-0.39	200.0	0.52	0.12	0.000	0.21
250.0	0.91	0.24	0.000	-0.51	275.0	0.67	0.14	0.000	0.15
300.0	1.23	0.35	0.000	-0.57	350.0	0.81	0.14	-0.002	0.07
362.5	2.14	0.75	-0.002	-0.67	400.0	0.93	0.14	-0.002	0.01
375.0	2.46	1.00	-0.004	-0.69	450.0	1.11	0.11	-0.003	0.08
400.0	3.28	2.25	-0.006	-0.73	475.0	1.26	-0.03	-0.004	0.11
425.0	4.31	5.80	-0.006	-0.90	512.5	1.84	-1.38	-0.004	0.14
437.5	-	-	-	-	525.0	-	-	-	-

Table A.3.14. Load deflection data for series 14.

SPECIMEN											
S14-2-3						S14-2-4					
LOAD	DEFLECTION					LOAD	DEFLECTION				
P	vert.	lat.	d_w	d1	d2	P	vert.	lat.	dw	d1	d2
kN	mm	mm	mm	mm	mm	kN	mm	mm	mm	mm	mm
0.0	0.00	0.00	0.000	0.00	0.00	0.0	0.00	0.00	0.000	0.00	0.00
50.0	0.27	-0.03	-0.002	0.03	0.07	50.0	0.69	0.01	0.000	0.25	-0.30
125.0	0.53	-0.01	-0.003	0.05	0.09	100.0	0.83	0.05	-0.002	0.25	-0.33
200.0	0.74	0.02	-0.004	0.05	0.08	200.0	1.04	0.09	-0.003	0.21	-0.38
275.0	1.06	0.05	-0.006	0.03	0.01	300.0	1.24	0.12	-0.004	0.16	-0.45
325.0	1.60	0.09	-0.007	-0.04	-0.10	400.0	1.46	0.15	-0.005	0.08	-0.53
350.0	2.11	0.18	-0.008	-0.09	-0.14	475.0	1.68	0.19	-0.006	0.00	-0.59
400.0	3.35	0.82	-0.008	-0.15	-0.23	500.0	1.84	0.27	-0.006	-0.11	-0.58
425.0	4.07	2.01	-0.008	-0.24	-0.27	525.0	2.18	0.62	-0.008	-0.30	-0.50
450.0	4.81	4.61	-0.008	-0.38	-0.29	550.0	2.64	2.54	-0.009	-0.63	-0.35
462.5	-	-	-	-	-	538.8	-	-	-	-	-

Table A.3.14. Load deflection data for series 14 (continued).

SPECIMEN										
S15-0-1					S15-0-2				
LOAD	DEFLECTION				LOAD	DEFLECTION			
P	vert.	lat.	d1	d2	P	vert.	lat.	d1	d2
kN	mm	mm	mm	mm	kN	mm	mm	mm	mm
0.0	0.00	0.00	0.00	0.00	0.0	0.00	0.00	0.00	0.00
25.0	0.26	0.03	0.38	0.38	25.0	0.47	0.06	0.43	0.65
75.0	0.52	0.09	0.38	0.38	50.0	0.60	0.14	0.42	0.67
125.0	0.71	0.10	0.36	0.36	100.0	0.77	0.22	0.40	0.70
175.0	0.92	0.10	0.35	0.34	200.0	1.04	0.27	0.41	0.78
225.0	1.27	0.10	0.31	0.32	300.0	1.47	0.31	0.41	0.86
275.0	1.88	0.09	0.30	0.21	350.0	1.49	0.35	0.39	0.90
312.5	2.75	0.13	0.32	0.08	575.0	1.64	0.44	0.35	0.98
337.5	3.77	0.21	0.33	-0.12	400.0	1.94	0.74	0.22	1.19
362.5	5.02	0.42	0.26	-0.10	425.0	2.59	2.49	0.05	1.73
375.0	-	-	-	-	437.5	-	3.69	-	-
SPECIMEN									
S15-2-1					S15-2-2				
LOAD	DEFLECTION				LOAD	DEFLECTION			
P	vert.	lat.	d1	d2	P	vert.	lat.	d1	d2
kN	mm	mm	mm	mm	kN	mm	mm	mm	mm
0.0	0.00	0.00	0.00	0.00	0.0	0.00	0.00	0.00	0.00
50.0	0.27	0.07	0.21	0.28	50.0	0.18	0.02	0.56	0.57
150.0	0.56	0.11	0.25	0.32	100.0	0.33	0.02	0.62	0.62
250.0	0.87	0.18	0.25	0.31	225.0	0.59	0.01	0.70	0.68
300.0	1.10	0.27	0.24	0.24	350.0	0.85	0.02	0.70	0.70
350.0	1.57	0.49	0.19	0.08	425.0	1.01	0.03	0.70	0.70
387.5	2.14	0.83	0.17	-0.08	475.0	1.18	0.02	0.70	0.69
412.5	2.77	1.54	0.14	-0.15	500.0	1.42	0.08	0.57	0.73
437.5	3.78	4.94	-0.03	-0.21	537.5	2.05	0.76	0.04	0.89
450.0	4.74	17.84	-0.34	0.09	556.3	2.60	3.08	-0.19	1.06
456.3	-	-	-	-	562.5	-	-	-	-

Table A.3.15. Load deflection data for series 15.

SPECIMEN											
S16-6-1						S16-6-2					
LOAD	DEFLECTION					LOAD	DEFLECTION				
P	vert.	lat.	d_w	d1	d2	P	vert.	lat.	d_w	d1	d2
kN	mm	mm	mm	mm	mm	kN	mm	mm	mm	mm	mm
0.0	0.00	0.00	0.000	0.00	0.00	0.0	0.00	0.00	0.000	0.00	0.00
50.0	0.26	0.08	0.000	0.11	0.09	50.0	0.35	0.03	0.000	0.70	0.69
125.0	0.52	0.12	0.000	0.00	-0.02	100.0	0.54	0.01	0.000	0.75	0.69
225.0	0.85	0.21	0.001	-0.03	-0.03	175.0	0.78	-0.02	-0.001	0.80	0.67
300.0	1.22	0.28	-0.003	-0.03	-0.10	300.0	1.10	-0.05	-0.002	0.83	0.58
350.0	1.80	0.32	-0.005	-0.04	-0.18	425.0	1.38	-0.08	-0.003	0.83	0.52
400.0	2.90	0.51	-0.007	-0.06	-0.24	475.0	1.50	-0.11	-0.004	0.82	0.49
425.0	3.57	1.01	-0.007	-0.08	-0.22	500.0	1.61	-0.16	-0.005	0.81	0.49
450.0	4.27	2.24	-0.007	-0.14	-0.26	525.0	1.72	-0.31	-0.005	0.77	0.50
475.0	5.06	5.40	-0.007	-0.30	-0.21	537.5	1.82	-0.65	-0.006	0.72	0.54
487.5	5.82	10.86	-0.007	-0.63	0.04	550.0	2.22	-	-0.007	-	-
SPECIMEN											
	S16-2-1						S16-2-2				
LOAD	DEFLECTION					LOAD	DEFLECTION				
P	vert.	lat.	d_w	d1	d2	P	vert.	lat.	dw	d1	d2
kN	mm	mm	mm	mm	mm	kN	mm	mm	mm	mm	mm
0.0	0.00	0.00	0.000	0.00	0.00	0.0	0.00	0.00	0.000	0.00	0.00
50.0	0.28	0.01	-0.001	0.04	-0.04	25.0	0.21	0.04	0.000	0.22	0.23
100.0	0.47	0.01	-0.002	0.11	-0.03	75.0	0.49	0.04	0.000	0.17	0.20
200.0	0.77	0.05	-0.004	0.24	0.08	175.0	0.77	0.04	-0.001	0.18	0.30
250.0	0.92	0.10	-0.005	0.26	0.12	275.0	1.05	0.06	-0.003	0.21	0.41
300.0	1.21	0.22	-0.006	0.27	0.14	375.0	1.30	0.08	-0.005	0.21	0.44
350.0	1.89	0.61	-0.008	0.27	0.16	400.0	1.37	0.10	-0.006	0.20	0.43
375.0	2.50	1.00	-0.009	0.24	0.14	425.0	1.46	0.17	-0.006	0.19	0.43
400.0	3.40	2.80	-0.010	0.19	0.17	450.0	1.59	0.34	-0.006	0.15	0.44
412.5	4.14	6.16	-0.011	0.04	0.31	475.0	1.89	1.51	-0.007	0.04	0.58
425.0	-	-	-	-0.24	-	487.5	2.61	7.91	-0.007	0.31	1.28

Table A.3.16. Load deflection data for series 16.

SPECIMEN						
S17-25-1						
LOAD	DEFLECTION					
P	vert.	lat.	d_{wV}	d_{wH}	d1	d2
kN	mm	mm	mm	mm	mm	mm
0.0	0.00	0.00	0.000	0.000	0.00	0.00
12.5	0.21	0.05	0.007	-0.001	0.75	0.77
25.0	0.33	0.10	0.029	-0.002	0.94	0.95
37.5	0.46	0.17	0.066	-0.002	1.09	1.07
50.0	0.56	0.21	0.126	-0.002	1.14	1.15
62.5	0.67	0.23	0.205	-0.002	1.18	1.25
75.0	0.83	0.25	0.355	-0.002	1.23	1.40
87.5	0.96	0.27	0.510	-0.002	1.27	1.55
100.0	-	-	-	-	-	-
SPECIMEN						
S17-25-2						
LOAD	DEFLECTION					
P	vert.	lat.	d_{wV}	d_{wH}	d1	d2
kN	mm	mm	mm	mm	mm	mm
0.0	0.00	0.00	0.000	0.000	0.00	0.00
5.0	0.08	0.00	-0.001	0.000	-0.01	-0.05
10.0	0.16	0.01	-0.004	0.000	-0.03	-0.08
30.0	0.40	0.14	-0.026	0.000	0.03	-0.11
60.0	0.66	0.28	-0.038	0.000	0.03	-0.26
90.0	0.93	0.42	-0.090	0.000	0.03	-0.39
100.0	1.00	0.54	-0.126	0.000	0.03	-0.39
110.0	1.12	0.61	-0.306	0.000	0.04	-0.29
120.0	1.28	0.64	-0.486	0.000	0.04	-0.18
135.0	1.59	0.67	-1.088	0.001	0.03	0.05
137.5	-	-	-	-	-	-

Table A.3.17. Load deflection data for series 17.

SPECIMEN						
S17-75-1						
LOAD	DEFLECTION					
P	vert.	lat.	d_{wV}	d_{wH}	d_1	d_2
kN	mm	mm	mm	mm	mm	mm
0.0	0.00	0.00	0.000	0.000	0.00	0.00
20.0	0.22	0.04	0.000	-0.001	-0.07	-0.03
50.0	0.47	0.11	-0.001	-0.001	-0.03	-0.04
90.0	0.70	0.20	-0.010	0.001	-0.03	-0.09
130.0	0.92	0.28	-0.025	0.007	-0.03	-0.17
150.0	1.03	0.30	-0.039	0.011	-0.05	-0.20
160.0	1.09	0.30	-0.059	0.013	-0.07	-0.20
180.0	1.23	0.25	-0.113	0.018	-0.10	-0.17
200.0	1.39	0.22	-0.151	0.027	-0.15	-0.12
210.0	1.52	0.17	-0.169	0.039	-0.18	-0.04
220.0	-	-	-	-	-	-
SPECIMEN						
S17-75-2						
LOAD	DEFLECTION					
P	vert.	lat.	d_{wV}	d_{wH}	d_1	d_2
kN	mm	mm	mm	mm	mm	mm
0.0	0.00	0.00	0.000	0.000	0.00	0.00
10.0	0.15	0.10	-0.001	0.000	0.03	0.13
40.0	0.46	0.25	-0.006	0.000	0.00	-0.02
75.0	0.76	0.36	-0.020	0.000	-0.13	-0.29
105.0	0.92	0.42	-0.032	0.000	-0.19	-0.37
135.0	1.08	0.45	-0.049	0.000	-0.25	-0.43
165.0	1.24	0.47	-0.074	0.000	-0.25	-0.45
190.0	1.42	0.47	-0.140	0.000	-0.25	-0.44
210.0	1.66	0.47	-0.216	0.000	-0.24	-0.35
220.0	1.77	0.47	-0.232	0.002	-0.24	-0.30
225.0	-	0.49	-	-	-	-

Table A.3.17. Load deflection data for series 17 (continued).

SPECIMEN					
1		2		3	
LOAD P kN	DEF. vert. mm	LOAD P kN	DEF. vert. mm	LOAD P kN	DEF. vert. mm
0.0	0.000	0.0	0.000	0.0	0.000
3.0	0.226	1.0	0.208	1.0	0.204
30.0	0.288	4.0	0.234	10.0	0.260
60.0	0.362	15.0	0.282	30.0	0.302
80.0	0.434	40.0	0.362	50.0	0.350
95.0	0.522	70.0	0.446	70.0	0.438
111.0	0.632	85.0	0.500	85.0	0.526
118.0	0.710	100.0	0.576	100.0	0.648
124.0	0.830	112.0	0.698	110.0	0.880
128.0	0.988	120.0	0.956	112.0	1.031
130.0	-	124.0	-	114.0	-

Table A.3.18. Load deflection data to series 18.

SERIES 3		SERIES 4		SERIES 4		SERIES 5	
Specimen No.	Initial max. lat. deflect. (mm)	Specimen No.	Initial max. lat. deflect. (mm)	Specimen No.	Initial max. lat. deflect. (mm)	Specimen No.	Initial max. lat. deflect. (mm)
S3-100-1	0.5	S4-50-1	0.0	S4-300-1	1.5	S5-75-1	1.5
S3-100-2	0.0	S4-50-2	0.0	S4-300-2	1.5	S5-100-1	1.5
S3-200-1	0.5	S4-100-1	0.0	S4-400-1	0.5	S5-150-1	0.0
S3-200-2	0.5	S4-100-2	0.0	S4-400-2	0.5	S5-150-2	1.0
S3-300-1	4.0	S4-150-1	0.0	S4-500-1	0.5	S5-200-1	0.0
S3-300-2	2.0	S4-150-2	1.0	S4-500-2	2.0	S5-250-1	0.5
S3-400-1	0.5	S4-200-1	0.0	S4-600-1	1.5	S5-300-1	1.0
S3-400-2	0.0	S4-200-2	1.5	S4-600-2	2.0	S5-300-2	1.0
S3-500-1	1.0	S4-250-1	0.0			S5-300-3	1.0
S3-500-2	2.0	S4-250-2	1.0				

SERIES 6		SERIES 7		SERIES 12		SERIES 8	
Specimen No.	Initial max. lat. deflect. (mm)	Specimen No.	Initial max. lat. deflect. (mm)	Specimen No.	Initial max. lat. deflect. (mm)	Specimen No.	Initial max. lat. deflect. (mm)
S6-150-1	0.0	S7-6-150-1	1.0	S12-5-1	1.5	S8-45-1	0.5
S6-300-1	1.5	S7-6-300-1	0.0	S12-7-1	1.5	S8-90-1	1.0
		S7-10-150-1	1.0	S12-9-1	0.0	S8-135-1	0.0
		S7-10-300-1	1.0	S12-11-1	0.5	S8-180-1	2.0
		S7-13-150-1	0.0	S12-13-1	0.0	S8-45-2	2.0
		S7-13-300-1	0.5	S12-15-1	0.0	S8-90-2	1.5
		S7-16-150-1	1.5	S12-13-2	0.5	S8-135-2	1.0
		S7-16-300-1	0.5	S12-15-2	0.5	S8-180-2	2.0
		S7-20-150-1	0.5				
		S7-20-300-1	1.5				

SERIES 13		SERIES 9		SERIES 9		SERIES 10	
Specimen No.	Initial max. lat. deflect. (mm)	Specimen No.	Initial max. lat. deflect. (mm)	Specimen No.	Initial max. lat. deflect. (mm)	Specimen No.	Initial max. lat. deflect. (mm)
S13-30-1	0.0	S9-1-1	0.0	S9-5-3	0.0	S10-7-1	0.0
S13-30-2	0.0	S9-1-2	0.0	S9-6-1	0.0	S10-7-2	0.0
S13-50-1	0.0	S9-1-3	0.0	S9-6-2	0.0	S10-6-1	0.0
S13-50-2	1.0	S9-2-1	0.0	S9-6-3	0.5	S10-6-2	0.0
S13-70-1	1.5	S9-2-2	0.0	S9-7-1	0.0	S10-5-1	0.0
S13-70-2	1.5	S9-2-3	0.0	S9-7-2	0.0	S10-5-2	0.5
S13-90-1	2.0	S9-3-1	0.0	S9-7-3	0.5	S10-4-1	1.5
S13-90-2	3.0	S9-3-2	0.0			S10-4-2	0.0
S13-110-1	6.0	S9-3-3	0.0			S10-3-1	0.5
S13-110-2	2.5	S9-4-1	0.0			S10-3-2	1.0
S13-130-1	4.5	S9-4-2	0.0			S10-2-1	0.5
S13-130-2	3.5	S9-4-3	0.0			S10-2-2	1.0
S13-140-1	2.0	S9-5-1	0.0			S10-1-1	0.5
S13-140-2	2.0	S9-5-2	0.0			S10-1-2	1.5

SERIES 5a		SERIES 14		SERIES 15&16		SERIES 17	
Specimen No.	Initial max. lat. deflect. (mm)	Specimen No.	Initial max. lat. deflect. (mm)	Specimen No.	Initial max. lat. deflect. (mm)	Specimen No.	Initial max. lat. deflect. (mm)
S5a-75-1	1.0	S14-0-1	0.5	S15-0-1	0.0	S17-75-1	0.0
S5a-300-1	0.5	S14-0-2	0.0	S15-0-2	0.0	S17-75-2	0.0
		S14-0-3	0.0	S15-2-1	0.5	S17-25-1	0.0
		S14-0-4	0.0	S15-2-2	0.0	S17-25-2	0.0
		S14-2-1	0.5	S16-6-1	0.0		
		S14-2-2	0.0	S16-6-2	0.0		
		S14-2-3	0.0	S16-2-1	0.0		
		S14-2-4	0.0	S16-2-2	0.0		

Table A.3.19. Initial lateral deflections.

APPENDIX 4

This appendix contains the load deflection graphs selected to represent each series of tests as presented in Chapter 6. The load deflection data for all the specimens are presented in Appendix 3. With the strut tests in the subsidiary series the deflections are plotted against the axial stress in the strut rather than against the applied load.

The positions of the deflections presented are given for the appropriate specimen in Chapter 3.

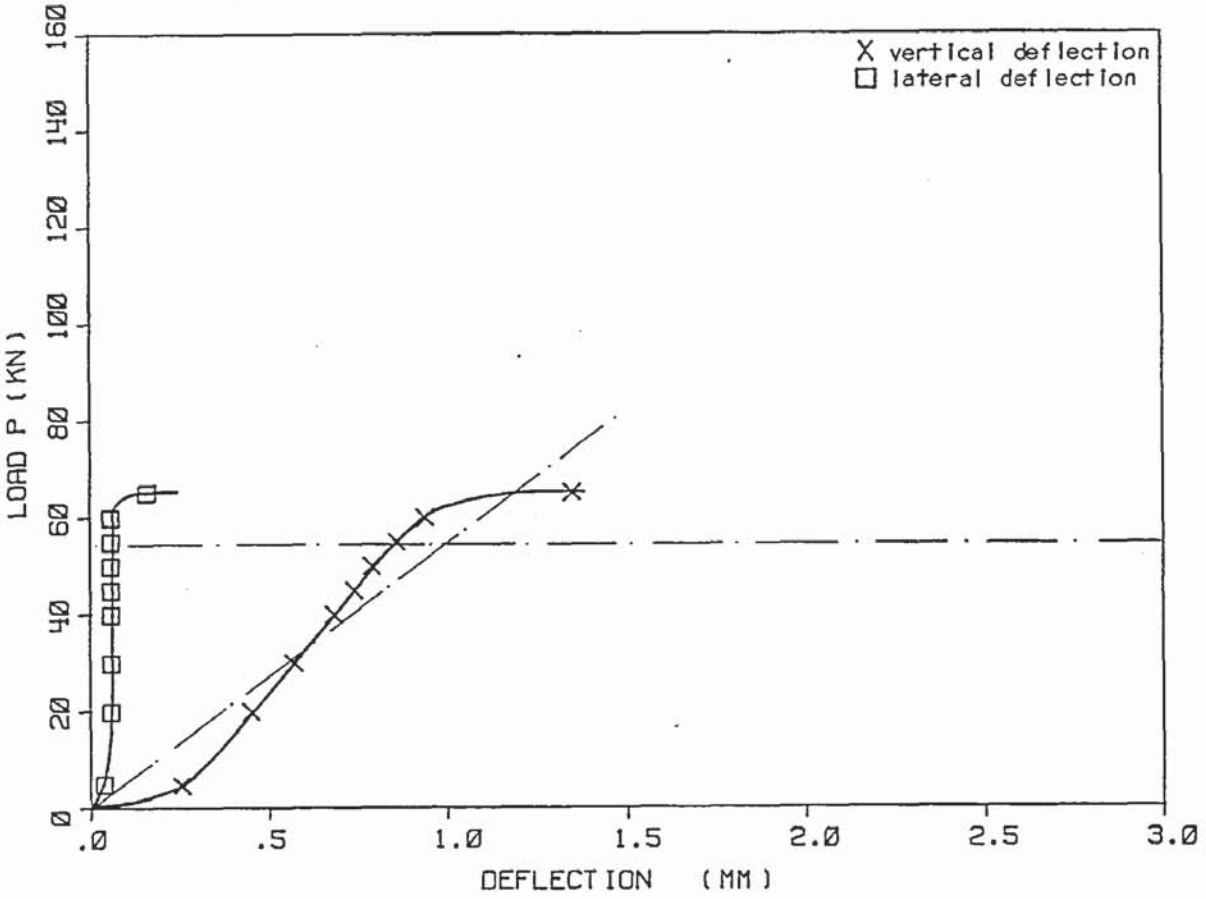

Figure A.4.1. The total vertical and mid-lateral deflections of specimen S3-100-2.

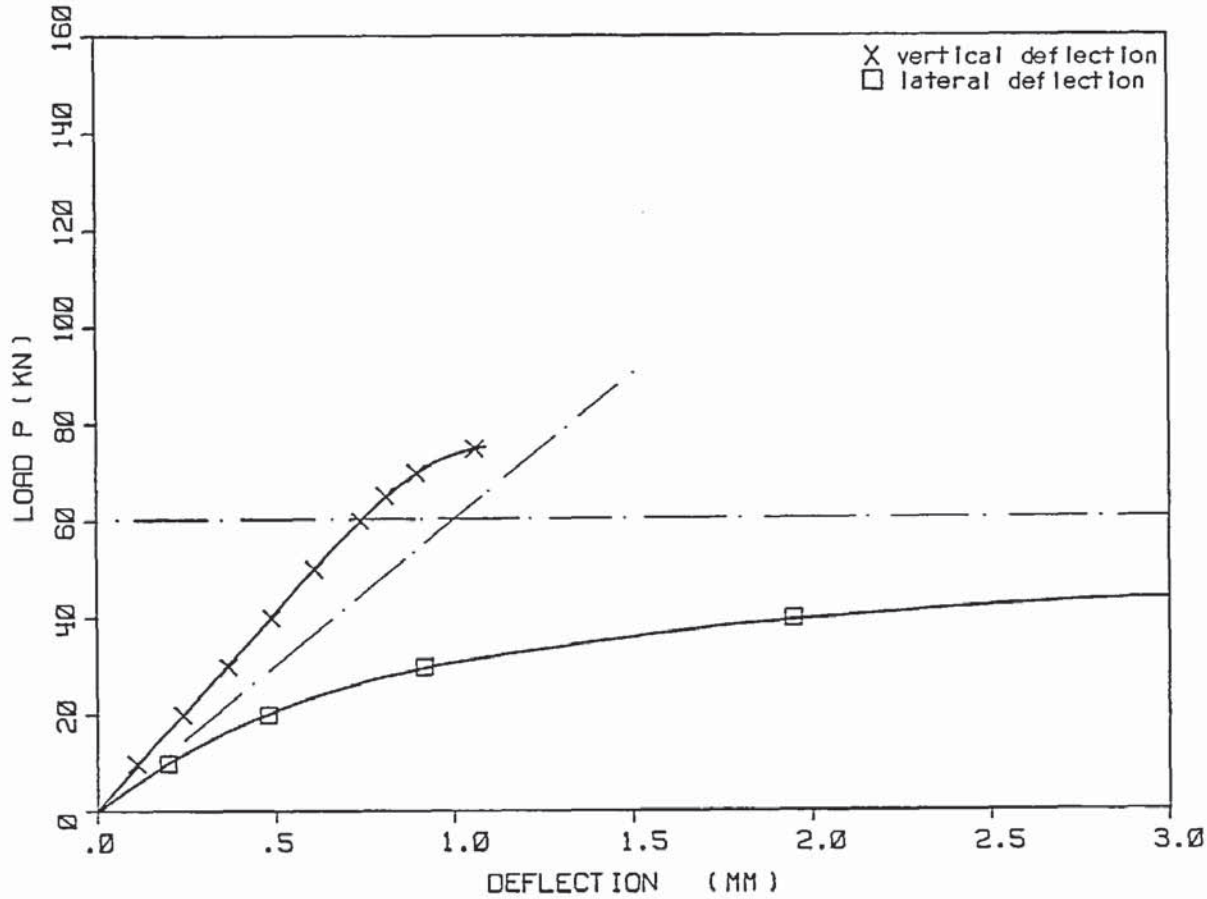

Figure A.4.2. The total vertical and mid-lateral deflections of specimen S3-500-2.

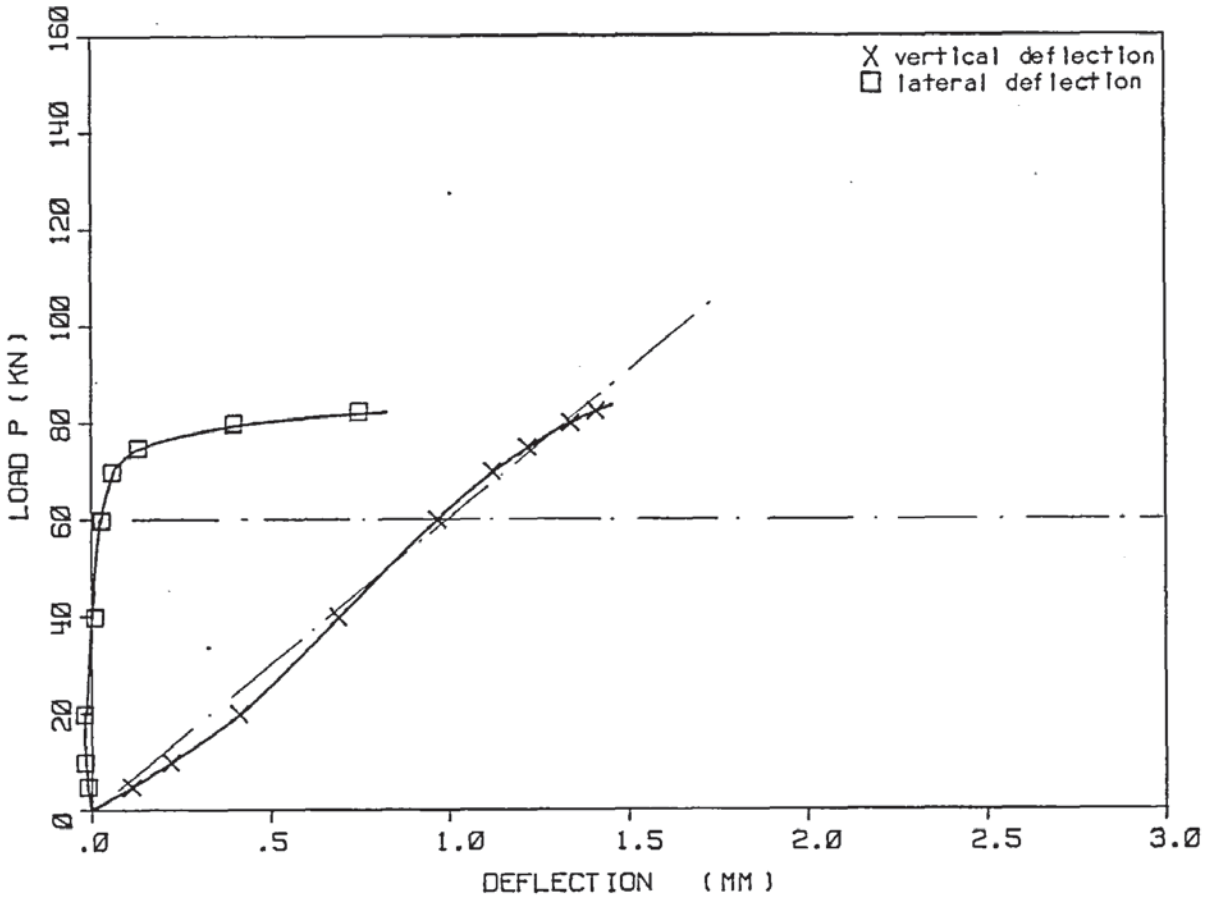

Figure A.4.3. The total vertical and mid-lateral deflections of specimen S4-150-2.

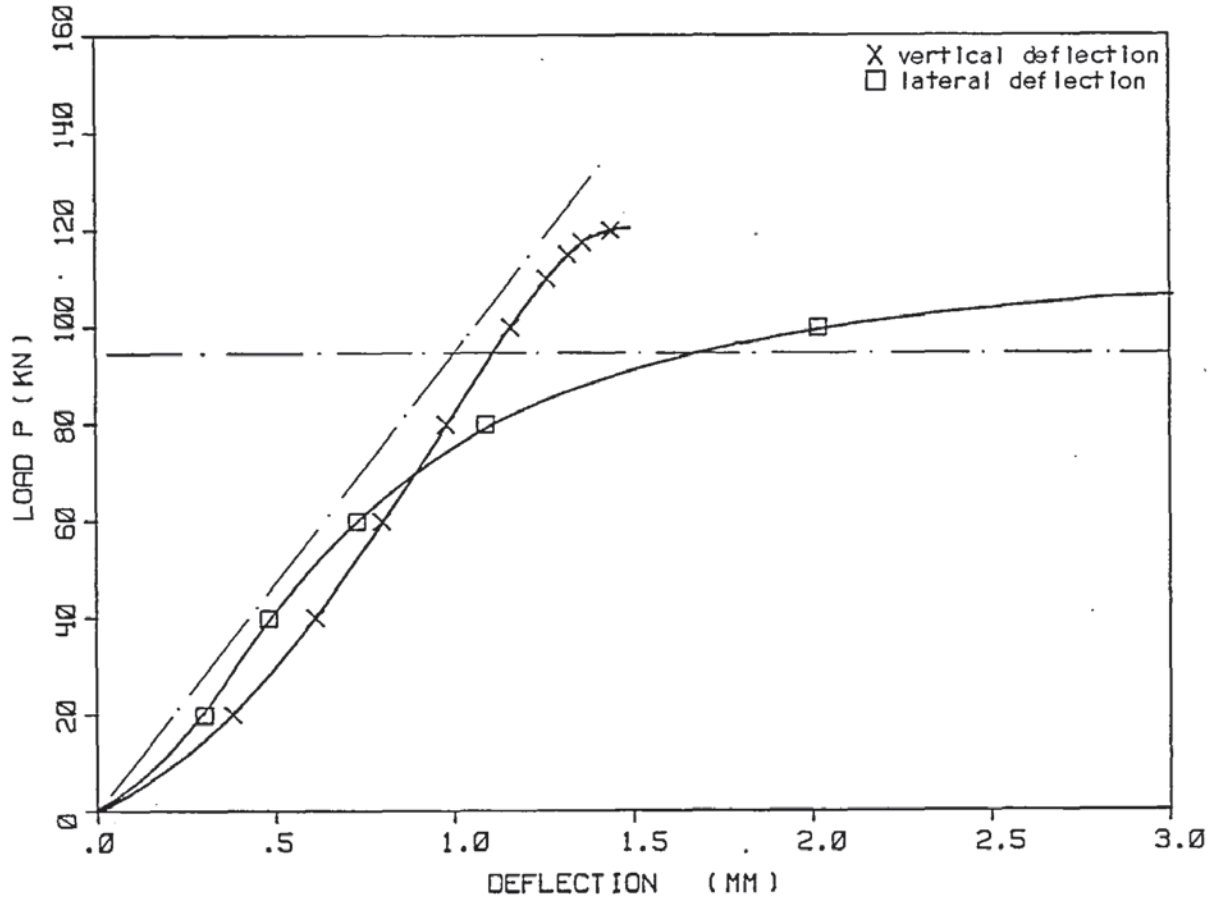

Figure A.4.4. The total vertical and mid-lateral deflections of specimen S4-500-2.

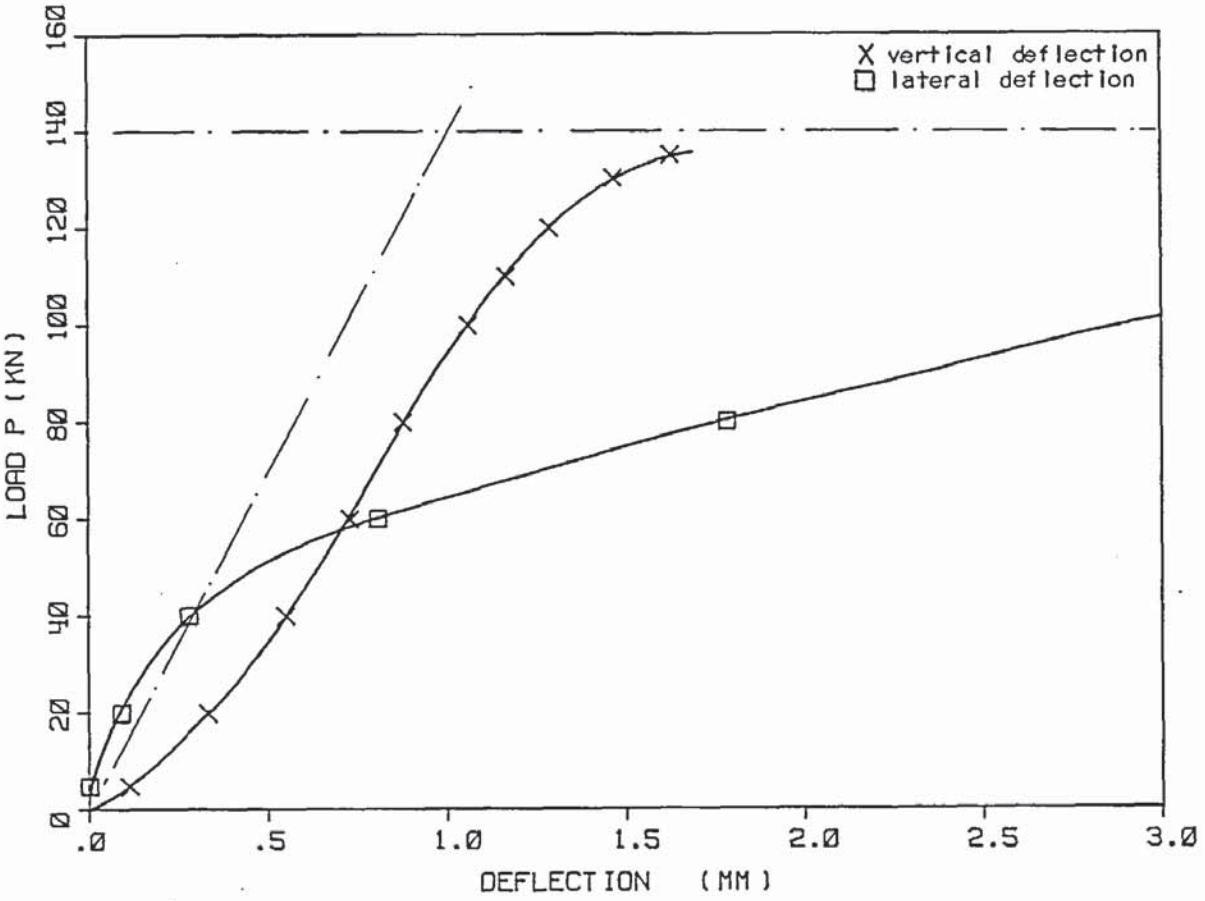

Figure A.4.5. The total vertical and mid-lateral deflections of specimen S5-75-1.

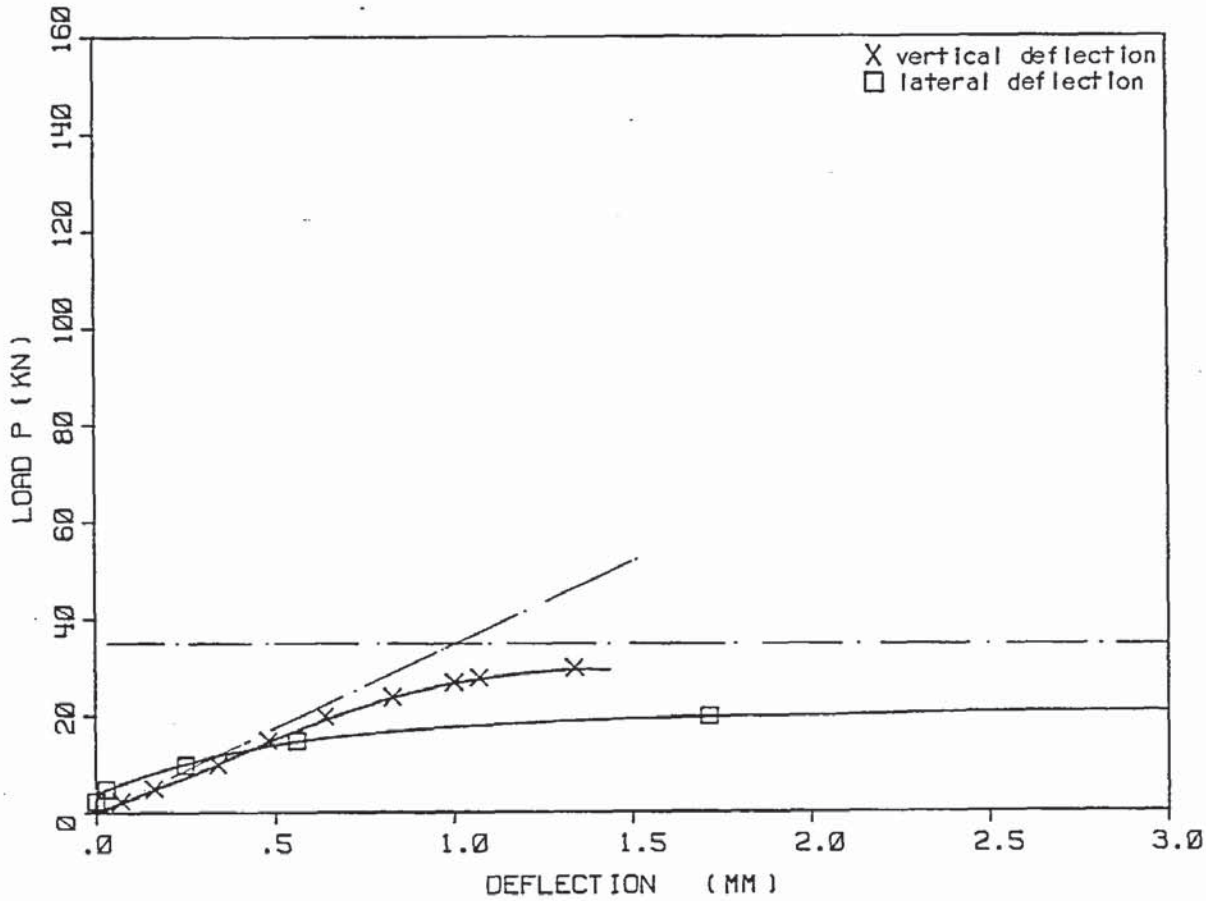

Figure A.4.6. The total vertical and mid-lateral deflections of specimen S5-300-2.

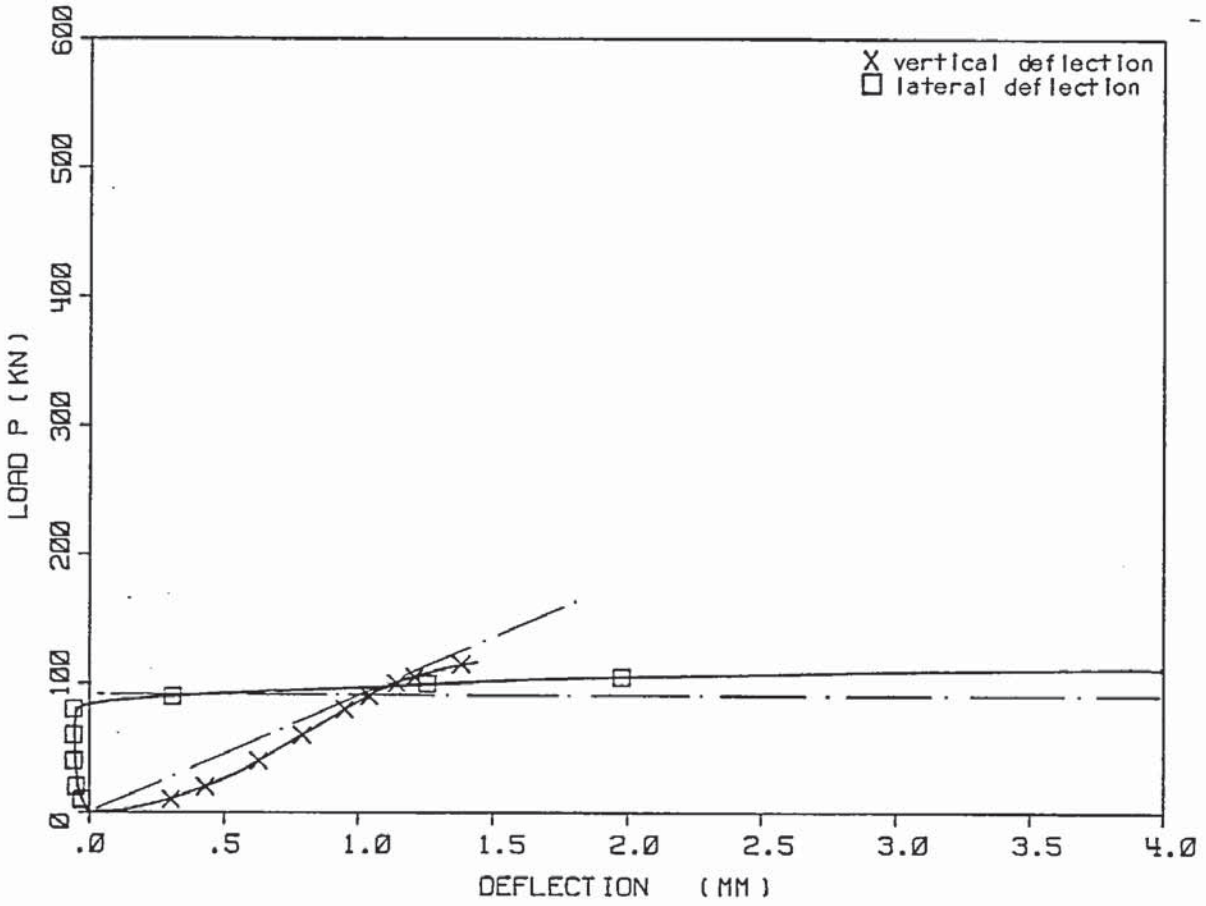

Figure A.4.7. The total vertical and mid-lateral deflections of specimen S12-5-1.

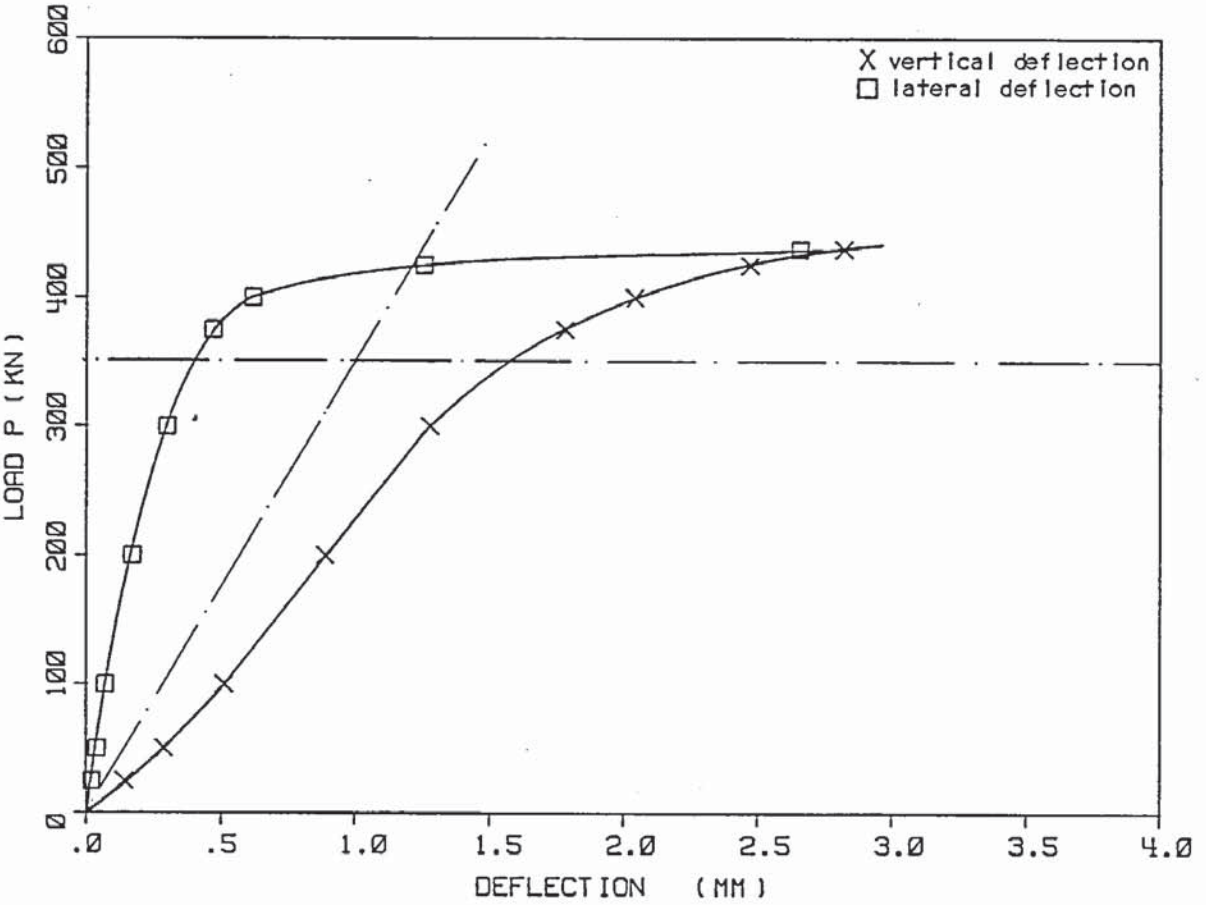

Figure A.4.8. The total vertical and mid-lateral deflections of specimen S12-9-1.

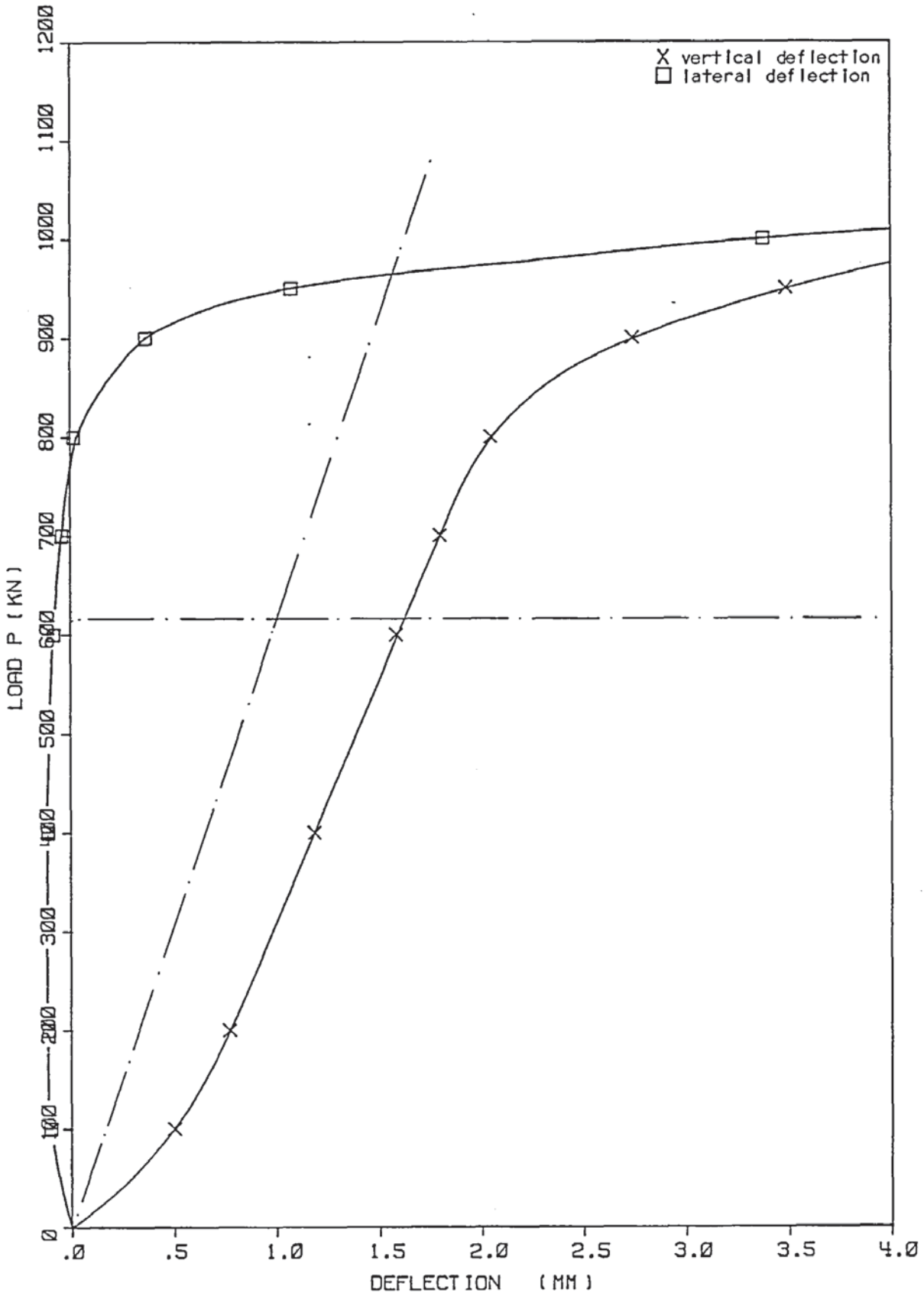

Figure A.4.9. The total vertical and mid-lateral deflections of specimen S12-15-2.

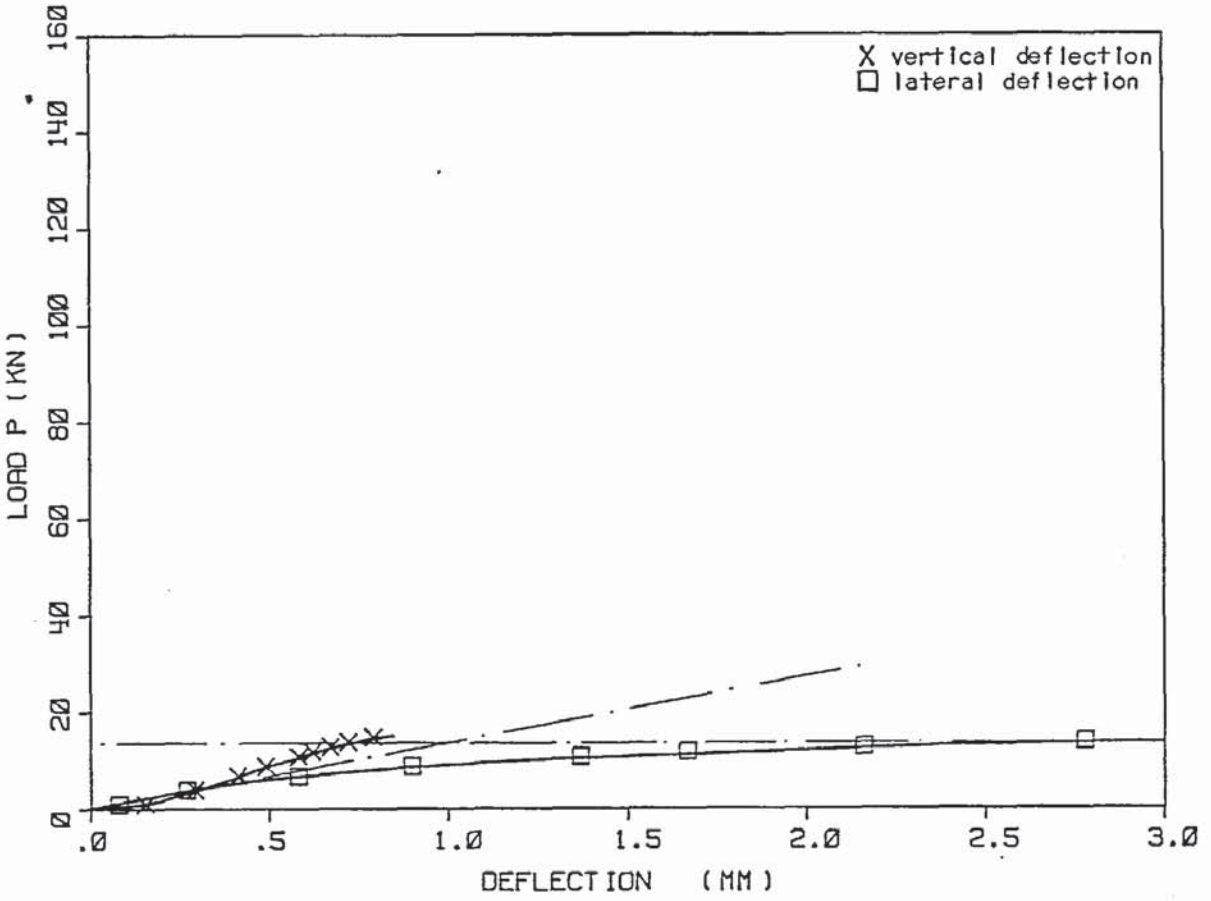

Figure A.4.10. The total vertical and mid-lateral deflections of specimen S8-45-2.

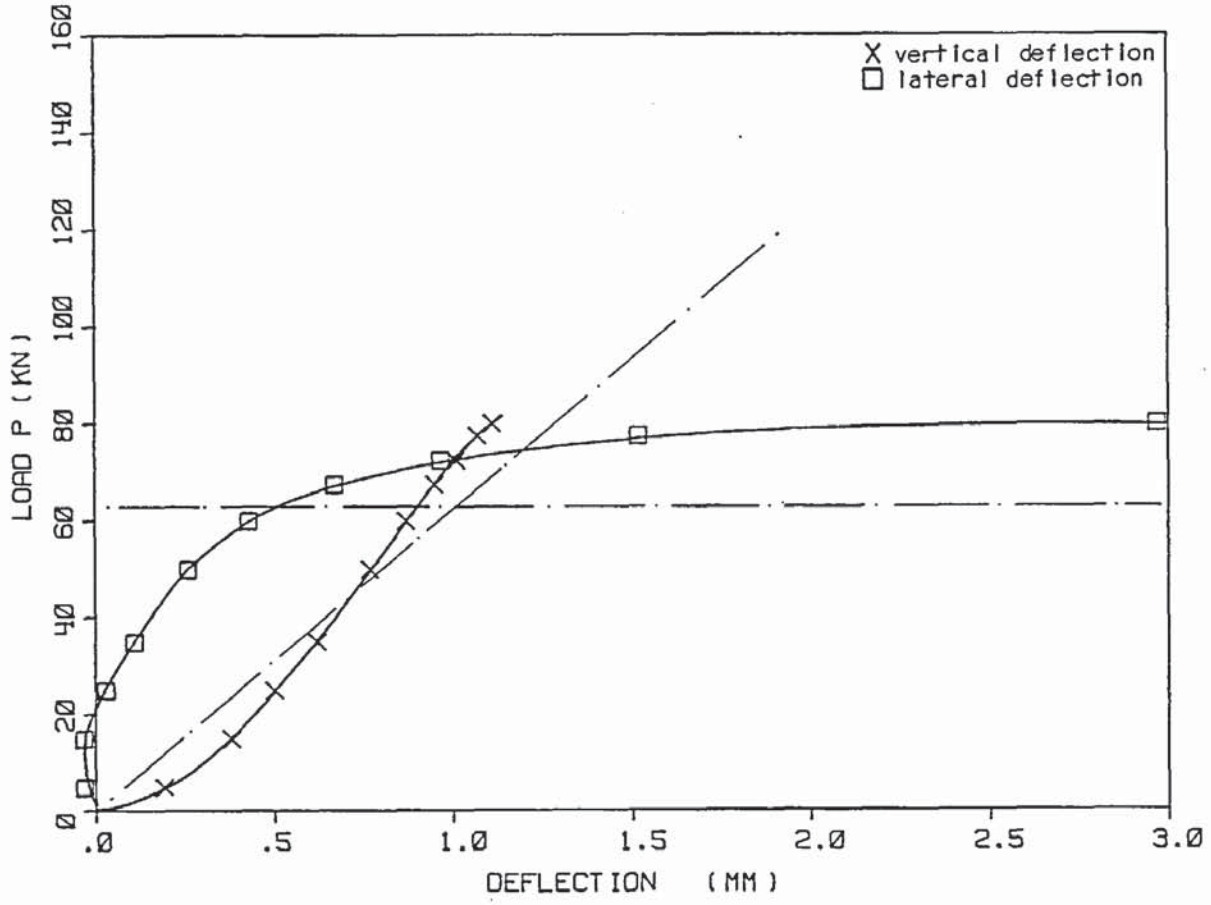

Figure A.4.11. The total vertical and mid-lateral deflections of specimen S8-135-2.

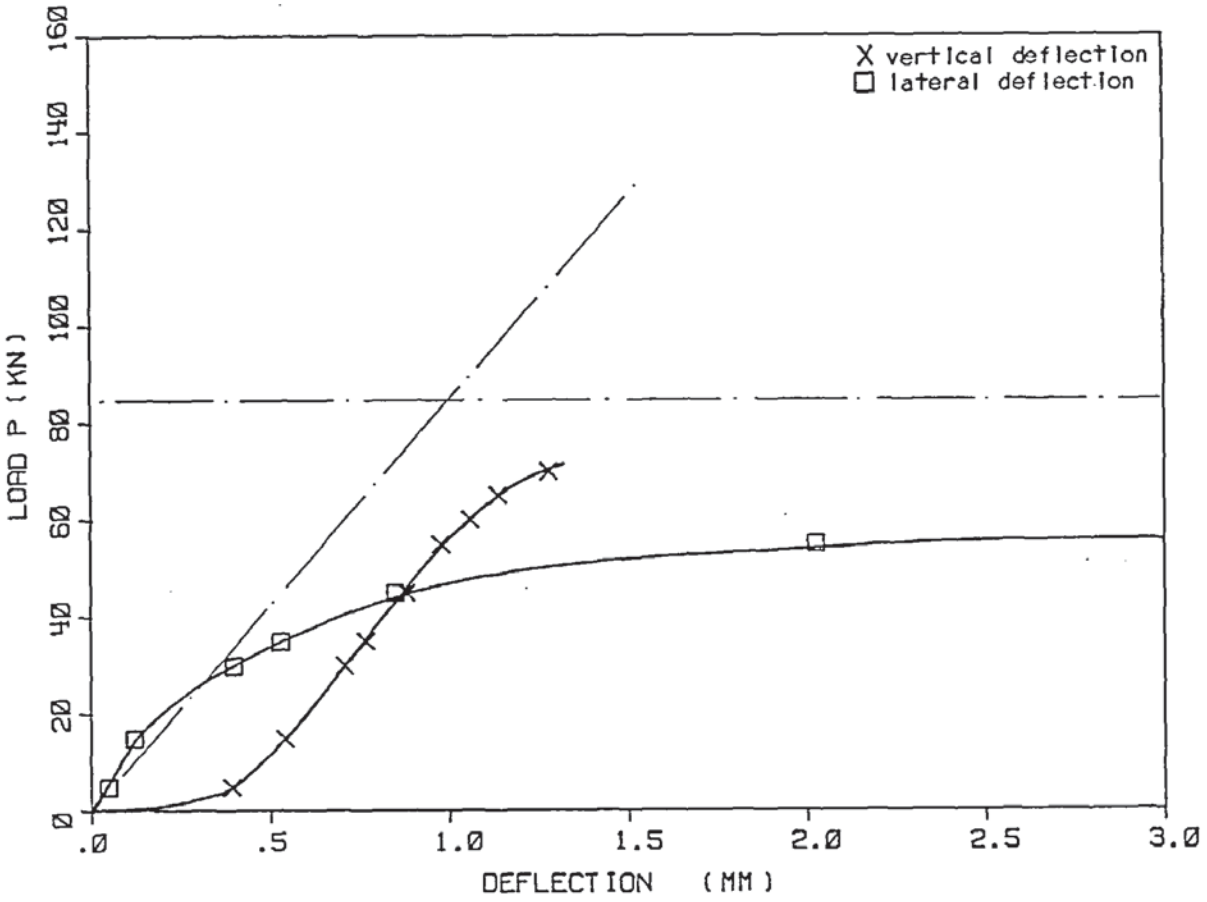

Figure A.4.12. The total vertical and mid-lateral deflections of specimen S8-180-2.

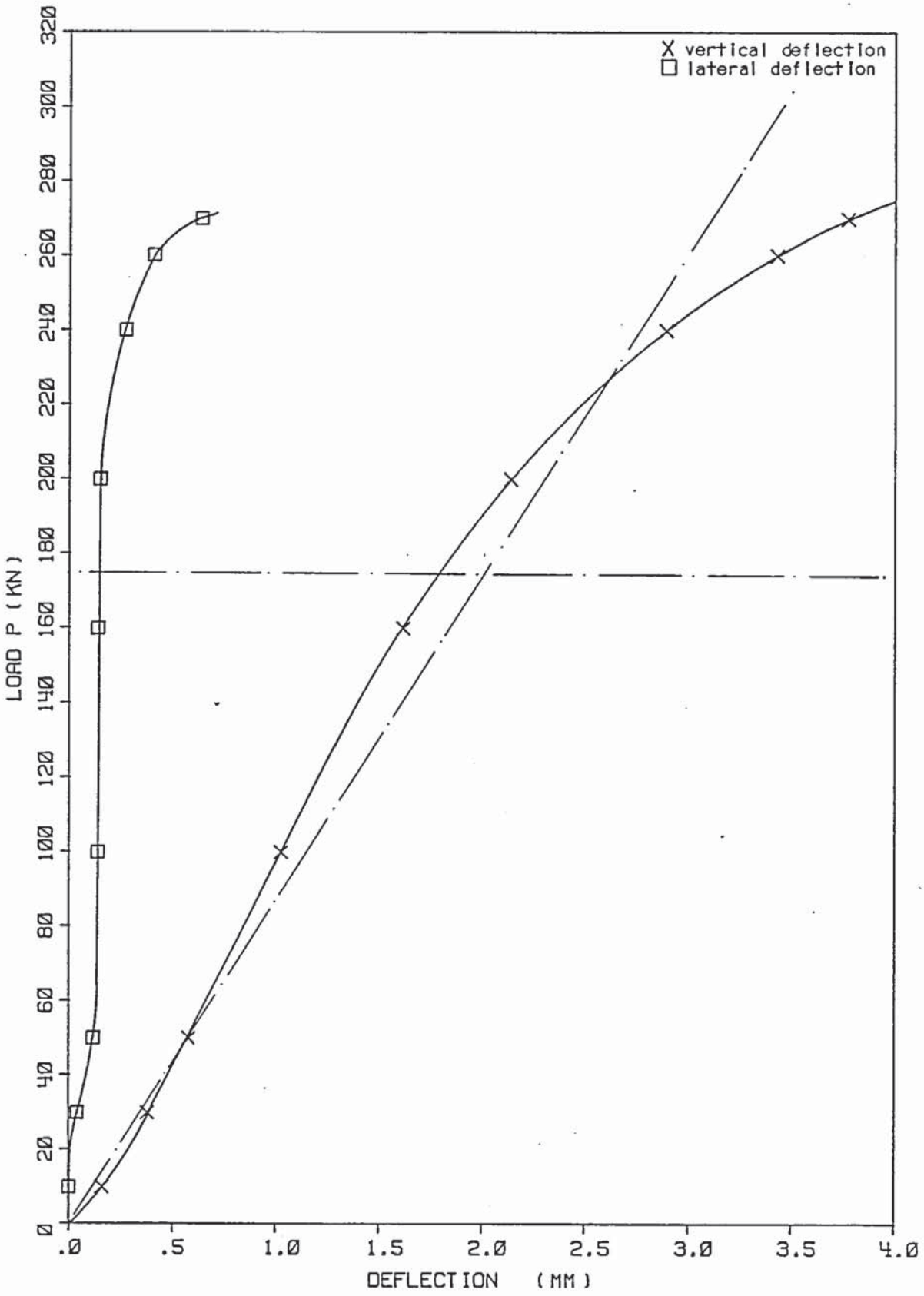

Figure A.4.13. The total vertical and mid-lateral deflections of specimen S13-30-1.

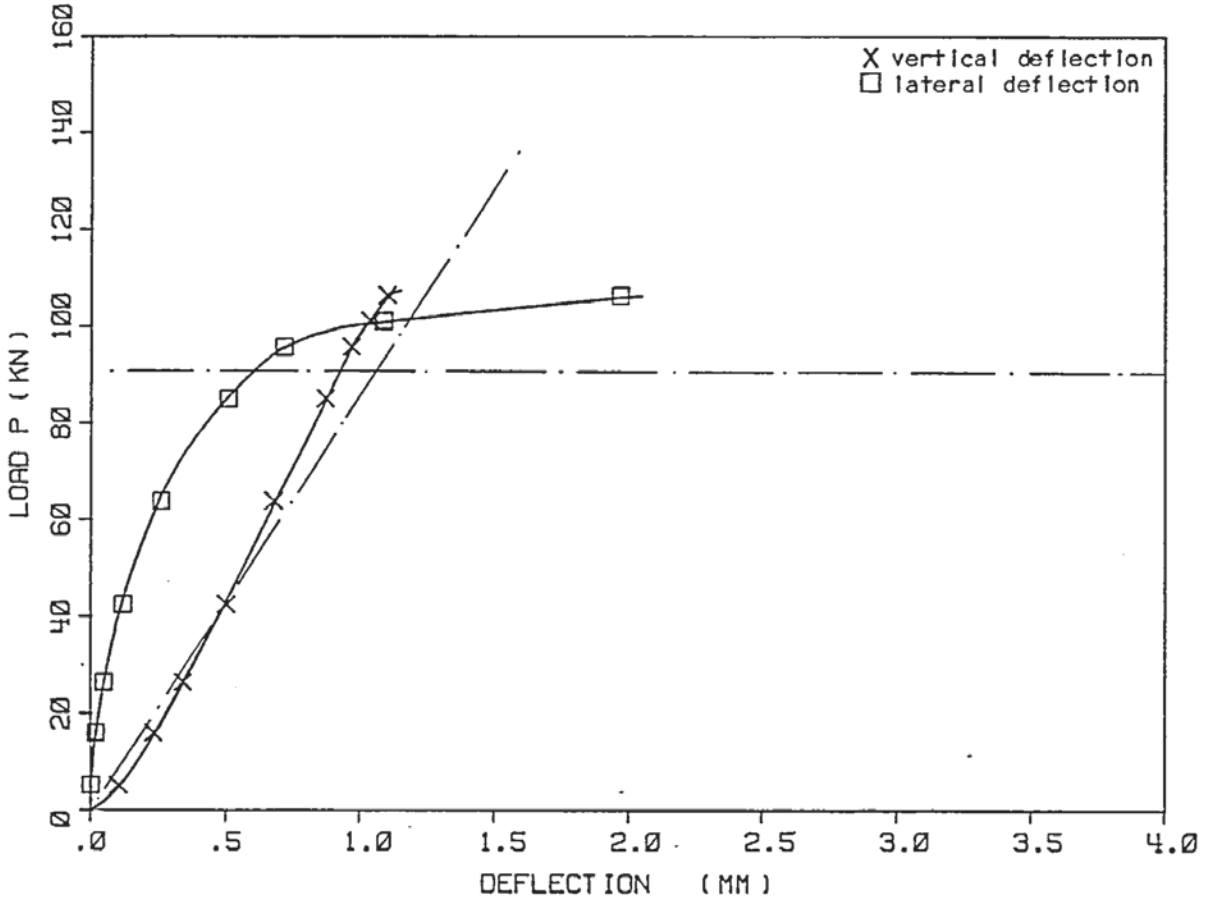

Figure A.4.14. The total vertical and mid-lateral deflections of specimen S13-70-2.

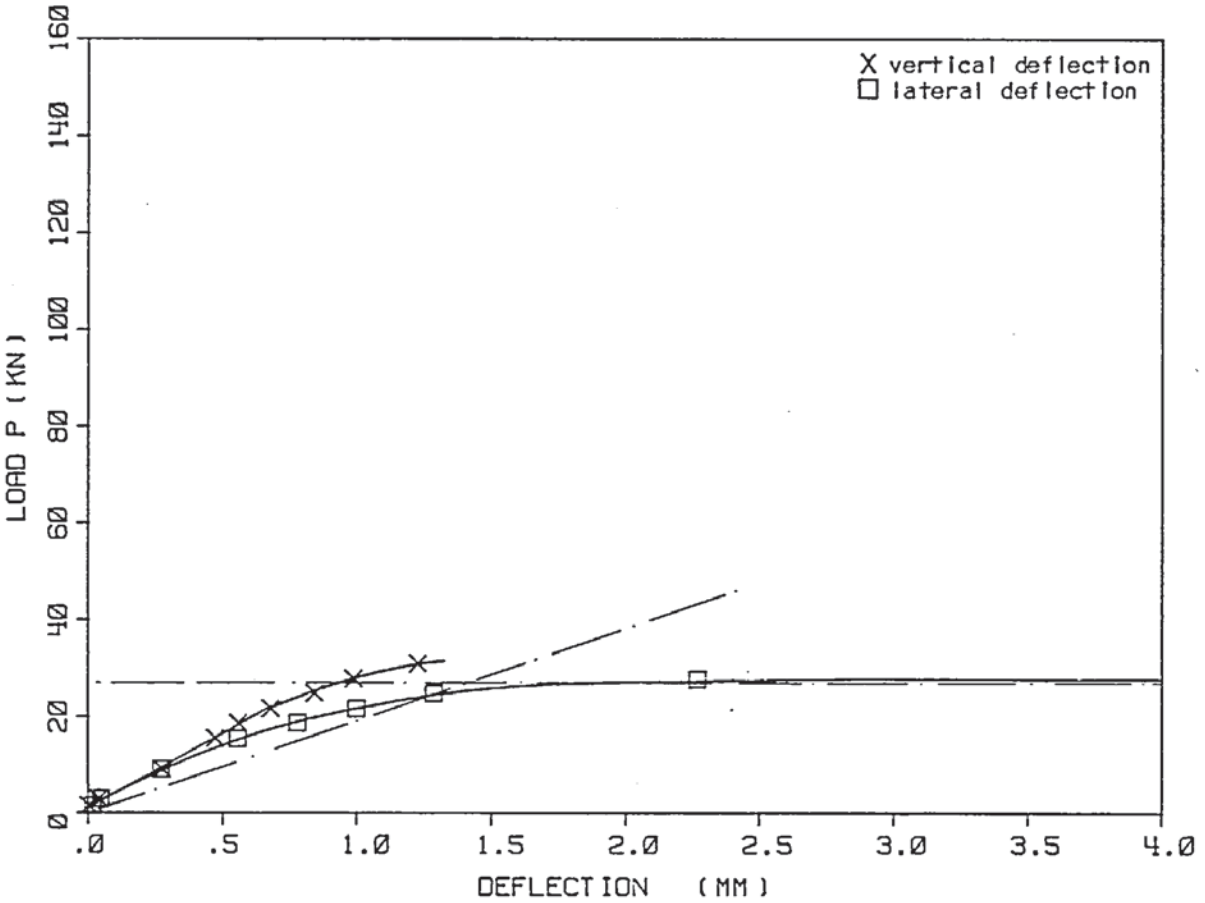

Figure A.4.15. The total vertical and mid-lateral deflections of specimen S13-140-2.

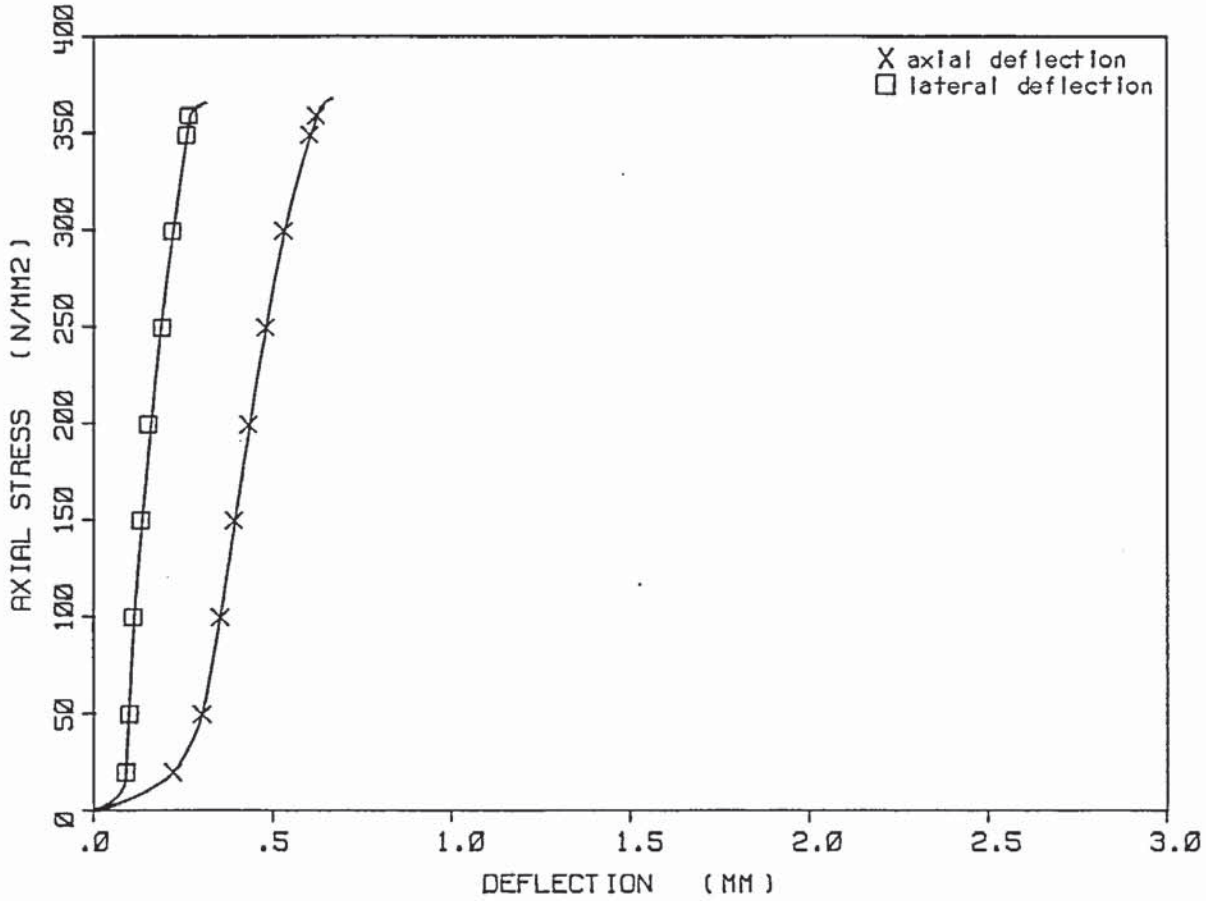

Figure A.4.16. The axial and mid-lateral deflections of specimen S9-1-2.

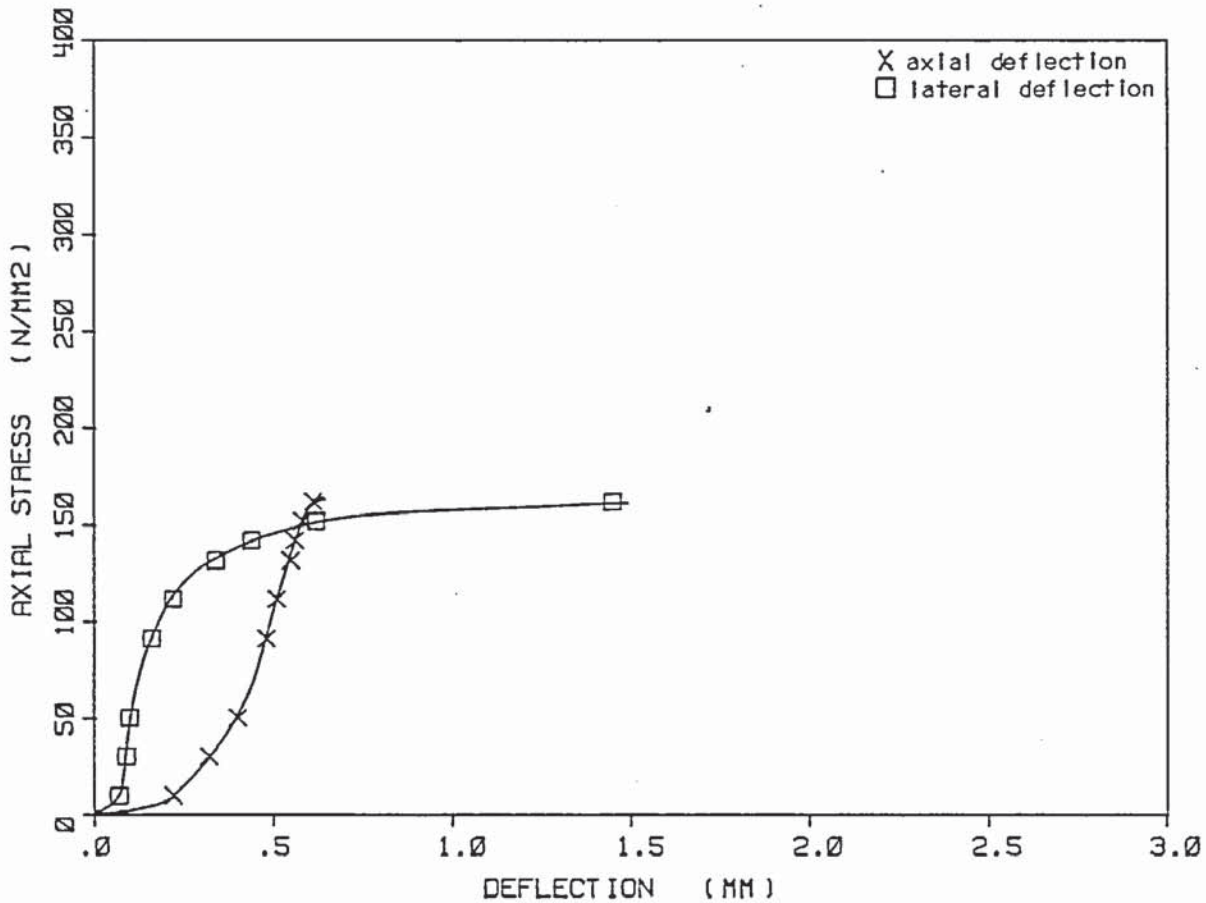

Figure A.4.17. The axial and mid-lateral deflections of specimen S9-4-2.

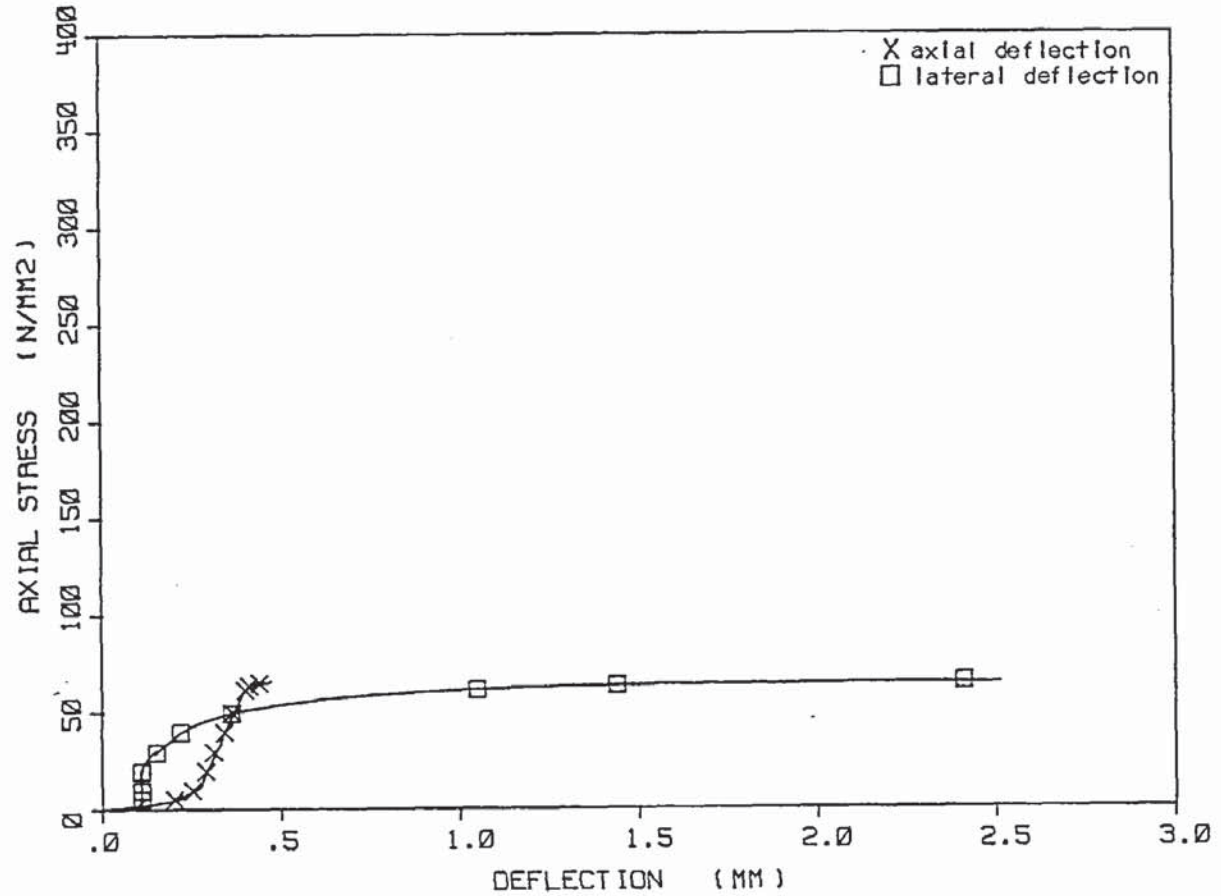

Figure A.4.18. The axial and mid-lateral deflections of specimen S9-7-2.

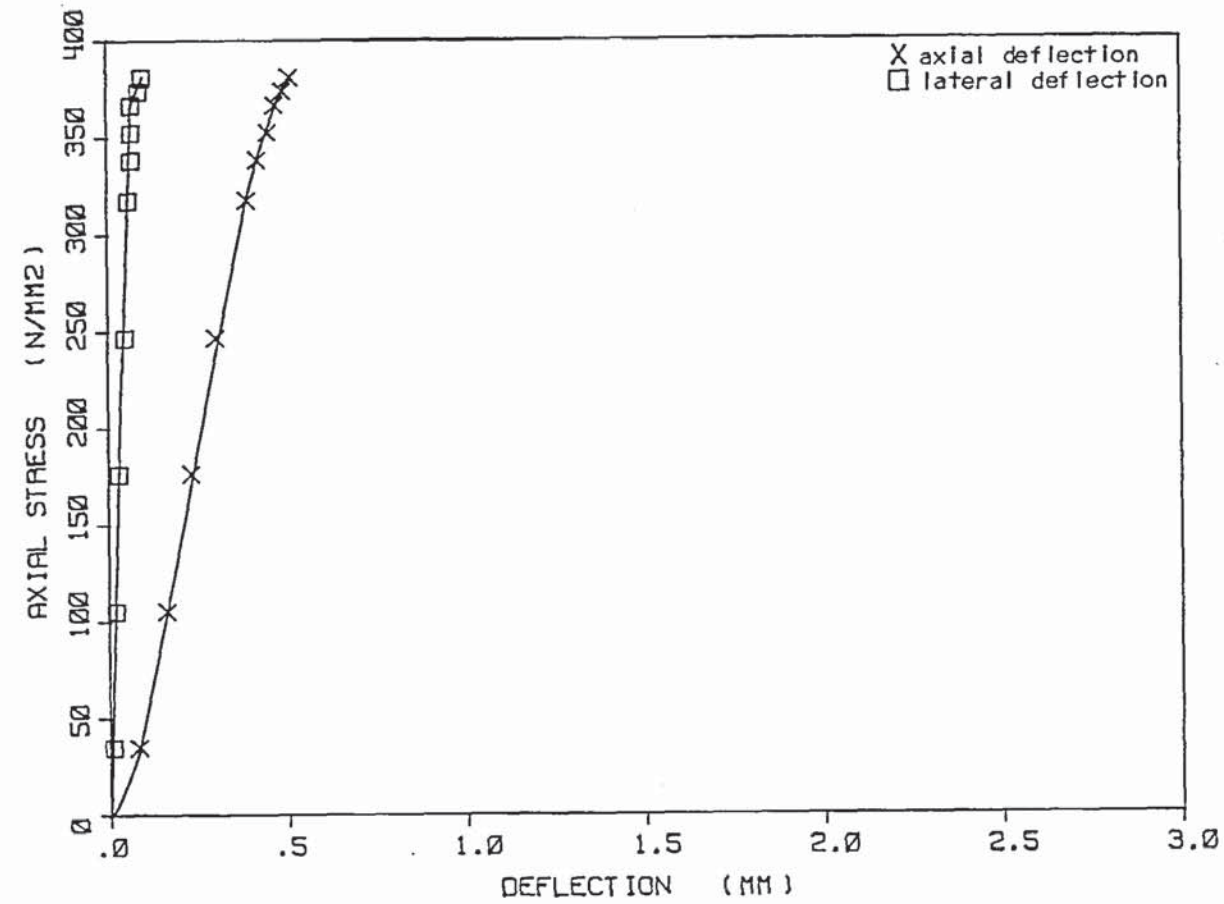

Figure A.4.19. The axial and mid-lateral deflections of specimen S10-7-2.

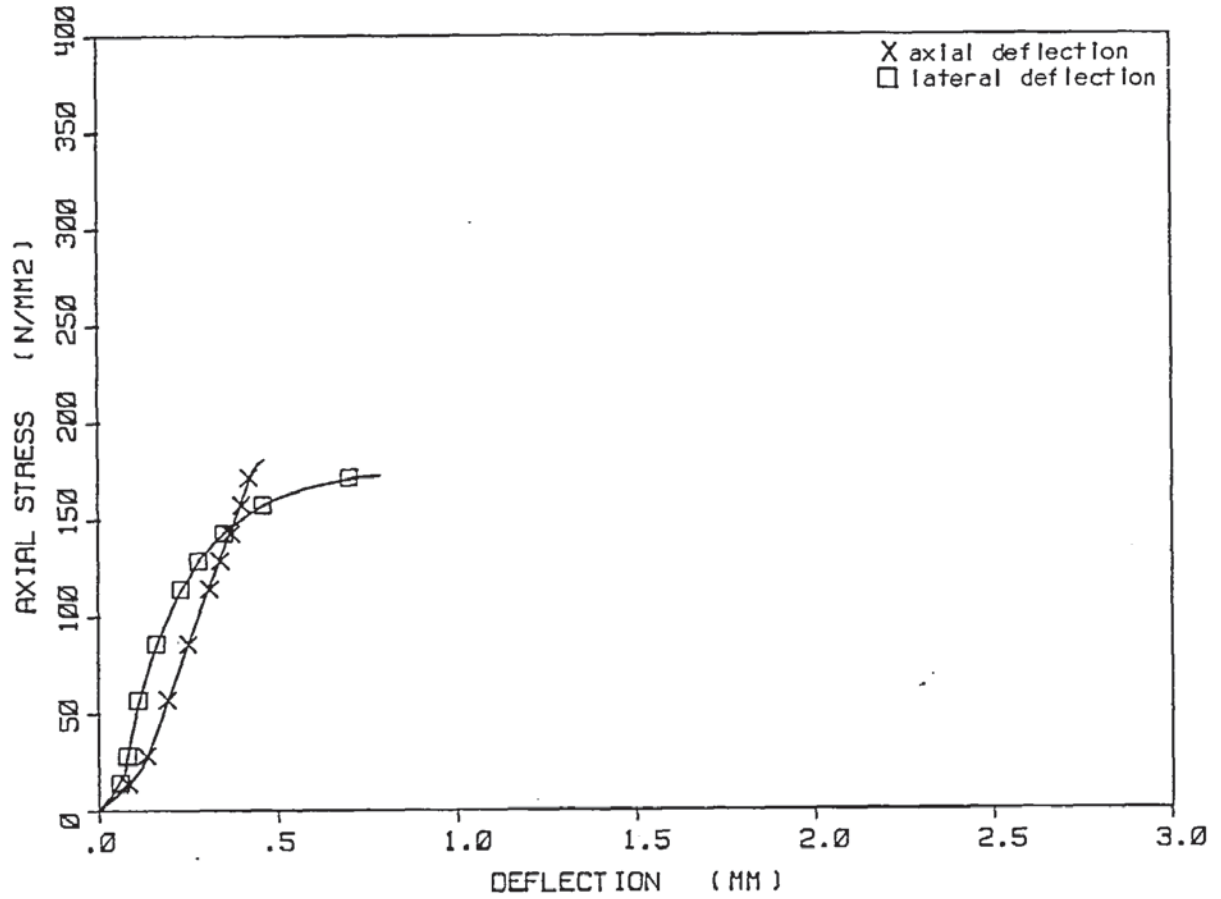

Figure A.4.20. The axial and mid-lateral deflections of specimen S10-4-1.

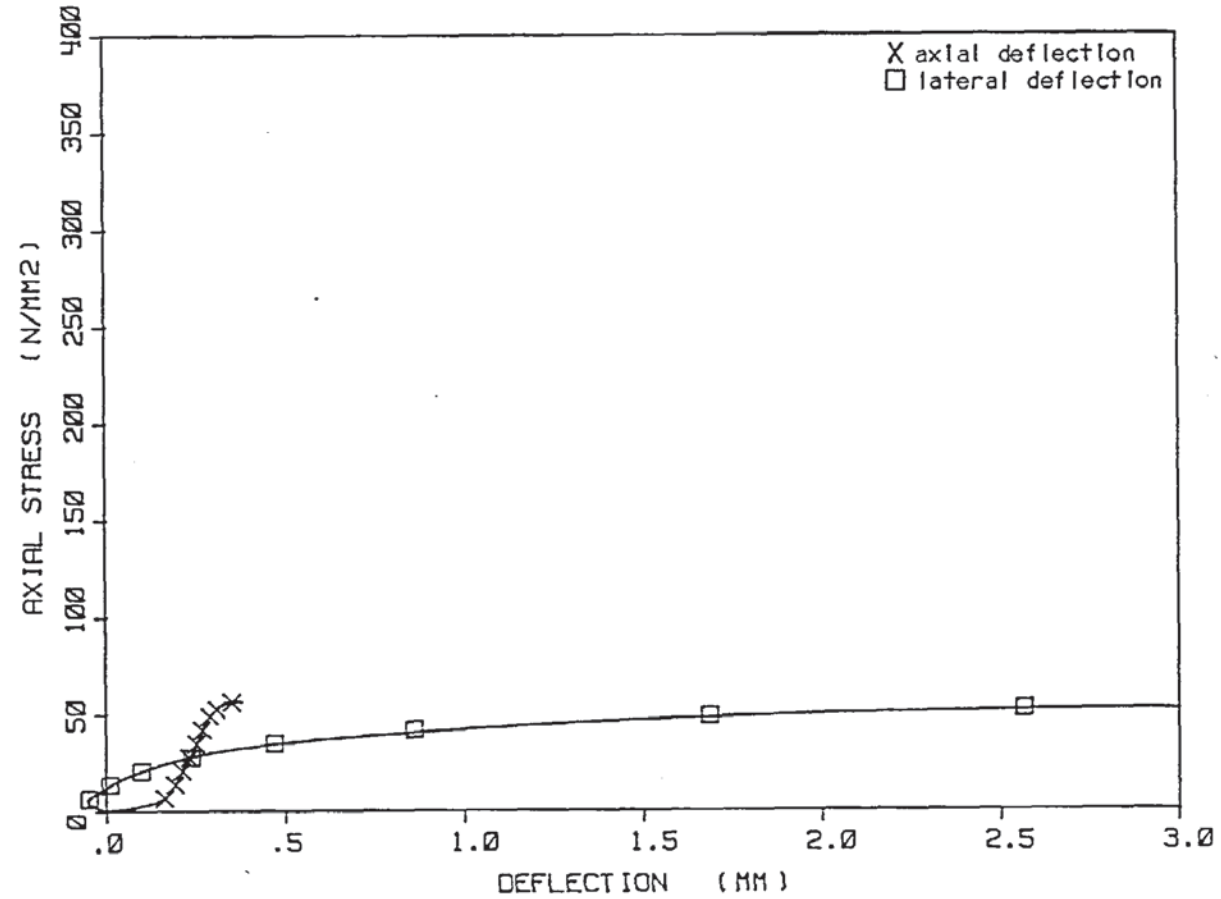

Figure A.4.21. The axial and mid-lateral deflections of specimen S10-1-1.

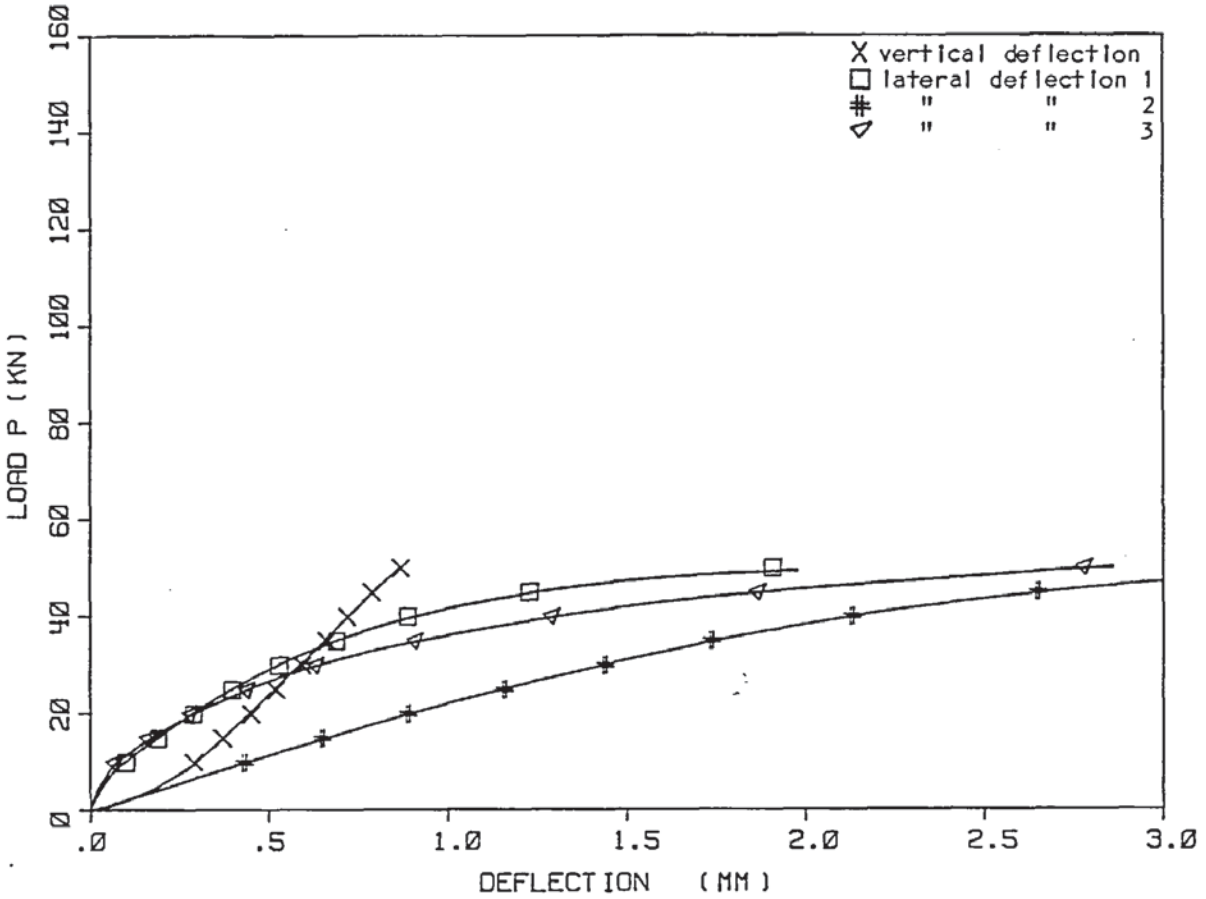

Figure A.4.22. The total vertical and mid-lateral deflections of specimen S11-150-1.

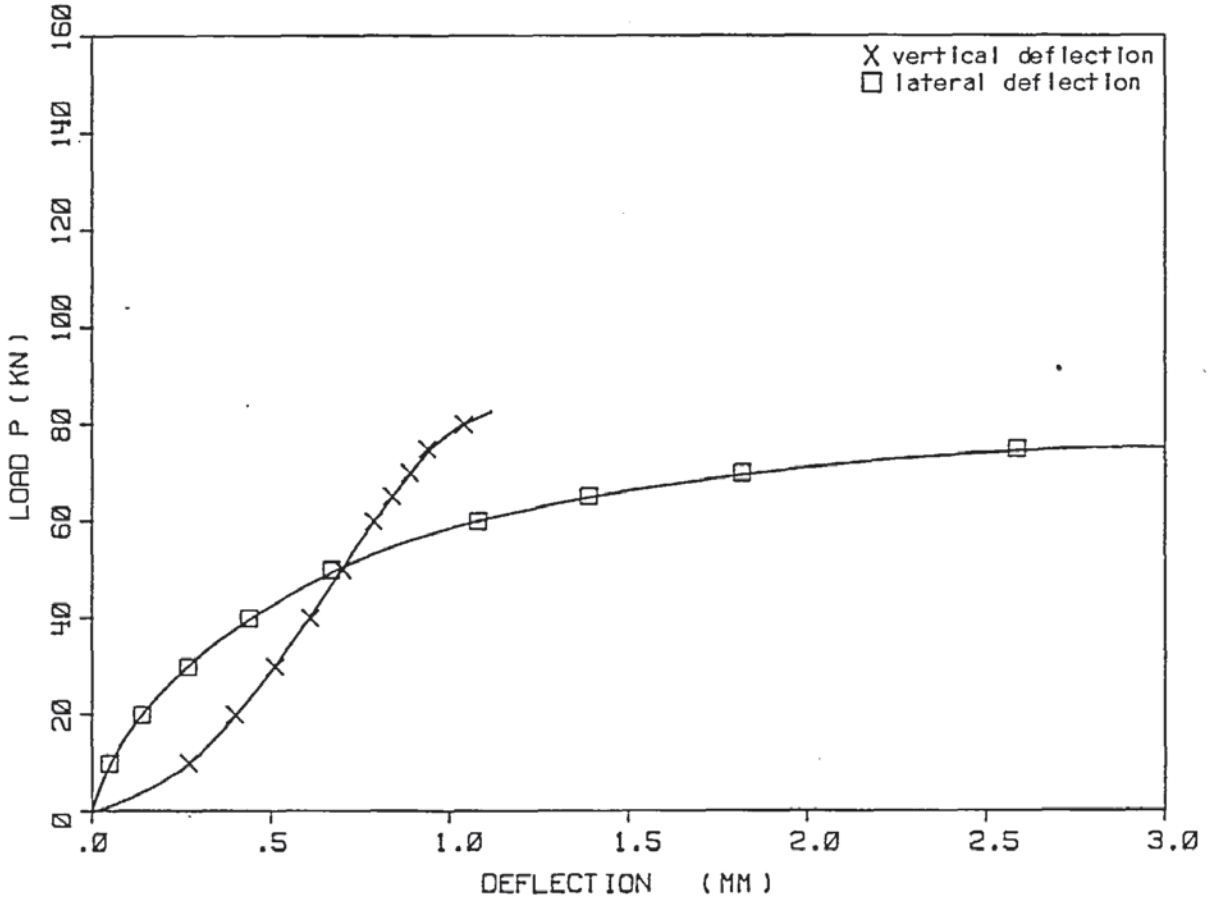

Figure A.4.23. The total vertical and mid-lateral deflections of specimen S2-0-1.

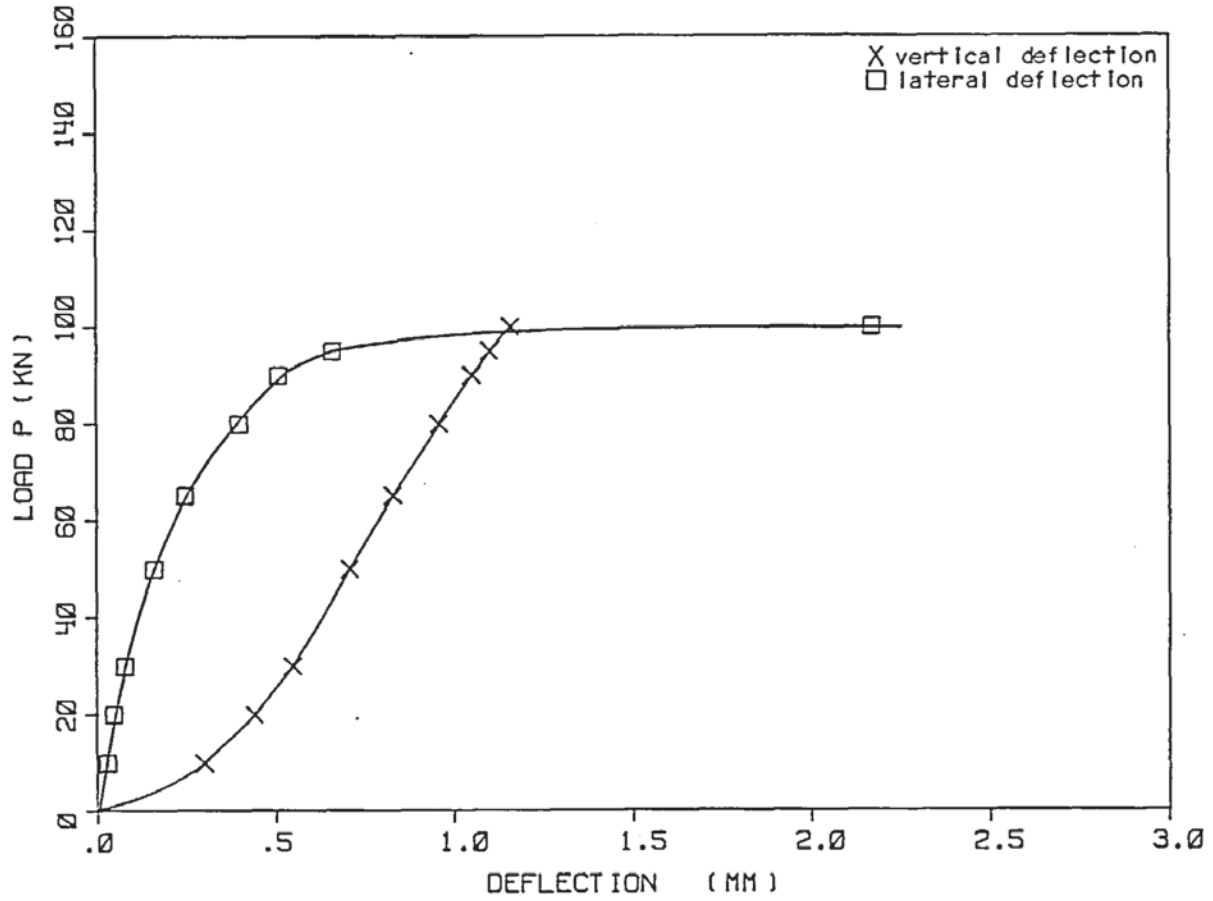

Figure A.4.24. The total vertical and mid-lateral deflections of specimen S2-0-2.

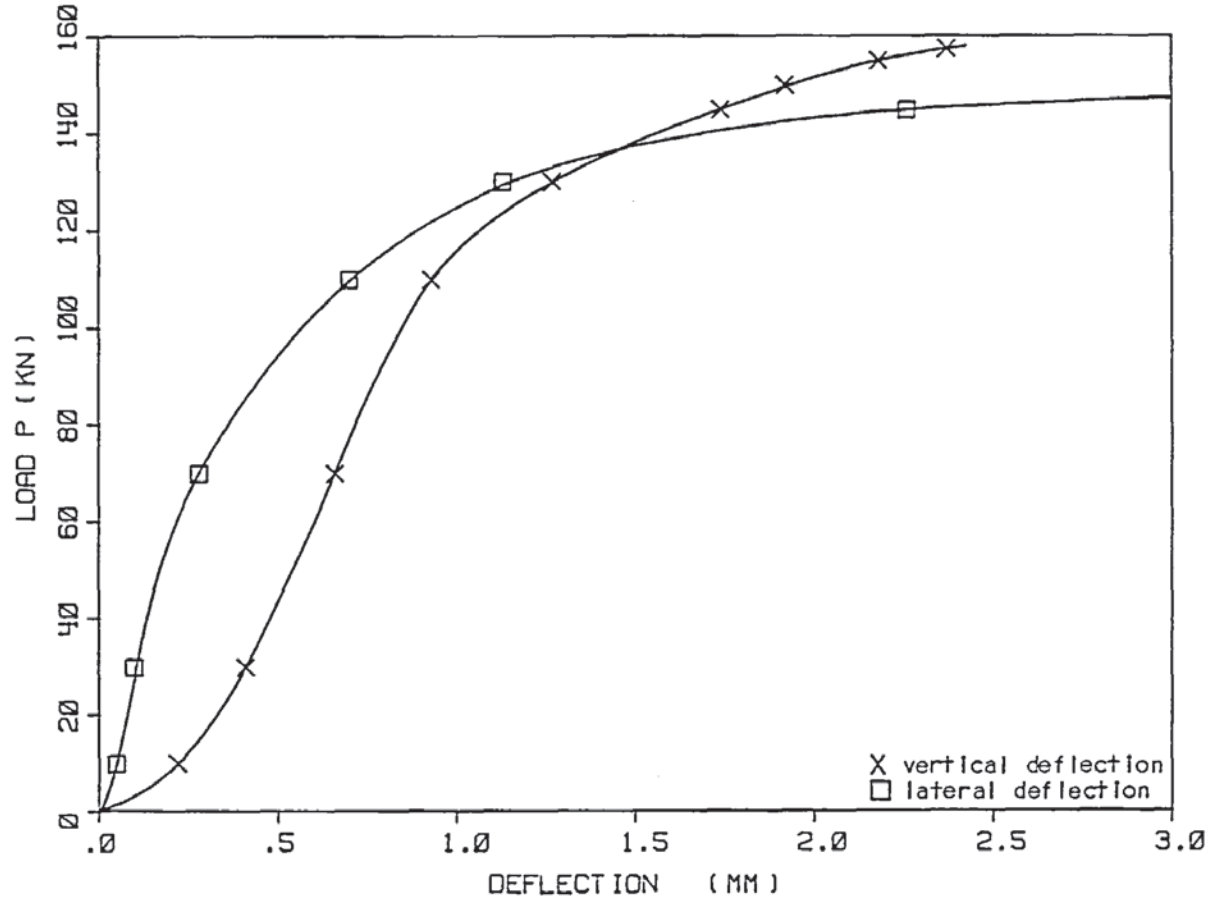

Figure A.4.25. The total vertical and mid-lateral deflections of specimen S5a-75-1.

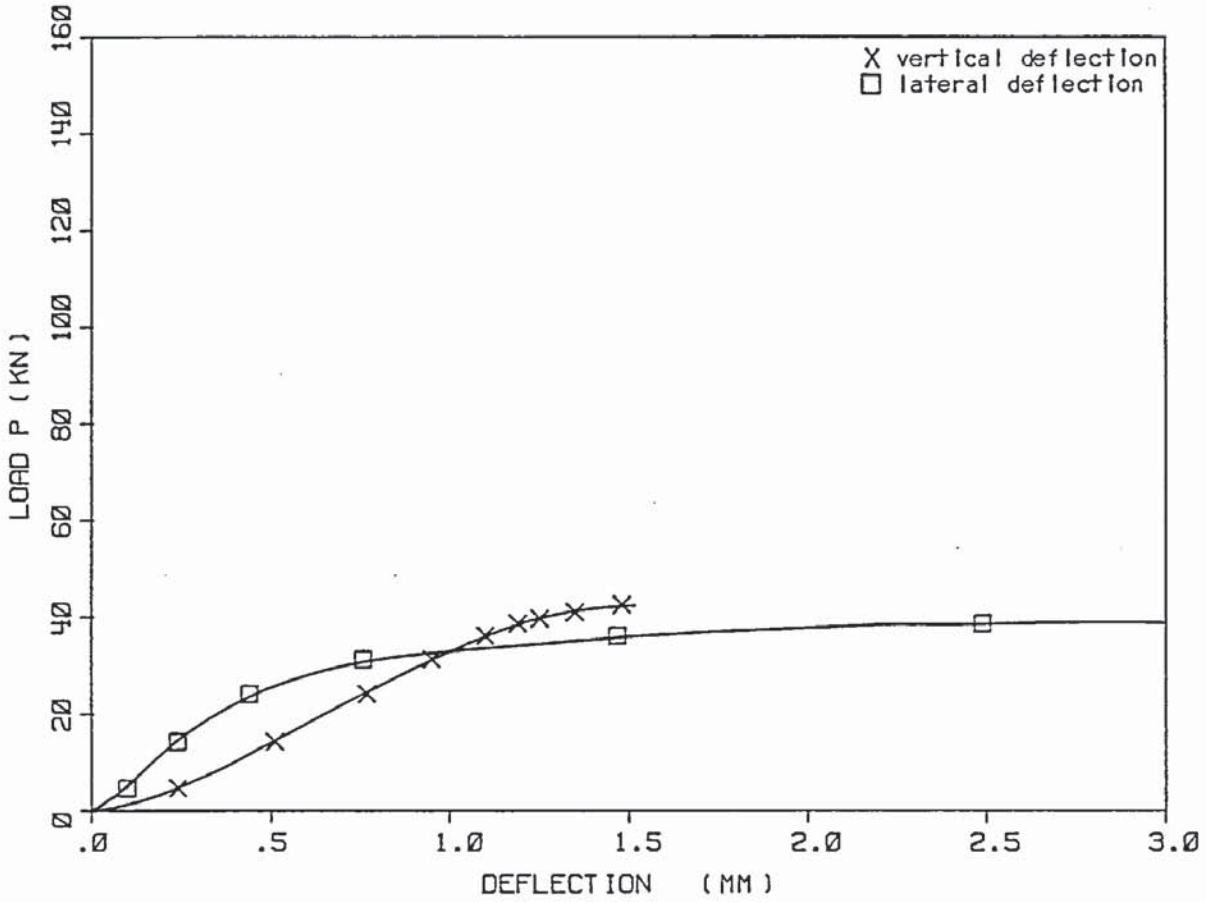

Figure A.4.26. The total vertical and mid-lateral deflections of specimen S5a-300-1.

APPENDIX 5

This appendix contains the tables of the strain gauge data for the main series, subsidiary and the weld series respectively. A considerable number of strain gauge readings were taken with the aid of data logging facilities (see Appendix 1 for details of equipment and computer programs). From each pair of strain gauges the average stress across that particular section was calculated as described in section 6.5.2.1. Out of all the data only the stresses that best represented the change in stress distribution throughout the tests are tabulated and presented in this Appendix.

With the gusset plates only the average stresses are tabulated and they are presented first. With the loaded plates the individual stresses are tabulated in addition to their average and are presented afterwards. The rosette strain gauge data for the gusset plates are tabulated at the end of this Appendix. Only the results are presented where all the gauges were within the yield stress.

The gauge positions for each specimen are presented in Chapter 3. Compressive stresses are taken to be positive.

Note that in the following tables:-

at least one of the strain gauges was reading beyond the yield strain and so the average stress was calculated as described in section 6.?.

† the strain gauge readings were taken as the specimen was failing.

* the stress is beyond the yield stress.

STRAIN GAUGE PAIR NUMBERS	SPECIMEN S5-75-1								
	LOAD kN								
	30	50	80	100	110	120	125	130	135
1-5	45.5	82.0	138.1	186.1	218.7	261.1	304.3	368.2#	378.0#
2-6	40.6	71.7	136.2	204.0	250.7	299.3	348.5#	378.0#	378.0#
10-16	26.5	61.1	93.5	138.0	170.0	208.8	238.4#	262.2#	267.9#
3-7	16.5	29.5	51.7	63.4	67.1	64.8	58.9	50.0	26.4
4-8	7.1	8.4	-18.8	-51.7	-73.9	-101.4	-123.0	-147.8	-184.6#

Table A.5.1. Average stress (N/mm2) across the width of plate S5-75-1.

STRAIN GAUGE PAIR NUMBERS	SPECIMEN S5-150-1				
	LOAD kN				
	30	60	65	70	70†
15-24	33.3	75.8	103.9	176.2	378.0#
6-13	45.9	111.3	183.9	298.3#	320.8#
18-27	49.0	120.8	212.9#	250.4#	191.8#
7-14	45.2	104.2	119.2	101.1#	44.6#
21-30	46.1	54.1	-3.6	-58.9#	-73.4#

Table A.5.2. Average stress (N/mm2) across the width of plate S5-150-1.

STRAIN GAUGE PAIR NUMBERS	SPECIMEN S5-150-1				
	LOAD kN				
	30	60	65	70	70†
1-8	17.0	29.8	22.9	10.0	-4.1
2-9	16.3	16.5	8.2	-32.0#	-49.3#
3-10	13.8	54.2	101.1#	125.0#	265.7#
4-11	11.1	44.4	74.4#	96.7#	151.0#
5-12	9.0	29.1	52.8	94.9#	119.8#
17-26	7.0	15.0	17.1	30.0	108.0

Table A.5.3. Average stress (N/mm2) along the supported edge of plate S5-150-1.

STRAIN GAUGE PAIR NUMBERS	SPECIMEN S5-150-2				
	LOAD kN				
	30	62.5	67.5	70.0	71.6
31-52	52.4	144.9	227.1#	273.4#	258.6#
13-27	49.8	129.5	164.5	158.0#	104.6#
34-55	52.1	81.8	55.2#	8.3#	-42.5#
73-76	33.9	86.5	110.7	163.3	366.2#
12-26	49.3	133.4	185.9	274.3#	330.4#
37-58	56.3	149.5	193.6	234.7#	218.7#
40-61	48.0	109.6	118.1	114.6#	36.1#
43-64	59.0	74.6	45.5	5.1#	-105.1#
46-67	59.0	150.7	191.3	245.2#	246.1#
14-28	41.3	93.8	103.8	106.1	92.3
49-70	24.5	14.8	-14.1	-52.2	-105.4

Table A.5.4. Average stress (N/mm2) across the width of plate S5-150-2.

STRAIN GAUGE PAIR NUMBERS	SPECIMEN S5-150-2				
	LOAD kN				
	30	62.5	67.5	70	71.6
1-15	18.0	31.6	27.8	20.5	-0.2
2-16	18.0	21.7	8.5	-6.2	-38.9
3-7	19.7	13.7	-8.3	-31.9	-75.0
4-18	20.8	60.6	53.9	47.1	14.5#
5-19	17.8	63.5	82.0#	70.5#	67.7#
6-20	12.8	58.2	96.3#	104.5#	114.7#
7-21	-0.2	13.7	27.8	64.1	98.7#
72-75	-9.2	-27.2	-33.4	-34.1	-

Table A.5.5. Average stress (N/mm2) along the supported edge of plate S5-150-2.

STRAIN GAUGE PAIR NUMBERS	SPECIMEN S5-300-1					
	LOAD kN					
	15	20	25	28	29	29.9
1-5	5.1	8.1	15.1	29.6	51.6	216.2
2-6	19.1	34.9	72.7	130.5	186.2#	266.7#
10-16	36.2	65.1	140.0#	196.0#	207.1#	173.2#
3-7	58.0	107.2	169.5#	155.4#	127.0#	80.0#
4-8	90.4	151.7#	121.0#	74.7#	58.7#	44.3#

Table A.5.6. Average stress (N/mm2) across the width of plate S5-300-1.

STRAIN GAUGE PAIR NUMBERS	SPECIMEN S5-300-2			
	LOAD kN			
	15	20	22	23
1-6	12.8	17.5	19.4	20.5
2-7	21.3	31.8	39.3	44.7
3-8	35.0	52.9	66.4	76.7
4-9	52.8	80.3	106.4	128.0#
5-10	72.2	139.2	167.5#	168.0#

Table A.5.7. Average stress (N/mm2) across the width of plate S5-300-2.

STRAIN GAUGE PAIR NUMBERS	SPECIMEN S5-300-3					
	LOAD kN					
	15	22.5	28	30	31	32
1-12	5.8	9.9	14.5	20.9	30.3	73.3
2-13	14.5	24.7	52.6	86.3	117.7	218.2#
3-14	29.8	48.5	93.6	135.3	163.7	222.8#
4-15	55.9	85.6	119.6	131.2	132.7	128.7
5-16	97.2	139.4	128.0	94.3	69.4	20.7

Table A.5.8. Average stress (N/mm2) across the width of plate S5-300-3.

STRAIN GAUGE PAIR NUMBERS	SPECIMEN S6-150-1					
	LOAD kN					
	30	70	80	87.5	92.5	95
1-24	30.7	79.4	108.4	136.1	193.7	299.4#
2-25	45.9	119.3	182.3	232.1	281.0#	320.0#
3-26	48.7	129.2	208.6	244.1#	254.6#	266.4#
4-27	44.3	111.7	129.2	133.3#	117.3#	4.1#
5-28	41.9	71.0	7.4	-24.7#	-55.1#	-79.0#

Table A.5.9. Average stress (N/mm2) across the width of plate S6-150-1.

STRAIN GAUGE PAIR NUMBERS	SPECIMEN S6-300-1							
	LOAD kN							
	10	20	25	27.5	31	32	33	34.8
1-24	4.0	9.6	8.7	9.7	34.1	89.5	171.2	378.0#
2-25	12.9	31.1	53.0	75.3	194.5	310.5#	351.9#	371.6#
3-26	19.7	51.5	101.7	145.9	244.6#	250.7#	240.6#	197.6#
4-27	34.2	79.8	133.0	153.6#	133.6#	98.6#	78.7#	55.7#
5-28	46.2	107.6	99.9	67.8#	-18.6#	-36.2#	-41.4#	-47.3#

Table A.5.10. Average stress (N/mm2) across the width of plate S6-300-1.

STRAIN GAUGE PAIR NUMBERS	SPECIMEN S7-10-150-1			
	LOAD kN			
	15	45	65	70
1-6	12.3	39.0	57.7	66.3
2-7	24.2	78.6	132.3	161.1
3-8	27.4	80.0	120.9	125.0
4-9	19.7	58.0	86.2	93.5
5-10	5.5	18.4	15.0	2.4

Table A.5.11. Average stress (N/mm2) across the width of plate S7-10-150-1.

STRAIN GAUGE PAIR NUMBERS	SPECIMEN S13-50-1						
	LOAD kN						
	39.2	58.7	78.3	97.9	130.5	169.7	215.4
1-6	43.0	70.3	96.3	127.8	197.4	245.0#	245.0#
2-7	67.6	110.2	157.0	210.2	245.0#	245.0#	245.0#
3-8	75.6	125.4	162.9	196.1	245.0#	245.0#	245.0#
4-9	36.6	57.7	66.8	84.6	116.9	153.8	245.0#
5-10	12.9	16.4	14.5	13.8	8.2	-5.5	17.5

Table A.5.12. Average stress (N/mm2) across the width of plate S13-50-1.

STRAIN GAUGE PAIR NUMBERS	SPECIMEN S13-70-1					
	LOAD kN					
	26.6	47.9	69.2	90.8	106.4	111.7
1-10	29.9	53.4	79.6	113.4	143.7	179.0
2-11	48.7	97.6	149.7	222.3#	245.0#	245.0#
3-12	47.1	81.3	154.8	233.0#	232.1#	224.4#
4-13	32.7	55.5	81.3	107.0	157.7#	151.8#
5-14	27.2	47.9	70.5	92.8	107.4#	109.5#

Table A.5.13. Average stress (N/mm2) across the width of plate S13-70-1.

STRAIN GAUGE PAIR NUMBERS	SPECIMEN S13-70-1					
	LOAD kN					
	26.6	47.9	69.2	90.8	106.4	111.7
6-15	81.7	173.1	245.0#	245.0#	245.0#	245.0#
7-16	37.4	59.7	84.3	101.9	82.7	12.6
5-14	27.2	47.9	70.5	92.8	107.9#	109.5#
8-17	5.6	8.3	7.0	0.5	-23.3	-64.1
9-18	-8.1	-22.6	-34.9	-51.2	-61.4#	-177.1#

Table A.5.14. Average stress (N/mm2) along the free edge of plate S13-70-1.

STRAIN GAUGE PAIR NUMBERS	SPECIMEN S13-110-1 LOAD kN					
	16.0	31.9	39.9	45.2	47.9	50.5
1-12	23.3	54.6	81.2	107.9	130.1	173.1#
2-13	32.0	84.7	129.3	166.4#	183.0#	192.0#
3-14	34.7	92.5	140.1	160.0#	168.2#	171.9#
4-15	33.1	68.3	98.1#	109.5#	110.1#	106.8#
5-16	23.7	26.2	33.0#	28.9#	27.6#	31.0#

Table A.5.15. Average stress (N/mm2) across the width of plate S13-110-1.

STRAIN GAUGE PAIR NUMBERS	SPECIMEN S13-110-1 LOAD kN					
	16.0	31.9	39.9	45.2	47.9	50.5
6-17	30.1	42.5	44.6	43.8	38.4	33.8
7-18	28.7	13.2	-20.2	-45.7	-66.2	-84.0
8-19	30.7	71.9#	52.7#	39.3#	28.7#	20.9#
5-16	23.7	26.2	33.0#	28.9#	27.6#	31.0#
9-20	23.2	22.8	5.3	-10.8	-26.0	-37.8
10-21	10.8	12.1	-0.6	-12.5	-24.8	-38.5
11-22	-3.5	-8.9	-9.9	-10.2	-9.6	-10.8

Table A.5.16. Average stress (N/mm2) along the free edge of plate S13-110-1.

STRAIN GAUGE PAIR NUMBERS	SPECIMEN S13-130-1 LOAD kN			
	20.9	33.9	43.1	44.4
1-14	23.4	39.9	62.6	72.7
2-16	36.4	61.3	99.8	115.6
3-16	42.6	70.0	108.9	122.5
4-17	47.9	77.5	103.0	106.1#
5-18	70.5	114.5	118.9#	109.2#

Table A 5.17. Average stress (N/mm2) across the width of plate S13-130-1.

STRAIN GAUGE PAIR NUMBERS	SPECIMEN S13-130-1 LOAD kN			
	20.9	33.9	43.1	44.4
6-19	18.8	30.3	35.3	37.0
7-20	20.6	32.9	35.8	35.3
8-21	36.6	53.6	42.4	33.8
9-22	57.2	90.1	73.7	59.5
5-18	70.5	114.5	118.9#	109.2#
10-23	50.9	80.8	81.6	74.5
11-24	10.0	13.8	9.6	7.2
12-25	-6.0	-9.9	-12.6	-13.0
13-26	0.1	0.0	-0.4	-0.5

Table A.5.18. Average stress (N/mm2) along the free edge of plate S13-130-1.

STRAIN GAUGE PAIR NUMBERS	SPECIMEN S11-150-1 LOAD kN 20	40	50	55
1-9	45.8	93.4	117.8	152.4
2-10	60.4	125.6	164.9	233.2
3-11	63.3	131.3	177.0	279.1
4-12	64.5	135.1	188.7	168.7
5-13	49.6	103.0	133.0	112.2
6-14	35.6	64.6	66.1	49.9
7-15	12.8	20.3	25.1	13.2
8-16	1.7	3.7	6.2	10.8

Table A.5.19. Average stress (N/mm2) in each strip of the multi-strip plate S11-150-1.

STRAIN GAUGE PAIR NUMBERS	SPECIMEN S5a-75-1 LOAD kN 40	110	140	150	155	157.5	160
1-6	42.5	125.4	167.3	189.7	213.2	248.6	306.4
2-7	34.3	102.5	137.9	168.4	226.9	303.5#	349.8#
3-8	23.0	71.0	98.7	127.6	169.8	208.1	244.0
4-9	16.5	49.3	65.7	79.5	89.6	95.8	99.0
5-10	9.6	25.7	18.4	-11.6	-67.7	-114.7	-156.5

Table A.5.20. Average stress (N/mm2) across the width of plate S5a-75-1.

STRAIN GAUGE PAIR NUMBERS	SPECIMEN S5a-300-1 LOAD kN 9.7	26.6	33.9	38.7	41.1	42.6	44.3
1-6	17.4	46.3	59.3	72.8	92.5	106.3	149.1
2-7	29.2	74.5	94.7	120.4	167.8	201.8	282.3
3-8	24.4	73.3	96.5	121.3	158.6	175.8	193.0
4-9	40.3	100.0	125.3	148.8	161.2	164.6	156.7
5-10	48.2	123.3	150.6	156.6	127.0	111.1	73.9

Table A.5.21. Average stress (N/mm2) across the width of plate S5a-300-1.

SPECIMEN S5-150-2									
STRAIN GAUGE PAIR NUMBERS	LOAD kN								
	30			62.5			67.5		
	GAUGE			GAUGE			GAUGE		
	1st.	2nd.	Average	1st.	2nd.	Average	1st.	2nd.	Average
9-10	-7.3	-0.4	-3.9	-33.6	9.9	-11.9	-48.3	13.0	-17.7
8-11	-3.6	-12.0	-7.8	-22.6	-12.8	-17.7	-34.2	-12.0	-23.0
22-25	-0.8	-6.3	-3.6	-14.2	-3.6	-8.9	-25.6	-1.0	-13.3
23-24	-7.7	-0.0	-3.9	-28.1	5.3	-11.4	-38.7	7.9	-15.4

SPECIMEN S5-150-2						
STRAIN GAUGE PAIR NUMBERS	LOAD kN					
	70			71.6		
	GAUGE			GAUGE		
	1st.	2nd.	Average	1st.	2nd.	Average
9-10	-65.6	17.5	-24.1	-91.5	22.8	-34.4
8-11	-48.3	-12.0	-30.2	-64.0	-16.9	-40.5
22-25	-38.9	- 1.8	-20.4	-57.3	- 8.7	-33.0
23-24	-53.0	12.0	-20.5	-81.1	19.1	-31.0

Table A.5.22. Stresses (N/mm2) in loaded plate of specimen S5-150-2.

SPECIMEN S5-300-3									
STRAIN GAUGE PAIR NUMBERS	LOAD kN								
	15			22.5			28		
	GAUGE			GAUGE			GAUGE		
	1st.	2nd.	Average	1st.	2nd.	Average	1st.	2nd.	Average
6-17	-4.8	-9.7	-7.3	-7.3	-16.1	-11.7	-9.7	-23.0	-16.4
7-18	-3.4	-14.2	-8.8	-6.1	-22.2	-14.2	-2.0	-38.7	-20.4
8-19	1.4	-16.5	-7.6	1.8	-26.1	-12.2	6.3	-40.9	-17.3
9-20	9.3	-26.9	-8.8	13.2	-39.7	-13.3	19.3	-50.7	-15.7
10-21	17.9	-33.6	-7.9	28.7	-52.0	-11.7	41.6	-68.1	-13.3
11-22	16.5	-25.0	-4.3	25.2	-36.7	-5.8	32.4	-45.4	-6.5

SPECIMEN S5-300-3									
STRAIN GAUGE PAIR NUMBERS	LOAD kN								
	30			31			32		
	GAUGE			GAUGE			GAUGE		
	1st.	2nd.	Average	1st.	2nd.	Average	1st.	2nd.	Average
6-17	-10.6	-30.5	-20.6	-10.6	-35.0	-22.8	-9.3	-47.1	-28.2
7-18	3.6	-54.2	-25.3	8.9	-67.7	-29.4	28.5	-100.5	-36.0
8-19	12.7	-54.4	-21.0	18.7	-65.4	-23.4	39.3	-93.8	-27.3
9-20	23.8	-56.7	-16.5	26.7	-61.3	-17.3	36.9	-70.1	-16.6
10-21	47.5	-74.4	-13.5	49.5	-77.3	-13.9	55.8	-81.1	-12.7
11-22	35.2	-48.5	-6.7	36.9	-50.5	-6.8	38.9	-52.0	-6.6

Table A.5.23. Stresses (N/mm2) in loaded plate of specimen S5-300-3.

SPECIMEN S6-300-1									
STRAIN GAUGE PAIR NUMBERS	LOAD kN								
	20			25			27.5		
	GAUGE			GAUGE			GAUGE		
	1st.	2nd.	Average	1st.	2nd.	Average	1st.	2nd.	Average
6-29	-2.6	-27.3	-15.0	-3.0	-39.3	-21.2	-2.4	-48.7	-25.6
7-30	1.6	-21.0	-9.7	5.7	-39.7	-17.0	10.8	-55.8	-22.5
8-31	3.6	-26.1	-11.3	15.7	-53.8	-19.1	28.7	-77.5	-24.4
9-32	15.9	-40.1	-12.1	31.2	-68.1	-18.5	45.4	-90.9	-22.8
10-33	26.9	-46.5	-9.8	32.2	-54.6	-11.2	33.6	-58.7	-12.6
11-34	20.1	-27.5	-3.7	27.9	-37.9	-5.0	31.2	-43.2	- 6.0
12-35	2.2	-28.1	-13.0	4.6	-40.5	-18.0	6.7	-49.5	-21.4
13-36	5.5	-26.9	-10.7	19.7	-49.3	-14.8	34.6	-69.7	-17.6
14-37	33.6	-37.3	-1.8	41.2	-48.1	-3.5	45.0	-54.8	-4.9
15-38	-6.5	-22.4	-14.5	-8.7	-33.0	-20.9	-9.5	-41.4	-25.5
16-39	-3.6	-22.4	-13.0	-0.0	-39.9	-20.0	3.8	-54.4	-25.3
17-40	9.1	-30.5	-10.7	21.6	-58.5	-18.5	35.2	-82.1	-23.5
18-41	18.9	-38.3	-9.7	34.6	-66.6	-16.0	47.9	-89.7	-20.9
19-42	23.4	-46.0	-11.3	26.7	-54.2	-13.8	28.1	-57.9	-14.9
20-43	31.2	-35.0	-1.9	35.8	-44.2	-4.2	37.3	-48.9	-5.8
21-44	-11.2	-14.6	-12.9	-16.1	-20.6	-18.4	-17.7	-26.1	-21.9
22-45	15.5	-31.8	-8.2	31.6	-60.5	-14.5	46.7	-84.6	-19.0
23-46	26.5	-37.7	-5.6	32.8	-47.9	-7.6	36.5	-53.6	-8.6

SPECIMEN S6-300-1									
STRAIN GAUGE PAIR NUMBERS	LOAD kN								
	31			32			33		
	GAUGE			GAUGE			GAUGE		
	1st.	2nd.	Average	1st.	2nd.	Average	1st.	2nd.	Average
6-29	9.5	-88.1	-39.3	34.0	-132.3	-49.2	37.9	-181.9	-57.0
7-30	52.6	-124.4	-35.9	11.7	-200.2	-44.3	178.0	-278.9*	
8-31	107.8	-176.4	-34.3	173.5	-245.9	-36.2	225.8	-299.0*	
9-32	106.4	-164.1	-28.9	143.7	-204.9	-30.6	172.1	-236.1	-32.0
10-34	37.3	-62.6	-12.7	40.9	-67.3	-13.2	47.5	-72.8	-12.7
11-34	38.3	-45.4	-3.6	41.8	-51.6	-4.9	45.0	-56.7	-5.9
12-35	24.0	-83.6	-29.8	56.0	-123.6	-33.8	98.9	-171.1	-36.1
13-36	117.0	-163.5	-23.3	184.5	-235.9	-25.7	240.0	-294.5*	
14-37	57.9	-69.5	-5.8	66.6	-77.7	-5.6	75.4	-84.8	-4.7
15-38	2.4	-79.5	-38.6	27.5	-123.3	-47.9	62.4	-172.9	-55.3
16-39	47.1	-125.6	-39.3	105.8	-201.8	-47.8	170.5	-274.9*	
17-40	116.6	-184.5	-34.0	184.3	-255.5	-35.6	238.8	-311.6	-36.4
18-41	111.5	-164.3	-26.4	149.0	-204.1	-27.6	176.4	-233.7	-28.7
19-42	33.6	-62.0	-14.2	37.7	-66.2	-14.3	42.0	-71.7	-14.9
20-43	46.7	-58.3	-5.8	50.7	-63.2	-6.3	53.8	-67.7	-7.0
21-44	-5.3	-55.8	-30.6	25.4	-95.4	-35.0	66.4	-142.1	-37.9
22-45	131.7	-186.6	-27.5	199.2	-262.0	-31.4	253.5*	-322.8*	
23-46	45.4	-66.8	-10.7	51.6	-74.6	-11.5	57.3	-81.1	-11.9

Table A.5.24. Stresses (N/mm2) in loaded plate of specimen S6-300-1.

SPECIMEN	S6-150-1								
STRAIN GAUGE PAIR NUMBERS	LOAD kN								
	30			70			80		
	GAUGE			GAUGE			GAUGE		
	1st.	2nd.	Average	1st.	2nd.	Average	1st.	2nd.	Average
6-29	8.3	-30.3	-11.0	21.8	-74.8	-26.5	32.2	-106.4	-37.1
7-30	1.0	-16.1	-7.6	1.8	-41.4	-19.8	0.4	-66.0	-32.8
8-31	-6.1	3.2	-1.5	-9.5	3.4	-3.1	-9.3	-4.6	-7.0
9-32	-5.3	7.9	1.3	-7.9	18.5	5.3	-10.1	20.8	5.4
10-33	2.6	-0.0	1.3	9.3	1.0	5.2	15.5	4.2	9.8
11-34	-1.2	-6.3	-3.8	-2.2	-4.8	-3.5	-2.4	-4.2	-3.1
12-35	19.9	-33.6	-6.9	47.5	-78.3	-15.4	67.5	-109.5	-21.0
13-36	-16.5	7.3	-4.5	-39.3	18.1	-10.6	-44.4	15.9	-14.3
14-37	1.2	-1.4	-0.1	2.8	-2.4	0.2	-0.8	-1.2	-1.0
15-38	5.9	-28.7	-11.4	18.3	-73.6	-27.7	27.7	-103.8	-38.1
16-39	1.6	-15.0	-6.7	6.5	-40.3	-16.9	13.6	-64.0	-25.2
17-40	-4.8	2.2	-1.3	-8.7	2.8	-3.0	-10.4	-5.5	-8.0
18-41	-4.8	9.1	2.2	-10.1	20.1	5.0	-13.4	22.4	4.5
19-42	-1.2	-0.4	-0.8	-1.4	0.2	-0.6	-2.4	4.0	0.8
20-43	1.0	0.4	-0.7	0.4	2.4	1.4	-0.8	4.0	1.6
21-44	12.8	-22.2	-4.7	37.7	-66.0	-14.2	49.3	-91.3	-21.0
22-45	-16.7	7.7	-4.5	-40.7	19.3	-10.7	-46.2	14.2	-16.0
23-46	-0.4	-1.0	-0.7	-1.2	-2.6	-1.9	-2.6	-2.0	-2.3

SPECIMEN	S6-150-1								
STRAIN GAUGE PAIR NUMBERS	LOAD kN								
	87.5			92.5			95		
	GAUGE			GAUGE			GAUGE		
	1st.	2nd.	Average	1st.	2nd.	Average	1st.	2nd.	Average
6-29	42.4	-132.9	-45.3	67.3	-174.1	-53.4	242.3	-694.8*	
7-30	-0.0	-84.2	-42.1	-1.0	-111.3	-56.2	-6.3	-196.8	-101.6
8-31	-10.1	-9.7	-9.9	-12.6	-16.9	-14.8	-17.9	-29.3	-23.6
9-32	-11.6	22.0	5.2	-12.8	23.2	5.2	-19.1	18.7	-0.2
10-33	22.0	6.3	14.2	34.2	10.6	22.4	93.0	19.1	56.1
11-34	-2.8	-3.8	-3.3	-2.6	-2.0	-2.3	-2.6	-1.2	-1.9
12-35	83.8	-136.0	-26.1	115.6	-180.0	-32.2	295.3*	-516.0*	
13-36	-49.1	13.4	-17.9	-53.8	10.8	-21.5	-55.0	-3.2	-29.1
14-37	-1.2	-1.4	-1.3	-3.8	-0.2	-2.0	-11.4	3.6	-3.9
15-38	36.5	-129.5	-46.5	59.5	-157.8	-49.2	278.8	-667.9	
16-39	19.9	-83.6	-31.9	32.6	-111.1	-39.3	98.3	-209.4	-55.6
17-40	-10.8	-11.6	-11.2	-14.8	-18.1	-16.5	-20.3	-34.0	-27.2
18-41	-14.4	23.0	4.3	-15.2	23.2	4.0	-22.8	18.3	-2.3
19-42	-3.6	5.7	1.1	-5.0	8.9	2.0	-9.5	17.5	4.0
20-43	0.4	4.6	2.5	0.6	5.7	3.2	0.4	6.5	3.5
21-44	62.0	-114.8	-26.4	91.1	-156.6	-32.8	304.3*	-493.5*	
22-45	-50.3	11.0	-19.7	-56.7	7.3	-24.7	-56.7	-16.5	-36.6
23-46	-4.4	-2.4	-3.4	-6.5	-2.0	-4.3	-14.2	3.4	-5.4

Table A.5.25. Stresses (N/mm2) in loaded plate of specimen S6-150-1.

SPECIMEN	S7-6-150-1								
STRAIN GAUGE PAIR NUMBERS	LOAD kN								
	15			45			65		
	GAUGE		Average	GAUGE		Average	GAUGE		Average
	1st.	2nd.		1st.	2nd.		1st.	2nd.	
1-3	-5.9	-22.8	-14.4	-32.0	-63.2	-47.6	-46.5	-90.1	-68.3
2-4	5.7	-21.2	-7.8	3.2	-71.3	-34.1	6.5	-101.9	-47.7

SPECIMEN	S7-6-150-1								
STRAIN GAUGE PAIR NUMBERS	LOAD kN								
	70			74.4					
	GAUGE		Average	GAUGE		Average	GAUGE		Average
	1st.	2nd.		1st.	2nd.		1st.	2nd.	
1-3	-48.7	-101.5	-74.6	-66.8	-136.8	-101.8			
2-4	11.2	-111.3	-50.1	18.3	-147.4	-64.6			

Table A.5.26. Stresses (N/mm2) in loaded plate of specimen S7-6-150-1.

SPECIMEN	S7-10-150-1								
STRAIN GAUGE PAIR NUMBERS	LOAD kN								
	15			45			65		
	GAUGE		Average	GAUGE		Average	GAUGE		Average
	1st.	2nd.		1st.	2nd.		1st.	2nd.	
11-18	-1.4	-7.8	-4.6	-9.5	-24.2	-17.1	-27.1	-40.4	-33.8
12-19	-5.9	-16.9	-11.4	-19.7	-50.3	-35.0	-35.2	-81.5	-58.4
13-20	-4.6	-10.1	-7.4	-14.0	-35.2	-24.6	-22.4	-63.8	-43.1
14-21	5.5	-10.1	-2.3	22.2	-34.8	-6.3	40.3	-64.2	-12.0
15-22	7.9	-3.8	2.1	27.5	-6.9	10.3	33.0	-3.0	15.0
16-23	-0.0	-2.2	-1.1	3.0	-7.3	-2.2	6.5	-13.2	-3.4
17-24	0.6	-0.0	0.3	1.6	0.4	1.0	1.8	0.2	1.0

SPECIMEN	S7-10-150-1		
STRAIN GAUGE PAIR NUMBERS	LOAD kN		
	70		
	GAUGE		Average
	1st.	2nd.	
11-18	-39.7	-46.7	-43.2
12-19	-45.0	-97.6	-71.3
13-20	-25.6	-81.5	-53.8
14-21	43.8	-78.1	-17.2
15-22	31.0	1.2	16.1
16-23	8.3	-16.9	-4.3
17-24	3.0	-0.0	1.5

Table A.5.27. Stresses (N/mm2) in loaded plate of specimen S7-10-150-1.

SPECIMEN	S7-13-150-1								
STRAIN GAUGE PAIR NUMBERS	LOAD kN								
	15			30			45		
	GAUGE		Average	GAUGE		Average	GAUGE		Average
	1st.	2nd.		1st.	2nd.		1st.	2nd.	
1-3	5.0	-9.1	-2.1	5.5	-18.7	-6.6	1.6	-35.2	-16.8
2-4	17.7	-22.6	-2.5	25.9	-44.0	-9.1	24.6	-74.4	-24.9

SPECIMEN	S7-13-150-1					
STRAIN GAUGE PAIR NUMBERS	LOAD kN					
	65			70†		
	GAUGE		Average	GAUGE		Average
	1st.	2nd.		1st.	2nd.	
1-3	-5.5	-93.0	-49.3	25.6	-148.8	-61.6
2-4	28.1	-174.9	-73.4	70.7	-274.7	-102.0

Table A.5.28. Stresses (N/mm2) in loaded plate of specimen S7-13-150-1.

SPECIMEN	S7-16-150-1								
STRAIN GAUGE PAIR NUMBERS	LOAD kN								
	20			50			65		
	GAUGE			GAUGE			GAUGE		
	1st.	2nd.	Average	1st.	2nd.	Average	1st.	2nd.	Average
1-3	-0.1	-22.2	-11.2	3.7	-57.3	-26.8	4.7	-74.8	-35.1
2-4	8.4	-27.7	-9.7	25.1	-65.6	-20.3	32.3	-85.4	-26.6

SPECIMEN	S7-16-150-1								
STRAIN GAUGE PAIR NUMBERS	LOAD kN								
	70			100			120t		
	GAUGE			GAUGE			GAUGE		
	1st.	2nd.	Average	1st.	2nd.	Average	1st.	2nd.	Average
1-3	7.2	-80.1	-36.5	16.5	-120.9	-52.4	13.7	-157.0	-71.7
2-4	35.9	-89.9	-27.0	55.7	-127.0	-35.7	46.6	-152.3	-52.9

Table A.5.29. Stresses (N/mm2) in loaded plate of specimen S7-16-150-1.

SPECIMEN	S5-150-1								
LOAD P kN	Z_1 GAUGE No.	Average Stress components N/mm2			Max. shear stress N/mm2	Principal stress N/mm2		Angle of Rotation rotation from f_z	
		f_x	f_z	f_y		f_3	f_1	θ	to
30	15	-0.4	33.3	7.0	30.2	33.5	-26.9	3.47	f_3
"	18	22.4	49.5	1.5	39.0	50.9	-27.0	-7.77	f_3
"	21	20.3	46.1	13.8	29.0	46.2	-12.2	-3.20	f_3
60	15	4.7	75.8	15.0	66.1	76.0	-56.3	2.23	f_3
"	18	55.2	120.8	13.8	88.7	123.2	-54.2	-6.70	f_3
"	21	15.5	54.1	20.9	36.0	54.2	-17.8	2.13	f_3

Table A.5.30. Rosette strain gauge data for plate S5-150-1.

SPECIMEN		S5-150-2							
LOAD P kN	Z_1 GAUGE No.	Average Stress components N/mm² fx	fz	fy	Max. shear stress N/mm²	Principal stress f3	N/mm² f1	Angle of rotation θ	Rotation from fz to
30	30	-24.8	16.8	52.4	38.6	52.5	-24.9	42.83	f3
"	33	-15.1	19.8	52.1	33.6	52.1	-15.1	43.87	f3
"	36	-29.4	31.2	56.3	46.3	59.9	-32.9	33.76	f3
"	39	-19.5	31.0	48.0	37.6	52.0	-23.4	31.82	f3
"	42	-13.6	17.9	44.0	28.9	44.2	-13.8	42.32	f3
"	45	-29.7	45.0	59.0	53.7	68.4	-39.1	27.76	f3
"	48	- 8.1	17.9	24.5	18.9	27.2	-10.7	29.73	f3
"	73	13.2	33.9	- 9.2	33.8	35.8	-31.8	-9.65	f3
50	30	-40.8	28.5	91.9	66.4	92.0	-40.9	43.74	f3
"	33	-23.7	34.3	81.3	52.7	81.6	-24.0	41.98	f3
"	36	-49.7	50.0	96.8	77.6	101.4	-54.4	35.07	f3
"	39	-32.5	50.5	81.5	62.6	87.2	-38.1	32.76	f3
"	42	-25.5	30.2	77.9	51.8	78.1	-25.6	42.80	f3
"	45	-50.4	75.6	101.4	90.9	116.4	-65.4	28.28	f3
"	48	-12.1	27.1	36.0	28.4	40.3	-16.5	28.86	f3
"	73	22.5	60.6	-17.6	61.4	64.0	-59.0	-9.53	f3
55	30	-44.0	31.9	104.1	74	104.1	-44.1	44.27	f3
"	33	-24.8	40.5	88.3	57.2	89.0	-25.5	40.58	f3
"	36	-54.9	56.4	109.9	87.2	114.8	-59.8	35.38	f3
"	39	-36.0	55.2	92.5	69.7	98.0	-41.5	33.63	f3
"	42	-30.1	31.8	86.3	58.2	86.4	-30.2	43.16	f3
"	45	-56.3	83.9	114.7	101.5	130.7	-72.4	28.69	f3
"	49	-12.0	27.1	35.0	28.2	39.8	-16.7	28.20	f3
"	73	25.7	68.9	-21.0	70.4	72.8	-68.1	-9.67	f3
62.5	30	-38.8	49.4	144.9	91.8	145.0	-38.8	-43.86	f1
"	33	-20.5	55.2	81.8	56.7	87.3	-26.1	32.16	f3
"	36	-64.0	72.4	149.5	110.8	153.6	-68.0	37.24	f3
"	39	-45.6	48.0	109.6	79.2	111.2	-47.2	39.19	f3
"	42	-35.1	16.4	74.6	54.9	74.8	-35.2	-43.27	f1
"	45	-70.7	100.5	150.7	126.2	166.2	-86.3	30.65	f3
"	48	- 6.6	17.1	14.8	16.8	21.0	-12.8	19.8	f3
"	73	36.3	86.5	-27.2	87.7	92.4	-83.2	-10.61	f3

Table A.5.31. Rosette strain gauge data for plate S5-150-2.

SPECIMEN		S5-75-1							
LOAD P kN	Z_1 GAUGE No.	Average Stress components N/mm² fx	fz	fy	Max. shear stress N/mm²	Principal stress f3	N/mm² f1	Angle of rotation θ	Rotation from fz to
50	10	52.1	47.3	-19.8	47.5	63.7	-31.4	-24.57	f3
"	13	38.9	56.0	2.0	40.0	60.5	-19.6	-13.74	f3
80	10	86.5	93.5	-23.0	82.5	114.3	-50.8	-20.79	f3
"	13	77.0	89.5	-23.6	80.4	107.2	-53.7	-19.36	f3
110	10	125.9	170.0	-12.7	132.9	189.5	-76.3	-15.70	f3
"	13	111.0	94.0	-64.3	112.3	135.9	-89.2	-25.57	f3

Table A.5.32. Rosette strain gauge data for plate S5-75-1.

SPECIMEN		S5-300-1							
LOAD P kN	Z_1 GAUGE No.	Average Stress components N/mm² fx	fz	fy	Max. shear stress N/mm²	Principal stress f3	N/mm² f1	Angle of rotation θ	Rotation from fz to
20	10	11.7	65.1	51.4	39.0	70.5	- 7.5	15.31	f3
"	13	20.8	52.6	15.3	34.6	52.7	-16.6	-2.28	f3

Table A.5.33. Rosette strain gauge data for plate S5-300-1.

APPENDIX 6

This appendix contains a design summary and design examples.

A.6.1 Design summary

Gusset plate design - ultimate limit slate

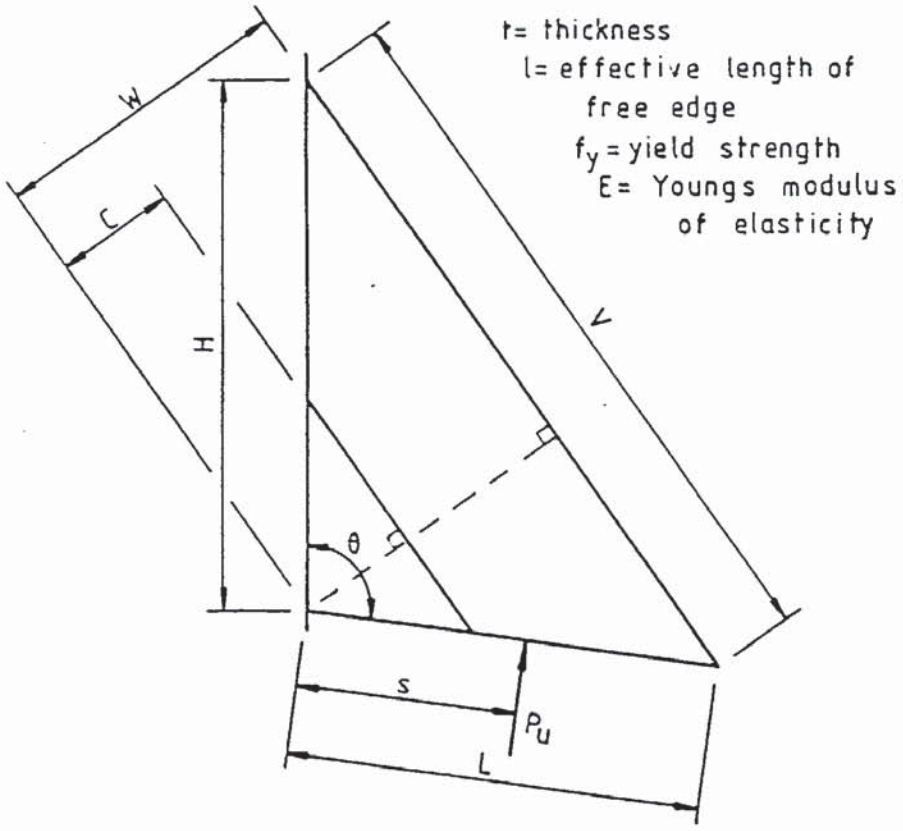

Required:- t

Known from other considerations:- θ, H, L, C, s, f_y, E & P_u

Calculate:-

$$V = \sqrt{L^2 + H^2 - 2.L.H.\cos\theta} \quad ; \text{ (For } \theta = 90°;\ V = \sqrt{L^2 + H^2}\text{)}$$

$$W = \frac{L.H.\sin\theta}{V} \quad ; \text{ (For } \theta = 90°;\ W = \frac{L.H.}{V}\text{)}$$

$$Z = \left\{\left[\frac{V}{2.W.\tan\theta/2} - 1\right]\frac{C}{W} + 1\right\}, \text{ but } \theta > 90°; \text{ (For } C = 0;\ Z = 1\text{)}$$

$$\ell = Z.W.\tan\theta/2, \text{ but } \theta > 90°; \text{ (For } \theta = 90°;\ \ell = Z.W.\text{)}$$

Calculate for use with tables:-

$$\frac{Pu.s}{\ell.W^2.E} \; ; \; \frac{fy}{E}; \; \frac{C}{W}$$

Obtain t/ℓ from design Tables (i.e. Table 8.1 or 8.2 if C = 0). This then gives the value of t required.

Slenderness ratio check:-

acceptable if $\frac{t}{\ell} > 21.65 \times 10^{-3}$

Gusset plate weld design

Obtain R′ using values of:-

$$\frac{fy}{E}; \; \frac{C}{W}; \; \frac{t}{\ell}$$

Obtain $\frac{R'}{\ell.W.E}$ from design Tables (i.e Table 8.3 or 8.4 if C = 0). This then gives the value of R′ required.

Shear force in loaded edge weld:-

$$F_{w\ell} = R'(\cos \gamma_\ell' - \mu \sin \gamma_\ell')$$

where $\gamma_\ell' = [\sin^{-1}(W/L) - 90 + \theta/2]C/W + 90 - \theta/2$

($= 90 - \theta/2$; when C = 0)

Fillet weld size required either side of loaded edge:-

$$t_{w\ell} = \frac{F_{w\ell}}{\sqrt{2}\, f_t . L . (1-C/W)}$$

Shear force in supported edge weld:-

$$F_{wh} = R'(\cos \gamma_h' - \mu \sin \gamma_h')$$

where $\gamma_h' = [\sin^{-1}(W/H) - 90 + \Theta/2]C/W + 90 - \Theta/2$

($= 90 - \Theta/2$; when $C = 0$)

Fillet weld size required either side of supported edge:-

$$t_{wh} = \frac{F_{wh}}{\sqrt{2}\, t_t . H (1-C/W)}$$

Loaded plate design check

The loaded plate size is usually determined by other constraints. The following is only intended as a check against it failing at its supported end.

Shear force at supported end:-

$$R_y = R' \sin \gamma_\ell' - P_u$$

$$\text{Shear stress } f_q = \frac{R_y}{T.B}$$

Axial force at supported end:-

$$R_x = R' \cos \gamma'_{\ell}$$

$$\text{Axial stress } f_a = \frac{R_x}{T.B}$$

Design of loaded plate support weld

If the loaded plate is welded to the support then the weld must be designed to carry the loads the loaded plate is subjected to.

$$\text{i.e. shear load} = R_y$$

$$\text{axial load} = R_x$$

Notes on ultimate limit state design stress

The ultimate limit state design strength for grade steel is given in Table 5.7.1 of the British draft steel code (2) less $20N/mm^2$ for sections fabricated from plates by welding.

The ultimate limit state design strength of a fillet weld is given in Section 14.6.3.11 of BS 5400: Part 3: 1982. The stress in a weld, based on the resultant of all shear forces acting on any part of it, and the effective area of such part, should not exceed the capacity f_t given by:

$$f_t = 0.215 (f_y + 455) \text{ for side fillets}$$

$$f_t = 0.334 (f_y + 455) \text{ for end fillets}$$

$$f_t = 0.239 (f_y + 455) \text{ for all other welds}$$

where f_y is the nominal yield stress of the weaker part joined.

Example 1

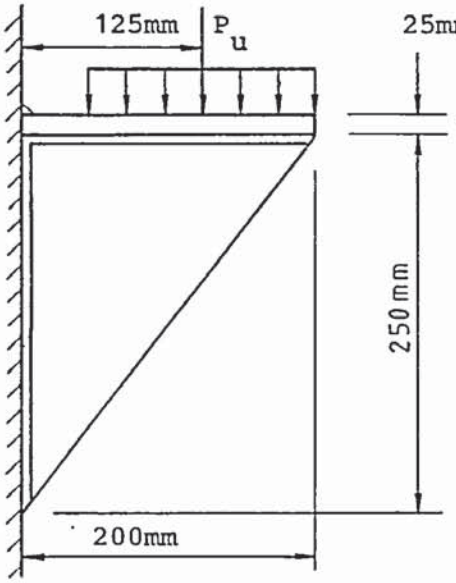

B = 150mm
Θ = 90°
H = 250mm
L = 200mm
C = 0
s = 125
f_y = 200N/mm^2
E = 206KN/mm^2
P_u = 280KN

A 90° bracket on a column supports a load of 280KN at the ultimate limit state. The thickness of the mild steel gusset plate and the size of the welds are required.

Gusset plate thickness:

$$V = \sqrt{L^2 + H^2} = \sqrt{200^2 + 250^2} = 320.2\text{mm}$$

$$W = \frac{L.H}{V} = \frac{200 \times 250}{320.2} = 156.2\text{mm}$$

$$Z = 1$$

$$\ell = Z.W = 156.2\text{mm}$$

$$\frac{Pu.s}{\ell.W^2.E} = \frac{280 \times 125}{156.2 \times 156.2^2 \times 206} = 44.58 \times 10^{-6}$$

$$\frac{f_y}{E} = \frac{200}{206 \times 10^3} = 0.9709 \times 10^{-3}$$

$$\frac{C}{W} = \frac{0}{156.2} = 0$$

From Table 8.2

$$\frac{t}{\ell} = 95.18 \times 10^{-3}$$

$$\therefore t = 95.18 \times 10^{-3} \times 156.2 = 14.8\text{mm}$$

$$\frac{t}{\ell} > 21.65 \times 10^{-3} \text{ therefore slenderness O.K.}$$

use 15mm thick plate

Gusset plate welds:

From Table 8.4

$$\frac{R'}{\ell.W.E} = 90.48 \times 10^{-6}$$

$$\therefore R' = 90.48 \times 10^{-6} \times 156.2 \times 156.2 \times 206 \times 10^{3}$$

$$= 454759\text{N}$$

$$= 454.8\text{kN}$$

Shear force in longitudinal weld

$$F_{w\ell} = R'(\cos \gamma'_{\ell} - \mu . \sin \gamma'_{\ell})$$

now $\gamma'_{\ell} = 90 - \theta/2 = 45°$

assume no friction i.e. $\mu = 0$

$$\therefore F_{w\ell} = 454.8 (\cos 45°) = 321.6\text{kN}$$

Fillet weld size required either side of loaded edge

$$t_{w\ell} = \frac{F_{w\ell}}{\sqrt{2}.f_t.L.(1-C/W)}$$

$$= \frac{321.6 \times 10^3}{\sqrt{2} \times 152 \times 200} = 7.5\text{mm}$$

Shear force in supported edge weld

$$F_{w\ell} = R'(\cos \gamma'_h - \mu.\sin \gamma')$$

$$= 454.8(\cos 45) - 321.6\text{kN}$$

Fillet weld size required either side of supported edge

$$t_{wh} = \frac{F_{wh}}{\sqrt{2}.f_t.H.(1-C/W)}$$

$$= \frac{321.6 \times 10^3}{\sqrt{2} \times 152 \times 250} = 6.0\text{mm}$$

Use 8mm fillet weld along both sides of the loaded and supported edges.

Loaded plate design check:

Shear force at supported end

$$R_y = R'\sin \gamma'_\ell - Pu$$

$$= 454.8 \sin 45 - 280 = 41.6\text{kN}$$

$$f_q = \frac{R_y}{T.B} = \frac{41.6 \times 10^3}{25 \times 150} = 11\ \text{N/mm}^2 \quad \text{O.K.}$$

Axial force at supported end

$$R_x = R' \cos \gamma'_{\ell}$$

$$= 454.8 \cos 45° = 321.6\text{kN}$$

$$f_a = \frac{321.6 \times 10^3}{25 \times 150} = 85.76 \text{ N/mm}^2 \quad \text{O.K.}$$

The loaded plate is adequate

Design of loaded plate support weld:

Assume a top fillet weld the full width of the loaded plate.

$$\text{Combined loading } R_c = \sqrt{R_x^2 + R_y^2} = \sqrt{321.6^2 + 41.6^2} = 324.3\text{kN}$$

$$t_w = \frac{\sqrt{2}\, R_c}{f_t . B} = \frac{\sqrt{2}.324.3 \times 10^3}{235 \times 150} = 13\text{mm}$$

To be consistent with the gusset plate welds, use 8mm fillet weld on top and bottom for the full width of the loaded plate.

Example 2

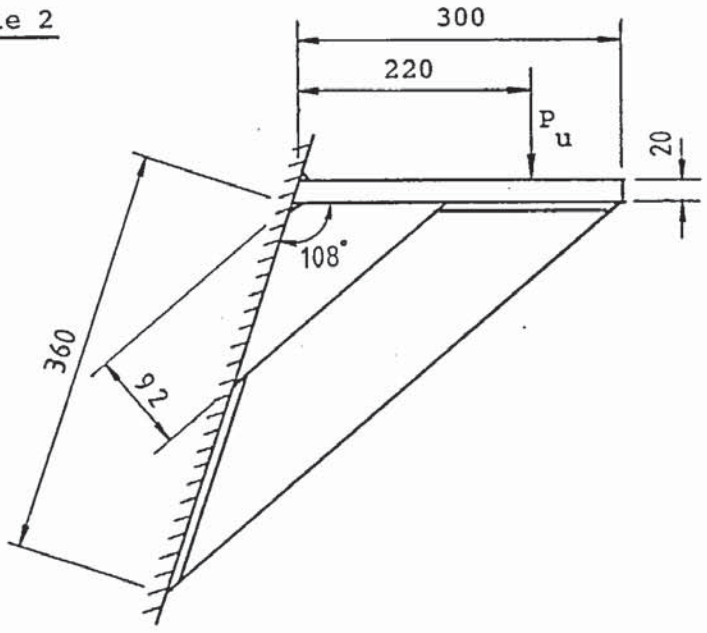

B	=	150mm
Θ	=	108°
H	=	360
L	=	300
C	=	92
s	=	220
f_y	=	200N/mm^2
E	=	206kN/mm^2
P_u	=	150kN

A bracket on an inclined column supports a load of 150kN at the ultimate limit state. The inside corner has been omitted to allow room for pipework. The thickness of the mild steel gusset plate and the size of the welds are required.

Gusset plate thickness:

$$V = \sqrt{L^2 + H^2 - 2.L.H \cos \theta}$$

$$= \sqrt{300^2 + 360^2 - 2 \times 300 \times 360 \times \cos 108^\circ}$$

$$= 535\text{mm}$$

$$W = \frac{L.H \sin \theta}{V} = \frac{300 \times 360 \times \sin 108^\circ}{535.1}$$

$$= 192\text{mm}$$

$$Z = \left\{\left[\frac{V}{2.W.\tan \theta/2} - 1\right] \frac{C}{W} + 1\right\}, \text{ but } \theta > 90^\circ$$

as $\theta = 108^\circ$ then θ is taken to be 90° in this equation.

$$Z = \left\{\left[\frac{535}{2 \times 192 \times \tan 90/2} - 1\right] \frac{92}{192} + 1\right\}$$

$$= 1.1884$$

$$\ell = Z.W.\tan \theta/2, \text{ but } \theta > 90^\circ$$

$$= 1.1884 \times 192 \times \tan 90/2$$

$$= 228\text{mm}$$

$$\frac{Pu.s}{\ell.W^2} = \frac{150 \times 10^3 \times 220}{228 \times 192^2} = 3.9262 \text{ N/mm}^2$$

$$f_y = 200 \text{ N/mm}^2$$

$$\frac{C}{W} = \frac{92}{192} = 0.479$$

From Table 8.1

$$\frac{t}{\ell} = 59.57 \times 10^{-3}$$

$$\therefore t = 59.57 \times 10^{-3} \times 228 = 13.6\text{mm}$$

$$\frac{t}{\ell} > 21.65 \times 10^{-3} \text{ therefore slenderness O.K.}$$

use 15mm thick plate 100mm wide.

Gusset plate welds:

From Table 8.3

$$\frac{R'}{\ell.W} = 5.365 \text{ N/mm}^2$$

$$R' = 5.365 \times 228 \times 192$$

$$= 234841 \text{ N}$$

$$= 234.8 \text{ kN}$$

Shear force in longitudinal weld

$$\gamma'_{\ell} = [\sin^{-1}(W/L) - 90 + \theta/2]C/W + 90 - \theta/2$$

$$= [\sin^{-1}(192/300) - 90 + 108/2]0.479 + 90 - 108/2$$

$$= 37.816$$

$$F_{w\ell} = R'(\cos \gamma'_{\ell} - \mu. \sin \gamma'_{\ell}$$

Assume no friction.

$$F_{w\ell} = 234.8 \cos 37.816$$

$$= 185.5 \text{ kN}$$

Fillet weld size required either side of loaded edge

$$t_{w\ell} = \frac{F_{w\ell}}{\sqrt{2}.f_t\, L(1-C/W)}$$

$$= \frac{185.5 \times 10^3}{\sqrt{2} \times 152 \times 300(1-0.479)}$$

$$= 5.5\text{mm}$$

Shear force in supported edge weld

$$\gamma'_h = [\sin^{-1}(W/H) - 90 + \theta/2]C/W + 90 - \theta/2$$

$$= [\sin^{-1}(192/360) - 90 + 108/2]0.479 + 90 - 108/2$$

$$= 34.195°$$

$$F_{wh} = R'(\cos \gamma'_h - \mu.\sin \gamma'_h)$$

$$= 234.8\ (\cos 34.145°)$$

$$= 194.2\text{kN}$$

Fillet weld size required either side of supported edge

$$t_{wh} = \frac{F_{wh}}{\sqrt{2}.f_t H(1-C/W)}$$

$$= \frac{194.2 \times 10^3}{\sqrt{2} \times 152 \times 360(1-0.479)}$$

$$= 4.8\text{mm}$$

Use 6mm fillet weld along both sides of the loaded and supported edges.

Loaded plate design check:

Shear forces at supported end

$$R_y = R' \sin \gamma'_\ell - Pu$$

$$= 234.8 \sin 37.816 - 150 = -6\text{kN}$$

$$f_q = \frac{R_y}{T.B} = \frac{6 \times 10^3}{20 \times 150} = 2 \text{ N/mm}^2 \text{ O.K.}$$

The loaded plate is adequate.

Design of loaded plate support weld:

Assume a top and bottom fillet weld the full width of the loaded plate

$$\text{Combined loading } R_c = \sqrt{R_x^2 + R_y^2}$$

$$= \sqrt{185.5^2 + 6^2}$$

$$= 185.6\text{kN}$$

$$t_w = \frac{R_c}{\sqrt{2}.f_t.B} = \frac{185.6 \times 10^3}{\sqrt{2} \times 235 \times 150} = 3.7$$

Use a 4mm fillet weld on top and bottom for the full width of the loaded plate. Alternatively to be consistent with the gusset plate welds use a full length 6mm fillet weld on top and a 40mm length on the underside.

REFERENCES

1. British Standard 449 (1969) The use of structural steel in buildings.

2. British Standard Institution - Draft standard specification for the structural use of steelwork in buildings, part 1, (November 19

3. van Dowen, A.A. Welded and bolted connections. 2nd International ECCS Symposium. New developments in steel construction, 1978.

4. Jensen, C.D. Welded structural brackets, Journal of the American Welding Society, October 1936, Vol. 15, No10.

5. Priest, M.H. The practical design of welded steel structures, Journal of the American Welding Society, August 1933, pp9-23.

6. American Welding Society welding handbook, 5th edition, section 5, Applications of welding, London, Macmillan, 1967.

7. Beedle, L.S., Tall, L. and Galambos, T.V. - Structural steel design, New York, The Ronald Press Company, 1st edition, pp550-555.

8. Salmon, C.G. and Johnson, J. - Steel structures; design and behaviour, 2nd edition, New York, Harper and Row, 1980.

9. Salmon, C.G. - Analysis of triangular bracket type plates, A.S.C.E. (Mech. Div) Vol. 88, No EM6 Proc. Paper 3363, pp41-87, December 1962.

10. Bulson, P.S. The stability of flat plates, Elsevier, 1971.

11. Timoshenko, S.P. and Gere J.M. - Theory of elastic stability, McGraw Hill Book Co. Inv., New York, 2nd edition, 1961, p348.

12. Salmon, C.G., Buettner, D.R. and O'Sheridan, T.C. - Laboratory investigation of unstiffened triangular bracket plates. Proc. A.S.C.E. (Struct. Div.), Vol. 90, pp257-278, April 1964.

13. Steel designer's manual - 4th edition, London, Crosby Lockwood Staples, 1972.

14. MacGinley, T.J. - Structural steelwork calculations and detailing, Butterworths, London, 1973.

15. Martin, L.H. - Methods for the limit state design of triangular steel gusset plates, Building and Environment, Vol. 14, pp147-155, 1979.

16. British Standard 5400 : Part 3, Code of practice for design of steel bridges.